MOLECULAR PHYSIOLOGY IN MOLLUSCS OF ECONOMIC OR ECOLOGICAL IMPORTANCE

EDITED BY: Xiaotong Wang and Youji Wang

PUBLISHED IN: Frontiers in Physiology and Frontiers in Marine Science

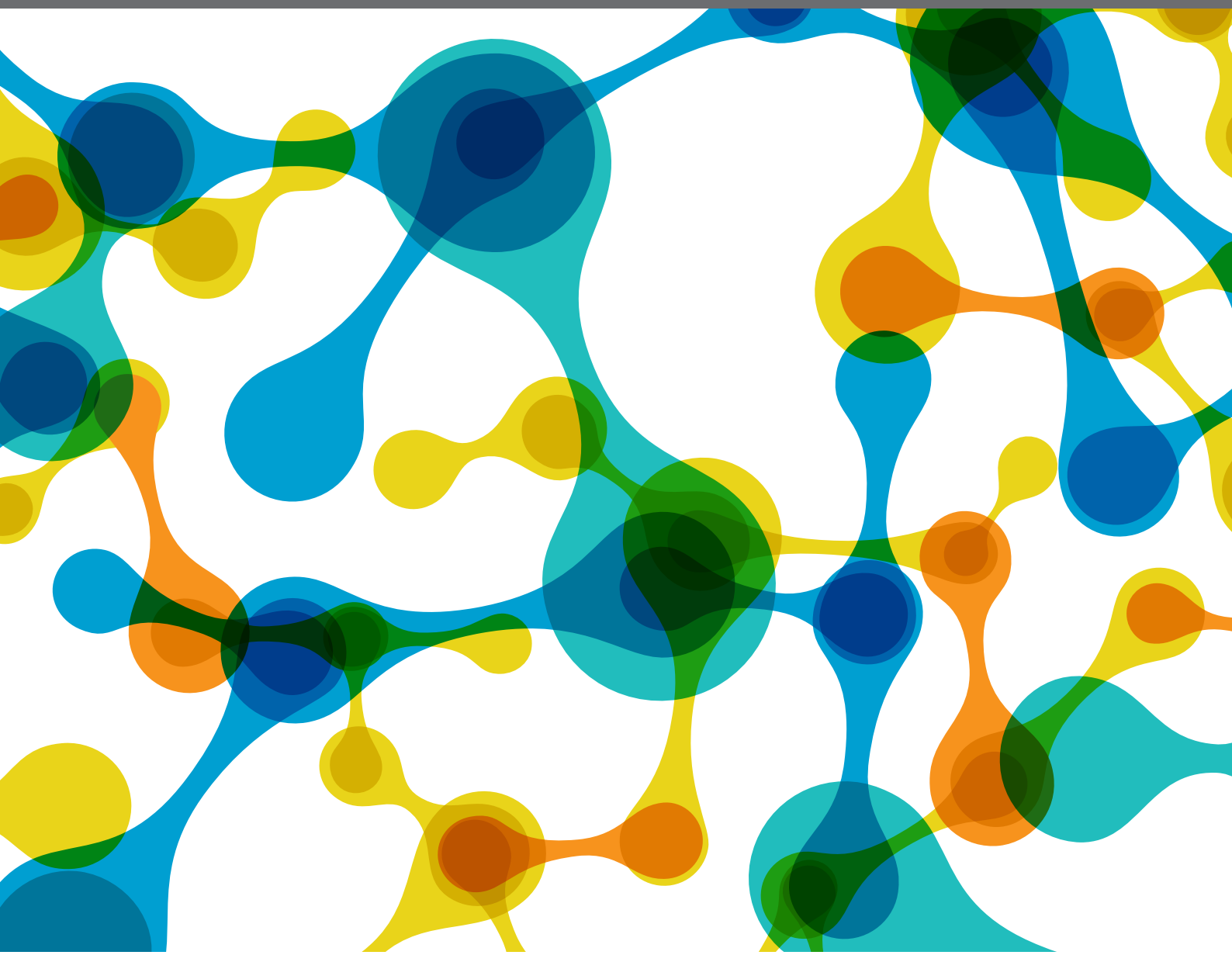

frontiers Research Topics

ISSN 1664-8714
ISBN 978-2-88963-135-3
DOI 10.3389/978-2-88963-135-3

About Frontiers

Frontiers is more than just an open-access publisher of scholarly articles: it is a pioneering approach to the world of academia, radically improving the way scholarly research is managed. The grand vision of Frontiers is a world where all people have an equal opportunity to seek, share and generate knowledge. Frontiers provides immediate and permanent online open access to all its publications, but this alone is not enough to realize our grand goals.

Frontiers Journal Series

The Frontiers Journal Series is a multi-tier and interdisciplinary set of open-access, online journals, promising a paradigm shift from the current review, selection and dissemination processes in academic publishing. All Frontiers journals are driven by researchers for researchers; therefore, they constitute a service to the scholarly community. At the same time, the Frontiers Journal Series operates on a revolutionary invention, the tiered publishing system, initially addressing specific communities of scholars, and gradually climbing up to broader public understanding, thus serving the interests of the lay society, too.

Dedication to Quality

Each Frontiers article is a landmark of the highest quality, thanks to genuinely collaborative interactions between authors and review editors, who include some of the world's best academicians. Research must be certified by peers before entering a stream of knowledge that may eventually reach the public - and shape society; therefore, Frontiers only applies the most rigorous and unbiased reviews.
Frontiers revolutionizes research publishing by freely delivering the most outstanding research, evaluated with no bias from both the academic and social point of view. By applying the most advanced information technologies, Frontiers is catapulting scholarly publishing into a new generation.

What are Frontiers Research Topics?

Frontiers Research Topics are very popular trademarks of the Frontiers Journals Series: they are collections of at least ten articles, all centered on a particular subject. With their unique mix of varied contributions from Original Research to Review Articles, Frontiers Research Topics unify the most influential researchers, the latest key findings and historical advances in a hot research area! Find out more on how to host your own Frontiers Research Topic or contribute to one as an author by contacting the Frontiers Editorial Office: researchtopics@frontiersin.org

MOLECULAR PHYSIOLOGY IN MOLLUSCS OF ECONOMIC OR ECOLOGICAL IMPORTANCE

Topic Editors:
Xiaotong Wang, Ludong University, China
Youji Wang, Shanghai Ocean University, China

Image: Xiaotong Wang.

As the largest marine phylum, molluscs comprise ~23% of all named marine organisms. Many molluscs have economic or ecological importance. With the development of molecular biology and omics techniques, significant gains have been made for molecular physiology in molluscs of economic or ecological importance.

Citation: Wang, X., Wang, Y., eds. (2019). Molecular Physiology in Molluscs of Economic or Ecological Importance. Lausanne: Frontiers Media.
doi: 10.3389/978-2-88963-135-3

Table of Contents

frontiers in Physiology

EDITORIAL
published: 06 September 2019
doi: 10.3389/fphys.2019.01131

Editorial: Molecular Physiology in Molluscs

Xiaotong Wang[1]* *and Youji Wang*[2]

[1] School of Agriculture, Ludong University, Yantai, China, [2] College of Fisheries and Life Science, Shanghai Ocean University, Shanghai, China

Keywords: mollusc, physiological process, morphological character, molecular mechanism, interaction with other factors

Editorial on the Research Topic

Molecular Physiology in Molluscs

Molluscs are second only to arthropods in terms of the number of living animal species and are the largest marine phylum, comprising ∼23% of all named marine organisms. Many molluscs have economic importance. Much progress has been made in the study of molluscan physiology, with two Nobel Prizes having been awarded for research on molluscan physiology (neurophysiology). Researching the giant axon of the squid, Professors A. L. Hodgkin and A. F. Huxley revealed the mechanisms involved in nerve impulses and, as a result, were awarded the Nobel Prize for Physiology or Medicine in 1963 (Wilbur and Yonge, 1964). Professor Eric Kandel, sharing the Nobel Prize for Physiology or Medicine 2000, found that, as snails learned, chemical signals changed the structure of the connections between cells (synapses), where the signals are sent and received, indicating that short- and long-term memories are formed by different signals (Kandel, 2005). Despite these prominent results, many obstacles remain in molluscan physiology research, such as the short domestication time, observation difficulties, absence of appropriate instruments and model animals, particularly the lack of a proliferative cell line. The embryonic cell line developed from the snail *Biomphalaria glabrata* (Bge) is the only existing cell line originating from a molluscan species (Yoshino et al., 2013). Compared with aquatic vertebrates, such as fish, the study of the functional validation of physiology-related genes has lagged behind in molluscs. However, with the development of molecular biology and omics techniques, molluscan physiology research has made significant gains over the past few years. The editorial office of Frontiers suggested that we should bring together related developments from other researchers, and publish a Research Topic on "molecular physiology in molluscs" in Frontiers in Physiology. At last, all 19 papers were published in this topic. These papers, united in this Research Topic, cover a broad thematic range and mainly focus on the molecular mechanisms of molluscan physiology.

In recent years, ocean acidification (OA), caused by further increases in atmospheric CO_2 partial pressure (Diaz et al., 2018), has become a hot Research Topic. Given that the main component of the external shells of mollusc (Marin et al., 2008) or internal bones (Marschner et al., 2013) or statoliths (Kaplan et al., 2013) is calcium carbonate, molluscs might be sensitive to ocean acidification (Parker et al., 2013; Wang et al., 2017; Campanati et al., 2018). Cao et al. reveal that OA reduced the resistance of Pacific oyster *Crassostrea gigas* to *Vibrio splendidus* challenge because of the increased energy expenditure, whereas Liao et al. report the energy metabolism and antioxidant responses of the Yesso scallop (*Patinopecten yessoensis*) under OA, reporting the tissue-specific effects related to energy metabolism. However, Kriefall et al. had different opinions about the physiological responses on seawater acidification because they found that far future OA levels have observable, but not severe, impacts on *Crepidula fornicata* larvae.

Cardiac-related physiology of molluscs is an interesting subject. Chen et al. show different transcriptomic responses to thermal stress in heat-tolerant and heat-sensitive Pacific abalones

OPEN ACCESS

Edited by:
Anna Di Cosmo,
University of Naples Federico II, Italy

Reviewed by:
Varvara Dyakonova,
Koltzov Institute of Developmental Biology, Russia
Roger P. Croll,
Dalhousie University, Canada

***Correspondence:**
Xiaotong Wang
wangxiaotong999@163.com

Specialty section:
This article was submitted to Aquatic Physiology, a section of the journal Frontiers in Physiology

Received: *31 May 2019*
Accepted: *16 August 2019*
Published: *06 September 2019*

Citation:
Wang X and Wang Y (2019) Editorial: Molecular Physiology in Molluscs. Front. Physiol. 10:1131. doi: 10.3389/fphys.2019.01131

indicated by cardiac performance, providing insight into the different heat-response strategies used by these animals. Cardiac indices were a novel approach used to investigate the scallop, *Chlamys farreri*. In their study, Xing et al. demonstrate that heart rate is a good indicator of thermal limit, whereas heart amplitude might indicate optimal growth temperature, and the rate-amplitude product could be an index of myocardial oxygen consumption, which provides basic information on the factors that might impact cardiac performance in scallops.

Via byssal threads, bivalves, such as mussels and scallops, can adhere to a variety of hard substrates under wet conditions (Amini et al., 2017; Waite, 2017). However, byssus adhesion is also an important cause of aquatic biofouling. In their paper, Li et al. focused on molecular bases of adhesive mechanisms of byssus in the highly invasive fouling mussel *Limnoperna fortunei*; their results will be of use to develop strategies against biofouling by freshwater organisms. Zhang et al. characterize an atypical metalloproteinase inhibitor-like protein (Sbp8-1) from the byssus of *C. farreri*, suggesting that Sbp8-1 might act as a crosslinker in the scallop byssus. This study also provides inspiration for the design of water-resistant materials.

Salinity is a primary physical factor affecting not only the distribution and physiological metabolism of molluscs (Jones et al., 2019), but also the areas suitable for the aquaculture of marine species. Jia and Liu report the molecular characterization of full-length Na^+/K^+-ATPase cDNA in Pacific abalone *Haliotis discus hannai*, finding that sudden salinity changes affect *NAK* gene transcription activation, translation, and enzyme activity via a cAMP-mediated pathway. Compared with Pacific abalone, Hong Kong oyster *Crassostrea hongkongensis* has a wider range of salinity adaptation. Using *in situ* transcriptomes, Xiao et al. reveal divergent adaptive responses to hyper- and hyposalinity in *C. hongkongensis*, suggesting the adaptive plasticity of marine molluscs.

Hemocytes of molluscs are involved in not only various physiological functions, but also innate immunity (Serpentini et al., 2000; Ray et al., 2013; Wang et al., 2013). Brokordt et al. propose that the hemocyte energy metabolic capacity potentially underlies cellular and molecular immune responses in a reproduction–immunity tradeoff in the scallop *Argopecten purpuratus*. The functioning of the host immune system relies on the frequent renewal and appropriate functioning of hemocytes, but the underlying renewal mechanism remains elusive at the gene level. Zhou et al. identify a transcription factor, LIM homeobox 9 (ChLhx9), in *C. hongkongensis*, showing that it induces hemocyte apoptosis by activating apoptotic genes or pathways, providing new insights into the functioning of molluscan hemocytes.

For human beings, the accumulation of toxic substances in molluscs is a serious food safety problem (Ragi et al., 2017). However, it is also unclear how the accumulation of toxic substances in molluscs will affect their own physiological activities, and how these effects might be impacted by other environmental factors. Cao et al. carried out a comparative *in vivo* study of the toxicity of saxitoxin (STX) on *C. gigas* and *C. farreri*, identifying different biochemical and immunotoxicity biomarkers in these two bivalves. Shi et al. demonstrate that anthropogenic noise and toxicity of cadmium have synergetic effects on the feeding activity, metabolism, and ATP synthesis of the blood clam *Tegillarca granosa*, which might be caused by the addition of stress responses and neurotransmitter disturbances.

Given their economic importance, the nutrition and growth physiology of molluscs have always been a focus of molluscan aquaculture research. Li et al. identify and characterize key genes in the hedgehog pathway of *C. gigas*, analyzing their accumulation and RNA localization patterns, and showing that the hedgehog pathway could be involved in *C. gigas* myogenesis. Although important for bivalve aquaculture, no artificial diet for bivalves has been successfully developed (Knauer and Southgate, 1999). By using a gas chromatography time-of-flight mass spectrometry (GC–TOF/MS)-based metabolomics approach, Yang et al. compare the metabolomics responses of pearl oysters (*Pinctada fucata martensii*) fed a formulated diet indoors with those of oysters cultured with natural diet outdoors, finding that the formulated diet could be an appropriate substitute for a natural diet, although its nutrient levels are insufficient.

Triploid oysters have been marketed for some years (Gong et al., 2004; Kang et al., 2013). However, data on the differences in the nutritional value between diploid and triploid oysters are lacking. Qin et al. compare the biochemical composition and nutritional quality of diploid vs. triploid *C. hongkongensis*, reporting that triploid *C. hongkongensis* has a better nutritional value and taste compared with the diploid *C. hongkongensis* during the reproductive phase. Thus, the authors suggest that we should consume triploid oysters harvested during the summer breeding season.

Finally, Kong et al. identify and analyze two novel short peptidoglycan recognition proteins from the deep sea Vesicomyidae clam *Archivesica packardana*, while Chen et al. report the method of piggyBac transposon-mediated transgenesis for the first time in a mollusc (*C. gigas*). Li et al. introduce the traditional Chinese nouns of "Yin" and "Yang" into the study of molecular physiology, identifying Forkhead Box L2 (FOXL2) and Doublesex And Mab-3 Related Transcription Factor 1L (DMRT1L) as the "Yin" and "Yang" Genes for female and male gonadal differentiation, respectively, in the bivalve mollusc *Patinopecten yessoensis*. Thus, those authors proposed that molecular sex differentiation is established before morphological sex differentiation in this species.

Together, the papers forming this Research Topic highlight exciting recent achievements in the varied world of molecular physiology research in molluscs, which will positively impact our understanding of molluscan physiology and advance the aquaculture of this economically important group. In future, cell line and genome editing developments could strongly promote the further research into the molecular physiology of molluscs.

AUTHOR CONTRIBUTIONS

All authors listed have made a substantial, direct and intellectual contribution to the work, and approved it for publication.

FUNDING

This work was supported by National Key R&D Program of China (2018YFD0901400), the National Natural Science Foundation of China (41876193), the Key R&D Program of Shandong Province, China (2018GHY115027), Special Funds for Taishan Scholars Project of Shandong Province, China (tsqn201812094), the Shandong Provincial Natural Science Foundation, China (ZR2019MC002), the Modern Agricultural Industry Technology System of Shandong Province, China (SDAIT-14-03), and the Key R&D Program of Yantai City, China (2017ZH054).

REFERENCES

Amini, S., Kolle, S., Petrone, L., Ahanotu, O., Sunny, S., Sutanto, C. N., et al. (2017). Preventing mussel adhesion using lubricant-infused materials. *Science* 357, 668–673. doi: 10.1126/science.aai8977

Campanati, C., Dupont, S., Williams, G. A., and Thiyagarajan, V. (2018). Differential sensitivity of larvae to ocean acidification in two interacting mollusc species. *Mar. Environ. Res.* 141, 66–74. doi: 10.1016/j.marenvres.2018.08.005

Diaz, R., Lardies, M. A., Tapia, F. J., Tarifeno, E., and Vargas, C. A. (2018). Transgenerational Effects of pCO_2-driven ocean acidification on adult mussels mytilus chilensis modulate physiological response to multiple stressors in larvae. *Front. Physiol.* 9:1349. doi: 10.3389/fphys.2018.01349

Gong, N., Yang, H., Zhang, G., Landau, B. J., and Guo, X. (2004). Chromosome inheritance in triploid pacific oyster Crassostrea gigas Thunberg. *Heredity.* 93, 408–415. doi: 10.1038/sj.hdy.6800517

Jones, H. R., Johnson, K. M., and Kelly, M. W. (2019). Synergistic effects of temperature and salinity on the gene expression and physiology of Crassostrea virginica. *Integr Comp Biol.* 59, 306–319. doi: 10.1093/icb/icz035

Kandel, E. R. (2005). *Psychiatry, Psychoanalysis, and the New Biology of Mind.* Washington, DC: American Psychiatric Pub.

Kang, J. H., Lim, H. J., Kang, H. S., Lee, J. M., Baby, S., and Kim, J. J. (2013). Development of genetic markers for triploid verification of the pacific oyster, crassostrea gigas. *Asian Austr. J. Anim. Sci.* 26, 916–920. doi: 10.5713/ajas.2013.13108

Kaplan, M. B., Mooney, T. A., Mccorkle, D. C., and Cohen, A. L. (2013). Adverse effects of ocean acidification on early development of squid (Doryteuthis pealeii). *PLoS ONE* 8:e63714. doi: 10.1371/journal.pone.0063714

Knauer, J., and Southgate, P. C. (1999). A review of the nutritional requirements of bivalves and the development of alternative and artificial diets for bivalve aquaculture. *Rev. Fish. Sci.* 7:40. doi: 10.1080/10641269908951362

Marin, F., Luquet, G., Marie, B., and Medakovic, D. (2008). Molluscan shell proteins: primary structure, origin, and evolution. *Curr. Top. Dev. Biol.* 80, 209–276. doi: 10.1016/S0070-2153(07)80006-8

Marschner, L., Staniek, J., Schuster, S., Triebskorn, R., and Kohler, H. R. (2013). External and internal shell formation in the ramshorn snail *Marisa cornuarietis* are extremes in a continuum of gradual variation in development. *BMC Dev. Biol.* 13:22. doi: 10.1186/1471-213X-13-22

Parker, L. M., Ross, P. M., O'connor, W. A., Portner, H. O., Scanes, E., and Wright, J. M. (2013). Predicting the response of molluscs to the impact of ocean acidification. *Biology* 2, 651–692. doi: 10.3390/biology2020651

Ragi, A. S., Leena, P. P., Cheriyan, E., and Nair, S. M. (2017). Heavy metal concentrations in some gastropods and bivalves collected from the fishing zone of South India. *Mar. Pollut. Bull.* 118, 452–458. doi: 10.1016/j.marpolbul.2017.03.029

Ray, M., Bhunia, A. S., Bhunia, N. S., and Ray, S. (2013). Density shift, morphological damage, lysosomal fragility and apoptosis of hemocytes of Indian molluscs exposed to pyrethroid pesticides. *Fish. Shellfish Immunol.* 35, 499–512. doi: 10.1016/j.fsi.2013.05.008

Serpentini, A., Ghayor, C., Poncet, J. M., Hebert, V., Galera, P., Pujol, J. P., et al. (2000). Collagen study and regulation of the de novo synthesis by IGF-I in hemocytes from the gastropod mollusc, Haliotis tuberculata. *J. Exp. Zool.* 287, 275–284. doi: 10.1002/1097-010X(20000901)287:4<275::AID-JEZ2>3.0.CO;2-8

Waite, J. H. (2017). Mussel adhesion - essential footwork. *J. Exp. Biol.* 220, 517–530. doi: 10.1242/jeb.134056

Wang, X., Li, L., Zhu, Y., Du, Y., Song, X., Chen, Y., et al. (2013). Oyster shell proteins originate from multiple organs and their probable transport pathway to the shell formation front. *PLoS ONE* 8:e66522. doi: 10.1371/journal.pone.0066522

Wang, X., Wang, M., Jia, Z., Song, X., Wang, L., and Song, L. (2017). A shell-formation related carbonic anhydrase in Crassostrea gigas modulates intracellular calcium against CO2 exposure: implication for impacts of ocean acidification on mollusc calcification. *Aquat. Toxicol.* 189, 216–228. doi: 10.1016/j.aquatox.2017.06.009

Wilbur, K. M., and Yonge, C. M. (1964). *Physiology of Mollusca.* New York, NY: Academic Press.

Yoshino, T. P., Bickham, U., and Bayne, C. J. (2013). Molluscan cells in culture: primary cell cultures and cell lines. *Can. J. Zool.* 91, 391–404. doi: 10.1139/cjz-2012-0258

Conflict of Interest Statement: The authors declare that the research was conducted in the absence of any commercial or financial relationships that could be construed as a potential conflict of interest.

frontiers in Physiology

ORIGINAL RESEARCH
published: 12 July 2018
doi: 10.3389/fphys.2018.00880

Seawater Acidification Reduced the Resistance of *Crassostrea gigas* to *Vibrio splendidus* Challenge: An Energy Metabolism Perspective

*Ruiwen Cao[1,2,3], Yongliang Liu[1], Qing Wang[1,2], Dinglong Yang[1,2], Hui Liu[1,2], Wen Ran[1,2,3], Yi Qu[1,2,3] and Jianmin Zhao[1,2]**

[1] Muping Coastal Environmental Research Station, Yantai Institute of Coastal Zone Research, Chinese Academy of Sciences, Yantai, China, [2] Research and Development Center for Efficient Utilization of Coastal Bioresources, Yantai Institute of Coastal Zone Research, Chinese Academy of Sciences, Yantai, China, [3] University of Chinese Academy of Sciences, Beijing, China

OPEN ACCESS

Edited by:
Xiaotong Wang,
Ludong University, China

Reviewed by:
Wenguang Liu,
South China Sea Institute of Oceanology (CAS), China
Hongjun Li,
National Marine Environmental Monitoring Center, China
Camille Détrée,
Universidad Austral de Chile, Chile

***Correspondence:**
Jianmin Zhao
jmzhao@yic.ac.cn

Specialty section:
This article was submitted to Aquatic Physiology, a section of the journal Frontiers in Physiology

Received: 03 April 2018
Accepted: 19 June 2018
Published: 12 July 2018

Citation:
Cao R, Liu Y, Wang Q, Yang D, Liu H, Ran W, Qu Y and Zhao J (2018) Seawater Acidification Reduced the Resistance of Crassostrea gigas to Vibrio splendidus Challenge: An Energy Metabolism Perspective. Front. Physiol. 9:880. doi: 10.3389/fphys.2018.00880

Negative physiological impacts induced by exposure to acidified seawater might sensitize marine organisms to future environmental stressors, such as disease outbreak. The goal of this study was to evaluate if ocean acidification (OA) could reduce the resistance capability of the Pacific oyster (*Crassostrea gigas*) to *Vibrio splendidus* challenge from an energy metabolism perspective. In this study, the Pacific oyster was exposed to OA (pH 7.6) for 28 days and then challenged by *V. splendidus* for another 72 h. Antioxidative responses, lipid peroxidation, metabolic (energy sensors, aerobic metabolism, and anaerobic metabolism) gene expression, glycolytic enzyme activity, and the content of energy reserves (glycogen and protein) were investigated to evaluate the environmental risk of pathogen infection under the condition of OA. Our results demonstrated that following the exposure to seawater acidification, oysters exhibited an energy modulation with slight inhibition of aerobic energy metabolism, stimulation of anaerobic metabolism, and increased glycolytic enzyme activity. However, the energy modulation ability and antioxidative regulation of oysters exposed to seawater acidification may be overwhelmed by a subsequent pathogen challenge, resulting in increased oxidative damage, decreased aerobic metabolism, stimulated anaerobic metabolism, and decreased energy reserves. Overall, although anaerobic metabolism was initiated to partially compensate for inhibited aerobic energy metabolism, increased oxidative damage combined with depleted energy reserves suggested that oysters were in an unsustainable bioenergetic state and were thereby incapable of supporting long-term population viability under conditions of seawater acidification and a pathogen challenge from *V. splendidus*.

Keywords: ocean acidification, *Crassostrea gigas*, *Vibrio splendidus*, oxidative stress, energy metabolism, physiological response

Abbreviations: ACN, aconitate hydratase; AK, adenylate kinase; AMPK, AMP-activated protein kinase; Axin, Fu gene inhibition axis formation; COX, cytochrome c oxidase; COX 1, subunit 1 of cytochrome c oxidase; D-LDH X1, D-lactate dehydrogenase transcript variant X1 (mitochondrial); D-LDH X2, D-lactate dehydrogenase transcript variant X2 (mitochondrial); GLY, glycogen; HK, hexokinase; IDH, isocitrate dehydrogenase; PK, pyruvate kinase; PROT, protein; SCS, succinyl-CoA synthetase alpha subunit; SDH, succinate dehydrogenase; SIRT2, NAD-dependent deacetylase sirtuin-2.

INTRODUCTION

Increased atmospheric CO_2 concentrations caused by anthropogenic activities have and will continue to contribute to ocean acidification (OA), as about 30% of CO_2 is absorbed by the oceans (Sabine et al., 2004). The pH of surface seawater has already declined approximately 0.1 pH units compared with pre-industrial levels (Intergovernmental Panel on Climate Change, 2014). With further increases of atmospheric CO_2 partial pressure (pCO_2), surface ocean pH is predicted to decline by another 0.3–0.4 pH units by the end of this century (Caldeira and Wickett, 2005). Due to biogeochemical and biochemical processes, such as eutrophication, anthropogenic sulfur and nitrogen deposition, and the existence of a mid-salinity minimum buffer zone, pH in coastal and estuary areas is more variable than that in the open ocean (Doney et al., 2007; Cai et al., 2011; Hu and Cai, 2013).

Numerous studies have indicated that coastal ecosystems are under more serious threat from OA combined with other environmental stressors, including increased ocean temperature, pollution, and pathogenic challenge (Chen et al., 2015; Queirós et al., 2015; Gunderson et al., 2016; Moreira et al., 2016; Duckworth et al., 2017). Seawater acidification has been found to negatively affect physiological processes in mollusks such as calcification, respiration, filtration, acid–base regulation, and immune responses (Pörtner et al., 2004; Gazeau et al., 2013; Sui et al., 2015; Liu et al., 2016; Castillo et al., 2017; Zhao et al., 2017), which could lead to severe threats for their energy budget (Wang et al., 2015). As a consequence, the negative impact posed by acidified seawater might sensitize marine organisms to future environmental perturbations, such as pathogenic infection (Hooper et al., 2007; Ellis et al., 2015). However, few studies have investigated the integrated environmental impacts of OA and pathogen infection on marine organisms. *Vibrio*sis, one of the major bacterial diseases affecting fish, bivalves, and crustaceans, is caused by pathogenic *Vibrio* species and has posed a severe challenge to marine organisms inhabiting coastal and estuary areas (Beaz-Hidalgo et al., 2010). It is therefore urgently needed to investigate the environmental and ecological future of coastal and estuarine regions under acidified seawater and pathogenic *Vibrio* infection.

Marine bivalves are globally recognized as valuable species from ecological and economic perspectives (Dumbauld et al., 2009). The Pacific oyster, *Crassostrea gigas,* is an important aquaculture bivalve species inhabiting estuaries and intertidal regions, where they are constantly confronted with various environmental perturbations. As a result, oysters are believed to be highly tolerant to multiple environmental stressors (Dineshram et al., 2016). However, some strains of *Vibrio splendidus* have been associated with summer mortality of juvenile oysters *C. gigas* (Lacoste et al., 2001; Gay et al., 2004). In addition, recent studies have found that OA could lead to immune suppression of marine invertebrates, especially marine bivalves, which could sensitize these species to pathogen infection (Hernroth et al., 2011; Ivanina et al., 2014; Liu et al., 2016; Wang et al., 2016).

Previous studies have shown that both OA and pathogenic infection could induce disturbances in energy metabolism and oxidative stress in marine organisms (Canesi et al., 2010; Ellis, 2013; Liu et al., 2013; Ellis et al., 2014; Lesser, 2016). The bioenergetics sustainability under environmental perturbations is linked directly to an organism's fitness and has thus population-level consequences (Sokolova et al., 2012). Our proteomic study has also found that energy metabolism disturbance was correlated with oyster immunosuppression in response to seawater acidification and pathogens challenge (Cao et al., 2018). As a follow-up study, antioxidant enzyme activities (CAT, SOD, and GPx) and lipid peroxidation (LPO) were investigated in *C. gigas*. Moreover, the expression responses of genes related to energy sensors (Axin1, AMPKβ, and SIRT2), aerobic metabolism [TCA cycle enzymes, electron transport chain (ETC) components, and ATP turnover], and anaerobic metabolism (D-LDH X1 and D-LDH X2) combined with energy reserve content (GLY and PROT) were also investigated to assess the energy expenditure response, and further elucidated whether the altered oyster energy metabolism strategy was long-term sustainable in response to OA and/or *V. splendidus*.

MATERIALS AND METHODS

Ocean Acidification Perturbation Experiment

Adult Pacific oysters (8–11 cm in shell length) were collected from a local farm from Muping, Yantai, and Shandong Provinces of China (37°38′N and 121°59′E; pH 8.10 ± 0.03) in December 2016, and acclimated in the laboratory for 2 weeks before commencement of the experiment. During the acclimation period, the organisms were maintained at a temperature of 17.3 ± 0.2°C and pH 8.14 ± 0.02 in aerated seawater (salinity 31.2 ± 0.5). After the preliminary acclimation, oysters were exposed for four weeks to two levels of seawater pH (8.1 or 7.6), followed by a 72 h challenge treatments (non-injection, filter-sterilized seawater-injection, or *V. splendidus*-injection), for a total of six treatments. The selected pH levels were representative of the present-day condition (pH 8.1) and the predicted condition by the moderate scenarios of Forster et al. (2007) for the year 2250 (pH 7.6). For each treatment, 3 aquaria were used with 20 organisms per aquarium (60 individuals per treatment). The control seawater was bubbled with the atmospheric air. Seawater bubbled with air–CO_2 mixtures was adjusted through an air and CO_2 gas flow adjustment system and set as the elevated pCO_2 treatment (pH 7.6). Oysters were fed twice daily with a commercial algal blend (containing *Chlorella vulgaris* Beij and *Phaeodactylum tricornutum*).

During the exposure period, seawater was renewed every other day using pre-equilibrated seawater. No oyster mortality was observed during OA exposure. The pH of each container was monitored daily with a pH electrode (pH meter PB-10, Sartorius Instruments, Germany) calibrated with NBS standard pH solution. Salinity, temperature, and dissolved oxygen (DO) were determined daily by using an YSI meter (YSI® model 85, Yellow Springs, OH, United States). Water samples were

collected from each tank every week to determine total alkalinity (TA) by potentiometric titration (Gran, 1952). Other related parameters of the carbonate chemistry were calculated according to known values of pH and TA levels using the software CO_2SYS with the constants for seawater pH from Millero et al. (2006) and for KSO_4^-, from Dickson (1990). Seawater carbonate chemistry parameters of all treatments are presented in Supplementary Table S1.

Bacterial Challenge Experiment

Vibrio splendidus was cultured in 2216E medium at 28°C overnight, and centrifuged at 4000 *g* for 10 min at 25°C. Then the pellet was re-suspended in filter-sterilized (0.22 μm pore size) seawater (FSSW) and adjusted to a final concentration of 5×10^7 CFU mL^{-1}.

After 28 days of OA exposure, either 100 μL of FSSW (fssw-inj group) or 100 μL of *V. splendidus* suspension (5×10^6 CFU per oyster, *Vibrio*-inj group) was injected into the adductor muscle of oysters. Oysters without injection (non-inj group) were also sampled after OA exposure. After processing, the animals from each treatment were returned to respective aquariums for another 72 h. No oyster mortality was found during the infection period.

Sampling Procedure and Biochemical Analysis

At the end of the exposure period, six replicates of digestive glands and gills were sampled in each treatment. The tissues were immediately frozen in liquid nitrogen and stored at −80 °C until used for biochemical analyses. Meanwhile, six replicates of digestive glands were carefully excised and stored in RNAlater solution (Ambion, Austin, TX, United States) for subsequent RNA extraction.

Antioxidant Enzyme and Glycolytic Enzyme Activity Assay

Oyster gills were homogenized in phosphate buffer (50 mM potassium dihydrogen phosphate; 50 mM potassium phosphate dibasic; 1 mM EDTA; pH 7.0) and centrifuged at 10,000 *g* for 20 min at 4°C to obtain the supernatants. The resultant supernatants were subjected to antioxidant enzymes assays and LPO determination. Catalase (CAT) activity was determined according to the modified method of Vega-López et al. (2007), following the protocol proposed by Radi et al. (1991). This method evaluated the alteration in absorbance resulting from hydrogen peroxide (H_2O_2) degradation at 240 nm, with enzyme activity expressed as U mg^{-1} of PROT. Superoxide dismutase (SOD) activity was quantified using the method proposed by Beauchamp and Fridovich (1971), with some modifications adapted by Carregosa et al. (2014). One unit of SOD activity was defined as the amount of enzyme that caused 50% inhibition in the rate of nitroblue tetrazolium (NBT) chloride reduction and was expressed as U mg^{-1} of PROT. Glutathione peroxidase (GPx) activity was measured as described by Lawrence and Burk (1976). The method assessed the decrement in nicotinamide adenine dinucleotide phosphate (NADPH) concentration in an assay coupled to glutathione reductase (GR) that catalyzed NADPH oxidation at 340 nm. The results were expressed as U mg^{-1} of PROT. LPO levels were quantified by measuring the malondialdehyde (MDA) content, according to the method previously described by Ohkawa et al. (1979). MDA concentrations were measured spectrophotometrically at OD 532 nm and the results were expressed as nmol MDA mg^{-1} of PROT.

Enzymatic activities of HK and PK were determined in the digestive glands of OA and/or *V. splendidus*-exposed oysters. The activities of HK and PK were determined as described by Greenway and Storey (1999) and the results were expressed as U g^{-1} of PROT.

Energy Reserves

Glycogen content was measured by using the phenol-sulfuric acid method described by Yoshikawa (1959). A calibration curve was obtained by using glucose standards. PROT content was quantified following the Biuret method (Robinson and Hogden, 1940). Bovine serum albumin (BSA) was used as the standard material. The GLY and the PROT content was expressed as mg per g FW (fresh weight).

RT-PCR Analysis

The mRNA expression levels of eight genes related to energy metabolism (ACN, IDH, SDH, SCS, COX 1, COX, AK, ATP synthase subunit alpha Axin1, AMPKβ, SIRT2, D-LDH X1, and D-LDH X2) and two immune related genes (Integrin beta-1B and TNF) were determined in OA and/or *V. splendidus* exposed treatments. Total RNA was extracted with TRIzol reagent (Invitrogen, United States) following the manufacturer's instructions. DNase I (Promega, United States) treated RNA was used as a template for cDNA synthesis. A standard protocol was undertaken to perform quantitative real-time PCR program by using an Applied Biosystems 7500 fast Real-Time PCR System (Applied Biosystems, United States). The primers designed for quantitative RT-PCR are presented in Supplementary Table S3. A dissociation curve analysis of amplification products was performed at the end of each PCR to confirm that only one PCR product was amplified and detected. Expression of target genes was normalized with the elongation factor 1-alpha reference gene (de Lorgeril et al., 2011), which was stable in the current study ($p > 0.05$, coefficient of variation < 5%). The comparative $2^{-\Delta\Delta CT}$ method was used to analyze the expression level of the selected genes (Livak and Schmittgen, 2001).

Integrated Biomarker Response (IBR)

The "Integrated Biomarker Response version 2" (IBRv2) index was utilized to integrate multiple biochemical parameters into one general index representing the environmental stress level of different treatments (Sanchez et al., 2013). To calculate the IBRv2 values, individual biomarker data (Xi) were compared to reference data (X0) and log transformed to reduce variance: Yi = log Xi/X0. The general mean (μ) and SD of each biomarker Yi were computed for all treatments; Yi was standardized as Zi = (Yi−μ)/s. Biomarker deviation index (A) was calculated using the mean of the standardized biomarker response (Zi) and mean of reference biomarker data (Z0): Ai = Zi−Z0. For a single treatment, the biomarker deviation index (A) was presented

in star plots, representing the deviation of each investigated biomarker in OA and/or *V. splendidus* exposed groups, compared to the control group. The area above 0 reflected biomarker induction, and the area below 0 indicated a biomarker inhibition. In addition, the IBRv2 was calculated for each biomarker in each treatment: IBRv2 = $\Sigma|A|$.

Statistical Analysis

All measured biochemical parameters were presented as the mean ± SD. The raw data were assessed for normality and homogeneity of variances using the Shapiro–Wilk test and Bartlett's test, respectively. A two-way ANOVA followed by Fisher's least significant difference (LSD) *post hoc* analyses was performed on all data to test for significant differences ($p < 0.05$) between treatments. The analyses were carried out using SPSS version 23.0 (SPSS Inc., Chicago, IL, United States). ANOVA results for all studied parameters are displayed in Supplementary Tables S4, S5. Principal component analysis (PCA) was performed with CANOCO 5.0 software (Microcomputer Power Inc., United States) using gene expression data from OA and *V. splendidus* exposed oysters to assess the variability associated with energy metabolism and immune responses.

RESULTS

Antioxidant Enzyme Responses and Oxidative Damage

There was no significant change in any of the physiological parameters measured in fssw-inj-treated oysters compared to non-inj-treated oysters (Supplementary Table S2). As a result, the oysters treated with fssw-injection were set as the control in the present study. The antioxidant enzyme responses and oxidative damage under OA and/or *Vibrio* exposure are shown in **Figure 1**. CAT activity increased significantly in oysters treated with *Vibrio* at pH 7.6 ($p < 0.05$, **Figure 1A**). However, no significant changes in CAT activity were observed in oysters exposed to either OA or *Vibrio* alone. Similarly, there was no significant change in SOD activity among all four treatments (Control, *Vibrio*, OA, and *Vibrio*-OA groups; **Figure 1B** and Supplementary Table S4). Regarding GPx activity, significant inhibition effect was observed in oysters under combined OA and *Vibrio* exposure ($p < 0.05$, **Figure 1C**). Oysters showed significantly higher LPO levels in response to *Vibrio* challenge, either alone or combined with OA (**Figure 1D**). However, oysters exposed only to OA showed higher but not significantly different LPO levels compared to the control individuals (**Figure 1D** and Supplementary Table S4).

Glycolytic Enzyme Activities and Energy Reserves

No significant difference in HK activity was found among individuals in the four treatments (**Figure 2A**). However, the enzyme activity of PK was significantly increased in OA-treated oysters, regardless of *Vibrio* challenge ($p < 0.01$; **Figure 2B** and Supplementary Table S4). Further, as a major energy reserve, GLY content was significantly decreased in response to the combined exposure of OA and *V. splendidus* compared to other treatments ($p < 0.05$; **Figure 2C** and Supplementary Table S4). No significant change in GLY content was found in the digestive glands of oysters treated with either OA or *Vibrio*. However, PROT content was significantly lower in *Vibrio* and *Vibrio*-OA treatments compared to the control group (**Figure 2D**), while no apparent change was found in OA-treated oysters compared with the other three treatments.

Expression of Genes Related to Energy Metabolism and Immune Responses

The expression levels of genes related to aerobic metabolism, including the TCA cycle (ACN, IDH, SDH, and SCS), mitochondria electron transfer chain components (COX1 and COX), and ATP metabolism (ATP synthase subunit alpha and AK), and two immune factors (TNF and integrin beta-1B), were investigated in oysters under exposure of OA and/or *Vibrio* (**Figure 3**). The mRNA expression of TCA cycle-related genes (ACN, IDH, SDH, and SCS) was significantly inhibited under *Vibrio* challenge (**Figures 3A–D** and Supplementary Table S5). The expression level of two TCA cycle enzyme (SDH and SCS) transcripts was significantly inhibited under OA exposure without *Vibrio* challenge compared to the control individuals (**Figures 3C,D**). To the contrary, the mRNA expression of ATP metabolism related genes (ATP synthase and AK) were significantly stimulated under OA challenge without *Vibrio* infection compared to other treatments (**Figures 3G,H**).

The expression pattern of all genes tested in *Vibrio*-OA-treated oysters was similar to that of *Vibrio*-treated individuals. The expression level of most of the aerobic metabolism-related genes (IDH, SDH, SCS, and COX1) was depressed under combined exposure to OA and *Vibrio*, but OA individually did not elevate the inhibition effect (**Figures 3A–E** and Supplementary Table S5). ANOVA results also suggest that there is generally no significant interaction between OA and *Vibrio* challenges, with the exception of SCS, ATP synthase subunit alpha, and AK (Supplementary Table S5). The mRNA expression of ATP synthase subunit alpha and AK transcripts was significantly decreased in oysters under *Vibrio*-OA exposure compared to OA treatment, suggesting an antagonistic relationship between *Vibrio* and OA on the expression of these two genes (**Figures 3G,H**). The expression level of integrin beta-1B transcripts was not altered in response to OA and *Vibrio* challenges, individually or in combination (**Figure 3I**). *Vibrio* challenge significantly inhibited the expression of TNF transcripts, regardless of OA exposure (**Figure 3J**), while no significant change was observed in oysters under OA exposure alone.

The expression responses of genes related to metabolic sensors (Axin1, AMPKβ, and SIRT2) and anaerobic glycolysis (D-LDH X1 and D-LDH X2) were also investigated. Our results showed significantly elevated expression of all genes (Axin1, AMPKβ, SIRT2, D-LDH X1, and D-LDH X2) investigated under exposure to *Vibrio* and OA (**Figures 4A–E** and Supplementary Table S5). A significant stimulation effect was observed in the expression of AMPKβ transcripts of *Vibrio*-treated oysters (**Figure 4B**). In oysters treated with OA alone, the expression of all genes (AMPKβ, SIRT2, D-LDH X1, and D-LDH X2), with the

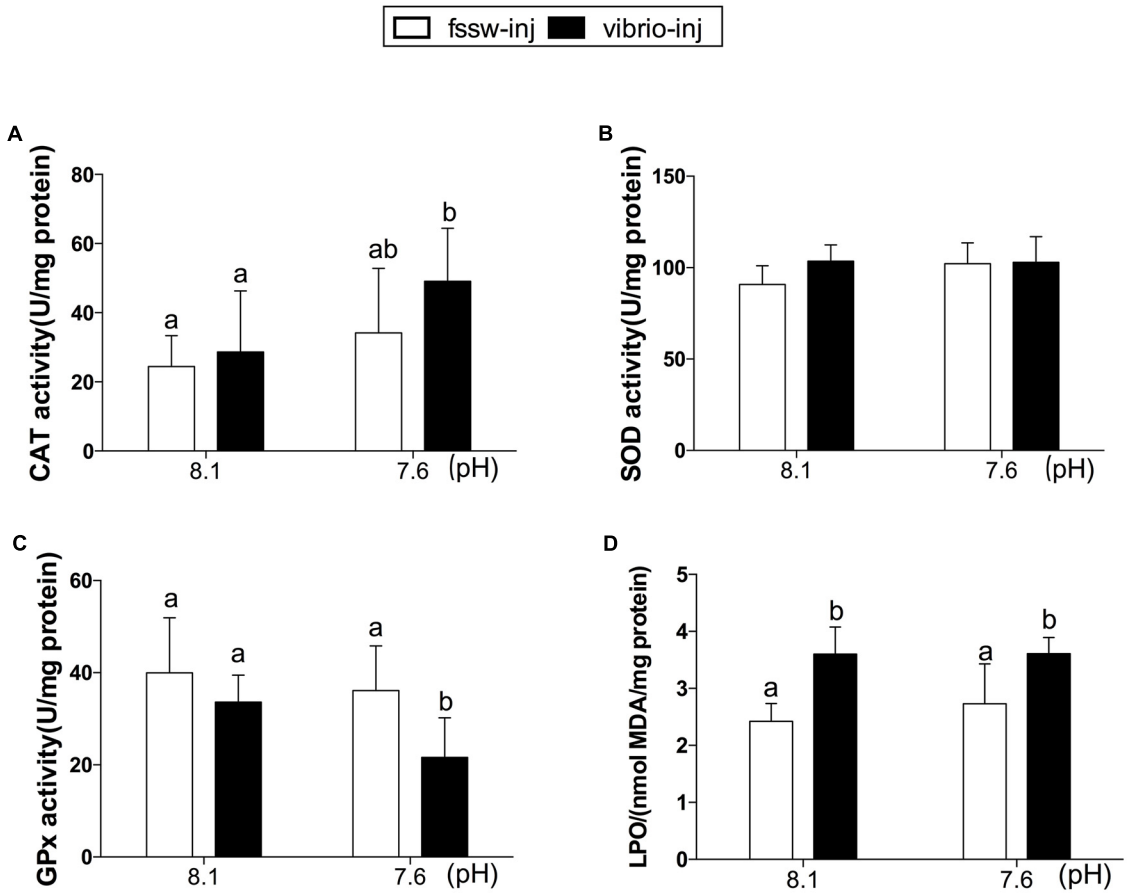

FIGURE 1 | Antioxidant enzyme activities and LPO levels in the gills of *C. gigas* post elevated pCO_2 and/or *V. splendidus* exposure. **(A)** CAT. **(B)** SOD. **(C)** GPx. **(D)** LPO. Each bar represents mean ± SD ($n = 6$). Different letters indicate significant differences among different treatments ($p < 0.05$).

exception of Axin1, was significantly elevated compared to the control group (**Figures 4B–E**). However, a significant interaction between OA and *Vibrio* was observed only in the expression of Axin1 transcripts (Supplementary Table S5).

Principal Component Analysis (PCA)

Principal component analysis was applied to all expression abundance data of aerobic energy metabolism-related genes and two immune genes from digestive glands (**Figure 5A**) and revealed 59.99% of the total variance. PC1 represented 40.53% of variance, highlighting the separation between non- and *Vibrio* exposed oysters. The second component (explaining only 19.46% of the variance) identified the separation of non-OA and OA exposure treatments without *Vibrio* challenge. Overall, PCA analysis provided further validation for the clustering of aerobic energy metabolism-related genes on the negative side of PC 1. Furthermore, PC 1 showed the clustering of *Vibrio* treatments in opposition to the expression elevation of all measured aerobic metabolism-related genes.

Additionally, PCA clustering of expression abundance data of energy metabolism-related (metabolic sensors, aerobic metabolism, and anaerobic metabolism) genes and two immune genes showed a total 51.85% variance (**Figure 5B**). PC1 expressed 35.93% variance, revealing separation between non- and *Vibrio*- exposed treatments. *Vibrio* and *Vibrio*-OA treatments correlated positively with metabolic sensor- and anaerobic metabolism-related genes and correlated negatively with aerobic metabolism-related genes. These results clearly demonstrated that in response to *Vibrio* challenge, either alone or combined with OA, oysters exhibited suppressed aerobic metabolism and stimulated aerobic metabolism.

Integrated Biomarker Response (IBR)

The IBR star plots present transformed data for each measured biochemical parameter (antioxidant enzymes and oxidative damage, glycolytic enzymes, and energy reserves) in oysters exposed to an OA and *Vibrio* challenge (**Figure 6A**). Star plots revealed that most of the parameters (CAT, GPx, HK, PROT, and GLY) showed higher response in oysters exposed to both *Vibrio* and OA than single stressor-treated individuals. The higher IBR index in oysters treated with *Vibrio*-OA, compared to single stressor-treated individuals, suggested that oysters were under severe stress in response to the combined exposure of *Vibrio* and OA. The integrated biomarker response (IBR) values in each

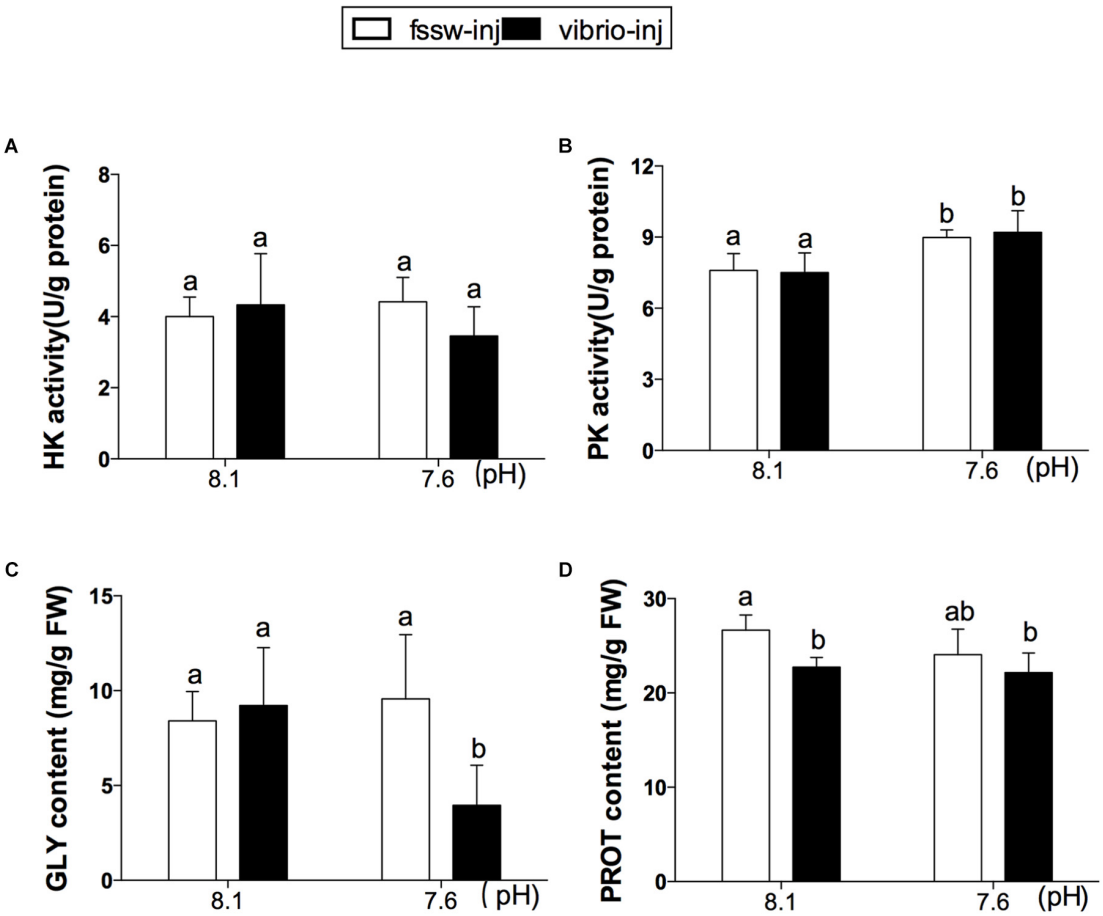

FIGURE 2 | Glycolytic enzyme activities and energy reserves in the digestive glands of *C. gigas* post elevated pCO_2 and/or *V. splendidus* exposure. **(A)** HK activity. **(B)** PK activity. **(C)** GLY content. **(D)** PROT content. Each bar represents mean ± SD ($n = 6$). Different letters indicate significant differences among different treatments ($p < 0.05$).

treatment are shown in **Figure 6B**. The IBR index was similar between the OA and *Vibrio* treatments, while the IBR index was exceedingly high in *Vibrio*-OA treatment compared to either the OA or *Vibrio* treatments alone. According to the IBR index, the rank order of treatments was: *Vibrio*-OA > *Vibrio* = OA.

DISCUSSION

Antioxidant Responses and Oxidative Damage

ROS are naturally produced and maintained at basal levels during cellular aerobic metabolism (Halliwell and Gutteridge, 1986). Numerous environmental stressors have been found to induce ROS production in marine invertebrates (Canesi et al., 2010; Tomanek et al., 2011; Zhu et al., 2011; Matoo et al., 2013; Ferreira et al., 2015). LPO, caused by excessive ROS production, is a major indicator of oxidative damage in organisms and a major contributor to the loss of cell function under environmental stress, including OA and pollutants (Moreira et al., 2016; Ricevuto et al., 2016; Valerio-García et al., 2017). In the present study, the LPO level increased significantly in *Vibrio*-treated oysters. Similarly, increased oxidative stress and altered antioxidant enzyme responses were observed in *Mytilus galloprovincialis* challenged with *V. splendidus* (Canesi et al., 2010). It has been shown that the adrenergic receptors and PKC-mediated pathways' activation induced by bacterial components were associated with ROS production (Dailianis et al., 2005; Ciacci et al., 2010). Meanwhile, antioxidant enzymes such as CAT and SOD were shown to remove excessive ROS in organisms under severe stress caused by environmental perturbations (Giarratano et al., 2014). Although the LPO level increased significantly in *V. splendidus* challenged oysters, no significant change was observed in the antioxidant enzyme activities (CAT, SOD, and GPx) in this study. These results suggest that inefficient activation of antioxidant defenses in *Vibrio*-treated oysters resulted in higher oxidative damage in these individuals compared to those in the control group.

However, the present findings demonstrated that oysters were able to increase the activities of antioxidant enzymes, such as CAT, to counteract the oxidative stress caused by combined exposure to OA and *Vibrio*. In contrast, the activity of GPx

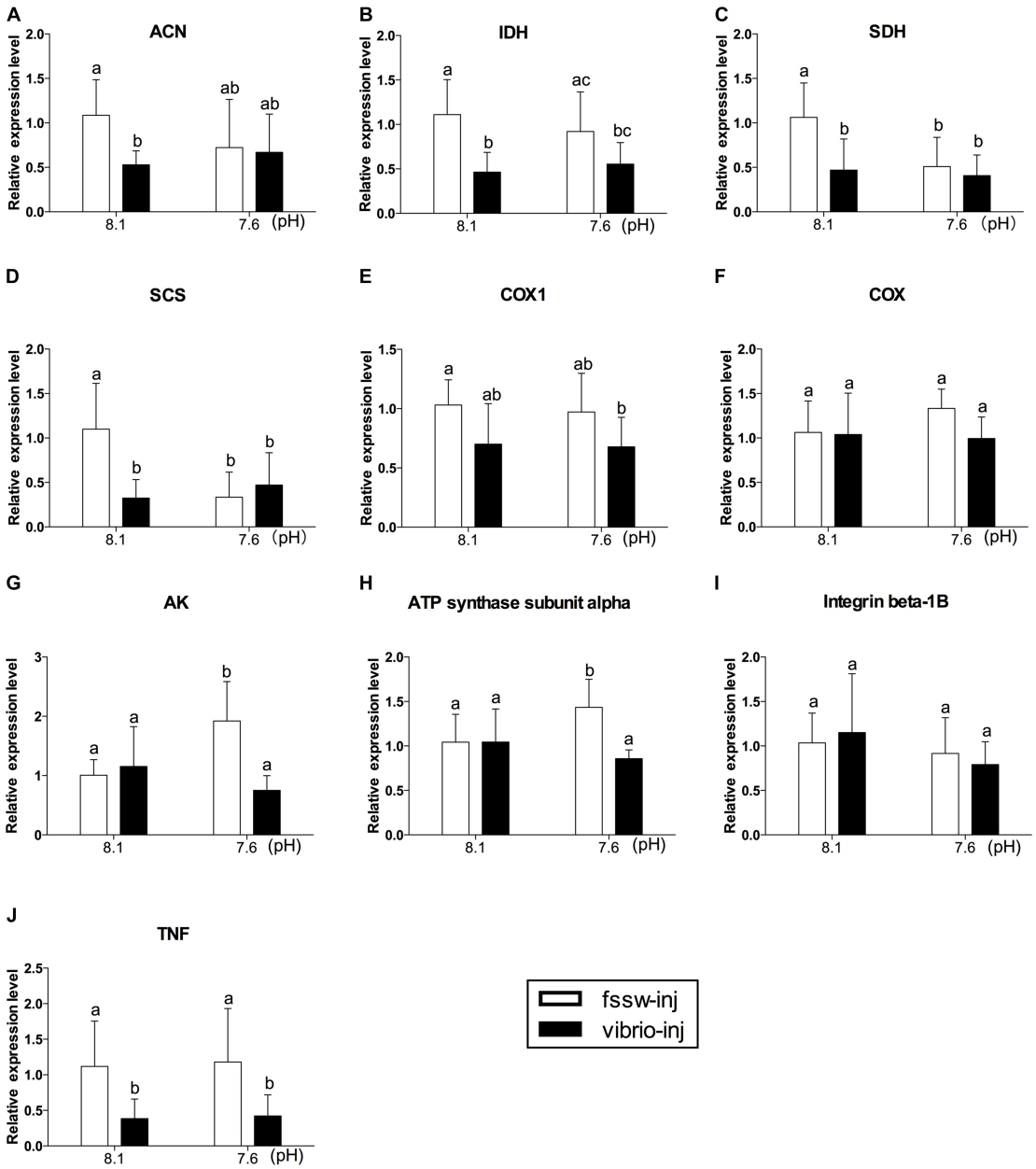

FIGURE 3 | The mRNA expression profiles of aerobic energy metabolism- and immune-related genes in the digestive glands of oysters post elevated pCO_2 and *V. splendidus* exposure. **(A)** ACN. **(B)** IDH. **(C)** SDH. **(D)** SCS. **(E)** COX 1. **(F)** COX. **(G)** AK. **(H)** ATP synthase subunit alpha. **(I)** Integrin beta-1B. **(J)** TNF. Each bar represents mean ± SD ($n = 6$). Different letters indicate significant differences among treatments ($p < 0.05$), and identical letters indicate no significant difference.

decreased significantly in the *Vibrio*-OA treatment. The inhibited responses of the antioxidant enzymes possibly suggested a failure of the antioxidant system in scavenging ROS, and thus resulted in the accumulation of the oxidative substance in the cells (Li et al., 2012). Accordingly, LPO level was increased significantly in response to the combined exposure to OA and *V. splendidus*.

Oxidative stress has been suggested to be involved in the toxic mechanism of seawater acidification (Benedetti et al., 2016; Moreira et al., 2016; Velez et al., 2016a). For example, a proteomic study on eastern oysters, *Crassostrea virginica*, suggested an induced oxidative stress after a 2-week exposure to elevated CO_2 concentration (∼357 Pa pCO_2; Tomanek et al., 2011). However, our results revealed that OA did not stimulate antioxidant responses and oxidative damage in oysters, indicating a low oxidative stress level in OA-exposed oysters. Similar results have also been found in two bivalve species, *C. virginica* and *Mercenaria mercenaria*, in which no persistent oxidative stress signal was observed during long-term exposure to OA (∼800 ppm CO_2; Matoo et al., 2013).

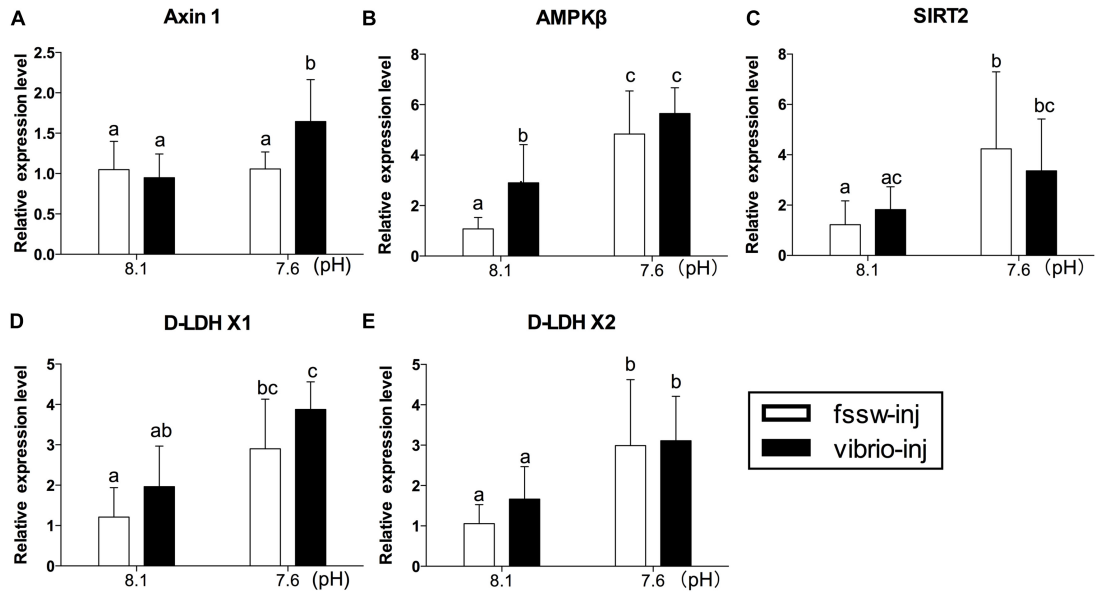

FIGURE 4 | The mRNA expression profiles of anaerobic energy metabolism- and energy sensing-related genes in the digestive glands of oysters post elevated pCO_2 and *V. splendidus* exposure. **(A)** Axin1. **(B)** AMPKβ. **(C)** SIRT2. **(D)** D-LDH X1. **(E)** D-LDH X2. Each bar represents mean ± SD ($n = 6$). Different letters indicate significant differences among treatments ($p < 0.05$), and identical letters indicate no significant difference.

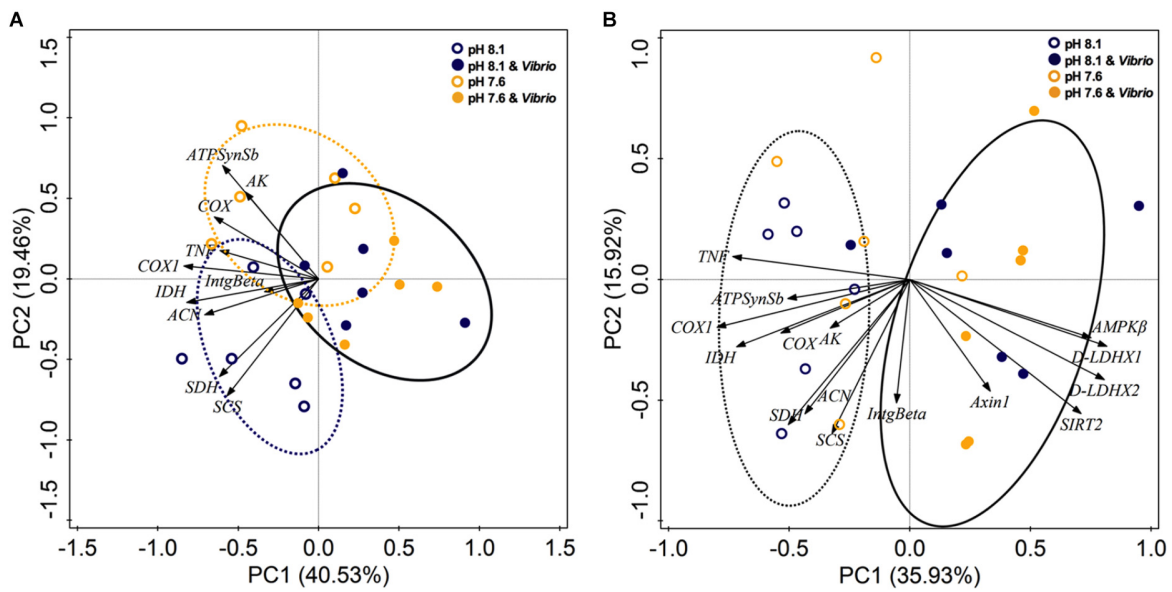

FIGURE 5 | (A) Principle component analysis (PCA) ordination biplot of ocean acidification and/or *V. splendidus* treatments for *C. gigas*, using expression data of genes related to aerobic metabolism and immune responses. **(B)** PCA ordination biplot of ocean acidification and/or *V. splendidus* treatments for *C. gigas*, using expression data of genes related to energy metabolism and immune responses.

In general, although OA alone did not induce significant changes in antioxidant enzyme activities, the combined exposure to OA and *Vibrio* led to higher oxidative stress compared to that of each stressor alone. This outcome was demonstrated by significantly altered antioxidant enzyme activities (CAT and GPx) and was expected as both OA exposure and *V. splendidus* challenge could lead to increased ROS production in oysters (Canesi et al., 2010; Tomanek et al., 2011). Above all, the results from this study demonstrated that excessive ROS production in oysters exposed to *Vibrio* alone or combined with an OA challenge induced cellular stress and oxidative damage and contributed therefore to the pathogenesis of *Vibriosis*.

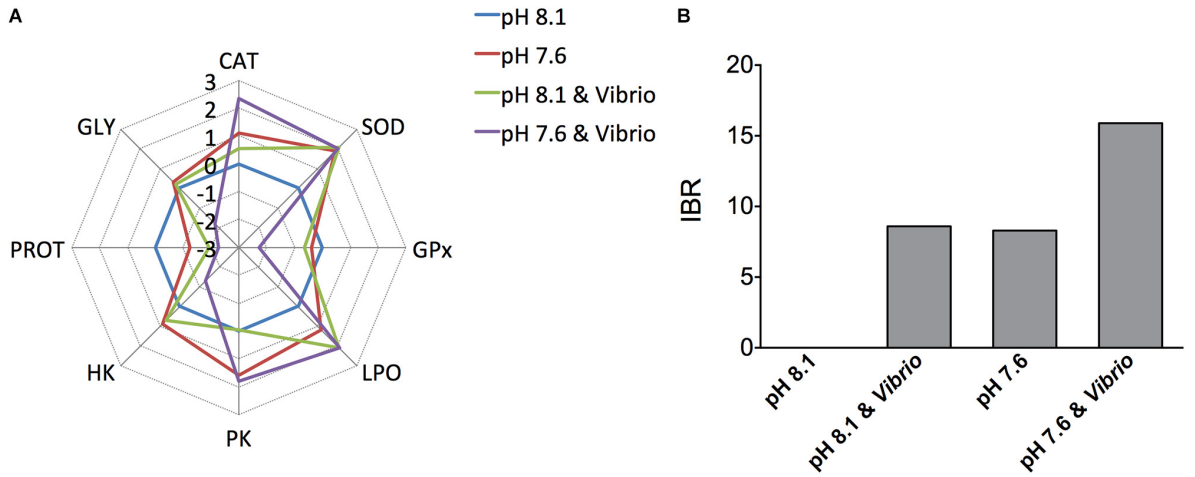

FIGURE 6 | Biomarker star plots and integrated biomarker response (IBR). **(A)** Biomarker star plots for each treatment displaying the general patterns of data variability. SOD, superoxide dismutase; CAT, catalase; GPx, glutathione peroxidase; LPO, lipid peroxidation; PK, pyruvate kinase; HK, hexokinase; PROT, protein; GLY, glycogen. **(B)** Calculated IBR index using the biochemical parameters measured in *C. gigas* after exposure to ocean acidification and/or *V. splendidus*.

Aerobic Metabolism and Energy Reserves

Energy metabolism biomarkers were vital for evaluating cellular energy status under environmental perturbations, and could be used to predict ecological consequences of stress exposure (Dong and Zhang, 2015). Under normal conditions, ATP supply via aerobic metabolism was sufficiently high to cover the maintenance costs, as well as energy costs of physiological activity, growth, and reproduction. However, severe environmental stress could lead to depressed aerobic metabolism in invertebrates (Giacomin et al., 2014; Dahlke et al., 2016; Zhao et al., 2017). Hence, the expression levels of aerobic metabolism-related genes were investigated in this study. Specifically, the TCA cycle served as the most important phase in respiratory process, oxidizing acetate into carbon dioxide (Fernie et al., 2004). ACN, IDH, SDH, and SCS are essential enzymes that participate in the mitochondrial TCA cycle. COX1 and COX are components of the mitochondria ETC (Wikstrom, 1977). Two ATP metabolic genes, including ATP synthase subunit alpha and AK, were also investigated in the oyster *C. gigas*.

A growing body of evidence has suggested that OA could disrupt the energy balance of mollusks by impairing key processes associated with high energy expenditure, such as immunity, development, acid–base homeostasis maintenance, and antioxidant processes (Lannig et al., 2010). A disturbance in energy metabolism by OA could sensitize bivalves to other environmental perturbations such as pathogen infection (Ivanina and Sokolova, 2015; Hernroth et al., 2016). In this study, the suppressed expression of two genes (SDH and SCS) in OA-treated oysters suggested only a mild inhibition effect of OA on aerobic energy metabolism. The increased mRNA expression of ATP synthase subunit alpha and AK might be associated with increased ATP turnover rates in OA treatment, which suggested a partial energy compensation for stress response in OA-treated oysters. In addition, enhanced glycolysis, indicated by increased PK activity, was observed in OA-treated oysters, which may supply the energy needed for acid–base homeostasis maintenance and other stress responses in oysters under OA exposure. The two energy reserves (GLY and PROT) were not altered in oysters under OA exposure, suggesting the maintenance of energy homeostasis in this treatment. Above all, our results indicated that OA-exposed oysters might exploit increased glycolysis and ATP turnover to provide the energy needed for cellular homeostasis, thereby explaining the high resistance of this species to OA.

From our findings, *V. splendidus* challenge was the major factor affecting oyster energy metabolism. Aerobic energy metabolism was decreased in *Vibrio* and *Vibrio*-OA treatments, which was demonstrated by the significantly inhibited expression of most aerobic energy metabolic genes. PCA analysis further confirmed the inhibition effect on the expression of aerobic metabolism-related genes caused by *Vibrio* exposure, either alone or combined with OA (**Figure 5A**). Although aerobic metabolism was inhibited, decreased PROT content in oysters treated by *Vibrio* alone or combined with OA and decreased GLY levels in the *Vibrio*-OA treatment suggested a disturbed energy balance. In addition, PK catalyzes the final step of glycolysis, which plays an important role in GLY metabolism (Hemre et al., 2002). Increased PK activity found in the present study indicated enhanced levels of glycolysis in *Vibrio*-OA treatment. Similarly, GLY has been mobilized as a source of energy for cellular protection mechanisms under extreme salinities (Velez et al., 2016b).

Energy Sensors and Anaerobic Metabolism

Energy homeostasis in invertebrates could be maintained through cellular pathways involved in cellular energy status sensing and energy expenditure modulation (Han et al., 2013; Dong et al., 2014; Dong and Zhang, 2015; Jost et al., 2015). When cellular energy status was compromised, activation of

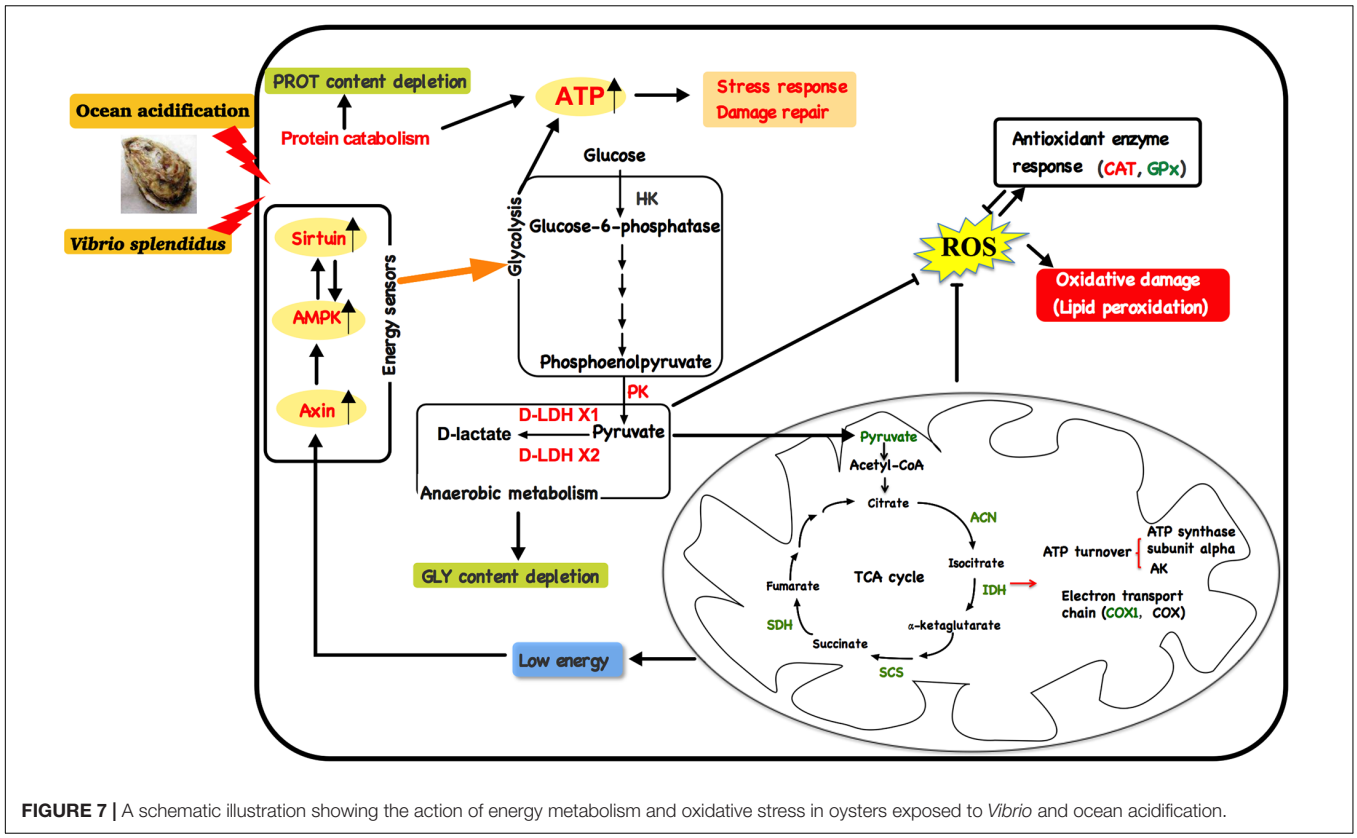

FIGURE 7 | A schematic illustration showing the action of energy metabolism and oxidative stress in oysters exposed to *Vibrio* and ocean acidification.

AMPK was initiated by assembling the Axin-AMPK-serine-threonine liver kinase B1 (LKB1) complex (Zhang et al., 2013). Histone/PROT deacetylase (SIRT) served as another metabolic sensor in cells under low energy status. The activation of energy metabolism sensors including Axin, AMPK, and SIRT could switch on the catabolic pathways (primarily lipid and glucose catabolism), resulting in ATP generation while simultaneously shutting down ATP consuming anabolic pathways (Cantó et al., 2009; Houtkooper et al., 2012; Hardie et al., 2016). In this study, the observed significantly elevated expression levels of metabolic sensors (Axin1, AMPKβ, and SIRT2) in oysters exposed to OA and/or *Vibrio* indicated activated catabolism and inhibited anabolic metabolism. This result could further explain the increased glycolytic enzyme activities found in *Vibrio*- and/or OA-treated oysters, and depleted GLY level in oysters treated by *Vibrio* alone or combined with OA. Positive correlation between the expression of metabolic sensing genes (Axin, AMPK, and SIRT) and glycolysis-related genes has also been observed in limpets, *Cellana toreuma* (Han et al., 2013; Dong et al., 2014).

Furthermore, D-LDH has the ability to catalyze the NADH-dependent interconversion of pyruvate and D-lactate in anabolic and catabolic pathways (Simon et al., 1989). In the present study, increased expression of D-LDH X1 and D-LDH X2 observed in OA and/or *Vibrio* exposed oysters verified our hypothesis that enhanced anaerobic glycolysis was initiated to compensate for depressed energy supplies caused by inhibition of aerobic metabolism. PCA results also indicated that metabolic sensors (Axin1, AMPKβ, and SIRT2) and anaerobic metabolism (D-LDH X1 and D-LDH X2) were negatively correlated with aerobic metabolic genes in *Vibrio*-treated oysters, regardless of OA.

While the metabolic rate and oxygen consumption were not measured in the present study, previous studies showed that OA could lead to succinate accumulation in both oyster gills and hepatopancreas, as measured by NMR-base metabolomics (Lannig et al., 2010), suggesting partial anaerobiosis of oysters under OA exposure. Furthermore, decreased oxygen consumption and metabolic rate were found in OA-exposed mussel *M. galloprovincialis* (Michaelidis et al., 2005). Michaelidis et al. (2005) also found that respiratory acidosis in the extracellular fluids of mussels might be associated with the reduction in aerobic scope and aerobic metabolism. In the meantime, reduction in energy reserves within bacterial challenged bivalve species has been observed in numerous studies (Dittman et al., 2001; Paillard et al., 2004; Flye-Sainte-Marie et al., 2007). Correspondingly, OA posed milder suppression on the aerobic metabolism and led to partial anaerobiosis in oysters, while bacterial challenge alone or combined with OA could lead to suppressed aerobic metabolism, partial anaerobiosis, and decreased energy reserves in oyster *C. gigas*. In addition, severely depleted energy reserves of *V. splendidus* challenged oysters under decreased pH might be associated with higher energy cost for the acid–base hemostasis maintenance and antioxidant responses.

Correlation of Energy Metabolism With Oxidative and Immune Response

Generally, oysters could suppress aerobic energy metabolism to decrease ROS production. Additionally, the suppressed energy metabolism and milder depleted energy reserves in *Vibrio*- or OA-treated oysters might be associated with the unaltered antioxidant enzyme response in these two treatments, as energy was mobilized to more urgent cellular stress responses, such as acid–base homeostasis and immune responses. Similarly, previous research has identified increased acid–base homeostasis maintenance under OA (Wang et al., 2017) and stimulated oxidative stress and immune responses under *V. splendidus* challenge in invertebrates (Canesi et al., 2010; Liu et al., 2013; Li et al., 2017). According to our previous proteomic results, a tradeoff between oxidative stress and energy metabolism was adopted by oysters in *Vibrio*-OA treatment (Cao et al., 2018). The ETC in mitochondria is a major site of ROS production (Chandel and Schumacker, 2000). In the *Vibrio*-OA group, both decreased abundance of ETC-related PROT expression found in our previous research and decreased mRNA expression of ETC-related gene COX1 in this study might suggest that a tradeoff exists between oxidative stress and energy metabolism.

In addition, as an immune factor, TNF played important roles in the immune functions of oysters. In this study, immune responses in oysters were perhaps suppressed as indicated by the significantly decreased expression of TNF transcripts. The depressed immune function in *Vibrio*-treated oysters could be associated with the disturbed energy metabolism caused by this treatment. Previous finding also suggested that *V. splendidus* challenge could lead to immunosuppression of marine invertebrates (Lacoste et al., 2001; Duperthuy et al., 2010).

Integrated Biomarker Response

The IBR index provides a global view of environmental stress by combining various biomarker signals (Beliaeff and Burgeot, 2002). Numerous laboratory experiments have adopted IBR index to better review and compare results between treatments (Qu et al., 2014; Xu et al., 2016; Valerio-García et al., 2017; Wang et al., 2018). Higher IBR values indicated more stressful conditions as the IBR index was considered to be a general description of "health status" (Leiniö and Lehtonen, 2005). In the present study, oysters exposed to the combination of both stressors displayed a greatly increased IBR value compared to each stressor alone. These results demonstrated that co-exposure is the most stressful condition, which was in coordination with the results that co-exposure induced more severe responses of oxidative stress and depleted energy reserves.

Recently, an energy metabolism model has been proposed by Sokolova et al. (2012), in which transition to partial anaerobiosis and metabolic rate depression are characteristics of organisms on the pessimum range of energy metabolism. As the balance of ATP supply and demand is disrupted in the pessimum range of energy metabolism, populations are unable to survive. Although OA-exposed oysters could maintain energy metabolism homeostasis in this study, the disturbed energy metabolism (decreased aerobic metabolism and increased anaerobic metabolism) led to decreased energy reserves under pathogen infection alone or combined with OA exposure, which was energetically unsustainable in the long run. Furthermore, OA might reduce the ability of oysters to resist infection by the pathogen *V. splendidus*, as indicated by the higher IBR value of combined exposure compared to a single stressor. As a consequence, marine bivalves are under severe threat from OA caused by global climate change and pathogen infection.

CONCLUSION

A schematic representation was developed to conclude the oxidative and energy metabolism responses of oysters exposed to OA and *Vibrio* (**Figure 7**). In brief, OA and *Vibrio* challenges could lead to suppressed aerobic metabolism, increased anaerobic metabolism, and oxidative stress. Compromised aerobic metabolism would lead to a low cellular energy condition, which could induce increased expression of metabolic sensors. In turn, anaerobic glycolysis and other catabolic metabolisms were enhanced to provide energy for cellular stress responses and damage repair, resulting in depleted energy reserves (GLY). PROT catabolism also increased to provide additional energy under stressful conditions, thereby causing depleted PROT levels. The increased oyster energy expenditure, in response to pathogen challenge along with exposure to acidified seawater, was expected, as important physiological processes such as immune responses, antioxidant responses, and acid–base homeostasis maintenance were stimulated. Above all, our results emphasize the deleterious effects of OA and pathogen infection on cellular stress and maintenance of metabolic homeostasis in marine invertebrates.

AUTHOR CONTRIBUTIONS

RC and JZ conceived and designed the experimental plan, analyzed the data, and drafted the manuscript. RC, YL, QW, DY, HL, WR, and YQ performed the experiments.

FUNDING

This research was supported by the grants from the Strategic Priority Research Program of the Chinese Academy of Sciences (XDA11020305), National Natural Science Foundation of China (No. 31172388), Key Research Program of the Chinese Academy of Sciences (Grant No. KZZDEW-14), Science and Technology Service Network Initiative (STS) Project (No. KFJ-STS-ZDTP-023), the Instrument Developing Project of the Chinese Academy of Sciences (YJKYYQ20170071), and the Youth Innovation Promotion Association, CAS (2016196).

SUPPLEMENTARY MATERIAL

The Supplementary Material for this article can be found online at: https://www.frontiersin.org/articles/10.3389/fphys.2018.00880/full#supplementary-material

REFERENCES

Beauchamp, C., and Fridovich, I. (1971). Superoxide dismutase: improved assays and an assay applicable to acrylamide gels. *Anal. Biochem.* 44, 276–287. doi: 10.1016/0003-2697(71)90370-8

Beaz-Hidalgo, R., Balboa, S., Romalde, J. L., and Figueras, M. J. (2010). Diversity and pathogenecity of *Vibrio* species in cultured bivalve molluscs. *Environ. Microbiol. Rep.* 2, 34–43. doi: 10.1111/j.1758-2229.2010.00135.x

Beliaeff, B., and Burgeot, T. (2002). Integrated biomarker response: a useful tool for ecological risk assessment. *Environ. Toxicol. Chem.* 21, 1316–1322. doi: 10.1002/etc.5620210629

Benedetti, M., Lanzoni, I., Nardi, A., d'Errico, G., Di Carlo, M., Fattorini, D., et al. (2016). Oxidative responsiveness to multiple stressors in the key Antarctic species, *Adamussium colbecki*: interactions between temperature, acidification and cadmium exposure. *Mar. Environ. Res.* 121, 20–30. doi: 10.1016/j.marenvres.2016.03.011

Cai, W.-J., Hu, X., Huang, W.-J., Murrell, M. C., Lehrter, J. C., Lohrenz, S. E., et al. (2011). Acidification of subsurface coastal waters enhanced by eutrophication. *Nat. Geosci.* 4, 766–770. doi: 10.1038/ngeo1297

Caldeira, K., and Wickett, M. E. (2005). Ocean model predictions of chemistry changes from carbon dioxide emissions to the atmosphere and ocean. *J. Geophys. Res. Oceans* 110:C09S04. doi: 10.1029/2004JC002671

Canesi, L., Barmo, C., Fabbri, R., Ciacci, C., Vergani, L., Roch, P., et al. (2010). Effects of *vibrio* challenge on digestive gland biomarkers and antioxidant gene expression in *Mytilus galloprovincialis*. *Comp. Biochem. Physiol. Part C Toxicol. Pharmacol.* 152, 399–406. doi: 10.1016/j.cbpc.2010.06.008

Cantó, C., Gerhart-Hines, Z., Feige, J. N., Lagouge, M., Noriega, L., Milne, J. C., et al. (2009). AMPK regulates energy expenditure by modulating NAD^+ metabolism and SIRT1 activity. *Nature* 458, 1056–1060. doi: 10.1038/nature07813

Cao, R., Wang, Q., Yang, D., Liu, Y., Ran, W., Qu, Y., et al. (2018). CO_2-induced ocean acidification impairs the immune function of the Pacific oyster against *Vibrio splendidus* challenge: an integrated study from a cellular and proteomic perspective. *Sci. Total Environ.* 625, 1574–1583. doi: 10.1016/j.scitotenv.2018.01.056

Carregosa, V., Velez, C., Soares, A. M., Figueira, E., and Freitas, R. (2014). Physiological and biochemical responses of three *Veneridae* clams exposed to salinity changes. *Comp. Biochem. Physiol. B Biochem. Mol. Biol.* 17, 1–9. doi: 10.1016/j.cbpb.2014.08.001

Castillo, N., Saavedra, L. M., Vargas, C. A., Gallardo-Escárate, C., and Détrée, C. (2017). Ocean acidification and pathogen exposure modulate the immune response of the edible mussel *Mytilus chilensis*. *Fish Shellfish Immunol.* 70, 149–155. doi: 10.1016/j.fsi.2017.08.047

Chandel, N. S., and Schumacker, P. T. (2000). Cellular oxygen sensing by mitochondria: old questions, new insight. *J. Appl. Physiol.* 88, 1880–1889.

Chen, S., Gao, K., and Beardall, J. (2015). Viral attack exacerbates the susceptibility of a bloom-forming alga to ocean acidification. *Glob. Change Biol.* 21, 629–636. doi: 10.1111/gcb.12753

Ciacci, C., Betti, M., Canonico, B., Citterio, B., Roch, P., and Canesi, L. (2010). Specificity of anti-*Vibrio* immune response through p38 MAPK and PKC activation in the hemocytes of the mussel *Mytilus galloprovincialis*. *J. Invertebr. Pathol.* 105, 49–55. doi: 10.1016/j.jip.2010.05.010

Dahlke, F. T., Leo, E., Mark, F. C., Pörtner, H.-O., Bickmeyer, U., Frickenhaus, S., et al. (2016). Effects of ocean acidification increase embryonic sensitivity to thermal extremes in Atlantic cod, *Gadus morhua*. *Glob. Change Biol.* 23, 1499–1510. doi: 10.1111/gcb.13527

Dailianis, S., Piperakis, S. M., and Kaloyianni, M. (2005). Cadmium effects on ROS production and DNA damage via adrenergic receptors stimulation: role of Na^+/H^+ exchanger and PKC. *Free Radic. Res.* 39, 1059–1070. doi: 10.1080/10715760500243765

de Lorgeril, J., Zenagui, R., Rosa, R. D., Piquemal, D., and Bachère, E. (2011). Whole transcriptome profiling of successful immune response to vibrio infections in the oyster *Crassostrea gigas* by digital gene expression analysis. *PLoS One* 6:e23142. doi: 10.1371/journal.pone.0023142

Dickson, A. G. (1990). Standard potential of the reaction: AgCl(s) + 12H2(g) = Ag(s) + HCl(aq), and the standard acidity constant of the ion HSO4- in synthetic sea water from 273.15 to 318.15 K. *J. Chem. Thermodyn.* 22, 113–127. doi: 10.1016/0021-9614(90)90074-Z

Dineshram, R., Chandramouli, K., Ko, G. W. K., Zhang, H., Qian, P.-Y., Ravasi, T., et al. (2016). Quantitative analysis of oyster larval proteome provides new insights into the effects of multiple climate change stressors. *Glob. Change Biol.* 22, 2054–2068. doi: 10.1111/gcb.13249

Dittman, D. E., Ford, S. E., and Padilla, A. (2001). Effects of *Perkinsus marinus* on reproduction and condition of the eastern oyster, *Crassostrea virginica*, depend on timing. *Mar. Ecol. Prog. Ser.* 20, 1025–1034. doi: 10.3354/dao02964

Doney, S. C., Mahowald, N., Lima, I., Feely, R. A., Mackenzie, F. T., Lamarque, J.-F., et al. (2007). Impact of anthropogenic atmospheric nitrogen and sulfur deposition on ocean acidification and the inorganic carbon system. *Proc. Natl. Acad. Sci. U.S.A.* 104, 14580–14585. doi: 10.1073/pnas.0702218104

Dong, Y., Han, G., and Huang, X. (2014). Stress modulation of cellular metabolic sensors: interaction of stress from temperature and rainfall on the intertidal limpet *Cellana toreuma*. *Mol. Ecol.* 23, 4541–4554. doi: 10.1111/mec.12882

Dong, Y., and Zhang, S. (2015). Ecological relevance of energy metabolism: transcriptional responses in energy sensing and expenditure to thermal and osmotic stresses in an intertidal limpet. *Funct. Ecol.* 30, 1539–1548. doi: 10.1111/1365-2435.12625

Duckworth, C. G., Picariello, C. R., Thomason, R. K., Patel, K. S., and Bielmyer-Fraser, G. K. (2017). Responses of the sea anemone, *Exaiptasia pallida*, to ocean acidification conditions and zinc or nickel exposure. *Aquat. Toxicol.* 182, 120–128. doi: 10.1016/j.aquatox.2016.11.014

Dumbauld, B. R., Ruesink, J. L., and Rumrill, S. S. (2009). The ecological role of bivalve shellfish aquaculture in the estuarine environment: a review with application to oyster and clam culture in West Coast (USA) estuaries. *Aquaculture* 290, 196–223. doi: 10.1016/j.aquaculture.2009.02.033

Duperthuy, M., Binesse, J., Le Roux, F., Romestand, B., Caro, A., Got, P., et al. (2010). The major outer membrane protein OmpU of *Vibrio splendidus* contributes to host antimicrobial peptide resistance and is required for virulence in the oyster *Crassostrea gigas*. *Environ. Microbiol.* 12, 951–963. doi: 10.1111/j.1462-2920.2009.02138.x

Ellis, R. P. (2013). *The Impact of Ocean Acidification, Increased Seawater Temperature and a Bacterial Challenge on the Immune Response and Physiology of the Blue Mussel, Mytilus edulis*. Plymouth: University of Plymouth.

Ellis, R. P., Spicer, J. I., Byrne, J. J., Sommer, U., Viant, M. R., White, D. A., et al. (2014). 1H NMR metabolomics reveals contrasting response by male and female mussels exposed to reduced seawater pH, increased temperature, and a pathogen. *Environ. Sci. Technol.* 48, 7044–7052. doi: 10.1021/es501601w

Ellis, R. P., Widdicombe, S., Parry, H., Hutchinson, T. H., and Spicer, J. I. (2015). Pathogenic challenge reveals immune trade-off in mussels exposed to reduced seawater pH and increased temperature. *J. Exp. Mar. Biol. Ecol.* 462, 83–89. doi: 10.1016/j.jembe.2014.10.015

Fernie, A. R., Carrari, F., and Sweetlove, L. J. (2004). Respiratory metabolism: glycolysis, the TCA cycle and mitochondrial electron transport. *Curr. Opin. Plant Biol.* 7, 254–261. doi: 10.1016/j.pbi.2004.03.007

Ferreira, N. G. C., Morgado, R., Santos, M. J. G., Soares, A. M., and Loureiro, S. (2015). Biomarkers and energy reserves in the isopod *Porcellionides pruinosus*: the effects of long-term exposure to dimethoate. *Sci. Total Environ.* 502, 91–102. doi: 10.1016/j.scitotenv.2014.08.062

Flye-Sainte-Marie, J., Pouvreau, S., Paillard, C., and Jean, F. (2007). Impact of brown ring disease on the energy budget of the Manila clam *Ruditapes philippinarum*. *J. Exp. Mar. Biol. Ecol.* 349, 378–389. doi: 10.1016/j.jembe.2007.05.029

Forster, P., Ramaswamy, V., Artaxo, P., Berntsen, T., Betts, R., Fahey, D. W., et al. (2007). "Changes in atmospheric constituents and in radiative forcing," in *Climate Change 2007: The Physical Science Basis. Contribution of Working Group I to the Fourth Assessment Report of the Intergovernmental Panel on Climate Change*, eds S. Solomon, D. Qin, M. Manning, Z. Chen, M. Marquis, K. B. Averyt, et al. (Cambridge: Cambridge University Press), 129–234.

Gay, M., Renault, T., Pons, A.-M., and Roux, F. L. (2004). Two *Vibrio splendidus* related strains collaborate to kill *Crassostrea gigas*: taxonomy and host alterations. *Dis. Aquat. Organ.* 62, 65–74.

Gazeau, F., Parker, L. M., Comeau, S., Gattuso, J.-P., O'Connor, W. A., Martin, S., et al. (2013). Impacts of ocean acidification on marine shelled molluscs. *Mar. Biol.* 160, 2207–2245. doi: 10.1007/s00227-013-2219-3

Giacomin, M., Jorge, M. B., and Bianchini, A. (2014). Effects of copper exposure on the energy metabolism in juveniles of the marine clam *Mesodesma mactroides*. *Aquat. Toxicol.* 152, 30–37. doi: 10.1016/j.aquatox.2014.03.025

Giarratano, E., Gil, M. N., and Malanga, G. (2014). Biomarkers of environmental stress in gills of ribbed mussel *Aulacomya atra atra* (Nuevo Gulf, Northern Patagonia). *Ecotoxicol. Environ. Saf.* 107, 111–119. doi: 10.1016/j.ecoenv.2014.05.003

Gran, G. (1952). Determination of the equivalence point in potentiometric titrations. Part II. *Analyst* 77, 661–670.

Greenway, S. C., and Storey, K. B. (1999). The effect of prolonged anoxia on enzyme activities in oysters (*Crassostrea virginica*) at different seasons. *J. Exp. Mar. Biol. Ecol.* 242, 259–272. doi: 10.1016/S0022-0981(99)00103-3

Gunderson, A. R., Armstrong, E. J., and Stillman, J. H. (2016). Multiple stressors in a changing world: the need for an improved perspective on physiological responses to the dynamic marine environment. *Annu. Rev. Mar. Sci.* 8, 357–378. doi: 10.1146/annurev-marine-122414-033953

Halliwell, B., and Gutteridge, J. M. C. (1986). Oxygen free radicals and iron in relation to biology and medicine: some problems and concepts. *Arch. Biochem. Biophys.* 246, 501–514. doi: 10.1016/0003-9861(86)90305-X

Han, G., Zhang, S., Marshall, D. J., Ke, C., and Dong, Y. (2013). Metabolic energy sensors (AMPK and SIRT1), protein carbonylation and cardiac failure as biomarkers of thermal stress in an intertidal limpet: linking energetic allocation with environmental temperature during aerial emersion. *J. Exp. Biol.* 216, 3273–3282. doi: 10.1242/jeb.084269

Hardie, D. G., Schaffer, B. E., and Brunet, A. (2016). AMPK: an energy-sensing pathway with multiple inputs and outputs. *Trends Cell Biol.* 26, 190–201. doi: 10.1016/j.tcb.2015.10.013

Hemre, G.-I., Mommsen, T. P., and Krogdahl, Å. (2002). Carbohydrates in fish nutrition: effects on growth, glucose metabolism and hepatic enzymes. *Aquac. Nutr.* 8, 175–194. doi: 10.1046/j.1365-2095.2002.00200.x

Hernroth, B., Baden, S., Tassidis, H., Hörnaeus, K., Guillemant, J., Bergström Lind, S., et al. (2016). Impact of ocean acidification on antimicrobial activity in gills of the blue mussel (*Mytilus edulis*). *Fish Shellfish Immunol.* 55, 452–459. doi: 10.1016/j.fsi.2016.04.007

Hernroth, B., Baden, S., Thorndyke, M., and Dupont, S. (2011). Immune suppression of the echinoderm *Asterias rubens* (L.) following long-term ocean acidification. *Aquat. Toxicol.* 103, 222–224. doi: 10.1016/j.aquatox.2011.03.001

Hooper, C., Day, R., Slocombe, R., Handlinger, J., and Benkendorff, K. (2007). Stress and immune responses in abalone: limitations in current knowledge and investigative methods based on other models. *Fish Shellfish Immunol.* 22, 363–379. doi: 10.1016/j.fsi.2006.06.009

Houtkooper, R. H., Pirinen, E., and Auwerx, J. (2012). Sirtuins as regulators of metabolism and healthspan. *Nat. Rev. Mol. Cell Biol.* 13, 225–238. doi: 10.1038/nrm3293

Hu, X., and Cai, W.-J. (2013). Estuarine acidification and minimum buffer zone—A conceptual study. *Geophys. Res. Lett.* 40, 5176–5181. doi: 10.1002/grl.51000

Intergovernmental Panel on Climate Change (Ed.). (2014). *Climate Change 2013 - The Physical Science Basis: Working Group I Contribution to the Fifth Assessment Report of the Intergovernmental Panel on Climate Change*. Cambridge: Cambridge University Press.

Ivanina, A. V., Hawkins, C., and Sokolova, I. M. (2014). Immunomodulation by the interactive effects of cadmium and hypercapnia in marine bivalves *Crassostrea virginica* and *Mercenaria mercenaria*. *Fish Shellfish Immunol.* 37, 299–312. doi: 10.1016/j.fsi.2014.02.016

Ivanina, A. V., and Sokolova, I. M. (2015). Interactive effects of metal pollution and ocean acidification on physiology of marine organisms. *Curr. Zool.* 61, 653–668. doi: 10.1093/czoolo/61.4.653

Jost, J. A., Keshwani, S. S., and Abou-Hanna, J. J. (2015). Activation of AMP-activated protein kinase in response to temperature elevation shows seasonal variation in the zebra mussel, *Dreissena polymorpha*. *Comp. Biochem. Physiol. A Mol. Integr. Physiol.* 182, 75–83. doi: 10.1016/j.cbpa.2014.11.025

Lacoste, A., Jalabert, F., Malham, S., Cueff, A., Gélébart, F., Cordevant, C., et al. (2001). A *Vibrio splendidus* strain is associated with summer mortality of juvenile oysters *Crassostrea gigas* in the Bay of Morlaix (North Brittany, France). *Dis. Aquat. Organ.* 46, 139–145.

Lannig, G., Eilers, S., Pörtner, H. O., Sokolova, I. M., and Bock, C. (2010). Impact of ocean acidification on energy metabolism of oyster, *Crassostrea gigas*—changes in metabolic pathways and thermal response. *Mar. Drugs* 8, 2318–2339. doi: 10.3390/md8082318

Lawrence, R. A., and Burk, R. F. (1976). Glutathione peroxidase activity in selenium-deficient rat liver. *Biochem. Biophys. Res. Commun.* 71, 952–958. doi: 10.1016/0006-291X(76)90747-6

Leiniö, S., and Lehtonen, K. K. (2005). Seasonal variability in biomarkers in the bivalves *Mytilus edulis* and *Macoma balthica* from the northern Baltic Sea. *Comp. Biochem. Physiol. Part C Toxicol. Pharmacol.* 140, 408–421. doi: 10.1016/j.cca.2005.04.005

Lesser, M. P. (2016). Climate change stressors cause metabolic depression in the blue mussel, *Mytilus edulis*, from the Gulf of Maine. *Limnol. Oceanogr.* 61, 1705–1717. doi: 10.1002/lno.10326

Li, Y., Li, M., Shi, J., Yang, X., and Wang, Z. (2012). Hepatic antioxidative responses to PCDPSs and estimated short-term biotoxicity in freshwater fish. *Aquat. Toxicol.* 120–121, 90–98. doi: 10.1016/j.aquatox.2012.04.016

Li, Y., Song, X., Wang, W., Wang, L., Yi, Q., Jiang, S., et al. (2017). The hematopoiesis in gill and its role in the immune response of Pacific oyster *Crassostrea gigas* against secondary challenge with *Vibrio splendidus*. *Dev. Comp. Immunol.* 71, 59–69. doi: 10.1016/j.dci.2017.01.024

Liu, S., Shi, W., Guo, C., Zhao, X., Han, Y., Peng, C., et al. (2016). Ocean acidification weakens the immune response of blood clam through hampering the NF-kappa β and toll-like receptor pathways. *Fish Shellfish Immunol.* 54, 322–327. doi: 10.1016/j.fsi.2016.04.030

Liu, X., Ji, C., Zhao, J., and Wu, H. (2013). Differential metabolic responses of clam *Ruditapes philippinarum* to *Vibrio anguillarum* and *Vibrio splendidus* challenges. *Fish Shellfish Immunol.* 35, 2001–2007. doi: 10.1016/j.fsi.2013.09.014

Livak, K. J., and Schmittgen, T. D. (2001). Analysis of relative gene expression data using Real-Time quantitative PCR and the $2-\Delta\Delta CT$ method. *Methods* 25, 402–408. doi: 10.1006/meth.2001.1262

Matoo, O. B., Ivanina, A. V., Ullstad, C., Beniash, E., and Sokolova, I. M. (2013). Interactive effects of elevated temperature and CO2 levels on metabolism and oxidative stress in two common marine bivalves (*Crassostrea virginica* and *Mercenaria mercenaria*). *Comp. Biochem. Physiol. A Mol. Integr. Physiol.* 164, 545–553. doi: 10.1016/j.cbpa.2012.12.025

Michaelidis, B., Ouzounis, C., Paleras, A., and Pörtner, H. O. (2005). Effects of long-term moderate hypercapnia on acid–base balance and growth rate in marine mussels *Mytilus galloprovincialis*. *Mar. Ecol. Prog. Ser.* 293, 109–118.

Millero, F. J., Graham, T. B., Huang, F., Bustos-Serrano, H., and Pierrot, D. (2006). Dissociation constants of carbonic acid in seawater as a function of salinity and temperature. *Mar. Chem.* 100, 80–94. doi: 10.1016/j.marchem.2005.12.001

Moreira, A., Figueira, E., Soares, A. M., and Freitas, R. (2016). The effects of arsenic and seawater acidification on antioxidant and biomineralization responses in two closely related *Crassostrea* species. *Sci. Total Environ.* 545–546, 569–581. doi: 10.1016/j.scitotenv.2015.12.029

Ohkawa, H., Ohishi, N., and Yagi, K. (1979). Assay for lipid peroxides in animal tissues by thiobarbituric acid reaction. *Anal. Biochem.* 95, 351–358. doi: 10.1016/0003-2697(79)90738-3

Paillard, C., Allam, B., and Oubella, R. (2004). Effect of temperature on defense parameters in Manila clam *Ruditapes philippinarum* challenged with *Vibrio tapetis*. *Dis. Aquat. Organ.* 59, 249–262. doi: 10.3354/dao059249

Pörtner, H. O., Langenbuch, M., and Reipschläger, A. (2004). Biological impact of elevated ocean CO2 concentrations: lessons from animal physiology and earth history. *J. Oceanogr.* 60, 705–718. doi: 10.1007/s10872-004-5763-0

Qu, R., Feng, M., Wang, X., Qin, L., Wang, C., Wang, Z., et al. (2014). Metal accumulation and oxidative stress biomarkers in liver of freshwater fish *Carassius auratus* following in vivo exposure to waterborne zinc under different pH values. *Aquat. Toxicol.* 150, 9–16. doi: 10.1016/j.aquatox.2014.02.008

Queirós, A. M., Fernandes, J. A., Faulwetter, S., Nunes, J., Rastrick, S. P. S., Mieszkowska, N., et al. (2015). Scaling up experimental ocean acidification and warming research: from individuals to the ecosystem. *Glob. Change Biol.* 21, 130–143. doi: 10.1111/gcb.12675

Radi, R., Beckman, J. S., Bush, K. M., and Freeman, B. A. (1991). Peroxynitrite-induced membrane lipid peroxidation: the cytotoxic potential of superoxide and nitric oxide. *Arch. Biochem. Biophys.* 288, 481–487. doi: 10.1016/0003-9861(91)90224-7

Ricevuto, E., Lanzoni, I., Fattorini, D., Regoli, F., and Gambi, M. C. (2016). Arsenic speciation and susceptibility to oxidative stress in the fanworm *Sabella spallanzanii* (Gmelin) (Annelida, Sabellidae) under naturally acidified conditions: an in situ transplant experiment in a Mediterranean CO_2 vent system. *Sci. Total Environ.* 544, 765–773. doi: 10.1016/j.scitotenv.2015.11.154

Robinson, H. W., and Hogden, C. (1940). The biuret reaction in the determination of serum proteins. 1. A study of the conditions necessary for the production of a stable color which bears a quantitative relationship to the protein concentration. *J. Biol. Chem.* 135, 707–725. doi: 10.1016/0003-9861(91)90224-7

Sabine, C. L., Feely, R. A., Gruber, N., Key, R. M., Lee, K., Bullister, J. L., et al. (2004). The oceanic sink for anthropogenic CO_2. *Science* 305, 367–371. doi: 10.1126/science.1097403

Sanchez, W., Burgeot, T., and Porcher, J.-M. (2013). A novel "Integrated Biomarker Response" calculation based on reference deviation concept. *Environ. Sci. Pollut. Res.* 20, 2721–2725. doi: 10.1007/s11356-012-1359-1

Simon, E. S., Plante, R., and Whitesides, G. M. (1989). D-lactate dehydrogenase. *Appl. Biochem. Biotechnol.* 22, 169–179. doi: 10.1007/BF02921743

Sokolova, I. M., Frederich, M., Bagwe, R., Lannig, G., and Sukhotin, A. A. (2012). Energy homeostasis as an integrative tool for assessing limits of environmental stress tolerance in aquatic invertebrates. *Mar. Environ. Res.* 79, 1–15. doi: 10.1016/j.marenvres.2012.04.003

Sui, Y., Hu, M., Huang, X., Wang, Y., and Lu, W. (2015). Anti-predatory responses of the thick shell mussel *Mytilus coruscus* exposed to seawater acidification and hypoxia. *Mar. Environ. Res.* 109, 159–167. doi: 10.1016/j.marenvres.2015.07.008

Tomanek, L., Zuzow, M. J., Ivanina, A. V., Beniash, E., and Sokolova, I. M. (2011). Proteomic response to elevated PCO_2 level in eastern oysters, *Crassostrea virginica*: evidence for oxidative stress. *J. Exp. Biol.* 214, 1836–1844. doi: 10.1242/jeb.055475

Valerio-García, R. C., Carbajal-Hernández, A. L., Martínez-Ruíz, E. B., Jarquín-Díaz, V. H., Haro-Pérez, C., and Martínez-Jerónimo, F. (2017). Exposure to silver nanoparticles produces oxidative stress and affects macromolecular and metabolic biomarkers in the goodeid fish *Chapalichthys pardalis*. *Sci. Total Environ.* 583, 308–318. doi: 10.1016/j.scitotenv.2017.01.070

Vega-López, A., Galar-Martínez, M., Jiménez-Orozco, F. A., García-Latorre, E., and Domínguez-López, M. L. (2007). Gender related differences in the oxidative stress response to PCB exposure in an endangered goodeid fish (*Girardinichthys viviparus*). *Comp. Biochem. Physiol. A Mol. Integr. Physiol.* 146, 672–678. doi: 10.1016/j.cbpa.2006.04.022

Velez, C., Figueira, E., Soares, A. M., and Freitas, R. (2016a). Combined effects of seawater acidification and salinity changes in *Ruditapes philippinarum*. *Aquat. Toxicol.* 176, 141–150. doi: 10.1016/j.aquatox.2016.04.016

Velez, C., Figueira, E., Soares, A. M., and Freitas, R. (2016b). Native and introduced clams biochemical responses to salinity and pH changes. *Sci. Total Environ.* 566–567, 260–268. doi: 10.1016/j.scitotenv.2016.05.019

Wang, C., Rong, H., Liu, H., Wang, X., Gao, Y., Deng, R., et al. (2018). Detoxification mechanisms, defense responses, and toxicity threshold in the earthworm *Eisenia foetida* exposed to ciprofloxacin-polluted soils. *Sci. Total Environ.* 612, 442–449. doi: 10.1016/j.scitotenv.2017.08.120

Wang, Q., Cao, R., Ning, X., You, L., Mu, C., Wang, C., et al. (2016). Effects of ocean acidification on immune responses of the Pacific oyster *Crassostrea gigas*. *Fish Shellfish Immunol.* 49, 24–33. doi: 10.1016/j.fsi.2015.12.025

Wang, X., Wang, M., Jia, Z., Qiu, L., Wang, L., Zhang, A., et al. (2017). A carbonic anhydrase serves as an important acid-base regulator in Pacific oyster *Crassostrea gigas* exposed to elevated CO_2: implication for physiological responses of mollusk to ocean acidification. *Mar. Biotechnol.* 19, 22–35. doi: 10.1007/s10126-017-9734-z

Wang, Y., Li, L., Hu, M., and Lu, W. (2015). Physiological energetics of the thick shell mussel *Mytilus coruscus* exposed to seawater acidification and thermal stress. *Sci. Total Environ.* 514, 261–272. doi: 10.1016/j.scitotenv.2015.01.092

Wikstrom, M. (1977). Proton pump coupled to cytochrome c oxidase in mitochondria. *Nature* 266, 271–273.

Xu, P., Zeng, G., Huang, D., Liu, L., Zhao, M., Lai, C., et al. (2016). Metal bioaccumulation, oxidative stress and antioxidant defenses in *Phanerochaete chrysosporium* response to Cd exposure. *Ecol. Eng.* 87, 150–156. doi: 10.1016/j.ecoleng.2015.11.029

Yoshikawa, H. (1959). *Glycogen. Rinsho Kagaku Kyosho*. Tokyo: Rinsho Ikagaku Kyodoisho, 150–152.

Zhang, Y.-L., Guo, H., Zhang, C.-S., Lin, S.-Y., Yin, Z., Peng, Y., et al. (2013). AMP as a low-energy charge signal autonomously initiates assembly of AXIN-AMPK-LKB1 complex for AMPK activation. *Cell Metab.* 18, 546–555. doi: 10.1016/j.cmet.2013.09.005

Zhao, X., Shi, W., Han, Y., Liu, S., Guo, C., Fu, W., et al. (2017). Ocean acidification adversely influences metabolism, extracellular pH and calcification of an economically important marine bivalve, *Tegillarca granosa*. *Mar. Environ. Res.* 125, 82–89. doi: 10.1016/j.marenvres.2017.01.007

Zhu, X., Zhou, J., and Cai, Z. (2011). The toxicity and oxidative stress of TiO_2 nanoparticles in marine abalone (*Haliotis diversicolor supertexta*). *Mar. Pollut. Bull.* 63, 334–338. doi: 10.1016/j.marpolbul.2011.03.006

Conflict of Interest Statement: The authors declare that the research was conducted in the absence of any commercial or financial relationships that could be construed as a potential conflict of interest.

frontiers in Marine Science

ORIGINAL RESEARCH
published: 30 August 2018
doi: 10.3389/fmars.2018.00312

Resilience of Atlantic Slippersnail *Crepidula fornicata* Larvae in the Face of Severe Coastal Acidification

*Nicola G. Kriefall[1], Jan A. Pechenik[2], Anthony Pires[3] and Sarah W. Davies[1]**

[1] Biology Department, Boston University, Boston, MA, United States, [2] Biology Department, Tufts University, Medford, MA, United States, [3] Biology Department, Dickinson College, Carlisle, PA, United States

Globally, average oceanic pH is dropping, and it will continue to decline into the foreseeable future. This ocean acidification (OA) will exacerbate the natural fluctuations in pH that nearshore ecosystems currently experience daily, potentially pushing marine organisms to their physiological limits. Adults of *Crepidula fornicata* (the Atlantic slippersnail) have proven remarkably resilient to many environmental changes, which is perhaps not surprising considering that they are common intertidally, have a geographically large native range, and have been extremely successful at invading coastal waters in many other parts of the world. However, the larvae of *C. fornicata* have been shown to be somewhat more vulnerable than adults to the effects of reduced pH. Research to date has focused on the physiological impacts of OA on *C. fornicata* larvae; few studies have explored shifts in gene expression resulting from changes in pH. In the present study, we examined the response of young (4-day old) *C. fornicata* larvae to two extreme OA treatments (pH 7.5 and 7.6) relative to pH 8.0, documenting both phenotypic and genome-wide gene expression responses. We found that rearing larvae at reduced pH had subtle influences on gene expression, predominantly involving downregulation of genes related to growth and metabolism, accompanied by significantly reduced shell growth rates only for larvae reared at pH 7.5. Additionally, 10-day old larvae that had been reared at the two lower pH levels were far less likely to metamorphose within 6 h when exposed to inducer. However, all larvae eventually reached similarly high levels of metamorphosis 24 h after settlement induction. Finally, there were no observed impacts of OA on larval mortality. Taken together, our results indicate that far future OA levels have observable, but not severe, impacts on *C. fornicata* larvae, which is consistent with the resilience of this invasive snail across rapidly changing nearshore ecosystems. We propose that future work should delve further into the physiological and transcriptomic responses of all life history stages to gain a more comprehensive understanding of how OA impacts the littoral gastropod *C. fornicata*.

Keywords: climate change, gastropod, invertebrates, calcium carbonate, aragonite, gene expression, *Crepidula fornicata*, ocean acidification

OPEN ACCESS

Edited by:
Youji Wang,
Shanghai Ocean University, China

Reviewed by:
Guangxu Liu,
Zhejiang University, China
Hyun Park,
Korea Polar Research Institute, South Korea

****Correspondence:***
Sarah W. Davies
daviessw@bu.edu

Specialty section:
This article was submitted to Aquatic Physiology, a section of the journal Frontiers in Marine Science

Received: *11 June 2018*
Accepted: *13 August 2018*
Published: *30 August 2018*

Citation:
Kriefall NG, Pechenik JA, Pires A and Davies SW (2018) Resilience of Atlantic Slippersnail Crepidula fornicata Larvae in the Face of Severe Coastal Acidification. Front. Mar. Sci. 5:312. doi: 10.3389/fmars.2018.00312

INTRODUCTION

Anthropogenic combustion of fossil fuels and the subsequent rise of atmospheric partial pressure of carbon dioxide (pCO_2) since the industrial revolution has introduced many threats to the marine world, including ocean acidification (OA) (Caldeira and Wickett, 2003; Bopp et al., 2013). The ocean's average pH has already declined by 0.13 units since 1765, undergoing seawater chemistry changes unobserved for hundreds of thousands, if not millions, of years (Petit et al., 1999; Pelejero et al., 2010). Furthermore, the International Panel on Climate Change (IPCC) predicts a steeper decline of another 0.2–0.4 units by the end of this century (Plattner et al., 2001; IPCC, 2013). In estuarine and intertidal nearshore ecosystems, this anthropogenic climate change threatens to exacerbate the already substantial daily fluctuations in pH and seawater chemistry experienced in coastal waters and alters the baselines of local environmental variability (Waldbusser and Salisbury, 2014). Understanding how marine organisms will respond to these forecasted changes is a pressing conservation issue and requires a multifaceted approach including a more mechanistic understanding behind observed responses (Kroeker et al., 2013).

In response to decreased pH, many shallow-water marine molluscs exhibit reduced calcification (Ries et al., 2009; Zhao et al., 2017) and shell growth (Berge et al., 2006) rates and experience higher mortality (Shirayama and Thornton, 2005). However, compared with adult life stages, larval stages of marine organisms are typically even more vulnerable to the effects of OA (Kurihara, 2008; Dupont and Thorndyke, 2009; Gazeau et al., 2013). Marine larvae lack defenses present in adulthood (Byrne, 2011), exhibit greater surface area to mass ratios than adults, and typically require more specific environmental conditions during development (Thorson, 1950; Hunt and Scheibling, 1997; Bechmann et al., 2011), contributing to their heightened vulnerability to the impacts of OA. Negative effects of OA on larval molluscs include morphological abnormalities, reduced growth, increased mortality, and delayed metamorphosis (Kurihara, 2008; Dupont and Thorndyke, 2009; Gazeau et al., 2013). Taken together, these effects highlight the importance of studying early life stages, given that reductions in fitness in response to OA during the larval stage could have broad-reaching implications for adult populations (Kurihara, 2008; Dupont and Thorndyke, 2009; Gazeau et al., 2013).

In contrast to the more extensively studied phenotypic effects of OA on invertebrate larvae, much less in known about the genetic mechanisms underlying these responses. However, we do know that changes in gene expression in response to OA can vary widely across taxa. In sea urchin and oyster larvae, OA dampens expression of suites of genes responsible for major cellular processes, including metabolism, biomineralization, and larval shell formation (O'Donnell et al., 2009; Todgham and Hofmann, 2009; Dineshram et al., 2012; De Wit et al., 2018). Similarly, Yang et al. (2017) found significant upregulation of a tyrosinase, which is a gene important for shell repair in oyster larvae. In contrast, Zippay et al. (2010) examined two shell formation genes in red abalone larvae and determined that they were not differentially expressed at reduced pH. Furthermore, Kelly et al. (2016) found that the decreased growth rates observed for California mussel larvae in response to OA did not correlate with changes in gene expression. Interestingly, a coccolithophore was able to increase calcification over 700 generations in response to high *p*CO2 and temperature, but without differentially expressing genes traditionally associated with calcification (Benner et al., 2013).

The Atlantic slippersnail, *Crepidula fornicata,* exemplifies a marine intertidal and estuarine invertebrate whose adults exhibit remarkable resilience to most predicted environmental conditions of climate change (Ries et al., 2009; Diederich and Pechenik, 2013; Noisette et al., 2016), yet whose early life stages appear somewhat more vulnerable (Noisette et al., 2014; Bashevkin and Pechenik, 2015; Maboloc and Chan, 2017). Indeed, fecundity can be higher for intertidal individuals than for neighboring subtidal individuals (Pechenik et al., 2017b) and higher fecundities have also been observed at the northern range extreme when compared to their range center (Pechenik et al., 2017a). Adult *C. fornicata* have even demonstrated increased calcification under intermediate pCO_2 conditions (605 and 903 ppm; Ries et al., 2009). Increased pCO_2 (750 μatm) has also been shown to have no significant effect on *C. fornicata* rates of respiration, ammonia excretion, or filtration; indeed, a significant decrease in calcification rate was not observed until these gastropods were placed under the extremely high pCO_2 of 1400 μatm (Noisette et al., 2016). Clearly *C. fornicata* adults appear remarkably robust in response to changes in pH when compared to other marine calcifying organisms (Ries et al., 2009; Noisette et al., 2014) and this resilience may help explain how *C. fornicata* has invaded diverse global environments and successfully established huge populations therein (Blanchard, 1997; Viard et al., 2006). In contrast to adult *C. fornicata*, early life stages have been shown to be relatively more negatively affected by environmental stressors. For instance, *C. fornicata* larvae under reduced pH exhibited decreased shell growth, their shells had more abnormalities, and their mineralization rates decreased (Noisette et al., 2014). A study on *C. fornicata's* congener, *C. onyx,* found no effect of reduced pH on larval mortality, but did similarly document reduced growth rates and increasingly porous shells (Maboloc and Chan, 2017).

While researchers are beginning to characterize the morphological effects of OA on *C. fornicata* larvae, gene expression responses under reduced pH conditions remain unexplored. To better understand the response of *C. fornicata* larvae to OA, this study first characterized a suite of phenotypic traits in response to three pH treatments (pH 8.0, 7.6, and 7.5) coupled with transcriptomic responses of larvae that had been reared at the different pH levels for 4 days, starting within 12 h of hatching. Given results from previous transcriptome studies of molluscs under OA (Dineshram et al., 2012; De Wit et al., 2018), we hypothesized that marked shifts in gene expression patterns early in development would be observed, including downregulation of genes related to growth and metabolism in combination with previously reported phenotypes of reduced shell growth rates in *C. fornicata* larvae (Noisette et al., 2014). The impact of acidification on time to competence for metamorphosis was also quantified; we predicted that time to competence would be prolonged even if growth rates were unaffected, as the onset

of competence relates to processes of differentiation rather than growth (Pechenik et al., 1996); delayed time to competence has previously been noted in other marine molluscs, eastern oyster and bay scallop (Talmage and Gobler, 2010). Conversely, we expected to see no impact of reduced pH on larval mortality, as has been observed in *C. onyx* larvae (Maboloc and Chan, 2017). Together, these results begin to explore the complexities of the effects of OA on an early life history stage of a highly invasive and resilient snail.

MATERIALS AND METHODS

Adult and Larval Collection

Several stacks of adult *C. fornicata* were collected on July 9th, 2016 from the intertidal region of Totten Inlet, Thurston Co., WA. At the height of summer, near-surface waters in southern Puget Sound exhibit extensive variation in pCO_2 (250–2200 μatm), leading to corresponding fluctuations in pH and the widespread occurrence of undersaturated conditions for aragonite ($\Omega_{ar} < 1$) (Reum et al., 2014; Bianucci et al., 2018). *C. fornicata* stacks were driven to the University of Washington Friday Harbor Laboratories, Friday Harbor, WA, where each stack of approximately 4–6 individuals was held unfed in a one-gallon glass jar of unfiltered seawater at room temperature (21–23°C); the seawater was mildly aerated and changed daily. Larvae used in this study hatched and were released naturally by a single brooding adult on the third day after adult collection. Veligers were collected by siphoning on to a 150 μm sieve shortly after release. Veligers in the present study may or may not have been full siblings, considering that a single brood of *C. fornicata* can have multiple sires (Dupont et al., 2006).

Seawater pH Manipulation and Carbonate Chemistry

Larvae were cultured in the Ocean Acidification Environmental Laboratory at the University of Washington Friday Harbor Laboratories. Incoming seawater was filtered at 1 μm and equilibrated overnight at 20°C by bubbling with ambient air (for pH 8.0) or with mixtures of CO_2 and CO_2-free air delivered by Aalborg GFC17 mass-flow controllers (for pH 7.5 and 7.6). Seawater pH was measured immediately before loading into culture jars with a Honeywell Durafet pH electrode calibrated to the total scale by the cresol purple spectrophotometric method described by Dickson et al. (2007). Headspaces of culture jars were continuously ventilated with the same gas mixtures used to condition the seawater pH treatments during the 2 day intervals between culture water changes. Temperature and salinity were measured with a YSI Pro Series 1030 meter. Seawater samples representing each treatment were fixed with mercuric chloride and titrated to determine total alkalinity (TA) using a Mettler DL15 automated titrator calibrated to certified reference materials (Dickson laboratory, Scripps Institution of Oceanography). pCO_2 and Ω_{ar} were estimated based on empirical measurements of pH and TA using CO_2Sys 2.1 (Pierrot et al., 2006). Seawater chemical and physical properties used in larval culture treatments are available in **Table 1**. pH levels of 7.5 and 7.6 were selected because these levels represent a tipping point between aragonite saturation (pH 7.6, $\Omega_{ar} \cong 1$) and undersaturation (pH 7.5, $\Omega_{ar} < 1$) for the seawater used in this study, given our values of salinity, temperature, and TA (**Table 1**). Aragonite undersaturation has been associated with shell dissolution in key calcifying organisms (Orr et al., 2005).

Larval Culture

Larvae were randomly distributed across pH treatments of 8.0, 7.6, and 7.5. Each pH treatment consisted of four replicate 800 mL jars each containing 200 larvae. Larvae were fed 15×10^4 cells mL^{-1} of Tahitian *Isochrysis galbana* (T-ISO), a diet that supports maximal growth rates in larvae of *C. fornicata* (e.g., Pechenik and Tyrell, 2015). T-ISO was concentrated by centrifugation and re-suspended in filtered seawater before addition to larval cultures to minimize transfer of algal growth medium. Larvae were reared for 12 days, and sub-sampled for transcriptome analyses on day 4. Food and culture seawater were changed every 2 days. To estimate mortality, live *C. fornicata* larvae were counted during water changes on days 2, 6, and 10 and the proportion surviving on days 6 and 10 were compared to the live count taken on day 2.

Shell Length and Growth Rate Measurements

Growth rates of veligers were measured as the change of shell length (μm) over time. Individuals were imaged using a Motic camera fitted to a Leica Wild M3C dissecting microscope, and shell lengths were measured in ImageJ. Twenty larvae were measured upon collection on the day of their hatch. After the brood was distributed into treatments, 20 larvae from each replicate culture jar were imaged and measured every 4 days until day 12 post-hatch. Larvae were blindly selected in order to avoid size biasing, and were returned to cultures after measurement.

Metamorphic Competence Measurements

When larvae were 10 days old, we exposed them to elevated levels of KCl (20 mM excess) in seawater to assess competence for metamorphosis (Pechenik and Heyman, 1987; Pechenik and Gee, 1993; Pechenik et al., 2007). For each assay, 10 larvae were taken from each of the four replicate cultures of the three pH treatments (n = 40/pH treatment). The groups of 10 larvae were each pipetted into a dish (50 mL) of 20 mM excess KCl in seawater and then into another dish of the same solution (20 mL), to avoid diluting the final test solution. Percent metamorphosis was assessed 6 h after the start of the experiment and again 24 h later; metamorphosis was signaled by the loss of the ciliated velum. These tests were conducted in seawater that was equilibrated to the ambient atmosphere (pH ∼8.0).

Statistical Analyses of Phenotypic Effects

All statistical tests were performed in the R environment (R Development Core Team, 2013). For larval growth, one-way ANOVAs and Tukey's *post hoc* tests were used to determine if significant differences in log-transformed cumulative growth

TABLE 1 | Summary of measurements (pH, salinity, and temperature) taken every 2 days per treatment, from hatching (day 0) through day 10 of the study.

Treatment (pH)	pH ± *SD*	Salinity (ppt) ± *SD*	Temperature (°C) ± *SD*	TA (μmol kg^{-1}) ± *SD*	pCO_2 (μatm) ± *SD*	Ω_{ar} ± *SD*
7.5	7.53 ± 0.02	29.73 ± 0.39	19.93 ± 0.18	2099.85 ± 3.30	1480.55 ± 72.05	0.83 ± 0.04
7.6	7.60 ± 0.01	29.55 ± 0.50	20.20 ± 0.37	2083.07 ± 15.95	1207.60 ± 20.43	0.98 ± 0.01
8.0	7.95 ± 0.03	29.53 ± 0.44	20.28 ± 0.12	2085.53 ± 13.33	504.97 ± 35.06	1.98 ± 0.11

Total alkalinity (TA) was measured on days 2 and 10. Partial pressure of carbon dioxide (pCO_2) and aragonite saturation state (Ω_{ar}) were calculated from TA and pH. A one-way ANOVA determined that there was no significant different in temperature across experimental treatments.

rates (μm/day) existed between treatments at each time interval. Rates were cumulative relative to initial measurements, which were defined as day of hatching. Proportions of larvae that metamorphosed were compared via a one-way ANOVA and Tukey's *post hoc* test at 6 and 24 h, respectively, after metamorphosis was induced in 10-day old larvae. Proportions of larvae surviving at 6 and 10 days, relative to day 2 counts were also compared via a one-way ANOVA and Tukey's *post hoc* test. All assumptions of parametric testing were explored using diagnostic plots in R (R Development Core Team, 2013).

RNA Isolation and Sequencing Preparation

To achieve a sufficient quantity of RNA for whole genome gene expression profiling, three groups of 15 four-day old larvae were sampled from each of the three experimental treatments (pH 7.5, 7.6, and 8.0). Total RNA was extracted from the nine samples (three treatments * three replicate groups of 15 larvae each) using RNAqueous kit (Ambion) per manufacturer's instructions with one additional step: 0.5 mm glass beads (BioSpec) were added to the vial of lysis buffer and samples were homogenized using a bead beater for 1 min. RNA quality was ascertained using gel electrophoresis by confirming the presence of ribosomal RNA bands, and 1500 ng of total RNA was used to create libraries. First, trace DNA contamination was eliminated by *DNase 1* (Ambion) digestion at 37°C for 45 min and then libraries were created as in Meyer et al. (2011) adapted for Illumina Hi-Seq sequencing (Dixon et al., 2015; Lohman et al., 2016). In brief, heat-sheared total RNA was transcribed into first-strand cDNA flanked by PCR primer sequences using oligo-dT containing primer, template-switching oligo (Matz et al., 1999) and SMARTScribe reverse transcriptase (Clontech). Complementary-DNA was then PCR-amplified and Illumina barcodes were incorporated using a secondary short PCR. Samples were equalized, pooled, and size-selected prior to sequencing (single-end (SE) 50 basepair (bp)) at Tufts Genomics.

Crepidula fornicata Transcriptome Annotation and Read Mapping

Previously published *C. fornicata* contigs (Henry et al., 2010) that were >500 bp in length were annotated by BLAST sequence homology searches against UniProt and Swiss-Prot NCBI NR protein databases with an *e*-value cutoff of e^{-5} and annotated sequences were assigned to Gene Ontology (GO) categories (The UniProt Consortium, 2015). Raw reads across libraries ranged from 14.2 to 25.2 million SE 50 bp sequences (**Table 2**). *Fastx_toolkit* was used to remove *Illumina TruSeq* adapters and poly(A)$^+$ tails. Sequences <20 bp in length with <90% of bases having quality cutoff scores >20 were also trimmed. In addition, PCR duplicates were removed via a custom perl script ensuring that each read that was mapped corresponded to a unique mRNA molecule. The resulting quality filtered reads were then mapped to the *C. fornicata* transcriptome using *Bowtie2.2.0* (Langmead and Salzberg, 2012). A per-sample counts file was generated using a custom perl script that sums up reads for all genes while discarding reads mapping to more than one gene. Total *C. fornicata* mapped reads ranged from 0.5 (pH 8.0) to 1.0 (pH 7.5) million with mapping efficiencies ranging from 24.4 to 26.3% (**Table 2**).

Gene Expression Analysis

Differential gene expression analyses were performed with *DESeq2* v. 1.6.3 (Love et al., 2014) in R v. 3.1.1 (R Development Core Team, 2013). First, data were tested for sample outliers using the *arrayQualityMetrics* package (Kauffmann et al., 2009) and no outliers were detected. Expression data were then normalized using the *rlog* function and these normalized data (N = 19,717 genes) were used to broadly characterize differences in gene expression across experimental treatments using a principal component analysis with the package *vegan* (Oksanen et al., 2016). Significance was assessed using the multivariate analysis of variance function, *adonis*, in the *vegan* package (Oksanen et al., 2016). Raw count data are available in **Supplementary Data Sheet 1**.

DESeq2 v. 1.6.3 was then used to identify differentially expressed genes (DEGs) consistently associated with the lower pH treatments (pH 7.5 and 7.6) relative to pH 8.0 using generalized linear models. *DESeq2* performed automatic

TABLE 2 | Summary of RNA libraries including raw single-end (SE) reads, trimmed (including de-duplication and quality filtering) reads, and mapped (to *C. fornicata* transcriptome) counts and percentages.

Sample	# SE reads	# After trimming	# Mapped	% Mapped
7.5A	25,224,357	3,222,928	789,550	24.50
7.5B	21,750,964	3,591,242	918,366	25.57
7.5C	22,895,862	4,078,245	1,027,861	25.20
7.6A	23,083,355	3,792,669	926,497	24.43
7.6B	16,184,588	3,239,532	816,054	25.19
7.6C	17,215,957	3,053,984	770,342	25.22
8.0A	15,364,186	2,393,789	612,258	25.58
8.0B	19,838,321	2,476,114	651,727	26.32
8.0C	14,229,958	1,839,873	480,153	26.10

independent filtering to remove low abundance transcripts, which maximizes the rate of DEG discovery post multiple testing correction at an alpha of 0.1. *P*-values for significance of contrasts between the lower pH treatments (pH 7.5 and 7.6) and pH 8.0 were generated based on Wald statistics and were adjusted for multiple testing using the false discovery rate method (Benjamini and Hochberg, 1995). Gene expression heatmaps of DEGs consistently associated with reduced pH were then generated with hierarchical clustering of expression profiles with the *pheatmap* package in R (Kolde, 2015). *DESeq2* results for both treatments are available in **Supplementary Data Sheet 2** (pH 7.6) and **Supplementary Data Sheet 3** (pH 7.5) while gene annotation information is available in **Supplementary Data Sheet 4**.

Gene ontology enrichment analysis was then performed using adaptive clustering of GO categories and Mann–Whitney U tests (GO-MWU) based on ranking of signed log *p*-values (Voolstra et al., 2011), which is particularly suitable for non-model organisms (Dixon et al., 2015). Results were plotted as dendrograms tracing the level of gene sharing between significant categories and direction of change in reduced pH treatments relative to pH 8.0 were indicated by text color. GO designation information can be found in **Supplementary Data Sheet 5**. GO enrichment results comparing pH 7.6 and 8.0 can be found in **Supplementary Data Sheet 6** (Cellular Component), 7 (Biological Process), and 8 (Molecular Function). GO enrichment results comparing pH 7.5 to 8.0 can be found in **Supplementary Data Sheet 9** (Cellular Component), 10 (Biological Process), and 11 (Molecular Function).

RESULTS

Rates of Larval Shell Growth

Crepidula fornicata larvae grew at a significantly slower rate in response to pH 7.5 at all three time-points after hatching when compared to larvae reared at pH 8.0, while larvae reared at pH 7.6 had a more variable response over time (**Table 3** and **Figure 1**). Specifically, on day 4, the cumulative growth rate was significantly lower for larvae reared in the pH 7.5 treatment compared to those reared at all other pH treatments (**Table 3** and **Figure 1B**). However, by day 8, larvae reared at both of the lower pH levels (7.5 and 7.6) were growing significantly more slowly than those reared at pH 8.0 (**Table 3** and **Figure 1C**). Lastly, by day 12, whereas mean shell growth rates were significantly lower for larvae reared at pH 7.5 when compared to those that had been reared at pH 7.6 and 8.0, there were no longer any significant differences in mean shell growth rates between larvae reared at pH 7.6 or 8.0 (**Table 3** and **Figure 1D**).

Metamorphic Competence 10 Days Post-hatching

The pH in which 10-day post-hatching *C. fornicata* larvae had been reared was shown to significantly affect their ability to metamorphose within the first 6 h of exposure to the 20 mM excess KCl inducer (**Table 4** and **Figure 2**). Larvae that had been reared at pH 7.6 or 7.5 exhibited significantly reduced metamorphosis at 6 h compared to larvae reared at pH 8.0 (**Table 4** and **Figure 2**). However, 24 h after larvae began exposure to the metamorphic inducer, larval pH treatment no longer had a significant effect on the extent of *C. fornicata* larval metamorphosis (**Table 4** and **Figure 2**).

Larval Survival

Proportions of living *C. fornicata* larvae on day 6 ranged from an average of 91.6 to 97.8% across treatments (**Figure 3**), but there were no statistical differences in mortality across treatments (**Table 5**). The same pattern of no impact of OA on larval mortality was also observed on day 10, when proportions of living larvae ranged from 86.8 to 91.0% (**Table 5** and **Figure 3**).

Larval Transcriptomic Responses to OA

Gene expression analyses revealed strong associations between *C. fornicata* larval expression levels of transcripts within each of the three pH treatments (*Adonis* $p = 0.003$, **Figure 4A**), suggesting that each treatment elicited a distinct transcriptomic stress response. Relative to pH 8.0, *C. fornicata* larvae reared at pH 7.6 differentially expressed (FDR-adjusted <0.1) 295 genes (38 were upregulated; 257 were downregulated), while larvae reared at pH 7.5 differentially expressed 55 genes (19 were upregulated; 36 were downregulated). Notably, most differentially expressed genes (DEGs) at both pH levels (pH 7.5 and 65.5%; pH 7.6 and 87.1%) were underrepresented relative to pH 8.0. A total of 33 DEGs were common to larvae reared at both reduced pH levels (**Figure 4B**). However, rearing larvae at pH 7.6 mounted a much stronger overall transcriptomic response when compared to pH 7.5. Differential gene expression and annotation information for each treatment is included in **Supplementary Data Sheets 2–4**.

TABLE 3 | Statistical analyses of the overall effect of pH treatment and between treatment comparisons, regarding cumulative larval growth rate (μm/day) per day of measurement (days 4, 8, and 12 post-hatching).

	Effect of pH treatment, 1-way ANOVA	Between treatment comparisons	Tukey's HSD *p*-value
Day 4	$F_{2,9} = 5.928$, $p = 0.0228$*		
		pH 7.6 vs. 7.5	0.0301*
		pH 8.0 vs. 7.5	0.0475*
		pH 8.0 vs. 7.6	0.9542
Day 8	$F_{2,9} = 13.3$, $p = 0.0021$*		
		pH 7.6 vs. 7.5	0.4282
		pH 8.0 vs. 7.5	0.0020**
		pH 8.0 vs. 7.6	0.0129*
Day 12	$F_{2,9} = 7.155$, $p = 0.0138$*		
		pH 7.6 vs. 7.5	0.0306*
		pH 8.0 vs. 7.5	0.0188*
		pH 8.0 vs. 7.6	0.9468

The level of significance is indicated by one or more asterisks ($p < 0.05$, **$p < 0.01$).*

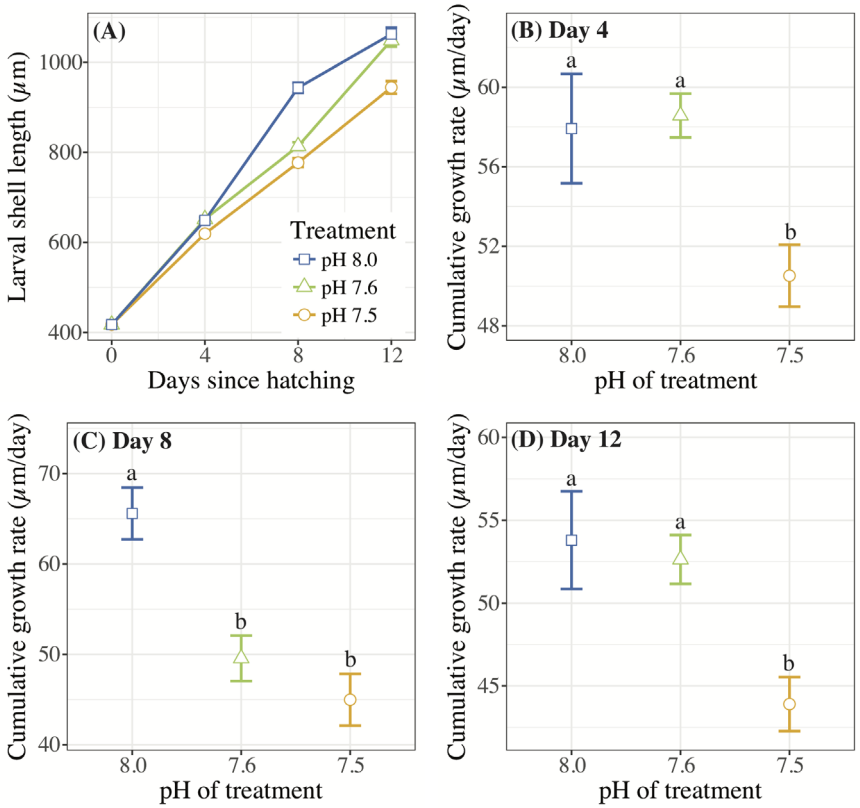

FIGURE 1 | (A) Mean *C. fornicata* larval shell lengths (in μm) +/– SE measured 0, 4, 8, and 12 days after hatching. Standard error bars are present for the mean of each treatment; however, these may be obscured by the mean values due to low variability between measurements. **(B–D)** Cumulative shell growth rates (μm/day) relative to initial (day 0) measurements compared at 4, 8, and 12 days. Different letters above bars (*i.e.,* "a" or "b") indicate significantly different means based on Tukey's test ($p < 0.05$).

Of the 33 DEGs in common across the two lower pH treatments, only 10 were annotated and, consistent with reduced pH causing an overall transcriptome downregulation, most of these DEGs were downregulated in larvae from reduced pH treatments relative to larvae reared at pH 8.0 (**Figure 4B**). These downregulated genes included genes associated with growth and metabolism (Epoxide hydrolase 1, Collagen alpha-1(II) chain, Cytochrome c oxidase subunits 2 and 3, tropomyosin, Collagen alpha-1(II) chain, Fibropellin-1), cell transport (Transmembrane protein 14C, actin-2), as well as a single gene involved in immunity (Thymosin beta-b) (**Figure 4B**). GO enrichment results are included in **Supplementary Data Sheets 5–11**.

Gene Ontology (GO) Enrichment in Response to OA

Functional enrichments between the two reduced pH treatments (7.5 and 7.6) and pH 8.0 allow for a general examination of the 'cellular component' (CC), 'biological process' (BP), and 'molecular function' (MF) categories that are being differentially regulated under reduced pH conditions. Consistent with *DESeq2* results, most GO enrichments were observed to be underrepresented relative to pH 8.0 (blue text; **Figure 5**). GO categories associated with ribosomal proteins (i.e., *ribosome;* GO:0005840, *small ribosomal subunit;* GO:0015935, *structural constituent of the ribosome;* GO:0003735), oxidative stress responses (i.e., *oxidoreductase;* GO:0016491), cytochrome-c oxidase (i.e., *cytochrome-c oxidase;* GO:0004129, *cytochrome complex;* GO:0017004), and translation activity

TABLE 4 | Statistical comparisons of the proportion of 10-day old larvae that metamorphosed 6 and 24 h post-induction of metamorphosis, including overall effect of pH treatment and between treatment comparisons.

	Effect of pH treatment, 1-way ANOVA	Between treatment comparisons	Tukey's HSD *p*-value
6 h	$F_{2,9} = 7.636$, $p = 0.0115$*		
		pH 7.6 vs. 7.5	0.7477
		pH 8.0 vs. 7.5	0.0388*
		pH 8.0 vs. 7.6	0.0124*
24 h	$F_{2,9} = 3.0$, $p = 0.1$		
		pH 7.6 vs. 7.5	0.1402
		pH 8.0 vs. 7.5	1.0000
		pH 8.0 vs. 7.6	0.1402

The level of significance is indicated by an asterisk ($p < 0.05$).*

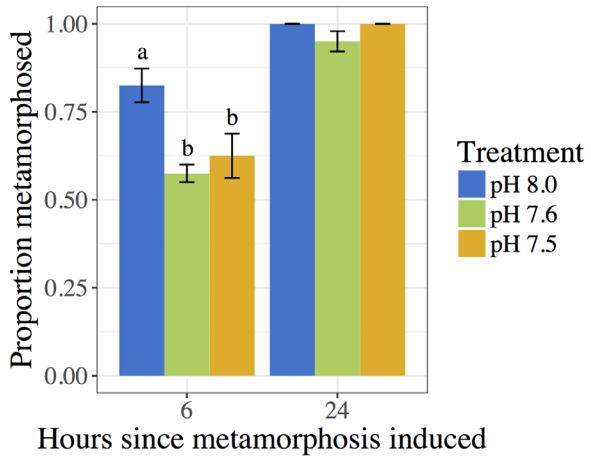

FIGURE 2 | Proportion of *C. fornicata* larval metamorphosis (induced with 20 mM KCl excess) after 6 and 24 h. Different letters above bars (*i.e.,* "a" or "b") indicate significantly different means based on Tukey's test ($p < 0.05$). If no letters exist above bars, no significant differences were observed based on Tukey's test ($p > 0.05$).

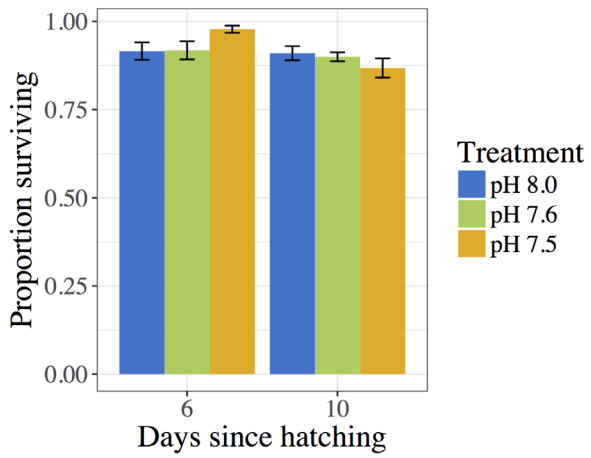

FIGURE 3 | Proportion of *C. fornicata* larval survival relative to day 2 as measured on days 6 and 10. Different letters above bars (*i.e.,* "a" or "b") indicate significantly different means based on Tukey's test ($p < 0.05$). If no letters exist above bars, no significant differences were observed based on Tukey's test ($p > 0.05$).

(i.e., *translation;* GO:0006412) were consistently downregulated in *C. fornicata* larvae under lower pH treatments compared to those that had been reared under the higher pH (8.0) (**Figure 5**).

DISCUSSION

Despite the extreme experimental levels of OA used in the present study, *C. fornicata* larvae were remarkably resilient, showing very low levels of mortality (**Figure 3**). Moreover, only the lowest pH treatment (pH 7.5) consistently affected larval shell growth rates (**Figure 1**), and short-term negative impacts of OA treatments on response to a metamorphic inducer were relieved within 24 h (**Figure 2**). Moreover, surprisingly few genes exhibited differential expression amongst the experimental treatments (**Figures 4**, **5**). Although we determined that reduced pH had a noticeable impact on some phenotypic and genotypic traits in *C. fornicata* larvae, the magnitude of the impact was relatively underwhelming. However, given that these pH conditions along with highly undersaturated aragonite are routinely experienced in Puget Sound (Reum et al., 2014; Bianucci et al., 2018), the subtle effects on physiology and transcriptomic responses perhaps might be expected for this highly resilient littoral gastropod.

OA Slows Growth Rates in *C. fornicata* Larvae

Only the lowest OA treatment of pH 7.5 consistently slowed growth of *C. fornicata* larvae significantly (**Figure 1**), indicating the substantial extent to which the baseline environmental pH of *C. fornicata* would have to change to impact larval growth. Interestingly, larvae reared in pH 7.6 demonstrated lower growth rates between days 4 and 8 (**Figure 1**). It appears that, in the current study, 7.6 lies close to a threshold, below which *C. fornicata* larval growth rates were affected over the entire course of development, rather than at certain time-points (**Figure 1**). Accordingly, larval growth rates in the pH 7.6 treatment recovered between days 8 and 12 (**Figure 1**). This pattern is best explained by the aragonite saturation state (Ω_{ar}) hovering around 1 in the pH 7.6 treatment, while lying well below 1 in the pH 7.5 treatment (**Table 1**).

While our results indicate that larvae reared at pH 7.6 withstood effects of OA quite well, despite an early lag in growth, related studies have observed different levels of tolerance. For instance, in 14-day old *C. onyx* larvae, Maboloc and Chan (2017) found that a pH reduction to just 7.71 elicited significant decreases in shell growth rates, perhaps highlighting species-specific differences. However, complex interactions were observed between OA and diet (Maboloc and Chan, 2017). In

TABLE 5 | Statistical comparisons between treatments of the cumulative proportion of surviving larvae on days 6 and 10 relative to initial counts on day 2.

	Effect of pH treatment, 1-way ANOVA	Between treatment comparisons	Tukey's HSD *p*-value
6 days	$F_{2,9} = 2.736$, $p = 0.118$		
		pH 7.6 vs. 7.5	0.1702
		pH 8.0 vs. 7.5	0.1537
		pH 8.0 vs. 7.6	0.9973
10 days	$F_{2,9} = 1.114$, $p = 0.37$		
		pH 7.6 vs. 7.5	0.5432
		pH 8.0 vs. 7.5	0.3679
		pH 8.0 vs. 7.6	0.9395

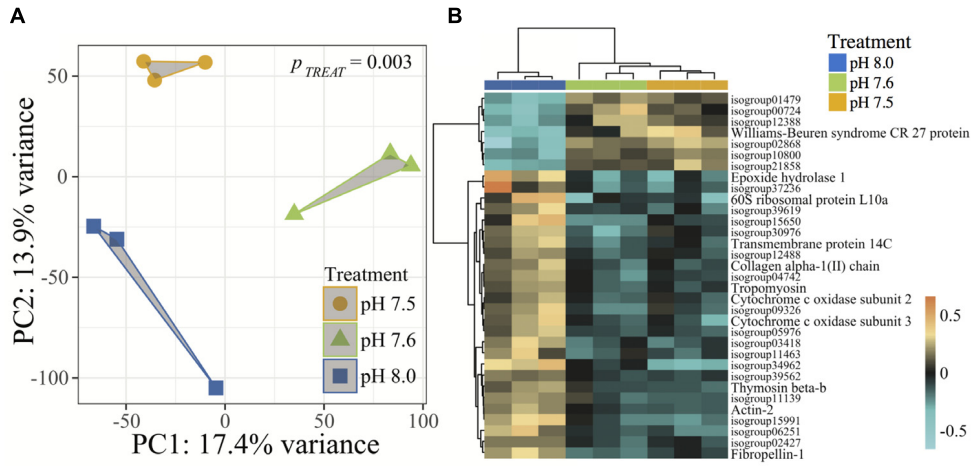

FIGURE 4 | (A) Principal component analysis (PCA) of all r-log transformed isogroups clustered by experimental treatment, demonstrating significantly different transcriptomic responses of 4-day old *C. fornicata* larvae across different pH treatments (*Adonis* p_{treat} = 0.003). Symbol colors represent treatment conditions: blue = pH 8.0, green = pH 7.6, and yellow = pH 7.5. **(B)** Heatmap for top DEGs (FDR-adjusted = 0.10) in common for both pH 7.6 and pH 7.5 relative to pH 8.0. Rows are genes and columns are independent RNAseq libraries (N = 15 larvae/library). The color scale is in $\log_2$ (fold change relative to the gene's mean). The trees are hierarchical clustering of genes and samples based on Pearson's correlation of their expression across samples and genes.

a study exposing *C. fornicata* to OA treatments (pH 7.82 and 7.56) over the entire course of development, from fertilization to hatching, larvae from reduced pH treatments were smaller at hatching than those under control conditions (Noisette et al., 2014), suggesting that OA impacted the reproductive or development process or that maternal effects were passed onto offspring. These two studies highlight the importance of considering other factors in addition to OA, such as pre-hatching events and diet, in future studies investigating the effects of OA on *C. fornicata*. Nevertheless, Noisette et al. (2014) conducted a literature review of the various effects of pH reductions on shell growth rates in mollusc larvae and concluded that the magnitude of diminished shell growth rates in larval *C. fornicata* was less than the observed losses across most other species, a result that corroborates the resilience to OA by *C. fornicata* larvae observed in the present study.

Larval *C. fornicata* Transcriptomic Depression in Response to OA

Here we observe that after 4 days, a pH difference of just 0.1 units elicited divergent transcriptomic responses between *C. fornicata* larvae exposed to reduced pH levels (7.5 and 7.6); both responses were statistically divergent from larval expression at pH 8.0 (**Figure 4**). Consistent with previous research on larval responses to OA in molluscs (Dineshram et al., 2012; De Wit et al., 2018), larvae maintained at reduced pH exhibited a dampening transcriptomic response, where most differentially expressed genes were downregulated relative to pH 8.0 (**Figure 4B**). Amongst annotated genes that were consistently downregulated in response to OA, most were associated with growth and metabolism (**Figure 4B**), which corroborates findings in oyster and sea urchin larvae reared under OA conditions (Todgham and Hofmann, 2009; Dineshram et al., 2012) and is supported by the theory that metabolism cutbacks help intertidal organisms cope with short-term stress (Portner and Farrell, 2008). GO analyses also demonstrated a pattern of transcriptomic depression, where most of the significantly enriched GO terms associated with metabolism and growth (e.g., ribosomal and mitochondrial functions, ATP-synthase activity) were downregulated relative to pH 8.0 (**Figure 5**).

Downregulation of genes associated with growth and metabolism is also consistent with our phenotypic results in terms of shell growth rate depression in larvae reared at pH 7.5 (**Figure 1**). However, on day 4 (the day of transcriptomic sampling), larvae reared at pH 7.6 showed more differential gene expression than larvae reared at pH 7.5, but without the same observed repression of shell growth (**Figures 1**, **5**). It is possible that the significant changes in gene expression on day 4 in the pH 7.6 treatment preclude the cumulative reduction in shell growth rates observed on day 8 of this experiment (**Figure 1**). Alternatively, pH 7.6 could represent a pH in which larvae were inducing many physiological changes to compensate for the pH treatment, which would be consistent with the observed fluctuations in shell growth rates observed at pH 7.6 and in the larger number of differentially enriched GO terms (**Figure 5**). Future work should focus on sampling *C. fornicata* larvae with increased temporal frequency to discern with more acuity the timing at which the strongest coinciding phenotypic and transcriptomic impacts are mounted in response to OA.

Additionally, *C. fornicata* larvae reared in the pH 7.6 treatment downregulated redox-regulation associated genes (see oxidoreductase and oxidation-reduction process in **Figure 5**), which are typically associated with the minimal cellular stress response (Kültz, 2005). It appears contradictory that marine

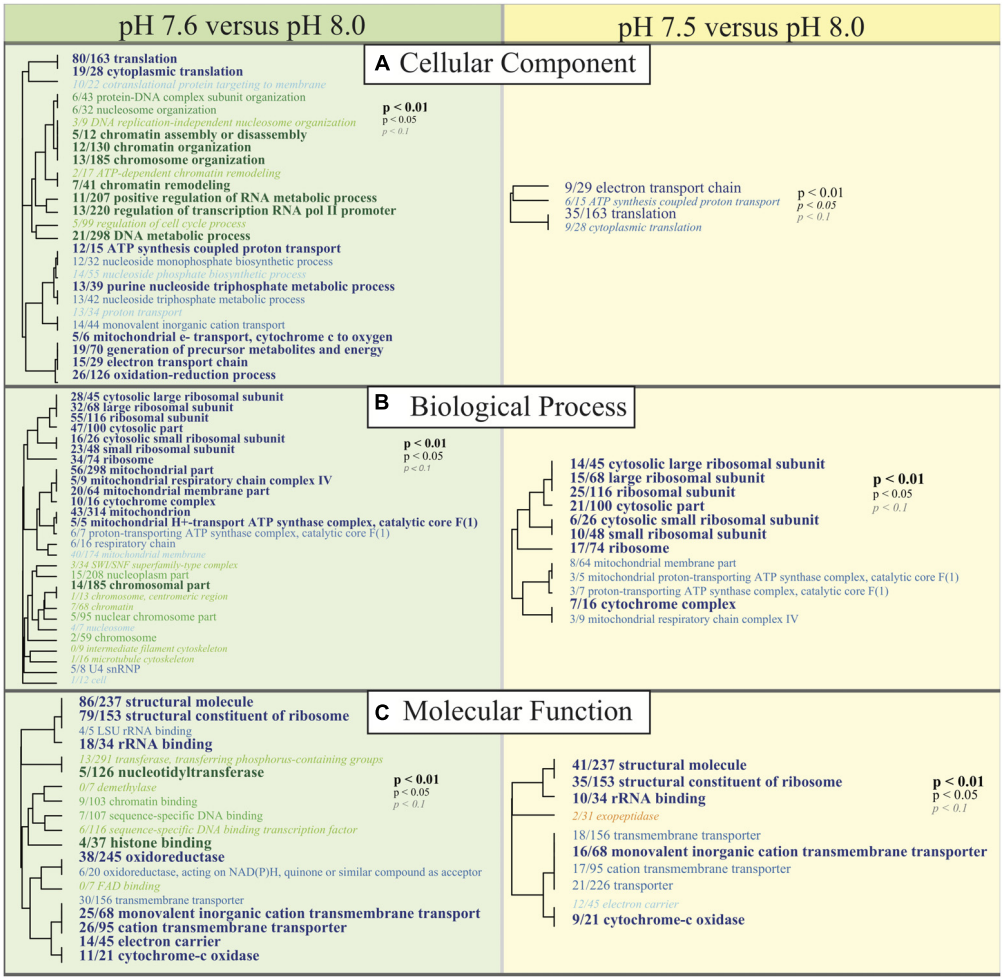

FIGURE 5 | Gene ontology (GO) categories significantly enriched for each pairwise comparison (Left: pH 7.6 vs. pH 8.0, Right: pH 7.5 vs. pH 8.0) by **(A)** 'cellular component,' **(B)** 'biological process,' and **(C)** 'molecular function' using Mann-Whitney U tests based on ranking of signed log *p*-values. Results are plotted as dendrograms tracing the level of gene sharing between significant categories. Direction of change is noted in color where those GO categories overrepresented in pH 8.0 conditions are colored as blue and those underrepresented in pH 8.0 conditions are colored as green and yellow.

organisms would downregulate these genes while under pH stress; indeed, upregulation rather than downregulation of redox functional processes has been reported in Emerald rockcod *Trematomus bernacchii* (Huth and Place, 2016) and in marine copepods (Lauritano et al., 2012) exposed to reduced pH. However, downregulation of stress response genes under OA conditions is shared among many other marine invertebrates, including purple sea urchin *Strongylocentrotus purpuratus* larvae (Todgham and Hofmann, 2009), *Saccostrea glomerata* oysters (Goncalves et al., 2017), Arctic copepods *Calanus glacialis* (Bailey et al., 2017), and coral *Acropora millepora* (Kaniewska et al., 2012). Downregulation of stress response genes may leave cells more vulnerable to the negative impacts of oxidative stress and protein denaturing (Todgham and Hofmann, 2009). Unexpectedly however, downregulation of stress response genes in response to OA did not present with any associated phenotypic impacts in *C. glacialis* copepods (Bailey et al., 2017), has been associated with pH-resistant oysters (Goncalves et al., 2017), and the *C. fornicata* larvae reared in the pH 7.6 treatment in the present study did not present with atypical growth rates at the time of transcriptome sampling, confirming that some pH-tolerant organisms typically downregulate redox-associated genes (Bailey et al., 2017).

OA Delays Larval Metamorphosis

Crepidula fornicata larvae, if competent, typically metamorphose within 6 h when exposed to seawater with KCl concentrations elevated by 15–20 mM (Pechenik and Heyman, 1987; Pechenik and Gee, 1993). In our study, a smaller percentage of larvae that had been reared at reduced pH metamorphosed in response to KCl within 6 h, but there was no significant effect of rearing conditions on percent metamorphosis by 24 h (**Figure 2**). The reduced response to excess KCl in the first 6 h for larvae reared at reduced pH could reflect a slightly longer time to become competent to metamorphose or interference with the functioning of the metamorphic pathway. This issue requires further study.

Similar and more extended delays in metamorphosis have been observed in other marine calcifiers, including hard clams, bay scallops, and coral larvae (Talmage and Gobler, 2010; Nakamura et al., 2011). In coral *Acropora digitifera* larvae, pH levels of 7.6 and 7.3 significantly reduced metamorphosis after both 2 h and 7 days of OA treatment, indicating that metamorphosis may be fully disrupted or severely delayed in these larvae (Nakamura et al., 2011). In the hard clam *Merceneria merceneria,* less than 7% of larvae metamorphosed after 14 days of development at pH 8.05, 7.80, and 7.53, compared to 51% metamorphosis in pH 8.17 (pre-industrial conditions) (Talmage and Gobler, 2010). After 12 days of development, 87% of bay scallop *Argopecten irradians* larvae metamorphosed in pre-industrial pH treatments as compared to 68% metamorphosis in pH 8.05 (Talmage and Gobler, 2010). Metamorphosis percentages in both species appeared approximately the same in all treatments by day 30 for *M. merceneria* and by day 19 for *A. irradians* (Talmage and Gobler, 2010). However, the current study did not examine percentage of metamorphosis while in natural seawater conditions, nor in the natural inducer of adult-conditioned seawater (Pechenik and Heyman, 1987; Pechenik and Gee, 1993).

While a slight temporal delay in metamorphosis of *C. fornicata* larvae may seem inconsequential, it is theorized that additional time spent in the water column will increase predation rates and size-specific mortality or could carry larvae away from suitable habitat prior to metamorphosis (Pechenik, 1999; Talmage and Gobler, 2010; Bashevkin and Pechenik, 2015). On the other hand, currents could carry larvae to more suitable habitat and further aid in the invasive dispersal potential of *C. fornicata* (Pechenik, 1999; Bashevkin and Pechenik, 2015). Future work should examine the interplay of the impacts of OA with the dynamics of larval settlement and predation rates.

CONCLUSION

Higher resistance to the negative impacts of environmental stressors when compared to native species is one of the defining characteristics of a successful invasive species (Lenz et al., 2011). Accordingly, in the presence of severe OA stress, *C. fornicata* larvae in the present study exhibited some deleterious but overall moderate effects, especially when compared with effects previously documented for other marine invertebrates. As oceans become more acidic, it is likely that *C. fornicata* populations, which are already able to withstand many extreme environmental conditions today (Diederich and Pechenik, 2013; Noisette et al., 2016) may be better able to outcompete native species. To actualize a more complete picture of how OA impacts *C. fornicata* early life stages, future work should more thoroughly characterize how quickly shifts in gene expression take place in response to OA, examine more diverse life stages, and consider the potential additional impacts of climate change (temperature and nutrient shifts). While the present study only considered the impact of reduced pH, Pechenik (1984) and Bashevkin and Pechenik (2015) found that warming temperatures favored *C. fornicata* larval growth, while Thieltges et al. (2004) suggested that colder temperatures have previously prevented range expansion of *C. fornicata* into northern Europe. Considering these results in conjunction with the present study, large populations of this resilient snail may be supported well into the future and perhaps even into new areas of the globe.

DATA AVAILABILITY STATEMENT

Detailed protocol of library preparation and associated bioinformatics can be found at https://github.com/z0on/tag-based_RNAseq. Protocol of gene ontology analysis can be found at https://github.com/z0on/GO_MWU. All annotation files for *Crepidula fornicata* transcriptome are available: http://sites.bu.edu/davieslab/data-code. Raw reads have been submitted to SRA under PRJNA471890. All phenotypic and seawater measurement datasets are available upon request.

AUTHOR CONTRIBUTIONS

AP and JP conceptualized the experimental design and carried out the organismal collections and phenotypic measurements. Transcriptomic data collection and analyses were performed by SD. Phenotypic data analyses were performed by NK. NK wrote the manuscript with contributions from SD, AP, and JP. All authors revised and approved the manuscript.

FUNDING

This research was supported by the National Science Foundation (CRI-OA-1416846 to Tufts University and CRI-OA-1416690 to Dickinson College). SD was a Simons Foundation Fellow of the Life Sciences Research Foundation (LSRF) during the time of transcriptome preparations and TagSeq libraries were prepared with LSRF funds.

ACKNOWLEDGMENTS

We thank Christine Choi, Rulaiha Taylor, and Alissa Resnikoff for assisting with maintenance of larval cultures, and Rebecca Guenther for support of seawater conditioning and chemical analysis in the Ocean Acidification Environmental Laboratory at the University of Washington Friday Harbor Laboratories. We also acknowledge the Marchetti and Castillo labs at UNC Chapel Hill for use of their lab spaces for the preparations of TagSeq libraries. Diane Cooper at Taylor Shellfish Co. kindly provided access to our adult field collection site.

SUPPLEMENTARY MATERIAL

The Supplementary Material for this article can be found online at: https://www.frontiersin.org/articles/10.3389/fmars.2018.00312/full#supplementary-material

REFERENCES

Bailey, A., De Wit, P., Thor, P., Browman, H. I., Bjelland, R., Shema, S., et al. (2017). Regulation of gene expression is associated with tolerance of the Arctic copepod *Calanus glacialis* to CO_2-acidified sea water. *Ecol. Evol.* 7, 7145–7160. doi: 10.1002/ece3.3063

Bashevkin, S. M., and Pechenik, J. A. (2015). The interactive influence of temperature and salinity on larval and juvenile growth in the gastropod *Crepidula fornicata* (L.). *J. Exp. Mar. Bio. Ecol.* 470, 78–91. doi: 10.1016/j.jembe.2015.05.004

Bechmann, R. K., Taban, I. C., Westerlund, S., Godal, B. F., Arnberg, M., Vingen, S., et al. (2011). Effects of ocean acidification on early life stages of shrimp (*Pandalus borealis*) and mussel (*Mytilus edulis*). *J. Toxicol. Environ. Health A* 74, 424–438. doi: 10.1080/15287394.2011.550460

Benjamini, Y., and Hochberg, Y. (1995). Controlling the false discovery rate: a practical and powerful approach to multiple testing. *J. R. Stat. Soc. Ser. B* 57, 289–300. doi: 10.2307/2346101

Benner, I., Diner, R. E., Lefebvre, S. C., Li, D., Komada, T., Carpenter, E. J., et al. (2013). *Emiliania huxleyi* increases calcification but not expression of calcification-related genes in long-term exposure to elevated temperature and pCO_2. *Philos. Trans. R. Soc. B Biol. Sci.* 368, 20130049–20130049. doi: 10.1098/rstb.2013.0049

Berge, J. A., Bjerkeng, B., Pettersen, O., Schaanning, M. T., and Øxnevad, S. (2006). Effects of increased sea water concentrations of CO_2 on growth of the bivalve *Mytilus edulis* L. *Chemosphere* 62, 681–687. doi: 10.1016/j.chemosphere.2005.04.111

Bianucci, L., Long, W., Khangaonkar, T., Pelletier, G., Ahmed, A., Mohamedali, T., et al. (2018). Sensitivity of the regional ocean acidification and carbonate system in Puget Sound to ocean and freshwater inputs. *Elem. Sci. Anth.* 6:22. doi: 10.1525/elementa.151

Blanchard, M. (1997). Spread of the slipper limpet *Crepidula fornicata* (L. 1758) in Europe. Current state and consequences. *Sci. Mar.* 61, 109–118.

Bopp, L., Resplandy, L., Orr, J. C., Doney, S. C., Dunne, J. P., Gehlen, M., et al. (2013). Multiple stressors of ocean ecosystems in the 21st century: projections with CMIP5 models. *Biogeosciences* 10, 6225–6245. doi: 10.5194/bg-10-6225-2013

Byrne, M. (2011). Impact of ocean warming and ocean acidification on marine invertebrate life history stages: vulnerabilities and potential for persistence in a changing ocean. *Oceanogr. Mar. Biol.* 49, 1–42. doi: 10.1016/j.marenvres.2011.10.00

Caldeira, K., and Wickett, M. E. (2003). Anthropogenic carbon and ocean pH. *Nature* 425:365. doi: 10.1038/425365a

De Wit, P., Durland, E., Ventura, A., and Langdon, C. J. (2018). Gene expression correlated with delay in shell formation in larval Pacific oysters (*Crassostrea gigas*) exposed to experimental ocean acidification provides insights into shell formation mechanisms. *BMC Genomics* 19:160. doi: 10.1186/s12864-018-4519-y

Dickson, A. G., Sabine, C. L., and Christian, J. R. (eds). (2007). "Guide to best practices for ocean CO_2 measurements," in *PICES Special. Publication,* (Sidney: North Pacific Marine Science Organization).

Diederich, C. M., and Pechenik, J. A. (2013). Thermal tolerance of *Crepidula fornicata* (Gastropoda) life history stages from intertidal and subtidal subpopulations. *Mar. Ecol. Prog. Ser.* 486, 173–187. doi: 10.3354/meps10355

Dineshram, R., Wong, K. K. W., Xiao, S., Yu, Z., Qian, P. Y., and Thiyagarajan, V. (2012). Analysis of Pacific oyster larval proteome and its response to high-CO_2. *Mar. Pollut. Bull.* 64, 2160–2167. doi: 10.1016/j.marpolbul.2012.07.043

Dixon, G. B., Davies, S. W., Aglyamova, G. V., Meyer, E., Bay, L. K., and Matz, M. V. (2015). Genomic determinants of coral heat tolerance across latitudes. *Science* 348, 1460–1462. doi: 10.1126/science.1261224

Dupont, L., Richard, J., Paulet, Y. M., Thouzeau, G., and Viard, F. (2006). Gregariousness and protandry promote reproductive insurance in the invasive gastropod *Crepidula fornicata*: evidence from assignment of larval paternity. *Mol. Ecol.* 15, 3009–3021. doi: 10.1111/j.1365-294X.2006.02988.x

Dupont, S., and Thorndyke, M. C. (2009). Impact of CO_2-driven ocean acidification on invertebrates early life-history – What we know, what we need to know and what we can do. *Biogeosci. Discuss.* 6, 3109–3131. doi: 10.5194/bgd-6-3109-2009

Gazeau, F., Parker, L. M., Comeau, S., Gattuso, J. P., O'Connor, W. A., Martin, S., et al. (2013). Impacts of ocean acidification on marine shelled molluscs. *Mar. Biol.* 160, 2207–2245. doi: 10.1007/s00227-013-2219-3

Goncalves, P., Thompson, E. L., and Raftos, D. A. (2017). Contrasting impacts of ocean acidification and warming on the molecular responses of CO_2-resilient oysters. *BMC Genomics* 18:431. doi: 10.1186/s12864-017-3818-z

Henry, J. J., Perry, K. J., Fukui, L., and Alvi, N. (2010). Differential localization of mRNAs during early development in the mollusc, *Crepidula fornicata*. *Integr. Comp. Biol.* 50, 720–733. doi: 10.1093/icb/icq088

Hunt, H. L., and Scheibling, R. E. (1997). Role of early post-settlement mortality in recruitment of benthic marine invertebrates. *Mar. Ecol. Prog. Ser.* 155, 269–301. doi: 10.3354/meps155269

Huth, T. J., and Place, S. P. (2016). Transcriptome wide analyses reveal a sustained cellular stress response in the gill tissue of *Trematomus bernacchii* after acclimation to multiple stressors. *BMC Genomics* 17:127. doi: 10.1186/s12864-016-2454-3

IPCC (2013). "Working group I contribution to the IPCC," in *Proceedings of the 5th Assessment Report Climate Change 2013: the Physical Science Basis*, (Cambridge: Cambridge University Press).

Kaniewska, P., Campbell, P. R., Kline, D. I., Rodriguez-Lanetty, M., Miller, D. J., Dove, S., et al. (2012). Major cellular and physiological impacts of ocean acidification on a reef building coral. *PLoS One* 7:e34659. doi: 10.1371/journal.pone.0034659

Kauffmann, A., Gentleman, R., and Huber, W. (2009). Array quality metrics - a bioconductor package for quality assessment of microarray data. *Bioinformatics* 25, 415–416. doi: 10.1093/bioinformatics/btn647

Kelly, M. W., Padilla-Gamiño, J. L., and Hofmann, G. E. (2016). High pCO_2 affects body size, but not gene expression in larvae of the California mussel (*Mytilus californianus*). *ICES J. Mar. Sci.* 73, 962–969. doi: 10.1093/icesjms/fsv184

Kolde, R. (2015). *Pheatmap: Pretty Heatmaps. R Packag. Version* 1.0.8. Available at: https://cran.r-project.org/web/packages/pheatmap/pheatmap.pdf

Kroeker, K. J., Kordas, R. L., Crim, R., Hendriks, I. E., Ramajo, L., Singh, G. S., et al. (2013). Impacts of ocean acidification on marine organisms: quantifying sensitivities and interaction with warming. *Glob. Chang. Biol.* 19, 1884–1896. doi: 10.1111/gcb.12179

Kültz, D. (2005). Molecular and evolutionary basis of the cellular stress response. *Annu. Rev. Physiol.* 67, 225–257. doi: 10.1146/annurev.physiol.67.040403.103635

Kurihara, H. (2008). Effects of CO_2-driven ocean acidification on the early developmental stages of invertebrates. *Mar. Ecol. Prog. Ser.* 373, 275–284. doi: 10.3354/meps07802

Langmead, B., and Salzberg, S. L. (2012). Fast gapped-read alignment with Bowtie 2. *Nat. Methods* 9, 357–359. doi: 10.1038/nmeth.1923

Lauritano, C., Procaccini, G., and Ianora, A. (2012). Gene expression patterns and stress response in marine copepods. *Mar. Environ. Res.* 76, 22–31. doi: 10.1016/j.marenvres.2011.09.015

Lenz, M., da Gama, B. A. P., Gerner, N. V., Gobin, J., Gröner, F., Harry, A., et al. (2011). Non-native marine invertebrates are more tolerant towards environmental stress than taxonomically related native species: results from a globally replicated study. *Environ. Res.* 111, 943–952. doi: 10.1016/j.envres.2011.05.001

Lohman, B. K., Weber, J. N., and Bolnick, D. I. (2016). Evaluation of TagSeq, a reliable low-cost alternative for RNAseq. *Mol. Ecol. Resour.* 16, 1315–1321. doi: 10.1111/1755-0998.12529

Love, M. I., Huber, W., and Anders, S. (2014). Moderated estimation of fold change and dispersion for RNA-seq data with DESeq2. *Genome Biol.* 15:550. doi: 10.1186/s13059-014-0550-8

Maboloc, E. A., and Chan, K. Y. K. (2017). Resilience of the larval slipper limpet *Crepidula onyx* to direct and indirect-diet effects of ocean acidification. *Sci. Rep.* 7:12062. doi: 10.1038/s41598-017-12253-2

Matz, M., Shagin, D., Bogdanova, E., Britanova, O., Lukyanov, S., Diatchenko, L., et al. (1999). Amplification of cDNA ends based on template-switching effect and step-out PCR. *Nucleic Acids Res.* 27, 1558–1560. doi: 10.1093/nar/27.6.1558

Meyer, E., Aglyamova, G. V., and Matz, M. V. (2011). Profiling gene expression responses of coral larvae (*Acropora millepora*) to elevated temperature and settlement inducers using a novel RNA-Seq procedure. *Mol. Ecol.* 20, 3599–3616. doi: 10.1111/j.1365-294X.2011.05205.x

Nakamura, M., Ohki, S., Suzuki, A., and Sakai, K. (2011). Coral larvae under ocean acidification: survival, metabolism, and metamorphosis. *PLoS One* 6:e14521. doi: 10.1371/journal.pone.0014521

Noisette, F., Bordeyne, F., Davoult, D., and Martin, S. (2016). Assessing the physiological responses of the gastropod *Crepidula fornicata* to predicted ocean acidification and warming. *Limnol. Oceanogr.* 61, 430–444. doi: 10.1002/lno.10225

Noisette, F., Comtet, T., Legrand, E., Bordeyne, F., Davoult, D., and Martin, S. (2014). Does encapsulation protect embryos from the effects of ocean acidification? The example of *Crepidula fornicata*. *PLoS One* 9:e93021. doi: 10.1371/journal.pone.0093021

O'Donnell, M. J., Todgham, A. E., Sewell, M. A., Hammond, L. M., Ruggiero, K., Fangue, N. A., et al. (2009). Ocean acidification alters skeletogenesis and gene expression in larval sea urchins. *Mar. Ecol. Prog. Ser.* 398, 157–171. doi: 10.3354/meps08346

Oksanen, J., Blanchet, F., Kindt, R., Legendre, P., and O'Hara, R. (2016). *Vegan: Community Ecology Package. R Packag.* 2.3-3. Available at: https://cran.r-project.org/web/packages/vegan/vegan.pdf

Orr, J. C., Fabry, V. J., Aumont, O., Bopp, L., Doney, S. C., Feely, R. A., et al. (2005). Anthropogenic ocean acidification over the twenty-first century and its impact on calcifying organisms. *Nature* 437, 681–686. doi: 10.1038/nature04095

Pechenik, J. A. (1984). The relationship between temperature, growth rate, and duration of planktonic life for larvae of the gastropod *Crepidula fornicata* (L.). *J. Exp. Mar. Biol. Ecol.* 74, 241–257. doi: 10.1016/0022-0981(84)90128-X

Pechenik, J. A. (1999). On the advantages and disadvantages of larval stages in benthic marine invertebrate life cycles. *Mar. Ecol. Prog. Ser.* 177, 269–297. doi: 10.3354/meps177269

Pechenik, J. A., Cochrane, D. E., Li, W., West, E. T., Pires, A., and Leppo, M. (2007). Nitric oxide inhibits metamorphosis in larvae of *Crepidula fornicata*, the slippershell snail. *Biol. Bull.* 213, 160–171. doi: 10.2307/25066632

Pechenik, J. A., Diederich, C. M., Browman, H. I., and Jelmert, A. (2017a). Fecundity of the invasive marine gastropod *Crepidula fornicata* near the current northern extreme of its range. *Invertebr. Biol.* 136, 394–402. doi: 10.1111/ivb.12194

Pechenik, J. A., Diederich, C. M., Chaparro, O. R., Montory, J. A., Paredes, F. J., and Franklin, A. M. (2017b). Differences in resource allocation to reproduction across the intertidal-subtidal gradient for two suspension-feeding marine gastropods: *Crepidula fornicata* and *Crepipatella peruviana*. *Mar. Ecol. Prog. Ser.* 572, 165–178. doi: 10.3354/meps12152

Pechenik, J. A., and Gee, C. C. (1993). Onset of metamorphic competence in larvae of the gastropod *Crepidula fomicata* (L.), judged by a natural and an artificial cue. *J. Exp. Mar. Biol. Ecol.* 167, 59–72. doi: 10.1016/0022-0981(93)90184-P

Pechenik, J. A., Hammer, K., and Weise, C. (1996). The effect of starvation on acquisition of competence and post- metamorphic performance in the marine prosobranch gastropod *Crepidula fornicata* (L.). *J. Exp. Mar. Biol. Ecol.* 199, 137–152. doi: 10.1016/0022-0981(96)00010-X

Pechenik, J. A., and Heyman, W. D. (1987). Using KCl to determine size at competence for larvae of the marine gastropod *Crepidula fornicata* (L.). *J. Exp. Mar. Biol. Ecol.* 112, 27–38. doi: 10.1016/S0022-0981(87)80012-6

Pechenik, J. A., and Tyrell, A. S. (2015). Larval diet alters larval growth rates and post-metamorphic performance in the marine gastropod *Crepidula fornicata*. *Mar. Biol.* 162, 1597–1610. doi: 10.1007/s00227-015-2696-7

Pelejero, C., Calvo, E., and Hoegh-Guldberg, O. (2010). Paleo-perspectives on ocean acidification. *Trends Ecol. Evol.* 25, 332–344. doi: 10.1016/j.tree.2010.02.002

Petit, J. R., Jouzel, J., Raynaud, D., Barkov, N. I., Barnola, J. M., Basile, I., et al. (1999). Climate and atmospheric history of the past 420,000 years from the Vostok ice core. Antarctica. *Nature* 399, 429–436. doi: 10.1038/20859

Pierrot, D., Lewis, E., and Wallace, D. W. R. (2006). MS Excel program developed for CO2 system calculations. ORNL/CDIAC-105a. *Carbon Dioxide Inf. Anal. Center* 4735, 1–17. doi: 10.3334/CDIAC/otg.CO2SYS_XLS_CDIAC105a

Plattner, G.-K., Joos, F., Stocker, T. F., and Marchal, O. (2001). Feedback mechanisms and sensitivities of ocean carbon uptake under global warming. *Tellus B* 53, 564–592. doi: 10.1034/j.1600-0889.2001.530504.x

Portner, H. O., and Farrell, A. P. (2008). Ecology: physiology and climate change. *Science* 322, 690–692. doi: 10.1126/science.1163156

R Development Core Team (2013). *R: A Language and Environment for Statistical Computing*. Vienna: R Foundation for Statistical Computing.

Reum, J. C. P., Alin, S. R., Feely, R. A., Newton, J., Warner, M., and McElhany, P. (2014). Seasonal carbonate chemistry covariation with temperature, oxygen, and salinity in a fjord estuary: implications for the design of ocean acidification experiments. *PLoS One* 9:e89619. doi: 10.1371/journal.pone.0089619

Ries, J. B., Cohen, A. L., and McCorkle, D. C. (2009). Marine calcifiers exhibit mixed responses to CO_2-induced ocean acidification. *Geology* 37, 1131–1134. doi: 10.1130/G30210A.1

Shirayama, Y., and Thornton, H. (2005). Effect of increased atmospheric CO_2 on shallow water marine benthos. *J. Geophys. Res.* 110, 1–7. doi: 10.1029/2004JC002618

Talmage, S. C., and Gobler, C. J. (2010). Effects of past, present, and future ocean carbon dioxide concentrations on the growth and survival of larval shellfish. *Proc. Natl. Acad. Sci. U.S.A.* 107, 17246–17251. doi: 10.1073/pnas.0913804107

The UniProt Consortium (2015). UniProt: a hub for protein information. *Nucleic Acids Res.* 43, D204–D212. doi: 10.1093/nar/gku989

Thieltges, D. W., Strasser, M., Van Beusekom, J. E. E., and Reise, K. (2004). Too cold to prosper - Winter mortality prevents population increase of the introduced American slipper limpet *Crepidula fornicata* in northern Europe. *J. Exp. Mar. Biol. Ecol.* 311, 375–391. doi: 10.1016/j.jembe.2004.05.018

Thorson, G. (1950). Reproductive and larval ecology of marine bottom invertebrates. *Biol. Rev.* 25, 1–45. doi: 10.1111/j.1469-185X.1950.tb00585.x

Todgham, A. E., and Hofmann, G. E. (2009). Transcriptomic response of sea urchin larvae *Strongylocentrotus purpuratus* to CO_2-driven seawater acidification. *J. Exp. Biol.* 212, 2579–2594. doi: 10.1242/jeb.032540

Viard, F., Ellien, C., and Dupont, L. (2006). Dispersal ability and invasion success of *Crepidula fornicata* in a single gulf: insights from genetic markers and larval-dispersal model. *Helgol. Mar. Res.* 60, 144–152. doi: 10.1007/s10152-006-0033-8

Voolstra, C. R., Sunagawa, S., Matz, M. V., Bayer, T., Aranda, M., Buschiazzo, E., et al. (2011). Rapid evolution of coral proteins responsible for interaction with the environment. *PLoS One* 6:e20392. doi: 10.1371/journal.pone.0020392

Waldbusser, G. G., and Salisbury, J. E. (2014). Ocean acidification in the coastal zone from an organism's perspective: multiple system parameters, frequency domains, and habitats. *Ann. Rev. Mar. Sci.* 6, 221–247. doi: 10.1146/annurev-marine-121211-172238

Yang, B., Pu, F., Li, L., You, W., Ke, C., and Feng, D. (2017). Functional analysis of a tyrosinase gene involved in early larval shell biogenesis in *Crassostrea angulata* and its response to ocean acidification. *Comp. Biochem. Physiol. Part B Biochem. Mol. Biol.* 206, 8–15. doi: 10.1016/j.cbpb.2017.01.006

Zhao, X., Shi, W., Han, Y., Liu, S., Guo, C., Fu, W., et al. (2017). Ocean acidification adversely influences metabolism, extracellular pH and calcification of an economically important marine bivalve, *Tegillarca granosa*. *Mar. Environ. Res.* 125, 82–89. doi: 10.1016/j.marenvres.2017.01.007

Zippay, M. L., Hofmann, G. E., and Hofman, G. E. (2010). Effect of pH on gene expression and thermal tolerance of early life history stages of red abalone (*Haliotis rufescens*). *J. Shellfish Res.* 29, 429–439. doi: 10.2983/035.029.0220

Conflict of Interest Statement: The authors declare that the research was conducted in the absence of any commercial or financial relationships that could be construed as a potential conflict of interest.

frontiers in Physiology

ORIGINAL RESEARCH
published: 21 January 2019
doi: 10.3389/fphys.2018.01967

Impact of Ocean Acidification on the Energy Metabolism and Antioxidant Responses of the Yesso Scallop (*Patinopecten yessoensis*)

Huan Liao[1,2], Zujing Yang[1], Zheng Dou[1], Fanhua Sun[1], Sihua Kou[1], Zhengrui Zhang[1], Xiaoting Huang[1] and Zhenmin Bao[1,3]*

[1] MOE Key Laboratory of Marine Genetics and Breeding, College of Marine Life Sciences, Ocean University of China, Qingdao, China, [2] College of Animal Biotechnology, Jiangxi Agricultural University, Nanchang, China, [3] Laboratory for Marine Fisheries Science and Food Production Processes, Qingdao National Laboratory for Marine Science and Technology, Qingdao, China

Ocean acidification (OA), which is caused by increasing levels of dissolved CO_2 in the ocean, is a major threat to marine ecosystems. Multiple lines of scientific evidence show that marine bivalves, including scallops, are vulnerable to OA due to their poor capacities to regulate extracellular ions and acid-based status. However, the physiological mechanisms of scallops responding to OA are not well understood. In this study, we evaluated the effects of 45 days of exposure to OA (pH 7.5) on the energy metabolism and antioxidant capability of Yesso scallops. Some biochemical markers related to energy metabolism (e.g., content of glycogen and ATP, activity of ATPase, lactate dehydrogenase, glutamate oxaloacetate transaminase, and glutamate-pyruvate transaminase), antioxidant capacity (e.g., reactive oxygen species level, activity of superoxide dismutase, and catalase) and cellular damage (e.g., lipid peroxidation level) were measured. Our results demonstrate that the effects of the reduced pH (7.5) on scallops are varied in different tissues. The energy reserves are mainly accumulated in the adductor muscle and hepatopancreas. Yesso scallops exhibit energy modulation by increasing lactate dehydrogenase activities to stimulate anaerobic metabolism. The highly active Na^+/K^+-ATPase and massive ATP consumption in the mantle and gill indicate that a large amount of energy was allocated for the ion regulation process to maintain the acid-base balance in the reduced-pH environment. Moreover, the increase in the reactive oxygen species level and the superoxide dismutase and catalase activities in the gill and adductor muscle, indicate that oxidative stress was induced after long-term exposure to the reduced-pH environment. Our findings indicate that the effects of OA are tissue-specific, and physiological homeostasis could be modulated through different mechanisms for Yesso scallops.

Keywords: ocean acidification, energy metabolism, oxidative stress, physiological response, scallop

OPEN ACCESS

Edited by:
Xiaotong Wang,
Ludong University, China

Reviewed by:
Nia M. Whiteley,
Bangor University, United Kingdom
Huaiping Zheng,
Shantou University, China

****Correspondence:***
Xiaoting Huang
xthuang@ouc.edu.cn

Specialty section:
This article was submitted to Aquatic Physiology, a section of the journal Frontiers in Physiology

Received: *02 September 2018*
Accepted: *31 December 2018*
Published: *21 January 2019*

Citation:
Liao H, Yang Z, Dou Z, Sun F, Kou S, Zhang Z, Huang X and Bao Z (2019) Impact of Ocean Acidification on the Energy Metabolism and Antioxidant Responses of the Yesso Scallop (Patinopecten yessoensis). Front. Physiol. 9:1967. doi: 10.3389/fphys.2018.01967

INTRODUCTION

Increasing amounts of anthropogenic CO_2 from the atmosphere dissolved in seawater has changed the overall seawater chemistry with a net increase in hydrogen (H^+) and bicarbonate ions (HCO_3^-) and a decrease in carbonate ions (CO_3^{2-}), which has already resulted in a 0.1 unit decline in seawater pH since the Industrial Revolution (Caldeira and Wickett, 2003, 2005; Sabine et al., 2004;

Feely, 2011; Perez et al., 2018). These changes are known as ocean acidification (OA). According to the prediction of the Intergovernmental Panel on Climate Change (IPCC), the pH of surface seawater could further decrease to 7.8 and 7.4 by the years 2100 and 2300, respectively (Caldeira and Wickett, 2003; Stocker, 2013). Many studies have confirmed that the predicted changes of seawater pH will have widespread negative effects on the structure, function and fitness of marine ecosystems (Feely, 2011; Uthicke et al., 2013). The variety of responses within and between taxa suggest that OA is a driver for substantial change in ocean ecosystems this century, potentially leading to long-term shifts in species composition (Pörtner and Farrell, 2008; Wittmann and Pörtner, 2013). As a result, understanding the potentials of maintaining physiological homeostasis will help predict biological stability and changes to rapid anthropogenic modifications of ecosystems and geosystems (Somero, 2010; Applebaum et al., 2014).

Marine bivalves, such as oyster, mussel, clam and scallop, are widely distributed, and they are economically and ecologically important (Gazeau et al., 2013; Kroeker et al., 2013). Scientific literature has revealed that most mollusk species are vulnerable to OA (Pörtner and Farrell, 2008; Wittmann and Pörtner, 2013). To regulate physiological homeostasis, energy is required in response to the environmental changes. Metabolic energy demands under acidification stress may exceed the energy supply from food or/and accrued energy resources, which might lead to a lack of adenosine triphosphate (ATP) to sustain routine metabolism (Lannig et al., 2010). However, some mollusks, such as bivalve fingernail clam *Sphaerium occidentale* and the cephalopod *Nautilus pompilius*, can overwhelm the capacity of systemic functions or inhibit the metabolic rate to conserve energy and to extend the survival time (Guppy, 1999). Recent studies have shown that modest increases in dissolved CO_2 (<1200 μatm) have little effect on metabolic rates, whereas extremely high levels of dissolved CO_2 (>5000 μatm) could depress metabolic rates (Michaelidis et al., 2005; Beniash et al., 2010; Hendriks et al., 2010; Thomsen and Melzner, 2010; Zhao et al., 2017b). As shown by Cao et al. (2018), Pacific oyster (*Crassostrea gigas*) modulates energy sources by inhibiting aerobic energy metabolism, stimulating anaerobic metabolism, and increasing glycolytic enzyme activity following exposure to a reduced pH value of 7.6 for 28 days. The clams *(Ruditapes philippinarum*) were reported to be able to maintain/regulate their physiological status and biochemical performance under reduced pH (7.3) for 28 days (Velez et al., 2016). However, in blue mussel *Mytilus edulis*, energy and protein metabolism were strongly affected by elevated pCO_2 (1,120, 2,400, or 4,000 μatm after 2 months of treatment) (Hüning et al., 2013). In addition, some recent transcriptomic analyses have indicated that marine bivalves implement a compensatory acid-base mechanism, metabolic depression and positive physiological responses to mitigate the effects of OA (Goncalves et al., 2016, 2017a,b; Li et al., 2016a,b; Peng et al., 2017).

Oxidative stress, the production and accumulation of reactive oxygen species (ROS), is an important component of the stress response for marine organism when exposed to environmental change (Lesser, 2006). In response to oxidative stress, a wide set of antioxidant systems including superoxide dismutase (SOD) and catalase (CAT) have evolved in marine organisms (Lesser, 2006). The oxidative stress response is prevalent in marine bivalves when exposed to elevated CO_2 levels. As shown in the mussel *M. galloprovincialis*, the oxidative status was negatively affected by reduced pH with an increase in antioxidant enzymes activity and ROS overproduction (Freitas et al., 2017). In the mussel *M. coruscus*, most biochemical indexes [SOD, CAT, glutathione peroxidase (GPx), acid phosphatase (ACP), and alkaline phosphatase (ALP)] measured in gills and hemocytes were increased when the mussels were subjected to reduced pH (Huang et al., 2018). Nevertheless, no persistent oxidative stress signal was observed during long-term (8–15 weeks) exposure to moderately elevated CO_2 (∼800 ppm CO_2) in hard shell clam *Mercenaria mercenaria* and eastern oyster *C. virginica* (Matoo et al., 2013). In addition, some studies have demonstrated that the key target genes associated with antioxidant defenses (ecSOD, catalase, and peroxiredoxin 6) were susceptible to OA in marine bivalves (Goncalves et al., 2016, 2017a,b; Li et al., 2016a,b; Wang et al., 2016).

All of these studies indicated that the metabolic effects and antioxidant responses varied among different marine species under elevated dissolved CO_2 seawater (Dupont et al., 2010; Hendriks et al., 2010; Kroeker et al., 2010). However, there was very limited information about the effects of OA on scallops (Benedetti et al., 2016; Haider et al., 2016; Nardi et al., 2018). The Yesso scallop (*Patinopecten yessoensis*) is an economically important shellfish in China, and the production is approximately 240,000 tons in 2016 (data from 2017 China Fishery Statistical Yearbook). The present study aimed to systematically assess the metabolic effects and antioxidant responses of Yesso scallops under present and future predicted sea surface pH. After 45 days of exposure to two pH levels (8.0 and 7.5), we measured some biochemical markers to determine the energy metabolism levels [assessed by the activity of ATPase, lactate dehydrogenase (LDH), glutamate oxaloacetate transaminase (GOT) and glutamate-pyruvate transaminase (GPT), content of glycogen (GLY) and ATP]; antioxidant capacity (ROS, CAT, and SOD); and cellular damage [measured by the lipid peroxidation (LPO) level] of four tissues (adductor muscle, mantle, gill, and hepatopancreas). The findings of the current study can improve our understanding of the physiological mechanisms involved in regulating energy metabolism and antioxidant responses in marine bivalves when exposed to elevated CO_2 levels.

MATERIALS AND METHODS

Experimental Animals Collection and Acclimation

Samples of 2-year-old Yesso scallops were collected from Haiyi Seeds Co., LTD, in Shandong province, China, in September 2017. The scallops without shell damage were transported on ice to the laboratory and acclimated for 1 week in a recirculated aquarium system equipped with a filtering system (pH 8.0, temperature 18°C, and salinity 30.2‰). During the acclimation period, all

scallops were fed twice daily with *Nitzschia closterium* (40,000 cells /animal), and the seawater was changed daily.

Ocean Acidification Stimulation and Seawater Chemistry Analysis

After 1 week of acclimation, the healthy scallops were randomly divided into two groups and placed in two different environments: the control group at a pH of 8.0 (current concentration of pCO_2) and the experimental group at a pH of 7.5 (representing the predicted water surface pH level of the twenty-first century) (Caldeira and Wickett, 2003; Stocker, 2013). For each treatment, there were three replicates of ∼50-L tanks, holding ten scallops each. The reduced pH value (pH 7.5) was maintained by vigorously bubbling ambient air or a CO_2 gas mixture. The CO_2 gas mixture was obtained by mixing CO_2-free air and pure CO_2 gas at known flow rates using flow controllers (Zhao et al., 2017a). The pH of seawater was monitored using a pH meter (Sartorius PB-10) to ensure no substantial change in pH during the experiment. The other seawater parameters including salinity, temperature and dissolved oxygen (DO) were measured daily by a multi-parameter water quality meter (HORIBA U-52, Japan). The total alkalinity (TA) was monitored once a week by potentiometric titration (Anderson and Robinson, 1946). The carbonate system parameters were calculated using CO2SYS software (Pierrot et al., 2006), and the seawater parameters for the experimental exposures are given in **Table 1**.

Biochemical Assays

After 45 days of experiments, six scallops per treatment were collected at random. Four tissues, including the adductor muscle, mantle, gill and hepatopancreas were collected from each specimen and stored at −80°C until further analyses. For GLY content determination, the tissues were added to an alkaline solution (1:3, w:v) in boiling water for 20 min, aiming to destroy all components except GLY. For the remaining biochemical markers, the tissues were added to an ice-cold physiological saline solution (1:9, w:v) and homogenized by ultrasonic treatment (0°C, 360 Watt). The homogenization was then centrifuged for 10 min at 2500 rpm and 4°C. The supernatants were stored at −80°C or immediately used to determine the content of ROS and ATP, the LPO levels, and the activities of SOD, CAT, GOT, GPT, LDH, and ATPase.

All of the enzymatic activities and biochemical assays were analyzed following the instructions of kits from the Nanjing Jiancheng Bioengineering Institute. Optical density values were measured using a microplate reader (Infinite 200 pro, Tecan). The results of the enzymatic activities were expressed as the unit per gram or unit per milligram of protein (U/g or U/mg protein).

Reactive oxygen species production was quantified using 2,7-dichlorofluorescin diacetate (DCFH-DA) treatment (Eruslanov and Kusmartsev, 2010). DCFH-DA is a non-polar dye, and it is converted into the polar derivative DCFH by cellular esterases that are non-fluorescent but would be oxidized by ROS to form highly fluorescent DCF (Burow and Valet, 1987). The fluorescence intensity was positively correlated with the ROS content, which was measured at the excitation and emission wavelengths of 500 and 530 nm, respectively. The results were referred to the standard curve drawn by positive control of the reactive oxygen donor with gradient concentrations.

The LPO levels were determined by measuring malondialdehyde (MDA). The quantitative measurement of MDA was based on the reaction of MDA and thiobarbituric acid (TBA). The reaction product MDA-TBA2 was measured at 532 nm (Janero, 1990).

The SOD activity was measured by the WBT-1 method (Peskin and Winterbourn, 2000). The tetrazolium salt WST-1 was converted into water-soluble WST-1 formazan by a superoxide radical generated by the conversion of xanthine to uric acid and hydrogen peroxide (H_2O_2) by xanthine oxidase. Meanwhile, the existence of SOD reduced the concentrations of the superoxide anion radical and thereby lowered the formation rate of WST-1. The absorbance of the final product was measured at 450 nm after 20 min of incubation at 37°C. The results are expressed in unit per milligram of protein (U/mg protein). One unit of SOD activity corresponded to the enzyme quantity when the SOD inhibition rate reached 50% under the assay conditions.

The CAT activity was determined on the basis of the ammonium molybdate method (Góth, 1991). CAT acted on catalyzing the H_2O_2 degradation reaction, which was terminated by adding ammonium molybdate. Moreover, ammonium molybdate and H_2O_2 reacted rapidly in forming a yellow complex, which was measured at 405 nm. One unit of CAT activity was defined as the degradation of 1 μmol H_2O_2 per second per milligram of tissue protein.

The GLY content was quantified according to the anthrone colorimetric method (Carroll et al., 1956). After treatment in concentrated sulfuric acid, GLY dehydrated and produced glycolaldehyde. Subsequently, the production was reacted with anthrone and formed blue compounds, which contained a maximum absorption peak at a wavelength of 620 nm.

TABLE 1 | Water chemistry parameters during 45 days of incubation of *P. yessoensis*.

Treatment	Measured parameters				Calculated parameters		
	pH_{NBS}	T (°C)	Sal (‰)	TA(μmol/kg)	*p*CO2(μatm)	Ωc	Ωa
Control	8.01 ± 0.02	18.35 ± 0.21	30.27 ± 0.25	2282.67 ± 149.70	546.66 ± 71.81	3.5 ± 0.33	2.17 ± 0.21
CO_2-incubation	7.51 ± 0.01	18.66 ± 0.30	30.47 ± 0.17	2260.1 ± 66.10	2217.91 ± 87.75	1.16 ± 0.06	0.72 ± 0.03

pH_{NBS}, pH calibrated with National Bureau of Standard scale; T, temperature; Sal, salinity; TA, total alkalinity; pCO_2, partial pressure of CO_2; Ωc and Ωa, saturation state of calcite and aragonite, respectively. Data are presented as the means ± standard deviations.

The LDH activity was measured by the trace enzyme labeling method (Weeks and Johnson, 1977), which is based on the function of LDH in catalyzing the formation of pyruvate. The pyruvate was reacted with 2, 4-dinitrophenylhydrazine in a terminal indicator reaction to form the characteristic brown color of the corresponding 2, 4-dinitrophenylhydrazone pyruvate, which was measured colorimetrically at 440 nm. One unit of LDH activity was defined as the formation of 1 μmol pyruvate per 15 min per gram protein.

The ATP content was determined according to the phosphomolybdic acid colorimetry method (Chen and Sun, 2002). It is an indirect method for determining the ATP level. In brief, creatine kinase was added to catalyze the formation of phosphocreatine from ATP and creatine, and then the product was detected at 636 nm.

The ATPase activity was quantified following the protocol of the ATP enzyme test kit (Na^+/K^+-ATPase and Ca^{2+}/Mg^{2+}-ATPase) from Nanjing Jiancheng Bioengineering Institute, which was based on ATPase function in decomposing ATP to produce ADP and inorganic phosphorus. The activity of ATPase was judged by the amount of inorganic phosphorus, which was interacted with a phosphorus-fixing agent for 30 min at 37°C. The absorbance was measured at 660 nm when the product cooled to room temperature, and one unit of ATPase was defined as the product of 1 μmol inorganic phosphorus per hour per milligram of protein.

The GPT and GOT activities were quantified following the method of Reitman and Frankel (1957). The activity of GPT or GOT was measured by mixing tissue suspension with the corresponding substrate. Both enzymes were acted on catalyzing the transamination of substrate and the formation of pyruvate. After a 30-min interaction at 37°C, 2, 4-dinitrophenylhydrazine solution was added to stop the transamination and reacted with pyruvate for 20 min at 37°C. Subsequently, the reaction liquid was mixed with NaOH solution for 15 min at room temperature. The optical density was read at 505 nm. The results were referred to the standard curve drawn by the pyruvate standard solution with gradient concentrations and expressed in unit per gram of protein.

Statistical Analysis

The statistical analyses of the data were preformed using SPSS software (version 20.0). The data collected from this study are expressed as the means ± standard deviation ($N = 6$). A one-way analysis of variance (ANOVA) and Tukey's test were used to differentiate between the means. Tests were considered significant at $p < 0.05$.

RESULTS

The levels of ROS, LPO, SOD and CAT in the adductor muscles, mantles, gills and hepatopancreas of scallops exposed to reduced-pH seawater and ordinary seawater (control) are illustrated in **Figure 1**. The levels of ROS in all tested organs were generally higher in the scallops exposed to reduced-pH seawater compared with the control group. The results of the statistical analyses demonstrate that the ROS levels in the gills and hepatopancreas were significantly higher ($p < 0.05$) in the scallops exposed to reduced-pH seawater than in the control group. For the LPO levels, no significant difference ($p > 0.05$) was observed in all organs between the scallops exposed to reduced-pH seawater and the control group. The SOD activities in the adductor muscles and hepatopancreas were significantly higher ($p < 0.05$) in the scallops exposed to reduced-pH seawater than in the control group. However, the SOD activities in the gills was significantly lower ($p < 0.05$) in the scallops exposed to reduced-pH seawater (6.19 ± 0.46 U $mgprot^{-1}$) than in the control group (130.06 ± 33.73 U $mgprot^{-1}$). For the CAT activities, the scallops exposed to reduced-pH seawater demonstrated significantly higher ($p < 0.05$) CAT activity in the adductor muscles (99.96 ± 36.95 U $mgprot^{-1}$) compared with the scallops in the control group (14.58 ± 2.80 U $mgprot^{-1}$).

The effects of reduced pH on different types of ATPase were varied in the four tissues (**Figures 2A,B**). The activities of Na^+/K^+-ATPase in the mantles and gills of the scallops exposed to reduced-pH seawater were significantly higher ($p < 0.05$) than in the respective organs of the scallops in the control group. The Ca^{2+}/Mg^{2+}-ATPase activity in the gills of the scallops exposed to reduced-pH seawater (5.13 ± 0.39 μmolPi $mgprot^{-1}$ h^{-1}) were significantly lower ($p < 0.05$) than in the gills of the scallops in the control group (7.98 ± 0.42 μmolPi $mgprot^{-1}$ h^{-1}). For ATP contents, the scallops exposed to reduced-pH seawater demonstrated significantly lower ($p < 0.05$) ATP contents in the mantles (168.13 ± 52.79 μmol $gprot^{-1}$) compared with the scallops in the control group (483.86 ± 91.41 μmol $gprot^{-1}$) (**Figure 2C**).

The results of the statistical analyses demonstrated that the GLY content in the adductor muscles was significantly lower ($p < 0.05$) in the scallops exposed to reduced-pH seawater (2.06 ± 0.52 mg g^{-1}) compared with the control group (4.32 ± 0.53 mg g^{-1}). However, the GLY content in the hepatopancreas was significantly higher ($p < 0.05$) in the scallops exposed to reduced-pH seawater (5.70 ± 0.38 mg g^{-1}) compared with the control group (4.58 ± 0.09 mg g^{-1}) (**Figure 3A**). The LDH activities in the adductor muscles of the scallops exposed to reduced-pH seawater (1565.31 ± 0.01 U $gprot^{-1}$) were significantly higher ($p < 0.05$) than in the adductor muscles of the scallops in the control group (861.53 ± 134.71 U $gprot^{-1}$) (**Figure 3B**).

For the GOT and GPT activities, no significant difference ($p > 0.05$) was observed in the adductor muscles, mantles and gills between the scallops exposed to reduced-pH seawater and the control group. However, the GPT activity in the hepatopancreas was significantly lower ($p < 0.05$) in the scallops exposed to reduced-pH seawater (5227.44 ± 817.48 U $gprot^{-1}$) compared with the control group (8294.14 ± 628.25 U $gprot^{-1}$) (**Figure 4**).

DISCUSSION

Ocean acidification caused by increased CO_2 emission to the atmosphere has been showed in all areas of the ocean including

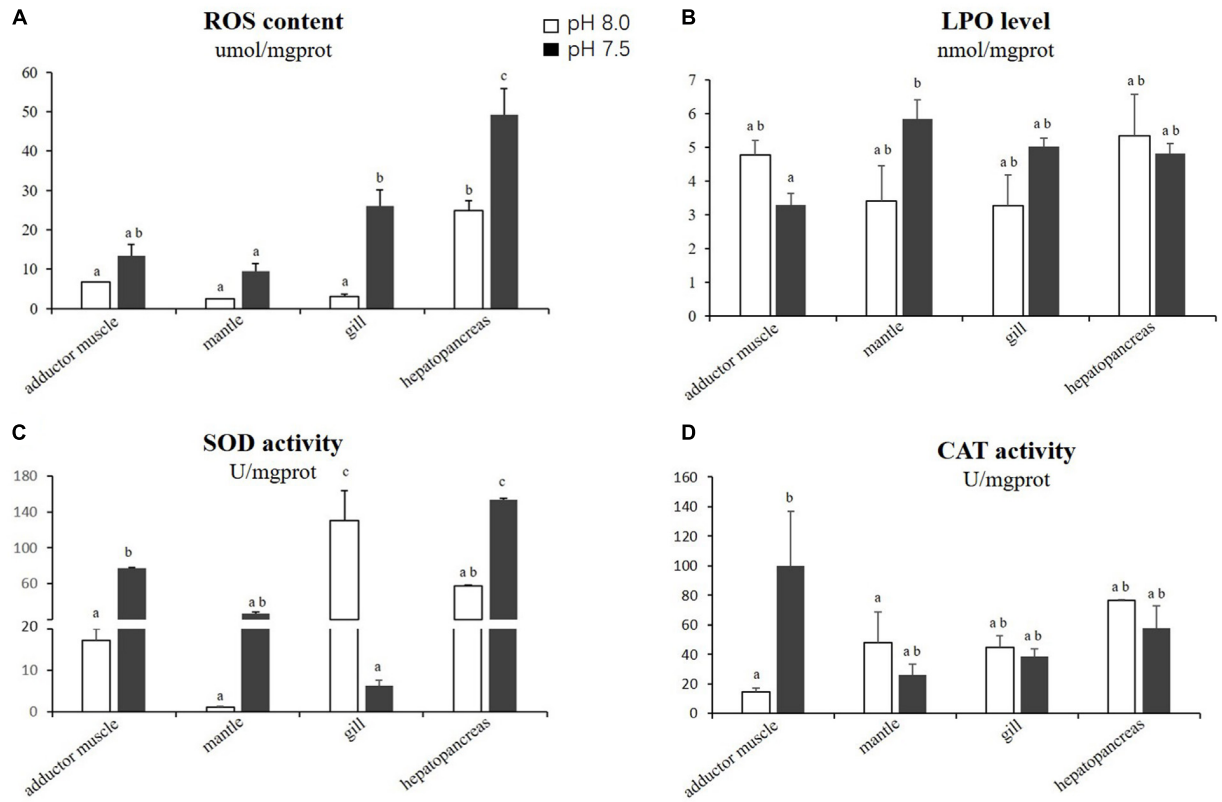

FIGURE 1 | Oxidative stress-related parameters in four tissues of *P. yessoensis* exposed to different pH levels (7.5 and 8.0). **(A)** ROS. **(B)** LPO. **(C)** SOD. **(D)** CAT. Each bar represents the means ± standard deviations ($n = 6$). Different letters indicate significant differences among different treatments ($p < 0.05$).

deep sea and coastal waters (Orr et al., 2005; Wittmann and Pörtner, 2013). The impacts of OA are more substantial in coastal waters, where the ecosystem responses to OA could have the most severe implications for mankind (Doney et al., 2007; Feely et al., 2008, 2009, 2010; Wootton et al., 2008; Zhai et al., 2012). Coastal organisms show diverse responses to elevated seawater pCO_2 (Pörtner and Farrell, 2008; Ries et al., 2009; Hendriks et al., 2010; Wittmann and Pörtner, 2013). The Yesso scallop is an economically important marine shellfish. This species has long been cultivated in the coastal ocean of China, Japan, and Russia (Shumway and Parsons, 2006). However, the potential effects of OA on the physiology of Yesso scallop is still unknown. Thus, the current study aims to evaluate the effects of OA on the scallop based on physiological and biochemical markers.

As a major form of energy storage in cells, GLY supplies energy quickly through glycolysis and oxidative phosphorylation. Adequate glycogen storage in muscle is important to support the optimal movement of muscle (Jensen and Richter, 2012). In the current study, low pH stress resulted in a decrease in glycogen level but an increase in LDH activity in the adductor muscles of scallops. A similar observation has been reported in *C. gigas*, where the GLY level in muscle tissue decreased after exposure to low pH seawater (Lannig et al., 2010). On the other hand, under stressful environments, LDH is an important enzyme that accelerates ATP production through anaerobic processes to maintain energy homeostasis (Strahl et al., 2011). The combined effects of elevated LDH activity and decreased GLY level in muscle tissues suggest that OA accelerates glycolysis, which might be an energy strategy of the Yesso scallop to fuel the high energy demand. The hepatopancreas is another important energy storage organ, and it plays an important role in energy homeostasis of the blood circulation system (Barber and Blake, 1985). The rising in GLY content in the hepatopancreas of the Yesso scallop during reduced-pH exposure suggests that some of the lactic acids from the muscle tissues entered the hepatopancreas through the blood circulation system, where they were then resynthesized to GLY for energetic conservation.

The transaminase GPT plays a key role in mobilizing L-amino acids for gluconeogenesis, and it acts as a link between carbohydrate and protein metabolism under altered physiological, pathological, and induced environmental stress conditions (Ramaswamy et al., 2015). However, the influences of acidification on GPT activity varies by species. A study on the thick shell mussel *M. coruscus* found that the activity of GPT in the gill and digestive gland increased when exposed to reduced-pH seawater (Hu et al., 2015). The current study recorded a contradictory result, where the GPT activity decreased in *P. yessoensis* under the reduced-pH treatment. The hepatopancreas is a major organ for gluconeogenesis. The

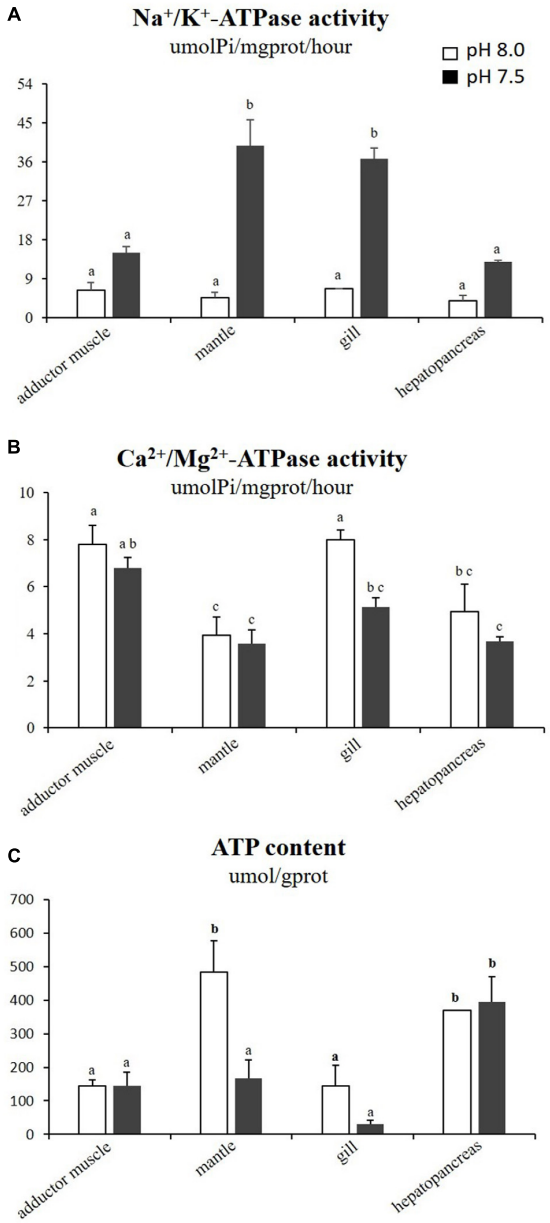

FIGURE 2 | Activities of Na^+/K^+-ATPase **(A)**, Ca^{2+}/Mg^{2+}-ATPase **(B)**, and ATP content **(C)** in four tissues of *P. yessoensis* exposed to different pH levels (7.5 and 8.0). Each bar represents the means ± standard deviations ($n = 6$). Different letters indicate significant differences among different treatments ($p < 0.05$).

decrease in GPT activity suggests a reduced turnover of amino acids and protein synthesis in the hepatopancreas of *P. yessoensis*.

In the mantle of *P. yessoensis* after OA exposure, a significant decrease in the ATP level was observed. Nevertheless, the GLY content and LDH activity varied slightly, indicating that glycolysis was not affected. Interestingly, the Na^+/K^+-ATPase activity, increased significantly and sharply in the reduced-pH exposure. The enzyme Na^+/K^+-ATPase is the main motor of cellular and extracellular acid-base balance and thus acts as an important ion regulatory player, and it may be related to the capability of each species to acclimate to pH fluctuations (Melzner et al., 2009; Velez et al., 2016). The highly active Na^+/K^+-ATPase and massive consumption of ATP in the mantle of *P. yessoensis* suggest that a large amount of energy in the mantle was allocated to the ion regulation process to maintain the acid-base balance in the reduced-pH environment. In the mantle of the oyster *C. gigas* following OA-exposure (pH ∼ 7.7) for 1 month, both the ATP content and alanine levels decreased, but the Na^+/K^+-ATPase activities were not affected. The authors suggested that alanine is transaminated to pyruvate, which together with ATP is used to build up phosphoenolpyruvate (PEP), with PEP as the substrate entering the gluconeogenetic pathway (Lannig et al., 2010). Other than the mantle, the Na^+/K^+-ATPase activities in the gill of *P. yessoensis* were also elevated after OA exposure. On the other hand, the reduced-pH treatment decreased the Ca^{2+}/Mg^{2+}-ATPase activity without affecting the ATP content in the gills of Yesso scallops. Therefore, it is reasonable to believe that the Yesso scallop could shift the use of its ion regulation mechanism by reducing the Ca^{2+}/Mg^{2+}-ATPase activity and increasing the Na^+/K^+-ATPase activity simultaneously to regulate the acid-base balance under low pH exposure. A similar result has been documented in Atlantic cod (*Gadus morhua*), where a shift in the use of ion regulation mechanisms occurred toward enhanced Na^+/H^+-exchange and $HCO^3{}^-$ transport at high PCO_2 (2200 μatm), paralleled by higher Na^+/K^+-ATPase activities, which did not affect the total gill energy consumption and left the whole animal energy budget unaffected (Kreiss et al., 2015).

Reactive oxygen species production is an important internal defense mechanism in bivalves such as *Mytilus edulis*, *Cerastoderma edule,* and *Ensis siliqua* (Wootton et al., 2003; Terahara and Takahashi, 2008). When the ROS content exceeds the antioxidant capacity, the excess ROS may lead to cell oxidative damages, such as DNA damage, membrane lipid damage and enzyme inactivation (Cheng et al., 2004a,b). Increasing ROS content and active peroxidase activities after low pH exposure have been reported in *M. coruscus*, *C. ariakensis,* and *C. gigas* (Bouilly et al., 2006; Gagnaire et al., 2006; Donaghy et al., 2009; Wang et al., 2016; Wu et al., 2016). In the current study, exposure to reduced-pH seawater led to high ROS production in the gill and hepatopancreas of *P. yessoensis*. The gill plays a vital role in respiration, and the hepatopancreas is a major organ for metabolism. These two organs have been shown to be sensitive to environmental stress in bivalves (Farcy et al., 2009; Lockwood et al., 2010). The high ROS content indicates that the oxidative stress occurred in the gill and hepatopancreas of Yesso scallops.

The levels of LPO, SOD, and CAT enzyme activities have been used as biomarkers to assess oxidative stress (Livingstone, 2001; Soldatov et al., 2007; Velez et al., 2016). In our study, the lipid peroxidation level did not change significantly in the reduced-pH group, suggesting that the reduced-pH treatment has little effect on the lipid peroxidation. A similar result was reported in the clam, *R. philippinarum* (Velez et al., 2016). However, the SOD activities were elevated in the adductor muscles and hepatopancreas but decreased in the gill of *P. yessoensis*

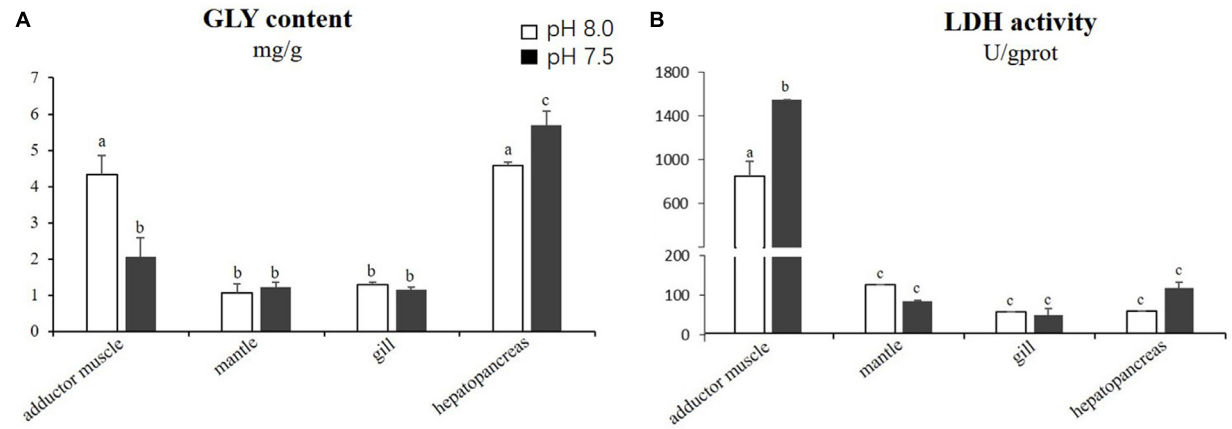

FIGURE 3 | Energy related parameters: GLY content **(A)** and LDH activity **(B)** in four tissues of *P. yessoensis* exposed to different pH levels (7.5 and 8.0). Each bar represents the means ± standard deviations (n = 6). Different letters indicate significant differences among different treatments ($p < 0.05$).

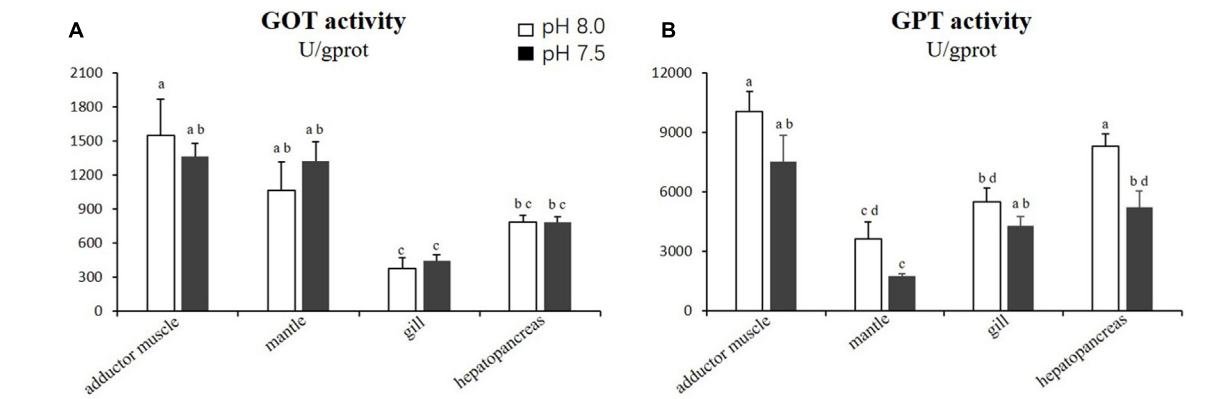

FIGURE 4 | Activities of GOT **(A)** and GPT **(B)** in four tissues of *P. yessoensis* exposed to different pH levels (7.5 and 8.0). Each bar represents the means ± standard deviations (n = 6). Different letters indicate significant differences among different treatments ($p < 0.05$).

after exposure to a reduced-pH seawater. The induction of SOD, a primary scavenger of O_2^- generated during stress condition, could inhibit the accumulation of oxygen radicals during exposure to low pH seawater. The weakening SOD activity in the gill tissue could indicate oxidative stress. Furthermore, the increased SOD activity resulted in a high level of H_2O_2, which should stimulate CAT activity. In our study, the activity of CAT increased in the adductor muscles, which could have been stimulated by the increased SOD activity.

CONCLUSION

The findings of the present study demonstrate that a reduction in seawater pH to 7.5 can potentially interfere with the energetic metabolism and antioxidant responses of scallops. Alteration of the energy demand or reserve has been observed in Yesso scallops after exposure to a reduced-pH environment. The muscle glycogen was decomposed and the activity of LDH increased, leading to suppressed aerobic metabolism and increased anaerobic metabolism. At the same time, the content of glycogen increased in the hepatopancreas, indicating that scallops were able to reserve some energy when exposed to a reduced-pH environment. In addition, the high Na^+/K^+-ATPase activities in the mantle and gill suggest that energy was allocated to ion transport in maintaining the intracellular and extracellular acid-base balance. Moreover, increased oxidative stress was also induced after long-term exposure to reduced-pH seawater. Overall, our findings are useful for a better understanding of the biochemical strategies and biological limitations of scallop if the ocean acidification worsens as predicted.

AUTHOR CONTRIBUTIONS

HL, XH, and ZB conceived and designed the experiments, analyzed the data, and drafted the manuscript. HL, ZY, ZD, FS, SK, and ZZ performed the experiments.

FUNDING

This research was funded by the National Natural Science Foundation of China (41676132 and U1706203), the Fundamental Research Funds for the Central Universities (201562018 and 201762016), the Earmarked Fund for Modern Agro-industry Technology Research System (CARS-49), the Seed Improvement Project of Shandong Province (2017LZGC009), and the Key Research and Development Program of Shandong Province (2016ZDJQ0208).

REFERENCES

Anderson, D. H., and Robinson, R. J. (1946). Rapid electrometric determination of alkalinity of sea water using glass electrode. *Ind. Eng. Chem.* 18, 767–769. doi: 10.1021/i560160a011

Applebaum, S. L., Pan, T. C. F., Hedgecock, D., and Manahan, D. T. (2014). Separating the nature and nurture of the allocation of energy in response to global change. *Integr. Comp. Biol.* 54, 284–295. doi: 10.1093/icb/icu062

Barber, B. J., and Blake, N. J. (1985). Intra-Organ Biochemical transformations associated with oogenesis in the bay scallop, *Argopecten irradians* concentricus (Say), as Indicated by 14 C incorporation. *Biol. Bull.* 168, 39–49. doi: 10.2307/1541172

Benedetti, M., Lanzoni, I., Nardi, A., d'Errico, G., Carlo, M. D., Fattorini, D., et al. (2016). Oxidative responsiveness to multiple stressors in the key antarctic species, *Adamussium colbecki*: interactions between temperature, acidification and cadmium exposure. *Mar. Environ. Res.* 121, 20–30. doi: 10.1016/j.marenvres.2016.03.011

Beniash, E., Ivanina, A., Lieb, N. S., Kurochkin, I., and Sokolova, I. M. (2010). Elevated level of carbon dioxide affects metabolism and shell formation in oysters *Crassostrea virginica*. *Mar. Ecol. Prog.* 419, 95–108. doi: 10.3354/meps08841

Bouilly, K., Gagnaire, B., Bonnard, M., Thomasguyon, H., Renault, T., Miramand, P., et al. (2006). Effects of cadmium on aneuploidy and hemocyte parameters in the Pacific oyster, *Crassostrea gigas*. *Aqua. Toxicol.* 78, 149–156. doi: 10.1016/j.aquatox.2006.02.028

Burow, S., and Valet, G. (1987). Flow-cytometric characterization of stimulation, free radical formation, peroxidase activity and phagocytosis of human granulocytes with 2,7-dichlorofluorescein (DCF). *Eur. J. Cell Biol.* 43, 128–133.

Caldeira, K., and Wickett, M. E. (2003). Oceanography: anthropogenic carbon and ocean pH. *Nature* 425:365. doi: 10.1038/425365a

Caldeira, K., and Wickett, M. E. (2005). Ocean model predictions of chemistry changes from carbon dioxide emissions to the atmosphere and ocean. *J. Geophys. Res.* 110:C09S04. doi: 10.1029/2004JC002671

Cao, R., Liu, Y., Wang, Q., Yang, D., Liu, H., Ran, W., et al. (2018). Seawater acidification reduced the resistance of *Crassostrea gigas* to *Vibrio splendidus* challenge: an energy metabolism perspective. *Front. Physiol.* 9:880. doi: 10.3389/fphys.2018.00880

Carroll, N. V., Longley, R. W., and Roe, J. H. (1956). The determination of glycogen in liver and muscle by use of anthrone reagent. *J. Biol. Chem.* 220, 583–593.

Chen, Z., and Sun, C. (2002). Contect of ATP in RBC detect by CPK. *J. Pract. Med. Tech.* 9, 908–909.

Cheng, W., Fengming, J., and Chen, J. C. (2004a). The immune response of Taiwan abalone *Haliotis diversicolor supertexta* and its susceptibility to *Vibrio parahaemolyticus* at different salinity levels. *Fish Shellfish Immunol.* 16, 295–306. doi: 10.1016/S1050-4648(03)00111-6

Cheng, W., Hsiao, I. S., Hsu, C.-H., and Chen, J.-C. (2004b). Change in water temperature on the immune response of Taiwan abalone *Haliotis diversicolor supertexta* and its susceptibility to *Vibrio parahaemolyticus*. *Fish Shellfish Immunol.* 17, 235–243. doi: 10.1016/j.fsi.2004.03.007

Donaghy, L., Kim, B. K., Hong, H. K., Park, H. S., and Choi, K. S. (2009). Flow cytometry studies on the populations and immune parameters of the hemocytes of the Suminoe oyster, *Crassostrea ariakensis*. *Fish Shellfish Immunol.* 27, 296–301. doi: 10.1016/j.fsi.2009.05.010

Doney, S. C., Mahowald, N., Lima, I., Feely, R. A., Mackenzie, F. T., Lamarque, J., et al. (2007). Impact of anthropogenic atmospheric nitrogen and sulfur deposition on ocean acidification and the inorganic carbon system. *Proc. Natl. Acad. Sci.* 104, 14580–14585. doi: 10.1073/pnas.0702218104

Dupont, S., Dorey, N., and Thorndyke, M. (2010). What meta-analysis can tell us about vulnerability of marine biodiversity to ocean acidification? *Estuar. Coast. Shelf Sci.* 89, 182–185. doi: 10.1016/j.ecss.2010.06.013

Eruslanov, E., and Kusmartsev, S. (2010). Identification of ROS using oxidized DCFDA and flow-cytometry. *Methods Mol. Biol.* 594, 57–72. doi: 10.1007/978-1-60761-411-1_4

Farcy, E., Voiseux, C., Lebel, J. M., and Fiévet, B. (2009). Transcriptional expression levels of cell stress marker genes in the Pacific oyster *Crassostrea gigas* exposed to acute thermal stress. *Cell Stress Chaperones* 14, 371–380. doi: 10.1007/s12192-008-0091-8

Feely, R. A. (2011). "Ocean acidification, the other CO2 Problem". *Am. Fish. Soc.* 3, 1–59. doi: 10.4319/lol.2011.rfeely_sdoney.5

Feely, R. A., Alin, S. R., Newton, J., Sabine, C. L., Warner, M., Devol, A., et al. (2010). The combined effects of ocean acidification, mixing, and respiration on pH and carbonate saturation in an urbanized estuary. *Estuar. Coast. Shelf Sci.* 88, 442–449. doi: 10.1016/j.ecss.2010.05.004

Feely, R. A., Doney, S. C., and Cooley, S. R. (2009). Ocean acidification: present conditions and future changes in a high-CO_2 world. *Oceanography* 22, 36–47. doi: 10.5670/oceanog.2009.95

Feely, R. A., Sabine, C. L., Hernandez-Ayon, J. M., Ianson, D., and Hales, B. (2008). Evidence for upwelling of corrosive "acidified" water onto the continental shelf. *Science* 320, 1490–1492. doi: 10.1126/science.1155676

Freitas, R., Marchi, L. D., Bastos, M., Moreira, A., Velez, C., Chiesa, S., et al. (2017). Effects of seawater acidification and salinity alterations on metabolic, osmoregulation and oxidative stress markers in *Mytilus galloprovincialis*. *Ecol. Indic.* 79, 54–62. doi: 10.1016/j.ecolind.2017.04.003

Gagnaire, B., Frouin, H., Moreau, K., Thomasguyon, H., and Renault, T. (2006). Effects of temperature and salinity on haemocyte activities of the Pacific oyster, *Crassostrea gigas* (Thunberg). *Fish Shellfish Immunol.* 20, 536–547. doi: 10.1016/j.fsi.2005.07.003

Gazeau, F., Parker, L. M., Comeau, S., Gattuso, J. P., O'connor, W. A., Martin, S., et al. (2013). Impacts of ocean acidification on marine shelled molluscs. *Mar. Biol.* 160, 2207–2245. doi: 10.1007/s00227-013-2219-3

Goncalves, P., Anderson, K., Thompson, E. L., Melwani, A., Parker, L. M., Ross, P. M., et al. (2016). Rapid transcriptional acclimation following transgenerational exposure of oysters to ocean acidification. *Mol. Ecol.* 25, 4836–4849. doi: 10.1111/mec.13808

Goncalves, P., Jones, D. B., Thompson, E. L., Parker, L. M., Ross, P. M., and Rafttos, D. A. (2017a). Transcriptomic profiling of adaptive responses to ocean acidification. *Mol. Ecol.* 26, 5974–5988. doi: 10.1111/mec.14333

Goncalves, P., Thompson, E. L., and Rafttos, D. A. (2017b). Contrasting impacts of ocean acidification and warming on the molecular responses of CO2-resilient oysters. *BMC Genomics* 18:431. doi: 10.1186/s12864-017-3818-z

Góth, L. (1991). A simple method for determination of serum catalase activity and revision of reference range. *Int. J. Clin. Chem.* 196:143. doi: 10.1016/0009-8981(91)90067-M

Guppy, M. (1999). Metabolic depression in animals: physiological perspectives and biochemical generalizations. *Biol. Rev. Camb. Philos. Soc.* 74, 1–40. doi: 10.1017/S0006323198005258

Haider, F., Falfushynska, H., Ivanina, A. V., and Sokolova, I. M. (2016). Effects of pH and bicarbonate on mitochondrial functions of marine bivalves. *Comp. Biochem. Physiol.* 198, 41–50. doi: 10.1016/j.cbpa.2016.03.021

Hendriks, I. E., Duarte, C. M., and Ivarez, M. (2010). Vulnerability of marine biodiversity to ocean acidification: a meta-analysis. *Estuar. Coast. Shelf Sci.* 86, 157–164. doi: 10.1016/j.ecss.2009.11.022

Hu, M., Li, L., Sui, Y., Li, J., Wang, Y., Lu, W., et al. (2015). Effect of pH and temperature on antioxidant responses of the thick shell mussel *Mytilus coruscus*. *Fish Shell. Immunol.* 46, 573–583. doi: 10.1016/j.fsi.2015.07.025

Huang, X., Liu, Y., Liu, Z., Zhao, Z., Dupont, S., Wu, F., et al. (2018). Impact of zinc oxide nanoparticles and ocean acidification on antioxidant responses of *Mytilus coruscus*. *Chemosphere* 196, 182–195. doi: 10.1016/j.chemosphere.2017.12.183

Hüning, A. K., Melzner, F., Thomsen, J., Gutowska, M. A., Krämer, L., Frickenhaus, S., et al. (2013). Impacts of seawater acidification on mantle gene expression patterns of the Baltic Sea blue mussel: implications for shell formation and energy metabolism. *Mar. Biol.* 160, 1845–1861. doi: 10.1007/s00227-012-1930-9

Janero, D. R. (1990). Malondialdehyde and thiobarbituric acid-reactivity as diagnostic indices of lipid peroxidation and peroxidative tissue injury. *Free. Radic. Biol. Med.* 9:515. doi: 10.1016/0891-5849(90)90131-2

Jensen, T. E., and Richter, E. A. (2012). Regulation of glucose and glycogen metabolism during and after exercise. *J. Physiol.* 590, 1069–1076. doi: 10.1113/jphysiol.2011.224972

Kreiss, C. M., Michael, K., Lucassen, M., Jutfelt, F., Motyka, R., Dupont, S., et al. (2015). Ocean warming and acidification modulate energy budget and gill ion regulatory mechanisms in Atlantic cod (*Gadus morhua*). *J. Comp. Physiol.* 185, 767–781. doi: 10.1007/s00360-015-0923-7

Kroeker, K. J., Kordas, R. L., Crim, R., Hendriks, I. E., Ramajo, L., Singh, G. S., et al. (2013). Impacts of ocean acidification on marine organisms: quantifying sensitivities and interaction with warming. *Glob. Chang. Biol.* 19, 1884–1896. doi: 10.1111/gcb.12179

Kroeker, K. J., Kordas, R. L., Crim, R., and Singh, G. G. (2010). Meta-analysis reveals negative yet variable effects of ocean acidification on marine organisms. *Ecol. Lett.* 13, 1419–1434. doi: 10.1111/j.1461-0248.2010.01518.x

Lannig, G., Eilers, S., Pörtner, H. O., Sokolova, I. M., and Bock, C. (2010). Impact of ocean acidification on energy metabolism of oyster, *Crassostrea gigas* - changes in metabolic pathways and thermal response. *Mar. Drugs* 8, 2318–2339. doi: 10.3390/md8082318

Lesser, M. P. (2006). Oxidative stress in marine environments: biochemistry and physiological ecology. *Annu. Rev. Physiol.* 68, 253–278. doi: 10.1146/annurev.physiol.68.040104.110001

Li, S., Huang, J., Liu, C., Liu, Y., Zheng, G., Xie, L., et al. (2016a). Interactive effects of seawater acidification and elevated temperature on the transcriptome and biomineralization in the pearl oyster *Pinctada fucata*. *Environ. Sci. Technol.* 50, 1157–1165. doi: 10.1021/acs.est.5b05107

Li, S., Liu, C., Huang, J., Liu, Y., Zhang, S., Zheng, G., et al. (2016b). Transcriptome and biomineralization responses of the pearl oyster *Pinctada fucata* to elevated CO2 and temperature. *Sci. Rep.* 6:18943. doi: 10.1038/srep18943

Livingstone, D. R. (2001). Contaminant-stimulated reactive oxygen species production and oxidative damage in aquatic organisms. *Mar. Pollut. Bull.* 42, 656–666. doi: 10.1016/S0025-326X(01)00060-1

Lockwood, B. L., Sanders, J. G., and Somero, G. N. (2010). Transcriptomic responses to heat stress in invasive and native blue mussels (genus *Mytilus*): molecular correlates of invasive success. *J. Exp. Biol.* 213, 3548–3558. doi: 10.1242/jeb.046094

Matoo, O., Ivanina, A., Ullstad, C., Beniash, E., and Sokolova, I. (2013). Interactive effects of elevated temperature and CO2 levels on metabolism and oxidative stress in two common marine bivalves (*Crassostrea virginica* and *Mercenaria mercenaria*). *Comp. Biochem. Physiol.* 164, 545–553. doi: 10.1016/j.cbpa.2012.12.025

Melzner, F., Göbel, S., Langenbuch, M., Gutowska, M. A., Pörtner, H. O., and Lucassen, M. (2009). Swimming performance in Atlantic Cod (*Gadus morhua*) following long-term (4-12 months) acclimation to elevated seawater P(CO2). *Aqua. Toxicol.* 92, 30–37. doi: 10.1016/j.aquatox.2008.12.011

Michaelidis, B., Ouzounis, C., Paleras, A., and Pörtner, H. O. (2005). Effects of long-term moderate hypercapnia on acid–base balance and growth rate in marine mussels *Mytilus galloprovincialis*. *Mar. Ecol. Prog.* 293, 109–118. doi: 10.3354/meps293109

Nardi, A., Benedetti, M., Fattorinia, D., and Regolia, F. (2018). Oxidative and interactive challenge of cadmium and ocean acidification on the smooth scallop *Flexopecten glaber*. *Aqua. Toxicol.* 196, 53–60. doi: 10.1016/j.aquatox.2018.01.008

Orr, J. C., Fabry, V. J., Aumont, O., Bopp, L., Doney, S. C., Feely, R. M., et al. (2005). Anthropogenic ocean acidification over the twenty-first century and its impact on calcifying organisms. *Nature* 437, 681–686. doi: 10.1038/nature04095

Peng, C., Zhao, X., Liu, S., Shi, W., Han, Y., Guo, C., et al. (2017). Ocean acidification alters the burrowing behaviour, Ca2+/Mg2+-ATPase activity, metabolism, and gene expression of a *bivalve* species, *Sinonovacula constricta*. *Mar. Ecol. Prog.* 575, 107–117. doi: 10.3354/meps12224

Perez, F. F., Fontela, M., García-Ibáñez, M. I., Mercier, H., Velo, A., Lherminier, P., et al. (2018). Meridional overturning circulation conveys fast acidification to the deep Atlantic Ocean. *Nature* 554, 515–518. doi: 10.1038/nature25493

Peskin, A. V., and Winterbourn, C. C. (2000). A microtiter plate assay for superoxide dismutase using a water-soluble tetrazolium salt (WST-1). *Clin. Chim. Acta* 293, 157–166. doi: 10.1016/S0009-8981(99)00246-6

Pierrot, D., Lewis, E., Wallace, R., Wallace, D., Wallace, W., and Wallace, D. W. R. (2006). *MS Excel Program Developed for CO2 System Calculations*. Oak Ridge, TN: Carbon Dioxide Information Analysis Center.

Pörtner, H. O., and Farrell, A. P. (2008). Ecology: physiology and climate change. *Science* 322, 690–692. doi: 10.1126/science.1163156

Ramaswamy, M., Thangavel, P., and Panneer Selvam, N. (2015). Glutamic oxaloacetic transaminase (GOT) and glutamic pyruvic transaminase (GPT) enzyme activities in different tissues of *Sarotherodon mossambicus* (Peters) exposed to a carbamate pesticide, carbaryl. *Pestic. Sci.* 55, 1217–1221. doi: 10.1002/(SICI)1096-9063(199912)55:12<1217::AID-PS78>3.0.CO;2-G

Reitman, S., and Frankel, S. (1957). A colorimetric method for the determination of serum glutamic oxalacetic and glutamic pyruvic transaminases. *Am. J. Clin. Pathol.* 28, 56–63. doi: 10.1093/ajcp/28.1.56

Ries, J. B., Cohen, A. L., and McCorkle, D. C. (2009). Marine calcifiers exhibit mixed responses to CO2-induced ocean acidification. *Geology* 37, 1131–1134. doi: 10.1130/G30210A.1

Sabine, C. L., Feely, R. A., Gruber, N., Key, R. M., Lee, K., Bullister, J. L., et al. (2004). The oceanic sink for anthropogenic CO2. *Science* 305, 367–371. doi: 10.1126/science.1097403

Shumway, S. E., and Parsons, G. J. (2006). *Scallops: Biology, Ecology and Aquaculture*. Amsterdam: Elsevier.

Soldatov, A. A., Gostiukhina, O. L., and Golovina, I. V. (2007). Antioxidant enzyme complex of tissues of the *bivalve Mytilus galloprovincialis* lam. under normal and oxidative-stress conditions: a review. *Appl. Biochem. Microbiol.* 43, 621–628. doi: 10.1134/S0003683807050092

Somero, G. N. (2010). The physiology of climate change: how potentials for acclimatization and genetic adaptation will determine 'winners' and 'losers'. *J. Exp. Biol.* 213, 912–920. doi: 10.1242/jeb.037473

Stocker, T. (2013). "IPCC, 2013: Climate Change 2013," in *The Physical Science Basis. Contribution of Working Group I to the Fifth Assessment Report of the Intergovernmental Panel on Climate Change*, eds T. F. Stocker, D. Qin, G.-K. Plattner, M. Tignor, S. K. Allen, J. Boschung, (New York, NY: Cambridge University Press).

Strahl, J., Dringen, R., Schmidt, M. M., Hardenberg, S., and Abele, D. (2011). Metabolic and physiological responses in tissues of the long-lived bivalve Arctica islandica to oxygen deficiency. *Comp. Biochem. Physiol.* 158, 513–519. doi: 10.1016/j.cbpa.2010.12.015

Terahara, K., and Takahashi, K. G. (2008). Mechanisms and immunological roles of apoptosis in molluscs. *Curr. Pharm. Des.* 14, 131–137. doi: 10.2174/138161208783378725

Thomsen, J., and Melzner, F. (2010). Moderate seawater acidification does not elicit long-term metabolic depression in the blue mussel *Mytilus edulis*. *Mar. Biol.* 157, 2667–2676. doi: 10.1007/s00227-010-1527-0

Uthicke, S., Momigliano, P., and Fabricius, K. E. (2013). High risk of extinction of benthic foraminifera in this century due to ocean acidification. *Sci. Rep.* 3:1769. doi: 10.1038/srep01769

Velez, C., Figueira, E., Soares, A. M., and Freitas, R. (2016). Combined effects of seawater acidification and salinity changes in *Ruditapes philippinarum*. *Aquat. Toxicol.* 176, 141–150. doi: 10.1016/j.aquatox.2016.04.016

Wang, Q., Cao, R., Ning, X., You, L., Mu, C., Wang, C., et al. (2016). Effects of ocean acidification on immune responses of the Pacific oyster *Crassostrea gigas*. *Fish Shellfish Immunol.* 49, 24–33. doi: 10.1016/j.fsi.2015.12.025

Weeks, L. E., and Johnson, J. H. (1977). Lactate dehydrogenase determination method. U.S. Patent No 4,006,061. St. Louis, MO: Monsanto Company.

Wittmann, A. A., and Pörtner, H. (2013). Sensitivities of extant animal taxa to ocean acidification. *Nat. Clim. Chang.* 3, 995–1001. doi: 10.1038/NCLIMATE1982

Wootton, E. C., Dyrynda, E. A., and Ratcliffe, N. A. (2003). *Bivalve* immunity: comparisons between the marine mussel (*Mytilus edulis*), the edible cockle

(*Cerastoderma edule*) and the razor-shell (*Ensis siliqua*). *Fish Shellfish Immunol.* 15, 195–210. doi: 10.1016/S1050-4648(02)00161-4

Wootton, J. T., Pfister, C. A., and Forester, J. D. (2008). Dynamic patterns and ecological impacts of declining ocean pH in a high-resolution multi-year dataset. *Proc. Natl. Acad. Sci.* 105, 18848–18853. doi: 10.1073/pnas.0810079105

Wu, F., Lu, W., Shang, Y., Kong, H., Li, L., Sui, Y., et al. (2016). Combined effects of seawater acidification and high temperature on hemocyte parameters in the thick shell mussel *Mytilus coruscus*. *Fish Shellfish Immunol.* 56, 554–562. doi: 10.1016/j.fsi.2016.08.012

Zhai, W., Zhao, H., Zheng, N., and Xu, Y. (2012). Coastal acidification in summer bottom oxygen-depleted waters in northwestern-northern Bohai Sea from June to August in 2011. *Chin. Sci. Bull.* 57, 1062–1068. doi: 10.1007/s11434-011-4949-2

Zhao, X., Guo, C., Han, Y., Che, Z., Wang, Y., Wang, X., et al. (2017a). Ocean acidification decreases mussel byssal attachment strength and induces molecular byssal responses. *Mar. Ecol. Prog. Ser.* 565, 67–77. doi: 10.3354/meps11992

Zhao, X., Shi, W., Han, Y., Liu, S., Guo, C., Fu, W., et al. (2017b). Ocean acidification adversely influences metabolism, extracellular pH and calcification of an economically important marine *bivalve*. *Tegillarca granosa*. *Mar. Environ. Res.* 125, 82–89. doi: 10.1016/j.marenvres.2017.01.007

Conflict of Interest Statement: The authors declare that the research was conducted in the absence of any commercial or financial relationships that could be construed as a potential conflict of interest.

frontiers in Physiology

ORIGINAL RESEARCH
published: 09 January 2019
doi: 10.3389/fphys.2018.01895

Different Transcriptomic Responses to Thermal Stress in Heat-Tolerant and Heat-Sensitive Pacific Abalones Indicated by Cardiac Performance

*Nan Chen[1,2], Zekun Huang[1,3,4], Chengkuan Lu[3,4], Yawei Shen[1,3,4], Xuan Luo[1,3,4], Caihuan Ke[1,3,4] and Weiwei You[1,3,4]**

[1] State Key Laboratory of Marine Environmental Science, Xiamen University, Xiamen, China, [2] College of the Environment and Ecology, Xiamen University, Xiamen, China, [3] College of Ocean and Earth Sciences, Xiamen University, Xiamen, China, [4] State-Province Joint Engineering Laboratory of Marine Bioproducts and Technology, College of Ocean and Earth Sciences, Xiamen University, Xiamen, China

The Pacific abalone *Haliotis discus hannai* is one of the most economically important mollusks in China. Even though it has been farmed in southern China for almost 20 years, summer mortality remains the most challengeable problem for Pacific abalone aquaculture recently. Here, we determined the different heat tolerance ability for five selective lines of *H. discus hannai* by measuring the cardiac performance and Arrhenius breakpoint temperature (ABT). The Red line (RL) and Yangxia line (YL) were determined as the most heat-sensitive and most heat-tolerant line, respectively. Heart rates for RL were significantly lower than those of the YL at the same temperature ($p < 0.05$). The differentially expressed genes (DEGs), which were enriched in several pathways including cardiac muscle contraction, glutathione metabolism and oxidative phosphorylation, were identified between RL and YL at control temperature (20°C) and heat stress temperature (28.5°C, the ABT of the RL) by RNA-seq method. In the RL, 3370 DEGs were identified between the control and the heat-stress temperature, while only 1351 DEGs were identified in YL between these two temperature tests. Most of these DEGs were enriched in the pathways such as protein processing in endoplasmic reticulum, nucleotide binding and oligomerization domain (NOD) like receptor signaling, and ubiquitin mediated proteolysis. Notably, the most heat-tolerant line YL used an effective heat-protection strategy based on moderate transcriptional changes and regulation on the expression of key genes.

Keywords: Pacific abalone, heat stress, cardiac performance, ABT, transcriptome

OPEN ACCESS

Edited by:
Xiaotong Wang,
Ludong University, China

Reviewed by:
Li Li,
Institute of Oceanology (CAS), China
Vengatesen Thiyagarajan,
The University of Hong Kong, Hong Kong

***Correspondence:**
Weiwei You
wwyou@xmu.edu.cn

Specialty section:
This article was submitted to Aquatic Physiology, a section of the journal Frontiers in Physiology

Received: *10 July 2018*
Accepted: *17 December 2018*
Published: *09 January 2019*

Citation:
Chen N, Huang Z, Lu C, Shen Y, Luo X, Ke C and You W (2019) Different Transcriptomic Responses to Thermal Stress in Heat-Tolerant and Heat-Sensitive Pacific Abalones Indicated by Cardiac Performance. Front. Physiol. 9:1895. doi: 10.3389/fphys.2018.01895

INTRODUCTION

The Pacific abalone (*Haliotis discus hannai*) is one of the most economically important mollusk species in China. The Pacific abalone is endemic to the coastal areas of Eastern Asia, including Northern China, Korea, and Japan (Li et al., 2007; Li J. et al., 2012; Chen N. et al., 2017). The large-scale Pacific abalone farming began in the late 1980s to cope with the decreasing of wild resources and increasing market demand (Guo et al., 1999; Li et al., 2007). Originally, most abalone

farms were situated in coastal areas within or close to the range of wild abalone. However, new varieties of the Pacific abalone had been successfully introduced to locations outside of the endemic range since 2000, including subtropical areas such as Fujian province (Deng et al., 2008). In 2016, China produced nearly 140,000 tons of abalone, and Fujian accounted for 80% of that total production (Guo and Zhao, 2017). However, the water temperature in Fujian is much higher than that in the natural habitat of the Pacific abalone, which put tremendous pressure on abalone. The warmer temperature not only reduce oxygen solubility but increase the mollusk's metabolic rate (Hamburger et al., 1994; Hoegh-Guldberg and Bruno, 2010; Vaquer-Sunyer and Duarte, 2011), which may trigger a rising number of oxygen deficient. The immune response of abalone could also be affected by the elevated temperature associated with increased in its susceptibility to disease outbreak (Cheng et al., 2004; Dang et al., 2012). Especially in summer, these influences would be more serious and the mass mortality occurred frequently (Liang et al., 2014). Therefore, it is important to explore how the abalone respond to the heat stress and whether different strategies are taken to adapt to the high temperature.

How do organisms response to the environmental change is one of the basic question for environmental physiology. Recently, advances in biotechnology have allowed experiments aimed at assessing this question to become increasingly reductionist, by relating changes in environment to genome-scale phenomena (Evans, 2015). Transcriptomics has been one of the popular methods because it can be used to compare the gene expression of different tissues and development stages with various treatment, even without the need for a reference genome (Martin and Wang, 2011; Shiel et al., 2015). The different trait related transcriptome studies had been widely performed on abalone (Franchini et al., 2011; van der Merwe et al., 2011; Valenzuela-Munoz et al., 2013; Choi et al., 2015; Picone et al., 2015; Valenzuela-Miranda et al., 2015; Harney et al., 2016). However, previous work on heat tolerance in the abalone was limited. Transcriptome-wide scans of the red abalone (*H. rufescens*) from three environmentally distinct regions were analyzed, and some loci associated with the heat response were identified (Wit and Palumbi, 2013). In the green lip abalone (*H. laevigata*), transcriptome analyses indicated that the heat shock protein 70 (HSP 70) gene family was strongly associated with heat response (Shiel et al., 2015). The related genes and transposable elements that respond quickly and effectively to summer heat stress (20°C) have been identified in heat-resistant green lip abalone line (Shiel et al., 2017). In southern China, ambient water temperatures can be over 28°C in summer, which was much higher than those published abalone heat test on red and green lip abalones. It would be very interesting to conduct the transcirptome analyses for the Pacific abalone under such high temperature and analyze whether there are similar or different heat response mechanism on different abalone species.

Different environments may exert strong selection pressures on different populations, leading to local adaptations to particular conditions (Hereford, 2009; North et al., 2011; Wit and Palumbi, 2013). Typically, such natural selection should produce phenotypes sensitive or resistant to a particular environmental stressor. In ectothermic organisms, physiological performance is sensitive to ambient temperature variation and is closely linked with the organismal heat tolerance (Portner et al., 2006; Clark et al., 2008). The Arrhenius breakpoint temperature (ABT) of cardiac performance has been used as an indicator for heat tolerance in porcelain crabs (*Petrolisthes*) (Stillman and Somero, 1996), marine snail (*Tegula*) (Stenseng et al., 2005), limpets (*Cellana*) (Dong and Williams, 2011; Han et al., 2013), and scallops (Xing et al., 2016). The ABT also has been shown to be a credible, non-invasive indicator of heat tolerance in abalone (Chen et al., 2016; Alter et al., 2017).

The study's objective was to identify differences in patterns of gene expression between heat-sensitive and heat-tolerant abalones when subjected to heat stress on subtropical area. We first aimed to assess heat tolerance with ABT measurements in various selective lines of *H. discus hannai*. Based on this assessment, we were able to identify heat-sensitive and heat-tolerant abalone lines, and to conduct transcriptome analyses. We also aimed to identify genes or pathways associated with heat response in abalones by comparing gene expression patterns between sensitive and tolerant lines. The results might provide clues as to how abalone cope with life at high temperature, increase our understanding of the thermal response patterns of the Pacific abalone and highlighted potentially important genes or pathways for future study.

MATERIALS AND METHODS

Experimental Animals

Five Pacific abalone selective lines were used in this research for the heat tolerance assessment: Yangxia line (YL), Dongshan line (DL), Red line (RL), Changdao line (CL) and Japanese line (JL). 50 individuals with the same size (4.5–6 cm) from each line were selected, labeled and cultured in a recirculating system for 7 days acclimation. Temperature, dissolved oxygen and salinity were kept at 20°C, 6 mg/L and 32, respectively. All abalones were fed once each day with fresh seaweed and all the residual food particles and fecal debris were removed 12 h before the start of the experiment.

Cardiac Performance

Sixteen individuals of each line were randomly selected, and crystal dishes (diameter = 20.0 cm, height = 9.5 cm) were used for abalone to settle. Fresh seawater was added into the dishes, and the dissolved oxygen concentration was kept by delivering air from a compressor to each dish. To measure real-time body temperature, a fine thermometer was inserted between the foot and the crystal dish. The crystal dish was immersed in a water bath, and the temperature of the seawater in the dish was increased using the water bath on the rate of approximately 0.1°C min^{-1}.

The non-invasive method was used for heart rate measurement (Depledge and Andersen, 1990; as modified by Chelazzi et al., 1999; Dong and Williams, 2011). To detect heart beats, an infrared sensor was glued to each shell above

the heart (Krazy Glue, Westerville, OH, United States). The fluctuations of heart beat were amplified, filtered and recorded by an infrared signal amplifier (AMP03, Newshift, Leiria, Portugal) and Powerlab (8/35, ADInstruments, March-Hugstetten, Australia). All heart rate data were monitored and analyzed with LabChart v8.0. The ABT was defined as the temperature at which the heart rate decreased dramatically. To determine the ABT, we used regression analyses to generate the best fit lines on both side of a putative break point (Stillman and Somero, 1996). To construct Arrhenius plots, heart rates were transformed to the natural logarithm of beats min^{-1}. Temperatures are shown as 1000/K (Kelvin temperatures). To test the significance of differences in ABT and maximum heart rate among lines, we used one-way analyses of variance (ANOVAs) in SPSS v17.0. We considered $p < 0.05$ statistically significant.

Heat Stress Experiments

Based on mean ABT for each line, we could distinguish the heat-sensitive lines from the heat-tolerant lines. The ABT of the most sensitive line was selected as the thermal stressor. We randomly selected an additional 24 specimens, 12 from the most heat-tolerant line and 12 from the most heat-sensitive line. Half of all specimens (6 per line) were randomly assigned to the control group. All others were assigned to experimental group. For heat exposure, the abalones were transferred to the experimental tank from the acclimation condition (20°C) directly, in which the temperature was set as ABT of most sensitive line prior to the experiment. The heat stress lasted for 2 h and the control group was kept at 20°C at the same time. All the abalones were dissected at the end of experiments and gills were immediately frozen in liquid nitrogen and stored at −80°C until use.

RNA Preparation and Sequencing

Total RNA was extracted from the gills of the 24 samples using Trizol reagent (Gibco BRL, United States). To check the purity and integrity of RNA, the Nanophotometer® spectrophotometer (IMPLEN, Westlake Village, CA, United States) and RNA Nano 6000 Assay Kit of the Agilent Bioanalyzer 2100 system (Agilent Technologies, Santa Clara, CA, United States) were used. Based on these results, we selected three individuals with the best RNA quality of six samples from each of the four groups (sensitive line/tolerant line × heat stress/control) for transcriptomic analyses. Library preparation and sequencing were performed by Novogene (Beijing, China). We obtained an average of ∼52.8 million raw reads per specimen (maximum: 63.0 million raw reads; minimum: 44.8 million raw reads).

De novo Transcriptome Assembly and Annotation

Raw reads were cleaned by removing ambiguous reads (those with > 10% ambiguous nucleotides) and low-quality reads (those consist of more than half bases whose quality scores < 10) to achieve clean reads. All clean data were assembled with Trinity r20140413p1 (Grabherr et al., 2011), with min_kmer_cov set to 2 and other parameters set to defaults. The longest transcript for each gene was considered to represent this gene and named unigene. Unigenes were used for all subsequent annotations.

To comprehensively annotate the assemblies, transcripts were compared to several public databases: Nt (NCBI non-redundant nucleotide sequences), Nr (NCBI non-redundant protein sequences), and Swiss-Prot using BLAST+ v2.2.28+ (e-value = 1e-5; Altschul et al., 1990); GO (Gene Ontology) with BLAST2GO (e-value = 1e-10; Götz et al., 2008); and KO (KEGG Orthologs) with KAAS r140224 (e-value = 1e-10; Mao et al., 2005; Moriya et al., 2007).

Quantification and Differential Analysis of Gene Expression

The *de novo* assembled transcriptome was used as a reference for read mapping and gene expression profiling. To identify differential gene expression, the sequence reads for each specimen were mapped back to the assembled transcriptome using RSEM v1.2.1.5 (bowtie2 set mismatch = 0; Li and Dewey, 2011). The gene expression levels were based on FPKM values (expected number of Fragments Per Kilobase of transcript sequence per Millions base pairs sequenced). We compared differential gene expression between pairs of groups with DESeq v1.10.1 in R (Anders and Huber, 2012). The strict filter (p-value < 0.05 and |log2 (fold change)| > 1) was set as the threshold for significant differential expression. We performed four analyses to identify differential gene expression between the two lines or stress conditions: (I) the heat-sensitive line vs. the heat-tolerant line at the control temperature; (II) the heat-sensitive line vs. the heat-tolerant line at the heat stress temperature; (III) the heat-sensitive line at the control temperature vs. the heat stress temperature; and (IV) the heat-tolerant line at the control temperature vs. the heat stress temperature.

Functional Annotation and Transcript Validation

Gene Ontology (GO) enrichment analysis of the differentially expressed genes (DEGs) was implemented by the GOseq v1.10.0 in R packages (Young et al., 2010). GOseq is based on Wallenius non-central hyper-geometric distribution, which adjusts for DEG gene length bias. We used KOBAS v2.0.12 (Mao et al., 2005) to test the statistically significant enrichment of DEGs in KEGG pathways.

The further validation for the RNA-seq results was conducted by real-time quantitative PCR (RT-PCR) with all the 24 individuals which were prepared in Section "Heat Stress Experiments." The expression levels of 10 genes which selected from intriguing pathways were quantified. Based on the reference unigene sequences, we designed gene-specific primers with Primer Premier v5.0 (**Supplementary Table S1**). First-strand cDNA was synthesized with a PrimeScript RT reagent Kit (TaKaRa, Dalian, China), and qRT-PCR was performed with a ThermoDyNAmo Flash SYBR Green qPCR Kit (Thermo Scientific, United States) on an ABI 7500 Fast Real-Time PCR system (Applied Biosystems, United States), following the manufacturer's instructions. Gene expression was normalized

based on the expression of 18S and β-actin. Relative gene expression was then calculated using the $2^{-\Delta\Delta CT}$ method.

RESULTS

Cardiac Performance and ABT Measurement

The cardiac performance at different temperatures were shown by the Arrhenius plots (**Figure 1A**). The cardiac performance could be divided into two phases. Abalone heart rates initially increased slowly with rising water temperature. As water temperature continued to rise, incidents of arrhythmia were observed. Heart rates decreased abruptly as soon as the water temperature exceeded a critical value (the ABT). The ABTs for the YL, DL, RL, JL, and CL were 31.9 ± 0.7, 29.5 ± 1.7, 28.5 ± 1.8, 29.5 ± 1.2, and 30.4 ± 0.6°C, respectively (**Figure 1B**) using regression analysis. The ABT of the YL was significantly higher than that of the DL, RL, and JL. The ABT of the CL was also significantly higher than that of the RL. The YL was the most tolerant to heat stress, while the RL was most sensitive. Therefore, the individuals from YL and RL were selected for transcriptome analysis, and 28.5°C (RL's ABT) was set as heat stress temperature. Heart capacity also differed between the RL and YL. Heart rates of RL specimens were lower than those of YL at the same temperature. The maximum of heart rates was also significantly different (Duncan's *post hoc* analysis, $p = 0.001$; RL: 54.75 ± 6.90 beats min^{-1} and YL: 75.14 ± 7.29 beats min^{-1}).

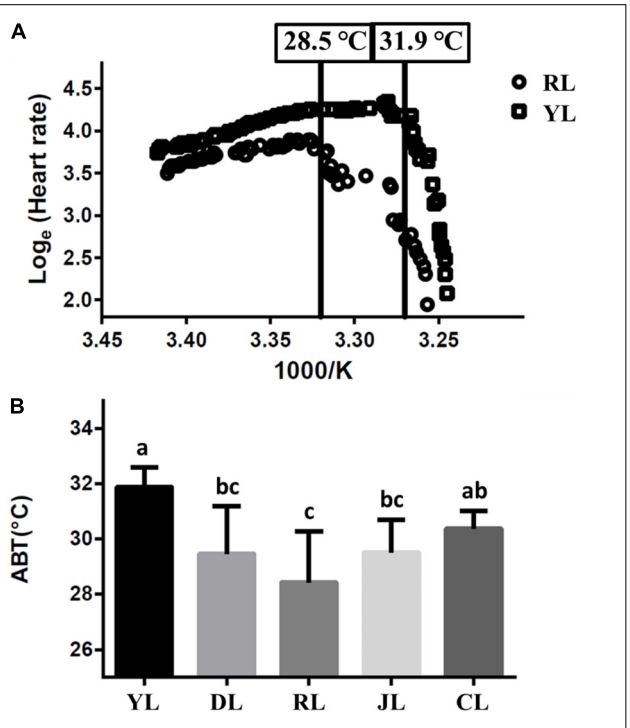

FIGURE 1 | The Arrhenius breakpoint temperature (ABT) for different Pacific abalone lines. **(A)** The Arrhenius plots for YL and RL. **(B)** The ABTs for the five selective lines. Bars labeled with different letters are significantly different ($p < 0.05$).

De novo Assembly and RNA-seq Mapping

After filtering, a total of 43.2 to 60.3 million clean reads for each sample were obtained. The *Trinity* assembly generated 227,066 transcirpts and 161,135 unigenes, with the minimum length of 201 bp and the maximum length of 17 kb. Only 27.26% of all unigenes could be annotated in one or more databases. Approximately 70% of all reads were successfully mapped back to the reference transcriptome (68.12–72.33%) (**Supplementary Table S2**).

Differentially Expressed Genes (DEGs)

We identified 535 DEGs between the heat-tolerant and heat-sensitive lines at the control temperature (20°C), and 492 DEGs at the heat stress condition. Of these DEGs, 150 were differentially expressed at both temperatures (**Figure 2A**). However, more genes were differentially expressed between the two temperatures as compared to those between the two lines. In the YL, 1351 DEGs were identified between the control and heat stress temperature: 1121 were up-regulated at the heat stress temperature as compared to the control, and 230 were down-regulated. Many more DEGs were identified in the RL. In the RL, 2217 DEGs

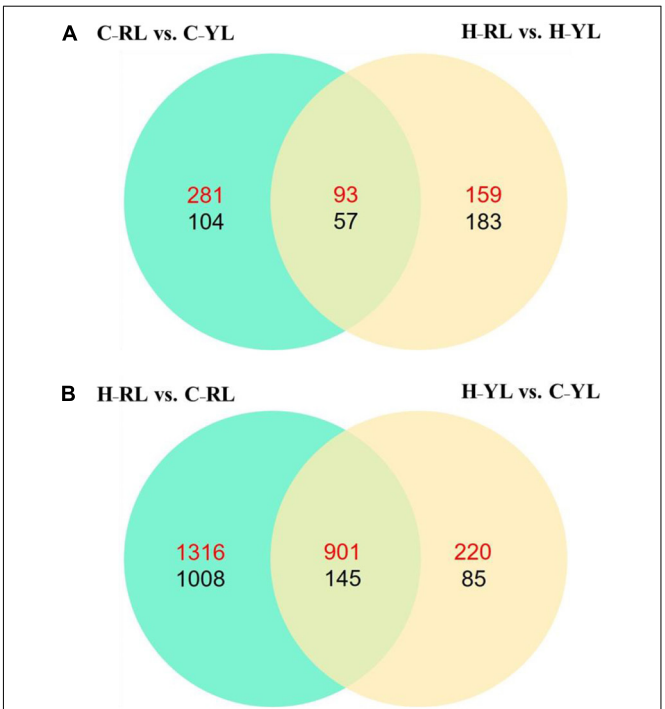

FIGURE 2 | The Venn diagram of significant differently expressed genes. **(A)** Comparison between different lines. **(B)** Comparison between control temperature and heat stress temperature. C_RL: RL at control temperature; C_YL: YL at control temperature; H_RL: RL at heat stress temperature; H_YL: YL at heat stress temperature. Up-regulated genes were numbered in red and down-regulated genes were numbered in black.

were up-regulated at the heat stress temperature as compared to the control, and 1153 genes were down-regulated (**Figure 2B**). Of these DEGs, 1046 genes were differentially expressed in both lines.

Gene Ontology (GO) Enrichment Analysis

The genes differentially expressed between the RL and YL were enriched in several interesting GO terms, including organic substance metabolic process, macromolecule metabolic process, hydrolase activity, and binding (**Figure 3**). Between control and heat stress treatment, the DGEs were significantly enriched in protein binding, ion binding, biological regulation, and intracellular membrane-bounded organelle for RL (**Figure 4A**) and transcription factor complex, intracellular membrane-bounded organelle, protein complex for YL (**Figure 4B**). Of these, nearly twice as many genes were enriched for each term in the RL as compared to YL (**Supplementary Table S3**).

KEGG Pathway Enrichment Analysis

Within KEGG pathway analysis, the results showed that the DEGs between the RL and YL were most enriched in the following five pathways: pancreatic secretion, cardiac muscle contraction, protein digestion and absorption, oxidative phosphorylation, and Parkinson's disease (**Figure 5**). Between the control and heat stress temperature, DEGs were most significantly enriched in the protein processing in endoplasmic reticulum pathway: 40 RL and 29 YL DEGs were enriched in this pathway. Several other pathways were also significant up-regulated, including ubiquitin mediated proteolysis, apoptosis, nucleotide binding, and oligomerization domain (NOD-like) receptor signaling pathway and TNF signaling pathway (**Figures 6A,B**).

Heat Shock Protein Family

Several genes in the HSP gene family were enriched in multiple pathways. Indeed, the expression levels of 35 HSP genes were significantly different between control and heat stressed specimens (**Figure 7** and **Table 1**). Of these, 20 HSP genes were differentially expressed in both abalone lines, 11 were differentially expressed in the RL only, and 4 were differentially expressed in the YL only. The degree of up-regulation also differed among the differentially expressed HSP genes: from

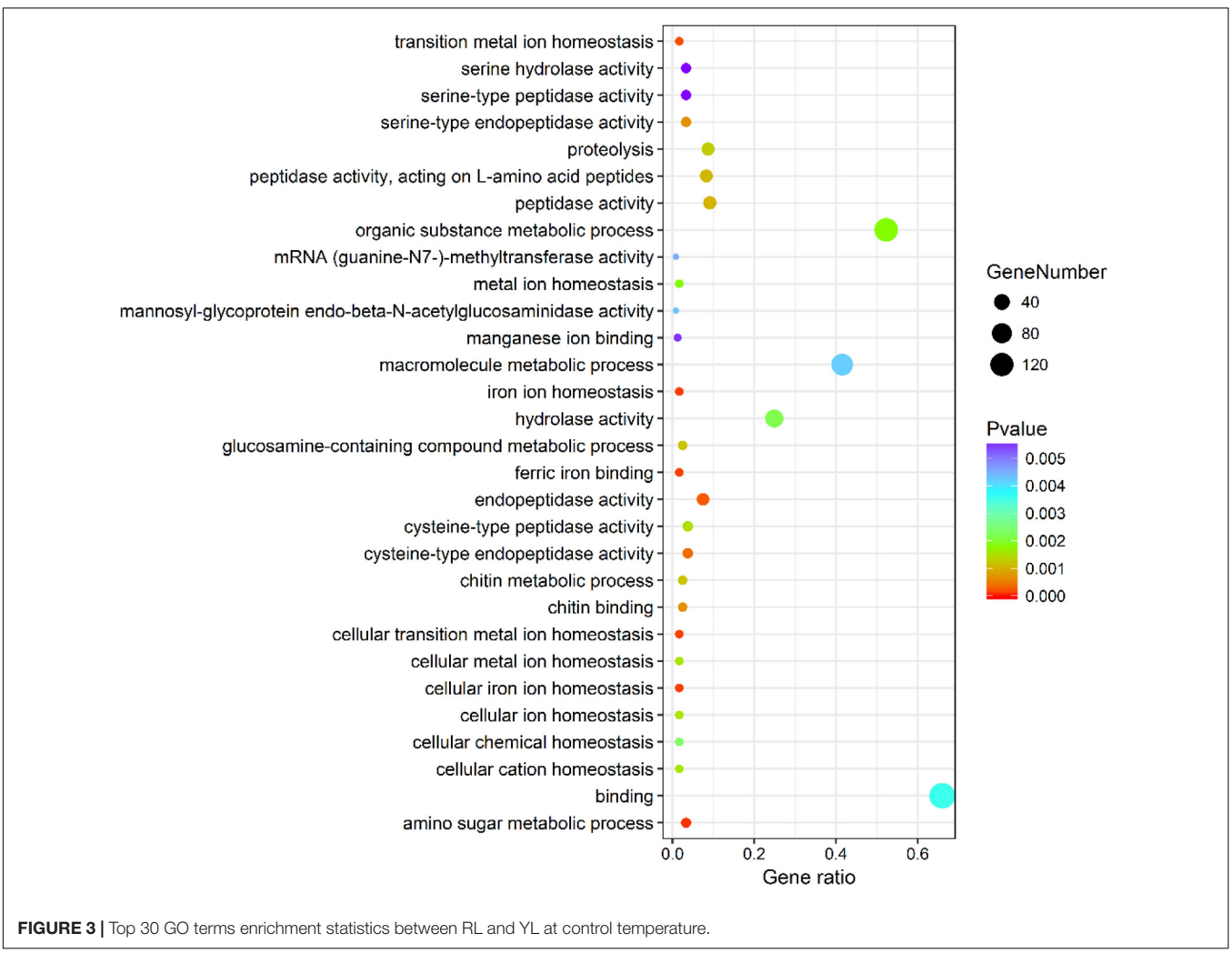

FIGURE 3 | Top 30 GO terms enrichment statistics between RL and YL at control temperature.

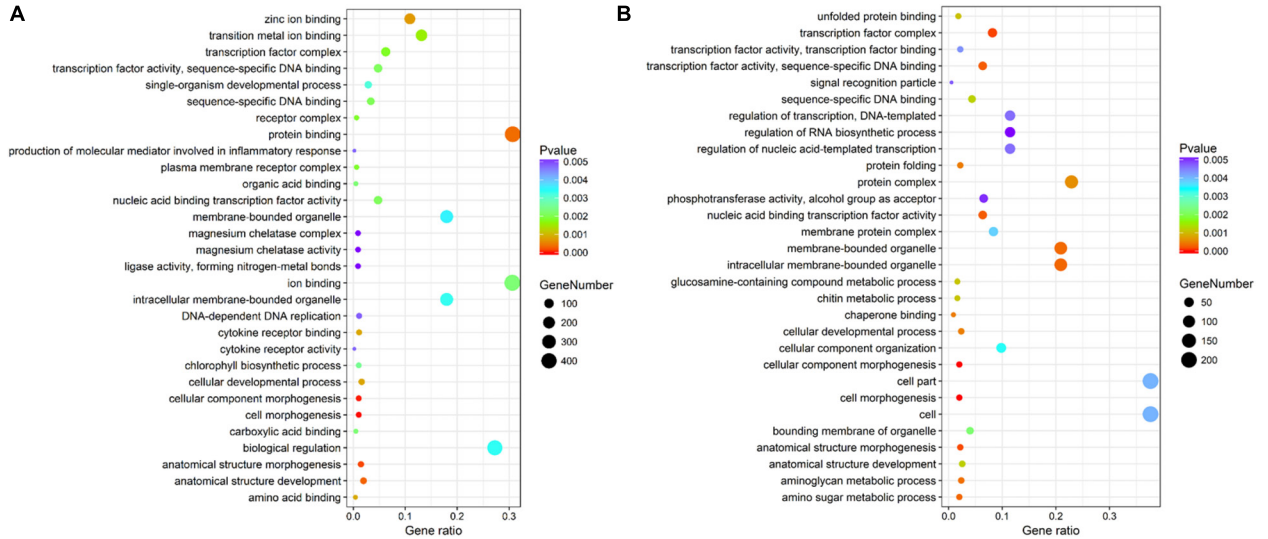

FIGURE 4 | Top 30 GO terms enrichment statistics between control and heat stress temperature. **(A)** Terms enrichment in RL. **(B)** Terms enrichment in YL.

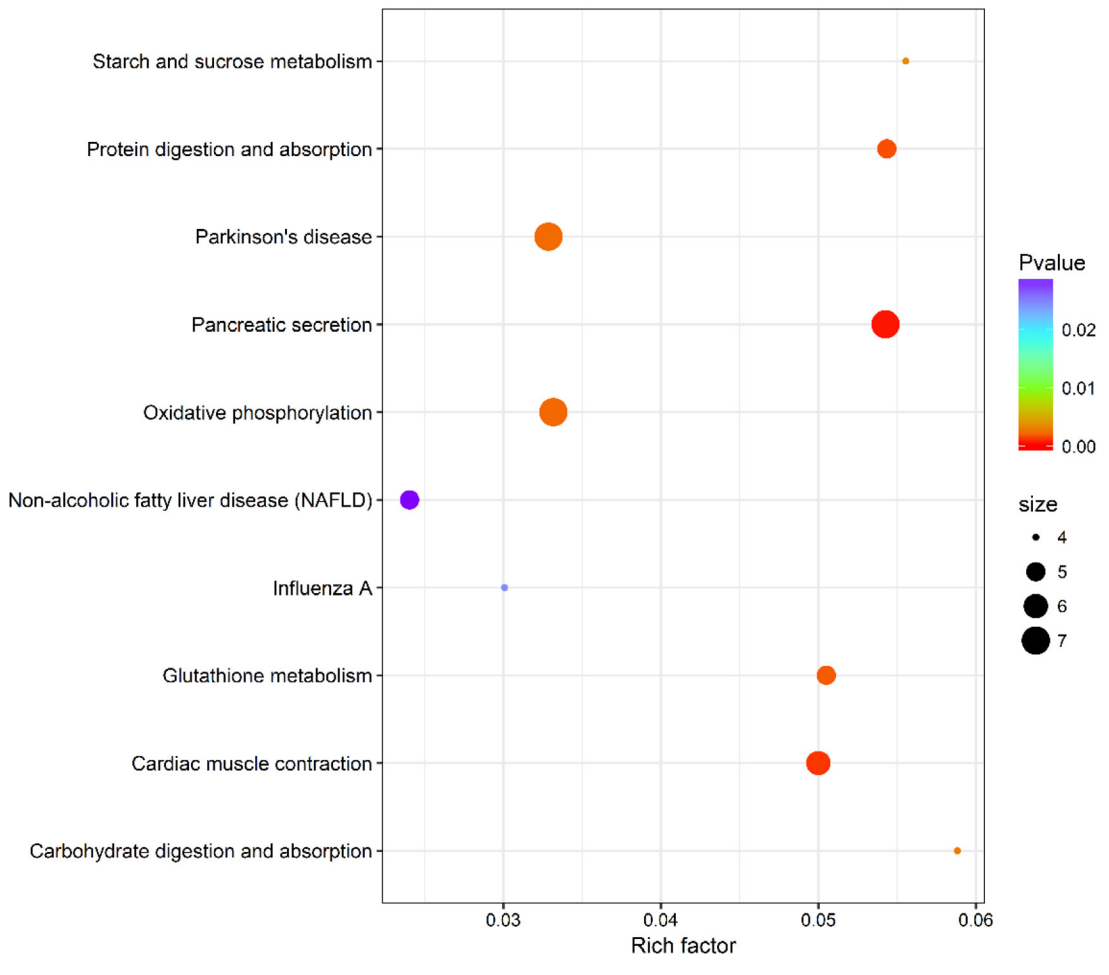

FIGURE 5 | Top 10 pathways enrichment statistics between RL and YL at control temperature.

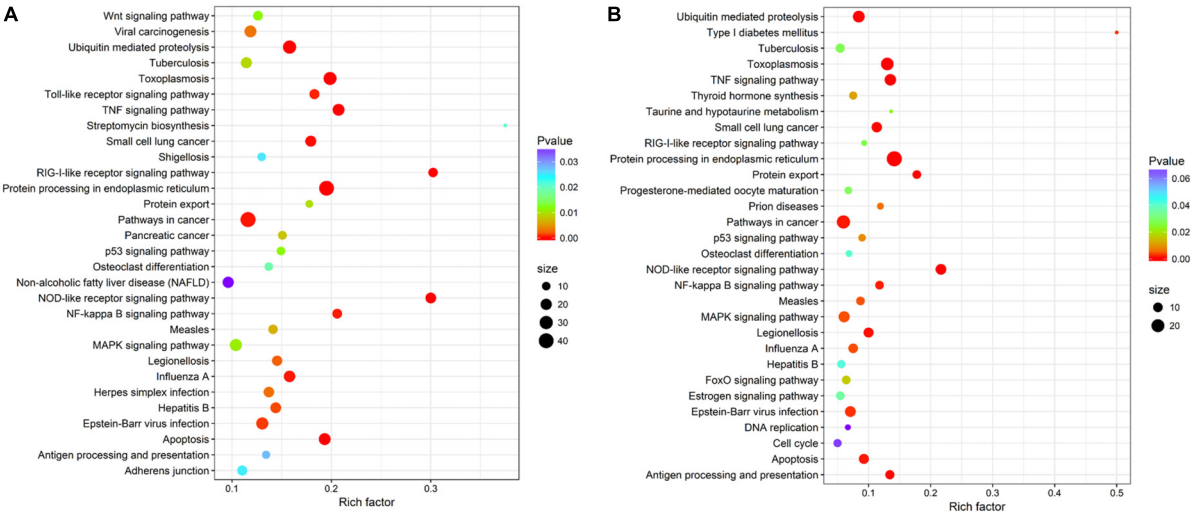

FIGURE 6 | Top 30 pathways enrichment statistics between control and heat stress temperature. **(A)** Pathway enrichment in the RL. **(B)** Pathway enrichment in the YL.

1.6-fold (log_2 Fold Change) (DnaJ homolog subfamily C member 7) to 11.9-fold (small heat shock protein 26) in RL and 2.9-fold (stress-70 protein, mitochondrial) to 11.4-fold (Heat shock 70 kDa protein) in YL.

Ubiquitin-Mediated Proteolysis Pathway

Ubiquitination serves as a versatile post-translational modification in all eukaryotic species. As shown in **Figure 8**, a total of 32 genes that involved in this pathway expressed differently. Of these, 16 genes and 30 genes were up regulated significantly in YL and RL, respectively.

Antioxidant Genes

Heat stress can result in oxidative stress as the formation of reactive oxygen species (ROS). There were several genes (including catalase, superoxide dismutase, peroxiredoxin 5) related to antioxidant system that annotated in this study (**Figure 9**) and only one catalase gene (c92672_g3) was up-regulated at heat stress temperature of both lines.

Real-Time Quantitative PCR Validation

We used 10 genes that were differentially expressed between the control and heat stress temperatures for qRT-PCR validation. These DEGs included HSP90 (c_95969_g1), HSP70 (c_92061_g1) and cyclin B (c_86983_g1). The patterns of gene expression indicated by the qRT-PCR and RNA-seq analyses were similar (**Figure 10**).

DISCUSSION

Cardiac Performance and Heat Tolerance Assessment

In ectothermic animals, temperature is the main variable which controls the rate of most metabolic processes (Morash and Alter, 2015). Increased temperatures can diminish oxygen solubility and change the metabolic rates (Hoegh-Guldberg and Bruno, 2010; Vaquer-Sunyer and Duarte, 2011). It thus becomes difficult for the organism to obtain sufficient oxygen to sustain aerobic scope, both with respect to providing metabolic fuel and to removing metabolic waste products at high temperature (Somero, 2012). Aerobic scope drops when the maximum metabolic rate fails to keep pace with the routine metabolic rate as temperature increases (Portner and Knust, 2007; Casselman et al., 2012). For many marine ectotherms, heat-stress tolerance is based on the ability to maintain normal aerobic scope in elevated water temperatures (Portner et al., 2006; Portner, 2010; Han et al., 2013). In gastropods, this capacity is largely dependent on heart function; the ABT of cardiac performance has thus been used as an effective indicator of heat tolerance in gastropods (Han et al., 2013; Chen et al., 2016).

We found that the five tested different Pacific abalone lines had different levels of heat tolerance. There were nearly 3.5°C difference between the most temperature-tolerant line (YL) and the most temperature-sensitive line (RL). At high water temperature, even a 1°C difference would affect abalone survival (Chen et al., 2016). The ABT for RL was 28.5 ± 1.8°C, which means RL abalone's cardiac function is approaching the limit at this temperature. Thus, at 28.5°C, cardiac function in an RL individual is approaching the maximum, while the individuals of YL could maintain normal oxygen supply and cardiac function at the same temperature. The cardiac muscle contraction pathway was significantly down-regulated when compared control of RL to control of YL by RNA-seq results. Only six genes, including myosin light chain 4 (MYL 4) were involved in this pathway, *MYL 4* is particularly notable because this gene regulates several critical biological processes, including heart contraction force, muscle organ development, and cardiac muscle contraction. The MYL 4 protein is down-regulated in failing human hearts, as compared to normal human hearts (Li W. et al., 2012). To verify

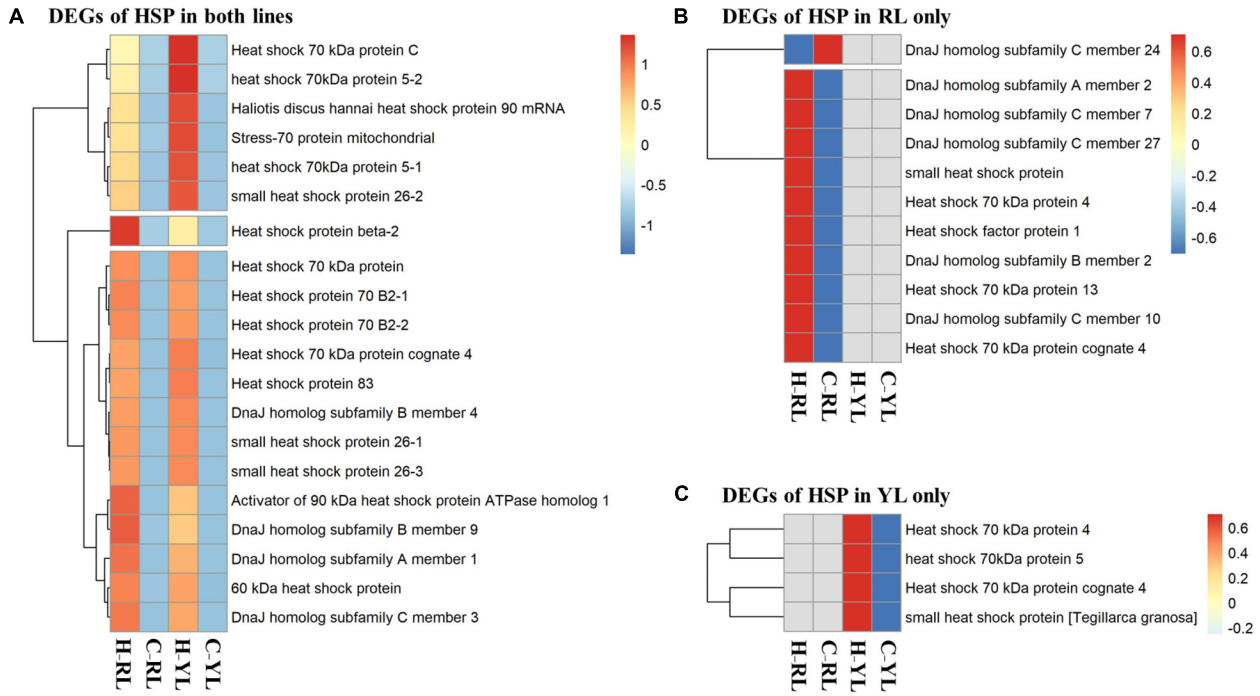

FIGURE 7 | Heatmaps of differentially expressed heat shock protein (HSP) genes. **(A)** Genes differentially expressed in both lines. **(B)** Genes differentially expressed in the RL only. **(C)** Genes differentially expressed in the YL only.

the difference in cardiac function, further study of the expression level of myosin family gene in the abalone heart is necessary.

The Identified Different Expression Genes

Between the RL and the YL, 535 DEGs were identified at the control temperature, and 492 DEGs were identified at the heat-stress temperature. However, more genes were differentially expressed between the control and heat-stress temperatures: 1351 DEGs in YL and 3370 DEGs in RL. This increase transcriptome fluctuation in the more temperature-sensitive line has been shown in other organisms, including copepod (*Tigriopus californicus*; Schoville et al., 2012), coral (*Acropora hyacinthus*; Barshis et al., 2013), snail (*Chlorostoma funebralis*; Gleason and Burton, 2015), and redband trout (*Oncorhynchus mykiss gairdneri*; Chen Z. et al., 2017). Indeed, the increased heat-tolerance seems to be based on the moderate transcriptional changes under heat stress (Bita et al., 2011). Here, twice as many RL DEGs were enriched per GO term as compared to YL DEGs. However, it is possible that this discrepancy is due to the higher level of physiological stress experienced by the less thermally tolerant individuals. Thus, we speculated that the more effective protection strategy was not only based on fine-tuned but the more effective expression response in the heat-tolerant abalone line. In this research, we observed a higher degree change of gene expression in the YL, as compared to the RL in some key genes including HSP family.

The different physiological stress might also be indicated by the down-regulated pathways: cell cycle and DNA replication. In face of stress condition, cells often delayed the DNA replication and cell division in favor of cytoprotective functions (Jonas et al., 2013). More genes (**Table 2**) were down-regulated in sensitive line vs. tolerant line (9 vs. 5), which mean the cells of RL might be subjected to more severe suppression.

HSP Family

Genes in the "Protein processing in endoplasmic reticulum" pathway, including many HSP genes, were significantly up-regulated. HSPs are highly conserved proteins that act as molecular chaperones to protect normal proteins from degeneration, catalyze the folding of normal proteins and the refolding of abnormal proteins, remove irreversibly damaged proteins, and help maintain cellular homeostasis (Snyder et al., 2001; Farcy et al., 2007; Liang et al., 2014). The molecular chaperones (HSP70, HSP90, and other HSPs) are one of the most varied gene families affected by heat stress in mollusks (Lang et al., 2009; Lockwood et al., 2010; Chapman et al., 2011). The rapid response of HSPs to heat stress is an important part of the molluscan protection mechanism (Zhao and Jones, 2012). There were fewer HSP DEGs in the YL (24) as compared to the RL (31), but the average fold change ($\log_2$ fold change) was higher in the YL (7.0) than in the RL (5.4). This indicated that the heat response strategy used by the YL might be more effective.

The HSP40 gene family is another important group, which primary function is to act as co-chaperones for HSP70 (Gleason and Burton, 2015). HSP40s increase the HSP70 ATP-hydrolysis

TABLE 1 | Differentially expressed heat shock protein family genes.

Gene name	Readcount			Readcount		
	H_RL	C_RL	Log_2 fold change	H_YL	C_YL	Log_2 fold change
DEG in both lines						
60 kDa heat shock protein	22940.4	1697.5	3.8	20808.9	1119.9	4.2
Activator of 90 kDa heat shock protein ATPase homolog 1	5238.0	55.9	6.6	3873.5	50.9	6.2
DnaJ homolog subfamily A member 1	14258.0	185.5	6.3	11714.6	111.0	6.7
DnaJ homolog subfamily B member 4	71733.8	474.1	7.2	76468.9	365.2	7.7
DnaJ homolog subfamily B member 9	442.4	19.8	4.5	318.0	16.1	4.3
DnaJ homolog subfamily C member 3	1816.7	101.8	4.2	1586.5	83.3	4.3
Haliotis discus hannai heat shock protein 90 mRNA	18359.5	290.8	6.0	29654.7	230.6	7.0
Heat shock 70 kDa protein	517199.6	157.6	11.7	512778.1	193.8	11.4
Heat shock 70 kDa protein C	40.2	3.1	3.7	91.9	2.7	5.1
Heat shock 70 kDa protein cognate 4	200721.2	6687.8	4.9	224124.7	4084.2	5.8
Heat shock 70 kDa protein 5-1	89771.3	3321.8	4.8	135757.5	2553.6	5.7
Heat shock 70 kDa protein 5-2	124.3	11.6	3.4	257.6	13.5	4.3
Heat shock protein 70 B2-1	1026410.4	601.0	10.7	953619.4	531.1	10.8
Heat shock protein 70 B2-2	103617.9	120.2	9.8	98169.6	108.6	9.8
Heat shock protein 83	351431.0	6616.4	5.7	389863.4	4789.3	6.3
Heat shock protein beta-2	266.7	4.7	5.8	137.1	2.5	5.8
Small heat shock protein 26-1	104467.4	28.1	11.9	109373.2	42.0	11.3
Small heat shock protein 26-2	81010.9	25.4	11.6	118746.7	46.2	11.3
Small heat shock protein 26-3	754714.9	417.6	10.8	795488.0	395.2	11.0
Stress-70 protein, mitochondrial	4156.8	1003.4	2.1	6168.8	854.8	2.9
DEG in RL only						
DnaJ homolog subfamily A member 2	5218.5	1508.9	1.8			
DnaJ homolog subfamily B member 2	308.6	95.0	1.7			
DnaJ homolog subfamily C member 10	23.3	2.8	3.0			
DnaJ homolog subfamily C member 24	25.0	120.8	−2.3			
DnaJ homolog subfamily C member 27	42.0	7.7	2.4			
DnaJ homolog subfamily C member 7	3339.3	1067.1	1.6			
Heat shock 70 kDa protein 13	32.4	5.6	2.5			
Heat shock 70 kDa protein 4	133179.5	549.7	7.9			
Heat shock 70 kDa protein cognate 4	80171.5	1847.4	5.4			
Heat shock factor protein 1	235.3	44.7	2.4			
Small heat shock protein	112213.5	112.6	10.0			
DEG in YL only						
Heat shock 70 kDa protein 4				152438.4	406.7	8.6
Heat shock 70 kDa protein cognate 4				75878.2	1199.4	6.0
Heat shock 70 kDa protein 5				28.2	0.9	4.9
Small heat shock protein [Tegillarca granosa]				131461.7	144.5	9.8

RL, red line; YL, Yangxia line; C_RL, RL at control temperature; C_YL, YL at control temperature; H_RL, RL at heat stress temperature; H_YL, YL at heat stress temperature.

rate and strengthen the HSP70 activity fields (Misselwitz et al., 1998; Genevaux et al., 2007; Mayer, 2013). In thermotolerant cells, this interaction might increase protein thermostability and accelerate heat-damage recovery (Gebauer et al., 1997; Terada et al., 1997; Gleason and Burton, 2015). The gastropod *C. funebralis* exhibited the opposite reaction to heat stress (Gleason and Burton, 2015): 66.7% of all annotated HSP70s showed a significantly higher fold change in heat-sensitive lines, as compared to heat-tolerant lines, while the expression levels of 60% of all HSP40s were higher in the heat-tolerant lines. Here, more than 70% of common HSP70 and HSP40 genes that differentially expressed in both lines showed a higher fold change in the YL, as compared to the RL. This might be because *C. funebralis* inhabits intertidal areas, where water temperature fluctuation is more drastic (Gleason and Burton, 2015) than in the subtidal habitat of the abalone. Some gene families, such as HSP60, are pre-adapted in heat-tolerant lines (Gleason and Burton, 2015), which might serve as a preparative defense against frequent heat stress events. In addition, significant up-regulation of HSP40 combined with reasonable up-regulation of HSP70 expression might reduce the need for the heat-tolerant lines to up-regulate HSP70 as drastically as the heat-sensitive populations do. For abalones, ambient water temperature does not fluctuate so frequently. Thus, the higher fold change of HSP gene family

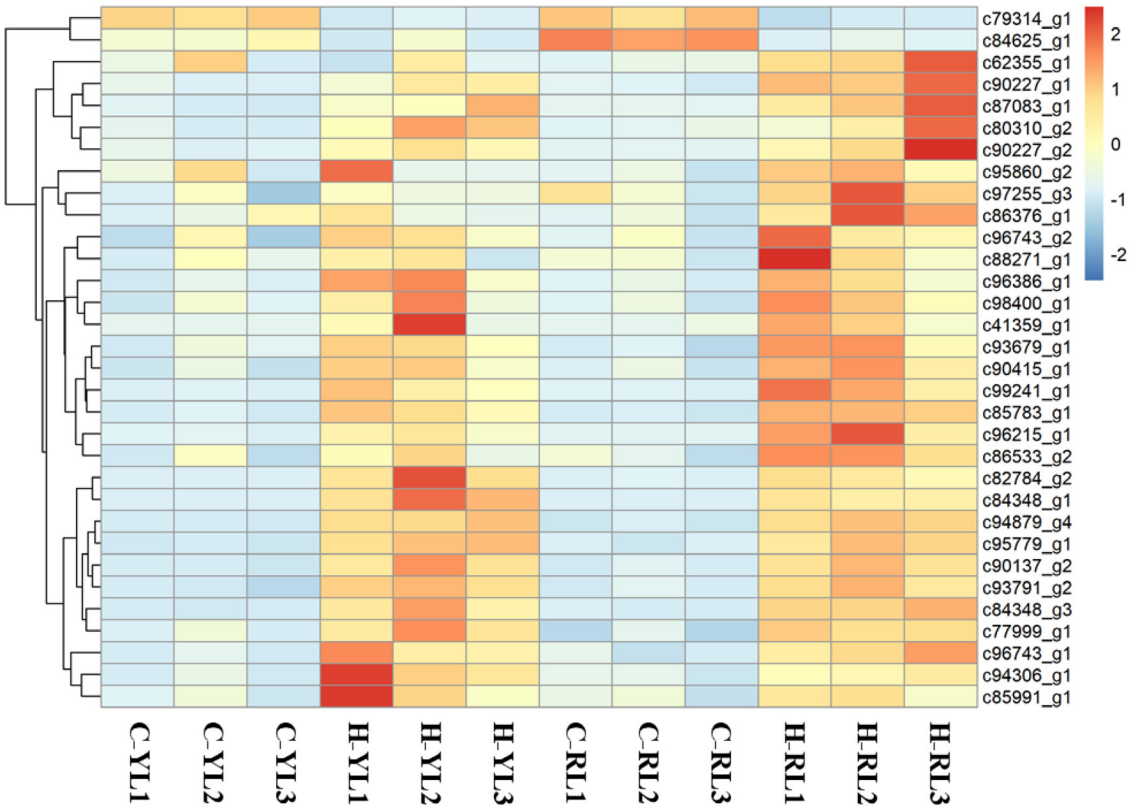

FIGURE 8 | Heatmap of genes involved in the ubiquitin-mediated proteolysis pathway.

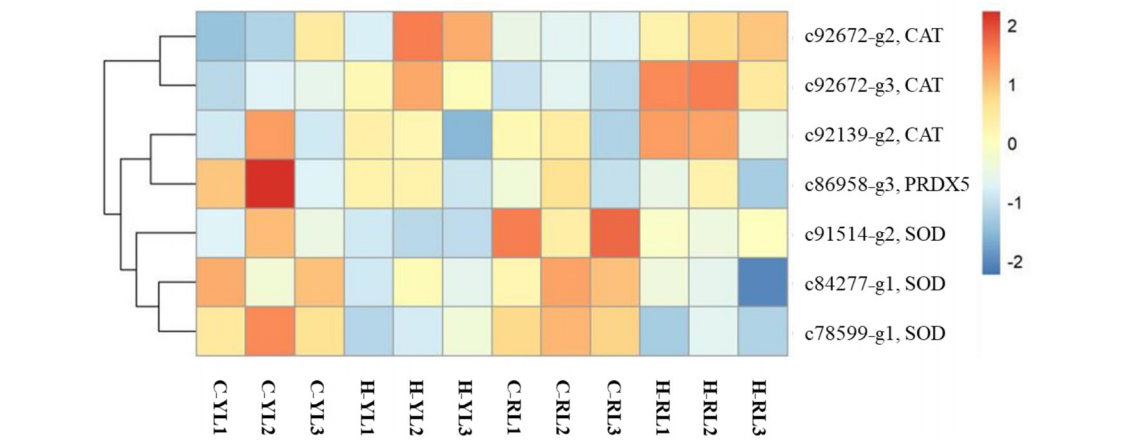

FIGURE 9 | Heatmap of differentially expressed antioxidant-related genes. CAT, catalase; SOD, superoxide dismutase; PRDX5, peroxiredoxin 5.

would be help to reduce the heat-damage more quickly in tolerant lines, which offered a more effective protection strategy.

Ubiquitin, Antioxidant-Related Genes and "Preadaptation"

Genes involved in the ubiquitin-mediated proteolysis pathway were considered as key transcription factors that respond to abiotic stresses, acting to clear irreparably damaged proteins (Glickman and Ciechanover, 2002; Kültz, 2005; Lyzenga and Stone, 2012). The up-regulation of genes involved in proteolysis has been reported in *Mytilus trossulus* (Lockwood et al., 2010), *Saccharina japonica* (Liu et al., 2015), and *Pyropia haitanensis* (Wang et al., 2018b). The RL and YL showed similar induction of many genes involved in this pathway. However, the less DEGs occurred in YL may also indicate these two lines endured

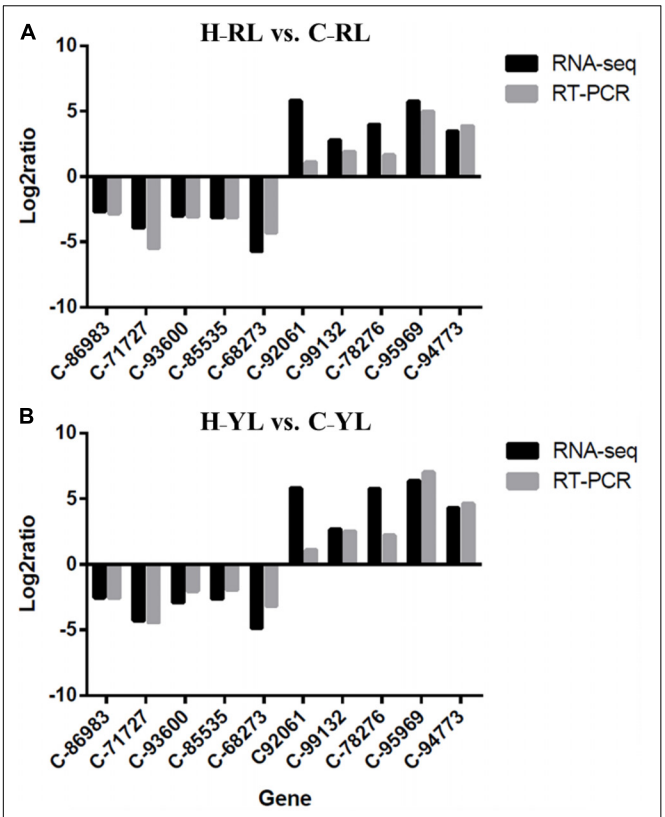

FIGURE 10 | Comparison of qRT-PCR and RNA-seq results. **(A)** H_RL vs. C_RL; **(B)** H_YL vs. C_YL.

different physiological stress. More irreparably damaged protein may be accumulated in RL. Therefore, for RL, more genes may be need to participate in this response that was helpful to transfer more ubiquitin to damaged protein and target them for degradation in time.

Heat stress can induce the overproduction of ROS (Abele et al., 2002; Heise et al., 2003; Yang et al., 2010; Cui et al., 2011). ROS are toxic to the cell as they cause damage to macromolecules (Kültz, 2005). Then, mitigating oxidative stress by increasing synthesis of antioxidants can increase thermal tolerance (Dilly et al., 2012). It has been demonstrated that the genes of antioxidant defense system were up regulated in the study of blue mussel (*M. galloprovincialis* and *M. trossulus*) (Lockwood et al., 2010), coral (*Acropora hyacinthus*) (Barshis et al., 2013), snail (*C. funebralis*) (Gleason and Burton, 2015) and *P. haitanensis* (Wang et al., 2018a). However, few genes related to antioxidant system could be annotated in this study (**Figure 9**). This might be explained by the stress exposure time. Wang et al. (2018b) found that the expression of antioxidant related genes showed gradual up-regulation with sustained high temperature in *P. haitanensis*. The significant fold changes were observed at 2- or 6-day time points. The heat stress last a total of 5.5 h in study of snail (*C. funebralis*) (Gleason and Burton, 2015) and it was more than 4 h in blue mussel (*M. galloprovincialis* and *M. trossulus*) (Lockwood et al., 2010). While, it was just 2 h in this study. Therefore, more stress time points were necessary for future studying the response of antioxidant system.

Besides acute responsiveness, the thermally tolerant snail (*C. funebralis*) individuals appeared to also utilize the "preadaptation" to cope with heat stress (Gleason and Burton, 2015). Some genes, including HSP60, partly of superoxide dismutase (SOD), glutathione peroxidase (GPx), and ubiquitin showed higher constitutive expression in tolerant populations and less up-regulated following heat stress compared with sensitive ones. While, as to these gene or related families, the higher constitutive expression was not found in the tolerant population (YL). Therefore, the preadaptation could not be the abalone's main strategy for coping with the heat stress. We speculated the better tolerance of YL may mostly rely on its precise coping strategy, which indicated by fine-tuning of transcirptome and stronger ability to regulate key genes.

TABLE 2 | Differentially expressed genes (DEGs) in cell cycle and DNA replication pathways.

Gene ID	Pathway	Log2 fold change		KO description
		H_RL vs. C_RL	H_YL vs. C_YL	
c68273_g1	Cell cycle	−5.7	−4.8	Cyclin A
c76770_g1	Cell cycle	−2.2	–	Polo-like kinase 1
c79314_g1	Cell cycle	−1.9	–	Anaphase-promoting complex subunit 12
c81134_g1	DNA replication	−2.2	–	Ribonuclease H2 subunit C
c86856_g2	DNA replication, cell cycle	−2.0	–	DNA replication licensing factor MCM6
c86983_g1	Cell cycle	−2.6	−2.5	Cyclin B
c88219_g1	DNA replication, cell cycle	–	−2.9	DNA replication licensing factor MCM3
c91413_g2	DNA replication	−1.8	–	Replication factor A2
c91496_g1	DNA replication, cell cycle	−1.8	–	DNA replication licensing factor MCM2
c93600_g1	DNA replication, cell cycle	−3.0	−2.9	DNA replication licensing factor MCM7
c94298_g1	DNA replication, cell cycle	−2.5	–	DNA replication licensing factor MCM5
c94298_g2	DNA replication, cell cycle	−3.1	−3.9	DNA replication licensing factor MCM5

C_RL, RL at control temperature; C_YL, YL at control temperature; H_RL, RL at heat stress temperature; H_YL, YL at heat stress temperature.

CONCLUSION

Our results suggest that the cardiac performance of thermally tolerant lines was less disrupted by high water temperatures stress. In addition, the heat-tolerant line employed a more effective strategy to cope with heat stress than the heat-sensitive line. This strategy included moderate changes in gene transcription and more effective regulation (such as more powerful to up-regulate the HSP family genes). Overall, our results provide insight into the different heat-response strategies employed by heat-tolerant and heat-sensitive abalone lines and these findings might provide some suggestions for further studies of heat-response mechanisms in mollusks. The key genes or pathways would be great indicator for our follow-up work. Combined these with the results with other studies, such as genome-wide association study (GWAS), would provide fundamental information for breeding of better heat-tolerant line.

ETHICS STATEMENT

The methods were carried out in accordance with the approved guidelines by Laboratory Animal Management and Ethics Committee of Xiamen University. All experimental procedures involving abalones were performed according to the Regulations for the Administration of Affairs Concerning Experimental Animals (Xiamen University, China; revised in November 2014).

AUTHOR CONTRIBUTIONS

CK and WY conceived and designed the experiments. NC, CL, and YS performed the experiments. NC and ZH analyzed the data. XL offered reagents and experiment animals. NC, CK, and WY wrote the manuscript. All authors has reviewed the manuscript.

FUNDING

This work was supported by grants from National Natural Science Foundation of China (Grant No. U1605213), Earmarked Fund for Modern Agro-Industry Technology Research System (Grant No. CARS-49), Key S & T Program of Fujian Province (Grant Nos. 2016NZ01010006 and 2016NZ0001-4), Shandong Province (Grant Nos. LJNY201709 and 2016GGH4513), Xiamen Southern Oceanographic Center (Grant No. 18GZY012HJ02), and China Postdoctoral Science Foundation (Grant No. 2017M622082).

SUPPLEMENTARY MATERIAL

The Supplementary Material for this article can be found online at: https://www.frontiersin.org/articles/10.3389/fphys.2018.01895/full#supplementary-material

REFERENCES

Abele, D., Heise, K., Portner, H. O., and Puntarulo, S. (2002). Temperature-dependence of mitochondrial function and production of reactive oxygen species in the intertidal mud clam *Mya arenaria*. *J. Exp. Biol.* 205, 1831–1841.

Alter, K., Andrewartha, S. J., Morash, A. J., Clark, T. D., Hellicar, A. D., Leon, R. I., et al. (2017). Hybrid abalone are more robust to multi-stressor environments than pure parental species. *Aquaculture* 478, 25–34. doi: 10.1016/j.aquaculture.2017.04.035

Altschul, S. F., Gish, W., Miller, W., Myers, E. W., and Lipman, D. J. (1990). Basic local alignment search tool. *J. Mol. Biol.* 215, 403–410. doi: 10.1016/S0022-2836(05)80360-2

Anders, S., and Huber, W. (2012). *Differential Expression of RNA-Seq Data at the Gene Level–the DESeq Package*. Heidelberg: European Molecular Biology Laboratory (EMBL).

Barshis, D. J., Ladner, J. T., Oliver, T. A., Seneca, F. O., Traylor-Knowles, N., and Palumbi, S. R. (2013). Genomic basis for coral resilience to climate change. *Proc. Natl. Acad. Sci. U.S.A.* 110, 1387–1392. doi: 10.1073/pnas.1210224110

Bita, C. E., Zenoni, S., Vriezen, W. H., Mariani, C., Pezzotti, M., and Gerats, T. (2011). Temperature stress differentially modulates transcription in meiotic anthers of heat-tolerant and heat-sensitive tomato plants. *BMC Genomics* 12:384. doi: 10.1186/1471-2164-12-384

Casselman, M. T., Anttila, K., and Farrell, A. P. (2012). Using maximum heart rate as a rapid screening tool to determine optimum temperature for aerobic scope in Pacific salmon *Oncorhynchus* spp. *J. Fish Biol.* 80, 358–377. doi: 10.1111/j.1095-8649.2011.03182.x

Chapman, R. W., Mancia, A., Beal, M., Veloso, A., Rathburn, C., and Blair, A. (2011). The transcriptome responses of the eastern oyster, *Crassostrea virginica*, to environmental conditions. *Mol. Ecol.* 20, 1431–1449. doi: 10.1111/j.1365-294X.2011.05018.x

Chelazzi, G., Williams, G. A., and Gray, D. R. (1999). Field and laboratory measurement of heart rate in a tropical limpet, *Cellana grata*. *J. Mar. Biol. Assoc. U.K.* 79, 749–751. doi: 10.1017/S0025315498000915

Chen, N., Luo, X., Gu, Y., Han, G., Dong, Y., You, W., et al. (2016). Assessment of the thermal tolerance of abalone based on cardiac performance in *Haliotis discus hannai*, *H. gigantea* and their interspecific hybrid. *Aquaculture* 465, 258–264. doi: 10.1016/j.aquaculture.2016.09.004

Chen, N., Luo, X., Lu, C., Ke, C., and You, W. (2017). Effects of artificial selection practices on loss of genetic diversity in the Pacific abalone, *Haliotis discus hannai*. *Aquac. Res.* 48, 4923–4933. doi: 10.1111/are.13311

Chen, Z., Farrell, A. P., Matala, A., and Narum, S. R. (2017). Mechanisms of thermal adaptation and evolutionary potential of conspecific populations to changing environments. *Mol. Ecol.* 27, 659–674. doi: 10.1111/mec.14475

Cheng, W., Hsiao, I. S., Hsu, C. H., and Chen, J. C. (2004). Change in water temperature on the immune response of Taiwan abalone *Haliotis diversicolor supertexta* and its susceptibility to *Vibrio parahaemolyticus*. *Fish Shellfish Immunol.* 17, 235–243. doi: 10.1016/j.fsi.2004.03.007

Choi, M., Kim, G., Kim, J., and Lim, H. K. (2015). Differentially-expressed genes associated with faster growth of the Pacific abalone, *Haliotis discus hannai*. *Int. J. Mol. Sci.* 16, 27520–27534. doi: 10.3390/ijms161126042

Clark, M. S., Fraser, K. P. P., and Peck, L. S. (2008). Lack of an HSP70 heat shock response in two Antarctic marine invertebrates. *Polar Biol.* 31, 1059–1065. doi: 10.1007/s12192-008-0014-8

Cui, Y., Du, Y., Lu, M., and Qiang, C. (2011). Antioxidant responses of *Chilo suppressalis* (Lepidoptera: Pyralidae) larvae exposed to thermal stress. *J. Therm. Biol.* 36, 292–297. doi: 10.1016/j.jtherbio.2011.04.003

Dang, V. T., Speck, P., and Benkendorff, K. (2012). Influence of elevated temperature on the immune response of abalone, *Haliotis rubra*. *Fish Shellfish Immunol.* 32, 732–740. doi: 10.1016/j.fsi.2012.01.022

Deng, Y. W., Liu, X., Wu, F. C., and Zhang, G. F. (2008). Experimental evaluation of heterobeltiosis and heterosis between two populations of Pacific abalone. *Acta Oceanol. Sin.* 27, 112–119.

Depledge, M. H., and Andersen, B. B. (1990). A computer-aided physiological monitoring-system for continuous, long-term recording of cardiac activity in selected invertebrates. *Comp. Biochem. Physiol. Part A Physiol.* 96, 473–477. doi: 10.1016/0300-9629(90)90664-E

Dilly, G. F., Young, C. R., Lane, W. S., Pangilinan, J., and Girguis, P. R. (2012). Exploring the limit of metazoan thermal tolerance via comparative proteomics: thermally induced changes in protein abundance by two hydrothermal vent polychaetes. *Proc. R. Soc. B* 279, 3347–3356. doi: 10.1098/rspb.2012.0098

Dong, Y. W., and Williams, G. A. (2011). Variations in cardiac performance and heat shock protein expression to thermal stress in two differently zoned limpets on a tropical rocky shore. *Mar. Biol.* 158, 1223–1231. doi: 10.1007/s00227-011-1642-6

Evans, T. G. (2015). Considerations for the use of transcriptomics in identifying the 'genes that matter' for environmental adaptation. *J. Exp. Biol.* 218, 1925–1935. doi: 10.1242/jeb.114306

Farcy, E., Serpentini, A., Fievet, B., and Lebel, J. M. (2007). Identification of cDNAs encoding HSP70 and HSP90 in the abalone *Haliotis tuberculata*: transcriptional induction in response to thermal stress in hemocyte primary culture. *Comp. Biochem. Physiol. Part B Biochem. Mol. Biol.* 146, 540–550. doi: 10.1016/j.cbpb.2006.12.006

Franchini, P., van der Merve, M., and Roodt-Wilding, R. (2011). Transcriptome characterization of the South African abalone *Haliotis midae* using sequencing-by-synthesis. *BMC Res. Notes* 4:59. doi: 10.1186/1756-0500-4-59

Gebauer, M., Zeiner, M., and Gehring, U. (1997). Proteins interacting with the molecular chaperone hsp70/hsc70: physical associations and effects on refolding activity. *FEBS Lett.* 417, 109–113. doi: 10.1016/S0014-5793(97)01267-2

Genevaux, P., Georgopoulos, C., and Kelley, W. L. (2007). The hsp70 chaperone machines of *Escherichia coli*: a paradigm for the repartition of chaperone functions. *Mol. Microbiol.* 66, 840–857. doi: 10.1111/j.1365-2958.2007.05961.x

Gleason, L. U., and Burton, R. S. (2015). RNA-seq reveals regional differences in transcriptome response to heat stress in the marine snail *Chlorostoma funebralis*. *Mol. Ecol.* 24, 610–627. doi: 10.1111/mec.13047

Glickman, M. H., and Ciechanover, A. (2002). The ubiquitin-proteasome proteolytic pathway: destruction for the sake of construction. *Physiol. Rev.* 82, 373–428. doi: 10.1152/physrev.00027.2001

Götz, S., García-Gómez, J. M., Terol, J., Williams, T. D., Nagaraj, S. H., Nueda, M. J., et al. (2008). High-throughput functional annotation and data mining with the Blast2GO suite. *Nucleic Acids Res.* 36, 3420–3435. doi: 10.1093/nar/gkn176

Grabherr, M. G., Haas, B. J., Yassour, M., Levin, J. Z., Thompson, D. A., Amit, I., et al. (2011). Full-length transcriptome assembly from RNA-Seq data without a reference genome. *Nat. Biotechnol.* 29, 644–652. doi: 10.1038/nbt.1883

Guo, X. M., Ford, S. E., and Zhang, F. S. (1999). Molluscan aquaculture in China. *J. Shellfish Res.* 18, 19–31.

Guo, Y. F., and Zhao, W. W. (2017). *China Fishery Statistical Yearbook, 2017*. Beijing: China agriculture press.

Hamburger, K., Dall, P. C., and Lindegaard, C. (1994). Energy metabolism of *Chironomus anthracinus* (Diptera: Chironomidae) from the profundal zone of Lake Esrom, Denmark, as a function of body size, temperature and oxygen concentration. *Hydrobiologia* 294, 43–50. doi: 10.1007/BF00017624

Han, G. D., Zhang, S., Marshall, D. J., Ke, C. H., and Dong, Y. W. (2013). Metabolic energy sensors (AMPK and SIRT1), protein carbonylation and cardiac failure as biomarkers of thermal stress in an intertidal limpet: linking energetic allocation with environmental temperature during aerial emersion. *J. Exp. Biol.* 216, 3273–3282. doi: 10.1242/jeb.084269

Harney, E., Dubief, B., Boudry, P., Basuyaux, O., Schilhabel, M. B., Huchette, S., et al. (2016). *De novo* assembly and annotation of the European abalone *Haliotis tuberculata* transcriptome. *Mar. Genomics* 28, 11–16. doi: 10.1016/j.margen.2016.03.002

Heise, K., Puntarulo, S., Portner, H. O., and Abele, D. (2003). Production of reactive oxygen species by isolated mitochondria of the Antarctic bivalve *Laternula elliptica* (King and Broderip) under heat stress. *Comp. Biochem. Physiol. Part C Toxicol. Pharmacol.* 134, 79–90. doi: 10.1016/S1532-0456(02)00212-0

Hereford, J. (2009). A quantitative survey of local adaptation and fitness trade-offs. *Am. Nat.* 173, 579–588. doi: 10.1086/597611

Hoegh-Guldberg, O., and Bruno, J. F. (2010). The impact of climate change on the world's marine ecosystems. *Science* 328, 1523–1528. doi: 10.1126/science.1189930

Jonas, K., Liu, J., Chien, P., and Laub, M. T. (2013). Proteotoxic stress induces a cell-cycle arrest by stimulating lon to degrade the replication initiator DnaA. *Cell* 154, 623–636. doi: 10.1016/j.cell.2013.06.034

Kültz, D. (2005). Molecular and evolutionary basis of the cellular stress response. *Annu. Rev. Physiol.* 67, 225–257. doi: 10.1146/annurev.physiol.67.040403.103635

Lang, R. P., Bayne, D. J., Camara, M. D., Cunningham, C., Jenny, M. J., and Langdon, C. J. (2009). Transcriptome profiling of selectively bred Pacific oyster *Crassostrea gigas* families that differ in tolerance of heat shock. *Mar. Biotechnol.* 11, 650–668. doi: 10.1007/s10126-009-9181-6

Li, B., and Dewey, C. N. (2011). RSEM: accurate transcript quantification from RNA-Seq data with or without a reference genome. *BMC Bioinformatics* 12:323. doi: 10.1186/1471-2105-12-323

Li, J., He, Q., Sun, H., and Liu, X. (2012). Acclimation-dependent expression of heat shock protein 70 in Pacific abalone (*Haliotis discus hannai* Ino) and its acute response to thermal exposure. *Chin. J. Oceanol. Limnol.* 30, 146–151. doi: 10.1007/s00343-012-1026-x

Li, W., Rong, R., Zhao, S., Zhu, X., Zhang, K., Xiong, X., et al. (2012). Proteomic analysis of metabolic, cytoskeletal and stress response proteins in human heart failure. *J. Cell. Mol. Med.* 16, 59–71. doi: 10.1111/j.1582-4934.2011.01336.x

Li, Q., Shu, J., Yu, R., and Tian, C. (2007). Genetic variability of cultured populations of the Pacific abalone (*Haliotis discus hannai* Ino) in China based on microsatellites. *Aquac. Res.* 38, 981–990. doi: 10.1111/j.1365-2109.2007.01764.x

Liang, S., Luo, X., You, W., Luo, L., and Ke, C. (2014). The role of hybridization in improving the immune response and thermal tolerance of abalone. *Fish Shellfish Immunol.* 39, 69–77. doi: 10.1016/j.fsi.2014.04.014

Liu, F., Wang, W., Sun, X., Liang, Z., and Wang, F. (2015). Conserved and novel heat stress-responsive microRNAs were identified by deep sequencing in *Saccharina japonica* (Laminariales, Phaeophyta). *Plant Cell Environ.* 38, 1357–1367. doi: 10.1111/pce.12484

Lockwood, B. L., Sanders, J. G., and Somero, G. N. (2010). Transcriptomic response to heat stress in invasive and native blue mussels (genus *Mytilus*): molecular correlates of invasive success. *J. Exp. Biol.* 213, 3548–3558. doi: 10.1242/jeb.046094

Lyzenga, W. J., and Stone, S. L. (2012). Abiotic stress tolerance mediated by protein ubiquitination. *J. Exp. Bot.* 63, 599–616. doi: 10.1093/jxb/err310

Mao, X., Cai, T., Olyarchuk, J. G., and Wei, L. (2005). Automated genome annotation and pathway identification using the KEGG Orthology (KO) as a controlled vocabulary. *Bioinformatics* 21, 3787–3793. doi: 10.1093/bioinformatics/bti430

Martin, J. A., and Wang, Z. (2011). Next-generation transcriptome assembly. *Nat. Rev. Genet.* 12, 671–682. doi: 10.1038/nrg3068

Mayer, M. P. (2013). Hsp70 chaperone dynamics and molecular mechanism. *Trends Biochem. Sci.* 38, 507–514. doi: 10.1016/j.tibs.2013.08.001

Misselwitz, B., Staeck, O., and Rapoport, T. A. (1998). J proteins catalytically activate hsp70 molecules to trap a wide range of peptide sequences. *Mol. Cell* 2, 593–603. doi: 10.1016/S1097-2765(00)80158-6

Morash, A., and Alter, K. (2015). Effects of environmental and farm stress on abalone physiology: perspectives for abalone aquaculture in the face of global climate change. *Rev. Aquac.* 7, 1–27.

Moriya, Y., Itoh, M., Okuda, S., Yoshizawa, A. C., and Kanehisa, M. (2007). KAAS: an automatic genome annotation and pathway reconstruction server. *Nucleic Acids Res.* 35, W182–W185. doi: 10.1093/nar/gkm321

North, A., Pennanen, J., Ovaskainen, O., and Laine, A. L. (2011). Local adaptation in a changing world: the roles of gene-flow, mutation, and sexual reproduction. *Evolution* 65, 79–89. doi: 10.1111/j.1558-5646.2010.01107.x

Picone, B., Rhode, C., and Roodt-Wilding, R. (2015). Transcriptome profiles of wild and cultured South African abalone, *Haliotis midae*. *Mar. Genomics* 20, 3–6. doi: 10.1016/j.margen.2015.01.002

Portner, H. O. (2010). Oxygen- and capacity-limitation of thermal tolerance: a matrix for integrating climate-related stressor effects in marine ecosystems. *J. Exp. Biol.* 213, 881–893. doi: 10.1242/jeb.037523

Portner, H. O., Bennett, A. F., Bozinovic, F., Clark, A., Lardies, M. A., Lucassen, M., et al. (2006). Trade-offs in thermal adaptation: the need for a molecular to ecological integration. *Physiol. Biochem. Zool.* 79, 295–313. doi: 10.1086/499986

Portner, H. O., and Knust, R. (2007). Climate change affects marine fishes through the oxygen limitation of thermal tolerance. *Science* 315, 95–97. doi: 10.1126/science.1135471

Schoville, S. D., Barreto, F. S., Moy, G. W., Wolff, A., and Burton, R. S. (2012). Investigating the molecular basis of local adaptation to thermal stress: population differences in gene expression across the transcriptome of the copepod *Tigriopus californicus*. *BMC Evol. Biol.* 12:170. doi: 10.1186/1471-2148-12-170

Shiel, B. P., Hall, N. E., Cooke, I. R., Robinson, N. A., and Strugnell, J. M. (2015). De novo characterization of the greenlip abalone transcriptome (*Haliotis laevigata*) with a focus on the heat shock protein 70 (HSP70) family. *Mar. Biotechnol.* 17, 23–32. doi: 10.1007/s10126-014-9591-y

Shiel, B. P., Hall, N. E., Cooke, I. R., Robinson, N. A., and Strugnell, J. M. (2017). Epipodial tentacle gene expression and predetermined resilience to summer mortality in the commercially important greenlip abalone, *Haliotis laevigata*. *Mar. Biotechnol.* 19, 191–205. doi: 10.1007/s10126-017-9742-z

Snyder, M., Girvetz, E., and Mulder, E. (2001). Induction of marine mollusk stress proteins by chemical or physical stress. *Arch. Environ. Contam. Toxicol.* 41, 22–29. doi: 10.1007/s002440010217

Somero, G. N. (2012). The physiology of global change: linking patterns to mechanisms. *Annu. Rev. Mar. Sci.* 4, 39–61. doi: 10.1146/annurev-marine-120710-100935

Stenseng, E., Braby, C. E., and Somero, G. N. (2005). Evolutionary and acclimation-induced variation in the thermal limits of heart function in congeneric marine snails (Genus *Tegula*): implications for vertical zonation. *Biol. Bull.* 208, 138–144. doi: 10.2307/3593122

Stillman, J., and Somero, G. (1996). Adaptation to temperature stress and aerial exposure in congeneric species of intertidal porcelain crabs (genus *Petrolisthes*): correlation of physiology, biochemistry and morphology with vertical distribution. *J. Exp. Biol.* 199, 1845–1855.

Terada, K., Kanazawa, M., Bukau, B., and Mori, M. (1997). The human DnaJ homologue dj2 facilitates mitochondrial protein import and luciferase refolding. *J. Cell Biol.* 139, 1089–1095. doi: 10.1083/jcb.139.5.1089

Valenzuela-Miranda, D., Del Rio-Portilla, M., and Gallardo-Escarate, C. (2015). Characterization of the growth-related transcriptome in California red abalone (*Haliotis rufescens*) through RNA-Seq analysis. *Mar. Genomics* 24, 199–202. doi: 10.1016/j.margen.2015.05.009

Valenzuela-Munoz, V., Araya-Garay, J. M., and Gallardo-Escarate, C. (2013). SNP discovery and high resolution melting analysis from massive transcriptome sequencing in the California red abalone *Haliotis rufescens*. *Mar. Genomics* 10, 11–16. doi: 10.1016/j.margen.2012.12.003

van der Merwe, M., Franchini, P., and Roodt-Wilding, R. (2011). Differential growth-related gene expression in abalone (*Haliotis midae*). *Mar. Biotechnol.* 13, 1125–1139. doi: 10.1007/s10126-011-9376-5

Vaquer-Sunyer, R., and Duarte, C. M. (2011). Temperature effects on oxygen thresholds for hypoxia in marine benthic organisms. *Glob. Change Biol.* 17, 1788–1797. doi: 10.1111/j.1365-2486.2010.02343.x

Wang, W., Lin, Y., Teng, F., Ji, D., Xu, Y., Chen, C., et al. (2018a). Comparative transcriptome analysis between heat-tolerant and sensitive *Pyropia haitanensis* strains in response to high temperature stress. *Algal Res.* 29, 104–112. doi: 10.1016/j.algal.2017.11.026

Wang, W., Teng, F., Lin, Y., Ji, D., Xu, Y., Chen, C., et al. (2018b). Transcriptomic study to understand thermal adaptation in a high temperature-tolerant strain of *Pyropia haitanensis*. *PLoS One* 13:e0195842. doi: 10.1371/journal.pone.0195842

Wit, P., and Palumbi, S. R. (2013). Transcriptome-wide polymorphisms of red abalone (*Haliotis rufescens*) reveal patterns of gene flow and local adaptation. *Mol. Ecol.* 22, 2884–2897. doi: 10.1111/mec.12081

Xing, Q., Li, Y., Guo, H., Yu, Q., Huang, X., Wang, S., et al. (2016). Cardiac performance: a thermal tolerance indicator in scallops. *Mar. Biol.* 163:244. doi: 10.1007/s00227-016-3021-9

Yang, L., Huang, H., and Wang, J. (2010). Antioxidant responses of citrus red mite, *Panonychus citri* (McGregor) (Acari: Tetranychidae), exposed to thermal stress. *J. Insect Physiol.* 56, 1871–1876. doi: 10.1016/j.jinsphys.2010.08.006

Young, M. D., Wakefield, M. J., Smyth, G. K., and Oshlack, A. (2010). Gene ontology analysis for RNA-seq: accounting for selection bias. *Genome Biol.* 11:R14. doi: 10.1186/gb-2010-11-2-r14

Zhao, L., and Jones, W. (2012). Expression of heat shock protein genes in insect stress responses. *Invertebrate Surviv. J.* 9, 93–101.

Conflict of Interest Statement: The authors declare that the research was conducted in the absence of any commercial or financial relationships that could be construed as a potential conflict of interest.

frontiers in Physiology

ORIGINAL RESEARCH
published: 22 March 2019
doi: 10.3389/fphys.2019.00293

Development of Novel Cardiac Indices and Assessment of Factors Affecting Cardiac Activity in a Bivalve Mollusc *Chlamys farreri*

Qiang Xing[1,2†], Lingling Zhang[1,2†], Yuqiang Li[1], Xinghai Zhu[1], Yangping Li[1], Haobing Guo[1], Zhenmin Bao[1,3] and Shi Wang[1,2]*

[1] MOE Key Laboratory of Marine Genetics and Breeding, College of Marine Life Sciences, Ocean University of China, Qingdao, China, [2] Laboratory for Marine Biology and Biotechnology, Qingdao National Laboratory for Marine Science and Technology, Qingdao, China, [3] Laboratory for Marine Fisheries Science and Food Production Processes, Qingdao National Laboratory for Marine Science and Technology, Qingdao, China

OPEN ACCESS

Edited by:
Xiaotong Wang,
Ludong University, China

Reviewed by:
Xiaoxu Li,
South Australian Research and Development Institute, Australia
Yun-wei Dong,
Xiamen University, China

***Correspondence:**
Shi Wang
swang@ouc.edu.cn

[†] These authors have contributed equally to this work

Specialty section:
This article was submitted to Aquatic Physiology, a section of the journal Frontiers in Physiology

Received: 13 August 2018
Accepted: 06 March 2019
Published: 22 March 2019

Citation:
Xing Q, Zhang L, Li Y, Zhu X, Li Y, Guo H, Bao Z and Wang S (2019) Development of Novel Cardiac Indices and Assessment of Factors Affecting Cardiac Activity in a Bivalve Mollusc Chlamys farreri. Front. Physiol. 10:293. doi: 10.3389/fphys.2019.00293

Cardiac activity has been widely used in marine molluscs as an indicator for their physiological status in response to environmental changes, which is, however, largely less studied in scallops. Here, we monitored cardiac performance of Zhikong scallop *Chlamys farreri* using an infrared-based method, and evaluated the effects of several biotic (shell height, total weight, and age) and environmental factors (circadian rhythm and temperature) on scallop heart rate (HR), amplitude (HA), and rate-amplitude product (RAP). Results revealed that size has a significant effect on both HR (negative) and HA (positive), but RAP values are similar in different sized scallops. Age also affects scallop cardiac performance, significantly for HR, but not for HA or RAP. Circadian rhythm affects cardiac activity, with significant elevation of HR, HA and RAP during 1:00–8:00 and 17:00–19:00. With seawater temperature elevation, HR peaks at 30.03 ± 0.23°C, HA at 15.08 ± 0.02°C, and RAP at 15.10 ± 0.19 and 30.12 ± 0.28°C. This suggests HR is a good indicator for thermal limit, whereas HA may indicate optimal growth temperature, and RAP could be an index of myocardial oxygen consumption to indicate myocardium stress. Our study provides basic information on the factors that may affect scallop cardiac performance. It also elucidates the feasibility of HA and RAP as cardiac indices in marine molluscs.

Keywords: scallop, heart rate, heart amplitude, rate-amplitude product, physiological trait

INTRODUCTION

Cardiovascular function conveys important information about whether an organism will survive, and how well they adapt to external environments. As an important parameter of cardiac activity, heart rate (HR) is widely used in vertebrates for evaluating physiological status. For example, HR is an independent predictor of cardiovascular and overall mortality in human (Caetano and Delgado, 2015). In Atlantic cod *Gadus morhua*, HR is also an important indicator for evaluating influences of short-term and prolonged exposure to hypoxia (Petersen and Gamperl, 2010). Similarly in invertebrates, such as Arthropoda (Wilkens et al., 1974; Bamber and Depledge, 1997;

Frederich and Pörtner, 2000) and Mollusca (Stenseng and Braby, 2005; Dong and Williams, 2011; Xing et al., 2016), HR is widely applied to study the cardiac responses to various environmental factors, including temperature, salinity, heavy metals, as well as oil contamination. For instance, the changing pattern of HR during temperature challenge has been extensively studied in marine molluscs (Widdows, 1973; Dong and Williams, 2011; Xing et al., 2016), suggesting HR is a good indicator of thermal limits in these animals. Effect of salinity fluctuations on HR of *Hiatella arctica* and *Modiolus modiolus* reveals a significant HR reduction in the initial response to salinity change, and different HR responses during reacclimation depending on the species and salinities (Bakhmet et al., 2012). The impact of heavy metals on organisms can also be investigated by recording the changes of HR. Exposure to copper results in the decay of HR as a function of copper concentration in blue mussel *Mytilus edulis* (Curtis et al., 2000), and bradycardia was observed in limpet *Patella vulgata* exposed to copper and zinc (Marchan et al., 1999). Fluctuations of HR in blue mussels under varying oil product concentrations also reflect the impact of oil contamination on bivalve bioindicators (Bakhmet et al., 2008). All these above indicate that HR is a stable cardiac parameter widely used in vertebrates and invertebrates.

Except for the environmental factors, some biotic factors such as body size, age, and gender also influence cardiac performance. In crustacean *Carcinus maenas*, HR is dependent on body size, with small crabs having a faster HR than the large ones (Ahsanullah and Newell, 1971). Similarly, a significantly negative relationship between HR and shell length was observed in limpet *Patella vulgate* (Santini et al., 2000). In cockroach *Gromphadorhina portentosa*, HR also scales negatively with body size (Streicher et al., 2012). Besides, decline in HR with age was found in human, and gender has a significant effect on HR at age <50 years (Umetani et al., 1998). Consequently, a systematic evaluation on the effects of environmental factors as well as biotic factors on cardiac activity will assist in a better understanding of the physiological status of the organisms investigated.

Based on the in-depth investigation on human electrocardiogram (ECG), there are other parameters besides HR in the ECG which can also provide valuable information on cardiac activity. For example, amplitudes of the P-QRS-T waves represent the variation in membrane potential during the depolarization or repolarization of different pumping chambers. There are also PR interval which reflects conduction through the atrioventricular node, and QT interval that represents the time taken for ventricular depolarization and repolarization. Most importantly, these parameters have been widely used in the clinical diagnosis of various cardiovascular diseases. In contrast, previous studies on cardiac performance in molluscs generally focus on HR, which may provide incomplete information on their cardiac activity.

Bivalves, including clams, oysters, mussels, and scallops, are a large group of molluscs consisting of ∼14,000 species worldwide (Appeltans et al., 2012). They can accumulate different contaminants from ambient water and therefore serve as bioindicators. In addition, some bivalves are of commercial importance, such as Pacific oyster *Crassostrea gigas*, Zhikong scallop *Chlamys farreri*, and Yesso scallop *Patinopecten yessoensis*. Considering their ecological and economic importance, study on the cardiac activity in these animals could benefit ecological surveys as well as aquacultural industry. In this study, we measured the cardiac performance of Zhikong scallop and examined the effects of several biotic factors (shell height, total weight, and age) and environmental factors (temperature and circadian rhythm) on cardiac parameters – heart rate (HR), amplitude (HA), and rate-amplitude product (RAP). It should facilitate a better understanding on the scallops' physiological status under different conditions.

MATERIALS AND METHODS

Specimens Collection and Acclimation

All Zhikong scallops used in present study were collected from artificial scallop-rearing substrates installed in Xunshan Fishery Group Co., Rongcheng (37°17′18 N, 122°57′56 E).

For the study of size effect, 96 24-month-old healthy scallops with shell height varying from 40.25 to 67.02 mm and total weight ranging from 42.39 to 67.81 g, were collected, respectively. For the study of age effect, scallops with similar shell height (40.53 ± 2.87 mm) were collected for each age group (12-, 18-, and 24-month-old, >=24 specimens for each group) to avoid the interference of size factor. For the study of temperature effect, 24 scallops with similar shell height (48.69 ± 1.91 mm) were collected. For the study of circadian rhythm effect, 48 24-month-old scallops (24 as control group and 24 as treatment group) with similar shell height (52.53 ± 2.62 mm) were collected. To prevent potential genetic effect on the experiments, all individuals were sampled from a pool of various geographical populations including Yantai (37°55′06 N, 120°45′27 E), Weihai (37°17′18 N, 122°57′56 E), and Qingdao (36°06′25 N, 120°32′52 E and 35°57′39 N, 120°16′25 E).

After sample collection, encrusted organisms on scallop shells were removed. The scallops were placed in plastic tanks with filtered and aerated seawater at 15°C for 7 days for acclimation (Bakhmet et al., 2005). To avoid tank effects, all scallops were randomly maintained in several plastic tanks. The water was partially replaced on a daily basis. The animals were maintained without feeding to avoid specific dynamic action. Our experiments were conducted according to the guidelines and regulations established by the Ocean University of China and the local government.

Cardiac Performance Monitoring

Cardiac performance was monitored by the non-invasive method improved from the technique of Depledge and Andersen (1990). The monitor apparatuses mainly consist of CNY-70 (Newshift, Lisbon, Portugal), AMP 03 amplifier (Newshift, Lisbon, Portugal) and PowerLab 8/35 portable digital recording instrument (ADInstruments, Sydney, NSW, Australia), for signal obtaining, amplifying and recording, respectively. Consecutive cardiac activity waves were recorded using the LabChart software (ADInstruments, Sydney, NSW, Australia).

To detect the effects of size and age on cardiac performance, scallops were maintained at 15°C which is within the optimum

temperature range for their growth (14–22°C) (Yu et al., 2010). To investigate the effects of temperature on cardiac performance, scallops were kept in a 5 L beaker immersed in a water bath, allowing the temperature in the beaker to be increased from 5 to 37°C at a rate of 0.2°C per min. To detect the effects of circadian rhythm on cardiac performance, all scallops were kept at 15°C, with the control group being maintained under natural light (a light:dark period of 12 h:12 h), and the experimental group being kept in a darkroom.

Data Analysis

The heart rate (HR) was counted in beats per min (bpm) (Curtis et al., 2000), and the heart amplitude (HA) representing the peak values of ventricular contraction was calculated in voltage (V). RAP was calculated as HR times HA (bpm*V). For examining the effects of size on cardiac performance, a regression analysis was performed. To detect the effect of age on cardiac performance, one-way ANOVA was conducted followed by Duncan's test. The HR/HA/RAP increment rate with temperature was obtained for each individual by regression analysis. To compare the differences in HR/HA/RAP between control and experimental groups under circadian rhythm influence, independent sample *t*-tests were performed. Differences and correlations were considered significant when $P < 0.05$. All data were analyzed using SPSS 21.0 (IBM Corp., Armonk, NY, United States).

RESULTS

Effects of Size and Age on Cardiac Performance

We first evaluated the effects of size, including shell height and total weight on scallop cardiac performance. As shown in **Figures 1A,B**, scallops with shell height of 40.25–67.02 mm have an HR ranging between 19.39 and 27.12 bpm, and HA varying from 1.43 to 2.42 V. The average HR and HA are 22.50 bpm and 1.89 V, respectively. Interestingly, shell height decreases with HR ($r = -0.85$, $P < 0.001$), but increases with HA ($r = 0.79$, $P < 0.001$). The effects of total weight on cardiac performance are similar to that of shell height, with the correlation coefficient of −0.80 ($P < 0.001$) and 0.80 ($P < 0.001$) with HR and HA, respectively (**Figures 1C,D**). The above results suggest that size does affect scallop cardiac performance, and smaller scallops tend to have faster HR but lower HA. Further investigation was conducted on the relationship between size and RAP. As shown in **Figures 1E,F**, there is no significant correlation between them, indicating that scallops with different shell height and total weight tend to have similar levels of RAP. The average RAP is 42.34 ± 0.41 bpm*V for scallops with shell height ranging from 40.25 to 67.02 mm and 43.91 ± 0.38 bpm*V for scallops with total weight between 42.39 and 67.81 g, respectively.

We further examined variation of cardiac performance with scallop age. As shown in **Figure 2A**, HR of 12-, 18-, and 24-month-old Zhikong scallops are 22.08 ± 0.33, 23.11 ± 0.24, and 24.60 ± 0.27 bpm, respectively. The difference among age groups is significant [one-way ANOVA, $F_{(2,69)} = 20.229$, $P < 0.001$], suggesting older scallops have relatively faster HR. But age has no significant effect on HA [one-way ANOVA, $F_{(2,69)} = 0.061$, $P = 0.941$] (**Figure 2B**) or RAP [one-way ANOVA, $F_{(2,69)} = 1.986$, $P = 0.145$] (**Figure 2C**).

Effects of Seawater Temperature on Cardiac Performance

We then examined the changes in cardiac performance when temperature elevated from 5 to 37°C. As shown in **Figure 3A**, temperature has a significant effect on scallop HR. HR first increased with the elevation of temperature and the average increasing rate was 1.73 ± 0.04 bpm/°C. After reaching the peak (54.95 ± 4.27 bpm) at 30.03 ± 0.23°C, HR abruptly decreased down to an average of less than 10 bpm at 34°C, with a decreasing rate of 11.73 ± 0.35 bpm/°C. The single peak pattern was also observed in the response of HA to temperature elevation (**Figure 3B**). According to our data, significantly ($P < 0.05$) higher HA was found from 12 to 16°C, with the maximal HA (1.70 ± 0.02 V) at 15.08 ± 0.02°C. Before the peak, HA increased gradually with an average rate of 0.04 V/°C. Afterward, HA decreased abruptly at the rate of 0.10–17 V/°C, and then declined moderately at 0.01 V/°C until 37°C. **Figure 3C** showed the changes in RAP with temperature elevation. RAP increased with temperature elevation, reaching the first peak (40.01 ± 1.03 bpm*V) at 15.10 ± 0.19°C with an average increasing rate of 2.42 ± 0.07 bpm*V/°C, and the second peak (76.38 ± 4.27 bpm*V) at 30.12 ± 0.28°C with the rate of 2.42 ± 0.13 bpm*V/°C. Afterward, RAP decreased sharply down to less than 10 bpm*V at 34°C, with the rate of 16.36 ± 0.52 bpm*V/°C.

During temperature elevation, we observed various plethysmogram patterns (**Figure 4**). In contrast to the normal cardiac plethysmogram at 15°C (**Figure 4A**), most scallops showed bradycardia with HR as low as 7.06 bpm when submerged at a low temperature (5°C) (**Figure 4B**). When environmental temperature increased to 28°C, temporary cardiac arrest occurred (**Figure 4C**, blue arrow). At 29°C, strong fluctuation with irregular signals was observed (**Figure 4D**). At extremely high temperature (32°C), obvious decrease in HA until disappearance was seen, indicating occurrence of permanent cardiac arrest (**Figure 4E**). But if scallops promptly returned to the control temperature (15°C), heart beat resumed quickly (**Figure 4F**). Although the plethysmogram pattern seemed different from the normal pattern (**Figure 4A**), we assume it represents the recovery of cardiac activity from severe environments. The various plethysmograms recorded at different temperatures indicate that temperature has significant effect on cardiac activity of ectothermic marine bivalve.

Effect of Circadian Rhythm on Cardiac Performance

The effect of circadian rhythm on cardiac performance was also evaluated. As displayed in **Figure 5**, an average of 22.78 ± 0.27 bpm in HR, 1.81 ± 0.02 V in HA and

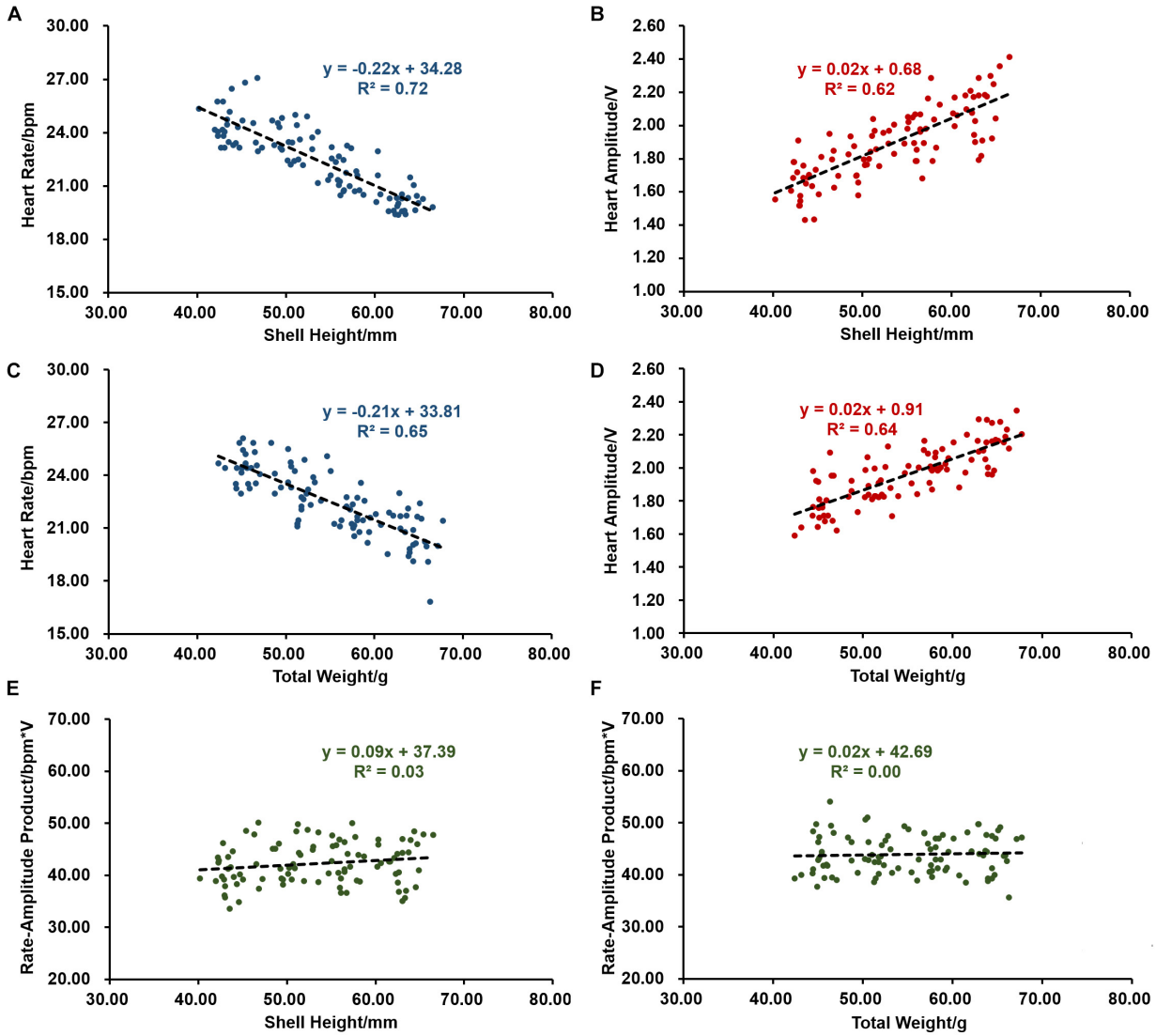

FIGURE 1 | The effects of size on cardiac activity (N = 96). **(A)** The negative correlation between heart rate (HR) and shell height. **(B)** The positive correlation between heart amplitude (HA) and shell height. **(C)** The negative correlation between HR and total weight. **(D)** The positive correlation between HA and total weight. **(E)** Correlation between rate-amplitude product (RAP) and shell height. **(F)** Correlation between RAP and total weight.

41.21 ± 1.66 bpm*V in RAP were recorded in the experimental group that constantly kept in the dark, and there is no significant difference in either HR, HA, or RAP during the 24 h period. In contrast, HR, HA, and RAP showed marked changes when scallops were exposed to natural light. Significantly higher HR was recorded during 1:00–8:00, with HR ranging from 27.16 ± 0.96 to 30.54 ± 0.80 bpm. Correspondingly, we found HA and RAP were significantly higher during this period, with the values ranging from 1.98 ± 0.03 to 2.37 ± 0.03 V, and 53.77 ± 3.52 to 72.37 ± 2.86 bpm*V, respectively. There is another small peak during 17:00–19:00 in HR, HA and RAP curves, with the maximal value of 29.35 ± 1.65 bpm in HR, 2.30 ± 0.05 V in HA, and 67.51 ± 6.14 bpm*V in RAP at 18:00. The above results suggest circadian rhythm has a significant effect on scallop cardiac activity, and HR and HA exhibit coordinate changes under natural light.

DISCUSSION

Research on cardiac performance has been widely conducted in marine molluscs, such as limpets (Pirro et al., 1999; Santini et al., 2000; Dong and Williams, 2011) mussels (Widdows, 1973; Bakhmet et al., 2005, 2008), oyster (Park et al., 2004) and clams (Taylor, 1976; Bakhmet et al., 2012). It has been demonstrated that mollusc cardiac performance can be affected by many factors, such as body size (Santini et al., 2000), environmental temperature (Widdows, 1973; Santini et al., 2000;

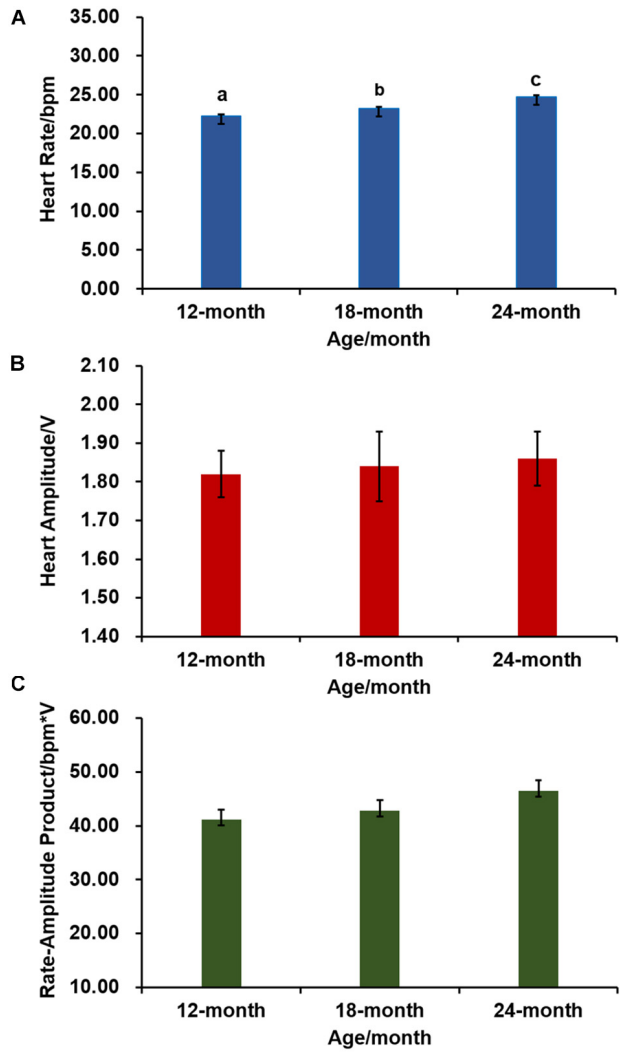

FIGURE 2 | The effect of age on cardiac activity (N = 24 for each group). **(A)** HR of Zhikong scallops with different ages. Different letters indicate significant differences ($P < 0.05$). **(B)** HA of Zhikong scallops with different ages. **(C)** RAP of Zhikong scallops with different ages.

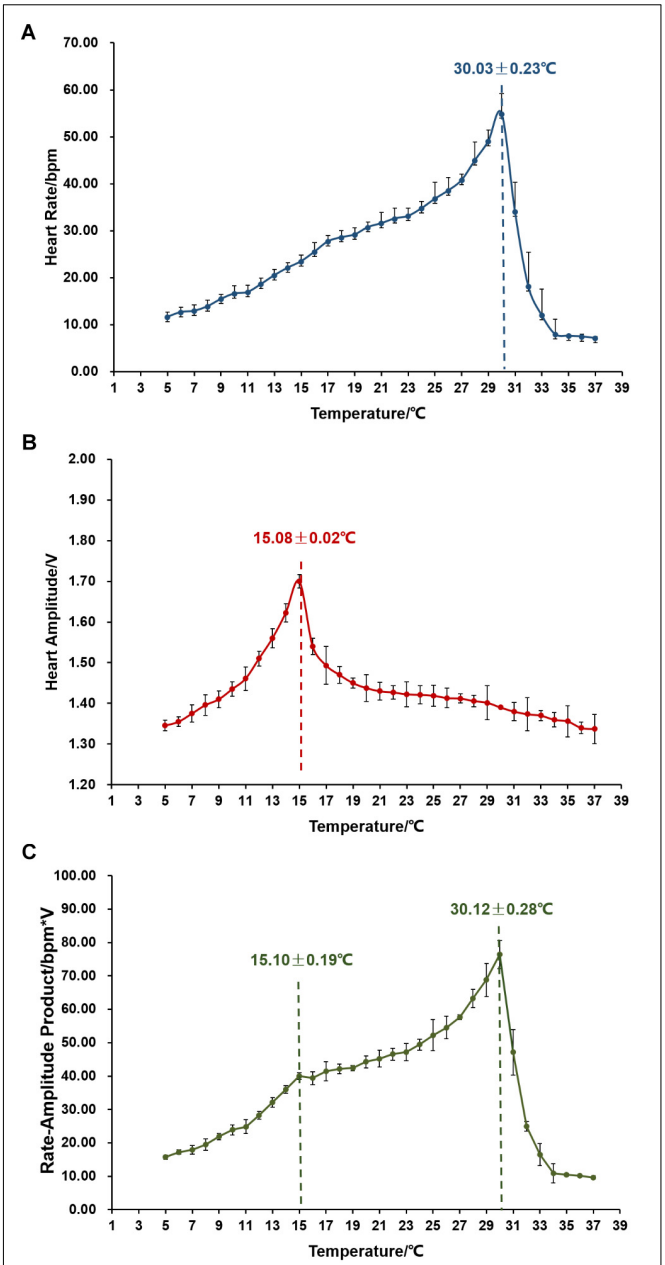

FIGURE 3 | The effect of temperature on cardiac activity (N = 24). **(A)** Effects of environmental temperature on scallop HR. The vertical line indicates Arrhenius break temperature (ABT). **(B)** Variations in HA in response to temperature elevation. The vertical line indicates the turning temperature when HA reaches the maximum. **(C)** Changing patterns of RAP with temperature elevation. The vertical line indicates the two peaks in RAP curve.

Dong and Williams, 2011), salinity (Berger and Kharazova, 1997; Bakhmet et al., 2012), food supply (Widdows, 1973), heavy metals and ammonia (Marchan et al., 1999; Curtis et al., 2000). But current knowledge on marine molluscs' cardiac responses to environmental factors is based on variations in HR mainly due to two reasons. First, it is widely accepted that HR is a good indicator of physiological status in various animals. Second, HR is relatively stable and easy to calculate. In present study, we developed two cardiac indices – HA and RAP, and evaluated the variation of HR, HA and RAP in response to several biotic and environmental factors. This would contribute to a more comprehensive understanding of scallops' cardiac activity.

Based on our study, size has significant effects on both HR and HA. There is a significant negative correlation between HR and shell height, as well as total weight. The similar trend of shell height and total weight with HR is expected because previous studies have revealed that these two factors are highly correlated (Du et al., 2016, 2017). Size-dependence of HR was also reported in blue mussel *M. edulis* (Sukhotin et al., 2003) and limpet *P. vulgate* (Santini et al., 2000). It suggests the negative relationship between size and HR may widely exist in various molluscs. Although the effect of size on HA is unknown in

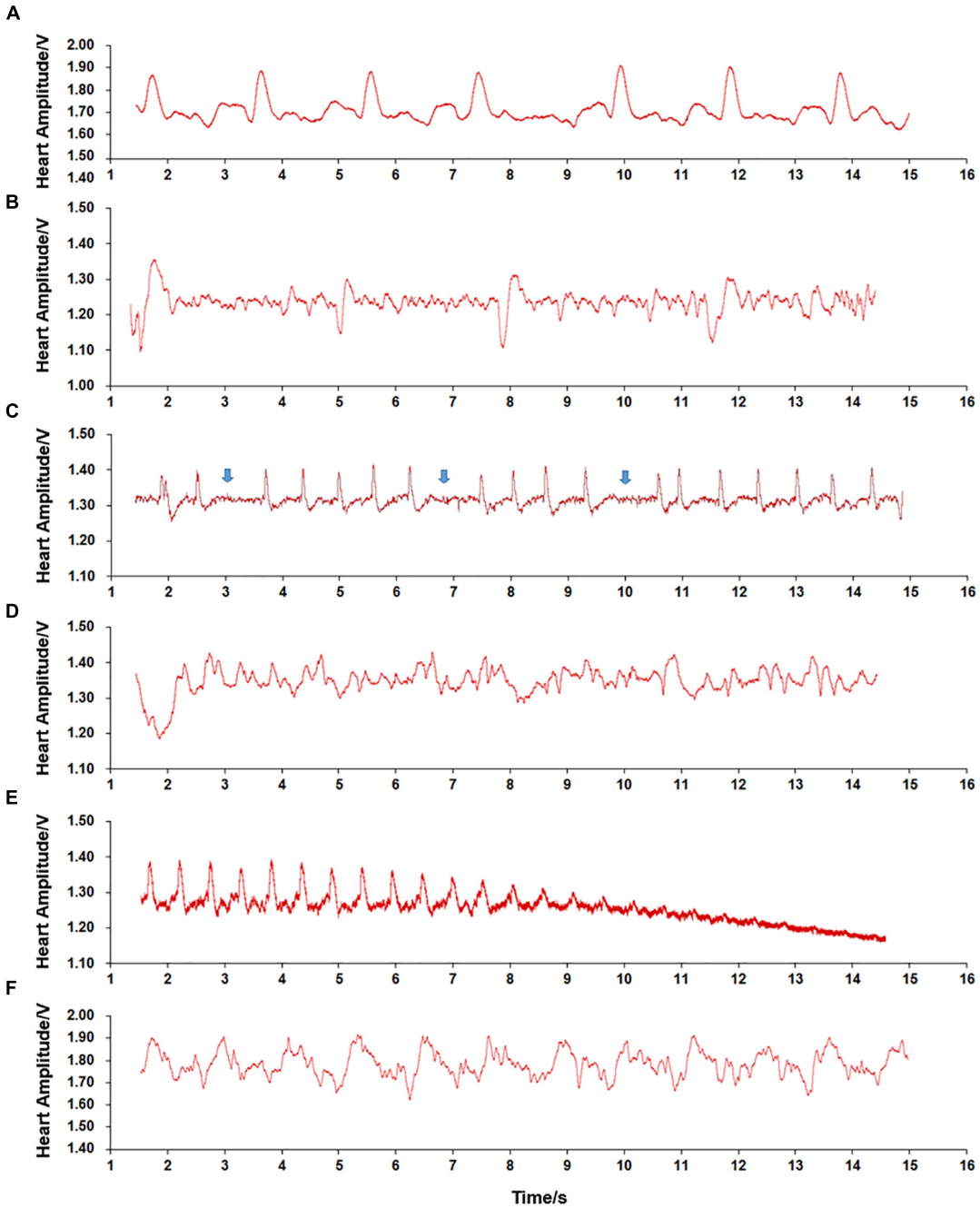

FIGURE 4 | Plethysmograms of cardiac performance recorded during temperature challenge. **(A)** Regular signal pattern recorded in scallops submerged in 15°C seawater. **(B)** Bradycardia recorded in scallops submerged at low temperature (5°C). **(C)** Temporary cardiac arrest recorded in scallops submerged at relatively high temperature (28°C). **(D)** Irregular signal pattern recorded in scallops submerged at high temperature (29°C). **(E)** Cardiac arrest recorded in scallops submerged at 32°C. **(F)** Regular signal pattern recorded in scallops returned to control temperature (15°C).

other molluscs, scallop HA positively correlates with size. It is noteworthy that RAP remains similar in different sized scallops, suggesting the opposite relationship of HR and HA with size may be a compromise between different sized scallops.

According to our data, age only affects HR but not HA or RAP, with older scallops having significantly faster HR. This is contrary to a report in freshwater mussels, in which obvious decline in HR with age increase was observed (Motley, 1934). Although the molecular mechanism of distinct relationships between HR and age in the two bivalves is unknown, it is an interesting phenomenon worthy of further research.

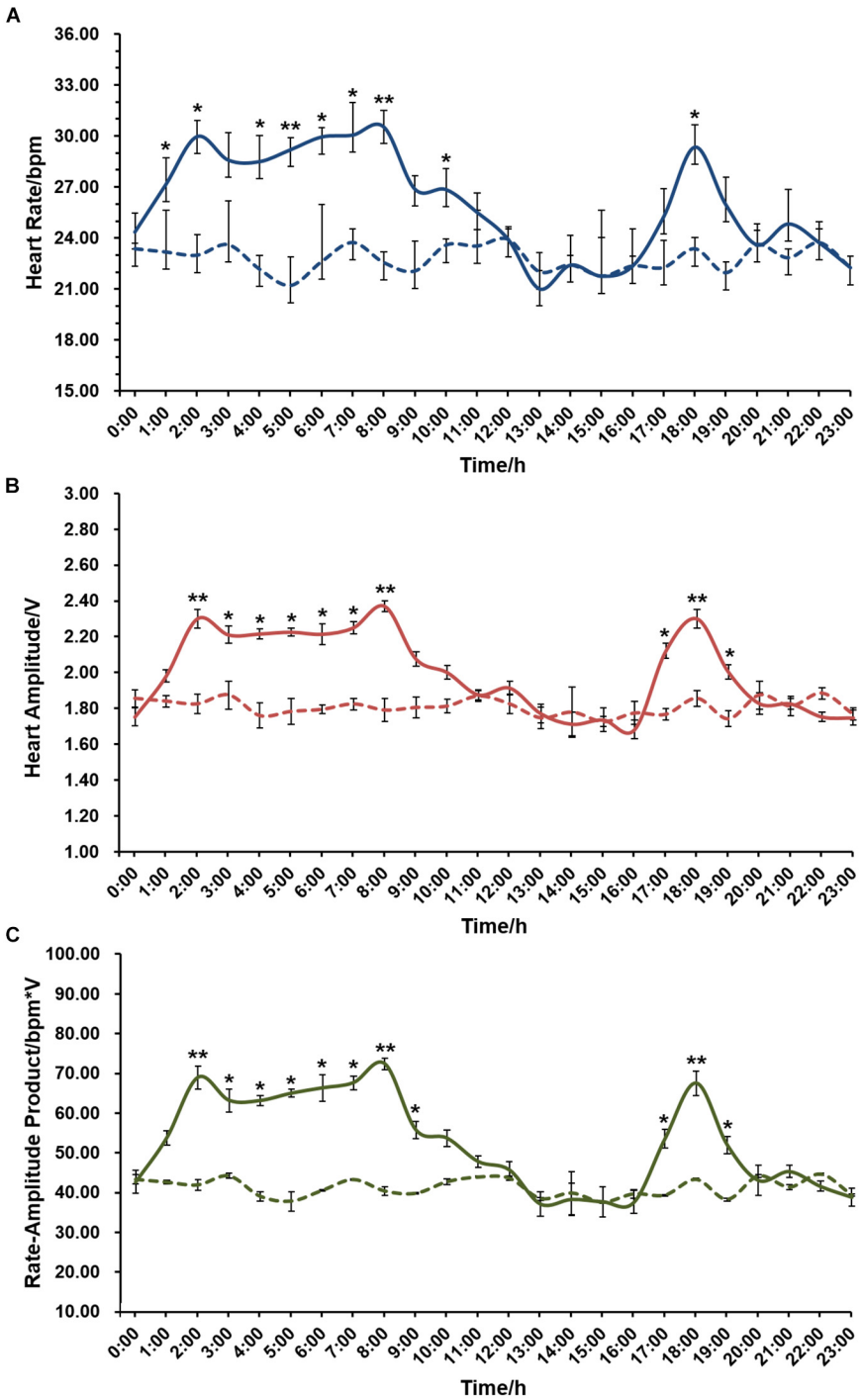

FIGURE 5 | The effect of circadian rhythm on cardiac activity of scallop (N = 24 for each group). **(A)** The effect of circadian rhythm on HR. **(B)** The effect of circadian rhythm on HA. **(C)** The effect of circadian rhythm on RAP. The x-axis represents a 24 h-period from midnight (0:00) to 11 pm (23:00). The solid and dotted curves indicate HR/HA/RAP monitored under natural light (a light:dark period of 12 h:12 h) and in a darkroom, respectively. *Indicates $P < 0.05$; **indicates $P < 0.01$.

The independence of RAP with scallop size and age inspires us to consider the possible similarity between scallop RAP and human rate-pressure product (HR*BP, RPP) because RPP is a marker of cardiac function which is relatively stable in healthy people irrespective of height or age (Hui et al., 2000; Overend et al., 2000; Mota et al., 2012). That being said, unlike amplitudes of the P-QRS-T waves in human ECG, HA may represent blood pressure (BP). Moreover, as an index of myocardial oxygen

consumption, RPP has strong correlation with the maximal oxygen consumption and is an indicator of myocardium stress (Overend et al., 2000; Mota et al., 2012). This indicates RAP may also be used to measure the workload or oxygen demand of the heart in scallop.

Temperature has been found to be a major environmental factor that affects HR of various marine molluscs (Widdows, 1973; Santini et al., 2000; Dong and Williams, 2011). In Zhikong scallop, temperature has significant effects on HR, HA and RAP. The temperature at which maximal HR reaches – Arrhenius break temperature (ABT), is 30.03 ± 0.23°C, close to the thermal endurance limit of Zhikong scallop we reported before (Xing et al., 2016). Interestingly, a peak in HA was also observed during temperature elevation, which is at 15.08 ± 0.02°C, very close to the optimal growth temperature (15.6–16.0°C) of Zhikong scallop (Wang, 1981). We therefore speculate that recording HA variations during temperature elevation could be an accurate method for assessing an organism's optimal growth temperature. Similar two peaks were found in RAP curve, one at 15.10 ± 0.19°C and the other at 30.12 ± 0.28°C. This suggests that maximal oxygen consumption may be relatively low when seawater temperature is lower than the optimal growth temperature (1st peak); with the increase of temperature, maximal oxygen consumption increases gradually; cardiac workload reaches the maximum at the organism's thermal tolerance temperature (2nd peak); afterward, aerobic metabolism decreases due to the inability of the heart to function beyond this critical temperature.

Although the effect of circadian rhythm on mollusc cardiac performance has never been reported before, we found that in scallops, circadian rhythm has a similar effect on HR, HA, and RAP. The same two peaks were found in HR, HA, and RAP curves, with the first one spanning across an 8 h-period from 1:00 to 8:00, and the other across a 3 h-period from 17:00 to 19:00, indicating Zhikong scallops are primarily active at night. This fluctuation pattern is very similar to the daily rhythm of oxygen consumption rate of Zhikong scallop (Zhang et al., 2001) and another bivalve *Coelomactra antiquate* (Meng et al., 2005). Since 8:00 and 18:00 correspond to the natural light shifting, we assume the rhythm of cardiac activity may be related to the changes in light sensed by scallop eyes (Li et al., 2017; Palmer et al., 2017; Wang et al., 2017), and/or the accustomed foraging behavior. From the molecular point of view, origin of biological rhythms consists of clock genes organized in negative and positive feedback loops (Cermakian and Sassonecorsi, 2000; Partch et al., 2014), thus investigation on expression variation of these genes in the daily cycle could help understanding the molecular bases of circadian rhythm of cardiac activity.

To sum up, our study revealed that all the investigated factors including size, age, environmental temperature and circadian rhythm have significant effects on scallop cardiac performance, therefore, these factors should be taken into account in the experimental design. But genetic background could potentially affect cardiac performance (Fujino et al., 1984) and should not be ignored. Our study also suggests that HA could be another informative parameter in the infrared-based cardiac activity measurement. Investigating variation in HA during temperature elevation could be a fast and accurate way for assessing optimal growth temperature of a given mollusc. Moreover, RAP may be an index of myocardial oxygen consumption and could be used to indicate myocardium stress in response to various environmental changes. Considering the variability of cardiac performance among different molluscs, feasibility of HA and RAP as indicators of physiological status in other organisms remains to be studied.

ETHICS STATEMENT

All applicable international, national, and/or institutional guidelines for the care and use of animals were followed.

AUTHOR CONTRIBUTIONS

SW, LZ, and ZB conceived and designed the experiments. YaL and HG collected the samples. QX, YuL, and XZ performed the experiments. QX and LZ analyzed the data. QX, LZ, and SW wrote the manuscript. All authors have read and approved the final manuscript.

FUNDING

This work was supported by National Natural Science Foundation of China (31702341), the Major basic research projects of Shandong Natural Science Foundation (ZR2018A07), and Fundamental Research Funds for the Central Universities (201762001 and 201841001).

REFERENCES

Ahsanullah, M., and Newell, R. (1971). Factors affecting the heart rate of the shore crab *Carcinus maenas* (L.). *Comp. Biochem. Phys. A* 39, 277–287. doi: 10.1016/0300-9629(71)90084-3

Appeltans, W., Ahyong, S. T., Anderson, G., Angel, M. V., Artois, T., Bailly, N., et al. (2012). The magnitude of global marine species diversity. *Curr. Biol.* 22, 2189–2202. doi: 10.1016/j.cub.2012.09.036

Bakhmet, I. N., Berger, V. J., and Khalaman, V. V. (2005). The effect of salinity change on the heart rate of *Mytilus edulis* specimens from different ecological zones. *J. Exp. Mar. Biol. Eco.* 318, 121–126. doi: 10.1016/j.jembe.2004.11.023

Bakhmet, I. N., Fokina, N. N., Nefedova, Z. A., and Nemova, N. N. (2008). Physiological-biochemical properties of blue mussel *Mytilus edulis* adaptation to oil contamination. *Environ. Monit. Assess.* 155, 581–591. doi: 10.1007/s10661-008-0457-5

Bakhmet, I. N., Komendantov, A. J., and Smurov, A. O. (2012). Effect of salinity change on cardiac activity in *Hiatella arctica* and *Modiolus modiolus*, in the white sea. *Polar biol.* 35, 143–148. doi: 10.1007/s10661-008-0457-5

Bamber, S. D., and Depledge, M. H. (1997). Responses of shore crabs to physiological challenges following exposure to selected environmental contaminants. *Aquat. Toxicol.* 40, 79–92. doi: 10.1016/S0166-445X(97)00040-4

Berger, V. J., and Kharazova, A. (1997). Mechanisms of salinity adaptations in marine molluscs. *Hydrobiologia* 355, 115–126. doi: 10.1023/A:1003023322263

Caetano, J., and Delgado, A. J. (2015). Heart rate and cardiovascular protection. *Eur. J. Intern. Med.* 26, 217–222. doi: 10.1016/j.ejim.2015.02.009

Cermakian, N., and Sassonecorsi, P. (2000). Multilevel regulation of the circadian clock. *Nat. Rev. Mol. Cell Biol.* 1, 59–67. doi: 10.1038/35036078

Curtis, T. M., Williamson, R., and Depledge, M. H. (2000). Simultaneous, long-term monitoring of valve and cardiac activity in the blue mussel *Mytilus edulis* exposed to copper. *Mar. Biol.* 136, 837–846. doi: 10.1007/s002270000297

Depledge, M., and Andersen, B. (1990). A computer-aided physiological monitoring system for continuous, long-term recording of cardiac activity in selected invertebrates. *Comp. Biochem. Phys. A* 96, 473–477. doi: 10.1016/0300-9629(90)90664-E

Dong, Y. W., and Williams, G. A. (2011). Variations in cardiac performance and heat shock protein expression to thermal stress in two differently zoned limpets on a tropical rocky shore. *Mar. Biol.* 158, 1223–1231. doi: 10.1007/s00227-011-1642-6

Du, M., Fang, J., Gao, Y., Fang, J., and Jiang, Z. (2017). Correlation and path analysis of quantitative traits of different-age *Chlamys farreri*. *J. Fish. China* 41, 580–587. doi: 10.11964/jfc.20160610463

Du, M. R., Fang, J. G., Bao, Z. M., Gao, Y. P., Fang, J. H., and Jiang, Z. J. (2016). Correlation and path cofficient analysis for *Chlamys farreri* cultured in different sea areas. *Oceanol. Limnol. Sin.* 5, 963–970. doi: 10.11693/hyhz20160100011

Frederich, M., and Pörtner, H. O. (2000). Oxygen limitation of thermal tolerance defined by cardiac and ventilatory performance in spider crab, Maja squinado. *Am. J. Physiol. Regul. Integr. Comp. Physiol.* 279, R1531–R1538. doi: 10.1046/j.1365-201X.1999.00525.x

Fujino, K., Yamamori, K., and Okumura, S. I. (1984). Heart-rate responses of the pacific abalone against water temperature changes [*haliotis discus* hannai]. *Bull. Japan. Soc. Sci. Fish.* 50, 1671–1676. doi: 10.2331/suisan.50.1671

Hui, S. C., Jackson, A. S., and Wier, L. T. (2000). Development of normative values for resting and exercise rate pressure product. *Med. Sci. Sport Exerc.* 32, 1520–1527. doi: 10.1097/00005768-200008000-00023

Li, Y., Sun, X., Hu, X., Xun, X., Zhang, J., Guo, X., et al. (2017). Scallop genome reveals molecular adaptations to semi-sessile life and neurotoxins. *Nat. Commun.* 8:1721. doi: 10.1038/s41467-017-01927-0

Marchan, S., Davies, M. S., Fleming, S., and Jones, H. D. (1999). Effects of copper and zinc on the heart rate of the limpet *Patella vulgata* L. *Com. Biochem. Phys. A* 123, 89–93. doi: 10.1016/s1095-6433(99)00043-4

Meng, X., Dong, Z., Cheng, H., Li, X., and Li, J. (2005). Oxygen consumption and ammonia-N excretion rates of *Coelomactra* antiquata. *J. Appl. Ecol.* 16, 2435–2438. doi: 10.1360/biodiv.050058

Mota, J., Soares-Miranda, L., Silva, J. M., Dos Santos, S. S., and Vale, S. (2012). Influence of body fat and level of physical activity on rate-pressure product at rest in preschool children. *Am. J. Hum. Biol.* 24, 661–665. doi: 10.1002/ajhb.22294

Motley, H. L. (1934). Physiological studies concerning the regulation of heartbeat in freshwater mussels. *Phys. Zool.* 7, 62–84. doi: 10.1086/physzool.7.1.30151214

Overend, T. J., Versteegh, T. H., Thompson, E., Birmingham, T. B., and Vandervoort, A. A. (2000). Cardiovascular stress associated with concentric and eccentric isokinetic exercise in young and older adults. *J. Gerontol.* 55, B177–B182. doi: 10.1093/gerona/55.4.B177

Palmer, B. A., Taylor, G. J., Brumfeld, V., Gur, D., Shemesh, M., Elad, N., et al. (2017). The image-forming mirror in the eye of the scallop. *Science* 358, 1172–1175. doi: 10.1126/science.aam9506

Park, K. H., Kim, Y.-S., Chung, E.-Y., Choe, S.-N., and Choo, J.-J. (2004). Cardiac responses of *Pacific oyster Crassostrea gigas* to agents modulating cholinergic function. *Comp. Biochem. Phys. C* 139, 303–308. doi: 10.1016/j.cca.2004.12.009

Partch, C. L., Green, C. B., and Takahashi, J. S. (2014). Molecular architecture of the mammalian circadian clock. *Trends Cell Biol.* 24, 90–99. doi: 10.1016/j.tcb.2013.07.002

Petersen, L., and Gamperl, A. (2010). Effect of acute and chronic hypoxia on the swimming performance, metabolic capacity and cardiac function of Atlantic cod (*Gadus morhua*). *J. Exp. Biol.* 213, 808–819. doi: 10.1242/jeb.033746

Pirro, M. D., Santini, G., and Chelazzi, G. (1999). Cardiac responses to salinity variations in two differently zoned mediterranean limpets. *Comp. Biochem. Phys. B* 169, 501–506. doi: 10.1007/s003600050248

Santini, G., Williams, G. A., and Chelazzi, G. (2000). Assessment of factors affecting heart rate of the limpet *Patella vulgata* on the natural shore. *Mar. Biol.* 137, 291–296. doi: 10.1007/s002270000339

Stenseng, E., and Braby, C. (2005). Evolutionary and acclimation-induced variation in the thermal limits of heart function in congeneric marine snails (*Genus Tegula*): implications for vertical zonation. *Biol. Bull.* 208, 138–144. doi: 10.2307/3593122

Streicher, J. W., Cox, C. L., and Birchard, G. F. (2012). Non-linear scaling of oxygen consumption and heart rate in a very large cockroach species (*Gromphadorhina portentosa*): correlated changes with body size and temperature. *J. Exp. Biol.* 215 (Pt 7), 1137–1143. doi: 10.1242/jeb.061143

Sukhotin, A., Lajus, D., and Lesin, P. (2003). Influence of age and size on pumping activity and stress resistance in the marine bivalve *Mytilus edulis* L. *J. Exp. Mar. Biol. Ecol.* 284, 129–144. doi: 10.1016/s0022-0981(02)00497-5

Taylor, A. (1976). The cardiac responses to shell opening and closure in the bivalve *Arctica islandica* (L.). *J. Exp. Biol.* 64, 751–759.

Umetani, K., Singer, D. H., McCraty, R., and Atkinson, M. (1998). Twenty-four hour time domain heart rate variability and heart rate: relations to age and gender over nine decades. *J. Am. Coll. Cardiol.* 31, 593–601. doi: 10.1016/S0735-1097(97)00554-8

Wang, S., Zhang, J., Jiao, W., Li, J., Xun, X., Sun, Y., et al. (2017). Scallop genome provides insights into evolution of bilaterian karyotype and development. *Nat. Ecol. Evol.* 1:0120. doi: 10.1038/s41559-017-0120

Wang, Z. (1981). Study on artificial seedling and experimental rearing of Zhikong scallop *Chlamys farreri*. *J. Dalian Fish.* 2, 1–12.

Widdows, J. (1973). Effect of temperature and food on the heart beat, ventilation rate and oxygen uptake of *Mytilus edulis*. *Mar. Biol.* 20, 269–276. doi: 10.1007/BF00354270

Wilkens, J. L., Wilkens, L. A., and Mcmahon, B. R. (1974). Central control of cardiac and scaphognathite pacemakers in the crab, cancer magister. *Comp. Biochem. Phys. A* 90, 89–104. doi: 10.1007/BF00698370

Xing, Q., Li, Y., Guo, H., Yu, Q., Huang, X., Wang, S., et al. (2016). Cardiac performance: a thermal tolerance indicator in scallops. *Mar. Biol.* 163:244. doi: 10.1007/s00227-016-3021-9

Yu, Z., Yang, H., Liu, B., Xu, Q., Xing, K., and Zhang, L. (2010). Growth, survival and immune activity of scallops, *Chlamys farreri* Jones et Preston, compared between suspended and bottom culture in Haizhou Bay, China. *Aquac. Res.* 41, 814–827. doi: 10.1111/j.1365-2109.2009.02358.x

Zhang, Y., Wang, Q., Liu, Z., Yang, A., Gong, X., and Li, F. (2001). Oxygen consumption rate comparison between triploid and diploid scallop, *Chlamys* (Azumapecten) *farreri*. *Mar. Fish. Res.* 22, 19–24. doi: 10.3969/j.issn.1000-7075.2001.01.004

Conflict of Interest Statement: The authors declare that the research was conducted in the absence of any commercial or financial relationships that could be construed as a potential conflict of interest.

frontiers in Physiology

ORIGINAL RESEARCH
published: 16 April 2018
doi: 10.3389/fphys.2018.00418

Byssus Structure and Protein Composition in the Highly Invasive Fouling Mussel *Limnoperna fortunei*

Shiguo Li[1], *Zhiqiang Xia*[1,2], *Yiyong Chen*[1,3], *Yangchun Gao*[1,3] *and Aibin Zhan*[1,3]*

[1] *Research Center for Eco-Environmental Sciences, Chinese Academy of Sciences, Beijing, China,* [2] *Department of Biological Sciences, Great Lakes Institute for Environmental Research, University of Windsor, Windsor, ON, Canada,* [3] *College of Resources and Environment, University of Chinese Academy of Sciences, Chinese Academy of Sciences, Beijing, China*

Biofouling mediated by byssus adhesion in invasive bivalves has become a global environmental problem in aquatic ecosystems, resulting in negative ecological and economic consequences. Previous studies suggested that mechanisms responsible for byssus adhesion largely vary among bivalves, but it is poorly understood in freshwater species. Understanding of byssus structure and protein composition is the prerequisite for revealing these mechanisms. Here, we used multiple methods, including scanning electron microscope, liquid chromatography–tandem mass spectrometry, transcriptome sequencing, real-time quantitative PCR, inductively coupled plasma mass spectrometry, to investigate structure, and protein composition of byssus in the highly invasive freshwater mussel *Limnoperna fortunei*. The results indicated that the structure characteristics of adhesive plaque, proximal and distal threads were conducive to byssus adhesion, contributing to the high biofouling capacity of this species. The 3,4-dihydroxyphenyl-α-alanine (Dopa) is a major post-transnationally modification in *L. fortunei* byssus. We identified 16 representative foot proteins with typical repetitive motifs and conserved domains by integrating transcriptomic and proteomic approaches. In these proteins, Lfbp-1, Lffp-2, and Lfbp-3 were specially located in foot tissue and highly expressed in the rapid byssus formation period, suggesting the involvement of these foot proteins in byssus production and adhesion. Multiple metal irons, including Ca^{2+}, Mg^{2+}, Zn^{2+}, Al^{3+}, and Fe^{3+}, were abundant in both foot tissue and byssal thread. The heavy metals in these irons may be directly accumulated by *L. fortunei* from surrounding environments. Nevertheless, some metal ions (e.g., Ca^{2+}) corresponded well with amino acid preferences of *L. fortunei* foot proteins, suggesting functional roles of these metal ions by interacting with foot proteins in byssus adhesion. Overall, this study provides structural and molecular bases of adhesive mechanisms of byssus in *L. fortunei*, and findings here are expected to develop strategies against biofouling by freshwater organisms.

Keywords: *Limnoperna fortunei*, biofouling, foot protein, byssus adhesion, proteome, transcriptome, ultrastructure, metal ion

OPEN ACCESS

Edited by:
Youji Wang,
Shanghai Ocean University, China

Reviewed by:
Maria Violetta Brundo,
Università degli Studi di Catania, Italy
Qiong Shi,
Beijing Genomics Institute (BGI), China
Ali Miserez,
Nanyang Technological University, Singapore

***Correspondence:**
Aibin Zhan
zhanaibin@hotmail.com;
azhan@rcees.ac.cn

Specialty section:
This article was submitted to Aquatic Physiology, a section of the journal Frontiers in Physiology

Received: *03 February 2018*
Accepted: *04 April 2018*
Published: *16 April 2018*

Citation:
Li S, Xia Z, Chen Y, Gao Y and Zhan A (2018) Byssus Structure and Protein Composition in the Highly Invasive Fouling Mussel Limnoperna fortunei. Front. Physiol. 9:418. doi: 10.3389/fphys.2018.00418

INTRODUCTION

Adhesion is the major process to form a sessile lifestyle in numerous aquatic species. Bivalve, one of the representative taxonomic groups that have strong adhesive abilities (Babarro and Comeau, 2014; Flammang et al., 2016; Kamino, 2016), can adhere to a variety of hard substrates under wet conditions with byssal threads secreted by foot glands (Waite, 2017). Byssus offers promising performance and potential to inspire underwater adhesive (Ahn, 2017), while byssus adhesion is a fundamental cause of aquatic biofouling and invasions. Large-scale biofouling, especially formed by highly invasive bivalves, poses serious threats to aquatic ecosystems, aquaculture facilities, and maritime industries (Amini et al., 2017). Such biofouling can cause corrosion of underwater facilities, water pollution, and changes in aquatic ecosystems, thus resulting in significantly ecological pollution and economic impacts (Amini et al., 2017). Therefore, deep understanding of byssus adhesion in bivalves is crucial for effectively mitigating these negative environmental impacts induced by fouling organisms, particularly by aquatic invasive species.

Byssus adhesion has been well-studied in marine mussels, especially in the genus *Mytilus*, revealing the structural characteristics of byssus and the roles of foot proteins and metal ions in byssus adhesion (Waite and Tanzer, 1981; Benedict and Waite, 1986; Waite, 1986; Zhao and Waite, 2006; Hwang et al., 2010; Yu et al., 2011; Wei et al., 2013). Marine mussel byssus is composed of proteinaceous threads, including distal thread, proximal thread, and adhesive plaque. The byssal thread is surrounded by a protective cuticle layer and supported by a collagen fiber core (Holten-Andersen et al., 2007, 2009b; Reddy and Yang, 2015). This well-structured byssus is mainly maintained by foot proteins secreted by foot glands (Wei et al., 2013). More than ten foot proteins, including collagens (preCol-NG, preCol-C, and preCol-D), thread matrix proteins (Ptmp and Tmp), and mussel foot proteins (Mfp-1-Mfp-6), have been isolated and identified from marine mussels (Waite, 2017). Mfp-1, which is mainly distributed on the surface of byssal thread, plays a protective function. Mfp-3, Mfp-5, and Mfp-6 are located in the underside of adhesive plaque, participating in byssal adhesion. Both Mfp-2 and Mfp-4 connect adhesive plaque and byssal thread and are involved in thread connection. Post-transnationally modified amino acid residues such as L-β-3,4-dihydroxyphenyl-α-alanine (Dopa) are enriched in foot proteins, contributing to byssal cohesive and adhesive interactions by formatting cross-links (Nicklisch and Waite, 2012). Furthermore, metal ions such as Ca^{2+} and Fe^{3+} bind to and interact with specific amino acids in adhesion-related proteins, playing critical roles in protein self-assembly, structure maintenance, and Dopa cross-linking (Holten-Andersen et al., 2009a; Seguin-Heine et al., 2014; Liu et al., 2015; Li S. G. et al., 2017). These results comprehensively show that byssus adhesion is a multi-level complex process, and elements at different levels (e.g., structure, protein, and metal ion) play their crucial roles in such a complex process.

Interestingly, numerous studies showed that elements involved at different levels largely varied among species, suggesting that species- and/or taxonomic group-specific mechanisms of byssus adhesion should be deeply investigated in organisms of interest. For example, a study on the scallop *Chlamys farreri* identified seven byssal proteins (Sbp1-Sbp7) and their associated genes, and intriguingly such proteins showed limited homologies to the currently known ones in mussels (Miao et al., 2015). Genomic analyses for this species highlighted that the expanded tyrosinases enabled rapid byssal formation (Guerette et al., 2013; Li Y. L. et al., 2017). Among fourteen byssal proteins identified from the pearl oyster *Pinctada fucata,* none of them could match Mfps or Sbps (Liu et al., 2015). Regarding the structure of byssus, a great number of nano-cavities were found in the inner core of distal thread in *P. fucata*, while such a structure was not observed in marine mussels and scallops (Liu et al., 2015; Reddy and Yang, 2015). Moreover, differences in both the type of metal ions and contents were also found among these marine bivalves (Seguin-Heine et al., 2014; Liu et al., 2015; Li S. G. et al., 2017).

Compared with marine species, byssus has been rarely studied in freshwater bivalves, though its adhesive mechanisms have been suggested to be species-specific. For example, two former studies identified a total of 12 novel foot proteins (Dpfp1-Dpfp12) from the freshwater mussel *Dreissena polymorpha*, showing great difference from foot proteins in marine bivalves. Ultrastructure difference was also found between *D. polymorpha* and marine mussels (Xu and Faisal, 2008; Gilbert and Sone, 2010; Farsad and Sone, 2012; Gantayet et al., 2013). So far, reasons are still not clear for such a high level of differences in adhesive mechanisms among bivalves, particularly between marine and freshwater species, largely owing to the lack of available information in freshwater species. It is therefore of great necessity to study byssus structure and protein composition in more freshwater counterparts, particularly under the circumstances that many freshwater bivalves have largely expanded their distribution ranges and caused severe biofouling problems in both native and invasive ranges, such as the golden mussel *Limnoperna fortunei* and *Dreissena* mussels (Zhan et al., 2012).

The golden mussel *L. fortunei* is a small-sized freshwater bivalve in the family Mytilidae with strong invasiveness. It is native to Southeast Asia and has invaded many freshwater ecosystems in Asia high-latitude regions and South America since 1990s (Zhan et al., 2012; Xia et al., 2017). *L. fortunei* often forms dense mussel beds by cross connecting among individuals or adhering to submersed substrates, causing severe problems such as pipe occlusion, water flow reduction, filter, and heat exchanger blocking and concrete corrosion in natural structures and manmade facilities (Boltovskoy et al., 2015). Such a severe biofouling problem has caused subsequent economic damages (Ohkawa et al., 1999a; Boltovskoy et al., 2015). In addition, due to its powerful filtering capacity, the invasion, and biofouling of *L. fortunei* can alter the structure and stability of freshwater ecosystems (Welladsen et al., 2011; Boltovskoy et al., 2015; Xu et al., 2015). A few studies have tried to investigate foot structure and proteins of *L. fortunei*, and to explore potential mechanisms of byssus adhesion in such a high-impact species. For example, microscopic observation revealed that secretory cells in the groove on ventral portion of foot

tissue in *L. fortunei* could secret mucous to produce byssal threads, indicating a cytological mechanism of byssus formation (Andrade et al., 2015). Two candidate glue proteins (i.e., Lffp-1 and Lffp-2) were successfully isolated from *L. fortunei* foot tissue (Ohkawa et al., 1999b; Ohkawa and Nomura, 2015), while only one foot protein gene, *LfFP-2*, has been fully sequenced (Uliano-Silva et al., 2014). Despite such research progress, the mechanism of byssus adhesion at multiple levels such as byssus structure, protein composition and metal ion in *L. fortunei* remains largely unexploited. Such a gap hinders not only better understanding of the difference in byssus adhesion between marine and freshwater bivalves, but also exploring prevention strategies against biofouling caused by this species.

Recently, the dual transcriptomic and proteomic approach has emerged as the best way to identify novel adhesion-related proteins in animals (Guerette et al., 2013; Hennebert et al., 2015). In this study, multiple analyses were conducted to study byssus in the golden mussel *L. fortunei*, from structural characteristic, protein composition and gene expression to metal ions that may participate in crucial processes of byssus formation and adhesion. Specifically, inductively coupled plasma mass spectrometry (ICP-MS) was employed to determine metal ion content and liquid chromatography–tandem mass spectrometry (LC-MS/MS), transcriptome sequencing, and real-time quantitative PCR (RT-qPCR) to identify foot proteins in foot tissue and byssal thread. The interactions of foot proteins and metal ions were demonstrated by analyzing amino acid preference and metal ion contents. Byssus ultrastructure, which is primarily maintained by interactions between foot proteins and metal ions, was observed using light microscope (LM) and scanning electron microscope (SEM). Nitroblue tetrazolium (NBT)/Glycinate staining were used to analyze the existence of Dopa modification in byssus. This structure and protein composition study is expected to provide significant backgrounds for deeply understanding the underlying mechanisms of byssus adhesion in the highly invasive *L. fortunei*.

MATERIALS AND METHODS

Sample Collection and Experimental Design

Adult golden mussels *L. fortunei* with medium size (1.5–2.0 cm) were collected from Shisanling Reservoir, Beijing, China (40°15′ N, 116°15′ E) in June 2017. Mussels were transported to laboratory within 2 h after collection under low temperature (∼15°C). Before downstream analyses, all mussels were cultured in a circulating aquarium at 20 ± 1°C for 1 week and daily fed with pure culture of algae *Chlorella* sp.

Multiple methods on foot tissue and byssal thread were used to clarify the mechanism of byssus adhesion in *L. fortunei*. To prepare newly secreted byssal thread, live mussels were carefully cut from original byssal threads and placed on glass slides to allow them to re-attach. The most important compositions involved in byssus adhesion, foot protein and metal ion were identified and further analyzed in foot and newly secreted byssus. Byssus ultrastructure associated with these two compositions was observed and characterized.

Foot tissue was dissected from live mussels using disinfected surgical blades, washed three times with double deionized water (ddH_2O), rapidly frozen with liquid nitrogen and preserved at −80°C. Meanwhile, whole byssal threads, including proximal thread, distal thread, and adhesive plaque, were collected from the same mussels, washed with ddH_2O and preserved at −80°C. The foot tissues and byssal threads from 30 mussels were pooled together as a mixed sample for total RNA and protein extraction.

Newly secreted byssal threads with whole structure were randomly dissected from 10 individuals. Byssal thread samples were then washed three times with ddH_2O, placed in a petri dish and preserved at 4°C for morphological observation. In addition, byssal threads with whole structure were dissected, washed three times with ddH_2O water, air-dried at room temperature and preserved in a sealed desiccator. Byssal threads from 30 individuals were pooled together as a biological replicate and three replicates were used for metal ion determination.

Foot, mantle, gonads, visceral mass, adductor muscle, and gill were collected, washed three times with RNase-free water, immediately frozen with liquid nitrogen and preserved at −80°C for tissue-specific gene expression analysis. In addition, byssal threads from 150 mussels were carefully removed and these mussels were randomly divided into three 50-individual groups. Each group was then cultured in a 20 L aerated tank under 20 ± 1°C for 7 days. The number of newly produced byssus was recorded daily. Foot tissues were collected from 10 individuals per tank on the 1st, 3rd, 5, and 7th day, respectively. These foot samples were washed three times with RNase-free water, immediately frozen with liquid nitrogen and preserved at −80°C for expression analysis for foot protein genes. Foot tissues from 10 individuals were pooled together as a biological replicate and three replicates were used for the above gene expression analyses.

Light Microscopy (LM) and Scanning Electron Microscopy (SEM)

To analyze byssus structure, byssus samples were observed with a Light Microscope (CX41, Olympus, Tokyo, Japan). The proximal thread, distal thread, and adhesive plaque of each sample were photographed and recorded with CellSens Standard (Olympus, Tokyo, Japan). Meanwhile, byssal threads were sputter-coated with gold particles for 60 s in Rotary Pumped Sputter Coater (E1010, Hitachi, Tokyo, Japan) and observed using a Scanning Electron Microscope (SEM, FEI Quanta 200, Netherlands) following the previously described method (Li S. G. et al., 2017).

Dopa Staining Analysis

To confirm the existence of *post-translational* modification Dopa in byssus of *L. fortunei,* byssal thread and adhesive plaque samples were stained with nitroblue tetrazolium (NBT)/Glycinate following Qin et al. (2016). Briefly, the golden mussel samples were raised in an aquarium with glass slides at the bottom. After adhesion on the slides, the byssus was extracted from mussel body and then scraped away from slides. The integrated byssus samples were secreted into slices with five micron thick using the classical paraffin section method. The obtained byssus slices

were subsequently stained with NBT/Glycinate solution (0.24 mmol/L NBT in 2 mol/L potassium glycinate, pH 10) in the dark for 2 h at 25°C. After staining, the slides were washed with sterilized water for three times and then observed using a light microscope (CX41, Olympus, Tokyo, Japan). Three slides were considered as three biological replicates and at least 10 byssal threads were observed for each replicate.

De Novo Transcriptome Sequencing

To identify adhesion-related genes, total RNA of foot tissue samples was extracted using mirVana miRNA Isolation Kit (Ambion Inc, Austin, Tex, USA) following the manufacturer's instructions. RNA integrity was evaluated using Agilent 2100 Bioanalyzer (Agilent Technologies, Santa Clara, CA, USA). Total RNA with integrity number (RIN) $\geq$ 7 was used for downstream analyses. A cDNA library was constructed using TruSeq Stranded mRNA LTSample Prep Kit (Illumina, San Diego, CA, USA) according to manufacturer's instructions and sequenced on the Illumina Sequencing Platform HiSeqTM 2500 (Illumina, San Diego, CA, USA). The sequenced results were spliced by TRINITY software (Grabherr et al., 2011) with paired-end method. TGICL software was used to remove redundancy and get a set of final unigene as reference sequences. Raw data of *L. fortunei* foot transcriptome has been deposited into Sequence Read Archive (SRA) in NCBI (accession number SRP125019). These obtained sequences were subsequently submitted to Basic Local Alignment Search Tool (BLAST) against NR database (ftp://ftp.ncbi.nih.gov/blast/db) and Swiss-Prot database (http://www.uniprot.org/downloads) for functional annotation. A cutoff E-value $\leq 1.0e^{-5}$ was used to identify the most representative annotation. Clusters of Orthologous Groups for Eukaryotic Complete Genomes (COG) and Kyoto Encyclopedia of Genes and Genomes (KEGG) annotation were also performed using previously described methods (Hou et al., 2017; Li S. G. et al., 2017) with the cutoff E-value $\leq 1.0e^{-5}$. Typical unigenes with high homologies to the reported adhesion-related proteins in this transcriptome were selected and compared with other bivalve species using homologous alignment methods (Guerette et al., 2013; DeMartini et al., 2017). Homologous alignments for foot proteins were conducted using BioEdit version 7.2.5 (Hall, 1999) and Jalview online bioinformatics tool (http://www.jalview.org/). Repetitive motifs were predicted by RADAR tool (https://www.ebi.ac.uk/Tools/pfa/radar/) and conserved domains were predicted by PROSITE tool (http://prosite.expasy.org/).

Protein Extraction and Mass Spectrometry Analysis

To analyze protein composition of byssal thread, foot tissue, and byssal thread samples were grinded in liquid nitrogen. Total foot and byssal proteins were extracted using the acetone precipitation method. Briefly, the grinded sample was put into a centrifuge tube, added cool acetone containing 10% trichloroacetic acid (TCA) and then precipitated at −20°C for 2 h. The precipitation was collected by centrifugation at 20,000 g for 10 min at 15°C, washed with 100% acetone and precipitated for another 30 min at −20°C. This precipitation protocol was repeated for three times. Subsequently, 500 μL L3 solution (1 mM PMSF, 2 mM EDTA and 10 mM DTT) was added into the tube following 5 min ultrasound lysis. The ultrasonic program included pulse on for 2 s and pulse off for 3 s at 180 W. The resulted sample was then 20,000 g centrifuged at 15°C for 30 min and supernatant was collected. The Bradford method was used for the protein quantitation. Specifically, 20 μg extracted proteins were separated by routine Sodium Dodecyl Sulfate Polyacrylamide Gel Electrophoresis (SDS-PAGE, 12%) and stained with Coomassie Blue R-250.

Candidate regions were selected from the SDS-PAGE gel and digested by trypsin using the acetonitrile and ammonium bicarbonate method. The digested peptides were further identified by Liquid Chromatography–tandem Mass Spectrometry (LC-MS/MS) using Ultimate 3000 RSLCnano System coupled to Q Exactive Mass Spectrometer (Thermo Scientific, Waltham, USA). The obtained data was further searched against Mollusca UniProt database (http://www.uniprot.org/taxonomy/6447) and the unigene library was generated from the foot transcriptome using MASCOT 2.3.02 (Matrix Science, London, UK). Experimental operation and data analysis were based on the methods described in our previous studies (Li et al., 2016; Li S. G. et al., 2017). The results with Unique Peptide $\geq$ 2, Coverage $\geq$ 30 and Score $\geq$ 100 were considered as representative foot proteins in foot and byssus. Subsequently, the results synchronously presented in foot transcriptome, foot proteome and byssus proteome were screened and considered as the most representative foot proteins. Amino acid compositions of these proteins were analyzed using ProtParam tool (http://web.expasy.org/protparam/). Repetitive motifs were predicted by RADAR tool (https://www.ebi.ac.uk/Tools/pfa/radar/) and domains were predicted by PROSITE tool (http://prosite.expasy.org/).

Real-Time Quantitative PCR (RT-qPCR)

Expressions of foot protein genes were analyzed using the RT-qPCR method. Foot tissue samples were grinded in liquid nitrogen. Total RNA isolation, purification and quantification were conducted using methods by Li S. G. et al. (2017). PrimeScript™ RT Reagent Kit (Takara, Tokyo, Japan) was used to synthesize cDNA following the manufacturer's instructions. A 20-μL reaction containing 0.4 μM of each primer, 1.0 μL of cDNA, and AceQ qPCR SYBR® Green Master Mix (Vazyme, Nanjing, China) was carried out on a LightCycler® 96 System (Roche Diagnostics, Mannheim, Germany). Thermal program included 1 cycle of 95°C for 600 s; 40 cycles of 95°C for 10 s and 60°C for 30 s; 1 cycle of 95°C for 10 s, 65°C for 30 s and 95°C for 10 s. The *LfACTIN* gene was used as the internal reference (Uliano-Silva et al., 2014). For tissue-specific analyses, the adductor muscle was used as the control tissue. For gene expression profile analysis, foot tissues from pre-cultured mussels were used as the day 0 control. Relative expression levels of these genes were calculated by the $2^{-\Delta\Delta CT}$ method (Livak and Schmittgen, 2001). Specific primers for all the genes (Table S1) were designed using Primer3 version 4.1.0 (http://primer3.ut.ee/).

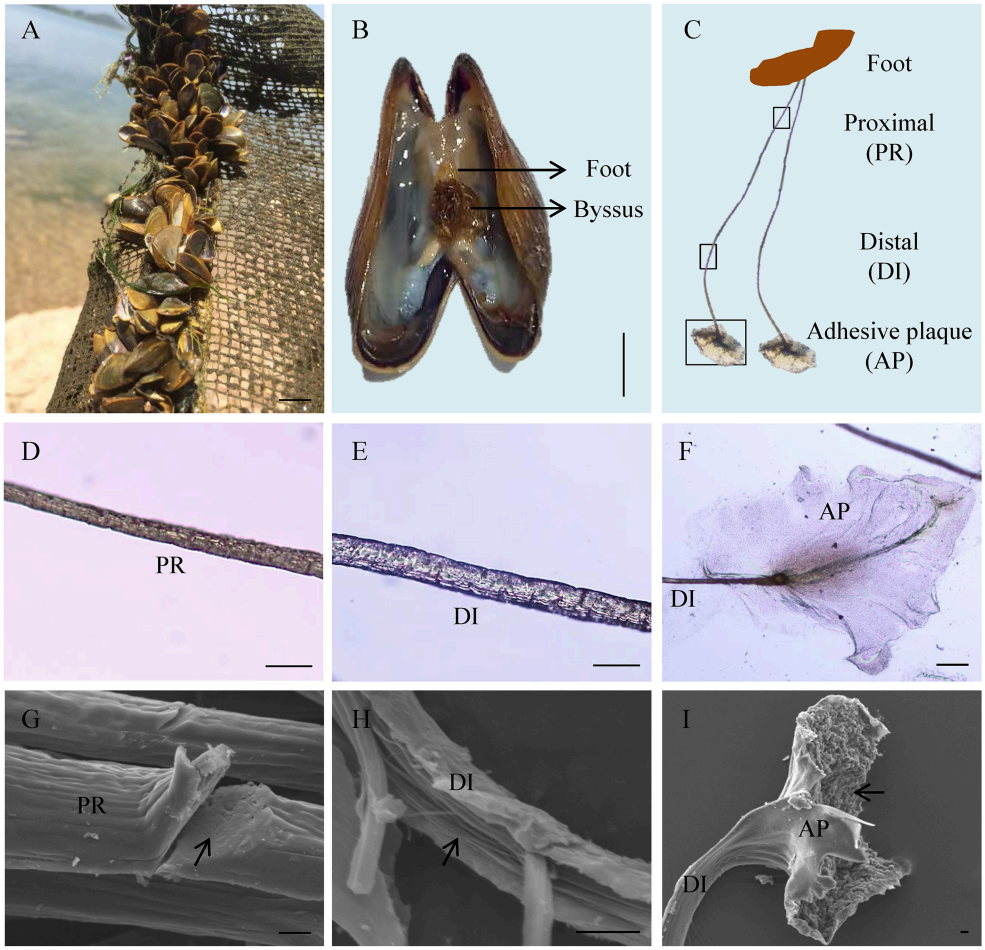

FIGURE 1 | Byssus morphology and structure of the golden mussel *Limnoperna fortunei*. **(A)** *L. fortunei* living in natural freshwater. **(B)** Photograph showing the position and morphology of foot and byssus. **(C)** The structure of byssal threads. PR, Proximal thread; DI, Distal thread; AP, Adhesive plaque. The black boxes indicate the observation regions for **(D–F)**. **(D)** Light photograph for the PR region. **(E)** Light photograph for the DI region. **(F)** Light photograph for the AP region. **(G)** Scanning electron micrograph for the PR region. The arrow indicates the compact ultrastructure of PR. **(H)** Scanning electron micrograph for the DI region. The arrow indicates the fibroid ultrastructure of DI. **(I)** Scanning electron micrograph for the AP region. The arrow indicates the rough underside of AP facing to substratum. Bar scale is 1 cm in **(A,B)**, 50 μm in **(D–F)**, and 10 μm in **(G–I)**.

Inductively Coupled Plasma Mass Spectrometry (ICP-MS)

To analyze metal ion composition and content, byssal thread, and foot tissue samples were firstly hydrolyzed in a mix of nitric acid (HNO_3) and hydrogen peroxide solution (H_2O_2, 30%) at 90°C for 3 h, respectively. Metal ion contents were determined using Inductively Coupled Plasma Mass Spectrometry (ICP-MS, Agilent 7500c, New Castle, DE, USA) with a micro-nebulizer following the protocol by Li S. G. et al. (2017) The determined metal elements included calcium, magnesium aluminum, iron, zinc, manganese, lead, copper, mercury, boron, molybdenum, nickel, and molybdenum. These metal ions were suggested to play key roles in byssus performance in bivalves (Seguin-Heine et al., 2014; Liu et al., 2015). Metal ion contents were presented as mg metal·g tissue^{-1} for foot tissues and mg metal·g byssus^{-1} for byssal threads. The percentage of each metal ion in the total contents of metal ions in both foot tissue and byssal thread samples were also calculated.

Statistical Analysis

Statistical analyses of data were obtained from three biological replicates and expressed as mean ± standard deviation (SD). Differences in gene expression levels and byssus numbers were accessed using one-way ANOVA with the significance level at $^*p < 0.05$. Micrographs were processed in Adobe Photoshop CS4 11.0 software and figures were drawn using SigmaPlot version 12.5 (Systat Software, San Jose, CA, USA).

RESULTS

Byssus Morphology and Structure

Adult *L. fortunei* could robustly adhere on underwater substrates *via* byssus in natural environments (**Figure 1A**). The byssus,

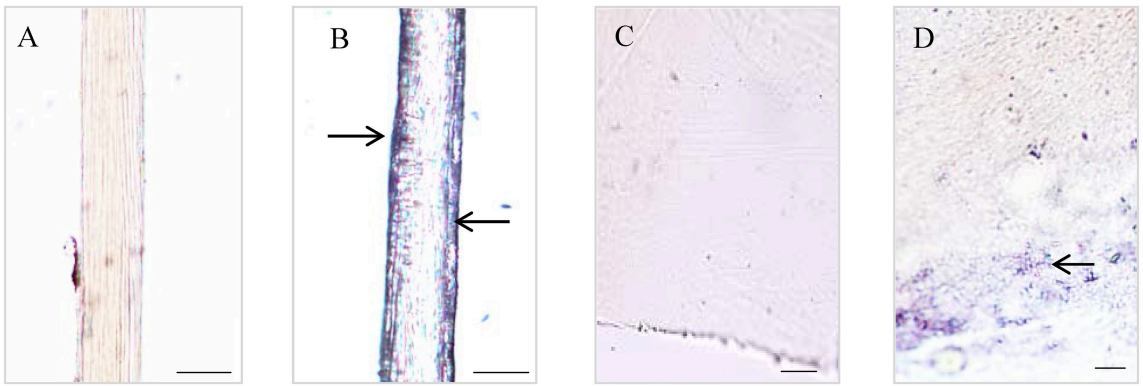

FIGURE 2 | Histological staining observations on different parts of *Limnoperna fortunei* byssus. Light micrographs of byssal thread longitudinal section before **(A)** and after **(B)** nitroblue tetrazolium (NBT)/Glycinate staining. Light micrographs of adhesive plaque transverse section before **(C)** and after **(D)** NBT/Glycinate staining. The arrows indicate the distribution regions of Dopa-containing proteins stained by NBT/Glycinate. Bar scale is 20 μm in **(A**,**B)**, and 10 μm in **(C,D)**.

which was secreted by foot tissue (**Figure 1B**), was 1.0–1.5 cm in length and could be divided into three parts: proximal thread, distal thread, and adhesive plaque (**Figure 1C**). Diameter of a byssal thread increased from proximal (15–20 μm) to distal end (25–30 μm, **Figures 1D,E**). At the distal end, an elliptical adhesive plaque with dramatically larger surface area (around 0.08 cm^2) allowed *L. fortunei* to fully attach to hard substrates (**Figure 1F**). SEM observation illustrated two distinct structures of a byssal thread: an outer cuticle and an inner fibrous core. The cuticle was smooth and fibers were closely aligned in the proximal thread, forming a compact structure (**Figure 1G**). Unlike proximal thread, the distal thread was a loosely organized structure with distinct boundary among inner filamentary fibers (**Figure 1H**). The cuticle of the adhesive plaque was smooth, while the underside attaching to substratum was rough with numerous cavities distributed along the thread (**Figure 1I**).

Dopa Staining Analysis

The Dopa-containing proteins stained by NBT/Glycinate had liner distributions in the longitudinal section of byssal thread (**Figure 2**) and were located at the outer sheath (**Figures 2A,B**). However, in adhesive plaque they were flocculent structures and located at the bottom of adhesive plaque transverse section (**Figures 2C,D**). These results suggest the potential locations of Dopa-containing foot proteins in different parts of byssus.

Transcriptome Sequencing and Adhesion-Related Gene Screening

A total of 73,231,128 nt raw data and 72,686,438 clean sequence reads were obtained from foot tissues, and the percentage of base number with Phred > 30 (Q30) in total bases is 92.89% (Table S2), yielding 92,951 unigenes with an average length of 681 bp and a N50 of 946 bp (Table S3 and Figure S1). A total of 26,262 (28.25%) and 21,624 (23.26%) unigenes were annotated to NR and Swiss-Prot database, respectively. Due to the lack of availability of freshwater species, the retrieved species were mainly confined in marine invertebrates such as *Crassostrea gigas*, *Lottia gigantea*, *Lingula anatina*, *Aaplysia californica,* and *Octopus bimaculoides* in NR database (E-value ≤ 1.0e-5, Figure S2) and vertebrates such as *Homo sapiens*, *Mus musculus*, *Rattus norvegicus,* and *Danio rerio* in Swiss-Prot database (E-value ≤ 1.0e-5, Figure S3).

A total of 17,871 (19.23%) unigenes were assigned to COG terms (Figure S4 and Table S4). The most representative terms for COG analysis were "Post-transcriptional modification, protein turnover, chaperone," "General function prediction only," "Function unknown," and "Signal transduction mechanism." Meanwhile, a total of 9,368 unigenes (10.08%) were assigned to KEGG terms (Figure S5 and Table S5). The most representative terms for KEGG analysis were "Transport and catabolism" and "Cell growth and death" in "Cellular process," "Signal transduction" in "Environmental information processing" and "Nervous system," "Immune system" and "Endocrine system" in "Organismal system".

In total, eight typical adhesion-related genes, which contained 12 unigenes, were obtained from the foot transcriptome (**Table 1**). These genes encoded foot/byssal proteins (*FP-1, FP-2, FP-3*), thread matrix protein (*TMP*), proximal thread matrix protein (*PTMP*), and precollagen (*preCOL-NG, preCOL-P,* and *preCOL-D*). These adhesion-related unigenes were well-annotated to corresponding homologs in marine mussels *M. coruscus*, *M. galloprovincialis,* and *M. edulis* with an average identity of 45.25%. Alignment analysis indicated that the foot proteins encoded by these genes in *L. fortunei* contained typical domains and motifs of known mussel foot proteins, such as EGF domain in foot protein 2, vWFA domain in proximal thread matrix protein and GXX motif in thread matrix protein and precollagens (**Figure 3**).

LC-MS/MS and Foot Proteins Identification

Proteins were successfully extracted from foot tissue and byssal thread of *L. fortunei*. Totally, 11 clear regions with a molecular weight range of 10–150 KD were dissected from SDS-PAGE gels for foot and byssal proteins (Figure S6). LC-MS/MS analysis detected 18 byssal proteins from byssal thread (Table S6) and 81 proteins from foot tissue (Table S7), respectively. By integrating

TABLE 1 | Typical adhesion-related genes in foot transcriptome of the golden mussel *Limnoperna fortunei*.

Unigene	Symbol	Length (bp)	Description	E-value	Identity (Amino acid)	Domain / motif	Swiss-id
comp98491_c0_seq1	BP-1	510	|AKI87984.1|byssal protein-1 [*Mytilus coruscus*]	7.0e-35	(70/135) 51.85%	—	sp|P33450|FAT_DROME
comp113423_c0_seq1	FP-2	363	|BAQ74176.1|putative foot protein-2 [*Limnoperna fortunei*]	1.0e-19	(106/108) 98.15%	EGF	sp|Q14517|FAT1_HUMAN
comp117406_c1_seq2	FP-2	524	|BAQ74176.1|putative foot protein-2 [*Limnoperna fortunei*]	5.0e-26	(132/133) 99.25%	EGF	sp|Q2PZL6|FAT4_MOUSE
comp155923_c0_seq1	FP-2	549	|AAX23970.1|foot protein 2 [*Mytilus edulis*]	4.0e-14	(56/140) 40.00%	EGF	sp|Q25464|FP2_MYTGA
comp119431_c0_seq1	FP-2	1111	|AAX23970.1|foot protein 2 [*Mytilus edulis*]	5.0e-88	(173/337) 51.34%	EGF	sp|Q25464|FP2_MYTGA
comp112372_c0_seq2	BP-3	1199	|AKI87986.1|byssal protein-3 [*Mytilus coruscus*]	3.0e-34	(55/129) 42.64%	—	sp|P49013|FBP3_STRPU
comp102200_c0_seq2	BP-3	696	|AKI87986.1|byssal protein-3 [*Mytilus coruscus*]	1.0e-24	(55/129) 42.64%	—	—
comp119176_c1_seq3	TMP	1399	|AAC33847.1|thread matrix protein [*Mytilus edulis*]	9.0e-28	(21/35) 60.00%	GXX motif	—
comp107331_c0_seq3	PTMP-1a	999	|AAL83537.1|proximal thread matrix protein 1 variant a [*Mytilus edulis*]	5.0e-12	(51/151) 33.77%	vWFA	sp|A2AX52|CO6A4_MOUSE
comp119875_c0_seq1	proCOL-NG	1571	|ALA16018.1|precollagen NG [*Mytilus coruscus*]	3.0e-12	(125/220) 56.82%	GXX motif	sp|A6H584|CO6A5_MOUSE
comp120266_c1_seq1	proCOL-P	2866	|AAM34600.1|precollagen-P [*Mytilus galloprovincialis*]	3.0e-13	(44/133) 33.08%	GXX motif	sp|Q14050|CO9A3_HUMAN
comp124514_c0_seq1	proCOL-D	2246	|AAB96638.1|precollagen D [*Mytilus edulis*]	1.0e-147	(44/131) 33.59%	GXX motif	sp|P27393|CO4A2_ASCSU

The "—" indicates no characterized domain.

adhesion-related unigenes, foot proteins and byssal proteins, a total of 16 foot proteins were identified (**Table 2**, Figure S7). These proteins could be classified into four types: (1) foot/byssal proteins, such as foot protein-2 (Lffp-2), byssal protein-1 (Lfbp-1), and byssal protein-3 (Lfbp-3); (2) enzymes: such as byssal peroxidase-like proteins (type 1, 2, and 4) and protease inhibitor-like protein-D2; (3) cellular framework proteins, such as tubulin alpha chain, histone H2B, and ribosomal proteins (type S3 and S14); and (4) other associated proteins, such as tropomyosin, p-glycoprotein, heat shock protein 70 (HSP 70), and byssal HSP-like protein 1. These adhesives proteins exhibited high homologies to known foot/byssal proteins in bivalves. In addition, Ala, Asp, Gly, Glu, Leu, Ser, Thr, and Val were the most abundant amino acids. The abundances of these amino acids were between 6 and 18%. Multiple repetitive motifs were found in these foot proteins. Distinct functional domains were also predicted, such as epidermal growth factor (EGF) domain in foot protein-2, ALPHA-TUBLIN domain in tubulin alpha chain, TROPOMYOSIN domain in tropomyosin, and HSP-70 domain in heat shock protein 70.

Expression Profiles of the Foot Protein Genes

RT-qPCR results indicated that the expression of selected foot protein genes was tissue-specific (**Figure 4A**). The foot/byssal protein genes *BP-1, FP-2,* and *BP-3* were specifically expressed in foot and their expression levels were 350.62-, 1484.25-, and 165.43-fold higher than that in adductor muscle, respectively. *TUB, HSP-70,* and *BPLP-2* also expressed in foot tissue but their expressions were more concentrated in other tissues. The relative expression levels of *TUB, HSP-70,* and *BPLP-2* were 84.38-fold higher in mantle, 190.01-fold higher in gonads and 125.89-fold higher in gonads than that in adductor muscle, respectively ($p < 0.05$). Byssal threads rapidly regenerated at early stages after removing original byssus and leveled off after 5 days (**Figure 4B**), indicating a platform period for the total number of byssal threads. The expression levels of all selected foot protein genes increased with byssus production but reached highest levels at different rates. Specifically, *HSP-70* reached its highest expression level on day 1 and maintained this level from day 1 to day 7. The expression level of *BP-3* exhibited a sharp increase on day 1 and reached the highest level on day 5. The expression levels of *TUB, BP-1, FP-2,* and *BPLP-2* sharply increased since day 3 and reached their highest levels on day 3, day 7, day 3 and day 7, respectively. It was thus clear that the expression profiles of *BP-1, FP-2,* and *BP-3* were closely related to byssus regeneration, suggesting that these genes play key roles in byssus formation.

Ion Composition and Content

All 13 metal ions were tested from foot tissue and byssal thread samples with similar percentages (**Table 3**). Ca^{2+}, Mg^{2+}, Zn^{2+}, Al^{3+}, and Fe^{3+} were the most abundant metal ions in foot tissue with the content order of Ca^{2+} (35.59 mg·g tissue^{-1}) > Mg^{2+} (26.37 mg·g tissue^{-1}) > Zn^{2+} (23.28 mg·g tissue^{-1}) > Al^{3+} (3.48 mg·g tissue^{-1}) > Fe^{3+} (1.65 mg·g tissue^{-1}), while Ca^{2+}, Mg^{2+}, Zn^{2+}, Al^{3+}, and Fe^{3+} were the most abundant metal ions in byssal threads with the content order of Mg^{2+}

(3.81 mg·g byssus^{-1}) > Ca^{2+} (3.58 mg·g byssus^{-1}) > Al^{3+} (1.16 mg·g byssus^{-1}) > Fe^{3+} (0.92 mg·g byssus^{-1}) > Zn^{2+} (0.32 mg·g byssus^{-1}).

DISCUSSION

Byssus morphology is largely similar among bivalves, but its ultrastructure can greatly vary among these species. In this study, byssal threads of the golden mussel *L. fortunei* became increasingly less compact from the proximal end to the distal end, which was consistent with previous studies on *D. polymorpha* (Farsad and Sone, 2012), *M. edulis* and *M. galloprovincialis* (Suhre et al., 2014; Reddy and Yang, 2015). This structure is important for mussel's self-reducing behavior, largely improving migration and predator-prey escape abilities by byssus de-adhesion and re-adhesion (Waite, 2017). The compact proximal end allows large numbers of byssal threads secretion in limited areas of foot tissues, and the less compact distal end facilitates inner fibers to spread out to form larger adhesive plaques, which may be both beneficial for byssus production and adhesion. Highly oriented structures in distal threads were considered to be related to byssus extensibility and stiff (Gosline et al., 2002; Farsad and Sone, 2012), representing firm byssus adhesion in *L. fortunei*. In addition, SEM results illustrated a highly porous adhesive plaque in *L. fortunei*, and such a structure was also observed in other mussel species such as *D. polymorpha* (Farsad and Sone, 2012), *M. edulis* (Benedict and Waite, 1986), and *M. californianus* (Waite, 1986). The number of cavities on adhesive plaque was suggested to be associated with adhesion ability as such cavities could participate in the formation of foot proteins by regulating protein coacervation (Waite et al., 2005). This view was supported by empirical evidence, for example, *M. californianus* has more pores in adhesive plaques than *M. edulis*, because the former lived in more turbulent intertidal environments (Waite, 1986). The abundant cavities may be conducive for *L. fortunei* to rapidly adhere and adapt to a new underwater environment. It is thus clear that the well-formed byssus structure of *L. fortunei* may increase invasive and fouling risks.

Structural integrity and adhesive properties of byssus are determined by foot proteins. Typical mussel adhesion-related foot proteins contain foot/byssal proteins (Mfps), collagen gland proteins (proCOLs) and thread matrix proteins (TPMs, Waite, 2017). In this study, the homologous genes coding these foot proteins were obtained from *L. fortunei* foot transcriptome. Sequence analyses indicated that these genes have conserved adhesion-related domains, such as EGF domain in *FP-2* and GXX domain in preCols. So far, more than six foot/byssal protein genes have been identified to be responsible for byssus adhesion, while only three of them (*BP-1*, *FP-2,* and *BP-3*) were isolated from *L. fortunei*. Interestingly, these *L. fortunei* foot protein genes showed low similarities to those found in other mussels. All results suggest a high level of species-specificity of these genes in bivalves. Indeed, adhesion-related proteins were diverse among aquatic organisms and even among bivalves (Miao et al., 2015), and most of them have more than one homologous genes. Such high polymorphism was suggested to explain the outstanding adaptabilities of mussels to a variety of substrata (Warner and Waite, 1999), which may be crucial to successful invasions and fouling by *L. fortunei*. Compared with other marine mussels, the foot/byssal proteins of *L. fortunei* were deficient in LC-MS/MS results, where only Lfbp-1, Lffp-2, and Lfbp-3 were identified, further demonstrating the high diversity of foot proteins in bivalves. In addition, proCOLs and TMPs were also absent in foot and byssus proteomes of *L. fortunei*. Collectively, three possible reasons may explain the absence of these proteins: (1) A major problem may be sample preparation, since the total foot tissue but not a limited region around the foot gland was used as the sample to conduct transcriptome sequencing. The whole foot sample can generate abundant transcripts to cover the relative low transcription of those genes for byssus synthesis and adhesion (Zhang et al., 2017). (2) These foot proteins may be different from known ones in structure and/or amino acid composition, thus it is difficult to be dissolved into the extraction solutions. (3) The widely distributed repetitive motifs may disturb protein enzymolysis and subsequently data search. Similar issues have been found in *M. coruscus* and *C. farreri* when their foot/byssal proteins were extracted (Miao et al., 2015; Qin et al., 2016). Acid-Urea methods were widely used by these studies to extract proteins from byssus because the generally major proteins in byssus (i.g. cross-linked proteins) were not simply isolated. However, this study confirmed that acetone precipitation method may be also effective in extracting foot and byssal proteins from mussel byssus. In addition, NBT/ Glycinate staining indicated that Dopa was located both in byssal thread and adhesive plaque of *L. fortunei*. The Dopa location regions of this species were consistent with that of the marine mussel *M. coruscus* (Qin et al., 2016), suggesting the basic characteristic of mussel Dopa-containing foot proteins.

By comparing foot transcriptome, foot proteome and byssal proteome, a total of 16 representative foot proteins and their coding genes were identified from *L. fortunei*. The homologs of these foot proteins have been proven to participate in byssus formation and interface adhesion in marine bivalves (Gantayet et al., 2014; Liu et al., 2015; Miao et al., 2015; Waite, 2017). The 16 proteins possessed abundant repetitive motifs. Motifs and modifications are the common features of adhesion-related proteins in marine mussels and scallops (Miao et al., 2015; Qin et al., 2016). Repetitive motifs often form regular or specific secondary structures (Taylor et al., 1994), which could promote interactions among foot proteins in *L. fortunei*. COG analysis indicated that the "Post-transcriptional modification, protein turnover, and chaperone" term was significantly enriched in foot transcriptome of *L. fortunei*. Modification plays a key role in byssus adhesion, for example, oxidation of Dopa (i.e., Dopa to dopaquinone) weakened adhesion of Mfps to substratum surfaces (Nicklisch et al., 2016), but strengthen cross-links among foot proteins during plaque formation (Yu et al., 2011). Staining analysis suggested that Dopa-containing proteins were located in byssal thread and adhesive plaque, which strongly supports the COG result. Carbamidomethyl modification, however, has not been well-studied on its specific function in regulating byssus adhesion though it was also identified in *C. farreri* byssus (Miao

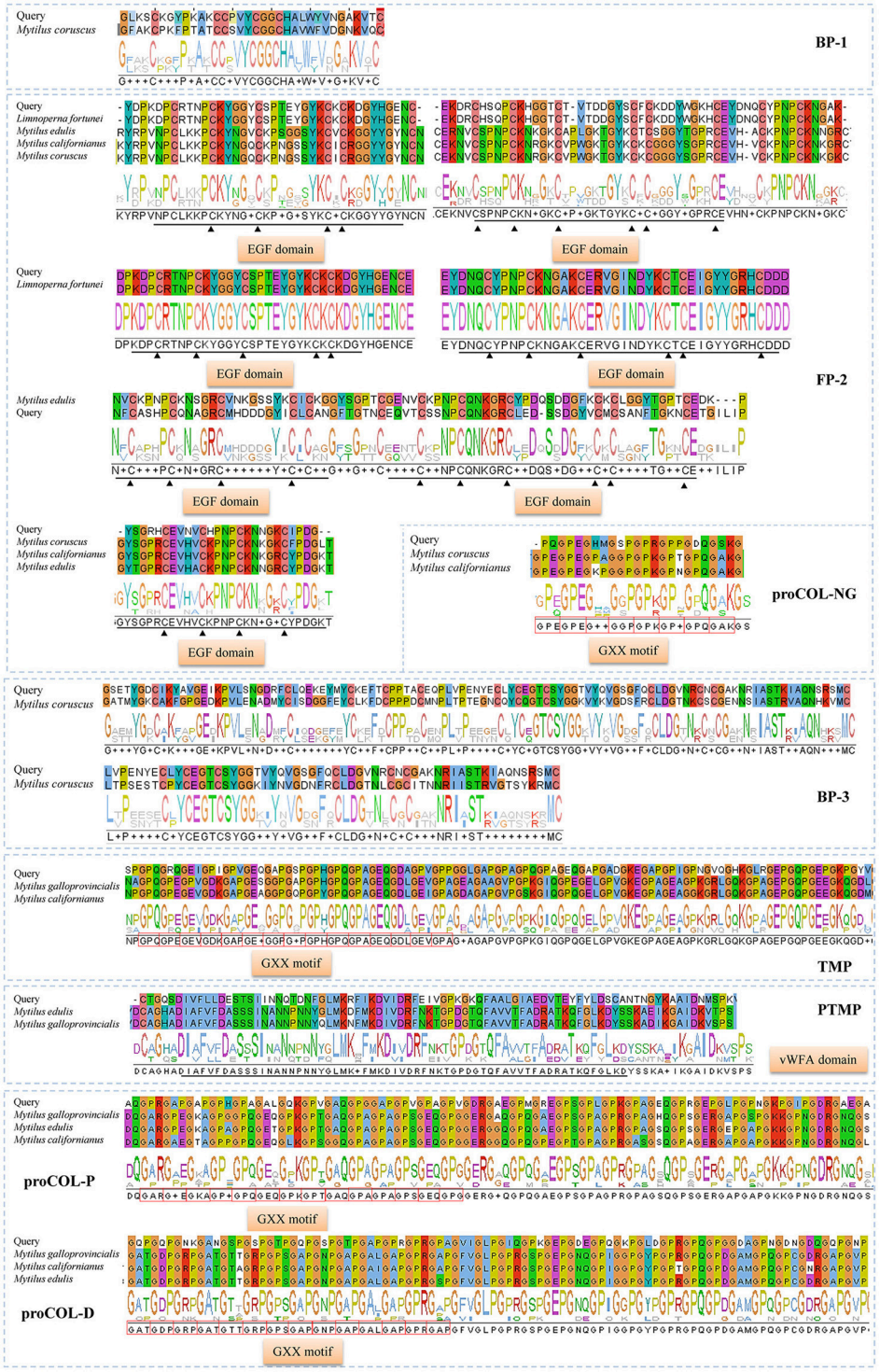

FIGURE 3 | Homologous alignments of foot protein genes identified from foot transcriptome of *Limnoperna fortunei*. Alignment result for each gene contains similarity regions of amino acids (shadow) and consensus logo (below the shadow). The regions marked by black straight lines and triangles are conserved EGF domains and the red boxes indicate GXX motifs. The amino acid sequences used for these alignments are as follows. Bp-1: *Mytilus coruscus* [AKI87984.1]; Fp-2: *Limnoperna fortunei* [BAO74176.1], *Mytilus edulis* [AAX23970.1], *Mytilus californianus* [AST36139.1] and *Mytilus coruscus* [ALA16015.1]; Bp-3: *Mytilus coruscus* [AKI87986.1]; proCOL-NG: *Mytilus coruscus* [ALA16018.1] and *Mytilus californianus* [ABW90433.1]; proCOL-D: *Mytilus galloprovincialis* [AAM34601.1], *Mytilus californianus* [ABW90432.1] and *Mytilus edulis* [AAB96638.1]; proCOL-P: *Mytilus galloprovincialis* [AAM34600.1], *Mytilus edulis* [AAB80719.1], and *Mytilus californianus* [ABW90434.1]; TMP: *Mytilus galloprovincialis* [AHI47022.1] and *Mytilus californianus* [ABW90433.1]; PTMP: *Mytilus edulis* [AAL83537.1] and *Mytilus galloprovincialis* [AAL17974.1].

TABLE 2 | The most representative foot proteins identified from the golden mussel *Limnoperna fortunei*.

Accession	Description	Score	Coverage	Unique Peptide	Amino acid composition	Domain	Matched Unigene
O96064	Paramyosin [*Mytilus galloprovincialis*]	1746.57	30.09	19	Ala (9.43%) Gln (7.51%) Gly (13.29%) Val (11.36%) Pro (6.64%)	—	comp124156_c0_seq1
A0K0YAX7	Filament-like protein-2 [*Mytilus coruscus*]	1284.48	40.88	14	Ala (7.92%) Asp (6.78%) Glu (7.32%) Gly (8.56%) Leu (7.37%) Pro(6.21%) Ser (7.45%) Thr (7.34%) Val (6.56%)	—	comp126030_c0_seq8
K1QQ68	Tubulin alpha chain [*Crassostrea gigas*]	1010.37	41.46	2	Ala (6.42%) Asp (6.71%) Glu (7.78%) Gly (8.74%) Leu (6.11%) Pro (7.34%) Ser (7.02%) Thr (6.14%) Val (7.33%)	ALPHA-TUBULIN	comp39206_c0_seq1
Q9GZ70	Tropomyosin [*Perna viridis*]	778.09	45.07	15	Ala (7.27%) Asp (7.04%) Glu (9.29%) Gly (7.25%) Leu (6.53%) Pro (6.46%) Ser (7.52%) Thr (6.02%) Val (7.28%)	TROPOMYOSIN	comp116888_c0464_seq2
A0K0YB30	Protease inhibitor-like protein-D2 [*Mytilus coruscus*]	571.54	241.99	2	Ala (9.22%) Asp (7.31%)Glu (7.25%) Gly (6.54%) Leu (10.32%) Pro (6.12%) Ser (6.94%) Thr (9.17%)	—	comp102054_c0_seq3
F0V4B3	Byssal protein-1 [*Mytilus galloprovincialis*]	445.72	8.96	2	Ala (9.61%) Asp (6.38%) Ile (6.01%) Leu (9.63%) Ser (3.57%) Thr (8.03%) Val (7.59%)	—	comp98491_c0_seq1
A024FCK3	Putative foot protein-2 [*Limnoperna fortunei*]	439.32	37.39	2	Ala (7.10%) Arg (6.54%) Asn (9.50%) Leu (7.72%) Met (7.74%) Phe (8.28%) Pro (9.45%) Val (10.10%)	EGF	comp119431_c0_seq1
A193DU97	Byssal HSP-like protein 1 [*Mytilus coruscus*]	340.48	38.51	2	Ala (7.44%) Asp (6.91%) Glu (6.43%) Gly (10.57%) Leu (6.91%) Pro (6.85%) Val (8.52%)	—	comp126799_c1_seq1
U5Y6N6	P-glycoprotein [*Perna viridis*]	300.07	36.31	4	Arg (6.12%) Asp (7.08%) Gln (10.21%) Gly (6.11%) Leu (8.17%) Pro (6.10%) Ser (10.22%) Val (8.24%)	—	Comp43007_c0_seq1
K1P7X2	40S ribosomal protein S14 [*Crassostrea gigas*]	288.09	88.32	2	Asp (9.04%) Gln (7.67%) Glu (14.13%) Gly (12.83%) Leu (11.45%) Ser (7.73%) Val (6.43%)	—	comp106676_c0_seq1
Q6PTI3	Byssal protein-3 [*Mytilus californianus*]	191.99	10.06	2	Asn (10.31%) Glu (7.40%) Gly (11.84%) Leu (14.70%) Thr (10.31%)	—	comp112372_c0_seq2
A193DUA2	Byssal peroxidase-like protein 2 [*Mytilus coruscus*]	190.68	201.35	2	Ala (7.70%) Asp (7.67%) Glu (8.78%) Ile (9.92%) Leu (13.22%) Ser (7.71%)	AN_PEROXIDASE	comp125734_c0_seq1
K1PUQ5	Histone H2B [*Crassostrea gigas*]	180.88	35.77	4	Ala (6.77%) Asp (6.75%) Gly (10.20%) Ile (9.14%) Leu (14.78%) Lys (6.76%) Thr (8.03%) Val (9.12%)	—	comp155404_c0_seq1
V5LVI9	Heat shock protein 70 [*Vulcanidas* sp.]	178.37	37.46	2	Ala (10.90%) Asp (7.12%) Glu (10.37%) Gly (7.72%) Leu (9.31%) Lys (6.04%) Phe (6.62%) Thr (8.67%)	HSP-70	comp113462_c0_seq1
A193DUA3	Byssal peroxidase-like protein 4 [*Mytilus coruscus*]	168.44	83.59	4	Ala (12.79%) Asn (7.65%) Asp (6.42%) Glu (12.80%) Ile (11.53%) Leu (7.67%) Phe (6.42%)	—	comp119654_c0_seq1
Q70MM6	Ribosomal protein S3 [*Crassostrea gigas*]	112.65	58.18	3	Asn (9.80%) Asp (7.78%) Gly (11.79%) Leu (17.56%) Thr (11.83%)	—	comp113325_c0_seq1

The "—" indicates no characterized domain.

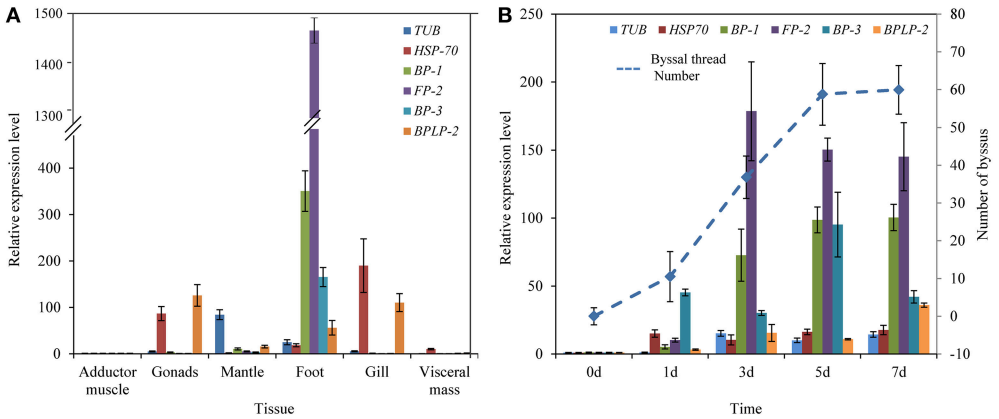

FIGURE 4 | Relative expression levels of six selective foot protein genes in different tissues **(A)** and byssus formation period **(B)** in the golden mussel *Limnoperna fortunei* detected by real-time quantitative PCR. *TUB*, Tubulin alpha chain; *HSP-70*, Heat shock protein 70; *BP-1*, Byssal protein-1; *FP-2*, Putative foot protein-2; *BP-3*, Byssal protein-3; *BPLP-2*, Byssal peroxidase-like protein 2. **(B)** The line chart indicates the changes in byssal thread numbers.

TABLE 3 | Metal ion contents in foot tissue and byssus of the golden mussel *Limnoperna fortunei* as detected by inductively coupled plasma mass spectrometry.

Organ	Metal ion content (Foot: mg·g tissue^{-1}/Byssus: mg·g byssus^{-1}) and percentage						
	Ca^{2+}	Mg^{2+}	Zn^{2+}	Fe^{3+}	Al^{3+}	Mn^{7+}	Pb^{4+}
Foot	35.59 ± 3.55	26.37 ± 3.29	23.28 ± 2.00	1.65 ± 0.34	3.48 ± 0.48	0.15 ± 0.23	(33.54 ± 4.21)×10^{-3}
Percentage	38.80%	28.75%	25.38%	1.80%	3.79%	0.16%	0.04%
Byssus	3.58 ± 0.44	3.81 ± 0.24	0.32 ± 0.05	0.92 ± 0.13	1.16 ± 0.28	0.16 ± 0.02	(20.40 ± 3.55)×10^{-3}
Percentage	34.09%	36.25%	3.02%	8.76%	11.02%	1.55%	0.15%
Organ	**Metal ion content (Foot: mg·g tissue^{-1}/ Byssus: mg·g byssus^{-1}) and percentage**						
	Cu^{2+}	Hg^{2+}	B^{3+}	Mo^{6+}	Ni^{2+}	Sr^{2+}	
Foot	0.08 ± 0.01	0.13 ± 0.03	0.13 ± 0.04	(2.14 ± 0.42)×10^{-3}	0.42 ± 0.36	0.41 ± 0.13	
Percentage	0.09%	0.14%	0.15%	< 0.01%	0.46%	0.45%	
Byssus	0.08 ± 0.01	(2.18 ± 0.53)×10^{-3}	0.31 ± 0.03	(1.36 ± 0.57)×10^{-3}	0.06 ± 0.01	0.09 ± 0.02	
Percentage	0.76%	0.02%	2.92%	0.01%	0.55%	0.89%	

et al., 2015). Interestingly, COG and KEGG analyses indicated that the annotated unigenes in *L. fortunei* foot transcriptome were significantly enriched in some signal transduction pathways. These results obtained here may provide valuable points to further study signal regulations of byssus adhesion, as the detailed molecular regulatory mechanisms for byssus adhesion in aquatic organisms remain elusive (Miao et al., 2015).

The three representative foot proteins, Lfbp-1, Lffp-2, and Lfbp-3 located at foot tissue, were highly expressed in the rapid byssus formation period, suggesting their crucial functions during byssus production. Two homologous proteins of them, bp-1 and bp-3, have been reported in *M. coruscus* but their functions have never been illuminated (Qin et al., 2016). Therefore, particular attention has been paid to Lffp-2 because the functions of its homologous proteins have been well-studied in marine mussels. The foot protein fp-2 was firstly identified from adhesive plaque in *M. edulis* (Reddy and Yang, 2015). It is the most abundant foot protein in inner part of adhesive plaque with a molecular weight of ∼45 KDa and a Dopa content of ∼5 mol%, accounting for 25% wet weight of plaque. It contains eleven EGF domains with abundant Ca^{2+} binding sites. Several homolog genes/proteins of *FP-2*/fp-2 have been isolated from mussels, including Pffp-2 from *L. fortunei* (Hwang et al., 2010; Uliano-Silva et al., 2014; Qin et al., 2016). The Pffp-2 is the only identified foot protein for which the open reading frame (ORF) has been sequenced so far (Uliano-Silva et al., 2014). In this study, the conserved EGF domain was found in Pffp-2, suggesting the potential adhesive function of this foot protein in *L. fortunei*. RT-qPCR analyses also strongly indicated that *PfFP-2* may be crucial to the adhesion of adhesive plaque in *L. fortunei*. Moreover, the specificities of other foot proteins such as enzymes and cellular fragment proteins were not as strong as foot/byssal proteins in the present study. It was reported that artificial contamination in the process of protein extraction could result in the presence of these proteins in byssus proteome (Qin et al., 2016). Whether these proteins in *L. fortunei* byssus are contamination is worth further studying in the future. However, these proteins might be involved in byssus adhesion because they were identified not only

in the byssus of *L. fortunei* but also in a variety of bivalves (Farsad and Sone, 2012; Gantayet et al., 2014; Miao et al., 2015; Qin et al., 2016).

The 16 representative foot proteins in *L. fortunei* have eight highly dominant amino acids. The abundances of these amino acids were between 6 and 18%, which were more than that in vertebrates (typically only 2–5% in vertebrate proteins), suggesting a high amino acid preference of these foot proteins. Such a high preference is similar to that found in freshwater mussel *D. polymorpha* (Gantayet et al., 2014) but dissimilar to that in marine mussel *M. oruscus* (Qin et al., 2016), suggesting the distinct amino acid preference between freshwater and marine species in foot proteins. Amino acids have strong metal ion binding capacity, for example, Glu and Asp most frequently bind to metal ions *via* charged or polar side chains (Golovin et al., 2005). Metal ions also can selectively bind to amino acids, for example, Ca^{2+} to Asn, Asp, Gly and Glu, Mg^{2+} to Glu and Asp, Fe^{3+} to His, Asp, Cys, Tyr and Glu, and Zn^{2+} to His and Cys (Lu et al., 2012). ICP-MS analysis demonstrated that Ca^{2+}, Mg^{2+}, Zn^{2+}, Al^{3+}, and Fe^{3+} were the most abundant metal ions in both foot tissue and byssal thread, which perfectly correspond to amino acid preference in the foot proteins of *L. fortunei*. Previous studies have found that mussel byssus and soft tissues had a strong ability to adsorb heavy metals, such as Ag, Ni, Mn, Fe, Zn, Hg, and Cd from surrounding environments by forming metal complexes between specific amino acids of foot proteins and heavy metals. Even after separation from mussels, the byssus still had a strong adsorption to these heavy metals (Szefer et al., 2002; Zhang et al., 2017). To a large extent, the detected high concentration of heavy metals in foot tissue and byssus in this study may be the result of metal accumulation by *L. fortunei*. In addition, metal ions such as Fe^{3+} and Ca^{2+} have significant impacts on the interactions between fp-2 and other foot proteins (e.g., Fp-3, Fp-4, and Fp−5) by binding to specific amino acid residues, forming the core function of adhesive plaques (Hwang et al., 2010; Lee et al., 2011). These metal ions also pose significant effects on self-assembly and Dopa oxidative cross-linking of adhesion-related proteins (Guo et al., 2015; Liu et al., 2016; Priemel et al., 2017). As mentioned above, Dopa has been observed in both byssal thread and adhesive plaque of *L. fortunei*. Therefore, we reasonably speculate that some metal ions play critical roles in byssus adhesion by interacting with amino acid residues in foot proteins of *L. fortunei,* which may also be the reason for the high concentration of other metal ions in byssus. (Taylor et al., 1994; Zhao and Waite, 2006; Harrington et al., 2009, 2010; Yu et al., 2011). More importantly, metal ions can affect byssus mechanical properties, as studies had shown that the strength of byssal threads varied with the metal ion concentrations in marine bivalves (Seguin-Heine et al., 2014; Li S. G. et al., 2017). These results illustrated the underlying roles of the interactions of metal ions and foot proteins in byssus adhesion, thus proving a valuable window of opportunity to manage biofouling through artificial intervention on these determining factors in either *L. fortunei* or other bivalve species such as *Dreissena* mussels (Gilbert and Sone, 2010; Gantayet et al., 2013; Rees et al., 2016).

CONCLUSIONS

Using multiple approaches, this study represents the first effort to clarify byssus structure, identify foot proteins and determine metal ions of foot tissue and byssus in the golden mussel *L. fortunei.* The obtained results suggest the structural characteristics of adhesive plaque, proximal, and distal threads highly conducive to byssus adhesion. Dopa is proved to be a *post-translational* modification in byssal thread and adhesive plaque. Sixteen representative foot proteins and their coding genes were identified from *L. fortunei*. In addition to heavy metals, potential interactions of these identified proteins and some specific metal ions may be important for byssus structural integrity and adhesive properties, indicating the key roles of foot proteins and metal ions involved in byssus adhesion. These results are beneficial to further reveal the molecular mechanism of *L. fortunei* byssus adhesion. Owing to the significant environmental implications, a comprehensive understanding on the mechanisms of byssus adhesion in freshwater mussels will facilitate to make strategies against biofouling of aquatic invasive organisms. In addition, the identified proteins from *L. fortunei* largely enrich the members of foot protein families in freshwater bivalves, providing abundant available genetic resources for underwater adhesives and antifouling materials studies.

ETHICS STATEMENT

This study did not involve endangered species and no specific permit was required for sampling.

AUTHOR CONTRIBUTIONS

SL and AZ designed and conducted the experiments. ZX, YG, and YC collected mussel samples. SL and AZ conducted data analyses and wrote the first version of this manuscript. SL, AZ, ZX, YG, and YC contributed to the completion of the manuscript.

FUNDING

This work was supported by Beijing Natural Science Foundation (No. 5182026), Youth Innovation Promotion Association, Chinese Academy of Sciences (2018054), and the National Natural Science Foundation of China (No. 31622011).

ACKNOWLEDGMENTS

The authors thank all editors and reviewers for insightful comments on the early versions of this manuscript.

SUPPLEMENTARY MATERIAL

The Supplementary Material for this article can be found online at: https://www.frontiersin.org/articles/10.3389/fphys.2018.00418/full#supplementary-material

REFERENCES

Ahn, B. K. (2017). Perspectives on mussel-inspired wet adhesion. *J. Am. Chem. Soc.* 139, 10166–10171. doi: 10.1021/jacs.6b13149

Amini, S., Kolle, S., Petrone, L., Ahanotu, O., Sunny, S., Sutanto, C. N., et al. (2017). Preventing mussel adhesion using lubricant-infused materials. *Science* 357, 668–673. doi: 10.1126/science.aai8977

Andrade, G. R., de Araújo, J. O. L. F., Nakamura Filho, A., Guañabens, A. C. P., Carvalho, M. D. D., and Cardoso, A. N. V. O. (2015). Functional Surface of the golden mussel's foot: morphology, structures and the role of cilia on underwater adhesion. *Mater. Sci. Eng. C* 54, 32–42. doi: 10.1016/j.msec.2015.04.032

Babarro, J. M. F., and Comeau, L. A. (2014). Byssus attachment strength of two mytilids in mono-specific and mixed-species mussel beds. *Biofouling* 30, 975–985. doi: 10.1080/08927014.2014.953941

Benedict, C. V., and Waite, J. H. (1986). Composition and ultrastructure of the byssus of *Mytilus edulis*. *J. Morphol.* 189, 261–270. doi: 10.1002/jmor.1051890305

Boltovskoy, D., Xu, M., and Nakano, D. (2015). "Impacts of *Limnoperna fortunei* on man-made structures and control strategies: General overview," in The *Limnoperna Fortunei: the Ecology, Distribution and Control of a Swiftly Spreading Invasive Fouling Mussel,* ed D. Boltovskoy (Cham: Springer International Publishing), 375–393.

DeMartini, D. G., Errico, J. M., Sjoestroem, S., Fenster, A., and Waite, J. H. (2017). A cohort of new adhesive proteins identified from transcriptomic analysis of mussel foot glands. *J. R. Soc. Interface* 14:0151. doi: 10.1098/rsif.2017.0151

Farsad, N., and Sone, E. D. (2012). Zebra mussel adhesion: structure of the byssal adhesive apparatus in the freshwater mussel, *Dreissena polymorpha*. *J. Struct. Biol.* 177, 613–620. doi: 10.1016/j.jsb.2012.01.011

Flammang, P., Demeuldre, M. L., Hennebert, E., and Santos, R. (2016). "Adhesive secretions in echinoderms: a review," in *The Biological Adhesives,* ed A. M.Smith (Cham: Springer International Publishing), 193–222.

Gantayet, A., Ohana, L., and Sone, E. D. (2013). Byssal proteins of the freshwater zebra mussel, *Dreissena polymorpha*. *Biofouling* 29, 77–85. doi: 10.1080/08927014.2012.746672

Gantayet, A., Rees, D. J., and Sone, E. D. (2014). Novel proteins identified in the insoluble byssal matrix of the freshwater zebra mussel. *Mar. Biotechnol.* 16, 144–155. doi: 10.1007/s10126-013-9537-9

Gilbert, T. W., and Sone, E. D. (2010). The byssus of the zebra mussel (*Dreissena polymorpha*): spatial variations in protein composition. *Biofouling* 26, 829–836. doi: 10.1080/08927014.2010.524298

Golovin, A., Dimitropoulos, D., Oldfield, T., Rachedi, A., and Henrick, K. (2005). MSDsite: a database search and retrieval system for the analysis and viewing of bound ligands and active sites. *Proteins Struct. Funct. Bioinf.* 58, 190–199. doi: 10.1002/prot.20288

Gosline, J., Lillie, M., Carrington, E., Guerette, P., Ortlepp, C., and Savage, K. (2002). Elastic proteins: biological roles and mechanical properties. *Philos. Trans. R. Soc. Lond. B Biol. Sci.* 357, 121–132. doi: 10.1098/rstb.2001.1022

Grabherr, M. G., Haas, B. J., Yassour, M., Levin, J. Z., Thompson, D. A., Amit, I., et al. (2011). Full-length transcriptome assembly from RNA-Seq data without a reference genome. *Nat. Biotechnol.* 29, 644–652. doi: 10.1038/nbt.1883

Guerette, P. A., Hoon, S., Seow, Y., Raida, M., Masic, A., Wong, F. T., et al. (2013). Accelerating the design of biomimetic materials by integrating RNA-Seq with proteomics and materials science. *Nat. Biotechnol.* 31, 908–915. doi: 10.1038/nbt.2671

Guo, Z. W., Ni, K. F., Wei, D. Z., and Ren, Y. H. (2015). Fe^{3+}-induced oxidation and coordination cross-linking in catechol-chitosan hydrogels under acidic pH conditions. *RSC Adv.* 5, 37377–37384. doi: 10.1039/C5RA03851K

Hall, T. A. (1999). BioEdit: a user-friendly biological sequence alignment editor and analysis program for Windows 95/98/NT. *Nucl. Acids. Symp.* 41, 95–98.

Harrington, M. J., Gupta, H. S., Fratzl, P., and Waite, J. H. (2009). Collagen insulated from tensile damage by domains that unfold reversibly: *in situ* X-ray investigation of mechanical yield and damage repair in the mussel byssus. *J. Struct. Biol.* 167, 47–54. doi: 10.1016/j.jsb.2009.03.001

Harrington, M. J., Masic, A., Holten-Andersen, N., Waite, J. H., and Fratzl, P. (2010). Iron-clad fibers: a metal-Based biological strategy for hard flexible coatings. *Science* 328, 216–220. doi: 10.1126/science.1181044

Hennebert, E., Maldonado, B., Ladurner, P., Flammang, P., and Santos, R. (2015). Experimental strategies for the identification and characterization of adhesive proteins in animals: a review. *Interface Focus* 5:20140064. doi: 10.1098/rsfs.2014.0064

Holten-Andersen, N., Fantner, G. E., Hohlbauch, S., Waite, J. H., and Zok, F. W. (2007). Protective coatings on extensible biofibres. *Nat. Mater.* 6, 669–672. doi: 10.1038/nmat1956

Holten-Andersen, N., Mates, T. E., Toprak, M. S., Stucky, G. D., Zok, F. W., and Waite, J. H. (2009a). Metals and the integrity of a biological coating: the cuticle of mussel byssus. *Langmuir* 25, 3323–3326. doi: 10.1021/la8027012

Holten-Andersen, N., Zhao, H., and Waite, J. H. (2009b). Stiff coatings on compliant biofibers: the cuticle of *Mytilus californianus* byssal threads. *Biochemistry* 48, 2752–2759. doi: 10.1021/bi900018m

Hou, J., Zhou, Y., Wang, C. J., Li, S., and Wang, X. K. (2017). Toxic effects and molecular mechanism of different types of silver nanoparticles to the aquatic crustacean *Daphnia magna*. *Environ. Sci. Technol.* 51, 12868–12878. doi: 10.1021/acs.est.7b03918

Hwang, D. S., Zeng, H., Masic, A., Harrington, M. J., Israelachvili, J. N., and Waite, J. H. (2010). Protein- and metal-dependent interactions of a prominent protein in mussel adhesive plaques. *J. Biol. Chem.* 285, 25850–25858. doi: 10.1074/jbc.M110.133157

Kamino, K. (2016). "Barnacle underwater attachment," in *The Biological Adhesives*, ed A. M.Smith (Cham: Springer International Publishing), 153–176.

Lee, B. P., Messersmith, P. B., Israelachvili, J. N., and Waite, J. H. (2011). Mussel-inspired adhesives and coatings. *Annu. Rev. Mater. Res.* 41, 99–132. doi: 10.1146/annurev-matsci-062910-100429

Li, S. G., Huang, J. L., Liu, C., Liu, Y. J., Zheng, G. L., Xie, L. P., et al. (2016). Interactive effects of seawater acidification and elevated temperature on the transcriptome and biomineralization in the pearl oyster *Pinctada fucata*. *Environ. Sci. Technol.* 50, 1157–1165. doi: 10.1021/acs.est.5b05107

Li, S. G., Liu, C., Zhan, A. B., Xie, L. P., and Zhang, R. Q. (2017). Influencing mechanism of ocean acidification on byssus performance in the pearl oyster *Pinctada fucata*. *Environ. Sci. Technol.* 51, 7696–7706. doi: 10.1021/acs.est.7b02132

Li, Y. L., Sun, X. Q., Hu, X. L., Xun, X. G., Zhang, J. B., Guo, X. M., et al. (2017). Scallop genome reveals molecular adaptations to semi-sessile life and neurotoxins. *Nat. Commun.* 8:1721. doi: 10.1038/s41467-017-01927-0

Liu, C., Li, S. G., Huang, J. L., Liu, Y. J., Jia, G. C., Xie, L. P., et al. (2015). Extensible byssus of *Pinctada fucata*: Ca^{2+}-stabilized nanocavities and a thrombospondin-1 protein. *Sci. Rep.* 5:15018. doi: 10.1038/srep15018

Liu, C., Xie, L. P., and Zhang, R. Q. (2016). Ca^{2+} mediates the self-assembly of the foot proteins of *Pinctada fucata* from the nanoscale to the microscale. *Biomacromolecules* 17, 3347–3355. doi: 10.1021/acs.biomac.6b01125

Livak, K. J., and Schmittgen, T. D. (2001). Analysis of relative gene expression data using real-time quantitative PCR and the $2^{-\Delta\Delta CT}$ method. *Methods* 25, 402–408. doi: 10.1006/meth.2001.1262

Lu, C. H., Lin, Y. F., Lin, J. J., and Yu, C. S. (2012). Prediction of metal ion-binding sites in proteins using the fragment transformation method. *PLoS ONE* 7:e39252. doi: 10.1371/journal.pone.0039252

Miao, Y., Zhang, L. L., Sun, Y., Jiao, W. Q., Li, Y. P., Sun, J., et al. (2015). Integration of transcriptomic and proteomic approaches provides a core set of genes for understanding of scallop attachment. *Mar. Biotechnol.* 17, 523–532. doi: 10.1007/s10126-015-9635-y

Nicklisch, S. C. T., Spahn, J. E., Zhou, H., Gruian, C. M., and Waite, J. H. (2016). Redox capacity of an extracellular matrix protein associated with adhesion in *Mytilus californianus*. *Biochemistry* 55, 2022–2030. doi: 10.1021/acs.biochem.6b00044

Nicklisch, S. C. T., and Waite, J. H. (2012). Mini-review: the role of redox in Dopa-mediated marine adhesion. *Biofouling* 28, 865–877. doi: 10.1080/08927014.2012.719023

Ohkawa, K., Nishida, A., Honma, R., Matsui, Y., Nagaya, K., Yuasa, A., et al. (1999a). Studies on fouling by the freshwater mussel *Limnoperna fortunei* and the antifouling effects of low energy surfaces. *Biofouling* 13, 337–350. doi: 10.1080/08927019909378389

Ohkawa, K., Nishida, A., Ichimiya, K., Matsui, Y., Nagaya, K., Yuasa, A., et al. (1999b). Purification and characterization of a dopa-containing protein from the foot of the Asian freshwater mussel, *Limnoperna fortunei*. *Biofouling* 14, 181–188. doi: 10.1080/08927019909378409

Ohkawa, K., and Nomura, T. (2015). "Control of *Limnoperna fortunei* fouling: Antifouling materials and coatings," in *The Limnoperna fortunei: The Ecology,*

Distribution and Control of a Swiftly Spreading Invasive Fouling Mussel, ed D. Boltovskoy (Cham: Springer International Publishing), 395–415.

Priemel, T., Degtyar, E., Dean, M. N., and Harrington, M. J. (2017). Rapid self-assembly of complex biomolecular architectures during mussel byssus biofabrication. *Nat. Commun.* 8:14539. doi: 10.1038/ncomms14539

Qin, C. L., Pan, Q., Qi, Q., Fan, M., Sun, J., Li, N. N., et al. (2016). In-depth proteomic analysis of the byssus from marine mussel *Mytilus coruscus*. *J. Proteomics* 144, 87–98. doi: 10.1016/j.jprot.2016.06.014

Reddy, N., and Yang, Y. (2015). "Mussel byssus fibers," in *The Innovative Biofibers from Renewable Resources,* eds N. Reddy and Y. Yang (Berlin; Heidelberg: Springer Berlin Heidelberg), 187–191.

Rees, D. J., Hanifi, A., Manion, J., Gantayet, A., and Sone, E. D. (2016). Spatial distribution of proteins in the quagga mussel adhesive apparatus. *Biofouling* 32, 205–213. doi: 10.1080/08927014.2015.1135426

Seguin-Heine, M., Lachance, A. E., Genard, B., Myrand, B., Pellerin, C., Marcotte, I., et al. (2014). Impact of open sea habitat on byssus attachment of suspension-cultured blue mussels (*Mytilus edulis*). *Aquaculture* 426–427, 189–196. doi: 10.1016/j.aquaculture.2014.02.006

Suhre, M. H., Gertz, M., Steegborn, C., and Scheibel, T. (2014). Structural and functional features of a collagen-binding matrix protein from the mussel byssus. *Nat. Commun.* 5:3392. doi: 10.1038/ncomms4392

Szefer, P., Frelek, K., Szefer, K., Lee, C. B., Kim, B. S., Warzocha, J., et al. (2002). Distribution and relationships of trace metals in soft tissue, byssus and shells of *Mytilus edulis* trossulus from the southern Baltic. *Environ. Pollut.* 120, 423–444. doi: 10.1016/S0269-7491(02)00111-2

Taylor, S. W., Waite, J. H., Ross, M. M., Shabanowitz, J., and Hunt, D. F. (1994). trans-2,3-cis-3,4-Dihydroxyproline, a new naturally occurring amino acid, is the sixth residue in the tandemly repeated consensus decapeptides of an adhesive protein from *Mytilus edulis*. *J. Am. Chem. Soc.* 116, 10803–10804. doi: 10.1021/ja00102a063

Uliano-Silva, M., Americo, J. A., Brindeiro, R., Dondero, F., Prosdocimi, F., and de Freitas Rebelo, M. (2014). Gene discovery through transcriptome sequencing for the invasive mussel *Limnoperna fortunei*. *PLoS ONE* 9:e102973. doi: 10.1371/journal.pone.0102973

Waite, J. H. (1986). Mussel glue from *Mytilus californianus* Conrad: a comparative study. *J. Comp. Physiol. B* 156, 491–496. doi: 10.1007/BF00691034

Waite, J. H. (2017). Mussel adhesion-essential footwork. *J. Exp. Biol.* 220, 517–530. doi: 10.1242/jeb.134056

Waite, J. H., Andersen, N. H., Jewhurst, S., and Sun, C. (2005). Mussel adhesion: finding the tricks worth mimicking. *J. Adhes.* 81, 297–317. doi: 10.1080/00218460590944602

Waite, J. H., and Tanzer, M. L. (1981). Polyphenolic substance of *Mytilus edulis*: novel adhesive containing L-Dopa and hydroxyproline. *Science* 212, 1038–1040. doi: 10.1126/science.212.4498.1038

Warner, S. C., and Waite, J. H. (1999). Expression of multiple forms of an adhesive plaque protein in an individual mussel, *Mytilus edulis*. *Mar. Biol.* 134, 729–734. doi: 10.1007/s002270050589

Wei, W., Yu, J., Broomell, C., Israelachvili, J. N., and Waite, J. H. (2013). Hydrophobic enhancement of Dopa-mediated adhesion in a mussel foot protein. *J. Am. Chem. Soc.* 135, 377–383. doi: 10.1021/ja309590f

Welladsen, H. M., Heimann, K., and Southgate, P. C. (2011). The effects of exposure to near-future levels of ocean acidification on activity and byssus production of the akoya pearl oyster, *Pinctada fucata*. *J. Shellfish Res.* 30, 85–88. doi: 10.2983/035.030.0112

Xia, Z. Q., Zhan, A. B., Gao, Y. C., Zhang, L., Haffner, G. D., and MacIsaac, H. J. (2017). Early detection of a highly invasive bivalve based on environmental DNA (eDNA). *Biol. Invasions* 20, 437–447. doi: 10.1007/s10530-017-1545-7

Xu, M. Z., Darrigran, G., Wang, Z. Y., Zhao, N., Lin, C. C., and Pan, B. Z. (2015). Experimental study on control of *Limnoperna fortunei* biofouling in water transfer tunnels. *J. Hydrol. Environ. Res.* 9, 248–258. doi: 10.1016/j.jher.2014.06.006

Xu, W., and Faisal, M. (2008). Putative identification of expressed genes associated with attachment of the zebra mussel (*Dreissena polymorpha*). *Biofouling* 24, 157–161. doi: 10.1080/08927010801975345

Yu, J., Wei, W., Danner, E., Ashley, R. K., Israelachvili, J. N., and Waite, J. H. (2011). Mussel protein adhesion depends on interprotein thiol-mediated redox modulation. *Nat. Chem. Biol.* 7, 588–590. doi: 10.1038/nchembio.630

Zhan, A., Perepelizin, P. V., Ghabooli, S., Paolucci, E., Sylvester, F., Sardia, P., et al. (2012). Scale-dependent post-establishment spread and genetic diversity in an invading mollusc in South America. *Divers. Distrib.* 18, 1042–1055. doi: 10.1111/j.1472-4642.2012.00894.x

Zhang, X. H., Ruan, Z. Q., You, X. X., Wang, J. T., Chen, J. M., Peng, C., et al. (2017). *De novo* assembly and comparative transcriptome analysis of the foot from Chinese green mussel (*Perna viridis*) in response to cadmium stimulation. *PLoS ONE* 12:e0176677. doi: 10.1371/journal.pone.0176677

Zhao, H., and Waite, J. H. (2006). Proteins in load-bearing junctions: the histidine-rich metal-binding protein of mussel byssus. *Biochemistry* 45, 14223–14231. doi: 10.1021/bi061677n

Conflict of Interest Statement: The authors declare that the research was conducted in the absence of any commercial or financial relationships that could be construed as a potential conflict of interest.

frontiers in Physiology

ORIGINAL RESEARCH
published: 23 May 2018
doi: 10.3389/fphys.2018.00597

Characterization of an Atypical Metalloproteinase Inhibitors Like Protein (Sbp8-1) From Scallop Byssus

Xiaokang Zhang[1†], Xiaoting Dai[1†], Lulu Wang[1], Yan Miao[1], Pingping Xu[1], Pengyu Liang[1], Bo Dong[1,2], Zhenmin Bao[1,3], Shi Wang[1,2], Qianqian Lyu[1,2] and Weizhi Liu[1,2]**

[1] MOE Key Laboratory of Marine Genetics and Breeding, College of Marine Life Sciences, Ocean University of China, Qingdao, China, [2] Laboratory for Marine Biology and Biotechnology, Qingdao National Laboratory for Marine Science and Technology, Ocean University of China, Qingdao, China, [3] Laboratory for Marine Fisheries Science and Food Production Processes, Qingdao National Laboratory for Marine Science and Technology, Qingdao, China

OPEN ACCESS

Edited by:
Xiaotong Wang,
Ludong University, China

Reviewed by:
Vengatesen Thiyagarajan,
The University of Hong Kong,
Hong Kong
Yongbo Bao,
Zhejiang Wanli University, China
Jian Hu,
Michigan State University,
United States

***Correspondence:**
Qianqian Lyu
lqqdo@163.com
Weizhi Liu
liuweizhi@ouc.edu.cn

[†] These authors have contributed equally to this work.

Specialty section:
This article was submitted to Aquatic Physiology, a section of the journal Frontiers in Physiology

Received: 09 March 2018
Accepted: 03 May 2018
Published: 23 May 2018

Citation:
Zhang X, Dai X, Wang L, Miao Y, Xu P, Liang P, Dong B, Bao Z, Wang S, Lyu Q and Liu W (2018) Characterization of an Atypical Metalloproteinase Inhibitors Like Protein (Sbp8-1) From Scallop Byssus. Front. Physiol. 9:597. doi: 10.3389/fphys.2018.00597

Adhesion is a vital physiological process for many marine molluscs, including the mussel and scallop, and therefore it is important to characterize the proteins involved in these adhesives. Although several mussel byssal proteins were identified and characterized, the study for scallop byssal proteins remains scarce. Our previous study identified two foot-specific proteins (Sbp7, Sbp8-1), which were annotated as the tissue inhibitors of metalloproteinases (TIMPs). Evolutionary analysis suggests that the *TIMP* genes of *Chlamys farreri* had gone through multiple gene duplications during evolution, and their potential functional roles in foot may have an ancient evolutionary origin. Focusing on the Sbp8-1, the sequence alignment and biochemical analyses suggest that Sbp8-1 is an atypical TIMP. One significant feature is the presence of two extra free Cys residues at its C-terminus, which causes the Sbp8-1 polymerization. Considering the fact that the no inhibitory activity was observed and it is mainly distributed in byssal thread and plaque, we proposed that this atypical Sbp8-1 may play as the cross-linker in scallop byssus. This study facilitates not only the understanding of scallop byssus assembly, also provides the inspiration of water-resistant materials design.

Keywords: scallop, byssus, TIMP, bioadhesion, cross-linker, Cysteine

INTRODUCTION

It is already well-known that adhesion is one of the most important physiological processes for marine molluscs, which is vital for food procurement, locomotion, defense, breeding and attachment (Gorb, 2008). In the marine environment, many organisms were adversely affected by tides and waves, and in response to this situation many marine molluscs have evolved their ability to live by adhering themselves to other materials (Yang et al., 2013). Like mussels and oysters can secrete adhesives and cement to affix themselves to the substratum (Wilker, 2011). Adhesive locomotion is an important strategy for gastropods, the mucus released from their foot play an important role in locomotion (Iwamoto et al., 2014). The tentacles in *Nautilus* can produce glue in a specialized glandular structure to pick up food

or attach to substrate for mating (von Byern et al., 2012). Therefore, adhesion widely exists in marine molluscs indicating this is a crucial physiological event for these organisms. In addition, it is obvious that the marine adhesion material exhibits remarkable adhesion ability with water-resistance properties, providing inspiration for the design of new materials to meet diverse application requirements (Aldred, 2013). Therefore, extensive amounts of efforts were put to characterize the adhesives from sessile organisms such as mussels, barnacles, or tube-dwelling worms (Naldrett and Kaplan, 1997; Taylor and Waite, 1997).

So far, several significant features for marine mollusc adhesives were discovered based on the characterized mollusc adhesives, including the mussels and barnacles. First, Presence of post-translational modifications (PTM): Several different types of PTM are detected for the studied marine bioadhesive proteins. For example, phosphorylated proteins (Zhao et al., 2005) and hydroxylated DOPA (Wang and Stewart, 2013) were found in the cement of sandcastle worm and *P. californica* respectively. Glycosylation was detected in byssal threads of marine mussels (Sun et al., 2002), and the tube feet disk nectin presented phosphorylation and glycosylation (Toubarro et al., 2016). Second, Metal ions are found to be critical for the marine adhesive materials. Elemental analysis of cured *P. californica* glue revealed relatively large quantities of Ca and Mg, which are complexed with the peptidyl-phosphates in the heterogeneous sub granules (Wang and Stewart, 2013). And Fe^{3+}-DOPA coordinative complexes were detected in the protective cuticle and bulk adhesive plaque of the byssus (Harrington et al., 2010). Third, so far, the identified marine adhesion proteins are non-conserved. For example, the protein compositions between scallop and mussel are significantly different, although they all belong to bivalves and adopt the byssus to attach to the substratum (Miao et al., 2015). Therefore, it is important to dissect and characterize the individual compositions of scallop byssus, which was important for the understanding its adhesive mechanisms.

Scallops produce and secrete specialized adhesives that work synergistically in water allowing them to attach themselves in marine environments. The secreted adhesive proteins solidified in sea water and shaped into byssus with excellent flexibility and toughness. In previous studies, we discovered 75 proteins from *Chlamys farreri* byssus based on transcriptomic approach and further identified seven foot-specific scallop byssal protein (Sbp) components based on proteomic approach (Miao et al., 2015). By sequence alignment, two proteins (Sbp7, Sbp8-1) were annotated as the tissue inhibitors of metalloproteinases (TIMPs) family. It is known that TIMPs can regulate important physiological activities by inhibiting metalloproteinases activity, which are proteinases that participate in extracellular matrix (ECM) degradation (Nagase and Woessner, 1999). In addition, it is suggested that TIMPs have other biological functions. For example, TIMPs are involved in erythroid-potentiating (Stetler-Stevenson et al., 1992) and cell growth–promoting (Hayakawa et al., 1992), and it is found that TIMPs can induce apoptosis and stimulate angiogenesis (Qi and Anand-Apte, 2015). TIMP also might be involved in antibacterial immune in mollusc (*Tegillarca granosa*) (Wang et al., 2012). Serine proteases and chorionic proteinase inhibitor from *Amphibalanus amphitrite* was identified, which is predicted to be possibly involved in either regulating the shell formation or functioning in immunity (Zhang et al., 2015). However, the knowledge for the discovered TIMP homologous (Sbp7, Sbp8-1) is insufficient, which precludes the understanding of its physiological function. Moreover, because TIMPs are present as multiple gene copies in the scallop genome, figuring out their evolutionary relationships may promote better understanding of expressional difference between different copies and provide insights into their potential functional divergence. Here our evolutionary analysis suggests that the TIMPs of *C. farreri* had gone through multiple gene duplications during evolution. Focusing on the Sbp8-1, which was mainly distributed in the byssal thread and plaque, detailed sequence alignment suggests that Sbp8-1 is an atypical TIMP with two extra free Cys residues at its C-terminus. More importantly, biochemical analysis in combination with mutagenesis suggests that two extra free Cys residues cause the Sbp8-1 polymerization. Finally considering the fact that the no inhibitory activity was observed, this atypical Sbp8-1 was proposed to function as the cross-linker in scallop byssus. This study will facilitate the biological function understanding of TIMP homologous (Sbp8-1) in byssus.

MATERIALS AND METHODS

Sample Collection

The adult *Chlamys farreri* used in this study were purchased from the market in Qingdao and the scallops were kept in the aquarium with circulating sea water at around 19°C. Frosted glass was laid on the bottom of the aquarium in order that the scallops can secret adhesives to form byssus. All experiments in this study were repeated at least three times.

Identification and Evolutionary Analysis of *TIMP* Genes

Putative *TIMP* genes in scallops and other molluscs were identified by performing blastp with an *e*-value threshold of $1e^{-5}$, using known *TIMP* genes of human and fly retrieved from NCBI protein database as queries. The conserved domain was identified by using the CDD tool[1]. And only the candidate genes containing NTR domain (Form complexes with metalloproteinases, such as collagenases, and irreversibly inactivate them) were kept for the following analysis. The identified TIMP protein sequences were aligned using clustalw in the MEGA 6.0 software (Tamura et al., 2013) and a phylogenetic tree of *TIMP* genes was constructed with the program MrBayes (ver3.2.6) (Huelsenbeck et al., 2001). The MCMC model-jumping method was performed to run for 1,000,000 generations with a sample frequency of 1000. In total, 1000 trees were produced, of which the first 250 were discarded as burn-in, while the remaining were summarized to get a consensus tree.

[1]https://www.ncbi.nlm.nih.gov/Structure/cdd/wrpsb.cgi

Expression Analysis

The expression levels of *TIMP* genes were retrieved from the RNA-seq datasets of *C. farreri* that were generated from a whole-genome sequencing project (Li et al., 2017), including eleven adult tissues/organs (adductor muscle, smooth muscle, foot, hepatopancreas, blood, kidney, female gonad, male gonad, gill, eye, and mantle) and three different foot regions (tip region, middle region, and root region). Illumina sequencing reads were mapped to the genome of *C. farreri* by using the STAR software (Dobin et al., 2013). HTSeq-count script (Anders et al., 2015) was used to count the total number of reads matching genic regions. Finally expression value was calculated as RPKM (reads per kilobase per million mapped reads) using the TMM algorithm in EdgeR software (Robinson et al., 2010). The expression level of a *TIMP* gene was represented by an average RPKM of three biological replicates. A *TIMP* gene was defined as foot specific if the following conditions were satisfied: foot RPKM >50 and foot RPKM/non-foot RPKM >100.

Rapid Amplification of cDNA Ends

In order to obtain the full-length sequences, 5′-RACE and 3′-RACE were carried out, and the primers were designed based on the known nucleic sequence of *Sbp8-1*(CF9441.24) as shown the primer 1 in **Table 1**. The forward primer of 5′-RACE and the backward primer of 3′-RACE are both used the UPM (Universal Primer Mix) from the kit. The 5′-cDNA and 3′-cDNA libraries were constructed using the SMARTer^{TM} RACE cDNA Amplification Kit (Clontech, CA). The resulting products were then cloned into PMD18-T vector to get the PMD18-T-Sbp8-1 plasmid, which was transformed into *E. coli* Top10. Finally, the positive clones were confirmed by sequencing.

Plasmid Construction and Recombinant Protein Expression and Purification

The *Sbp8-1* gene with termination codon and cleavage sites of restriction endonucleases (*Bam*HI, *Xho*I) were obtained by PCR amplification from the plasmid PMD18-T-Sbp8-1 using primer 2 shown in **Table 1**. The expression vector pET32a was utilized to construct recombinant plasmid, which was transformed into *E. coli* BL21(DE3) for expression. The cultures were grown in LB media with 0.1 mg·ml^{-1}Ampicillin at 37°C. When the OD_{600} of the cultures reached 0.6–0.8, the cells were induced by adding isopropyl-β-D-thiogalactopyranoside (IPTG) to a final concentration of 0.2 mM. Then, the cultures were grown at 16°C for 15 h. The cells were harvested by centrifuging 3,000 × *g* for 30 min at 4°C and the cell pellets were resuspended in 20 mL ice-cold binding buffer (20 mM Tris–HCl, 20 mM imidazole, 500 mM NaCl, pH 8.5). Cells were lysed by using a sonicator with 5 s pause every 10 s at 40% power for 25 min. The resulting sample was subsequently centrifuged (12,000 × *g*, 25 min, 4°C) to remove insoluble fractions.

The final supernatant was applied to pre-equilibrated Ni-NTA matrix and shaking gently at 4°C for 1 h. After washing with the binding buffer, Sbp8-1 protein was eluted using elution buffer containing 500 mM imidazole in binding buffer. The corresponding fractions were concentrated to 10 mg·ml^{-1} for further analysis. The resulting protein was loaded on HiPrep Sephacryl S-200 HR (GE) to monitor the protein polymerization, which was pre-equilibrated with the binding buffer without imidazole. The flow rate is 0.5 ml·min^{-1} and the peak fraction was collected and detected by SDS–PAGE. For the polyclonal antibody preparation, the fusion Trx tag of recombinant Sbp8-1 was removed by protease (Supplementary Figure 1).

Site-Directed Mutagenesis

QuikChange Site-Directed Mutagenesis Kit (Agilent technology, Santa Clara, CA, United States) was used to perform the site-directed mutagenesis. The primers M-C164S and M-C186S (**Table 1**) were used for the mutation of Sbp8-1^{C164S,C186S}. The expression and purification method of the mutant protein is the same as that of Sbp8-1.

Localization of Sbp8-1 in *Chlamys farreri* Byssus Based on Western Blot

Scallop Byssal Protein Extraction

Protein extraction was carried out according to the previous experimental method (Miao et al., 2015). The collected byssus from *Chlamys farreri* were rinsed several times with deionized water and cut into different parts as the picture showed (**Figure 3A**). Briefly, the corresponding fractions were grinded into powder in liquid nitrogen and incubated with extraction buffer (5% acetic (*v/v*), 6 M GdnHCl, 2 mM EDTA, 10 mM DTT) at 37°C for 1 h. After centrifugation (12,000 × *g*, 25 min, 4°C), supernatant was collected and dialyzed against 1% acetic acid (*v/v*) at 4°C. Finally, the extracted protein was dialyzed against deionized water and lyophilized.

Preparation of Polyclonal Antibody

The recombinant Sbp8-1 protein was excised from SDS–PAGE gel (Supplementary Figure 1) and ground thoroughly as the antigen. The samples were prepared using a typical procedure (Plumari et al., 2010). After four times immunization, the rabbits were sacrificed and serum was collected for antibody purification (ABclonal Biotechnology, Wuhan, China).

TABLE 1 | Primers used in this study.

Primer name	Forward(5′-3′)	Backward(5′-3′)
Primer 1	CAAGCGATATTGTCATCATTGGGAAAA	AGTGATGCCACAAACACCTTGGGAGT
Primer 2	CGGGATCCTGTACATGTAATCCATACCCAG	CCGCTCGAGTCAACAATCGTTGTCGGTC
M-C164S	CAGTAATTGAGTCTTTCAACAAAGAACGTTGCGTACCC	CGCAACGTTCTTTGTTGAAAGACTCAATTACTGTTGAATTATCG
M-C186S	GTGGACCGACAACGATTCTTGACTCGAGCACCAC	GTGGTGCTCGAGTCAAGAATCGTTGTCGGTCCAC

Western blot: Western blot analysis of the byssus protein extractions was performed. After electrophoresis, the proteins were electrotransferred to a PVDF membrane for 45 min at 100 V, and the membrane was blocked by incubating the membrane with 5% non-fat milk in Tris-buffered saline containing 0.1% Tween-20 (TBST) for 2 h. The membrane was then incubated overnight at 4°C with rabbit polyclonal anti-Sbp8-1 (1:500 dilution) in blocking solution. After rinsing with TBST, the membrane was incubated with diluted (1:5000) peroxidase-conjugated goat anti-rabbit IgG antibody (BBI, New York, United States) for 1 h. Finally, the membrane blots were developed using an enhanced chemiluminescence regent kit (BOSTER Biological Technology, Wuhan, China).

Peptide Mass Fingerprinting Derived From Gel Bands

The corresponding band was cut with a clean blade and subjected to trypsin digestion after destaining. After washing with 100 mM NH_4HCO_3, the gel pieces were rehydrated in 100 mM NH_4HCO_3 with 10 ng sequencing grade-modified trypsin (Promega, WI) at 37°C overnight. After digestion, the protein peptides were collected, and the gels were washed with 0.1% TFA in 60% ACN to collect the remaining peptides (Shevchenko et al., 2006). Then the samples were analyzed using Easy-nLC nano-flow HPLC system connected to Orbitrap Elite mass spectrometer (Thermo Fisher Scientific, CA, United States). Then the raw files were analyzed using the Proteome Discoverer 1.4 software (Thermo Fisher Scientific, CA, United States). The deduced Sbp8-1 sequence was used as the search template.

Detection of Metalloproteinase Inhibitory Activity

Succinylated gelatin and type IV collagenase (Sigma-Aldrich) were used for the metalloproteinase inhibitor activity test. The gelatin was succinylated using the method described previously (Rao et al., 1997). And the inhibition assay was carried out in the reaction system including 0.14 μM type IV collagenase and 240 μg succinylated gelatin in the presence or absent of Sbp8-1, the total volume was adjusted to 150 μL using 50 mM borate buffer. The reaction buffer was incubated at 37°C for 30 min, then reacted with 0.03% TNBSA and read at 450 nm after incubation at room temperature for 20 min and the relative enzyme activity was monitored.

Circular Dichroism Spectrum Detection

In order to verify whether the Sbp8-1 protein was folded correctly, the secondary structure of Sbp8-1 was detected by circular dichroism spectrum. The Sbp8-1 protein was digested with protease to remove the fusion tag. After purification, the resulting Sbp8-1 without Trx was dialyzed against phosphate buffer (0.01 M, pH 8.0 with 250 mM Na_2SO_4). The protein sample was injected into the quartz cell and then measured within the wavelengths ranging from 190 to 250 nm (detection step of 1 nm and a detection time interval of 0.5 s). During the test, the phosphate buffer was used as a control and the experiment was repeated three times.

Amino Acid Composition, Sequence Alignment and Structural Modeling

The TIMP-2 protein sequences with the highest structural similarity to the Sbp8-1 protein were selected for amino acid sequence alignment. The alignment was generated with ClustalW (**Figure 4**). The molecular weights and theoretical isoelectric points were analyzed on the Expasy server[2]. Signal peptide was predicted with SignalP 4.1 server[3].

RESULTS AND DISCUSSIONS

Evolutionary Analysis of *TIMP* Genes

To gain insights into the evolution of *TIMP* gene and its expression in different tissues of scallops, we conducted genome-wide search and identified thirteen *TIMP* genes in the *C. farreri* genome. In addition, thirteen *TIMP* genes were identified in scallop *Patinopecten yessoensis* and *oyster Crassostrea gigas* respectively, but none in other molluscs (*Lottia gigantea*, *Octopus bimaculoides*, and *Aplysia californica*). The number of TIMPs in bivalves is remarkably higher than those in other molluscs and non-molluscs (e.g., four TIMPs in human and one in fly) suggesting that *TIMP* gene family in bivalves had expanded notably during evolution.

Our previous study identified seven byssal proteins that were foot specific (Miao et al., 2015). Among them, two *TIMP*s (Sbp7, Sbp8-1) were discovered through our sequence alignment analysis. Phylogenetic analysis (**Figure 1A**) indicated the high diversity and deep evolutionary divergence of *TIMP*s in the bivalve lineage. Many clades contained *TIMP* genes from both scallops and oyster, implying that the duplication events of *TIMP* genes even occurred before the divergence of scallop and oyster lineages (∼425 million years ago) (Wang et al., 2017). The expression analysis of *TIMP*s in *C. farreri* (**Figure 1B**) revealed a substantial number of foot-specific *TIMP*s including Sbp7 and Sbp8-1, with remarkably higher expression levels in foot (RPKM: 70-9,000) than in other tissues (0.3–92.0; **Figure 1B**). These foot-specific *TIMP*s showed the dispersed distribution across the phylogenetic tree, suggesting that their potential functional roles in foot may have an ancient evolutionary origin. Analysis of the expression level of *Sbp8-1* (Cf9441.24) suggests that it is mainly secreted by the middle region and tip region of scallop foot (**Figure 2**). According to previous reports about the distribution of glands in the scallop foot (Gruffydd, 1978), Sbp8-1 protein may be secreted by the second type of mucous cell which is found all along the ventral surface of the middle region and tip region of the foot. Previous studies showed that different types of proteinase inhibitors were identified in the *Zebra mussel* (Xu and Faisal, 2008) and *Mytilus coruscus* byssus (Qin et al., 2016). Also, metalloproteinase inhibitor was identified in the soluble fraction from proximal thread (Qin et al., 2016). Collectively, these findings suggest that TIMP genes may play important roles for the assembly and function of byssus in bivalves, which is likely of ancient evolutionary origin.

[2]https://web.expasy.org/protparam/

[3]http://www.cbs.dtu.dk/services/SignalP/

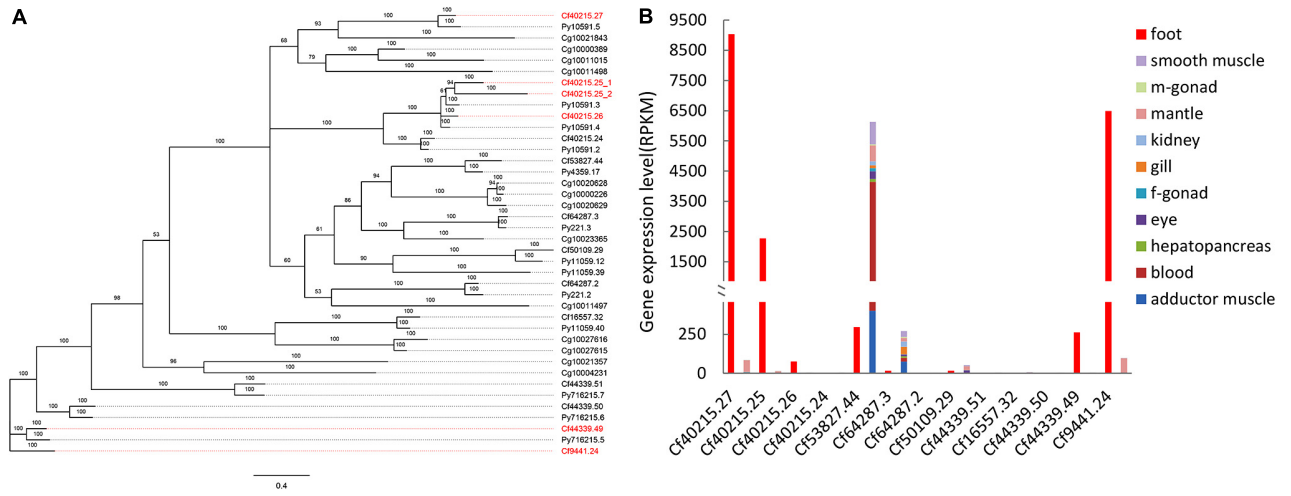

FIGURE 1 | Phylogenetic and expression analysis of *TIMP* genes. **(A)** Bayesian phylogenetic tree of *TIMP* genes in bivalves. Red gene names indicated the foot-specific TIMPs from *C. farreri*. CF: *Chlamy farreri*; PY: *Patinopecten yessoensis*; Cg: *Crassostrea gigas*. **(B)** Expression comparison of *C. farreri TIMP* genes between foot and a sum of other tissues (smooth muscle, male gonad, mantle, kidney, gill, female gonad, eye, hepatopancreas, blood, and adductor muscle).

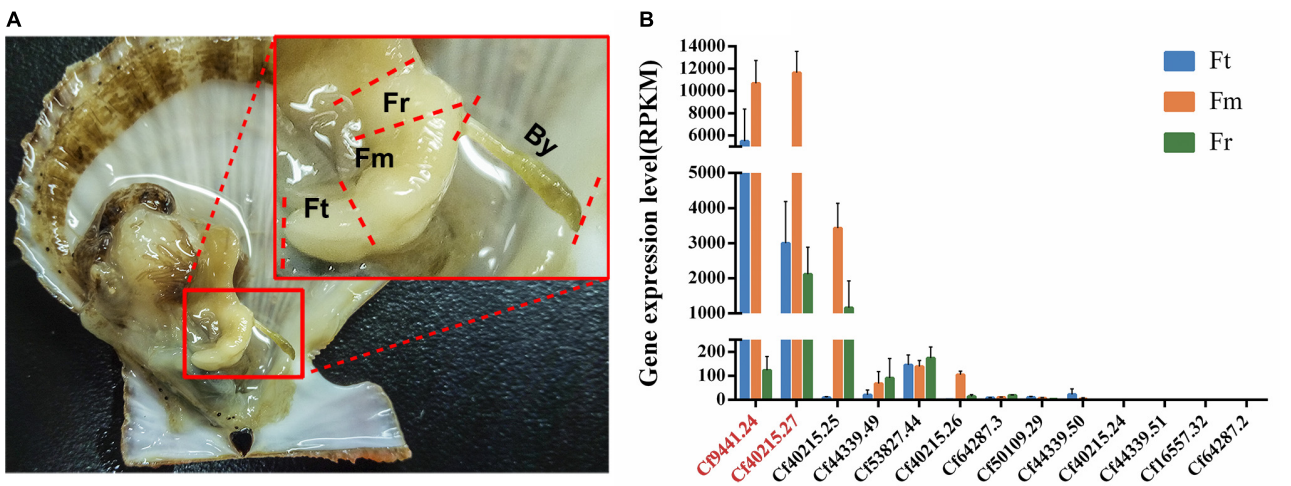

FIGURE 2 | Anatomical structure of *Chlamys farreri* foot and expression analysis of all of *TIMP* genes. **(A)** Anatomy of *C. farreri* and magnified display of *C. farreri* foot. It demonstrates the foot contains three different regions as labeled: Fr, root region of foot; Fm, middle region of foot; Ft, tip region foot; By, *C. farreri* byssus. **(B)** Expression levels of *C. farreri TIMP* genes across different foot regions. The genes labeled in red font encode Sbp8-1 (Cf9441.24) and Sbp7 (Cf40215.27) respectively, the standard errors were based on three biological replicates. This analysis indicates that the genes encoding Sbp8-1 and Sbp7 proteins were highly expressed in the middle region and tip region of *C. farreri* foot.

Distribution of Sbp8-1 in *C. farreri* Byssus

Detailed visualization demonstrates that the scallop byssus could be divided into four parts (**Figure 3A**) and the protein was extracted for these individual parts. The SDS–PAGE showed that similar protein compositions were observed for the byssal thread and plaque region (**Figure 3B**). They both contain four major bands with similar Mw (2 bands with Mw around 40 kDa and 2 bands with Mw around 20 kDa). And only one major band was observed with the Mw around 40 kDa for the sheathed region. However, the two major bands (1 band with Mw around 45 kDa and the other one with Mw >75 kDa) were observed for the root region. Similar to our previous observation, the overall scallop byssal thread protein was composed by three major fractions based on the Mw distribution (Miao et al., 2015). In sum, these observations indicate that protein composition vary in different parts of byssus.

To accurately map the distribution of individual compositions in byssus, the western-blot was carried out. Thereby, we first attempted to over-express these two proteins (Sbp7, Sbp8-1) to obtain as the antigen. However, poor expression level of Sbp7 precluded further investigation of this protein, and then the Sbp8-1 was chosen for the following assay. As shown in

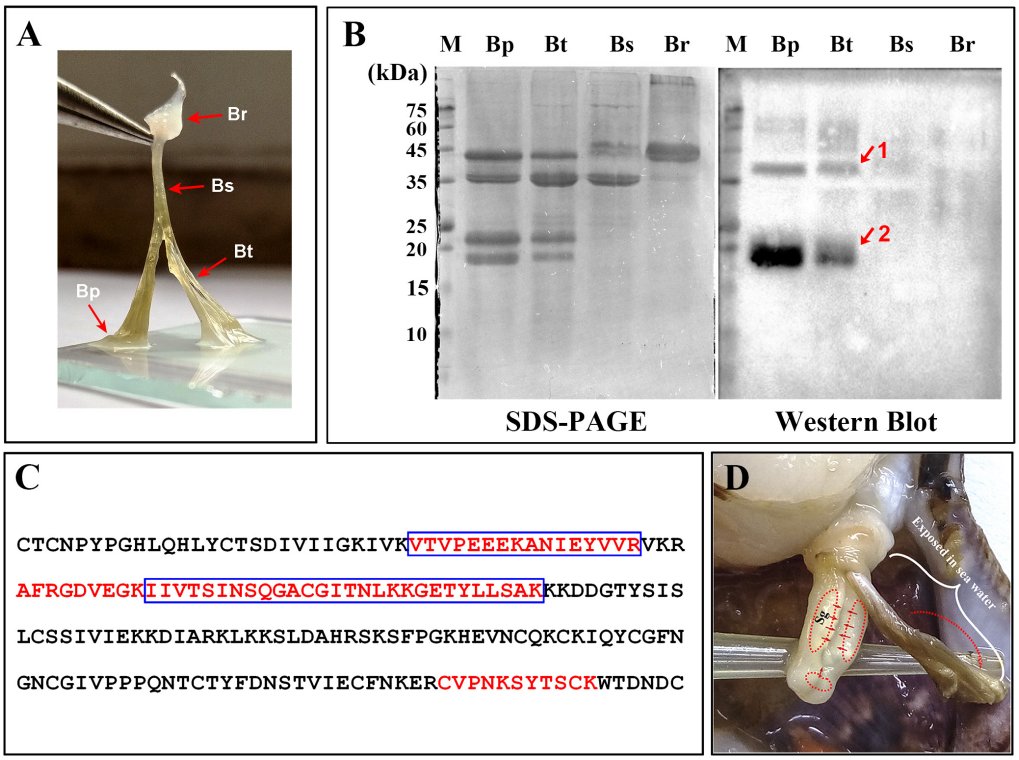

FIGURE 3 | Distribution of Sbp8-1 in *Chlamys farreri* byssus based on western blot. **(A)** Picture of *C. farreri* byssus showing it contains four regions; Br, byssal root region; Bs, byssal sheathed region; Bt, byssal thread region; Bp: byssal plaque region. **(B)** SDS–PAGE and western blot analysis of extracted byssal proteins. The red arrows and numbers indicate the corresponding bands for the further mass spectrometry analysis. **(C)** The identified unique peptide from the corresponding protein bands in **(B)**. The amino acids in the blue box are the peptides identified in Band 1 and the amino acids in the red font are the peptides identified in Band 2. **(D)** The secretion and distribution areas of Sbp8-1. Sg, secretory glands. The red solid arrow indicates the secretion areas of the Sbp8-1 in scallop foot based on the expression level analysis. The red dashed arrow indicates the distribution area of Sbp8-1 in scallop byssus based on the western blot analysis.

Figure 3B, the western-blot assay using the anti-Sbp8-1 antibody showed Sbp8-1 was discovered mainly in the byssal thread and plaque region, not in the others. However, two bands were observed for both lanes, one band (band 1) is around the 20 kDa, which is close to the Mw of Sbp8-1. Whereas the other band (band 2) is around the 40 kDa, which is one fold higher than the Mw of Sbp8-1. To further validate presence of Sbp8-1 in these two bands, the mass-spectroscopy was carried out. And the result demonstrates that 6 unique peptides were discovered for band 2 and 8 unique peptides for band 1 (**Figure 3C**). This further confirms that the Sbp8-1 was discovered mainly in the byssal thread and plaque region.

Taken together, it was found that the Sbp8-1 was mainly secreted in the scallop foot middle and tip region based on the expression pattern analysis (**Figure 2**), and finally distributed in the byssal thread and plaque region as depicted in **Figure 3D**. However, the transport pathway needs more investigation.

Amino Acid Composition and Sequence Alignment Analysis

Amino Acid Composition Analysis

The amino acid analysis for Sbp8-1, Sbp7 was summarized in **Figures 4C,D**. One significant feature for Sbp8-1 and Sbp7 compared to others structure-determined TIMPs is the relative high Lys content, which leads to their basic theoretical pI as shown in **Figure 4C**.

Sequence Alignment

Sequence alignment was performed as shown in **Figure 4A** for the two TIMPs from scallop byssal protein (Sbp8-1, Sbp7) with three structure-determined TIMPs (PDB:1BR9, human TIMP-2; PDB: 1BQQ, bovine TIMP-2; PDB:3CKI, human TIMP-3). First, it showed the low sequence similarity between the scallop byssal protein (Sbp8-1, Sbp7) and the other TIMPs (Sequence identity <30%); Furthermore, it was found that the C-terminal region is more divergent, and this might be functional relevant because the C-terminal of TIMP may enhance the inhibitory selectivity and binding efficiencies (Willenbrock et al., 1993). TIMP-2 binds to the hemopexin domain of proMMP-2 to form a tight complex through its C-terminal domain (Visse and Nagase, 2003). More surprising, two additional Cys residues are discovered (blue box in **Figure 4A**). Generally, the TIMPs have 6 disulfides formed by 12 conserved Cys residues (red box in **Figure 4A**). Previous study demonstrated that insertion of Cys residue in C-terminal of human TIMP-3 results in the human Sorsby's fundus dystrophy (SFD) disease. And the plausible molecular mechanism is the Cys insertion leads to

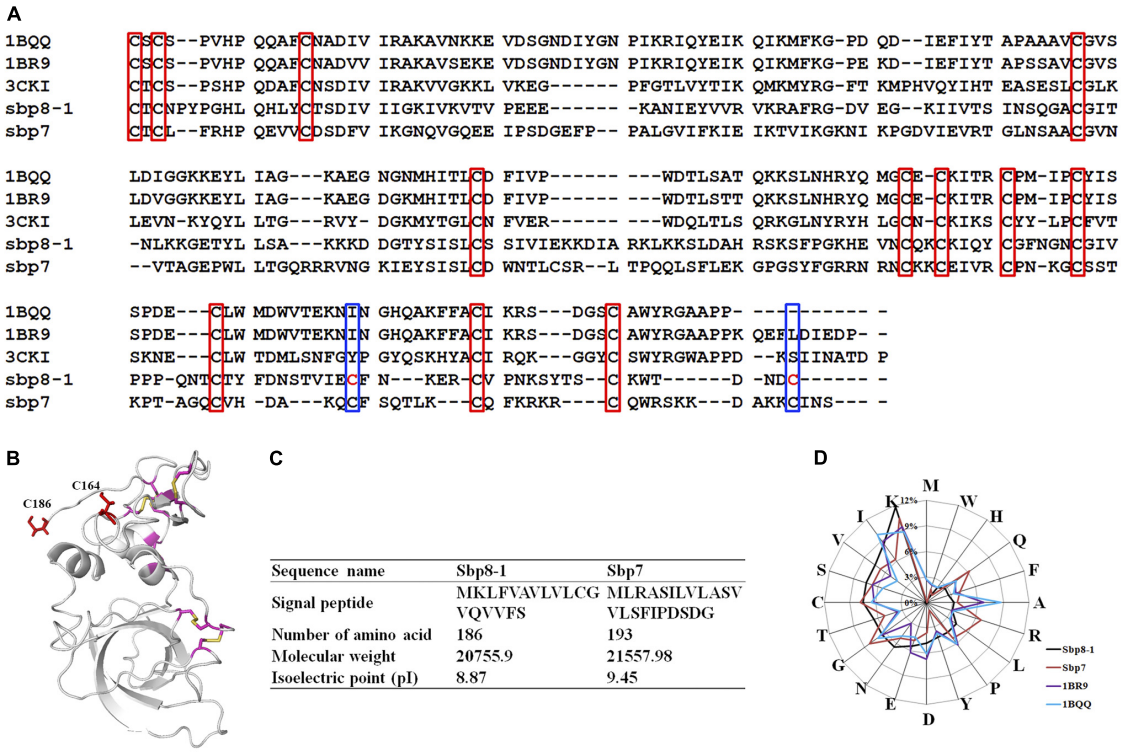

FIGURE 4 | Sequence Characteristics and the basic information of Sbp8-1 and Sbp7. **(A)** Multiple sequence alignments of the Sbp8-1 and Sbp7 with other structure determined TIMPs. Three others structure-determined TIMPs were chosen due to the relative high sequence similarity to either Sbp8-1 or Sbp7. They include the PDB: 1BR9, human TIMP-2; PDB: 1BQQ, bovine TIMP-2; PDB: 3CKI: human TIMP-3). Red boxes indicate the 12 conserved Cys residues and the blue boxes indicate two extra residues in the C-terminal of Sbp8-1. **(B)** The three-dimensional structural model of Sbp8-1 generated by I-Tasser (Yang et al., 2015) suggests that two extra Cys present in Sbp8-1 C-terminal do not form disulfide bonds. **(C,D)** Amino acid composition analysis of Sbp8-1 and Sbp7.

the formation of intermolecular disulfide bridges that cause protein polymerization (Stohr and Anand-Apte, 2012). Also, the structural model of Sbp8-1 generated using the I-Tasser server (Yang et al., 2015) suggests that two extra Cys residues (C164, C186) in Sbp8-1 C-terminal exist as free state (**Figure 4B**). In sum, the above analyses indicate the Sbp8-1 is an atypical TIMP, which might have distinct biochemical features and unique function in scallop byssus.

Biochemical Characterization of Recombinant Sbp8-1

Biochemical characterization demonstrates that Sbp8-1 is an atypical TIMP, which may function as the cross-linker in the scallop byssus as mentioned below.

Polymerization

The recombinant Sbp8-1 (with Trx fusion tag) was loaded on gel filtration chromatography using Hi–Prep Sephacryl S-200 HR (GE) to monitor the polymerization state. As expected, the Sbp8-1 was eluted in void volume (around 36 mL), indicating the polymerization occurs (**Figure 5**). To explore the relationship between the two additional Cys residues (**Figure 3A**) and the polymerization, two following assays were carried out. First, the DTT (10 mM) was added in the elution buffer and it turned out that the elution volume shifted to 60 mL, this suggests the presence of intermolecular disulfides might cause the polymerization, which may formed by the two C-terminal extra Cys residues. To confirm this hypothesis, the C164S and C186S double mutation was then generated. The mutant Sbp8-$1^{C164S,C186S}$ was reloaded on the gel filtration chromatography. The elution volume of Sbp8-$1^{C164S,C186S}$ shifted to the 62 mL as shown in **Figure 5**. Our analyses strongly indicate that Sbp8-1 is in the polymerization state, and this polymerization is caused by the two extra free Cys residues in the C-terminal region. It is known that the free thiol groups are typically important for the marine adhesives. For example, in mussel footprint protein mfp-6 with 11 mol% cysteine content, and most of them occur as free thiol (Lee et al., 2011). It is known that DOPA exists in the scallop byssal thread and plaque region (Li et al., 2017), it is therefore reasonable to propose that Sbp8-1 may function as the cross-linker through the interaction between free cysteine and DOPA.

Enzymatic Inhibitory Assay

The biological function annotation based on seqeunce alignment showed that the Sbp8-1 belongs to TIMP-2. Previous study showed that TIMP-2 can inhibit the activity of MMP-2 (type IV

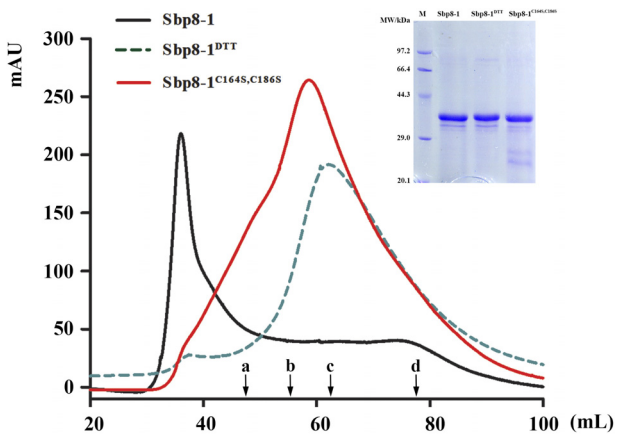

FIGURE 5 | Protein polymerization analysis based on gel filtration. The Sephacryl S-200 High Resolution column was used to evaluate the polymerization state. The solid black line represented the gel-filtration profile of Sbp8-1 running in the binding buffer and the dashed black line represented gel filtration profile of Sbp8-1 running with binding buffer with 10 mM DTT, while the solid red line represented the gel-filtration profile of Sbp8-1^{C164S,C186S}. The inset SDS–PAGE shows the purity of each sample. The black arrows indicate the elution volume at the peak of different molecular weight proteins. a, IgG (160 kDa); b, BSA (67 kDa); c, β-lactoglobulin (35 kDa); d, cytochrome C (12.4 kDa).

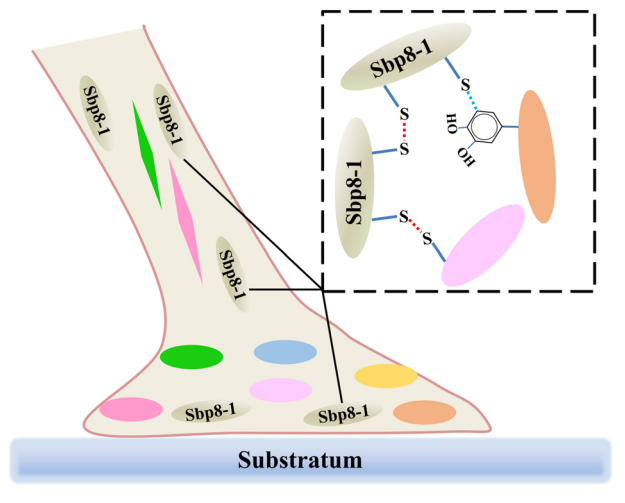

FIGURE 6 | Schematic illustration of the potential cross-linking role of Sbp8-1 protein in the scallop byssus. The left side is a schematic diagram of the structure of the byssus, in which different colors of ovals and diamonds represent different byssal protein components; The dotted box on the right shows the potential cross-linking between Sbp8-1 protein and other proteins.

collagenase) (Tuuttila et al., 1998). In order to test whether Sbp8-1 protein has inhibitory activity toward type IV collagenase, the succinylated gelatin method was used for the assay. However, it turned out that addition of either Sbp8-1 or the fusion tag control (Trx protein) will enhance the type IV collagenase activity (Supplementary Figure 2), suggests that the Sbp8-1 does not have the inhibitory activity toward type IV collagenase, which is different to the canonical human TIMP-2. To verify the folding of Sbp8-1 protein, the circular dichroism was carried out. The result (Supplementary Figure 3) showed that Sbp8-1 protein has obvious secondary structure. In summary, Sbp8-1 protein is an atypical TIMP without metalloproteinase inhibitor activity.

CONCLUSION

It is known that both the foot and byssus are crucial for scallop, and the exploration of the scallop byssus composition is the first key step to understand its biological function. Focusing on the TIMPs derived from scallop byssus, a comprehensive characterization of Sbp 8-1 was carried out for the first time. Evolutionary analysis suggests that the *TIMPs* genes of *Chlamys farreri* had gone through multiple gene duplications during evolution, and their potential functional roles in foot may have an ancient evolutionary origin. Focusing on the Sbp8-1, one of the discovered TIMPs from scallop byssus, sequence alignment and enzymatic inhibitory assay suggest that it is an atypical TIMPs. One significant feature is two extra free Cys residues in C-terminal of Sbp8-1. These two residues might form the intermolecular disulfides resulting in the sbp8-1 polymerization; considering its distribution, we proposed that the Sbp8-1 protein may play the cross-linking role in scallop byssus through the C-terminal extra Cys residues as shown in **Figure 6**.

AUTHOR CONTRIBUTIONS

WL, QL, SW, and XZ designed and performed the study and drafted the manuscript. SW, ZB, and LW were in charge of reviewing the data analysis during the manuscript submission process. YM, PX, XZ, and PL contributed experiment materials and analysis tools. XD, XZ, and PX collected the information and analyzed the data. BD and SW participated in study development.

FUNDING

This work was supported by National Natural Science Foundation of China (31472258, U1706203); Key Research and Development Plan of Shandong Province (2016GSF115008), and the Fundamental Research Funds for the Central Universities (201822024, 201841001, and 201762001).

ACKNOWLEDGMENTS

We are very grateful to Dr. Xiaoju Dou for the help of using laser scanning confocal microscope. The authors gratefully acknowledge Shanghai Omicsspace Biotechnology Co., Ltd., for technical assistance with the peptide/protein identification.

SUPPLEMENTARY MATERIAL

The Supplementary Material for this article can be found online at: https://www.frontiersin.org/articles/10.3389/fphys.2018.00597/full#supplementary-material

REFERENCES

Aldred, D. N. (2013). *Biological and Biomimetic Adhesives: Challenges and Opportunities*. Cambridge: Royal Society of Chemistry.

Anders, S., Pyl, P. T., and Huber, W. (2015). HTSeq–a python framework to work with high-throughput sequencing data. *Bioinformatics* 31, 166–169. doi: 10.1093/bioinformatics/btu638

Dobin, A., Davis, C. A., Schlesinger, F., Drenkow, J., Zaleski, C., Jha, S., et al. (2013). STAR: ultrafast universal RNA-seq aligner. *Bioinformatics* 29, 15–21. doi: 10.1093/bioinformatics/bts635

Gorb, S. N. (2008). Biological attachment devices: exploring nature's diversity for biomimetics. *Philos. Trans. A Math. Phys. Eng. Sci.* 366, 1557–1574. doi: 10.1098/rsta.2007.2172

Gruffydd, L. D. (1978). The byssus and byssus glands in *Chlamys islandica* and other scallops (Lamellibranchia). *Zool. Scr.* 7, 277–285. doi: 10.1111/j.1463-6409.1978.tb00611.x

Harrington, M. J., Masic, A., Holten-Andersen, N., Waite, J. H., and Fratzl, P. (2010). Iron-clad fibers: a metal-based biological strategy for hard flexible coatings. *Science* 328, 216–220. doi: 10.1126/science.1181044

Hayakawa, T., Yamashita, K., Tanzawa, K., Uchijima, E., and Iwata, K. (1992). Growth-promoting activity of tissue inhibitor of metalloproteinases-1 (TIMP-1) for a wide range of cells. A possible new growth factor in serum. *FEBS Lett.* 298, 29–32. doi: 10.1016/0014-5793(92)80015-9

Huelsenbeck, J. P., Ronquist, F., Nielsen, R., and Bollback, J. P. (2001). Bayesian inference of phylogeny and its impact on evolutionary biology. *Science* 294, 2310–2314. doi: 10.1126/science.1065889

Iwamoto, M., Ueyama, D., and Kobayashi, R. (2014). The advantage of mucus for adhesive locomotion in gastropods. *J. Theor. Biol.* 353, 133–141. doi: 10.1016/j.jtbi.2014.02.024

Lee, B. P., Messersmith, P. B., Israelachvili, J. N., and Waite, J. H. (2011). Mussel-inspired adhesives and coatings. *Annu. Rev. Mater. Res.* 41, 99–132. doi: 10.1146/annurev-matsci-062910-100429

Li, Y., Sun, X., Hu, X., Xun, X., Zhang, J., Guo, X., et al. (2017). Scallop genome reveals molecular adaptations to semi-sessile life and neurotoxins. *Nat. Commun.* 8:1721. doi: 10.1038/s41467-017-01927-0

Miao, Y., Zhang, L., Sun, Y., Jiao, W., Li, Y., Sun, J., et al. (2015). Integration of transcriptomic and proteomic approaches provides a core set of genes for understanding of scallop attachment. *Mar. Biotechnol. (NY)* 17, 523–532. doi: 10.1007/s10126-015-9635-y

Nagase, H. H., and Woessner, J. F. (1999). Matrix metalloproteinases. *J. Biol. Chem.* 274, 21491–21494. doi: 10.1074/jbc.274.31.21491

Naldrett, M. J., and Kaplan, D. L. (1997). Characterization of barnacle (*Balanus eburneus* and *B-cenatus*) adhesive proteins. *Mar. Biol.* 127, 629–635. doi: 10.1007/s002270050053

Plumari, M., Gellera, C., and Taroni, F. (2010). Production of polyclonal antibodies against protein antigens purified by electroelution from SDS-polyacrylamide gel. *Protoc. Exch.* doi: 10.1038/nprot.2010.27

Qi, J. H., and Anand-Apte, B. (2015). Tissue inhibitor of metalloproteinase-3 (TIMP3) promotes endothelial apoptosis via a caspase-independent mechanism. *Apoptosis* 20, 523–534. doi: 10.1007/s10495-014-1076-y

Qin, C. L., Pan, Q. D., Qi, Q., Fan, M. H., Sun, J. J., Li, N. N., et al. (2016). In-depth proteomic analysis of the byssus from marine mussel *Mytilus coruscus*. *J. Proteomics* 144, 87–98. doi: 10.1016/j.jprot.2016.06.014

Rao, S. K., Mathrubutham, M., Karteron, A., Sorensen, K., and Cohen, J. R. (1997). A versatile microassay for elastase using succinylated elastin. *Anal. Biochem.* 250, 222–227. doi: 10.1006/abio.1997.2223

Robinson, M. D., McCarthy, D. J., and Smyth, G. K. (2010). edgeR: a Bioconductor package for differential expression analysis of digital gene expression data. *Bioinformatics* 26, 139–140. doi: 10.1093/bioinformatics/btp616

Shevchenko, A., Tomas, H., Havlis, J., Olsen, J. V., and Mann, M. (2006). In-gel digestion for mass spectrometric characterization of proteins and proteomes. *Nat. Protoc.* 1, 2856–2860. doi: 10.1038/nprot.2006.468

Stetler-Stevenson, W. G., Bersch, N., and Golde, D. W. (1992). Tissue inhibitor of metalloproteinase-2 (TIMP-2) has erythroid-potentiating activity. *FEBS Lett.* 296, 231–234. doi: 10.1016/0014-5793(92)80386-U

Stohr, H., and Anand-Apte, B. (2012). A review and update on the molecular basis of pathogenesis of Sorsby fundus dystrophy. *Adv. Exp. Med. Biol.* 723, 261–267. doi: 10.1007/978-1-4614-0631-0_34

Sun, C., Lucas, J. M., and Waite, J. H. (2002). Collagen-binding matrix proteins from elastomeric extraorganismic byssal fibers. *Biomacromolecules* 3, 1240–1248. doi: 10.1021/bm0255903

Tamura, K., Stecher, G., Peterson, D., Filipski, A., and Kumar, S. (2013). MEGA6: molecular evolutionary genetics analysis version 6.0. *Mol. Biol. Evol.* 30, 2725–2729. doi: 10.1093/molbev/mst197

Taylor, S. W., and Waite, J. H. (1997). "Marine adhesives: from molecular dissection to application," in *Protein-Based Materials. Bioengineering of Materials*, eds K. McGrath and D. Kaplan (Boston, MA: Birkhäuser), 217–248.

Toubarro, D., Gouveia, A., Ribeiro, R. M., Simoes, N., da Costa, G., Cordeiro, C., et al. (2016). Cloning, characterization, and expression levels of the nectin gene from the tube feet of the sea urchin *Paracentrotus Lividus*. *Mar. Biotechnol. (NY)* 18, 372–383. doi: 10.1007/s10126-016-9698-4

Tuuttila, A., Morgunova, E., Bergmann, U., Lindqvist, Y., Maskos, K., Fernandez-Catalan, C., et al. (1998). Three-dimensional structure of human tissue inhibitor of metalloproteinases-2 at 2.1 A resolution. *J. Mol. Biol.* 284, 1133–1140. doi: 10.1006/jmbi.1998.2223

Visse, R., and Nagase, H. (2003). Matrix metalloproteinases and tissue inhibitors of metalloproteinases: structure, function, and biochemistry. *Circ. Res.* 92, 827–839. doi: 10.1161/01.RES.0000070112.80711.3D

von Byern, J., Wani, R., Schwaha, T., Grunwald, I., and Cyran, N. (2012). Old and sticky-adhesive mechanisms in the living fossil *Nautilus pompilius* (Mollusca. Cephalopoda). *Zoology (Jena)* 115, 1–11. doi: 10.1016/j.zool.2011.08.002

Wang, C. S., and Stewart, R. J. (2013). Multipart copolyelectrolyte adhesive of the sandcastle worm, *Phragmatopoma californica* (Fewkes): catechol oxidase catalyzed curing through peptidyl-DOPA. *Biomacromolecules* 14, 1607–1617. doi: 10.1021/bm400251k

Wang, Q., Bao, Y., Huo, L., Gu, H., and Lin, Z. (2012). A novel tissue inhibitor of metalloproteinase in blood clam *Tegillarca granosa*: molecular cloning, tissue distribution and expression analysis. *Fish Shellfish Immunol.* 33, 645–651. doi: 10.1016/j.fsi.2012.06.021

Wang, S., Zhang, J., Jiao, W., Li, J., Xun, X., Sun, Y., et al. (2017). Scallop genome provides insights into evolution of bilaterian karyotype and development. *Nat. Ecol. Evol.* 1:120. doi: 10.1038/s41559-017-0120

Wilker, J. J. (2011). Biomaterials: redox and adhesion on the rocks. *Nat. Chem. Biol.* 7, 579–580. doi: 10.1038/nchembio.639

Willenbrock, F., Crabbe, T., Slocombe, P. M., Sutton, C. W., Docherty, A. J., Cockett, M. I., et al. (1993). The activity of the tissue inhibitors of metalloproteinases is regulated by C-terminal domain interactions: a kinetic analysis of the inhibition of gelatinase A. *Biochemistry* 32, 4330–4337. doi: 10.1021/bi00067a023

Xu, W., and Faisal, M. (2008). Putative identification of expressed genes associated with attachment of the zebra mussel (*Dreissena polymorpha*). *Biofouling* 24, 157–161. doi: 10.1080/08927010801975345

Yang, B., Kang, D. G., Seo, J. H., Choi, Y. S., and Cha, H. J. (2013). A comparative study on the bulk adhesive strength of the recombinant mussel adhesive protein fp-3. *Biofouling* 29, 483–490. doi: 10.1080/08927014.2013.782541

Yang, J., Yan, R., Roy, A., Xu, D., Poisson, J., and Zhang, Y. (2015). The I-TASSER Suite: protein structure and function prediction. *Nat. Methods* 12, 7–8. doi: 10.1038/nmeth.3213

Zhang, G., He, L. S., Wong, Y. H., Xu, Y., Zhang, Y., and Qian, P. Y. (2015). Chemical component and proteomic study of the *Amphibalanus* (=*Balanus*) *amphitrite* shell. *PLoS One* 10:e0133866. doi: 10.1371/journal.pone.0133866

Zhao, H., Sun, C., Stewart, R. J., and Waite, J. H. (2005). Cement proteins of the tube-building polychaete *Phragmatopoma californica*. *J. Biol. Chem.* 280, 42938–42944. doi: 10.1074/jbc.M508457200

Conflict of Interest Statement: The authors declare that the research was conducted in the absence of any commercial or financial relationships that could be construed as a potential conflict of interest.

frontiers in Physiology

ORIGINAL RESEARCH
published: 07 September 2018
doi: 10.3389/fphys.2018.01244

Expression of Na^+/K^+-ATPase Was Affected by Salinity Change in Pacific abalone *Haliotis discus hannai*

Yanglei Jia[1,2,3] *and Xiao Liu*[1,2]*

[1] *Key Laboratory of Experimental Marine Biology, Institute of Oceanology and Center for Ocean Mega-Science, Chinese Academy of Sciences, Qingdao, China,* [2] *Laboratory for Marine Biology and Biotechnology, Qingdao National Laboratory for Marine Science and Technology, Qingdao, China,* [3] *University of Chinese Academy of Sciences, Beijing, China*

Na^+/K^+-ATPase (NKA) belongs to the P-type ATPase family, whose members are located in the cell membrane and are distributed in diverse tissues and cells. The main function of the NKA is to regulate osmotic pressure. To better understand the role of NKA in osmoregulation, we first cloned and characterized the full-length cDNAs of NKA α subunit and β subunit from Pacific abalone *Haliotis discus hannai* in the current study. The predicted protein sequence of the NKA α subunit, as the catalytic subunit, was well conserved. In contrast, the protein sequence of the β subunit had low similarity with those of other species. Phylogenetic analysis revealed that both the α and β subunits of the NKA protein of Pacific abalone were clustered with those of the Gastropoda. Then, the relationship between salinity changes and the NKA was investigated. Sudden salinity changes (with low-salinity seawater (LSW) or high-salinity seawater (HSW)) led to clear changes in ion concentration (Na^+ and K^+) in hemolymph; however, the relative stability of ion concentrations in tissue revealed that Pacific abalone has a strong osmotic pressure regulation ability when faced with these salinity changes. Meanwhile, the expression and activity of the NKA was significantly decreased (in LSW group) or increased (in HSW group) during the ion concentration re-establishing stages, which was consistent with the coordinated regulation of ion concentration in hemolymph. Moreover, a positive correlation between cyclic adenosine monophosphate (cAMP) concentrations and NKA mRNA expression (NKA activity) was observed in mantle and gill. Therefore, the sudden salinity changes may affect NKA transcription activation, translation and enzyme activity via a cAMP-mediated pathway.

Keywords: salinity, osmoregulation, ion transportation, Na^+/K^+-ATPase, cAMP

OPEN ACCESS

Edited by:
Youji Wang,
Shanghai Ocean University, China

Reviewed by:
Ahmet Regaib Oğuz,
Yüzüncü Yıl University, Turkey
Tsung-Han Lee,
National Chung Hsing University, Taiwan
Hajime Kitano,
Kyushu University, Japan
Yongbo Bao,
Zhejiang Wanli University, China

***Correspondence:**
Xiao Liu
liuxiao@qdio.ac.cn

Specialty section:
This article was submitted to Aquatic Physiology, a section of the journal Frontiers in Physiology

Received: *09 March 2018*
Accepted: *17 August 2018*
Published: *07 September 2018*

Citation:
Jia Y and Liu X (2018) Expression of Na^+/K^+-ATPase Was Affected by Salinity Change in Pacific abalone Haliotis discus hannai. Front. Physiol. 9:1244. doi: 10.3389/fphys.2018.01244

INTRODUCTION

Abalones are large marine snails in the family Haliotidae and the genus Haliotis belonging to the class Gastropoda of the phylum Mollusca (Lv, 1978; Appeltans et al., 2014; Cook, 2016). Pacific abalone *Haliotis discus hannai,* which is naturally distributed in the Northwest Pacific, is considered an important commercially fishery industry animal in China. The production in 2015 was about 115,397 metric tons, accounting for approximately 90% of the worldwide yield (Elliott, 2000; Gordon and Cook, 2004; Cook, 2016).

Temperature and salinity are the primary physical factors affecting the distribution and physiological metabolism of shellfish (Davenport et al., 1975; Burton, 1983; Navarro, 1988). Pacific abalone is a stenohaline species, and it is very sensitive to low salinity. The strain of P-97, which had experienced several generations of linearly selection since 1997, resulting in a significantly increased tolerance of temperature and salinity. The optimum growth salinity for the sixth generation of P-97 is approximately 24–36 part per thousand (ppt) (Kong et al., 2017).

The main factors related to osmotic pressure are H_2O and the concentrations of ions and bioorganic molecules. A cell's osmolarity is the sum of the concentrations of the various ion species and many proteins and other organic compounds inside the cell. The main ions include Na^+, K^+, Ca^{2+}, and Cl^-, and bioorganic molecules include free amino acids (Siebers et al., 1972; Amende and Pierce, 1980). Na^+ and Cl^- are the principal osmotically active solutes in the hemolymph. Contribution of Na^+ and Cl^- accounted for 47.7–51.6% and 37.1–42.2% of the total osmotic concentration of the hemolymph, respectively (Cheng et al., 2002). The combined contribution of Na^+ and Cl^- to the hemolymph osmolality is about 90%. It is suggested that the contribution of organic compounds like protein, free amino acid to the osmotic concentration of the hemolymph is much lower than that of ions. The movements of most ions through the membrane are mediated by membrane transport proteins which are specialized to varying degrees in the transport of specific ions. The transmembrane transport of Na^+ and Cl^- could be mediated by several channel proteins like sodium channels, some members of electroneutral cation-Cl cotransporters (solute carrier family, SLC12A) and many others. Na^+/K^+-ATPase (NKA) is one of the ion channels that using the energy derived from ATP hydrolysis to maintain the membrane potential by driving three sodium ions export and two potassium ions import across the plasma membrane against their electrochemical gradients. There is hence a net export of a single positive charge per pump cycle. In most animal cells, the NKA is responsible for about 1/5 of the cell's energy expenditure. The NKA is an integral membrane heterodimer belonging to the P-type ATPase family and it is an enzyme that found in the membranes of all animal cells (Hall and Guyton, 2006; Clausen et al., 2017). It is composed of two catalytic α subunits and two non-catalytic β subunits (Therien and Blostein, 2000). Although the β subunit has no catalytic activity, it is required for stabilization, maturation, and translocation of the catalytic α subunit to the plasma membrane (Beggah et al., 1997; Hasler et al., 1998; Rajasekaran et al., 2004). In addition, the β subunit also mediates the trans-dimerization of NKAs between neighboring cells, where they regulate the integrity of tight junctions (Rajasekaran and Rajasekaran, 2003; Babdinitz et al., 2009; Tokhtaeva et al., 2011). Furthermore, a third, non-essential subunit (the γ subunit) has been identified in mammals (Reeves et al., 1980). Thus far, four α, three β and one γ subunit isoforms have been identified in mammals, and several α and β subunits have been identified in fish (Mobasheri et al., 2000; Guynn et al., 2002).

Previous studies have determined that the influence of salinity on NKAs in many crustacean and vertebrates, such as fish, and NKA is highly sensitive to the changes in salinity (Mancera and McCormick, 2000; Richards et al., 2003; Pan et al., 2014; Pham et al., 2016). However, the responses of NKA were not consistently when faced with the changes of salinity in different species and the detailed mechanism is not clear yet. In *Litopenaeus vannamei*, NKA α-subunit gene transcript increased rapidly when the salinity decreased (Pan et al., 2014). Whereas in *Fundulus heteroclitus*, the increased salinity induced a rise in gill NKA activity 3 h after transfer (Mancera and McCormick, 2000). In *Oncorhynchus Mykiss*, five NKA α-isoforms were identified. High salinity stimulation decreased NKA α1a mRNA, but increased NKA α1b mRNA. The other 3 isoforms were not changed following salinity change (Richards et al., 2003). Moreover, there has been less research on NKA in mollusk. Many studies have confirmed that salinity change could stimulate the change in nervous endocrine (like dopamine (DA), noradrenaline (NE) and 5-hydroxytryptamine (5-HT)), thereby inducing the change in physiological function (Sommer and Mantel, 1991; Hoshijima and Hirose, 2007). Morris and Edwards (1995) also confirmed that the injection of DA or cyclic adenosine monophosphate (cAMP) have the same effect on NKA activity. These researches indicated that biogenic amines play a role in stimulating the NKA.

The action of most biogenic amines combine with the G protein-coupled receptor (GPCR) and is then mediated by the generation of intracellular cAMP, a very important second messenger in many biological processes. The cAMP molecule is a derivative of ATP and used for intracellular signal transduction in many different organisms, conveying the cAMP-dependent pathway (Bos, 2006). The predominant effect of cAMP is to activate a cAMP-dependent protein kinase (PKA). Four molecules of cAMP bind each dormant PKA holoenzyme, activating the kinase by releasing the catalytic subunits from a regulatory subunit-cAMP complex. Then, the catalytic subunit of PKA could get into the nucleus and subsequently regulate gene transcription. The detailed mechanisms between cAMP and NKA activity have been well studied in vertebrates like rats. Previous literatures reported that the enzyme activity of NKA is thought to be downregulated by cAMP via PKA-dependent phosphorylation of the catalytic subunit (Bertorello et al., 1991; Kurihara et al., 2000). Whereas in another study, PKA-mediated stimulation of NKA α subunit phosphorylation level likely participates in the cAMP-dependent stimulation of NKA activity (Kiroytcheva et al., 1999). Whether a salinity change could affect the content of cAMP and then regulate the gene expression and activity of NKA in Pacific abalone needs further research.

According to the literatures mentioned above, we could conclude that NKA may play an important role in salinity regulation and the responses of NKA were not consistent between different species. Moreover, the effect of salinity on NKA has not been reported in Pacific abalone. The present study described the molecular cloning and characterization of full-length NKA (α subunit and β subunit) cDNA from Pacific abalone (designated HdNKA) as well as its expression profile in various tissues. In addition, we then determined the influence of salinity on the expression and activity of HdNKA. Furthermore, we measured the concentration of ions and cAMP in both hemolymph and

tissues. The results were used to elucidate the correlation between cAMP and HdNKA (expression and activity) in Pacific abalone *Haliotis discus hannai*.

MATERIALS AND METHODS

Animal

Adult abalones (length: 40 ± 5 mm, weight: 4.8 ± 0.3 g) that derived from a selective breeding population known as P-97, which had experienced seven generations of selection since 1997 was obtained from a commercial farm in Xunshan, Weihai, China. After transported to the laboratory, animals were adapted for 1 week in tank filled with aerated normal seawater (NSW, salinity = 30.0 ppt) at 24.0 ± 0.5°C. Low salinity seawater (LSW, salinity = 20.0 ppt) was a blend of fresh water and NSW. High salinity seawater (HSW, salinity = 40.0 ppt) was a blend of NSW and marine life reef salt (Goe, Qingdao, China). Salinity was measured by water quality handheld instrument YSI pro30 (YSI, Yellow Springs, OH, United States). During the experimental period, the Pacific abalones were fed with a formulated commercial diet daily (Gold Feed, Weihai, China).

Experimental Design

As shown in **Figure 1**, Pacific abalones were transferred directly into four tanks filled with LSW or HSW (80 individuals per group, 20 individuals per tank). After the sudden transfer (all LSW and HSW treatment groups), animals were sampled at 0.25, 0.75, 1.5, 3, 6, 12, 24, and 48 h (8 individuals per point, 2 individuals per tank). Pacific abalones grown in NSW were sampled at 0 h, and these samples were regarded as the control. Pacific abalone was euthanized as previously described (Altenhein et al., 2002). The hemolymph (∼800 μl) was withdrawn from the sole side foot muscle and collected into 1.5 ml Eppendorf (EP) tubes carefully. Then, the hemolymph was centrifuged at 1000 rpm for 10 min (Heraeus Pico 21, 24 × 1.5/2.0 ml rotor, Thermo Scientific, Carlsbad, CA, United States). Supernatants were separated into a new tube and then stored at −80°C. Different tissues, including hepatopancreas, muscle, mantle and gill, were dissected. Tissues were washed with deionized water rapidly, wiped with filter paper and then evenly separated into several parts for the determination of ion concentration, cAMP concentration, and *Hdnka* expression and activity. The tissue was immersed into liquid nitrogen for quick freezing and then stored at −80°C. All animal experiments were performed with the approval of the Institutional Animal Ethics Committee of Institute of Oceanology, Chinese Academy of Sciences.

Preparation of Total RNA for the First Stranded Synthesis

Total RNA of each tissue was extracted with TRIzol Reagent (Cat No. 15596-026, Invitrogen, Carlsbad, CA, United States) according to the manufacturer's instructions. The concentration of RNA was determined by measuring the OD at 260 nm with the NanoDrop ND-1000 UV-Visible Spectrophotometer (Thermo Scientific, Carlsbad, MA, United States). The integrity was checked by separating the RNA on a 1% agarose gel and staining with Gel-Red (Cat No. D0139, Beyotime, Shanghai, China).

Cloning of the Full Length cDNA of Na^+/K^+-ATPase α Subunit and β Subunit

Total RNA extracted from different tissue at 0 h point was mixed and used for 5′ RACE and 3′ rapid-amplification of cDNA ends (RACE). First-strand cDNA were synthesized using SMARTer® RACE 5′/3′ Kit (Cat No. 634858, TAKARA, Dalian, China) following the manufacturer's instructions. On the basis of the fragments of NKA α subunit and β subunit gene obtained from transcriptome sequencing (unpublished data), the primers used for amplification of the full length of NKA α subunit and β subunit were designed using Primer Premier 5 (PREMIER Biosoft International, Palo Alto, CA, United States) following the kit protocol and synthesized by Beijing Genomics Institute (BGI) (**Table 1**). The PCR reaction was conducted in the following conditions: 5 cycles of denaturation (94°C for 30 s), annealing and elongation (72°C for 3 min); then 5 cycles of denaturation (94°C for 30 s), annealing (70°C for 30 s) and elongation (72°C for 3 min); finally, 25 cycles of denaturation (94°C for 30 s), annealing (68°C for 30 s) and elongation (72°C for 3 min). A final extension step was conducted at 72°C for 10 min. The PCR products were electrophoresed on a 1% agarose gel and staining with Gel-Red. Those bands with the expected sizes were extracted using NucleoSpin Gel and PCR Clean-Up Kit (Cat No. 740609.10, MACHEREY-NAGEL, Düren, Germany). The purified PCR products were then subcloned using In-Fusion HD Cloning Kit (Cat No. 638909, TAKARA, Dalian, China) and sequenced (Sanger dideoxy sequencing) in both directions.

Bioinformatics and Phylogenetic Analysis

The sequences were assembled using DNAMAN 9 (Lynnon Biosoft, San Ramon, CA, United States). Then the open reading frame (ORF) was analyzed. Amino acid sequences were aligned using the ClustalX2 (Larkin et al., 2007), and phylogenetic tree was carried out in MEGA 7.0 program using maximum likelihood (ML) method (Kumar et al., 2016). Bootstrap value was computed over 1000 replications. The similarity between different sequences was calculated by DNAMAN 9 software. The trans-membrane domains of protein sequence were predicted by the TMHMM Server v. 2.0[1] and MEMSAT3 and MEMSAT-SVM (Buchan et al., 2010). Sequences and accession numbers were shown in Supplementary Files.

Physiological and Biochemical Indexes Measurement

The frozen hemolymph was thawed on ice and recentrifuged at 5000 rpm for 10 min. The supernatant was separated into a new EP tube for hemolymph ion concentration measurements. Approximately 50 mg tissue was put in a glass homogenizer with

[1]http://www.cbs.dtu.dk/services/TMHMM

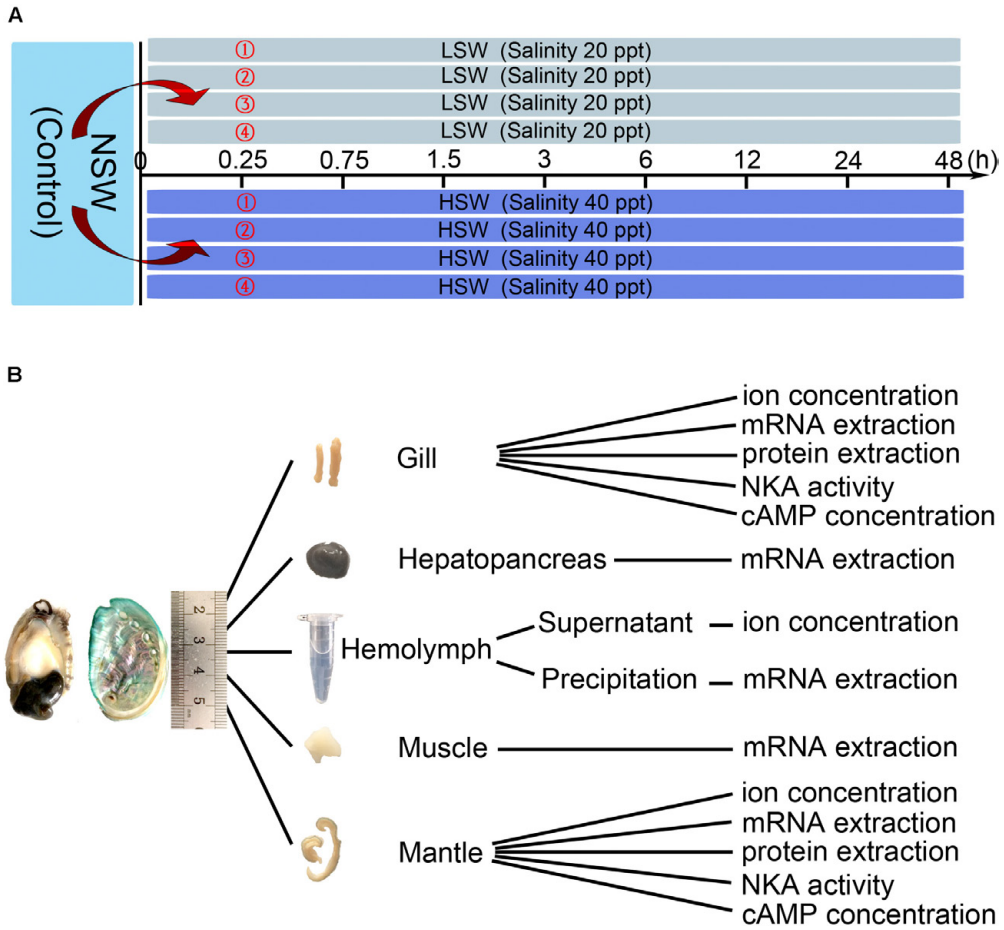

FIGURE 1 | Experimental design. **(A)** Treatment and sampling time points. **(B)** Application of sampled tissue.

TABLE 1 | List of primer sequences used in this study.

Primer name	Primer sequence (5′-3′)	Amplification target
NKAα-5′	***GATTACGCCAAGCTT*** CACTGGGTGTGACAGCATAGCGGTAG	For NKA α subunit 5′ RACE
NKAα-3′	***GATTACGCCAAGCTT*** CAGTTCAGCCCCATCACACTCTCCC	For NKA α subunit 3′ RACE
NKAβ-5′	***GATTACGCCAAGCTT*** CATAGCCTTGCTTTGGCAGGTACTCG	For NKA β subunit 5′ RACE
NKAβ-3′	***GATTACGCCAAGCTT*** TTCACCATTTGTCAGCACATTCCCA	For NKA β subunit 3′ RACE
UPM	CTAATACGACTCACTATAGGGCAAGCAGTGGTATCAACGCAGAGT	Universal Primer for RACE PCR
qactb-F	GGTATCCTCACCCTCAAGT	For actb q-PCR
qactb-R	GGGTCATCTTTTCACGGTTG	
qNKAα-F	TACATCCACCATCTGCTCG	For NKA α subunit q-PCR
qNKAα-R	AAGTTTGAATTCGGCCC	
qNKAβ-F	TAATGAGAACCTGGGTGAGA	For NKA β subunit q-PCR
qNKAβ-R	GATAAATACAAGGGGCGAC	

Letters in bold and italics indicate the nucleobase added to the 5′-end of GSP that used for In-Fusion cloning.

200 μl ice-cold deionized water and homogenized completely. Then, it was centrifuged at 5000 rpm for 10 min. The supernatant was transferred to a new EP tube. The supernatants were used for tissue ion concentration measurements. The tissues used for NKA activity were homogenized with normal saline (0.9%) and centrifuged at 5000 rpm for 10 min for collection of the supernatant. The tissue used to determine the cAMP concentration was homogenized with 0.1 M HCl and centrifuged at 13000 rpm for 10 min for collection of the supernatant. All of the homogenate steps were carried out on ice, and the centrifugal steps were carried out at 4°C. The supernatants were separated into new tubes and stored at −80°C. The protein concentrations

of supernatants after tissue homogenization were measured with a Protein Quantitative Reagent Kit-BCA Method (Cat No. P0010, Beyotime, Shanghai, China).

The concentration of Na^+ ions was determined using a Blood Sodium Concentration Assay Kit (Cat No. BC2805, Solarbio, Beijing, China). The concentration of K^+ ions was determined using a Potassium Assay Kit according to the manufacturer's instructions (Cat No. C001-2, Nanjing Jiancheng Bioengineering Institute, Nanjing, China). The activity of NKA was measured using a Na^+/K^+-ATPase assay kit (Cat No. A070-2, Nanjing Jiancheng Bioengineering Institute, Nanjing, China). The concentration of cAMP in tissue was measured with a cAMP Direct Immunoassay Kit (Colorimetric) (Cat No. K371-100, BioVision, Milpitas, CA, United States).

Q-PCR Analysis of Na^+/K^+-ATPase α Subunit and β Subunit

Q-PCR was used to determine the influence of salinity on the expression of NKA α subunit and β subunit. The first-strand cDNA used for q-PCR was synthesized using PrimeScript™ RT reagent Kit with gDNA Eraser (Cat No. RR047A, TAKARA, Dalian, China). SYBR® Premix Ex™ Taq II kit (Cat No. RR42LR, TAKARA, Dalian, China) was used to perform the PCR reactions. The primers designed using Primer Premier 5 following the manufacturer's instructions and synthesized by BGI (**Table 1**). The following PCR program was used: 95°C for 30 s, followed by 40 cycles of 95°C for 5 s, 60°C for 30 s. Melting curve was inserted to analyze the specific of PCR products. The q-PCR reaction was performed using the QuantStudio™ 6 Flex Real-Time PCR System (Applied Biosystems, Carlsbad, CA, United States). The amplicon sizes and amplification efficiency of primers used for q-PCR were shown in **Supplementary Figure S1**. In addition, the specificity of the primers that we used was measured (**Supplementary Figure S1**). The data were calculated with the $2^{-\Delta\Delta C_t}$ method. Beta-actin (actb, Accession number: AY380809.1) was used as the internal control and the initial group (0 h) was used as the normalized group.

Western Blotting Analysis of Na^+/K^+-ATPase α Subunit

The membrane proteins of each tissue were extracted with RIPA buffer (high) (Cat No. R0010, Solarbio, Beijing, China). The concentration of protein was measured with a Protein Quantitative Reagent Kit-BCA Method. Protein samples (extracted from mantle or gill at the same time point) were mixed depending on their concentration and then subjected to SDS-PAGE; the separated proteins were then electrophoretically transferred onto a PVDF membrane. In brief, the membrane was blocked with 5% skim milk in TBST at room temperature for 1 h. Then, the blots were incubated with primary antibodies against the NKA α subunit (1:500, ATP1A2 Rabbit Polyclonal, Cat. No. 16836-1-AP, Proteintech, Rosemont, IL, United States) overnight at 4°C, followed by incubation with appropriate peroxidase-conjugated secondary antibodies (1:3000, HRP Goat Anti-Rabbit IgG (H+L), Cat. No. AS014, ABclonal, Wuhan, China). Gray values were analyzed using ImageJ software. Actb served as an internal control (1:1000, ACTB Monoclonal Antibody, Cat. No. AC026, ABclonal, Wuhan, China), and the initial group (0 h) was used as the normalized group. The detail information and the specificity of primary antibody against HdNKA α and actb were shown in **Supplementary Figure S1**.

Statistical Analysis

Statistical analysis was performed with the Statistical Package for the Social Sciences, version 18.0 (SPSS Inc., Chicago, IL, United States). The results are presented as the means ± SEM, and differences were considered significant at the $P < 0.05$ level. The correlations between ion concentrations and salinity were analyzed using linear regression. Differences in all time-points and salinity groups were determined using two-way analysis of variance followed by multiple comparison tests. Since the data did not pass the Shapiro–Wilk normality test, Spearman's test was carried out to determine the correlation between cAMP concentration and *Hdnka* mRNA expression and HdNKA activity in mantle and gill.

RESULTS

Ion Concentration

The concentration of Na^+ and K^+ in LSW, HSW, and NSW were measured in order to test the differences in aquaculture waters with different salinities (**Figure 2A**). These data indicated that the ion concentration and salinity of seawater are positively correlated ($P < 0.0001$). A higher salinity represented a higher concentration of Na^+ and K^+. To gain more insight into the influence of salinity on the ionic concentration in hemolymph, we measured the concentrations of Na^+ and K^+ in hemolymph after the sudden treatment with LSW or HSW at different times (**Figures 2B,C**). From these data, we found that the ion concentrations of Na^+ and K^+ in samples treated with LSW gradually decreased as the treatment time increased. In contrast, the HSW treatment produced a significant increase in both Na^+ and K^+ concentrations ($P < 0.05$). In addition, the concentrations of Na^+ and K^+ in mantle and gill after the treatment at different times were measured (**Figures 2D,E**). These data showed that the trend in Na^+ and K^+ concentrations in the mantle and gill fluctuated, but no significant differences were observed between different groups after treatments with LSW and HSW ($P > 0.05$).

Sequence Analysis of Na^+/K^+-ATPase α Subunit and β Subunit

In the present study, all of the *Hdnka* α subunit and β subunit cDNA sequences were identified by RACE-PCR from the Pacific abalone. The nucleotides and deduced amino acid sequences are shown in **Figures 3**, **4**. The full-length cDNA of the *Hdnka* α subunit was 5098 bp long and contained a 5′ UTR of 312 bp, a 3′ UTR of 1690 bp with a poly (A) tail, and an ORF of 3096 bp encoding a polypeptide of 1032 amino acids (GenBank accession number: MG767304, **Figure 3**). The full-length cDNA of the

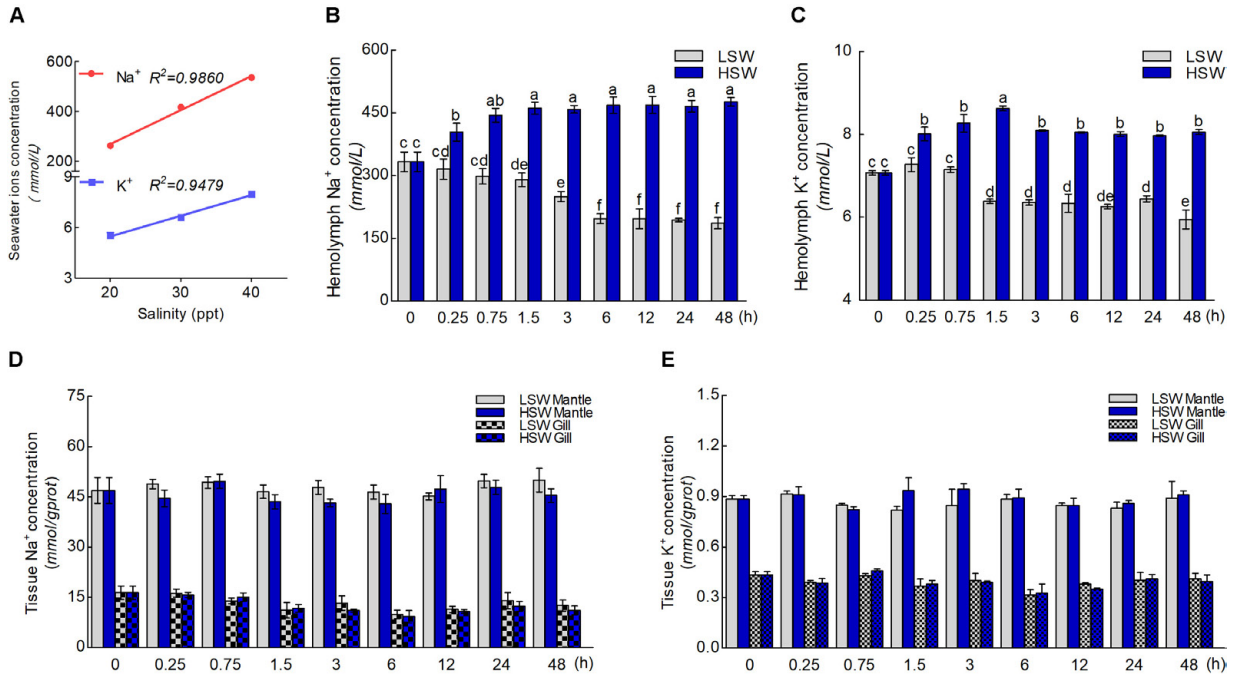

FIGURE 2 | Concentrations of Na^+ and K^+ ions. **(A)** The correlation between salinity and concentrations of Na^+ and K^+. **(B)** The concentration of Na^+ in hemolymph after the sudden salinity change at different times. **(C)** The concentration of K^+ in hemolymph after the sudden salinity change at different times. **(D)** The concentration of Na^+ in mantle and gill after the sudden salinity change at different times. **(E)** The concentration of K^+ in mantle and gill after the sudden salinity change at different times. Different letters on data indicate statistically significant differences between the results ($P < 0.05$). n = 4/time-point.

Hdnka β subunit was 3213 bp long and contained a 5′ UTR of 65 bp, a 3′ UTR of 2272 bp with a poly (A) tail, and an ORF of 876 bp encoding a polypeptide of 292 amino acids (GenBank accession number: MG767305, **Figure 4**).

The α subunit of NKA is the major catalytic unit. Multiple sequence alignments showed that the amino acid sequence of the *Hdnka* α subunit shared high similarity with those of Gastropoda (87.31–89.24%), Bivalvia (85.01–87.31%), Cephalopoda (85.27–85.76%) and *Homo sapiens* (73.55%). Transmembrane analysis showed that the high similarity regions of the sequence are the transmembrane regions (**Figure 5**). However, the multiple sequence alignments for the *Hdnka* β subunit amino acid sequences showed low similarity when compared with those of other species [Gastropoda (43.05–47.46%), Bivalvia (40.38–44.13%), Cephalopoda (40.85%) and *Homo sapiens* (23.96%)] (**Figure 6**). Phylogenetic tree analyses revealed that both the α subunit and β subunit of NKA in Pacific abalone clustered with those from other invertebrate species (especially those characterized in other marine Gastropoda and Bivalvia) (**Figures 7A,B**).

In terms of structure, TMHMM and MEMSAT3 and MEMSAT-SVM analysis showed that the *Hdnka* α subunit is a transmembrane protein. Transmembrane protein topology prediction showed that the transmembrane region possesses 10 transmembrane helices. Both the C-terminus and the N-terminus were localized on the intracellular side (**Figure 7C**). The β subunit of *Hdnka* is characterized by an intracellular N-terminus, followed by only one α-helix, and an extracellular C-terminus (**Figure 7D**). Furthermore, the extracellular domain was highly glycosylated (Nyblom et al., 2013).

Gene Expression of Na^+/K^+-ATPase α Subunit and β Subunit

The expression of the *Hdnka*α and β subunits occurred in all tissues examined (**Figures 7E,F**), including muscle, gill, mantle, hemolymph and hepatopancreas in NSW group. Muscle was used as the normalized group. The highest expression levels of both the *Hdnka* α and β subunits were found in mantle. The lowest expression level of the *Hdnka* α subunit was found in muscle, while that of the β subunit was found in hepatopancreas.

To evaluate the influence of salinity changes on *Hdnka* expression, we examined the mRNA levels of both the *Hdnka* α and β subunits in mantle and gill after sudden treatment with LSW or HSW at different times. The mRNA expression levels of the *Hdnka* α subunit increased slightly at the initial time, after the treatment of LSW, in mantle ($P > 0.05$) and gill ($P < 0.05$). However, as the time of treatment increased, the expression decreased. After treatment for approximately 1.5 h, the expression was reduced to its minimum. Then, the expression was slightly higher in mantle, but it was still significantly lower than the normal level ($P < 0.05$) (**Figures 8A,C**). In contrast, treatment with HSW first decreased the expression of the *Hdnka* α subunit slightly in gill ($P < 0.05$). However, the reduction in mantle was not significant ($P > 0.05$). After treatment for 6 h, there was a significant increase in this expression in both

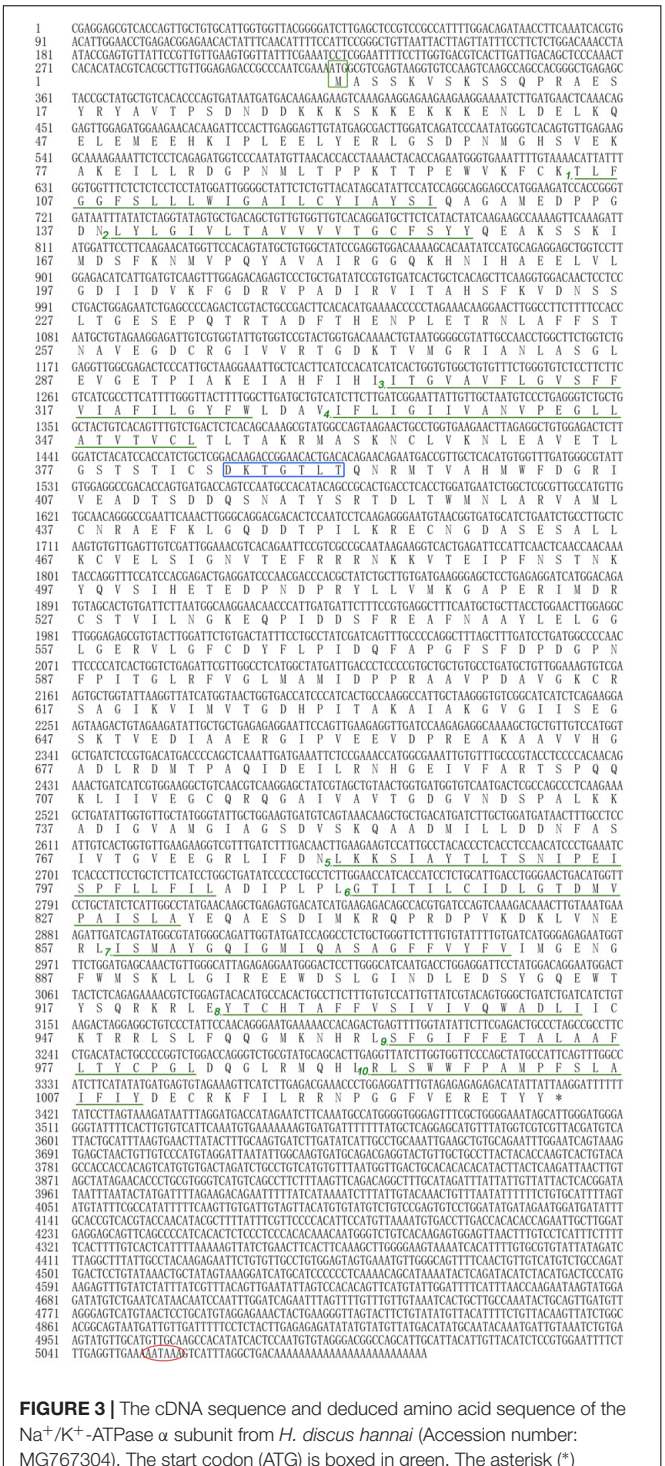

FIGURE 3 | The cDNA sequence and deduced amino acid sequence of the Na^+/K^+-ATPase α subunit from *H. discus hannai* (Accession number: MG767304). The start codon (ATG) is boxed in green. The asterisk (*) indicates the stop codon. The P-type ATPase motif is indicated by a blue box. A polyadenylation signal sequence AATAAA is circled with a red oval. The transmembrane regions are underlined with green and numbered (1–10).

these two tissues. This high expression pattern continued in the subsequent processing ($P < 0.05$). The influence of salinity on the mRNA level of the *Hdnka* β subunit was similar to its influence on the expression of the α subunit (**Figures 8B,D**).

Na^+/K^+-ATPase Activity

To further investigate whether the activity of HdNKA is under osmotic regulation, we carried out the measurement of HdNKA activity after the sudden treatment, including measuring in the tissues of mantle and gill (**Figures 8E,F**). From these data, we could find that at the initial period of the experiment, the activity of HdNKA was very stable. There was no difference between them ($P > 0.05$). However, as time progressed, a dramatic change occurred in the HdNKA activity. The LSW treatment led to a rapid reduction in expression in the tissues of both mantle and gill. In contrast, the activity of HdNKA was significantly increased in these tissues after the HSW treatment. These data indicated that the salinity had a significant influence on HdNKA activity in both mantle and gill.

Western Blotting Analysis

We used western blotting to determine whether the salinity change stimulation could affect the protein level of HdNKA. The amount of HdNKA α subunit protein in mantle and gill was examined after the LSW and HSW treatments and further measured by densitometry (**Figures 8G,H**). A highly significant reduction in HdNKA α subunit expression was found in the LSW treatment group relative to its level in the control. In contrast, the HSW treatment led an obvious increase in the expression of HdNKA α subunit. These data were consistent with the q-PCR results.

cAMP Concentration

To further explore the underlying molecular mechanism by which osmotic regulation leads to significant changes in HdNKA expression and activity after sudden treatment with different salinities, we examined the concentration of cAMP in both mantle and gill (**Figures 9A,B**). We found that the difference in cAMP concentration was statistically significant after the different salinity treatments at different times ($P < 0.05$). The results show that the cAMP concentration was significantly lower in the LSW-treated samples than in the control but higher in the HSW-treated group.

With the results of HdNKA enzyme activity and expression level (q-PCR) and the cAMP concentration in mantle and gill, we investigated the correlation between cAMP concentration, HdNKA activity and *Hdnka* α and β subunit mRNA expression levels. Statistical analysis showed that the cAMP concentration was moderately correlated with the *Hdnka* mRNA expression level (of both the α and β subunits) and the HdNKA activity, including in samples of mantle and gill ($P < 0.0005$) (**Figures 9C–F**).

DISCUSSION

One of the main objectives of the present study was to determine the role of the osmotic pressure regulation in Pacific abalone. The second objective was to investigate the possible mechanisms of HdNKA involved in this process. Therefore, the expression and activities of HdNKA in tissue were measured after treatment with either LSW or HSW.

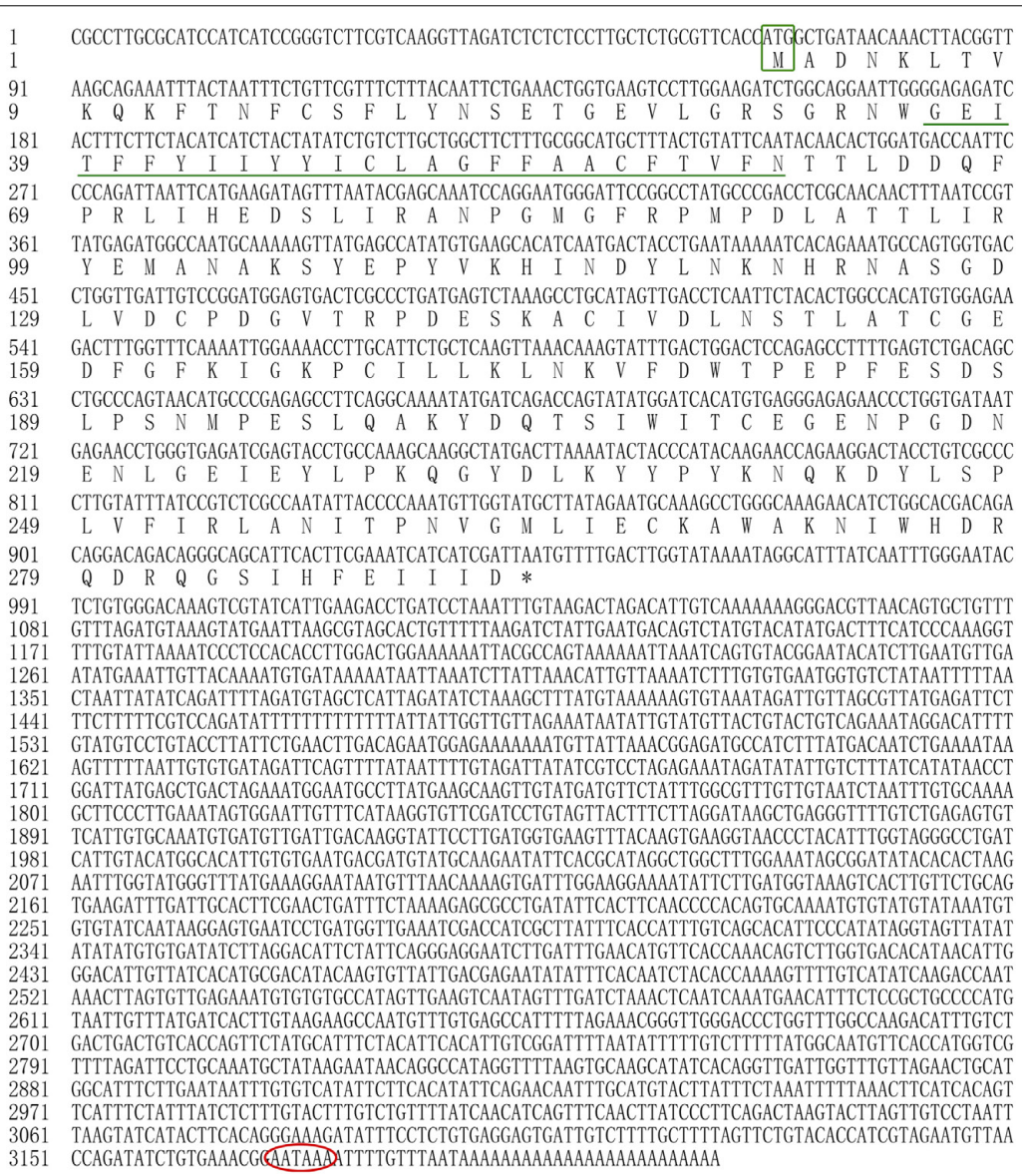

FIGURE 4 | The cDNA sequence and deduced amino acid sequence of the Na^+/K^+-ATPase β subunit from *H. discus hannai* (Accession number: MG767305). The start codon (ATG) is boxed in green. The asterisk (*) indicates the stop codon. A polyadenylation signal sequence AATAAA is circled with a red oval. The transmembrane region is indicated with green underline.

Pacific abalone belongs to the mollusk phylum. Similar to other invertebrates, it has an open circulatory system. In this system, fluid in a cavity called the hemocoel bathes the organs directly with oxygen and nutrients, and there is no distinction between blood and interstitial fluid (Monahan-Earley et al., 2013). This combined fluid is called hemolymph. Hemolymph is composed of water, inorganic salts (mostly sodium, chlorine, potassium and calcium), and organic compounds (mostly carbohydrates, proteins, and lipids) (Wyatt, 1961; Richards and Davies, 1977; Sowers et al., 2006). Hemolymph is analogous to the blood in vertebrates, which circulates in the interior of the body in direct contact with the animal's tissues. This arrangement means that all cells are surrounded by hemolymph. The ions in hemolymph act directly on the surfaces of the tissue cells. From the ion concentrations in hemolymph, we could find that salinity significant influenced the concentrations of Na^+ and K^+ in a clear time-dependent manner after sudden treatment with LSW. Moreover, with the progression of the treatment, the ion concentration remained at a low level. In contrast, the concentrations of these ions greatly increased when treated with HSW. These data were consistent with previous research in *Haliotis diversicolor supertexta* (Cheng et al., 2002). Sudden salinity changes directly changed the ion concentrations that surrounded tissue, and the balance between intracellular and extracellular electrical potentials was altered at the initial time. This sudden change may activate the stress response

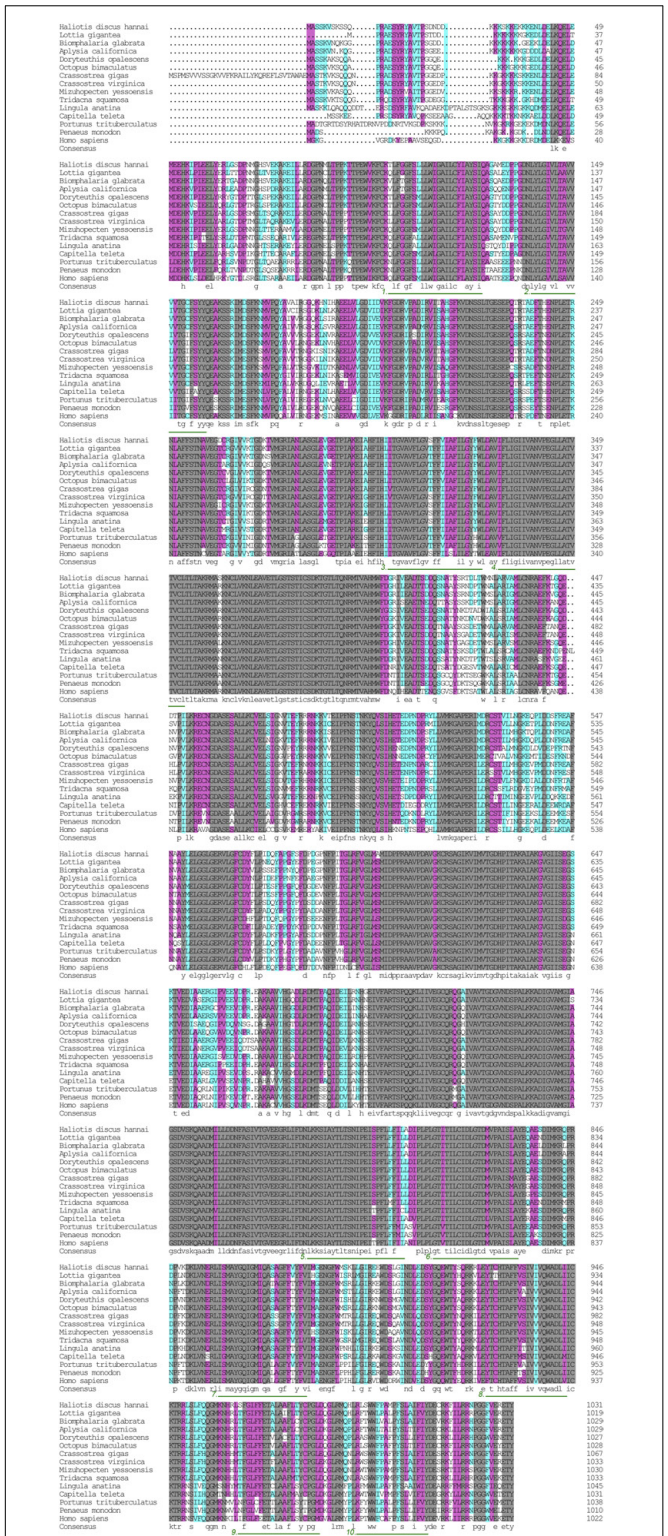

FIGURE 5 | Multiple alignment of the HdNKA α subunit sequence with NKA α subunit sequences deposited in GenBank. The amino acids highlighted in gray are identical in all sequences. The amino acids highlighted in pink are conserved more than 75%. The amino acids highlighted in cyan are conserved more than 50%. The regions underlined with green and numbered (1–10) are transmembrane regions.

of the organism. Ion concentrations may initially decrease after LSW treatment and increase after HSW treatment. When compared the ion concentrations in tissues, both the Na^+ and K^+ were basically maintained at the same level respectively (**Figures 2D,E**). Due to the complexity of cell osmoregulation, this stasis may be affected by the change in cell volume and the transmembrane transport of water molecules. Moreover, both the Na^+ and K^+ could be transported separately by several ion channels. There are also several channel proteins that can cotransport both Na^+ and K^+ at the same time. As an important ion transporter, the function of NKA in maintaining the ion concentration at a well-balanced level in Pacific abalone has never been reported.

Thus, our initial attempts were directed toward cloning the full-length cDNAs of the *Hdnka* α and β subunits. In the present study, only one α subunit and one β subunit of *Hdnka* cDNAs were identified from the Pacific abalone. Multiple sequence alignments showed that the amino acid sequence of the *Hdnka* α subunit had high similarity with those of other species. This result demonstrates that the gene is much conserved in evolution. The subunit composition of the NKA is tissue specific (Therien and Blostein, 1999). Nevertheless, its α subunit, the catalytic subunit, is common to all of the subtypes and possesses high sequence similarity with α subunits of other P-type ATPases, even the sarco/endoplasmic reticulum Ca^{2+}-ATPase (SERCA) and the gastric H^+/K^+-ATPase (Møller et al., 1996). This enzyme catalyzes the same reaction in different species. The conserved domain of the α subunit is the active site region of the enzyme. However, multiple sequence alignments of the β subunit amino acid sequences show that the sequences of this gene and those of other species share low similarity. The main function of NKA is pumping sodium out of cells while pumping potassium into cells via binding sites on the α subunit. Highly conserved amino acids sequences are thought to have functional value. Results of bioinformatics analysis indicated that the α subunit is the catalytic subunit of the NKA on another perspective.

Subunit α of NKA is the catalytic subunit. Therefore, most previous studies have particularly focused on this subunit in other species. The regulation of NKA under osmotic stress has been determined using the renal epithelial cell line NBL-1 (Ferrer-Martínez et al., 1996). This study indicated that the hypertonic shock increased the amount of NKA α subunit mRNA but had no influence on the β subunit levels. In addition, this stimulation was not correlated with significant changes in the amount of NKA α subunit protein. From the q-PCR data in our experiment, we found that after the treatment with LSW, the change in *Hdnka* α subunit expression could be divided into three stages. In the first phase, the expression slightly increased in both mantle ($P > 0.05$) and gill ($P < 0.05$). This difference indicates that gill is more sensitive when faced with salinity change. Moreover, the first phase is very ephemeral. This transient increase may due to the stress response of organism, which resulted from the sudden decrease of ion concentration in hemolymph. The rapid change resulted in electrical potential and altered the expression of NKA at the initial time. In the second phase, there is a rapid reduction of α subunit expression in these two tissues. To keep the normal biological function of the organism, the

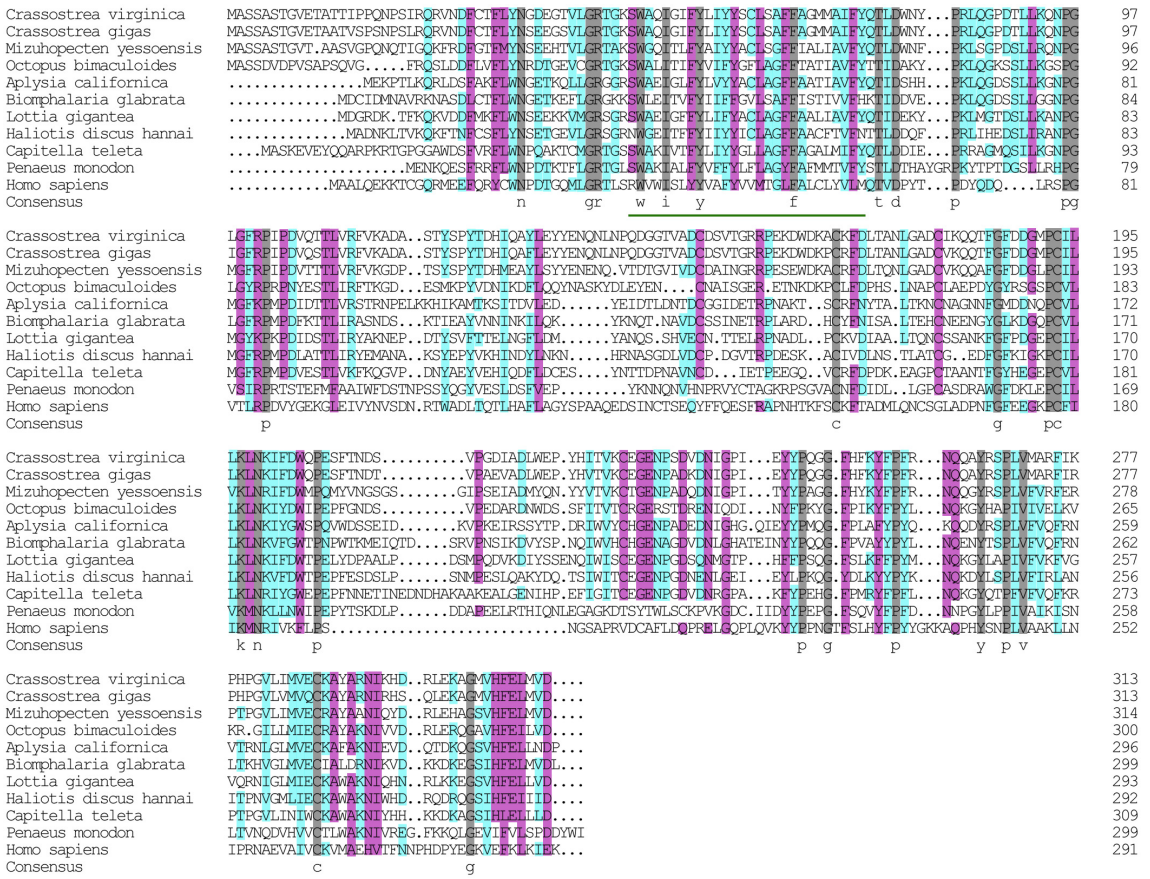

FIGURE 6 | Multiple alignment of the HdNKA β subunit sequences with NKA β subunit sequences deposited in GenBank. The amino acids highlighted in gray are identical in all sequences. The amino acids highlighted in pink are conserved more than 75%. The amino acids highlighted in cyan are conserved more than 50%.

intracellular ion concentration needs to be maintained within a certain physiological range, which leads to the significant reduction in NKA expression in later stage. In the last phase, expression increases slightly. In contrast, the HSW treatment led to a slight reduction in expression at the first stage. However, this period lasted longer than it did during the LSW treatment. These data indicated that Pacific abalone was more sensitive to low salinity than to high salinity. Then, there is a significant increase in expression. NKA α subunit expression changes in the euryhaline teleost *Fundulus heteroclitus* was also been divided into two phases in a previous publication: a stress period and an adjustment period. There were significant differences in the activity of NKA between these two periods (Mancera and McCormick, 2000). Moreover, there are many previous studies that showed that a change in salinity has no influence on the activity of NKA (Heijden et al., 1997; Kelly et al., 1999; Romao et al., 2001). These differences may due to the differences in the adaptability of different species to osmotic changes and their different modes of regulating osmotic pressure.

There is much less studies on the β subunit of NKA than on the NKA α subunit due to its lack of catalytic activity. Most of the research is on fish. Moreover, the conclusions about the effect of salinity on the β subunit are also inconsistent (Blasiole et al., 2003; Deane and Woo, 2005; Fiol et al., 2006). From the data of our experiment, we found that the influence of salinity changes on the expression of the *Hdnka* β subunit was consistent with the changes in the expression of the *Hdnka* α subunit. Furthermore, we also determined the expression of HdNKA at the protein level by western blot. Like the results from q-PCR, the HSW treatment increased the expression of HdNKA, and LSW treatment led a reduction in HdNKA expression. In contrast, the amount of NKA α subunit protein was not modified after hypertonic shock at any time tested, even when the biological activity of the pump was already enhanced, as in a previous study (Ferrer-Martínez et al., 1996). In addition, the activity of HdNKA was measured in our experiment. The activity of NKA in mantle was increased significantly by 3 h after transfer into HSW, but the levels of both mRNA (both α and β) and protein were not changed at the same time point (**Figures 8A,G**). The response of NKA activity to the salinity changes occurred a little earlier than that of gene expression. These data indicated that the increase in NKA activity is not due to only the accumulation of NKA. There may be some other factors. In gill, the protein abundance of the α subunit was slightly enhanced at 3 h after transfer into HSW (**Figure 8H**), but the patterns were different from those of the mRNA expression levels of α and β (non-changed; **Figures 8B,D**). These differences

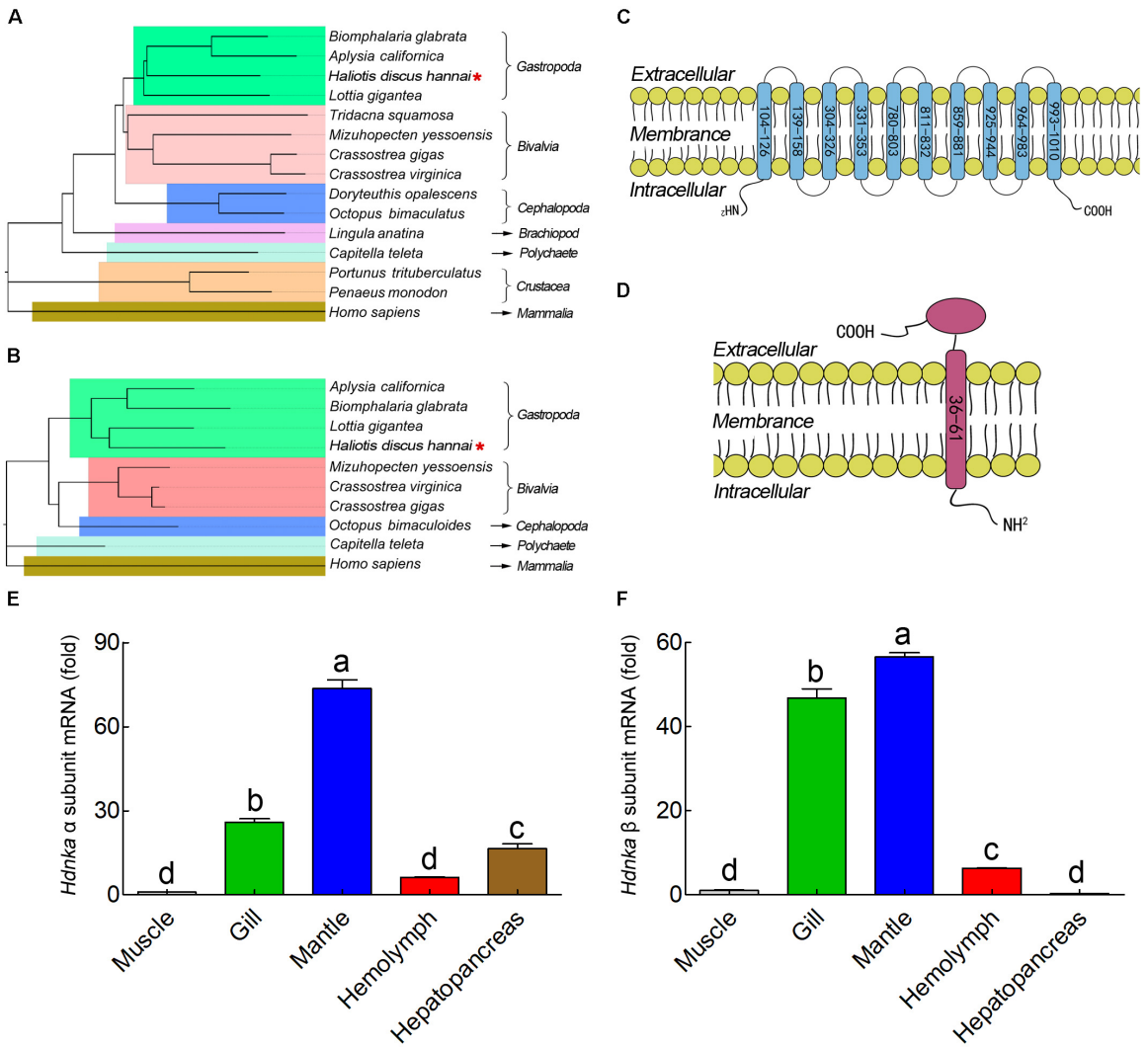

FIGURE 7 | Phylogenetic tree, transmembrane structure and expression profile analysis. **(A)** Phylogenetic tree analysis of HdNKA α subunit from Pacific abalone and NKA α subunits from other species. **(B)** Phylogenetic tree analysis of HdNKA β subunit from Pacific abalone and NKA β subunits from other species. **(C)** Topology model of the α subunit of HdNKA. The yellow spheroids represent the cell membrane, and the blue rod-like structure represents the transmembrane region. The numbers in the rod represent the amino acid sites. **(D)** Topology model of the HdNKA β subunit. The yellow spheroids represent the cell membrane. The red rod and oval structures represent the transmembrane region and highly glycosylated extracellular domain, respectively. The numbers in the rod represent the amino acid sites. **(E)** Transcript levels of *Hdnka* α subunit in the tissues obtained from Pacific abalone. **(F)** Transcript levels of *Hdnka* β subunit in the tissues obtained from Pacific abalone. Different letters on data indicate statistically significant differences between the results ($P < 0.05$). $n = 4$/time-point.

may be caused by the accuracy of the detection method. From these data, we concluded that 3–6 h is the critical time range. Due to the subtle effects of individual differences, the mix in protein samples may cause the slight increase at the 3 h time point. In summary, these data indicated that HdNKA was significantly regulated by the salinity change at both the mRNA and protein levels in Pacific abalone. The regulation process in Pacific abalone when faced with salinity changes mainly includes three stages: a passive stress response period, an active adjustment period and an adaptation period.

The regulation of NKA was divided into two categories, endogenous and exogenous. As an intracellular second messenger, cAMP could regulate the activity of NKA (Kiroytcheva et al., 1999). In conclusion, substances causing an increase in cAMP upregulate the activity of NKA. This study indicated that cAMP could regulate the NKA by PKA phosphorylation on the NKA α subunit in rat. However, in another study, the activity of NKA in rat was inhibited by cAMP (Kurihara et al., 2000). This research suggested that NKA activity could be regulated by a cAMP-dependent protein kinase that is anchored on the membrane via its anchoring protein. Unfortunately, both of these two reports did not determine the influence of cAMP on the expression of NKA at the mRNA level. Currently, little is known about whether salinity changes affect the concentration of cAMP in Pacific abalone. Moreover, the effect of cAMP on the expression of

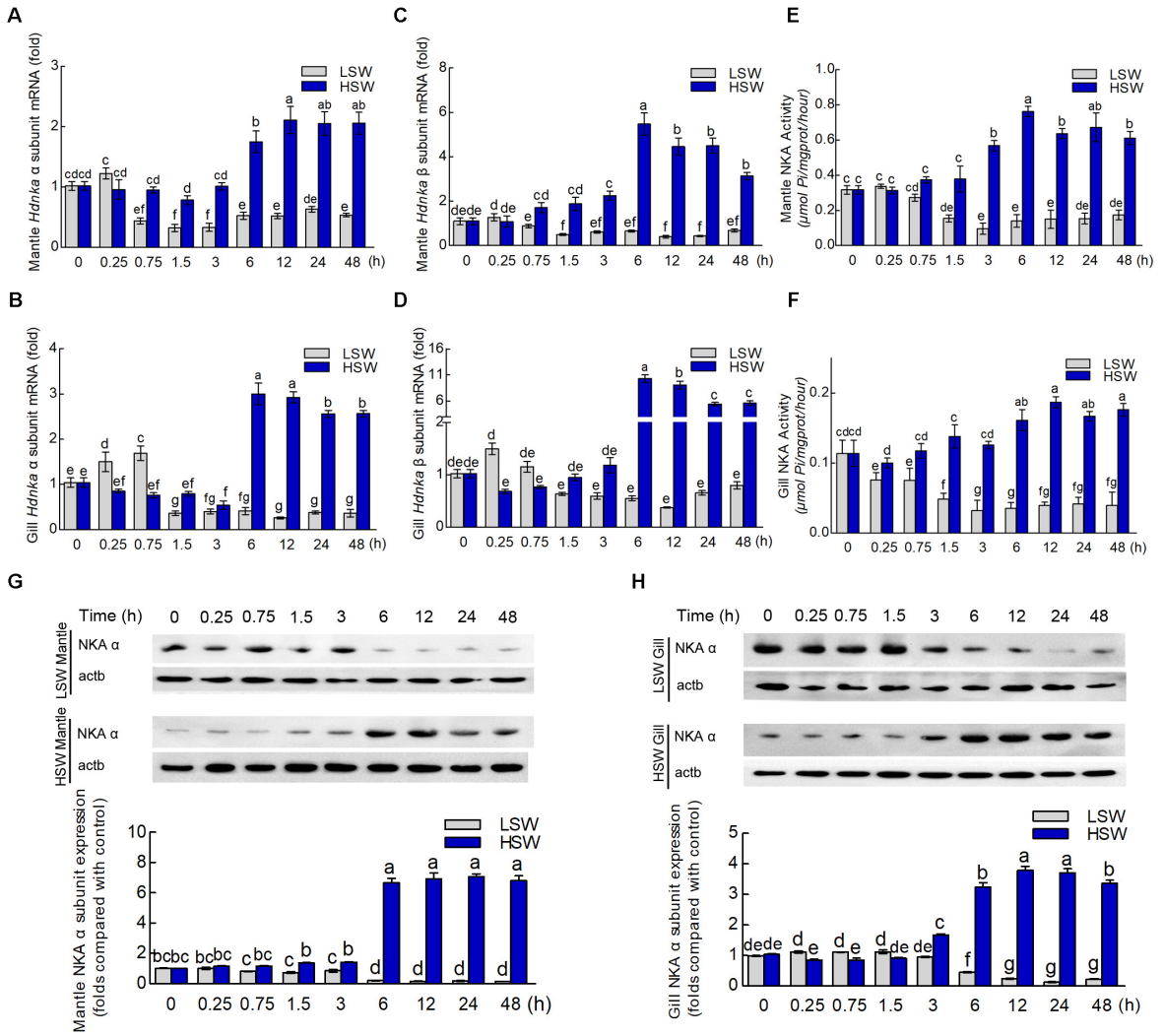

FIGURE 8 | Expression and activity analysis of Na^+/K^+-ATPase α and β subunits. **(A)** Influence of salinity changes on the mRNA level of the *Hdnka* α subunit in mantle. **(B)** Influence of salinity changes on the mRNA level of the *Hdnka* β subunit in mantle. **(C)** Influence of salinity changes on the mRNA level of the *Hdnka* α subunit in gill. **(D)** Influence of salinity changes on the mRNA level of the *Hdnka* β subunit in gill. **(E)** Influence of salinity changes on the activity of HdNKA in mantle. **(F)** Influence of salinity changes on the activity of HdNKA in gill. **(G)** Influence of salinity changes on the expression of the HdNKA α subunit in mantle determined with western blot. **(H)** Influence of salinity changes on the expression of the HdNKA α subunit in gill determined with western blot. Different letters on data indicate statistically significant differences between the results ($P < 0.05$). $n = 4$/time-point.

NKA is still unknown. Sommer and Mantel (1991)have reported that short-term acclimation of crabs to 40% seawater increased the cAMP content of the posterior gills from its value in the controls. Nonetheless, this result was not consistent with our findings. In the present study, the concentration of cAMP was measured after sudden treatment with LSW or HSW at different times. In both mantle and gill, the cAMP concentration was substantially lower after sudden treatment with LSW. In contrast, the HSW treatment increased the cAMP concentration rapidly. These findings suggested that a cAMP generation system is stimulated after salinity changes. The differences in the influence of salinity changes on the cAMP concentration may due to the differences between species. In addition, statistical analysis showed that the cAMP concentration was highly significant and positively correlated with the HdNKA activity and HdNKA expression in both mantle and gill samples in Pacific abalone.

In summary, the present study has identified the full-length of *Hdnka* α and β subunits in Pacific abalone *H. discus hannai*. From the data of our experiment, we found that NKA may play an important role during the process of osmotic pressure regulation in Pacific abalone. When faced with sudden salinity change, the responses of *Hdnka* α subunit could be divided into three stages: stress period, adjustment period and stable period. Moreover, the concentration of cAMP in mantle and gill were affected by salinity change. Changes in salinity may affect the synthesis of cAMP and then affect the transcription, translation, and enzyme activity

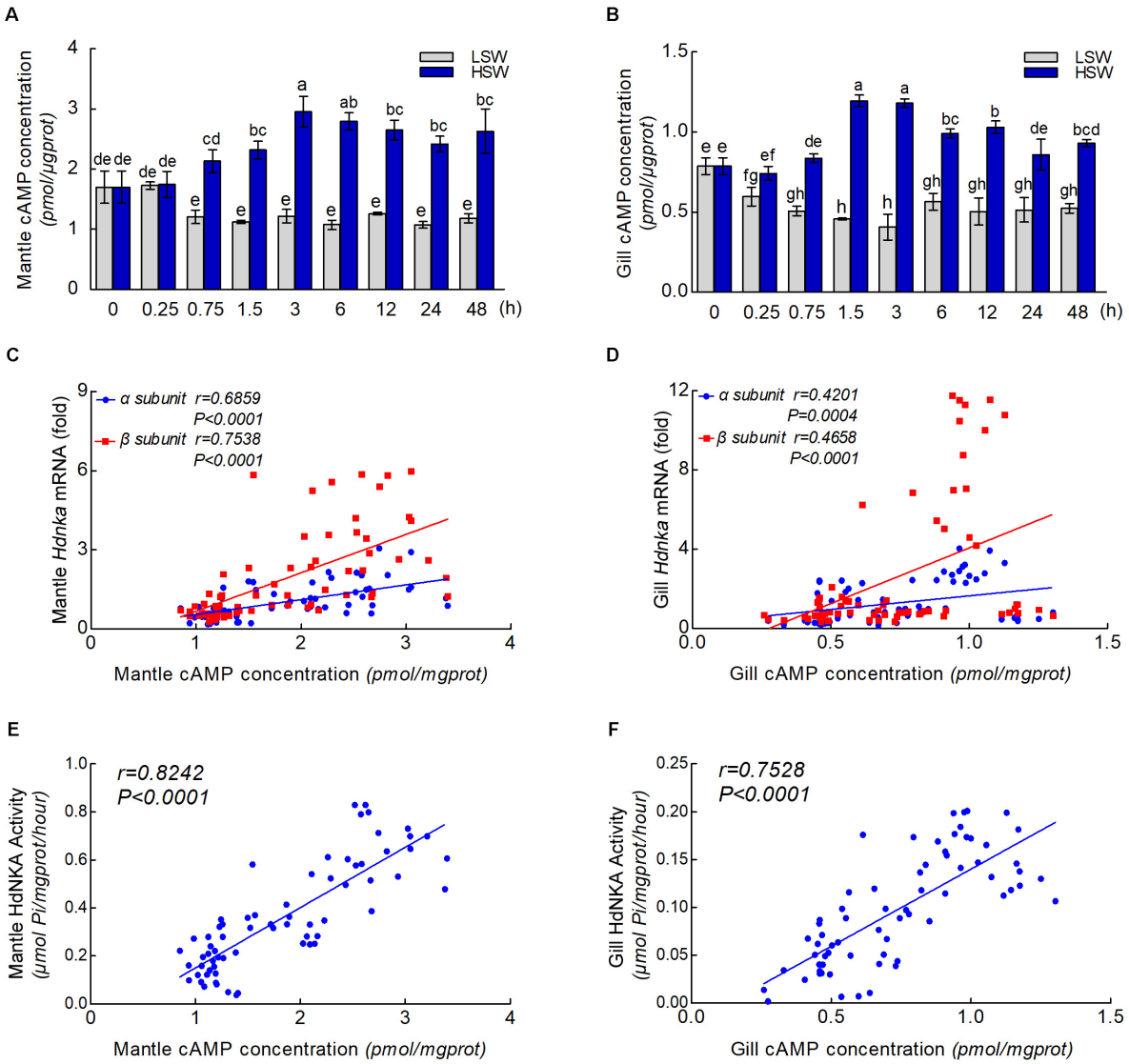

FIGURE 9 | cAMP concentrations and correlation analysis. **(A)** Influence of salinity changes on the concentration of cAMP in mantle. **(B)** Influence of salinity changes on the concentration of cAMP in gill. **(C)** Correlation analysis between cAMP concentration and *Hdnka* α and β subunit expression in mantle. **(D)** Correlation analysis between cAMP concentration and *Hdnka* α and β subunit expression in gill. **(E)** Correlation analysis between cAMP concentration and HdNKA activity in mantle. **(F)** Correlation analysis between cAMP concentration and HdNKA activity in gill. Different letters on data indicate statistically significant differences between the results ($P < 0.05$). n = 4/time-point.

of HdNKA. Further research is needed to determine whether salinity changes directly affect the HdNKA activity by the phosphorylation of PKA through the cAMP pathway in Pacific abalone. In addition, the role of the significant changes in non-catalytic subunit (the *Hdnka* β subunit) expression needs further investigation.

AUTHOR CONTRIBUTIONS

XL conceived and supervised the study. YJ performed most of the experiments and prepared the figures. YJ and XL analyzed the data and wrote the paper.

FUNDING

This work was supported in part by grants from the National Natural Science Foundation of China (41676152) and the Earmarked Fund for Agriculture Seed Improvement Project of Shandong Province (2017LZGC009).

SUPPLEMENTARY MATERIAL

The Supplementary Material for this article can be found online at: https://www.frontiersin.org/articles/10.3389/fphys.2018.01244/full#supplementary-material

REFERENCES

Altenhein, B., Markl, J., and Lieb, B. (2002). Gene structure and hemocyanin isoform HtH2 from the mollusc *Haliotis tuberculata* indicate early and late intron hot spots. *Gene* 301, 53–60. doi: 10.1016/S0378-1119(02)01081-8

Amende, L. M., and Pierce, S. K. (1980). Cellular volume regulation in salinity stressed molluscs: the response of *Noetia ponderosa* (Arcidae) red blood cells to osmotic variation. *J. Comp. Physiol.* 138, 283–289. doi: 10.1007/BF00691562

Appeltans, W., Bouchet, P., Boxshall, G., Fauchald, K., Gordon, D., Hoeksema, B., et al. (2014). *World Register of Marine Species. 2012*. Ostend: WoRMS.

Babdinitz, E., Albeck, S., Peleg, Y., Brumfeld, V., Gottschalk, K. E., and Karlish, S. J. (2009). A C-terminal lobe of the β subunit of Na,K-ATPase and H,K-ATPase resembles cell adhesion molecules. *Biochemistry* 48, 8684–8691. doi: 10.1021/bi900868e

Beggah, A. T., Jaunin, P., and Geering, K. (1997). Role of glycosylation and disulfide bond formation in the β subunit in the folding and functional expression of Na,K-ATPase. *J. Biol. Chem.* 272, 10318–10326. doi: 10.1074/jbc.272.15.10318

Bertorello, A. M., Aperia, A., Walaas, S. I., Nairn, A. C., and Greengard, P. (1991). Phosphorylation of the catalytic subunit of Na+,K+-ATPase inhibits the activity of the enzyme. *Proc. Natl. Acad. Sci. U.S.A.* 88, 11359–11362. doi: 10.1073/pnas.88.24.11359

Blasiole, B., Degrave, A., Canfield, V., Boehmler, W., Thisse, C., Thisse, B., et al. (2003). Differential expression of Na,K-ATPase α and β subunit genes in the developing zebrafish inner ear. *Dev. Dyn.* 228, 386–392. doi: 10.1002/dvdy.10391

Bos, J. L. (2006). Epac proteins: multi-purpose cAMP targets. *Trends Biochem. Sci.* 31, 680–686. doi: 10.1016/j.tibs.2006.10.002

Buchan, D. W., Ward, S. M., Lobley, A. E., Nugent, T. C. O., Bryson, K., and Jones, D. T. (2010). Protein annotation and modelling servers at University College London. *Nucleic Acids Res.* 38, W563–W568. doi: 10.1093/nar/gkq427

Burton, R. F. (1983). "Ionic regulation and water balance," in *The Mollusca-Physiology*, ed. K. M. Wilbur (Cambridge, MA: Academic Press), 293–350.

Cheng, W., Yeh, S. P., Wang, C. S., and Chen, J. C. (2002). Osmotic and ionic changes in Taiwan abalone *Haliotis diversicolor* supertexta at different salinity levels. *Aquaculture* 203, 349–357. doi: 10.1016/S0044-8486(01)00606-8

Clausen, M. V., Hilbers, F., and Poulsen, H. (2017). The structure and function of the Na,K-ATPase isoforms in health and disease. *Front. Physiol.* 8:371. doi: 10.3389/fphys.2017.00371

Cook, P. A. (2016). Recent trends in worldwide abalone production. *J. Shellfish Res.* 35, 581–583. doi: 10.2983/035.035.0302

Davenport, J., Gruffydd, D., and Beaumont, A. (1975). An apparatus to supply water of fluctuating salinity and its use in a study of the salinity tolerances of larvae of the scallop *Pecten maximus* L. *J. Mar. Biol. Assoc. U. K.* 55, 391–409. doi: 10.1017/S0025315400016015

Deane, E. E., and Woo, N. Y. S. (2005). Cloning and characterization of sea bream Na+-K+-ATPase α and β subunit genes: in vitro effects of hormones on transcriptional and translational expression. *Biochem. Biophys. Res. Commun.* 331, 1229–1238. doi: 10.1016/j.bbrc.2005.04.038

Elliott, N. G. (2000). Genetic improvement programmes in abalone: what is the future? *Aquac. Res.* 31, 51–59. doi: 10.1046/j.1365-2109.2000.00386.x

Ferrer-Martínez, A., Casado, F. J., and Felipe, A. M. (1996). Regulation of Na+,K+-ATPase and the Na+/K+/Cl- co-transporter in the renal epithelial cell line NBL-1 under osmotic stress. *Biochem. J.* 319, 337–342. doi: 10.1042/bj3190337

Fiol, D. F., Chan, S. Y., and Kültz, D. (2006). Identification and pathway analysis of immediate hyperosmotic stress responsive molecular mechanisms in tilapia (*Oreochromis mossambicus*) gill. *Comp. Biochem. Physiol. Part D Genomics Proteomics* 1, 344–356. doi: 10.1016/j.cbd.2006.08.002

Gordon, H. R., and Cook, P. A. (2004). World abalone fisheries and aquaculture update: supply and market dynamics. *J. shellfish Res.* 23, 935–940.

Guynn, S. R., Scofield, M. A., and Petzel, D. H. (2002). Identification of mRNA and protein expression of the Na/K-ATPase α1-, α2- and α3-subunit isoforms in Antarctic and New Zealand notothenid fishes. *J. Exp. Mar. Biol. Ecol.* 273, 15–32. doi: 10.1016/S0022-0981(02)00136-3

Hall, J. E., and Guyton, A. C. (2006). *Textbook of Medical Physiology*. St. Louis, Mo: Elsevier Saunders.

Hasler, U., Wang, X., Crambert, G., Béguin, P., Jaisser, F., Horisberger, J. D., et al. (1998). Role of β-subunit domains in the assembly, stable expression, intracellular routing, and functional properties of Na,K-ATPase. *J. Biol. Chem.* 273, 30826–30835. doi: 10.1074/jbc.273.46.30826

Heijden, A., Verbost, P., Eygensteyn, J., Li, J., Bonga, S., and Flik, G. (1997). Mitochondria-rich cells in gills of tilapia (*Oreochromis mossambicus*) adapted to fresh water or sea water: quantification by confocal laser scanning microscopy. *J. Exp. Biol.* 200, 55–64.

Hoshijima, K., and Hirose, S. (2007). Expression of endocrine genes in zebrafish larvae in response to environmental salinity. *J. Endocrinol.* 193, 481–491. doi: 10.1677/JOE-07-0003

Kelly, S. P., Chow, I. N., and Woo, N. Y. (1999). Alterations in Na+-K+-ATPase activity and gill chloride cell morphometrics of juvenile black sea bream (Mylio macrocephalus) in response to salinity and ration size. *Aquaculture* 172, 351–367. doi: 10.1016/S0044-8486(98)00505-5

Kiroytcheva, M., Cheval, L., Carranza, M. L., Martin, P. Y., Favre, H., Doucet, A., et al. (1999). Effect of cAMP on the activity and the phosphorylation of Na^+,K^+-ATPase in rat thick ascending limb of Henle. *Kidney Int.* 55, 1819–1831. doi: 10.1046/j.1523-1755.1999.00414.x

Kong, N., Liu, X., Li, J. Y., Mu, W. D., Lian, J. W., Xue, Y. J., et al. (2017). Effects of temperature and salinity on survival, growth and DNA methylation of juvenile Pacific abalone *Haliotis discus* hannai Ino. *Chin. J. Oceanol. Limnol.* 35, 1–11. doi: 10.1007/s00343-016-5185-z

Kumar, S., Stecher, G., and Tamura, K. (2016). Mega7: molecular evolutionary genetics analysis version 7.0 for bigger datasets. *Mol. Biol. Evol.* 33, 1870–1874. doi: 10.1093/molbev/msw054

Kurihara, K., Nakanishi, N., and Ueha, T. (2000). Regulation of $Na^{+-}K^{+-}$ATPase by cAMP-dependent protein kinase anchored on membrane via its anchoring protein. *Am. J. Physiol. Cell Physiol.* 279, C1516–C1527. doi: 10.1152/ajpcell.2000.279.5.C1516

Larkin, M. A., Blackshields, G., Brown, N. P., Chenna, R., McGettigan, P. A., McWilliam, H., et al. (2007). Clustal W and Clustal X version 2.0. *Bioinformatics* 23, 2947–2948. doi: 10.1093/bioinformatics/btm404

Lv, D. (1978). A study on the Haliotidae from the coast of China. *Stud. Mar. Sin.* 14, 89–100.

Mancera, J. M., and McCormick, S. D. (2000). Rapid activation of gill Na^+,K^+-ATPase in the euryhaline teleost *Fundulus heteroclitus*. *J. Exp. Zool.* 287, 263–274. doi: 10.1002/1097-010X(20000901)287:4<263::AID-JEZ1>3.0.CO;2-I

Mobasheri, A., Avila, J., Cózar-Castellano, I., Brownleader, M. D., Trevan, M., Francis, M. J., et al. (2000). Na^+,K^+-ATPase isozyme diversity; comparative biochemistry and physiological implications of novel functional interactions. *Biosci. Rep.* 20, 51–91. doi: 10.1023/A:1005580332144

Møller, J. V., Juul, B., and Le Maire, M. (1996). Structural organization, ion transport, and energy transduction of P-type ATPases. *Biochim. Biophys. Acta* 1286, 1–51. doi: 10.1016/0304-4157(95)00017-8

Monahan-Earley, R., Dvorak, A. M., and Aird, W. C. (2013). Evolutionary origins of the blood vascular system and endothelium. *J. Thromb. Haemost.* 11, 46–66. doi: 10.1111/jth.12253

Morris, S., and Edwards, T. (1995). Control of osmoregulation via regulation of Na^+K^+-ATPase activity in the amphibious purple shore crab *Leptograpsus variegatus*. *Comp. Biochem. Physiol. Part C Pharmacol.* 112, 129–136.

Navarro, J. M. (1988). The effects of salinity on the physiological ecology of *Choromytilus chorus* (Molina, 1782) (Bivalvia: Mytilidae). *J. Exp. Mar. Biol. Ecol.* 122, 19–33. doi: 10.1016/0022-0981(88)90209-2

Nyblom, M., Poulsen, H., Gourdon, P., Gourdon, P., Reinhard, L., Andersson, M., et al. (2013). Crystal structure of Na^+,K^+-ATPase in the Na^+-bound state. *Science* 342, 123–127. doi: 10.1126/science.1243352

Pan, L., Liu, H., and Zhao, Q. (2014). Effect of salinity on the biosynthesis of amines in *Litopenaeus vannamei* and the expression of gill related ion transporter genes. *J. Ocean Univ. China* 13, 453–459. doi: 10.1007/s11802-014-2013-y

Pham, D., Charmantier, G., Boulo, V., Wabete, N., Ansquer, D., Dauga, C., et al. (2016). Ontogeny of osmoregulation in the Pacific blue shrimp. *Comp. Biochem. Physiol. Part B Biochem. Mol. Biol.* 196, 27–37. doi: 10.1016/j.cbpb.2015.12.007

Rajasekaran, A. K., and Rajasekaran, S. A. (2003). Role of Na-K-ATPase in the assembly of tight junctions. *Am. J. Physiol. Ren. Physiol.* 285, F388–F396. doi: 10.1152/ajprenal.00439.2002

Rajasekaran, S. A., Gopal, J., Willis, D., Espineda, C., Twiss, J. L., and Rajasekaran, A. K. (2004). Na,K-ATPase β1-subunit increases the translation efficiency of the

α1-subunit in MSV-MDCK cells. *Mol. Biol. Cell* 15, 3224–3232. doi: 10.1091/mbc.E04-03-0222

Reeves, A. S., Collins, J. H., and Schwartz, A. (1980). Isolation and characterization of (Na,K)-ATPase proteolipid. *Biochem. Biophys. Res. Commun.* 95, 1591–1598. doi: 10.1016/S0006-291X(80)80080-5

Richards, J. G., Semple, J. W., Bystriansky, J. S., and Schulte, P. M. (2003). Na+/K+-ATPase α-isoform switching in gills of rainbow trout (*Oncorhynchus mykiss*) during salinity transfer. *J. Exp. Biol.* 206, 4475–4486. doi: 10.1242/jeb.00701

Richards, O. W., and Davies, R. (1977). *"Hymenoptera" in Imms' General Textbook of Entomology*. Berlin: Springer, 1175–1279.

oRomao, S., Freire, C., and Fanta, E. (2001). Ionic regulation and Na^+,K^+-ATPase activity in gills and kidney of the Antarctic aglomerular cod icefish exposed to dilute sea water. *J. Fish Biol.* 59, 463–468. doi: 10.1111/j.1095-8649.2001.tb00146.x

Siebers, D., Lucu, C., Sperling, K. R., and Eberlein, K. (1972). Kinetics of osmoregulation in the crab *Carcinus maenas*. *Mar. Biol.* 17, 291–303. doi: 10.1007/BF00366739

Sommer, M. J., and Mantel, L. H. (1991). Effects of dopamine and acclimation to reduced salinity on the concentration of cyclic AMP in the gills of the green crab, *Carcinus maenas* (L). *Gen. Comp. Endocrinol.* 82, 364–368. doi: 10.1016/0016-6480(91)90311-S

Sowers, A., Young, S., Grosell, M., Browdy, C., and Tomasso, J. (2006). Hemolymph osmolality and cation concentrations in *Litopenaeus vannamei* during exposure to artificial sea salt or a mixed-ion solution: relationship to potassium flux. *Comp. Biochem. Physiol. Part A Mol. Integr. Physiol.* 145, 176–180. doi: 10.1016/j.cbpa.2006.06.008

Therien, A. G., and Blostein, R. (1999). K+/Na+ antagonism at cytoplasmic sites of Na+-K+-ATPase: a tissue-specific mechanism of sodium pump regulation. *Am. J. Physiol.* 277, 891–898. doi: 10.1152/ajpcell.1999.277.5.C891

Therien, A. G., and Blostein, R. (2000). Mechanisms of sodium pump regulation. *Am. J. Physiol. Cell Physiol.* 279, C541–C566. doi: 10.1152/ajpcell.2000.279.3.C541

Tokhtaeva, E., Sachs, G., Souda, P., Bassilian, S., Whitelegge, J. P., Shoshani, L., et al. (2011). Epithelial junctions depend on intercellular trans-interactions between the Na,K-ATPase β1 Subunits. *J. Biol. Chem.* 286, 25801–25812. doi: 10.1074/jbc.M111.252247

Wyatt, G. R. (1961). The biochemistry of insect hemolymph. *Annu. Rev. Entomol.* 6, 75–102. doi: 10.1146/annurev.en.06.010161.000451

Conflict of Interest Statement: The authors declare that the research was conducted in the absence of any commercial or financial relationships that could be construed as a potential conflict of interest.

frontiers in Physiology

ORIGINAL RESEARCH
published: 26 October 2018
doi: 10.3389/fphys.2018.01491

Analysis of *in situ* Transcriptomes Reveals Divergent Adaptive Response to Hyper- and Hypo-Salinity in the Hong Kong Oyster, *Crassostrea hongkongensis*

Shu Xiao[1], Nai-Kei Wong[2], Jun Li[1], Yue Lin[1], Yuehuan Zhang[1], Haitao Ma[1], Riguan Mo[1], Yang Zhang[1] and Ziniu Yu[1]**

[1] CAS Key Laboratory of Tropical Marine Bio-Resources and Ecology, Guangdong Provincial Key Laboratory of Applied Marine Biology, South China Sea Institute of Oceanology, Chinese Academy of Sciences, Guangzhou, China, [2] State Key Discipline of Infection Diseases, Shenzhen Third People's Hospital, Shenzhen, China

OPEN ACCESS

Edited by:
Xiaotong Wang,
Ludong University, China

Reviewed by:
Alexssandro Geferson Becker,
Universidade Federal do Paraná, Brazil
Juan Antonio Martos-Sitcha,
University of Cádiz, Spain
Pierre Boudry,
Institut Français de Recherche pour l'Exploitation de la Mer (IFREMER), France

***Correspondence:**
Yang Zhang
yzhang@scsio.ac.cn
Ziniu Yu
carlzyu@scsio.ac.cn

Specialty section:
This article was submitted to Aquatic Physiology, a section of the journal Frontiers in Physiology

Received: *27 June 2018*
Accepted: *02 October 2018*
Published: *26 October 2018*

Citation:
Xiao S, Wong N-K, Li J, Lin Y, Zhang Y, Ma H, Mo R, Zhang Y and Yu Z (2018) Analysis of in situ Transcriptomes Reveals Divergent Adaptive Response to Hyper- and Hypo-Salinity in the Hong Kong Oyster, Crassostrea hongkongensis. Front. Physiol. 9:1491. doi: 10.3389/fphys.2018.01491

Crassostrea hongkongensis, a commercially valuable aquaculture species dwelling in estuaries along the coast of the South China Sea, is remarkable for its eurysalinity traits that enable its successful colonization of diverse osmotic niches ranging from near freshwater to seawater. In order to elucidate how this oyster copes with coastal waters with immense salinity differences, we performed *in situ* transcriptomic analysis (RNA-seq) to characterize the global expression patterns of oysters distributed across naturally formed salinity gradients in Zhenhai Bay along the northern coast of the South China Sea. Principal component analysis reveals distinct expression profiles of oysters living in the extreme conditions of hypo-salinity and hyper-salinity. Compared with the situation of optimal salinity for oyster growth, hypo-salinity mainly regulated expression of genes involved in FoxO and oxytocin signaling, tight junction and several immune pathways, while hyper-salinity altered gene expression implicated in amino acid metabolism, AMPK and PI3K-AKt signaling pathways, demonstrating the complexity and plasticity of transcriptomic expression underpinning oyster eurysalinity. Furthermore, the expression patterns of several genes correlated with salinity gradients reveals the fine-tuned coordination of molecular networks necessary for adaptive homeostasis in *C. hongkongensis*. In conclusion, a striking capacity and distinct patterns of transcriptomic expression contribute to eurysalinity adaptation in *C. hongkongensis*, which provides new mechanistic insights into the adaptive plasticity and resilience of marine mollusks.

Keywords: oysters, *Crassostrea hongkongensis*, adaptive plasticity, salinity, osmoregulation, transcriptomics

INTRODUCTION

Estuaries are dynamic and intricate ecosystems characterized by rapid periodic fluctuations in physical parameters such as salinity, oxygen levels and temperature. To cope with these challenging environmental oscillations, local marine organisms have evolved various adaptive strategies to enable survival and physiological plasticity. The Hong Kong oyster, *Crassostrea hongkongensis*, is

an endemic and commercially valuable aquaculture species that thrives along the northern coast of South China Sea (Lam and Morton, 2004). As benthic and sessile filter-feeders, the Hong Kong oyster has acquired a powerful capacity for adapting to the inherently dynamic estuarial habitats (Liu et al., 2013). Notably, this oyster exhibits remarkable eurysalinity traits, which allow it to survive in extreme conditions across salinity gradients from seawater down to near freshwater, making it one of the predominant estuarial inhabitants in the local region. The Hong Kong oyster typically thrives within a salinity range of 5–30 ppt and the optimal salinity levels for it are approximately 10–25 ppt. It therefore exhibits adaptive plasticity superior to that of common species such as *Crassostrea giga*, *Crassostrea angulata* and *Crassostrea sikamea* (Lam and Morton, 2004; Liu et al., 2013). Previous findings have shown that substantial genetic variation could arise across the various oyster populations cultivated in different salinity niches (Li et al., 2013; Ma et al., 2016). Therefore, the Hong Kong oyster serves as an excellent model for exploiting the molecular mechanisms underlying functional plasticity in response to extreme osmotic stresses in bivalves.

Recently, several studies have employed transcriptomic analysis to investigate the molecular basis of oyster osmotic regulation, though their scope has been limited to experimental manipulations within the laboratory (Meng et al., 2013; Zhao et al., 2014; Yan et al., 2017). Currently, there is a paucity of understanding about the regulatory mechanisms of oyster salinity acclimation *in situ*. In this present study, we have carefully designed field experiments to sample oysters from different osmotic niches which encompass a continuum from freshwater to seawater, with the explicit aim of capturing snapshots of active transcripts under *in situ* conditions. Zhenhai Bay in Guangdong province, China, was chosen as a representative estuary area of the northern South China Sea for field study, where salinity gradients are naturally formed along the coast and punctuated with seasonal changes. Hong Kong oyster's success to thrive in local intertidal niches has been attributed to a strong and vertically inherited capacity for osmotic regulation, eventually leading to the emergence of endemic populations of this species. This coastal area thus provides us an ideal sampling location to study salinity adaption of oysters. This study represents a systematic attempt to understand the molecular underpinnings of oyster adaptive response to extreme conditions of salinity *in situ*. Analysis of *in situ* transcriptomes was used accordingly to characterize the genomic response to extreme osmotic conditions, with the hope of gaining insights into the crucial molecular determinants or pathways that contribute to govern the physiological plasticity in the Hong Kong oyster.

MATERIALS AND METHODS

Ethics Statement

Crassostrea hongkongensis is neither an endangered nor protected species. Oyster handling was conducted in compliance with the guidelines and regulations established by the ethics committee of the CAS South China Sea Institute of Oceanology and the local government.

In situ Sample Collection

In situ oyster sampling was conducted in Zhenhai Bay, situated between the Wencun and Beidou towns in Taishan municipality, Guangdong province, China. Its specific geographical coordinates are 21.44–21.95° north latitude, and 112.24–112.65° east longitude. The bay has in excess of 80 km of shoreline with an array of substrates including clay, mud, sand, and concrete from urbanized areas. It is the only estuary of the local Nafu River.

The oysters used in this study were collected at November 12, 2017 from six locations within the salinity gradient map of the local coast. The overall sample collection comprised of 90 wild 1-year old oysters (15 oysters per site). The shell height (maximal hinge-lip distance) of the oyster sampled ranged from 6 to 8 cm. The gills of the oysters were processed for total RNA isolation *in situ* within 30 min after their harvest on site.

RNA Isolation From Gills

Total RNA was isolated from the gills of oysters collected from different locations by using TRIzol Reagent (Invitrogen, United States) following the manufacturer's instructions. The isolated RNA was incubated with RNase free DNase (Invitrogen, United States) to eliminate the potential genomic RNA contamination. The purity and concentration of RNA samples were determined by Nanodrop 2000 (Thermo Fisher Scientific, United States). RNA integrity was verified by using an Agilent 2100 BioAnalyzer (Agilent, United States) with an RIN (RNA integrity number) setting >8.5. The same RNA samples from five oyster at each site was pooling as one biological replication, and each site contains three biological replications.

Library Construction and RNA-seq

The cDNA library for Illumina sequencing was prepared by using a Truseq^{TM} RNA sample prep kit (Illumina). Briefly, mRNA was first enriched by using poly-T oligo-attached magnetic beads (Illumina), which was subsequently broken down into fragments (200–700 nt). The first and second strands of cDNA were synthesized by SuperScript II reverse transcriptase and DNA polymerase I, respectively. After that, the libraries were end-repaired and ligated with adaptors, and amplified with Phusion DNA polymerase. The quality of cDNA library was validated by TBS380 (PicoGreen) and the samples were then sequenced on a BGISEQ-500 sequencing platform (BGI, China).

Real-Time qPCR Validation

One microgram of total RNA was used in reverse transcription (RT) experiments with PrimeScript^{TM} RT Reagent Kit (TaKaRa, Japan). All primers used in this studies were listed in **Supplementary Table S4**. The real-time qPCR was performed at the platform of LightCycler 480 (Roche) with 20 μL reaction system including 10 μL of 2× Master Mix (Roche), 0.4 μL of each of primers (10 mM), 5 μL of 1:50 diluted cDNA, and PCR-grade water for the rest. The dissociation curve analysis was performed to confirm specificity of amplicons. Each sample was carried out in triplicates, and relative expression levels of target genes was calculated using methods of $2^{-\Delta\Delta Ct}$ through normalized

with reference gene GAPDH. Results were expressed as mean of log2 (fold-changes) to compare with the result obtained from RNA-seq.

Bioinformatics Pipeline

Data Filtering

Clean reads were obtained by filtering raw data with the software SOAPnuke, which include removal of adaptors, unknown base reads (unknown bases were more than 10%) and low quality reads (cases were the percentage of base whose quality is less than 15% or greater than 50% in a read). Clean reads were stored in the FASTQ format and used for quantitative analysis.

Gene Expression Analysis

Clean reads were mapped onto known *C. hongkongensis* transcriptome datasets (Tong et al., 2015) by using Bowtie2 (Langmead and Salzberg, 2012), and the resultant matched reads were calculated and normalized to RPKM by using the RESM software (Li and Dewey, 2011). Pearson correlation coefficients between whole samples were calculated by using R cor, and PCA (principal components analysis) was performed by using princomp. Statistical significance of differentially expressed genes (DEGs) was analyzed via DEseq2 methods based on negative binomial distribution with the following threshold settings: fold change $\geq$2.00 and adjusted *p*-value $\leq$ 0.05 (Love et al., 2014).

Gene Ontology Analysis

Differentially expressed gene were subjected to analyses of Gene Ontology (GO) and KEGG Orthology (KO), which were further classified according to official classification. GO functional enrichment was performed by using phyper of R and the *p*-value was calculated in hypergeometric test with the following formula:

$$P = 1 - \sum_{i=0}^{m-1} \frac{\binom{M}{i}\binom{N-M}{n-i}}{\binom{N}{n}}$$

Then, false discovery rate (FDR) was calculated for each *p*-value, and we defined FDR <0.01 as significantly enriched (Ye et al., 2006; Kanehisa et al., 2008).

RESULTS

Broad-Spectrum Tolerance of *C. hongkongensis* for Salinity Extremities

Crassostrea hongkongensis is one of the euryhaline species that can survive under extreme conditions of salinity ranging from 2 to 30 ppt, and preferentially live in estuarial habitats. Zhenhai Bay features naturally formed salinity gradients comprising near freshwater and seawater. The geographic coordinate and annual mean salinity were presented **Figure 1**, including P1 (21.94N, 112.48E, 5.0 $\pm$ 3.9 ppt), P2 (21.93N, 112.45E, 8.4 $\pm$ 4.1 ppt), P3 (21.92N, 112.42E, 13.7 $\pm$ 5.2 ppt); P4 (21.87N, 112.43E, 19.2 $\pm$ 5.1 ppt); P5 (21.77N, 112.52E, 23.1 $\pm$ 3.9 ppt); P6 (21.67N, 112.64E, 28.1 $\pm$ 4.2 ppt). Here, *C. hongkongensis* occupied niches of diverse osmotic conditions across this bay. To characterize the molecular mechanisms underlying salinity adaption of the Hong Kong oyster, six distinct oyster populations (P1–P6) were collected across these salinity gradients. The realtime salinity were P1, 5.5 ppt; P2, 8.8 ppt; P3, 13.5 ppt; P4, 18.3 ppt; P5, 22.4 ppt; P6, 28.5 ppt, which was consistent with annual mean salinity by and large.

Expression Patterns of Whole Transcriptomes

In our experimental design, 18 libraries were constructed from six populations. Each population contained three biological replicates. After sequencing and low quality filtration, a total of 352.65 million clean reads were obtained with an average of 24 million reads for individual samples (**Supplementary Table S1**), and the raw data were deposited into database with accession number (SRR7777763–SRR7777768). The percentages of total mapped reads and unique mapped reads were 76.79–83.15% and 73.59–80.64%, respectively (**Supplementary Table S1**). The Pearson correlation analysis of global expression profiles reveals that was observed a higher correlation within each population than that between different populations (**Figure 2A** and **Supplementary Figure S1**). PCA further suggests that the expression profiles of oysters collected from locations P2–P5 (salinity from 8.8 to 22.4 ppt) overlap with each other (**Figure 2B**).

Pathway Enrichments in Hypo-Salinity and Hyper-Salinity Adaptation

To analyze which genes or pathways were involved in response to hypo-salinity and hyper-salinity adaptation, the DEGs obtained via the DEseq2 methods with samples at P3 as a control. Accordingly, hypo-salinity (P1 vs P3) generated 3,731 of up-regulated DEGs and 3,042 of down-regulated DEGs, whereas hyper-salinity (P6 vs P3) resulted in 641 of up-regulated DEGs and 563 of down-regulated DEGs (**Supplementary Figures S2**, **S3**). Furthermore, we classified these DEGs into different signaling pathways using KEGG (**Supplementary Tables S2**, **S3**). The top 10 enriched pathways in response to salinity extremities are listed in the **Figure 3** to illustrate that hypo-salinity regulates many signaling pathways or processes, which include the FoxO signaling pathway, oxytocin signaling pathway, regulation of actin cytoskeleton, and tight junction. Concomitantly, several immune pathways are also influenced by hypo-salinity, including chemokine signaling pathway, pathogenic infection, platelet activation, etc. (**Figure 3A**). In contrast, oysters under hyper-salinity seem to follow a different pattern of regulation, which features pathways involved in arginine and proline metabolism, riboflavin metabolism, PI3K-Akt signaling, protein digestion and absorption, ECM receptor interaction, focal adhesion, neuroactive ligand receptor interaction and so on (**Figure 3B**). There are almost no identical categories between hypo- and hyper-salinity, implying that different regulatory mechanisms may be at work for salinity adaptation under distinct conditions.

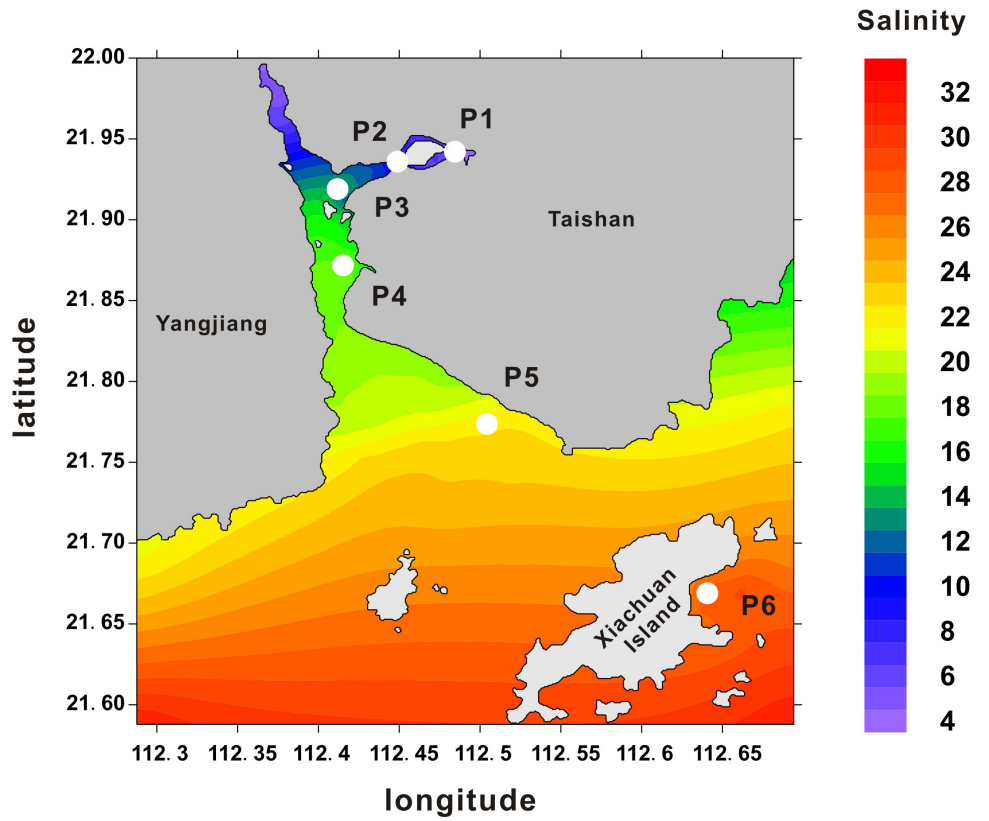

FIGURE 1 | Oyster sampling locations across salinity gradients in Zhenhai Bay. Heatmap shows the average salinity (ppt) measured in different sampling areas between Shenjing town and Xiachuan Island. The salinity data were collected from the local Taishan Marine and Fisheries Agency. Numerals in the *y*- and *x*-axis indicate the coordinates in latitude and longitude, respectively.

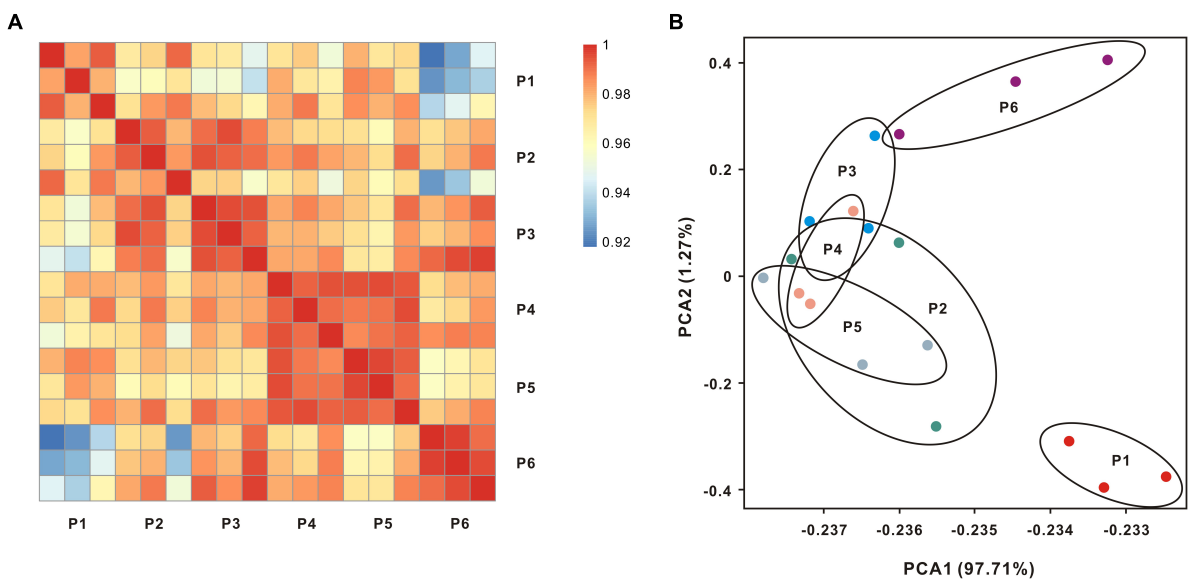

FIGURE 2 | Global transcript expression profiles of oysters living across salinity gradients. **(A)** Expression patterns of whole transcriptomes were analyzed by means of RNA-seq quantification. The heatmap shows the square of correlation between oysters collected from different locations. Each location contains three independent biological replicates. **(B)** Principal components analysis (PCA) using the normalized whole transcriptome expression.

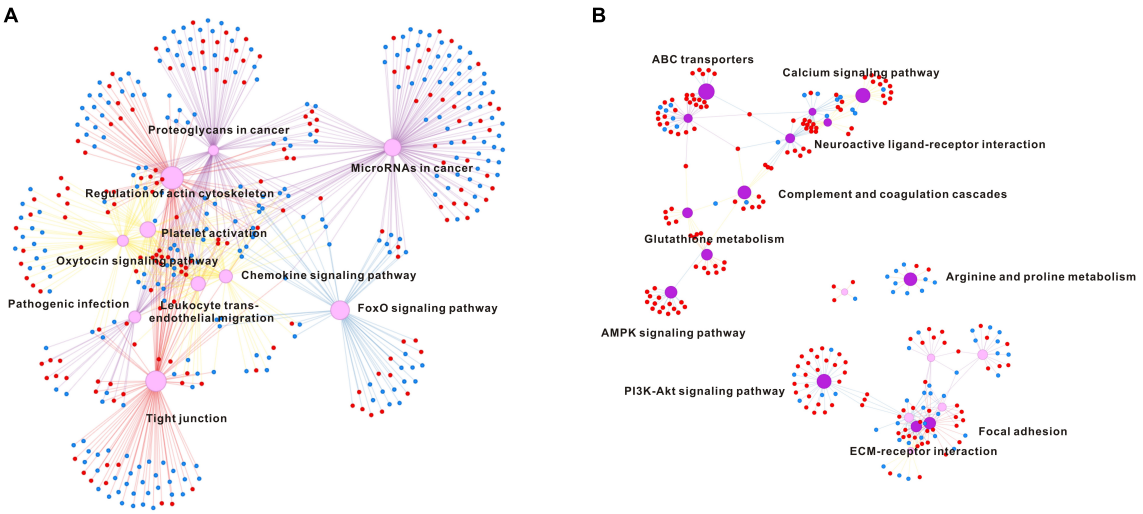

FIGURE 3 | Pathway enrichment analysis in hypo-salinity **(A)** and hyper-salinity **(B)** adaptation. The top 10 enriched pathways are shown in the network. The up-regulated and down-regulated genes are indicated in red dot and blue dot, respectively.

Osmotic Marker Genes

To precisely identify which genes are directly correlated with the oyster response to extreme conditions along the salinity gradients (that is, osmatic marker genes), we performed a whole transcriptomic correlation analysis between gene expression and salinity gradient. The heatmap shows the top 10 genes positively or negatively correlated with salinity extremities (**Figure 4**). Notably, the expression level of hypoxia inducible factor 1 α inhibitor, cholecystokinin receptor type α like and sulfotransferase 1α1-like gene significantly increased with salinity elevation, whereas the expression level of low density lipoprotein (LDL) receptor, calcium uptake protein 3 and neuronal acetylcholine receptor (AChR) β3 dramatically declined as salinity increased. All of these genes showed a high correlation with the salinity gradient ($p < 0.01$), strongly suggestive of functional importance as marker genes in osmotic adaptation.

RNA-Seq Validation by Real-Time qPCR

To validate the reliability of RNA-seq, 10 genes were selected to compare the expressional consistency between RNA-seq and Realtime PCR, including half of up-regulated DEGs and half of down-regulated DEGs. The scatter plot showed that the gene expression level are highly consistent ($R^2 = 0.912$, Pearson's correlation analysis, **Supplementary Figure S4**). Meanwhile, the references genes GAPDH wasn't affected by salinity fluctuation.

DISCUSSION

In estuaries, osmoregulation is an essential and highly complex process through which oysters sustain their physiological activities despite dramatic variation in salinity and diverse osmotic niches. Previous studies have attempted to investigate the osmotic adaptive response based on experimental models mimicking salinity stress in laboratory environments (Meng et al., 2013; Zhao et al., 2014; Yan et al., 2017). However, there is a dearth of empirical evidence to guide our understanding about how oysters adapt to salinity extremities under *in situ* conditions. To address this gap, *in situ* transcriptomes were analyzed to provide exciting glimpses into the active transcripts of samples collected in the field. Based on the PCA analysis, the total transcriptomic expression profile (P2–P5) were overlapped, which suggests that salinity levels of 8.8–22.4 ppt represent tolerable salinity limits for normal physiological activities. Beyond these limits, distinct gene expression profiles, as represented by oysters collected from P1 to P6, were found to explicitly diverge from the normal expression patterns seen for the locations of P2–P5. This transcriptomic divergence strongly suggests that adaptive gene expression networks are at work in the oysters' response to extreme conditions of salinity. Collectively, a total of 25.4% DEGs were identified in the Hong Kong oyster under extreme conditions of hypo- and hyper-salinity across naturally formed salinity gradients, which greatly exceeds the DGEs number previously reported for stimulation conditions used in the laboratory(Meng et al., 2013; Yan et al., 2017). Implicitly, this also means that the oysters have a much greater capacity and functional plasticity for salinity adaptation in the field environments than can be envisioned for laboratory manipulations. It is difficult to rule out the possibility that certain environmental factors may interfere the final results for *in situ* analysis when compared to tightly controlled modeling experiments in the laboratory. However, validity of the current *in situ* sampling methodology is in part justified on the ground that the sampling locations all lie within a narrow span of latitude with similar climate features (e.g., temperature); no obvious disease was found within this region, suggesting that salinity likely stands out as the most important variable for this studies. It then logically follows that the extreme conditions of hypo-salinity and hyper-salinity lead to distinct expression profiles. The crucial genes and pathways involved in

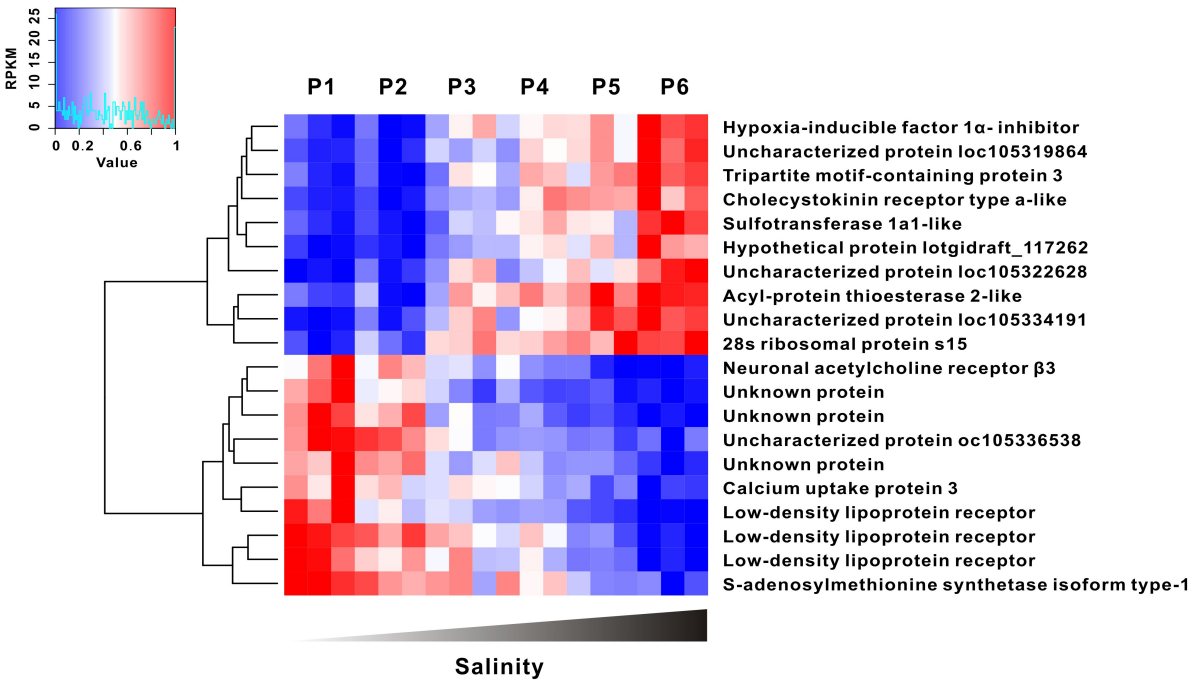

FIGURE 4 | Gene expression was highly correlated with salinity gradient. The top 10 of salinity positive and negative correlation genes were clustered ($|R^2| > 0.89$, $p < 0.01$).

signal transduction, actin cytoskeleton dynamics and adhesion, metabolism and immune defense are discussed as follows.

Signal Transduction

Strikingly, FoxO signaling pathway and oxytocin signaling pathway were observed to be mostly up-regulated by hypo-salinity. Indeed, both of these signaling pathways are conserved regulators for insulin signaling and glucose metabolism (Webb and Brunet, 2014; Elabd and Sabry, 2015; Watanabe et al., 2016), being consistent with that hypo-salinity promotes growth of oyster shell weight and size (our unpublished data). Moreover, FoxO transcription factors play a pivotal role in promoting the expression of genes involved in antioxidant defense (Klotz et al., 2015). Here, two target genes, namely, catalase and GADD45, were also increased in oysters subjected to hypo-salinity conditions. Previous evidence showed that catalase can catalyze the decomposition of hydrogen peroxide, a detrimental ROS (reactive oxygen species) when produced in excess, and protect host cells against the oxidative injury in the Hong Kong oyster (Zhang et al., 2011). GADD45 is another an oxidative stress response protein responsible for repairing oxidant induced DNA damage (Li et al., 2017). Thus, it seems reasonable to speculate that activation of FoxO signaling and its target genes may contribute to resolution of oxidative stress under hypo-salinity. It is interesting to note that extreme hypertonic stress reportedly activates FoxO signaling to result in lifespan extension (Lamitina and Strange, 2005; Anderson et al., 2016) in *Crassostrea elegans*, suggesting distinct adaptive strategies during the evolution. In contrast, hyper-salinity conditions led to inhibition of PI3K-Akt signaling pathway in the Hong Kong oyster, as evidenced by a suppression of phosphoinositide 3-kinase (PI3K), receptor tyrosine kinases (RTKs) and focal adhesion kinase (FAK). Taken into account that all of these signaling pathways are crucial for cell proliferation/growth with conserved functions in species from *Drosophila* to mammals, down-regulation of the pathways may partially account for hyper-salinity dependent growth suppression in the oysters.

Metabolism

Many euryhaline marine invertebrates have been reported to regulate their extracellular and intracellular osmolality in response to salinity fluctuations (Liu and Hellebust, 1976; Boone and Claybrook, 1977; Pierce, 1982; Eierman and Hare, 2014). Although oysters lack the ability for adjustment of extracellular fluids, they have a compensatory machinery for transporting osmotically active solutes to maintain osmotic hemostasis (Meng et al., 2013). Among them, free amino acids (FAAs) were shown to account for the majority of the total osmotically active solutes. In this light, metabolism of amino acid is thus anticipated to be critical for osmoregulation in this marine organism. Here, the metabolism pathways responsible for arginine and proline metabolism are regulated under hyper-salinity, suggesting functional significance of the amino acids in osmoregulation. Apart from amino acids metabolism, genes responsible for riboflavin metabolism were also observed to be increased as counter-measures against hyper-salinity. While there is a lack of evidence in animals, previous studies have shown that riboflavin can enhance organismal resistance to salinity stress

through augmenting organic solutes and ion uptake in plants (Azooz, 2009). So, it is tempting to speculate whether analogous mechanisms exist in oysters to enhance osmoregulation.

Immune Defense

Other than their prototypical roles in seawater filtration, gills are also a key contributor to host innate immunity in oysters (Dautremepuits et al., 2009; Zhang et al., 2015). We observed that immune response was elicited when Hong Kong oyster encountered hypo-salinity but not hyper-salinity. Similarly, such situations have also been reported in other oyster species, such as the Sydney rock oyster and Pacific oyster (Meng et al., 2013; Yan et al., 2017), suggesting that immune response can be elicited or sustained in oysters in hypo-salinity environments (Butt et al., 2006; Gagnaire et al., 2006). Chemokine signaling pathway is one of many crucial biological responses implicated therein. Importantly, chemokines promote changes in cellular morphology, or more specifically cell polarization, to thwart pathogenic infection, typically through the activation of JAK/STAT signaling (Mellado et al., 2001). In our study, the homologs of JAK/STAT were observed to be upregulated under hypo-salinity conditions in the Hong Kong oyster, suggesting that hypo-salinity environments could activate chemokine signaling pathway. Two factors may potentially account for this process. Firstly, coastal microbial abundance and density generally surpass that in the high-salinity ocean waters (Hassard et al., 2016), which may readily trigger off immune response and activate immune signaling pathways. Secondly, hypo-salinity may aggravate the stress from cell polarization in the gills, and *vice versa*, which enhances chemokine activation. However, both of these hypotheses need further validation. Additionally, other important immune pathways, pathogenic infection and platelet activation, were observed to be adaptively regulated under hypo-salinity conditions. Platelet activation are crucial to host inflammatory and immunomodulatory activities in vertebrates (Assinger, 2014). Despite limited knowledge established on its process of platelet activation, most homolog genes are present in oysters. Of note, adenylyl cyclase, a central signaling regulator known for catalyzing the conversion of ATP to cAMP (3',5'-cyclic AMP) and functioning as a key second massager in multiple physiological processes, was found to increase in mRNA expression under hypo-salinity. It has been recognized that cAMP signaling strongly influences host immune defense through regulating inflammatory response, phagocytosis and antimicrobial activities (Serezani et al., 2008). Additionally, cAMP improves host salinity tolerance by regulating NaCl and water absorption in aquatic animals, corroborating a dual role of cAMP in oyster hypo-salinity response (Tresguerres et al., 2014).

Other Osmoregulation Associated Genes

In additional, salinity correlation analysis reveals several marker genes whose expression seems tightly coupled with salinity fluctuations. For instance, hypoxia-inducible factors (HIFs) are master transcriptional factors for oxygen homeostasis in all animal species, including oysters (Lee et al., 2004; Helen, 2011; Piontkivska et al., 2011; Nguyen et al., 2013). Given that the solubility of oxygen declines with increasing salinity, long-term exposure to hyper-salinity favors the induction of hypoxia response (Lange et al., 1972). Consistent with this assumption, the hypoxia inducible factor 1 α inhibitor (HIF1AN) was observed to be upregulated as salinity increased, which may contribute to mitigation of HIF over-activity and maintenance of oxygen hemostasis. Moreover, another important salinity positive correlation marker gene was identified to be cholecystokinin receptor, which has been previously reported to regulate protein and fat digestion and control of energy balance (Wank, 1995). Up-regulation of cholecystokinin receptor in our findings would suggest that increased energy demand may ensue for living in a suboptimal environment above physiological salinity. In contrast, the expression of several marker genes was negatively correlated with the salinity gradient including three homologs of LDL receptor, neuronal AChR β3 and others. LDL receptors are associated with lipoproteins transfer and are functionally important for endocytosis and vesicles trafficking (Jeon and Blacklow, 2005). These proteins are also essential for innate immune defense, since lipoprotein deficiency results in increased susceptibility to bacterial infections (Peterson et al., 2008), which is consistent with increased ease of immune activation within a low salinity environment. In additional, salinity dependent down-regulation of neuronal AChRs suggests that the neurotransmitter may be directly involved in osmotic adaptation. Neuronal AChR responds to their cognate ligands neurotransmitter acetylcholine, and trigger the activation of second messenger (Albuquerque et al., 2009). Meanwhile, as a non-selective cation channel, AChRs could transport several different positively charged ions, including Na^+ and K^+, to keep intracellular ion homeostasis (Dani and Bertrand, 2007).

CONCLUSION

Here, our work represents a pioneering study on the regulatory mechanisms of oyster adaptive response to extreme conditions of salinity *in situ*. Distinct transcriptomic expression profiles were found among oysters living in extreme conditions across naturally formed salinity gradients. Diverse pathways including signal transduction, immune response, amino acid metabolism and others were altered in response to salinity fluctuations, revealing the striking complexity and plasticity of transcriptomic expression of oysters in eurysalinity adaptation.

AUTHOR CONTRIBUTIONS

YZ and SX conceived and designed the experiments. SX, JL, YL, YhZ, HM, and RM performed the experiments. SX, N-KW, YZ, and ZY analyzed the data. SX, N-KW, YZ, and YZ wrote the paper. All authors reviewed the manuscript.

FUNDING

This research was supported by the Guangdong Natural Science Funds for Distinguished Young Scholars (No. 2015A030306003), the National Science Foundation of China

(Nos. 31572640 and 31572661), Key Program of Administration of Ocean and Fisheries of Guangdong (Nos. A201501B and A201601A04), the Guangdong Special Support Program of Youth Scientific and Technological Innovation (No. 2015TQ01N139), and the Science and Technology Planning Project of Guangzhou, China (Nos. 2014B020202011, 2016B020233005, 201707010177, and 2017B030314052).

SUPPLEMENTARY MATERIAL

The Supplementary Material for this article can be found online at: https://www.frontiersin.org/articles/10.3389/fphys.2018.01491/full#supplementary-material

FIGURE S1 | Boxplot presents the expression profile of all samples.

FIGURE S2 | MA-plot shows the DGEs under hypo-salinity.

FIGURE S3 | MA-plot shows the DGEs under hyper-salinity.

FIGURE S4 | The correlation of gene expression between RNA-seq and Real-Time qPCR.

TABLE S1 | The transcriptome and mapping reads statistics.

TABLE S2 | The gene list and functional annotation of DGEs under hypo-salinity.

TABLE S3 | The gene list and functional annotation of DGEs under hyper-salinity.

TABLE S4 | The list of primer used in the validation.

REFERENCES

Albuquerque, E. X., Pereira, E. F., Alkondon, M., and Rogers, S. W. (2009). Mammalian nicotinic acetylcholine receptors: from structure to function. *Physiol. Rev.* 89, 73–120. doi: 10.1152/physrev.00015.2008

Anderson, E. N., Corkins, M. E., Li, J. C., Singh, K., Parsons, S., Tucey, T. M., et al. (2016). *C. elegans* lifespan extension by osmotic stress requires FUdR, base excision repair, FOXO, and sirtuins. *Mech. Ageing Dev.* 154, 30–42. doi: 10.1016/j.mad.2016.01.004

Assinger, A. (2014). Platelets and infection - an emerging role of platelets in viral infection. *Front. Immunol.* 5:649. doi: 10.3389/fimmu.2014.00649

Azooz, M. M. (2009). Foliar Application with Riboflavin (Vitamin B2) Enhancing the Resistance of *Hibiscus sabdariffa* L. (Deep Red Sepals Variety) to Salinity Stress. *J. Biol. Sci.* 9, 109–118. doi: 10.3923/jbs.2009.109.118

Boone, W. R., and Claybrook, D. L. (1977). The effect of low salinity on amino acid metabolism in the tissues of the common mud crab, *Panopeus herbstii* (Milne-Edwards). *Comp. Biochem. Physiol. Part A* 57, 99–106. doi: 10.1016/0300-9629(77)90357-7

Butt, D., Shaddick, K., and Raftos, D. (2006). The effect of low salinity on phenoloxidase activity in the Sydney rock oyster, *Saccostrea glomerata*. *Aquaculture* 251, 159–166. doi: 10.1016/j.aquaculture.2005.05.045

Dani, J. A., and Bertrand, D. (2007). Nicotinic acetylcholine receptors and nicotinic cholinergic mechanisms of the central nervous system. *Annu. Rev. Pharmacol. Toxicol.* 47, 699–729. doi: 10.1146/annurev.pharmtox.47.120505.105214

Dautremepuits, C., Marcogliese, D. J., Gendron, A. D., and Fournier, M. (2009). Gill and head kidney antioxidant processes and innate immune system responses of yellow perch (*Perca flavescens*) exposed to different contaminants in the St. Lawrence River, Canada. *Sci. Total Environ.* 407, 1055–1064. doi: 10.1016/j.scitotenv.2008.10.004

Eierman, L. E., and Hare, M. P. (2014). Transcriptomic analysis of candidate osmoregulatory genes in the eastern oyster *Crassostrea virginica*. *BMC Genomics* 15:503. doi: 10.1186/1471-2164-15-503

Elabd, S., and Sabry, I. (2015). Two birds with one stone: possible dual-role of oxytocin in the treatment of diabetes and osteoporosis. *Front. Endocrinol.* 6:121. doi: 10.3389/fendo.2015.00121

Gagnaire, B., Frouin, H., Moreau, K., Thomas-Guyon, H., and Renault, T. (2006). Effects of temperature and salinity on haemocyte activities of the Pacific oyster, *Crassostrea gigas* (Thunberg). *Fish Shellfish Immunol.* 20, 536–547. doi: 10.1016/j.fsi.2005.07.003

Hassard, F., Gwyther, C. L., Farkas, K., Andrews, A., Jones, V., Cox, B., et al. (2016). Abundance and distribution of enteric bacteria and viruses in coastal and estuarine sediments—a review. *Front. Microbiol.* 7:1692.

Helen, P. (2011). Molecular characterization and mRNA expression of two key enzymes of hypoxia-sensing pathways in eastern oysters *Crassostrea virginica* (Gmelin): hypoxia-inducible factor α (HIF-α) and HIF-prolyl hydroxylase (PHD). *Comp. Biochem. Physiol. Part D Genomics Proteom.* 2, 103–114. doi: 10.1016/j.cbd.2010.10.003

Jeon, H., and Blacklow, S. C. (2005). Structure and physiologic function of the low-density lipoprotein receptor. *Annu. Rev. Biochem.* 74, 535–562. doi: 10.1146/annurev.biochem.74.082803.133354

Kanehisa, M., Araki, M., Goto, S., Hattori, M., Hirakawa, M., Itoh, M., et al. (2008). KEGG for linking genomes to life and the environment. *Nucleic Acids Res.* 36, D480–D484.

Klotz, L. O., Sanchez-Ramos, C., Prieto-Arroyo, I., Urbanek, P., Steinbrenner, H., and Monsalve, M. (2015). Redox regulation of FoxO transcription factors. *Redox Biol.* 6, 51–72. doi: 10.1016/j.redox.2015.06.019

Lam, K., and Morton, B. (2004). The oysters of Hong Kong (Bivalvia: Ostreidae and Gryphaeidae). *Raffles Bull. Zool.* 52, 11–28.

Lamitina, S. T., and Strange, K. (2005). Transcriptional targets of DAF-16 insulin signaling pathway protect *C. elegans* from extreme hypertonic stress. *Am. J. Physiol. Cell Physiol.* 288, C467–C474. doi: 10.1152/ajpcell.00451.2004

Lange, R., Staaland, H., and Mostad, A. (1972). The effect of salinity and temperature on solubility of oxygen and respiratory rate in oxygen-dependent marine invertebrates. *J. Exp. Mar. Biol. Ecol.* 9, 217–229. doi: 10.1016/0022-0981(72)90034-2

Langmead, B., and Salzberg, S. L. (2012). Fast gapped-read alignment with Bowtie 2. *Nat. Methods* 9, 357–359. doi: 10.1038/nmeth.1923

Lee, J. W., Bae, S. H., Jeong, J. W., Kim, S. H., and Kim, K. W. (2004). Hypoxia-inducible factor (HIF-1)alpha: its protein stability and biological functions. *Exp. Mol. Med.* 36, 1–12. doi: 10.1038/emm.2004.1

Li, B., and Dewey, C. N. (2011). RSEM: accurate transcript quantification from RNA-Seq data with or without a reference genome. *BMC Bioinformatics* 12:323. doi: 10.1186/1471-2105-12-323

Li, D., Dai, C., Yang, X., Li, B., Xiao, X., and Tang, S. (2017). GADD45a Regulates Olaquindox-Induced DNA Damage and S-Phase Arrest in Human Hepatoma G2 Cells via JNK/p38 Pathways. *Molecules* 22:E24. doi: 10.3390/molecules22010124

Li, L., Wu, X., and Yu, Z. (2013). Genetic diversity and substantial population differentiation in *Crassostrea hongkongensis* revealed by mitochondrial DNA. *Mar. Genomics* 11, 31–37. doi: 10.1016/j.margen.2013.06.001

Liu, F., Rainbow, P. S., and Wang, W. X. (2013). Inter-site differences of zinc susceptibility of the oyster *Crassostrea hongkongensis*. *Aquat. Toxicol.* 132–133, 26–33. doi: 10.1016/j.aquatox.2013.01.022

Liu, M. S., and Hellebust, J. A. (1976). Effects of salinity and osmolarity of the medium on amino acid metabolism in *Cyclotella cryptica*. *Can. J. Bot.* 54, 938–948. doi: 10.1139/b76-098

Love, M. I., Huber, W., and Anders, S. (2014). Moderated estimation of fold change and dispersion for RNA-seq data with DESeq2. *Genome Biol.* 15:550. doi: 10.1186/s13059-014-0550-8

Ma, H. T., Xiao, S., Zhang, Y., Li, X. M., Li, J., and Yu, Z. N. (2016). Polymorphic microsatellite loci developed from the Hong Kong oyster (*Crassostrea hongkongensis*). *Genet. Mol. Res.* 15:4. doi: 10.4238/gmr.15048676

Mellado, M., Rodriguez-Frade, J. M., Manes, S., and Martinez, A. C. (2001). Chemokine signaling and functional responses: the role of receptor dimerization and TK pathway activation. *Annu. Rev. Immunol.* 19, 397–421. doi: 10.1146/annurev.immunol.19.1.397

Meng, J., Zhu, Q. H., Zhang, L. L., Li, C. Y., Li, L., She, Z. C., et al. (2013). Genome and transcriptome analyses provide insight into the euryhaline adaptation mechanism of *Crassostrea gigas*. *PLoS One* 8:e58563. doi: 10.1371/journal.pone.0058563

Nguyen, L. K., Cavadas, M. A., Scholz, C. C., Fitzpatrick, S. F., Bruning, U., Cummins, E. P., et al. (2013). A dynamic model of the hypoxia-inducible factor 1alpha (HIF-1alpha) network. *J. Cell Sci.* 126, 1454–1463. doi: 10.1242/jcs.119974

Peterson, M. M., Mack, J. L., Hall, P. R., Alsup, A. A., Alexander, S. M., Sully, E. K., et al. (2008). Apolipoprotein B is an innate barrier against invasive *Staphylococcus aureus* infection. *Cell Host Microbe* 4, 555–566. doi: 10.1016/j.chom.2008.10.001

Pierce, S. K. (1982). Invertebrate Cell-volume control mechanisms - a coordinated use of intracellular amino-acids and inorganic-ions as osmotic solute. *Biol. Bull.* 163, 405–419. doi: 10.2307/1541452

Piontkivska, H., Chung, J. S., Ivanina, A. V., Sokolov, E. P., Techa, S., and Sokolova, I. M. (2011). Molecular characterization and mRNA expression of two key enzymes of hypoxia-sensing pathways in eastern oysters *Crassostrea virginica* (Gmelin): hypoxia-inducible factor alpha (HIF-alpha) and HIF-prolyl hydroxylase (PHD). *Comp. Biochem. Physiol. Part D Genomics Proteom.* 6, 103–114. doi: 10.1016/j.cbd.2010.10.003

Serezani, C. H., Ballinger, M. N., Aronoff, D. M., and Peters-Golden, M. (2008). Cyclic AMP: master regulator of innate immune cell function. *Am. J. Respir. Cell Mol. Biol.* 39, 127–132. doi: 10.1165/rcmb.2008-0091TR

Tong, Y., Zhang, Y., Huang, J., Xiao, S., Zhang, Y., Li, J., et al. (2015). Transcriptomics analysis of *Crassostrea hongkongensis* for the discovery of reproduction-related genes. *PLoS One* 10:e0134280. doi: 10.1371/journal.pone.0134280

Tresguerres, M., Barott, K. L., Barron, M. E., and Roa, J. N. (2014). Established and potential physiological roles of bicarbonate-sensing soluble adenylyl cyclase (sAC) in aquatic animals. *J. Exp. Biol.* 217, 663–672. doi: 10.1242/jeb.086157

Wank, S. (1995). Cholecystokinin receptors. *Am. J. Physiol.* 269, G628–G646.

Watanabe, S., Wei, F. Y., Matsunaga, T., Matsunaga, N., Kaitsuka, T., and Tomizawa, K. (2016). oxytocin protects against stress-induced cell death in murine pancreatic beta-cells. *Sci. Rep.* 6:25185. doi: 10.1038/srep25185

Webb, A. E., and Brunet, A. (2014). FOXO transcription factors: key regulators of cellular quality control. *Trends Biochem. Sci.* 39, 159–169. doi: 10.1016/j.tibs.2014.02.003

Yan, L., Su, J., Wang, Z., Yan, X., Yu, R., Ma, P., et al. (2017). Transcriptomic analysis of *Crassostrea sikamea* x *Crassostrea angulata* hybrids in response to low salinity stress. *PLoS One* 12:e0171483. doi: 10.1371/journal.pone.0171483

Ye, J., Fang, L., Zheng, H. K., Zhang, Y., Chen, J., Zhang, Z. J., et al. (2006). WEGO: a web tool for plotting GO annotations. *Nucleic Acids Res.* 34, W293–W297. doi: 10.1093/nar/gkl031

Zhang, Y., Fu, D., Yu, F., Liu, Q., and Yu, Z. (2011). Two catalase homologs are involved in host protection against bacterial infection and oxidative stress in *Crassostrea hongkongensis*. *Fish Shellfish Immunol.* 31, 894–903. doi: 10.1016/j.fsi.2011.08.005

Zhang, Y., Sun, J., Mu, H., Li, J., Zhang, Y., Xu, F., et al. (2015). Proteomic basis of stress responses in the gills of the pacific oyster *Crassostrea gigas*. *J. Proteome Res.* 14, 304–317. doi: 10.1021/pr500940s

Zhao, X., Yu, H., Kong, L., Liu, S., and Li, Q. (2014). Comparative transcriptome analysis of two oysters, *Crassostrea gigas* and *Crassostrea hongkongensis* provides insights into adaptation to hypo-osmotic conditions. *PLoS One* 9:e111915. doi: 10.1371/journal.pone.0111915

Conflict of Interest Statement: The authors declare that the research was conducted in the absence of any commercial or financial relationships that could be construed as a potential conflict of interest.

frontiers in Physiology

ORIGINAL RESEARCH
published: 11 February 2019
doi: 10.3389/fphys.2019.00077

Reproduction Immunity Trade-Off in a Mollusk: Hemocyte Energy Metabolism Underlies Cellular and Molecular Immune Responses

Katherina Brokordt[1,2], Yohana Defranchi[1,2,3], Ignacio Espósito[1], Claudia Cárcamo[1,2], Paulina Schmitt[4], Luis Mercado[4], Erwin de la Fuente-Ortega[5] and Georgina A. Rivera-Ingraham[6]*

[1] Laboratory of Marine Physiology and Genetics, Centro de Estudios Avanzados en Zonas Áridas, Universidad Católica del Norte, Coquimbo, Chile, [2] Centro de Innovación Acuícola AquaPacífico, Universidad Católica del Norte, Coquimbo, Chile, [3] Magister en Ciencias del Mar, Universidad Católica del Norte, Coquimbo, Chile, [4] Grupo de Marcadores Immunológicos, Laboratorio de Genética e Immunología Molecular, Instituto de Biología, Pontificia Universidad Católica de Valparaíso, Valparaíso, Chile, [5] Departamento de Ciencias Biomédicas, Facultad de Medicina, Universidad Católica del Norte, Coquimbo, Chile, [6] Laboratoire Environnement de Petit Saut, HYDRECO, Kourou, French Guiana

OPEN ACCESS

Edited by:
Youji Wang,
Shanghai Ocean University, China

Reviewed by:
Tibor Kiss,
Hungarian Academy of Sciences, Hungary
Hu Baoqing,
Nanchang University, China

***Correspondence:**
Katherina Brokordt
kbrokord@ucn.cl;
katherina.brokordt@ceaza.cl

Specialty section:
This article was submitted to Aquatic Physiology, a section of the journal Frontiers in Physiology

Received: *04 September 2018*
Accepted: *22 January 2019*
Published: *11 February 2019*

Citation:
Brokordt K, Defranchi Y, Espósito I, Cárcamo C, Schmitt P, Mercado L, de la Fuente-Ortega E and Rivera-Ingraham GA (2019) Reproduction Immunity Trade-Off in a Mollusk: Hemocyte Energy Metabolism Underlies Cellular and Molecular Immune Responses. Front. Physiol. 10:77. doi: 10.3389/fphys.2019.00077

Immune responses, as well as reproduction, are energy-hungry processes, particularly in broadcast spawners such as scallops. Thus, we aimed to explore the potential reproduction-immunity trade-off in *Argopecten purpuratus*, a species with great economic importance for Chile and Peru. Hemocytes, key immunological cells in mollusks, were the center of this study, where we addressed for the first time the relation between reproductive stage, hemocyte metabolic energetics and their capacity to support immune responses at cellular and molecular levels. Hemocyte metabolic capacity was assessed by their respiration rates, mitochondrial membrane potential and citrate synthase (CS) activity. Cellular immune parameters such as the number of circulating and tissue-infiltrating hemocytes and their reactive oxygen species (ROS) production capacity were considered. Molecular immune responses were examined through the transcriptional levels of two pattern recognition receptors (*ApCLec* and *ApTLR*) and two anti-microbial effectors (*ferritin* and *big defensin*). Their expressions were measured in hemocytes from immature, matured and spawned scallops under basal, and one of the following challenges: (i) *in vitro*, where hemocytes were challenged with the β glucan zymosan, to determine the immune potentiality under standardized conditions; or (ii) *in vivo* challenge, using hemocytes from scallops injected with the pathogenic bacteria *Vibrio splendidus*. Results indicate a post-spawning decrease in the structural components of the immune system (hemocyte number/quality) and their potential capacity of performing immune functions (with reduced ATP-producing machinery and exhaustion of energy reserves). Both *in vitro* and *in vivo* challenges demonstrate that hemocytes from immature scallops have, in most cases, the best metabolic potential (increased CS activity) and immune performances, with for example, over threefold higher ROS production and tissue-infiltration capacity than those from mature and spawned scallops after the bacterial challenge. Agreeing

with cellular responses, hemocytes from immature individuals induced the highest levels of immune receptors and antimicrobial effectors after the bacterial challenge, while spawned scallops presented the lowest values. Overall, results suggest a trade-off between resource allocation in reproduction and the immune responses in *A. purpuratus*, with hemocyte energy metabolic capacity potentially underlying cellular and molecular immune responses. Further research would be necessary to explore regulatory mechanisms such as signaling pleiotropy which may potentially be underlying this trade-off.

Keywords: reproductive cost, scallop immunity, hemocyte metabolism, hemocyte respiration, scallop immune genes

INTRODUCTION

Both reproduction and immune defense are fitness associated traits with high energy demand (Lochmiller and Deerenberg, 2000; Schwenke et al., 2016). Because life-history evolution tends to optimize rather than maximize energy resources, reproduction, and immune response can be mutually constraining (Schwenke et al., 2016). Therefore, a trade-off between these two relevant processes may arise as a consequence of limiting energy availability.

Because scallops are broadcast spawners, they invest massively in reproduction to produce abundant energy-rich gametes in order to ensure fertilization success, and to allow early planktonic development without external food. In this group of bivalves, energy investment in reproduction has shown to reduce other vital processes such as swimming ability and escape response capacity (Brokordt et al., 2000a,b, 2003, 2006; Kraffe et al., 2008), and tolerance to environmental stress (Brokordt et al., 2015). In addition, post-reproduction mass mortalities have been reported for scallops and other marine bivalves (Tremblay et al., 1998; Xiao et al., 2005; Samain et al., 2007). For oysters, it has been proposed that mass mortality is the result of multiple factors including physiological imbalance associated with reproduction, aquaculture practices, and increased susceptibility to pathogens (Samain et al., 2007).

For a given animal, defense against pathogens is determined in part by its immune response capacity. Scallop's immune defense, like all invertebrates, relies on innate immunity mechanisms because they lack an adaptive immune system. Thus, they have developed a series of sophisticated and effective strategies to recognize and eliminate invading microorganisms (Loker et al., 2004; Song et al., 2015). These strategies include cascades of cellular and humoral immune responses that have been recently shown to be coordinated by a series of extracellular stimuli or messengers, cell receptors, signaling pathways and the regulation of the expression of antimicrobial effectors (Song et al., 2015; Oyanedel et al., 2016a,b).

Hemocytes in particular are involved in various physiological functions including nutrient storage and transport and tissue repair (Beninger et al., 2003; Donaghy et al., 2009), all processes which may be increased during gonad maturation (e.g., nutrient transport) and after spawning (e.g., gonad resorption). However, being the only circulating cells in mollusks, they also play a key immunity role, acting as sentry cells to induce the immune response. Hemocyte defense mechanisms include: (1) chemotaxis, (2) recognition of non-self-particles by soluble and membrane bound receptors, (3) activation of intracellular signaling cascades, (4) opsonization (i.e., secretion of soluble factors toward extracellular environment), (5) phagocytosis, and (6) intracellular degradation of foreign material (Donaghy et al., 2009). The chemotaxis process includes an active migration and infiltration of hemocytes toward the affected tissues. In vertebrates, it has been shown that mounting the initial immune response demands high levels of nutrients and energy due to the hypermetabolic state of the (energy-hungry) phagocytic immune cells (macrophages) involved (Lochmiller and Deerenberg, 2000). Also in invertebrates it was observed that the immune defense is energetically costly, requiring metabolic adaptation and reallocating energy from different tissues toward the immune system (Bajgar et al., 2015). In the scallop *Chlamys farreri* for example, mounting the immune defense against the pathogenic bacterium *Vibrio anguillarum* was observed to be mainly at the expense of glycogen stored in the adductor muscle and the digestive gland (Wang et al., 2012).

For bivalve molluscs, reproduction-immunity trade-offs have been investigated mainly in oysters, though solely through the assessment of cellular immune parameters (Cho and Jeong, 2005; Li et al., 2007; Samain et al., 2007; Wendling and Wegner, 2013). In contrast, this trade-off has been widely addressed in insects (reviewed by Schwenke et al., 2016). The main conclusions of these studies are that (i) physiological costs of reproduction frequently involve the decrease in both basal and induced levels of immunity and (ii) that the energetic requirements of reproduction and immunity indicate that the reallocation of a common energy source may be the basis for the trade-off between these traits (Schwenke et al., 2016). It is however important to remark that none of these studies have evaluated the reproduction-immunity trade-offs considering the various components of the reaction cascade associated with the immune response.

The scallop *Argopecten purpuratus* is one of the most cultured molluscs in countries such as Chile or Peru. In the former, collection of wild *A. purpuratus* is prohibited, and aquaculture production reached 19,018 tons by year 2000. In Peru, the production of this scallop represents the main aquaculture product of the country, and by 2014 represented 45,300 tons,

i.e., 56.4% of the total aquaculture production of the country (PromPerú, 2014). However, its production in these countries has gradually declined in part due to the increasing number of mass mortality events. In Chile alone, for the period 2000–2016 this decrease overpassed 84% of the total production (FAO, 2016). As in other bivalves, these mortality events usually coincide with the reproductive period but its causes have not been yet elucidated. Pathogenic infections cannot be ruled out as being partly responsible given that several studies have shown that vibriosis produces massive mortalities in *A. purpuratus* hatchery-reared larvae (Riquelme et al., 1996, 2000; Rojas et al., 2015). While *Vibrio splendidus* infection is still mainly recognized as a larval problem in *A. purpuratus*, it has more recently been identified as a pathogenic agent with fatal consequences for adult *Patinopecten yessoensis* scallops (Liu et al., 2013).

In this study, we aimed to explore a potential reproduction-immunity trade-off in *A. purpuratus*, contributing to the knowledge in (non-oyster) bivalves and in a species with great economic importance for countries such as Chile or Peru. Furthermore, we address for the first time this subject using a multi-approach methodology, avoiding relying solely on cellular immune parameters to have an overview of relation between bio-energetics and immunity/reproduction. To do this, *A. purpuratus* in different reproductive stages (immature, maturing, and spawned) were challenged with *V. splendidus*. Basal immunity and the capacity to mount the immune response after a challenge was assessed at the cellular level and at the transcriptional levels of immune genes encoding immune sensors and antimicrobial effectors. Considering that mollusk hemocytes have an active participation in immune response but also contribute in transporting nutrients to the growing gonad (Beninger et al., 2003), reproduction-immunity trade-offs may not only be energetic but also functional. Therefore, in this study we paid especial attention to the relation between the reproductive status on the hemocyte capacity to function as immune cells, by evaluating their metabolic capacity, and phagocytic [through reactive oxygen species (ROS) production] and tissue infiltration capacities after the challenge. Finally, these results were correlated with metabolic parameters, i.e., hemocyte respiration and mitochondrial membrane potential ($\Delta\omega m$). Overall, the results of this study will contribute to comprehend the potential reasons behind the increasingly frequent mortality events of *A. purpuratus* cultures and design adequate measures contributing to reduce the economic loss entailed by such events.

MATERIALS AND METHODS

Scallop Procurement and Holding Conditions

Adult *A. purpuratus* (70–80 mm shell height) with immature and mature gonads were obtained from the aquaculture facilities of the Universidad Católica del Norte (UCN) located at the Tongoy Bay in Coquimbo. It should be noted that as gonad maturation in *A. purpuratus* is somehow asynchronous, it is possible to simultaneously obtain scallops at different reproductive stages. Scallops were transported to the UCN laboratory in Coquimbo, and acclimated to laboratory conditions for 4 days, in 1,000 L tanks supplied with filtered, aerated, running seawater, and fed a diet composed of *Isochrysis galbana* and *Chaetoceros calcitrans* in equal amounts. Following acclimation, a group of mature scallops were stimulated to spawn by adding excess microalgae.

Bacteria Procurement

A pathogenic strain of *V. splendidus* (VPAP18) for *A. purpuratus* larvae (Rojas et al., 2015) was kindly donated by Dr. Rojas from the Microbiology Lab at UCN. The strain was maintained in Trypticase Soy Agar NaCl 3% and grown in Trypticase Soy broth NaCl 3% until exponential phase (DO_{600}: 0.2–0.4). Bacteria was then washed three times by centrifugation with 0.22 μm filtered sterilized seawater (SSW) and reconstituted in SSW at a DO_{600} of 0.09, corresponding to 1×10^7 CFU (colony forming units) $\times$ mL^{-1} as determined empirically in our laboratory. Bacterial concentrations were confirmed by a standard dilution plating technique.

Experimental Setup

Scallops from each reproductive stage (immature, mature, and spawned; n = 24 per reproductive status) were injected in the adductor muscle with either 100 μL of a sublethal dose of the VPAP18 strain (1×10^7 CFU $\times$ mL^{-1} as determined by preliminary LD50 assays) (n = 8 per reproductive condition), or with 100 μL of 0.22 μm filtered SSW, serving as injury control (n = 8 per reproductive condition). In parallel, naïve (undisturbed) adult scallops were also considered for assessing basal levels of immune parameters at each reproductive stage (n = 8 scallops per reproductive condition).

Hemolymph from each scallop was extracted from the adductor muscle 24 h post-injection. Preliminary assays showed that after 24 h post-challenge *A. purpuratus* presents the highest induction of immune response. One fraction of the hemolymph was used to determine the number of circulating hemocytes (TCH), their capacity to produce ROS, and their respiration rate capacity. The other hemolymph fraction was used to isolate hemocytes through centrifugation (600 $\times$ g for 5 min at 4°C). The resulting pellet was split into two parts and immediately frozen in liquid nitrogen and stored at −80°C. These hemocyte pellets were used for the analyses of the mitochondrial enzyme citrate synthase (CS) and protein content and for the analyses of gene transcriptional levels by RT-qPCR, respectively.

For each of the three reproduction stages and for naïve scallops only, we further used a small aliquot of hemolymph to carry out an *ex vivo* challenge of hemocytes as detailed later on (see section "Respiration Rates"). For these challenged hemocytes, we conducted respiration rate (RR) and mitochondrial membrane potential ($\Delta\omega m$) measurements.

Hemocyte Metabolism

Respiration Rates

Hemocyte RR were determined on fresh hemolymph samples collected from the adductor muscle of experimental scallops using a 3 mL cold syringe (needle 23G X 1"). Two types of respiration measurements were carried out using animals under the three different reproductive stages: (i) *ex vivo* challenge,

using naïve scallops which hemocytes were challenged with zymosan and (ii) *in vivo* challenge, using hemolymph samples from scallops subjected to the bacterial or SSW injection (as described in section "Experimental Setup"). For the first, samples consisted in 81 μL hemolymph to which 9 μL of either zymosan (zymosan A from *Saccharomyces cerevisiae*, Sigma, prepared in 1X PBS to a final concentration of 16 particles per hemocyte) or 1X PBS (for control purposes) was added. For the second, samples consisted of 90 μL of undiluted hemolymph. The *ex vivo* challenge aimed to assess the potential metabolic capacity to mount the defense response by the hemocytes from scallops at the three reproductive stages. We further reasoned that by exposing the hemocytes to a MAMP (microbe-associated molecular pattern) such as the β glucan zymosan, the tests would better allow comparing responses under controlled standardized conditions. On the other hand, the *in vivo* challenge with the bacteria would allow analyzing the metabolic cost of mounting the immune response under more realistic cellular/physiological conditions; and considering the time at which the associated immune molecules are induced.

To determine hemocyte RR, 90-μL glass metabolic chambers equipped with an oxygen sensor spots (OXSP5, sensor code SD7-541-207, Pyro-Science GmbH, Aachen, Germany) glued to the inner side of the chamber were used. Measurements were carried out as in Rivera-Ingraham et al. (2016). Briefly, chambers were filled with an hemolymph sample and were then closed, ensuring the absence of any air bubbles within the chamber and measurements were carried out at 20°C using a four-channel fiber optic oxygen meter (Firesting, Pyro-Science GmbH). All measurements started at an O_2 partial pressure (pO_2) of around 70–80%, the natural air saturation of the hemolymph sample after extraction and transfer to the metabolic chamber. The O_2 concentration in each of the chambers was registered each 5 s through the Pyro Oxygen Logger software as a functioning of declining pO_2. Four measurements were recorded in parallel, where hemocytes were allowed to respire until O_2 was completely consumed in the chamber, a process which took no more than 2 h. Between four and eight replicates were carried out for each developmental stage and experimental treatment. When possible, the critical pO_2 (p_cO_2), as defined by Tang (1933) and indicating the onset of anaerobic metabolism, was calculated using the equation by Duggleby (1984). RRs were calculated as a function of declining pO_2. Given the oxyconformity behavior of hemocytes, for statistical purposes RRs between 30 and 40% pO_2 were calculated by linear regression on plots representing oxygen concentration over time in the chamber. The 30–40% pO_2 interval was chosen as representative of the natural pO_2 in bivalve hemolymph according to the reports of Allen and Burnett (2008) and Handa et al. (2017, 2018). For each hemolymph sample tested, the number of hemocytes was quantified using a Neubauer cell-counting chamber to express RRs as nmol $O_2 \cdot min^{-1} \cdot$ million hemocytes^{-1}.

Citrate Synthase Activity

Apparent specific activity of the key mitochondrial enzyme CS was measured in hemocyte pellets from each scallop 24 h after the injections. The pellets were manually homogenized on ice in 8 volumes of homogenization buffer (pH 7.2) containing 50 mM imidazole-HCl, 2 mM EDTA-Na (ethylene dinitrilotetraacetic acid), 5 mM EGTA (ethyleneglycol 2 tetraacetic acid), 150 mM KCl, 1 mM dithiothreitol and 0.1% Tween-20. The homogenates were then centrifuged at 600 *g* at 4°C for 10 min. Conditions for enzyme assays were adapted from those used by Brokordt et al. (2000a) as follows (all concentrations in mmol L^{-1}): TRIS-HCl 75, oxaloacetate 0.3 (omitted for the control), DTNB (5,5-dithio-*bis*-2-nitrobenzoic acid, Ellman's reagent) 0.1, acetyl CoA 0.2, pH 8.0. Enzyme activities were measured at 20°C using a microplate spectrophotometer EPOCH (BioTek) to follow the absorbance changes at 412 nm to detect the transfer of sulfydryl groups from CoASH to DTNB. The molar extinction coefficients used for DTNB was 13.6. All assays were run in duplicate and the specific activities expressed in international units (IU, μmol of substrate converted to product per min) per mg of hemocyte wet mass.

Hemocyte Mitochondrial Membrane Potential

Hemocyte $\Delta\omega m$ was determined in fresh hemolymph samples, collected as previously described, from eight undisturbed scallops for each of the three developmental stages considered (n = 24). The sample was aliquoted into two inverted-microscope slides (30 μL per slide), which were maintained in humid chambers until their analysis to avoid sample evaporation. It was in these slides and in humid conditions that hemocytes were allowed to adhere on the microscope slides for 10 min, time after which, one of the aliquots was treated with 5.3 μL of zymosan (final concentration of 16 particles per hemocyte in SSW) while the other received the equivalent volume of SSW. After 15 min, the fluorophore JC-10 (52305, Enzo Life Sciences) diluted in DMSO was added to each of the two aliquots to obtain a final concentration of 5 μM (Donaghy et al., 2012). This fluorophore accumulates in mitochondria and exists under monomer form under low $\Delta\omega m$ conditions. JC-10 is excitable with an Ar lasser (488 nm), and while monomers exhibit a green fluorescence, JC-10 aggregates (occurring under higher $\Delta\omega m$ conditions), exhibit a red fluorescence. Due to hemocyte morphology and the fact that these may aggregate, a criteria for a common confocal plane was established. In the present study we used the plane of focus of hemocyte nuclei, and for this, the nucleus-staining fluorophore Hoechst 33342 (Chazotte, 2011; Invitrogen) was equally added to each sample (2 μL of a stock solution 1:100 in water). Samples were incubated with these two fluorophores simultaneously during 30 min, and were then visualized in a Zeiss LSM 800 confocal microscope (Carl Zeiss, Heidelberg, Germany) equipped with diode lasers. Visualization and imaging was carried out using a Plan-Neofluar 63x/1.3 Imm Korr objective. To avoid photobleaching, the areas of interest (i.e., those containing healthy looking, moderately packed and adhered hemocytes) were located using transmission light. Then, and for each of these selected areas, three single pictures were taken, with the following conditions and in the following order (increasing excitation energy): (i) Ex: 493 nm, Em: 410–533 nm to register the green fluorescence corresponding to JC-10 in monomer form (JC_{mon}); (ii) Ex: 488 nm, Em: 550–600 nm to register the red fluorescence corresponding to JC-10 in its aggregate form (JC_{agg}),

and (iii) Ex: 345 nm, Em: 400–467 nm to visualize hemocyte nuclei. Picture resolution was in all cases 512 × 512 pixels and 16 bit.

For each picture taken, only hemocytes with their nuclei in clear plane of focus (as evidenced by the Hoechst fluorescence) were considered for analysis. For each of these hemocytes, two regions of interest (ROIs) of approximately 0.5 um^2 were plotted in the areas with the highest JC_{agg} fluorescence. For each plotted ROI, two values were calculated: the average JC_{agg} (red) fluorescence and the average JC_{mon} (green) fluorescence. The relative $\Delta\omega m$ for a given ROI was calculated as the ratio JC_{agg} : JC_{mon}. The $\Delta\omega m$ for a given hemocyte was calculated as the average ratio for both ROIs. The values of a minimum of 10 hemocytes per hemolymph sample (20 hemocytes per scallop) were used for $\Delta\omega m$ determination in a given animal. All image analyses were carried out using the software Fiji (Bethesda, MD, United States)[1].

Hemocyte Immune Activity

Determination of Circulating Hemocytes

The total number of circulating hemocytes was measured in the hemolymph of each experimental scallop. To do this, two samples of 10 μL each were mixed with 10 μL of PBS 1X and 10 μl of 0.4% Trypan-blue staining. In each sample the number of hemocytes was quantified using a Neubauer cell-counting chamber.

Determination of Infiltrating Hemocytes

A polyclonal antibody against scallop hemocytes was generated in CF-1 mice (4–6 weeks old). Hemocytes were obtained from scallops challenged with a sublethal dose (1×10^7 CFU × mL^{-1}) of the VPAP18 strain for 24 h (see section "Experimental Setup"). Then, total proteins from hemocytes were extracted and quantified as described below (see section "Hemocyte Protein Content"). For antibody production, mice were subcutaneously injected at 1, 15, and 30 days with 250 μg of an hemocyte protein extract diluted 1:1 in FIS peptide (peptide sequence: FISEAIIHVLHSR), a T helper cell activator (Prieto et al., 1995), and 1:1 Freund's adjuvant (Thermo Scientific). The antiserum was collected on day 45, centrifuged at 700 *g* for 10 min and the supernatant was stored at −20°C. Antibody specificity was determined by western blot as described before (Schmitt et al., 2015) and the antibody capacity to detect hemocytes was determined in gills by immunofluorescence (**Supplementary Figure 1**).

Determination of the total number of infiltrating hemocytes in gonad tissues was performed by immunofluorescence analysis using the polyclonal antibody against whole hemocytes. For this, tissues were dissected under sterile conditions and fixed in Bouin's solution (0.9% picric acid, 9% formaldehyde, 5% acetic acid). Fixed samples were dehydrated through an ascending ethanol series and embedded in Histosec (Merck). Sections were cut at 5 μm using a rotary microtome (Leica RM 2235) and mounted on glass slides. Paraffin sections were cleared in Neoclear (Merck) and hydrated by incubations in a descending ethanol series. Then, paraffin sections were incubated overnight at 4°C with the anti-hemocyte antibody (1:100), PBS with 1% BSA. A second incubation was performed for 1 h at 20°C with goat anti-mouse Alexa Fluor 568-conjugated (Thermo Scientific) 1:200 in PBS/1% BSA. Control slides were incubated with the prebleed serum of mouse. The slides where analyzed using a Leica TCS SP5 II spectral confocal microscope (Leica Microsystems) and images were obtained with a Leica 40 × 1.25 Oil HCX PL APO CS lens (Leica Microsystems), using the autofluorescence of the fixed tissue as contrast. The examination was performed on at least three tissue sections from different scallops to ensure they were consistently reproducible. The number of infiltrated hemocytes into gonad tissues was manually counted in 5 (400×) fields per scallop using the ImageJ v1.52e software.

Reactive Oxygen Species (ROS) Production

Reactive oxygen species production was measured in the hemolymph (where the number of hemocytes was previously quantified) of each experimental scallop using the nitroblue tetrazolium (NBT) reduction assay modified from Malham et al. (2003). To do this, two hemolymph samples of 100 μL each was obtained per scallop. These were incubated during 30 min in 96-well culture plates for hemocyte adhesion, time after which 15 μL of zymosan (Sigma; in 1% PBS, final concentration of 16 particles per hemocyte) was added and incubated for 15 min to allow hemocytes to phagocyte. The supernatant was then removed and 90 μL of PBS 1X plus 10 μL of NBT (1 mg/mL in 1% PBS) were added, and incubated for 90 min in darkness. Supernatant was removed and hemocytes fixed with 100% methanol 100 μL during 3 min, followed by one wash with 70% methanol 100 μL for 5 min. Then 120 μL of 2 M KOH was added to disrupt hemocyte membrane, plus 140 μL DMSO to solubilize the formazan produced by the NBT. Optical density (OD) at 630 nm was measured on a microplate spectrophotometer (EPOCH, BioTek) and the results expressed as OD values per million $hemocytes^{-1}$. OD was corrected using wells that followed the same process but without hemocytes (negative controls).

Hemocyte Protein Content

Total protein was quantified in 0.03 g (wet mass) of hemocyte pellets from each scallop following Brokordt et al. (2015). Hemocytes were homogenized in 150 μL of homogenization buffer (32 mM Tris-HCl at pH 7.5, 2% SDS, 1 mM EDTA, 1 mM Pefabloc and 1 mM protease inhibitor cocktail; Sigma) and incubated for 5 min at 100°C. After this time, 100 μL of homogenization buffer were added to each sample and incubation was resumed for an additional 5 min. The homogenate was centrifuged at 10,600 *g* for 20 min. Total protein was quantified in a microplate spectrophotometer EPOCH (BioTek) at 562 nm in an aliquot of the supernatant using Micro-BCA kit.

Immune Genes

Transcriptional levels of four immune-related genes were analyzed in the hemocytes from each experimental scallop. Two of these genes correspond to two antimicrobial effectors: *ferritin-1* (*Apfer1*; GenBank Accession No. KT895278) and *big-defensin* (*ApBD1*; GenBank Accession No. KU499992), which

[1]https://fiji.sc/

were already characterized and validated as immune genes for *A. purpuratus* by our research group (Coba de la Peña et al., 2016; Oyanedel et al., 2016b; González et al., 2017). In addition, two cDNA sequences showing homologies with immune sensors, such as a toll-like receptor (*ApTLR*; GenBank Accession No. MH732641) and a C-type lectin (*ApCLec*; GenBank Accession No. MH732642) were identified by next generation sequencing from *A. purpuratus* RNA by the Illumina HiSeq4000 platform (unpublished data) and included in this analysis.

RNA Extraction and First Strand cDNA Synthesis

RNA from hemocyte pellets was extracted using TRIzol® reagent according to the manufacturer's instructions (Thermo Scientific). RNA was then treated with DNAse I (Thermo Scientific) during 15 min at room temperature and inactivated by heat, 10 min at 65°C, followed by a second precipitation with sodium acetate 0.3 M (pH 5.2) and isopropanol (1:1 v:v). The RNA obtained was quantified using an Epoch spectrophotometer (BioTek, Winooski, VT, United States), and integrity was verified by the visual inspection of rRNA bands in electrophoretically separated total RNA. The RNA was stored at −80°C for further use.

Reverse transcription (RT) of RNAs from hemocytes was carried out by AffinityScript QPCR cDNA Synthesis Kit (Stratagene, Santa Clara, CA, United States) following the manufacturer's protocol. RT of RNAs was done in equiproportions (i.e., from equal quantities of RNA) within all compared samples from each experiment.

Quantitative Real-Time PCR

The primers used in this study for quantitative real-time PCR (RT-qPCR) are listed in **Table 1**. Primers for the new *TLR* and *CLec* were designed using Primer3web version 4.1.0 (Untergasser et al., 2012) to have melting temperatures of 58 to 60°C and generate PCR products of 50 to 150 bp. For the *TLR*, the amplified region included a partial 3′-UTR sequence to ensure specific amplification of one *TLR* putative homolog. β-actin was used as endogenous control in order to normalize experimental results (Coba de la Peña et al., 2016; González et al., 2017).

Each RT-qPCR reaction contained 10 μL of Takyon Low ROX SYBR 2X (Nalgene®), 2 μL cDNA and 0.3 μM (final concentration) of each primer, in a final volume of 20 μL. RT-qPCRs were run in a Real-Time PCR System Agilent Technologies (Stratagene MX3000P). Initial denaturation time was 3 min at 95°C, followed by 40 PCR cycles of 95°C, 15 s and 60°C, 30 s. After the PCR cycles, the purity of the PCR product was checked by the analysis of its melting curve; the thermal profile for melting curve analysis consisted of denaturation for 15 s at 95°C, lowered to 55°C for 15 s and then increased to 95°C for 15 s with continuous fluorescence readings. During RT-qPCR, the efficiency of gene amplification were approximately equal to that of the housekeeping gene (as it was determined by slope calculation) and the comparative C_T method (also called $\Delta\Delta C_T$ method) (Pfaffl, 2001) was applied for relative quantification. Experiments included eight biological replicates and three technical replicates were performed.

Energetic Status

Muscle Carbohydrates

The energetic status of scallops at the three reproductive stages was evaluated through their content of total carbohydrates in the adductor muscle, the main energy storage tissue for these organisms (Brokordt and Guderley, 2004). To quantify total carbohydrates, samples of adductor muscles from each scallop were dried to a constant mass at 60°C. Dry tissues were then pulverized in a mortar and homogenized with deionized water at a proportion 1:1 (w/v). The phenol-sulfuric acid method described by Dubois et al. (1956) was used for total carbohydrate determinations. Its concentration was determined in a spectrophotometer (Variant Cary UV) at 490 nm using as standard a solution of glycogen in deionized water at a concentration of 50 $\mu g\ mL^{-1}$.

Statistical Analyses

Results are presented as means ± standard errors of the mean (SE). The Kolmogorov–Smirnov test was used to test normality while homoscedasticity was tested with the Levene test. Results meeting the requirements for parametric analyses were evaluated by a factorial analysis of variance (ANOVA), with the reproductive stage and challenge as factors, followed by an FDR-BY (false discovery rate) *post hoc* test (Benjamini and Yekutieli, 2001). When assumptions for parametric analyses were not met, a Kruskal–Wallis test was applied followed by *U*-Mann–Whitney pairwise comparisons. All statistical analyzes were conducted

TABLE 1 | Nucleotide sequences of the primers used for RT-qPCR of immune and housekeeping genes in Argopecten purpuratus.

Gene	Sequences (5′–3′)	Amplicon (bp)	Reference
ApTLR	F: CGACAAAACAGAGAAACAAATGGC	95	Present study
	R: GTGAACCTCAGTCCGTCAATCT		
ApCLec	F: CCTATGAACTATGCCTGCCGAT	76	Present study
	R: TTGTCCATCCGTTACAACCCAT		
Apfer1	F: CATCACCAACCTGAAACGTGTT	69	Coba de la Peña et al., 2016
	R: TACTCCAGGGATTCTTTGTCGTACA		
ApBD1	F: TGCCGTGTTCCAGATGA	101	González et al., 2017
	R: TACTCCAGGGATTCTTTGTCGTACA		
Ap β-actin	F: GAATCTGGCCCATCCATTGT	65	Coba de la Peña et al., 2016; González et al., 2017
	R: CGTTCTCGTGGATTTTTTTCAAGT		

using SPSS 15.0 (SPSS, Inc., Chicago, IL, United States) and R version 3.3.1 (R Core Team, 2016) with the "agricolae" package (De Mendiburu, 2017).

RESULTS

Hemocyte Metabolism

Hemocyte Respiration Rates

Ex vivo experimentations showed that, compared to spawned scallops, hemocyte RR was between 2- and 3.5-fold higher in immature and mature animals, respectively (F = 6.135; $P < 0.001$). Compared to their control (PBS) values, at the 30–40% pO_2 the zymosan challenge significantly increased hemocyte RR for immature (F = 11.983; P = 0.005), mature (F = 15.865; P = 0.001) and spawned scallops (K = 7.410; P = 0.006) by 1.9-, 2-, and 3.7-fold, respectively (**Figure 1A**). Post-challenge hemocytes from immature scallops showed the highest RR, and those from spawned the lowest RR (**Figure 1A**). The difference in RR between PBS and zymosan challenge increased with decreasing pO_2. Critical pO_2 values did not differ among hemocytes from different reproductive stages (F = 0.902; P = 0.424), and remained between 4 and 8% air saturation. However, challenging these hemocytes with zymosan caused p_cO_2 values to increase by roughly 2- and 3-fold in immature and mature scallops, respectively (F = 5.915; P = 0.011) (**Figure 1A**).

In vivo challenges evidenced that RRs varied among reproductive stages following the order immature = mature > spawned for all three treatments (basal: K = 6.400; P = 0.008; SSW: F = 4.830; P = 0.034; *V. splendidus:* K = 8.882; P = 0.012) (**Figure 1B**). In all cases, spawned scallops presented hemocytes with the lowest RRs, and *V. splendidus* challenged hemocytes in immature and mature animals had over sevenfold higher hemocyte RR than in spawned scallops. Treatment had no impact on RR of immature (F = 0.566; P = 0.579) mature (K = 3.714; P = 0.156) or spawned scallops (F = 1.732; P = 0.222) (**Figure 1B**).

Citrate Synthase Activity

The activity of the mitochondrial enzyme CS was measured in hemocytes and turned out to be different among scallops in the assessed reproductive stages (F = 17.32; $P < 0.0001$); but not between scallops at basal or injected either with *V. splendidus* or SSW (control) (F = 2.22; P = 0.118) (**Figure 2**). However, the interaction between the reproductive stage and immune status significantly affected hemocyte CS activity (F = 7.16; $P < 0.0001$). Regardless the immune condition, hemocytes from spawned scallops showed the lowest CS activity, while those from immature and mature scallops were similar. Under basal conditions, hemocytes from mature scallops showed the highest CS activity, but values were only significantly different from those obtained for SSW-injected mature scallops and spawned scallops under all immune conditions.

Hemocyte Mitochondrial Membrane Potential (Δωm)

JC-10 ratio results evidenced that undisturbed hemocyte Δωm did not differ among animals in different reproductive stages (F = 1.233; P = 0.313), showing an overall JC-10 ratio average of 1.36 (**Figure 3A**). However, when these hemocytes were challenged with zymosan, JC-10 ratio values significantly decreased in all cases by an average of 40% (**Figures 3A,B**). Under challenged conditions, the hemocytes from mature scallops had significantly the lowest Δωm (F = 4.764; P = 0.021) (**Figure 3A**). As shown in **Figure 3B**, the confocal analyses also allowed verifying that hemocytes had successfully phagocyted zymosan particles. Although phagocytic rate was not quantified, observations indicate that most frequently hemocytes had 1–2 phagocyted particles and a maximum of 4.

Hemocyte Immune Activity

Circulating Hemocytes

Total circulating hemocytes (TCH) changed with the reproductive status, the immune treatment, and with the interaction of these factors (**Figure 4A**). In general, TCH was lower in spawned than in immature and mature scallops

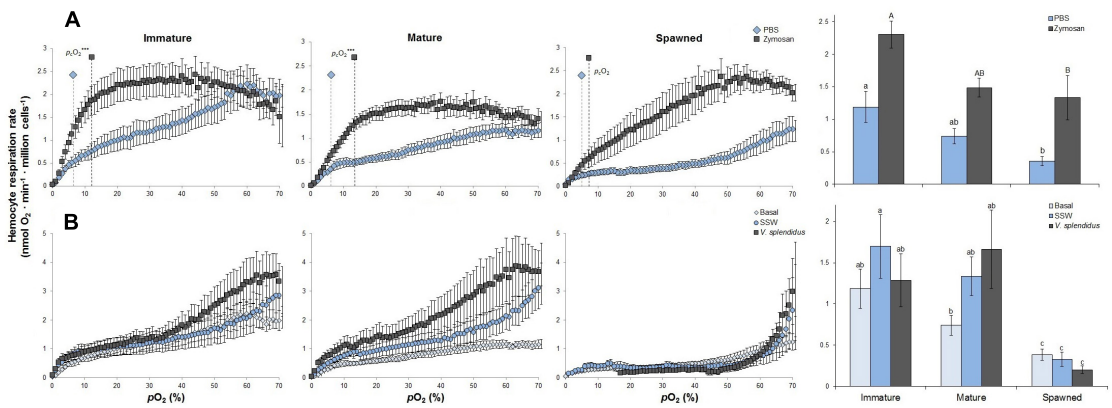

FIGURE 1 | Effects of **(A)** *in vitro* challenge with zymosan and **(B)** *in vivo* challenge with *Vibrio splendidus* on hemocyte respiration rates and critical O_2 (p_cO_2) (only for *in vitro*) from immature, mature, and spawned *Argopecten purpuratus* (n = 4–8 per condition and treatment). For bar graphs, values associated with the same letter belong to the same subset based on *a posteriori* multiple comparison test Student-Newman-Keuls. ***$P < 0.001$.

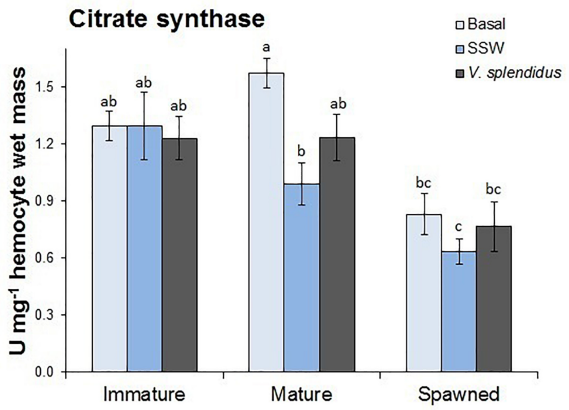

FIGURE 2 | Effects of *in vivo* challenge with *V. splendidus* on citrate synthase (CS) activity in hemocytes form immature, mature, and spawned *A. purpuratus*. Values associated with the same letter belong to the same subset based on a FDR-BY (false discovery rate) *post hoc* test (Benjamini and Yekutieli, 2001) (n = 4–8 per condition and treatment).

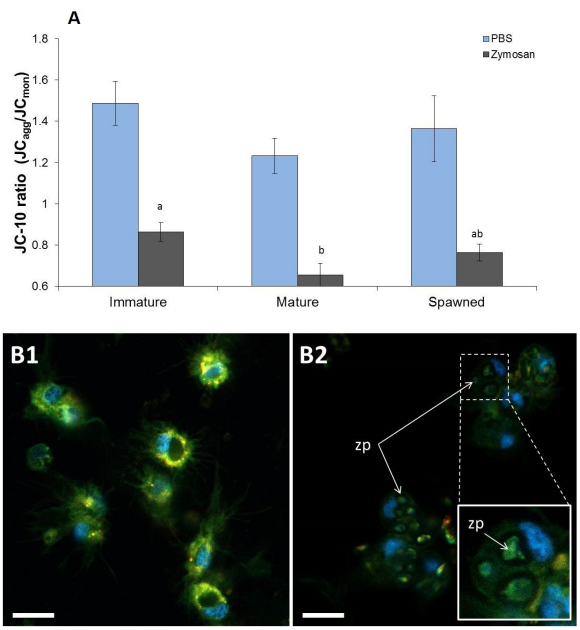

FIGURE 3 | Mitochondrial membrane potential from *A. purpuratus* hemocyte obtained through JC-10 staining (red and green fluorescence). **(A)** Values associated with the same letter belong to the same subset based on *a posteriori* multiple comparison test Student-Newman-Keuls. Challenge with zymosan caused in all cases a decrease in JC-10 ratios. **(B)** Subpanels 1 and 2 show representative images of hemocytes respectively without and with zymosan challenge. Blue fluorescence corresponds to Hoechst 33342 staining (nuclei-specific). Scale bars = 10 μm. Zp = phagocyted zymosan particles (n = 4–8 per condition and treatment).

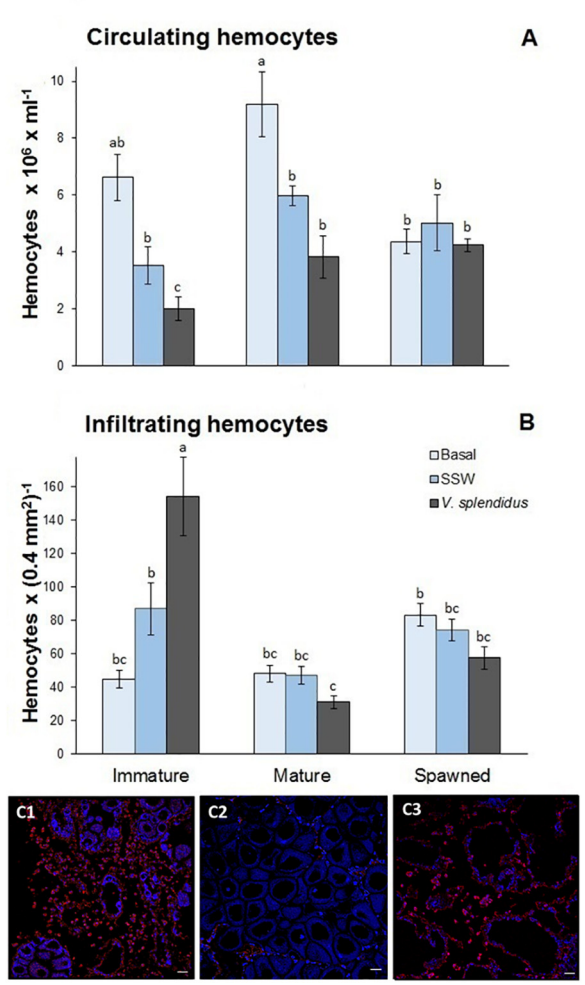

FIGURE 4 | Effects of *in vivo* challenge with *V. splendidus* on **(A)** the density of circulating hemocytes and **(B)** the number of the infiltrating hemocytes in immature, mature, and spawned *A. purpuratus*. Values associated with the same letter belong to the same subset based on a FDR-BY (false discovery rate) *post hoc* test (Benjamini and Yekutieli, 2001). **(C)** Representative images for the detection of infiltrating hemocytes in gonad tissue from *V. splendidus*-challenged scallops at different reproductive stages by immunofluorescence and confocal analysis. Alexa 568 goat anti-mouse antibody was used for hemocyte detection (in red) and autofluorescence was used as contrast (in blue). **(C1)** Immature; **(C2)** mature; **(C3)** spawned. Magnification 400X, scale bar: 25 μm (n = 4–8 per condition and treatment).

(F = 3.78; P = 0.048). Also, the lowest TCH was observed in scallops injected with *V. splendidus*, followed by SSW-injected animals at an intermediate level and finally, those in the basal status showing the highest amount of TCH (F = 14.09; P = 0.00002). Interestingly, only immature scallops decreased significantly TCH after *V. splendidus* injection (F = 2.60; P = 0.048), while mature and spawned scallops showed similar TCH to their injection control (SSW).

Infiltrating Hemocytes

Both the reproductive stage and its interaction with the immune treatment significantly affected the number of infiltrating hemocytes (respectively, F = 20.29, $P < 0.0001$; and F = 12.25, $P < 0.0001$) (**Figure 4B**). In general, the number of infiltrated hemocytes was the highest in immature scallops; among these, those scallops injected with *V. splendidus* showed the highest

numbers (**Figures 4B,C**). Mature and spawned scallops showed lower amounts of infiltrating hemocytes with no apparent differences among scallops at basal status or injected with SSW or the bacteria.

ROS Formation

Reactive oxygen species production by circulating hemocytes was affected by the reproductive status and immune treatment, and the interaction between these factors (**Figure 5**). Independent of the immune treatment, ROS production was the highest in the hemocytes from immature, followed by mature and spawned scallops ($F = 5.76$; $P = 0.006$). Independent of the reproductive status, ROS production was higher in hemocytes from scallops injected with *V. splendidus*, and no difference was detected between hemocytes from undisturbed or injected with SSW scallops ($F = 8.22$; $P = 0.0009$). Interestingly, hemocytes from immature scallops showed threefold higher ROS production capacity than those from mature and spawned scallops after the bacterial challenge ($F = 2.59$; $P = 0.047$).

Hemocyte Protein Content

The total protein concentration was assessed in circulating hemocytes as a proxy of their general energetic status. Only reproductive status significantly affected the protein content; being the hemocytes from spawned those with the lowest levels ($F = 22.47$; $P < 0.0001$) (**Figure 6**).

Immune Genes

Transcriptional levels of the four immune genes evaluated in hemocytes varied significantly with the reproductive status, the immune treatments or with the interaction between them (**Table 2**).

Transcriptional levels of *ApTLR* were significantly affected by the reproductive status, and the interaction between this and the immune treatment (**Figure 7** and **Table 2**). Regardless the immune treatment, immature scallops showed the highest *ApTLR* levels, the spawned individuals the lowest levels, and mature scallops was not different from either of these reproductive stages. The interaction analysis showed that only in immature scallop injected with *V. splendidus* transcriptional level of this immune receptor was significantly induced; while in mature and spawned scallop no differences of this gene was observed among immune treatments.

Relative levels of the *ApCLec* transcripts were affected by the immune treatment and the interaction between this and the reproductive status (**Figure 7** and **Table 2**). Independent of the

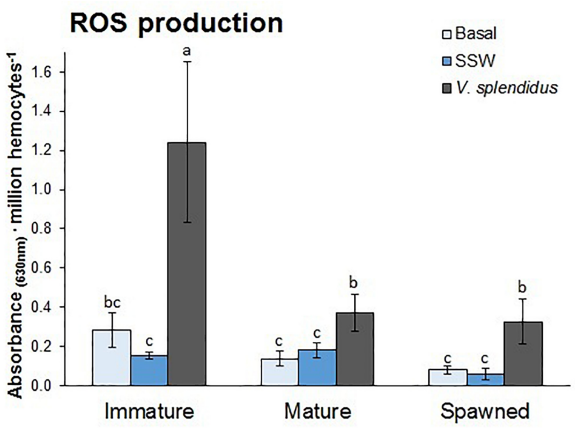

FIGURE 5 | Effects of *in vivo* challenge with *V. splendidus* on reactive oxygen species (ROS) formation in hemocytes from immature, mature, and spawned *A. purpuratus*. Values associated with the same letter belong to the same subset based on a FDR-BY (false discovery rate) *post hoc* test (Benjamini and Yekutieli, 2001) (n = 4–8 per condition and treatment).

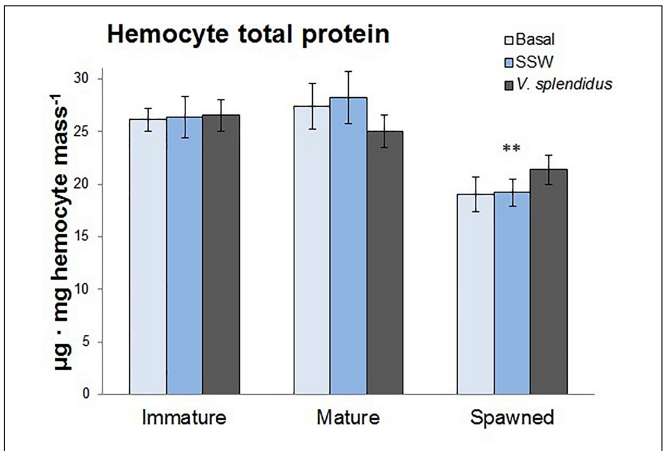

FIGURE 6 | Effects of *in vivo* challenge with *V. splendidus* on hemocyte total protein content in immature, mature, and spawned *A. purpuratus* (n = 4–8 per condition and treatment; $^{**}P < 0.001$).

TABLE 2 | Two-way ANOVAs to compare transcriptional levels of immune genes between *Argopecten purpuratus* scallop at different reproductive status and immune treatments.

Source	DF	*F*	*P*	Comparisons
ApTLR				
Reproductive status (RS)	2	4.36	0.0192*	I > M = S
Immune treatment (IT)	2	1.91	0.1611	
RS × IT	4	2.75	0.0411*	
ApCLec				
Reproductive status (RS)	2	1.82	0.175	
Immune treatment (IT)	2	3.89	0.028*	V > SSW = B
RS × IT	4	3.35	0.017*	
Apfer1				
Reproductive status (RS)	2	7.00	0.00225*	I = M > S
Immune treatment (IT)	2	13.62	0.00002*	V > SSW = B
RS × IT	4	2.90	0.03212*	
ApBD1				
Reproductive status (RS)	2	3.69	0.0349*	I = M > S
Immune treatment (IT)	2	5.215	0.0103*	V > SSW = B
RS × IT	4	11.144	0.000006*	

*Reproductive status factor: immature (I), mature (M), and spawned (S) scallop reproductive stages; immune treatments: injected with Vibrio splendidus (V), injected with sterilized seawater (SSW), not injected-basal status (B). n = 4–8 biological replicates per condition (each replicate include three technical replicates). *P < 0.05.*

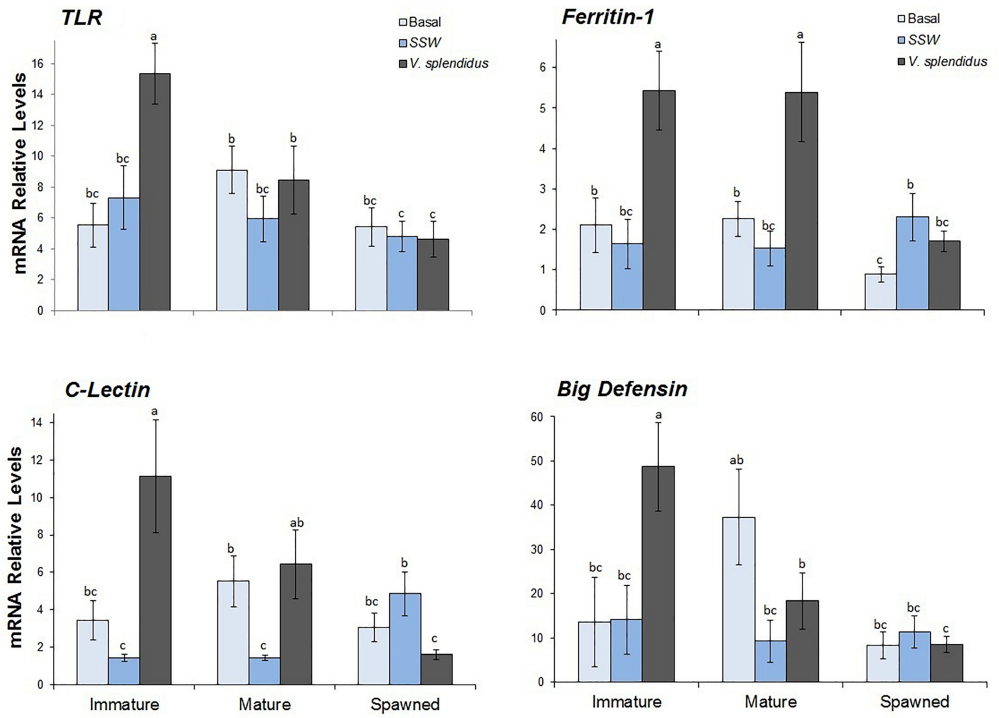

FIGURE 7 | Effects of *in vivo* challenge with *V. splendidus* on transcriptional levels of immune-related genes in hemocytes from immature, mature, and spawned *A. purpuratus*. Values associated with the same letter belong to the same subset based on a FDR-BY (false discovery rate) *post hoc* test (Benjamini and Yekutieli, 2001) (n = 4–8 per condition and treatment).

reproductive status, *ApCLec* transcriptional levels were higher in scallops injected with *V. splendidus* than in those injected with SSW; but the basal levels of this gene was similar to both injected treatments ($F = 3.89$; $P = 0.028$). The interaction analysis indicated that the levels of *ApCLec* was higher in immature *V. spendidus*-injected scallops. The injection with the bacteria also significantly induced the transcriptional levels of this gene in mature scallops, but only in comparison with their control SSW-injected. In contrast, in spawned scallops those injected with the bacteria showed the lowest levels of *ApCLec* transcripts, compared with the basal status or SWW-injected scallops.

The transcriptional levels of both effectors, *Apfer1* and *ApBD-1*, varied significantly with the reproductive stage, the immune treatment and the interaction between them (**Figure 7** and **Table 2**). For both genes immature scallops showed the highest relative levels, while no difference was observed between mature and spawned scallops. Also for both genes, regardless the reproductive status, those scallops injected with *V. splendidus* showed higher transcript levels than those injected with SSW or not subjected to injection, and these did not differ between them. The interaction analysis indicated that the levels of *Apfer1* was highest in bacteria-injected immature and mature scallops. *ApBD-1* also showed the highest levels in immature scallops injected with the bacteria; but interestingly, after gonad maturation basal transcriptional levels of *ApBD-1* also increased greatly, largely overpassing the levels of immature scallops under basal status.

Energetic Status

The energetic status of scallops at the three reproductive stages was evaluated through their carbohydrate reserves in the adductor muscle. Results showed that carbohydrate contents varied with the reproductive status ($F = 53.9$; $P < 0.0001$), but not with the immune status or the interaction between them (respectively, $F = 0.47$; $P = 0.62$; $F = 0.59$; $P = 0.47$) (**Figure 8**). Spawned scallops showed the lowest levels of carbohydrates in their adductor muscles, and no differences were observed between immature and mature scallops.

DISCUSSION

Empirical observations of reproduction-immunity tradeoffs have been made in some bivalve mollusks, mainly oysters (e.g., De Decker et al., 2011; Wendling and Wegner, 2013). However the hemocyte metabolic bases underlying this trade-off were not explored until now. As previously shown for oysters, in the present study we found a strong decrease in immune parameters after spawning in the scallop *A. purpuratus*, but the novelty of our results is that we additionally found that this decrease in their immune capacities was associated with a decrease in the aerobic metabolic capacity of hemocytes to mount immune responses at cellular and molecular levels. In general, our results showed that hemocytes from spawned scallops had lower respiration rates and capacity to produce ATP via the mitochondrial enzyme CS

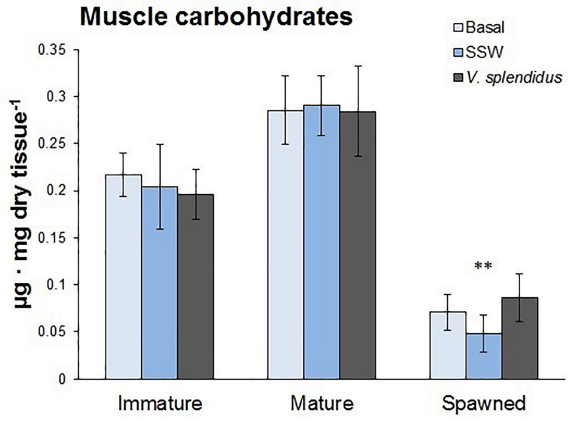

FIGURE 8 | Total carbohydrate content in the adductor muscle of immature, mature, and spawned *A. purpuratus* (n = 4–8 per condition and treatment; $^{**}P < 0.001$).

than hemocytes from immature and mature scallops at basal and after the bacterial challenge. This decreased metabolic capacity was paralleled with lower post-challenge hemocyte infiltration capacity and ROS production, as well as lower induction capacity of immune genes.

Hemocyte Basal Energy Status Decrease After Spawning Impacting the Potentiality of the Immune Response

Carbohydrate reserves play a central role in supplying energy for gametogenesis, thus other studies conducted on scallops have shown a strong reduction in these energy reserves after both gonadal maturation and spawning (Brokordt et al., 2000a,b; Martinez et al., 2000; Brokordt and Guderley, 2004). In the present study we only observed a reduction in muscle carbohydrates after spawning. This is in agreement with what has been previously reported in several other bivalve species in which glycogen storages reach their minimain post-spawning individuals (e.g., Li et al., 2009; Hong et al., 2014). In some other cases, this was accompanied with a reduction in tissue adenylate energy charge (indicator of metabolic potential available to the cell) (Li et al., 2007). Overall, our results demonstrate that spawning is an energy demanding process that occurs at the expense of other tissue reserves and metabolic potential. Furthermore, we here revealed that low energy reserves also corresponded with post-spawning scallops (under undisturbed (basal) conditions) having hemocytes with significantly lower protein content and decreased metabolic rates, the later evidenced by low RRs (between 4.4- and 5.8-fold lower than mature and immature scallops), and CS activity (decreased by 0.8-times).

While the number of infiltrating hemocytes in the gonads did not differ from those in immature and mature scallops, post-spawning caused a reduction in the number of circulating hemocytes. The same was observed in the clam *Ruditapes philippinarum,* which was due to an increase in hemocyte mortality rates and an increase in their infiltration in the gonadal tissue (e.g., Li et al., 2009; Hong et al., 2014). This increase in basal levels of infiltrating hemocytes after spawning can be associated with the fact that hemocytes play also a role in gonad restructuration and gamete resorption (Cho and Jeong, 2005; Li et al., 2007; Samain et al., 2007; Wendling and Wegner, 2013). In our study the decrease in circulating hemocytes after spawning was not paralleled with an increase in infiltrating hemocyte abundance in the gonad, which may be associated with an increase in hemocyte mortality or a post-spawning decline in the hematopoiesis capacity. To this, we may add the reduction in the nutritional quality of circulating hemocytes in post-spawning *A. purpuratus*, which may be the result of a decrease in the available energy stored for hemocyte production and/or metabolic capacity for protein synthesis.

Regarding transcriptional levels of immune-related genes under basal conditions, results revealed that both immune receptors (*ApTLR* and *ApCLec*) did not change with the reproductive status. However, a post-spawning decrease in the antimicrobial effectors (*Apfer1* and *ApBD1*) transcripts was observed. To the best of our knowledge changes in transcriptional levels of immune-related genes during the reproductive process have not been assessed before in other bivalve mollusks. Nonetheless, similar to our results, Li et al. (2007) registered a marked decrease in the hemolymph antimicrobial activity in post-spawning *Crassostrea gigas* measured under both basal and heat-shock conditions.

Besides innate immunity, ferritins in mollusks are involved in different functional roles. Among others, they play a crucial task in iron storage and homeostasis, regulating intracellular iron concentration, an essential micronutrient (Coba de la Peña et al., 2016). In *Pecten maximus* it was demonstrated that hemocytes work in the transport of iron mediated by ferritins especially during gamete proliferation (Beninger et al., 2003). Therefore, the observed reduction in the basal levels of *ferritin* in hemocytes from post-spawning scallops could be associated with a decrease in the need for this micronutrient. Still, we cannot discard a reduction in the capacity to synthetizes this molecule.

Interestingly, transcriptional levels of *ApBD1* were strongly overexpressed under basal conditions in mature scallops compared to immature and spawned scallops. Such high levels of this anti-microbial peptide (AMP) could be associated with a potential maternal transfer of immunity (i.e., passive immunity), which is considered to play an essential role in protecting the offspring against pathogens at early stages of life (Wang et al., 2015). Maternal transfers of several immune molecules have been observed in *C. farreri* (Yue et al., 2013; Wang et al., 2015). On the other hand, the low levels of *ApBD1* mRNA transcripts observed in hemocytes from undisturbed immature and spawned scallops, may be associated with the preponderant immune function of this molecule as AMP, thus its induction is expected to occur mostly under a microbial exposure.

Overall, the assessed immune parameters under basal status indicate a post-spawning decrease in the structural components of the immune system (number of hemocytes) and their potential capacity of performing immune functions as indicated by reduced ATP producing machinery as it will be further discussed

below. All these factors may well be pre-determining a decreased bio-energetic capacity for combatting pathogen exposure.

Hemocyte Bioenergetics and Immune Associated Responses Are Lower After Gonad Maturation and Spawning

Hemocyte key bioenergetic parameters such as their oxygen consumption, CS activity (a key enzyme for the regulation of ATP production), as well as the potential protonmotive force driving ATP synthesis (i.e., $\Delta\omega m$), were here evaluated to assess how these may be constrained by reproduction and its energy-demanding processes.

In general, hemocytes from immature scallops showed the best metabolic and immune performances, while these severely decreased in undisturbed post-spawning scallops and in bacteria-challenged mature animals. A bioenergetic characterization of hemocyte response to a standardized challenge (here zymosan particles) allowed us to determine the potentiality of these cells to counteract pathogen exposure. Despite the reproduction stage, this challenge caused hemocytes to significantly increase their RRs, likely aimed at increasing ATP formation to respond to the increased energy requirements and which would be responsible for the ∼1.8-fold drop in $\Delta\omega m$. However, the respiratory behavior of hemocytes from immature and mature scallops was very different from the one of spawned scallops. The first two showed high (and stable) O_2 consumption independent of environmental pO_2 until around 20% pO_2. Nevertheless, hemocytes from immature scallops maintained higher values than those from mature scallops, with average values of 2.3 to and 1.5 $nmolO_2\ min^{-1}$ million $cells^{-1}$, respectively. This response would allow hemocytes from these reproductive stages to maintain a sustained metabolic support for immune responses, in comparison with hemocytes from spawned scallops, which only maintain such levels of O_2 consumption to a pO_2 of ∼50%. Interestingly, hemocytes from immature scallops showed this post-challenge oxyregulatory-like behavior at ∼1.5-fold higher rates that hemocytes from mature scallops, which together with the higher $\Delta\omega m$ suggest a better bioenergetical status for supporting immune responses.

In vivo evaluation of hemocytes evidenced that regardless the challenge status, spawned scallops presented the cells with the lowest RR. Remarkably, *V. splendidus* challenged hemocytes from immature and mature scallops had over sevenfold higher RR than hemocyte from spawned animals. This general pattern coincides with CS activity, albeit only a tendency was observed on its activity in hemocytes after bacterial challenge. Additionally, as under basal conditions hemocytes from injected immature and mature scallops presented higher nutritious status, as indicated by their levels of total protein content. These results suggest that hemocytes from immature and mature scallops have a higher metabolic capacity to support immune response upon bacterial exposure. Compared to *ex vivo* RRs, these values are nevertheless significantly lower, and despite the different nature of both challenges, this is probably in part due to the fact that *in vivo* measures were done 24 h-post challenge where the energy-demand for immune responses are likely reduced. Thus, both *in vitro* and *in vivo* are here providing a good and complementary overview of the metabolic requirements of setting the immune response across time. To our knowledge, there are no other studies addressing hemocyte RR as a result of an *in vivo* challenge. However, contrarily to our results, a previous work by Cheng (1976) using hemocytes phagocytizing *ex vivo* heat-killed vegetative cells of *Bacillus megaterium* did not register any increase in hemocyte RR.

In their immune role during the infection process, hemocytes (and namely the number of circulating/infiltrating cells) provide a good overview of the degree of the immune response. As a result of an infection, a negative correlation between the density of circulating and tissue-infiltrating hemocytes after infection has been reported in several bivalves (Paillard et al., 1996; Cochennec-Laureau et al., 2003; Donaghy et al., 2009; Allam and Pales-Espinosa, 2016). This would be the result of the active movement of hemocytes toward the infection sites leading to an increase in tissue-infiltrated hemocytes; which would be generalized in the case of systemic infections such as those caused by most *Vibrio* species (Allam and Pales-Espinosa, 2016). In the present study the effects of exposure to *V. splendidus* on the number of circulating and infiltrating hemocytes was only evident in immature scallops, with the first decreasing by nearly twofold and the second increasing also in the same proportion. Compared with basal levels, *Vibrio*-challenged mature scallops also decreased the density of circulating hemocytes, but this was similar to the response to the injection with SSW (injury control). Curiously, this decrease in circulating hemocytes was not paralleled with an increase in infiltrating hemocytes as in immature scallops. This suggests that hemocytes in mature scallops have a lower infiltrating capacity in the gonad than immature scallops, although a higher infiltration in other tissue cannot be ruled out. Post-spawning scallops showed lower levels of both circulating and infiltrating hemocytes, with no apparent bacteria-induced changes, suggesting that hemocytes from scallops at this stage were less actively responding to the bacterial challenge, which would be coherent with their lower metabolic capacities.

The production of ROS by immune-stimulated hemocytes has been recognized in various bivalves (e.g., Pipe, 1992; Lambert et al., 2003; Buggé et al., 2007) as agents of internal defense, damaging potential pathogens during phagocytosis process. Our results in *A. purpuratus* showed that ROS production by hemocytes increased as a consequence of *V. splendidus* exposure in all reproductive stages, but the magnitude of this response was fairly different among them. After bacterial challenge, hemocytes of mature and spawned scallops increased their ROS production by 1- and 3-fold, respectively, whereas in comparison with the control conditions (SSW injection), it augmented by sevenfold in immature animals. Overall, both of the cellular immune parameters assessed reveal the hemocytes from immature scallops as having the best response.

Molecular immune responses were examined through the transcriptional levels of two hemocyte pattern recognition

receptors (*ApTLR* and *ApCLec*) and two anti-microbial effectors (*Apfer1* and *ApBD1*). In congruence with cellular responses, results exhibited that hemocytes from immature individuals induced the highest values after the bacterial challenge, most often followed by mature animals and with spawned scallops presenting the lowest values. Both receptors tested (*ApTLR* and *ApCLec* where here identified in *A. purpuratus* for the first time) were overexpressed after the *Vibrio*-challenge, but only when animals where immature. These results suggest that these receptors would be an important recognition component, potentially involved in the anti-bacterial immune defense of *A. purpuratus*. Interestingly, under challenge conditions, the AMP *ApBD1* transcriptional pattern followed a similar pattern of that shown by *ApTLR*. We recently showed that the expression of this AMP is regulated via a putative Rel/NF-kB signaling pathway in *A. purpuratus* (Oyanedel et al., 2016b), and present results suggest that this could be further mediated through the *ApTLR*. TLR signaling pathways have been found to mediate expression of antimicrobial effectors in other bivalve mollusks including scallops (Wang et al., 2011). Even so, herein we would like to bring up the importance of considering the animal reproductive status when characterizing immune pathways.

Like TLRs, lectins are critical components of innate immunity because of their pathogen pattern recognition and binding functions (Vasta et al., 2004). In scallops, a C-type lectin has only been previously characterized in *C. farreri* (Yang et al., 2010, 2011). Remarkably, these authors found that in addition to its recognition role, CfLec-1 also enhances the opsonization of hemocytes for the clearance of bacteria (Yang et al., 2011). In the present study, hemocytes from immature and mature scallops showed significant transcript inductions of *ApCLec* (in mature status only respect to their injury control) after the *Vibrio*-challenge. Thus, the expression profiles of isolated lectin suggest a functional capacity of these receptors during infectious challenge, but at a lower level in hemocytes from mature and not in post-spawning scallops.

Among their multiple functions, ferritins are involved in microbial elimination through an iron-withholding strategy: by storing host iron and preventing iron acquisition, bacterial growth, and proliferation is thereby inhibited (Ong et al., 2006). Ferritin induction by bacterial challenge has also been observed in other scallops such as *Mizuhopecten yessoensis* (Zhang et al., 2013; Sun et al., 2014). In a previous study we isolated and characterized *Apfer1*, and further reported its induction in response to inactivated *V. splendidus* (Coba de la Peña et al., 2016). The results of this study now add to the previous by showing that the induction of this gene also occurs upon the challenge with live *V. splendidus*, but only in hemocytes from immature and mature scallops.

Overall results regarding the immune-genes suggest a reduced molecular immune capacity in scallops after gonadal maturation and spawning, which is consistent with a reduced energy metabolic capacity of hemocytes under these stages. Energetically speaking this is not surprising, since gonadal maturation and spawning are energy-hungry processes, and a trade-off between reproduction and immunity would decrease the energy available for immune-related tasks. However, for post-spawning scallops, were the decrease in the immune capacity is most evident, we cannot rule out other regulatory mechanisms potentially underlying this trade-off such as signaling pleiotropy. In this regards, we suspect that the physiological trade-off between spawning and immunity in scallops may be regulated by neuroendocrine signals. For example, the spawning process of *A. purpuratus* has been shown to be modulated by the neuroendocrine system and specifically by catecholaminergic regulation (Martínez et al., 1996). This study revealed a striking increase of the catecholamines dopamine (DO) and norepinephrine (NE) during and after gamete release. Also a catecholaminergic regulation of immune response has been recently showed for oysters and scallops (Zhou et al., 2011; Song et al., 2015; Wang et al., 2018). In oysters, NE induces negative effects on hemocyte phagocytosis by means of their receptors (reviewed by Wang et al., 2018). Furthermore, a complete immune-related pathway from receptors to effectors has been recently shown to be modulated by microRNAs interacting with the neuroendocrine immunomodulation system (Chen et al., 2015). In scallops, Zhou et al. (2011) showed that high concentration of NE and epinephrine repressed the increase of antioxidants (superoxide dismutase and catalase) and lysozyme activities in hemolymph after a *V. anguillarum* challenge. Moreover, it has been observed that the α-adrenergic receptor on the surface of scallop hemocytes could be regulated at the transcriptional level during the immune response (reviewed by Song et al., 2015). It could transmit signals to regulate hemocyte phagocytosis and antibacterial function through the second messenger cAMP, and further modulate the induction of immune-related genes and the activity of immune-related enzymes in hemolymph (reviewed by Song et al., 2015). This information suggests that an increase of DO and/or NE during spawning of *A. purpuratus* could have reduced the immune activity of hemocytes and the transcriptional levels of immune-related genes, therefore further research is necessary to give light into this potential source of immune modulation.

Post-spawning Immune-Decrease: Role in Massive Mortality Events?

Argopecten purpuratus wild and cultured populations are currently experiencing large mortality events throughout its distribution range. These have been observed to often coincide with the spawning period of the species (see Brokordt et al., 2015 and references therein) but despite the economic importance of *A. purpuratus* cultures (PromPerú, 2014; FAO, 2016), the reasons behind these spawning-associated mortality events have not yet been elucidated.

The present study evidenced how reproduction is a period during which energy and immunity is significantly reduced, making mature and specially spawned *A. purpuratus* scallops more prone to pathogenic infection as it occurs in other bivalve species (Li et al., 2010; Hong et al., 2014). *Vibrio* is responsible for massive mortalities during the reproduction period in mollusks across the world (e.g., Travers et al., 2009) as well as being a

primary pathogen to many marine organisms (Reichelt et al., 1976). Thus, our results using *V. splendidus* provide an excellent basis for studying the role of this immunity-reproduction trade-off in the mortality events and elaborating adequate conservation measures targeting the amelioration of the bioenergetic capacity of the animals.

ETHICS STATEMENT

This study was carried out in accordance with the recommendations of the CCAC guidelines (https://www.ccac.ca/Documents/Standards/Policies/Ethics_of_animal_investigation.pdf). The protocol was approved by the CEAZA Bioethics Committee and supervised by CONICYT Bioethics Committee.

AUTHOR CONTRIBUTIONS

KB and PS contributed to the conception and design of the study. YD, IE, CC, GR-I, EdlF-O, and LM contributed to the acquisition of data. CC, YD, IE, and GR-I organized the database and performed the statistical analysis. KB and GR-I worked on analysis, interpretation of data, and wrote the first draft of the manuscript. PS wrote sections of the manuscript. All authors contributed to manuscript revision, read, and approved the submitted version.

FUNDING

This study was supported by FONDECYT-1170118 to KB, CC, PS, and LM.

ACKNOWLEDGMENTS

We are deeply grateful to Dr. Claudio Alvarez for his help with the immune-fluorescent essays. We also thank German Lira for his support with scallop maintenance and procurement. We thank the confocal facility (FONDEQUIP, EQM140100) from the Faculty of Medicine, Universidad Católica del Norte. Additional thanks go to the two referees for their comments on the original version of the manuscript.

SUPPLEMENTARY MATERIAL

The Supplementary Material for this article can be found online at: https://www.frontiersin.org/articles/10.3389/fphys.2019.00077/full#supplementary-material

FIGURE S1 | Validation of whole hemocytes antibody detection by Western blot and Immunofluorescence. **(A)**, Determination of antibody specificity against total protein extract from hemocytes 1. SDS PAGE, 2. Western blotting. **(B)**, merged confocal images for detection of infiltrating hemocytes in scallop gills by immunofluorescence. In blue, nuclei. In green, hemocyte detection. Scale bar, 7 μm.

REFERENCES

Allam, B., and Pales-Espinosa, E. (2016). Bivalve immunity and response to infections: are we looking at the right place? *Fish Shellfish Immunol.* 53, 4–12. doi: 10.1016/j.fsi.2016.03.037

Allen, S. M., and Burnett, L. E. (2008). The effects of intertidal air exposure on the respiratory physiology and the killing activity of hemocytes in the pacific oyster, *Crassostrea gigas* (Thunberg). *J. Exp. Mar. Biol. Ecol.* 357, 165–171. doi: 10.1016/j.jembe.2008.01.013

Bajgar, A., Kucerova, K., Jonatova, L., Tomcala, A., Schneedorferova, I., Okrouhlik, J., et al. (2015). Extracellular adenosine mediates a systemic metabolic switch during immune response. *PLoS Biol.* 13:e1002135. doi: 10.1371/journal.pbio.1002135

Beninger, P. G., Le Pennec, G., and Le Pennec, M. (2003). Demonstration of nutrient pathway from the digestive system to oocytes in the gonad intestinal loop of the scallop *Pecten maximus* L. *Biol. Bull.* 205, 83–92. doi: 10.2307/1543448

Benjamini, Y., and Yekutieli, D. (2001). The control of the false discovery rate in multiple testing under dependency. *Ann. Stat.* 29, 1165–1188. doi: 10.1186/1471-2105-9-114

Brokordt, K., Fernandez, M., and Gaymer, C. (2006). Domestication reduces the capacity to escape from predators. *J. Exp. Mar. Biol. Ecol.* 329, 11–19. doi: 10.1016/j.jembe.2005.08.007

Brokordt, K., and Guderley, H. (2004). Energetic requirements during gonad maturation and spawning in scallops: sex differences in *Chlamys islandica* (Muller 1776). *J. Shellfish Res.* 23, 25–32.

Brokordt, K., Pérez, H., Herrera, C., and Gallardo, A. (2015). Reproduction reduces HSP70 expression capacity in *Argopecten purpuratus* scallops subject to hypoxia and heat stress. *Aquat. Biol.* 23, 265–274. doi: 10.3354/ab00626

Brokordt, K. B., Guderley, H. E., Guay, M., Gaymer, C. F., and Himmelman, J. H. (2003). Sex differences in reproductive investment: maternal care reduces escape response capacity in the whelk *Buccinum undatum*. *J. Exp. Mar. Biol. Ecol.* 291, 161–180. doi: 10.1016/S0022-0981(03)00119-9

Brokordt, K. B., Himmelman, J. H., and Guderley, H. E. (2000a). Effect of reproduction on escape responses and muscle metabolic capacities in the scallop *Chlamys islandica* Muller 1776. *J. Exp. Mar. Biol. Ecol.* 251, 205–225.

Brokordt, K. B., Himmelman, J. H., Nusetti, O. A., and Guderley, H. (2000b). Reproductive investment reduces recuperation from exhaustive escape activity in the tropical scallop *Euvola ziczac*. *Mar. Biol.* 137, 857–865. doi: 10.1007/s002270000415

Buggé, D. M., Hégaret, H., Wikfors, G. H., and Allam, B. (2007). Oxidative burst in hard clam (*Mercenaria mercenaria*) haemocytes. *Fish Shellfish Immunol.* 23, 188–196. doi: 10.1016/j.fsi.2006.10.006

Chazotte, B. (2011). Labeling nuclear DNA with hoechst 33342. *Cold Spring Harb. Protoc.* 2011:prot5557. doi: 10.1101/pdb.prot5557

Chen, H., Wang, L., Zhou, Z., Hou, Z., Liu, Z., Wang, W., et al. (2015). The comprehensive immunomodulation of NeurimmiRs in haemocytes of oyster *Crassostrea gigas* after acetylcholine and norepinephrine stimulation. *BMC Genomics* 16:942. doi: 10.1186/s12864-015-2150-8

Cheng, T. C. (1976). Aspects of substrate utilization and energy requirement during molluscan phagocytosis. *J. Invertebrate Pathol.* 27, 263–268. doi: 10.1016/0022-2011(76)90156-7

Cho, S.-M., and Jeong, W.-G. (2005). Spawning impact on lysosomal stability of the Pacific oyster. *Crassostrea gigas*. *Aquaculture* 244, 383–387. doi: 10.1016/j.aquaculture.2004.12.013

Coba de la Peña, T., Cárcamo, C. B., Díaz, M. I., Brokordt, K. B., and Winkler, F. M. (2016). Molecular characterization of two ferritins of the scallop argopecten purpuratus and gene expressions in association with early development, immune response and growth rate. *Comp. Biochem. Physiol. B Biochem. Mol. Biol.* 198, 46–56. doi: 10.1016/j.cbpb.2016.03.007

Cochennec-Laureau, N., Auffret, M., Renault, T., and Langlade, A. (2003). Changes in circulating and tissue-infiltrating hemocyte parameters of European flat oysters, *Ostrea edulis*, naturally infected with *Bonamia ostreae*. *J. Invertebrate Pathol.* 83, 23–30. doi: 10.1016/S0022-2011(03)00015-6

De Decker, S., Normand, J., Saulnier, D., Pernet, F., Castagnet, S., and Boudry, P. (2011). Responses of diploid and triploid Pacific oysters *Crassostrea gigas* to

Vibrio infection in relation to their reproductive status. *J. Invertebrate Pathol.* 106, 179–191. doi: 10.1016/j.jip.2010.09.003

De Mendiburu, F. (2017). *Agricolae: Statistical Procedures for Agricultural Research. R package version 1.2–8*.

Donaghy, L., Kraffe, E., Le Goïc, N., Lambert, C., Volety, A. K., and Soudant, P. (2012). Reactive oxygen species in unstimulated hemocytes of the Pacific oyster *Crassotrea gigas*: a mitochondrial involvement. *PLoS One* 7:e46594. doi: 10.1371/journal.pone.0046594

Donaghy, L., Lambert, C., Choi, K., and Soudant, P. (2009). Hemocytes of the carpet shell clam (*Ruditapes decussatus*) and the Manila clam (*Ruditapes philippinarum*): current knowledge and future prospects. *Aquaculture* 297, 10–24. doi: 10.1016/j.aquaculture.2009.09.003

Dubois, M., Gilles, K. A., Hamilton, J. K., Rebers, P. T., and Smith, F. (1956). Colorimetric method for determination of sugars and related substances. *Anal. Chem.* 28, 350–356. doi: 10.1021/ac60111a017

Duggleby, R. G. (1984). Regression analysis of nonlinear Arrhenius plots: an empirical model and a computer program. *Comput. Biol. Med.* 14, 447–455. doi: 10.1016/0010-4825(84)90045-3

FAO (2016). *Estadísticas de Pesca y Acuicultura. Producción Mundial de Acuicultura 1950-2014 (FishstatJ)*. Rome: FAO.

González, R., Brokordt, K., Cárcamo, C. B., de la Peña, T. C., Oyanedel, D., Mercado, L., et al. (2017). Molecular characterization and protein localization of the antimicrobial peptide big defensin from the scallop Argopecten purpuratus after *Vibrio splendidus* challenge. *Fish Shellfish Immunol.* 68, 173–179. doi: 10.1016/j.fsi.2017.07.010

Handa, T., Araki, A., Kawana, K., and Yamamoto, K.-i (2018). Acid–base balance of hemolymph in pacific oyster *Crassostrea gigas* in normoxic conditions. *J. Natl. Fish. Univ.* 66, 103–110.

Handa, T., Araki, A., and Yamamoto, K.-i (2017). Oxygen and acid–base status of hemolymph in the pacific oyster *Crassostrea gigas* after cannulation of the adductor muscle. *J. Nat. Fish. Univ.* 66, 35–40.

Hong, H.-K., Donaghy, L., Park, H.-S., and Choi, K.-S. (2014). Influence of reproductive condition of the Manila clam *Ruditapes philippinarum* on hemocyte parameters during early post-spawning period. *Aquaculture* 434, 241–248. doi: 10.1016/j.aquaculture.2014.08.019

Kraffe, E., Tremblay, R., Belvin, S., LeCoz, J., Marty, Y., and Guderley, H. (2008). Effect of reproduction on escape responses, metabolic rates and muscle mitochondrial properties in the scallop *Placopecten magellanicus*. *Mar. Biol.* 156, 25–38. doi: 10.1007/s00227-008-1062-4

Lambert, C., Soudant, P., Choquet, G., and Paillard, C. (2003). Measurement of *Crassostrea gigas* hemocyte oxidative metabolism by flow cytometry and the inhibiting capacity of pathogenic vibrios. *Fish Shellfish Immunol.* 15, 225–240. doi: 10.1016/S1050-4648(02)00160-2

Li, Y., Qin, J. G., Abbott, C. A., Li, X., and Benkendorff, K. (2007). Synergistic impacts of heat shock and spawning on the physiology and immune health of *Crassostrea gigas*: an explanation for summer mortality in Pacific oysters. *Am. J. Physiol. Regul. Integr. Comp. Physiol.* 293, R2353–R2362. doi: 10.1152/ajpregu.00463.2007

Li, Y., Qin, J. G., Li, X., and Benkendorff, K. (2009). Spawning-dependent stress responses in pacific oysters *Crassostrea gigas*: a simulated bacterial challenge in oysters. *Aquaculture* 293, 164–171. doi: 10.1016/j.aquaculture.2009.04.044

Li, Y., Qin, J. G., Li, X., and Benkendorff, K. (2010). Assessment of metabolic and immune changes in postspawning Pacific oyster *Crassostrea gigas*: identification of a critical period of vulnerability after spawning. *Aquac. Res.* 41, e155–e165. doi: 10.1111/j.1365-2109.2010.02489.x

Liu, R., Qiu, L., Yu, Z., Zi, J., Yue, F., Wang, L., et al. (2013). Identification and characterisation of pathogenic *Vibrio splendidus* from Yesso scallop (*Patinopecten yessoensis*) cultured in a low temperature environment. *J. Invertebrate Pathol.* 114, 144–150. doi: 10.1016/j.jip.2013.07.005

Lochmiller, R. L., and Deerenberg, C. (2000). Trade-offs in evolutionary immunology: just what is the cost of immunity? *Oikos* 88, 87–98. doi: 10.1034/j.1600-0706.2000.880110.x

Loker, E. S., Adema, C. M., Zhang, S.-M., and Kepler, T. B. (2004). Invertebrate immune systems–not homogeneous, not simple, not well understood. *Immunol. Rev.* 198, 10–24. doi: 10.1111/j.0105-2896.2004.0117.x

Malham, S. K., Lacoste, A., Gélébart, F., Cueff, A., and Poulet, S. A. (2003). Evidence for direct link between stress and immunity in the mollusc *Haliotis tuberculata*. *J. Exp. Zool.* 295A, 136–144. doi: 10.1002/jez.a.10222

Martinez, G., Brokordt, K., Aguilera, C., Soto, V. V., and Guderley, H. (2000). Effect of diet and temperature upon muscle metabolic capacities and biochemical composition of gonad and muscle in *Argopecten purpuratus* Lamarck 1819. *J. Exp. Mar. Biol. Ecol.* 247, 29–49. doi: 10.1016/S0022-0981(00)00143-X

Martínez, G., Saleh, F., Mettifogo, L., Campos, E., and Inestrosa, N. (1996). Monoamines and the release of gametes by the scallop *Argopecten purpuratus*. *J. Exp. Zool.* 274, 365–372. doi: 10.1002/(SICI)1097-010X(19960415)274:6<365::AID-JEZ5>3.0.CO;2-M

Ong, S. T., Ho, J. Z. S., Ho, B., and Ding, J. L. (2006). Iron-withholding strategy in innate immunity. *Immunobiology* 211, 295–314. doi: 10.1016/j.imbio.2006.02.004

Oyanedel, D., González, R., Brokordt, K., Schmitt, P., and Mercado, L. (2016a). Insight into the messenger role of reactive oxygen intermediates in immunostimulated hemocytes from the scallop *Argopecten purpuratus*. *Dev. Comp. Immunol.* 65, 226–230. doi: 10.1016/j.dci.2016.07.015

Oyanedel, D., Gonzalez, R., Flores-Herrera, P., Brokordt, K., Rosa, R., Mercado, L., et al. (2016b). Molecular characterization of an inhibitor of NF-κB in the scallop *Argopecten purpuratus*: first insights into its role on antimicrobial peptide regulation in a mollusk. *Fish Shellfish Immunol.* 52, 85–93. doi: 10.1016/j.fsi.2016.03.021

Paillard, C., Ashton-Alcox, K. A., and Ford, S. E. (1996). Changes in bacterial densities and hemocyte parameters in eastern oysters, *Crassostrea virginica*, affected by juvenile oyster disease. *Aquat. Living Resour.* 9, 145–158. doi: 10.1051/alr:1996018

Pfaffl, M. W. (2001). A new mathematical model for relative quantification in real-time RT–PCR. *Nucleic Acids Res.* 29:e45. doi: 10.1093/nar/29.9.e45

Pipe, R. K. (1992). Generation of reactive oxygen metabolites by the haemocytes of the mussel *Mytilus edulis*. *Dev. Comp. Immunol.* 16, 111–122. doi: 10.1016/0145-305X(92)90012-2

Prieto, I., Hervás-Stubbs, S., García-Granero, M., Berasain, C., Riezu-Boj, J. I., Lasarte, J. J., et al. (1995). Simple strategy to induce antibodies of distinct specificity: application to the mapping of gp120 and inhibition of HIV-1 infectivity. *Eur. J. Immunol.* 25, 877–883. doi: 10.1002/eji.1830250403

PromPerú (2014). *Informe Anual 2014: Desenvolvimiento del Comercio Exterior Pesquero*. Cusco: Departamento de Productos Pesqueros de la Sub Dirección de Promoción Internacional de la Oferta Exportable.

R Core Team (2016). *R: a Language and Environment for Statistical Computing*. Vienna: R Foundation for Statistical Computing.

Reichelt, J. L., Baumann, P., and Baumann, L. (1976). Study of genetic relationships among marine species of the genera *Beneckea* and *Photobacterium* by means of in vitro DNA/DNA hybridization. *Arch. Microbiol.* 110, 101–120. doi: 10.1007/BF00416975

Riquelme, C., Araya, R., and Escribano, R. (2000). Selective incorporation of bacteria by *Argopecten purpuratus* larvae: implications for the use of probiotics in culturing systems of the Chilean scallop. *Aquaculture* 181, 25–30. doi: 10.1016/S0044-8486(99)00225-2

Riquelme, C., Hayashida, G., Araya, R., Uchida, A., Satomi, M., and Ishida, Y. (1996). Isolation of a native bacterial strain from the scallop *Argopecten purpuratus* with inhibitory effects against pathogenic vibrios. *J. Shellfish Res.* 15, 369–374.

Rivera-Ingraham, G. A., Nommick, A., Blondeau-Bidet, E., Ladurner, P., and Lignot, J.-H. (2016). Salinity stress from the perspective of the energy-redox axis: lessons from a marine intertidal flatworm. *Redox Biol.* 10, 53–64. doi: 10.1016/j.redox.2016.09.012

Rojas, R., Miranda, C. D., Opazo, R., and Romero, J. (2015). Characterization and pathogenicity of *Vibrio splendidus* strains associated with massive mortalities of commercial hatchery-reared larvae of scallop *Argopecten purpuratus* (Lamarck, 1819). *J. Invertebrate Pathol.* 124, 61–69. doi: 10.1016/j.jip.2014.10.009

Samain, J., Dégremont, L., Solechnik, P., Haure, J., Bédier, E., Ropert, M., et al. (2007). Genetically based resistance to summer mortality in the Pacific oyster (*Crassostrea gigas*) and its relationship with physiological, immunological characteristics and infection processes. *Aquaculture* 268, 227–256. doi: 10.1016/j.aquaculture.2007.04.044

Schmitt, P., Wacyk, J., Morales-Lange, B., Rojas, V., Guzmán, F., Dixon, B., et al. (2015). Immunomodulatory effect of cathelicidins in response to a beta-glucan in intestinal epitelial cells from rainbow trout. *Dev. Comp. Immunol.* 51, 160–169. doi: 10.1016/j.dci.2015.03.007

Schwenke, R. A., Lazzaro, B. P., and Wolfner, M. F. (2016). Reproduction–immunity trade-offs in insects. *Annu. Rev. Entomol.* 61, 239–256. doi: 10.1146/annurev-ento-010715-023924

Song, L., Wang, L., Zhang, H., and Wang, M. (2015). The immune system and its modulation mechanism in scallop. *Fish Shellfish Immunol.* 46, 65–78. doi: 10.1016/j.fsi.2015.03.013

Sun, Y., Zhang, Y., Fu, X., Zhang, R., Zou, J., Wang, S., et al. (2014). Identification of two secreted ferritin subunits involved in immune defense of Yesso scallop *Patinopecten yessoensis*. *Fish Shellfish Immunol.* 37, 53–59. doi: 10.1016/j.fsi.2014.01.008

Tang, P.-S. (1933). On the rate of oxygen consumption by tissues and lower organisms as a function of oxygen tension. *Q. Rev. Biol.* 8, 260–274. doi: 10.1086/394439

Travers, M.-A., Basuyaux, O., Le Goïc, N., Huchette, S., Nicolas, J. L., Koken, M., et al. (2009). Influence of temperature and spawning effort on *Haliotis tuberculata* mortalities caused by *Vibrio harveyi:* an example of emerging vibriosis linked to global warming. *Glob. Change Biol.* 15, 1365–1376. doi: 10.1111/j.1365-2486.2008.01764.x

Tremblay, R., Myrand, B., Sevigny, J.-M., Blier, P., and Guderley, H. (1998). Bioenergetic and genetic parameters in relation to susceptibility of blue mussels, *Mytilus edulis* (L.) to summer mortality. *J. Exp. Mar. Biol. Ecol.* 221, 27–58. doi: 10.1016/S0022-0981(97)00114-7

Untergasser, A., Cutcutache, I., Koressaar, T., Ye, J., Faircloth, B. C., Remm, M., et al. (2012). Primer3—new capabilities and interfaces. *Nucleic Acids Res.* 40:e115. doi: 10.1093/nar/gks596

Vasta, G. R., Ahmed, H., and Odom, E. W. (2004). Structural and functional diversity of lectin repertoires in invertebrates, protochordates and ectothermic vertebrates. *Curr. Opin. Struct. Biol.* 14, 617–630. doi: 10.1016/j.sbi.2004.09.008

Wang, L., Song, X., and Song, L. (2018). The oyster immunity. *Dev. Comp. Immunol.* 80, 99–118. doi: 10.1111/j.1742-4658.2007.05898.x

Wang, L., Yue, F., Song, X., and Song, L. (2015). Maternal immune transfer in mollusc. *Dev. Comp. Immunol.* 48, 354–359. doi: 10.1016/j.dci.2013.07.001

Wang, M., Yang, J., Zhou, Z., Qiu, L., Wang, L., Zhang, H., et al. (2011). A primitive Toll-like receptor signaling pathway in mollusk Zhikong scallop *Chlamys farreri*. *Dev. Comp. Immunol.* 35, 511–520. doi: 10.1016/j.dci.2010.12.005

Wang, X., Wang, L., Yao, C., Qiu, L., Zhang, H., Zhi, Z., et al. (2012). Alternation of immune parameters and cellular energy allocation of *Chlamys farreri* under ammonia-N exposure and *Vibrio anguillarum* challenge. *Fish Shellfish Immunol.* 32, 741–749. doi: 10.1016/j.fsi.2012.01.025

Wendling, C. C., and Wegner, K. M. (2013). Relative contribution of reproductive investment, thermal stress and Vibrio infection to summer mortality phenomena in Pacific oysters. *Aquaculture* 412, 88–96. doi: 10.1016/j.aquaculture.2013.07.009

Xiao, J., Ford, S. E., Yang, H., Zhang, G., Zhang, F., and Guo, X. (2005). Studies on mass summer mortality of cultured zhikong scallops (*Chlamys farreri* Jones et Preston) in China. *Aquaculture* 250, 602–615. doi: 10.1016/j.aquaculture.2005.05.002

Yang, J., Qiu, L., Wei, X., Wang, L., Wang, L., Zhou, Z., et al. (2010). An ancient C-type lectin in *Chlamys farreri* (CfLec-2) that mediate pathogen recognition and cellular adhesion. *Dev. Comp. Immunol.* 34, 1274–1282. doi: 10.1016/j.dci.2010.07.004

Yang, J., Wang, L., Zhang, H., Qiu, L., Wang, H., and Song, L. (2011). C-type lectin in *Chlamys farreri* (CfLec-1) mediating immune recognition and opsonization. *PLoS One* 6:e17089. doi: 10.1371/journal.pone.0017089

Yue, F., Zhou, Z., Wang, L., Ma, Z., Wang, J., Wang, M., et al. (2013). Maternal transfer of immunity in scallop *Chlamys farreri* and its trans-generational immune protection to offspring against bacterial challenge. *Dev. Comp. Immunol.* 41, 569–577. doi: 10.1016/j.dci.2013.07.001

Zhang, Y., Zhang, R., Zou, J., Hu, X., Wang, S., Zhang, L., et al. (2013). Identification and characterization of four ferritin subunits involved in immune defense of the Yesso scallop (*Patinopecten yessoensis*). *Fish Shellfish Immunol.* 34, 1178–1187. doi: 10.1016/j.fsi.2013.01.023

Zhou, Z., Wang, L., Shi, X., Zhang, H., Gao, Y., Wang, M., et al. (2011). The modulation of catecholamines to the immune response against bacteria *Vibrio anguillarum* challenge in scallop *Chlamys farreri*. *Fish Shellfish Immunol.* 31, 1065–1071. doi: 10.1016/j.fsi.2011.09.009

Conflict of Interest Statement: The authors declare that the research was conducted in the absence of any commercial or financial relationships that could be construed as a potential conflict of interest.

frontiers in Physiology

ORIGINAL RESEARCH
published: 28 May 2018
doi: 10.3389/fphys.2018.00612

The Molecular Mechanism Underlying Pro-apoptotic Role of Hemocytes Specific Transcriptional Factor Lhx9 in *Crassostrea hongkongensis*

Yingli Zhou[1,2], Fan Mao[1,2], Zhiying He[1,2], Jun Li[1], Yuehuan Zhang[1], Zhiming Xiang[1], Shu Xiao[1], Haitao Ma[1], Yang Zhang[1] and Ziniu Yu[1]**

[1] CAS Key Laboratory of Tropical Marine Bio-resources and Ecology, Guangdong Provincial Key Laboratory of Applied Marine Biology, South China Sea Institute of Oceanology, Chinese Academy of Sciences, Guangzhou, China, [2] University of Chinese Academy of Sciences, Beijing, China

OPEN ACCESS

Edited by:
Xiaotong Wang,
Ludong University, China

Reviewed by:
Mingjia Yu,
State Oceanic Administration, China
Li Li,
Institute of Oceanology (CAS), China
Dineshram Ram,
National Institute of Oceanography (CSIR), India

***Correspondence:**
Yang Zhang
yzhang@scsio.ac.cn
Ziniu Yu
carlzyu@scsio.ac.cn

Specialty section:
This article was submitted to Aquatic Physiology, a section of the journal Frontiers in Physiology

Received: 28 February 2018
Accepted: 07 May 2018
Published: 28 May 2018

Citation:
Zhou Y, Mao F, He Z, Li J, Zhang Y, Xiang Z, Xiao S, Ma H, Zhang Y and Yu Z (2018) The Molecular Mechanism Underlying Pro-apoptotic Role of Hemocytes Specific Transcriptional Factor Lhx9 in Crassostrea hongkongensis. Front. Physiol. 9:612. doi: 10.3389/fphys.2018.00612

Hemocytes are the central organ of immune defense against pathogens by means of inflammation, phagocytosis, and encapsulation in mollusks. The well-functioning of the host immune system relies on the hemocytes' task exertion and frequent renewal, but the underlying renewal mechanism remains elusive at the gene level. Here, we identified one transcription factor, LIM homeobox 9, in *Crassostrea hongkongensis* (*Ch*Lhx9) that could be involved in hemocyte apoptosis or renewal. *Ch*Lhx9 contains a homeodomain and two LIM domains. The expression profile of *Ch*Lhx9 showed that it was specific and had high expression in hemocytes, and it significantly increased under the bacterial challenge. RNA interference of *Ch*Lhx9 dramatically decreased the apoptosis rate of hemocytes when compared with a control group, which strongly implies its pro-apoptotic role in hemocytes. Furthermore, the genomic responses to the knockdown of *Ch*Lhx9 were examined through RNA-seq, which showed that multiple pathways associated with cell apoptosis, including the apoptosis pathway, hippo signal pathway and p53 signaling pathway, were significantly down-regulated. Meanwhile, seven of the key apoptotic genes were confirmed to be upregulated by *Ch*Lhx9, among which *Ch*ASPP1 (apoptosis stimulating protein of p53) was confirmed to induce hemocyte apoptosis strongly, which demonstrates that *Ch*ASPP1 was a downstream target mediated by *Ch*Lhx9 that caused apoptosis. In conclusion, tissue-specific transcription factor *Ch*Lhx9 induces hemocyte apoptosis through activating apoptotic genes or pathways, which could contribute to hemocyte renewal and immune defense in oysters.

Keywords: *Crassostrea hongkongensis*, hemocytes, apoptosis, *Ch*Lhx9, *Ch*ASPP1, RNAi, RNA-seq

INTRODUCTION

Hemocytes function in both cellular and humoral defenses, which is the main means for oysters to cope with infectious agents (Chu, 1988; Feng, 1988; Lavine and Strand, 2002; Arefin et al., 2015). Eliminating pathogens relies on the ability of hemocytes to recognize foreign targets and induce apoptotic cell death (Lavine and Strand, 2002; Sokolova, 2009). In addition, activation-induced hemocyte death, as the second safeguard against autoimmunity, prevents an excessive immune response (Feig and Peter, 2007). The apoptosis of hemocytes plays an essential role in homeostasis of the immune responses to ensure well-functioning of the oyster immune system in resisting foreign microbes (Opferman and Korsmeyer, 2003; Hildeman et al., 2007; Hughes et al., 2010; Ghosh et al., 2015). Therefore, the mechanism that underlies oyster hemocyte apoptosis has drawn a large amount of attention and studies to obtain a better understanding of oyster autoimmunity and disease management.

Homeobox genes, which encode homeodomain transcription factors, are involved in the regulation of apoptosis, cellular differentiation and developmental processes in many metazoans (Mcginnis et al., 1984; Lohmann et al., 2002; Pearson et al., 2005; Kocak et al., 2013). E2A-PBX1, a chimeric homeobox protein, paradoxically induces both thymocyte death and lymphoma in E2A-PBX1 transgenic mice (Dedera et al., 1993). During the development of *Drosophila*, homeobox genes Dfd and Abd-B induce localized apoptosis to maintain normal segment boundaries, and Dfd directly binds to the enhancer of the downstream cell death promoting gene reaper (White et al., 1994; Lohmann et al., 2002). Recently, more studies have revealed that Hox genes, a subset of the homeobox genes, play a pivotal role in cell apoptosis for vertebrates (Raman et al., 2000). HOX-C9 activates the intrinsic pathway of apoptosis to inhibit the growth of neuroblastoma (Kocak et al., 2013) and the overexpression of HOXB1 to induce the death of HL60 leukemic cells by upregulating caspase2 and downregulating MDM2 (Petrini et al., 2013).

Recently, our previous studies showed that one homeobox gene, Lhx9, was specific and highly expressed in hemocytes in Hong Kong oyster, *C. hongkongensis* (Tong et al., 2015), an economically important and filter-feeding species in the coastal waters of the South China Sea (Volety et al., 1999; Lam and Morton, 2003). Lhx9 contains two specialized cysteine-rich LIM domains that are involved in protein-binding interactions and a homeodomain that is involved in DNA-binding interactions and the transcription of downstream genes (Sanchezgarcia and Rabbitts, 1994; Dawid et al., 1995; Agulnick et al., 1996). In mammals, Lhx9 is important for the development of gonads and is responsible for the invasion of the epithelium into the mesenchyme (Birk et al., 2000). In invertebrate, a homologous gene of Lhx9 is expressed in accessory cells to control the early regulation of wing development (Bourgouin et al., 1992).

However, compared to studies in model organisms, the function of Lhx9 in mollusks is still unknown. Therefore, in this study, we cloned and functionally studied a molluscan Lhx9 homolog from *C. hongkongensis*. *Ch*Lhx9 knockdown oysters harbor a significantly lower apoptosis rate compared to control oysters. RNA-sequencing analysis of *Ch*Lhx9 knockdown oysters indicated that it participates in the regulation of several cellular process pathways that are associated with cell apoptosis. Importantly, we identified seven crucial apoptosis genes that are regulated by *Ch*Lhx9 and revealed that *Ch*ASPP1, the downstream gene of *Ch*Lhx9, induces the apoptosis of hemocytes. Thus, *Ch*Lhx9 serves as a tissue-specific transcription factor to induce the apoptosis of hemocytes by activating the expression of apoptotic genes in *C. hongkongensis*.

MATERIALS AND METHODS

Animals and Sample Collection

Healthy oysters (*C. hongkongensis*), which averaged 108 mm in shell height, were collected from Zhanjiang, Guangdong province, China, and kept in aerated seawater (18‰ salinity) at 25°C and fed with 0.8% *Tetraselmis suecica* and *Isochrysis galbana* for 1 week before processing. Different tissues (hemocytes, labial palps, heart, digestive gland, mantle, muscle, gonad, and gill tissues) were collected from at least three independent oysters for RNA extraction and flow cytometry. The collected samples were immersed in TRIzol, quickly frozen in liquid nitrogen, and then stored at −80°C until RNA isolation.

Pathogen Challenge and *in Vivo* RNA Interference (RNAi)

For the pathogen challenge, the oysters were randomly divided into three groups, the *Vibrio alginolyticus*, the *Staphylococcus haemolyticus* challenge groups and the PBS control group, with each group in separate tanks. Oysters in the two challenged groups were injected with 100 μL *V. alginolyticus* or *S. haemolyticus* (suspended in 0.1 M PBS at a concentration of 1.0×10^9 cells/mL) into the adductor muscle; oysters in the control group were injected with an equal volume of PBS. After treatment, the oysters were returned to the water tanks, and three individuals were randomly sampled at 3, 6, 12, 24, 48, and 72 h post-injection.

An *in vivo* dsRNAi experiment was conducted according to the previous reports (Liu et al., 2017). The oysters were divided randomly into two groups. In the experimental group, 100 μL of *Ch*Lhx9 dsRNA or *Ch*ASPP1 dsRNA (1 mg/μL) was injected into the adductor of each oyster. The oysters that received an injection of 100 μL EGFP dsRNA (1 mg/μL) were used as the control group. Hemocytes were sampled at 72 h post-injection. Then, 48 h after the knockdown of *Ch*Lhx9, the remaining oysters in the two groups received an injection of 100 μL of *V. alginolyticus* (suspended in 0.1 M PBS at a concentration of 1.0×10^9 cells/mL) in the adductor muscle. The hemocytes were harvested at 24 h post-challenge.

Cloning of *Ch*Lhx9 cDNA and Sequence Analysis

According to the sequence of *C. gigas* Lhx9 (GenBank accession number: XP011419207.1), gene-specific primers (**Supplementary Table S1**) were designed and used to clone

the cDNA of *Ch*Lhx9. The primer pairs *Ch*Lhx9-F1/R1, TakaraUPM/*Ch*Lhx9-R2 and *Ch*Lhx9-F2/TakaraUPM were used to amplify the ORF of *Ch*Lhx9, 5′UTR of *Ch*Lhx9 and 3′UTR of *Ch*Lhx9. The synthesis of cDNA templates and a PCR program were used according to the SMARTer® RACE 5′/3′ Kit (TaKaRa, Japan) recommendation. All of the PCR products were cloned into the pMD19-T vector (TaKaRa, Japan) for sequencing using an Applied Biosystems (ABI) 3730 DNASequencer. The full-length cDNA sequences were obtained by overlaying the three sequences of cDNA.

The deduced amino acid sequences of *Ch*Lhx9 were compared with previously published sequences of representative invertebrate and vertebrate Lhx9s. The sequences were analyzed based on nucleotide and protein databases using BLASTN and BLASTX, respectively[1]. The molecular weight and the theoretical isoelectric point were calculated using the Compute pI/Mw tool[2]. The protein secondary structure and domains were predicted using SMART[3]. Multiple sequence alignments and a phylogenetic tree were constructed using the MEGA7.0 software based on the alignment of the complete amino acid sequences. The cNLS Mapper[4] was used to predict the nuclear localization signals of *Ch*Lhx9, and Jalview software was used to generate the consensus sequence of the predicted NLS in *Ch*Lhx9 and the proved NLSs.

Cell Culture and Subcellular Localization

HEK 293T cells were maintained in Minimum Eagle's medium (Gibco, United States), which contained 10% fetal bovine serum (Gibco, United States) and 1× antibiotics (streptomycin and penicillin, Gibco) at 37°C in a humidified incubator of 5% CO_2. The ORF of *Ch*Lhx9 was inserted into the pEGFP-N1 vector (Promega, United States) to produce GFP-tagged *Ch*Lhx9 expression plasmids. The recombinant endo-free plasmids, including *Ch*Lhx9-GFP (200 ng) or pEGFP- N1 (200 ng), were transfected into HEK293T cells by using ViaFect Transfection Reagent (Promega, United States). Then, 48 h after transfection, the cells were washed with PBS twice, fixed with 4% paraformaldehyde at room temperature for 15 min, and then stained with DAPI for 5 min. After washing twice with PBS, cellular localization of the *Ch*Lhx9-GFP protein was observed by using fluorescence microscopy.

Apoptosis Check by Flow Cytometry

Hemocytes were harvested from oysters at 72 h post dsRNA injection. The apoptosis rate was detected by using the Annexin V-FITC detection kit (Vazyme, China) according to the manufacturer's instruction. In the reaction system, 100 μL of hemocytes, diluted with 100 μL of binding buffer, was incubated with 5 μL of Annexin V-FITC and 5 μL of propidium iodide for 10 min to mark early apoptotic cells and late-apoptotic or necrotic cells. After recollection and re-suspension, the hemocytes were immediately subjected to flow cytometer (Guava, United States) for apoptosis rate detection (10,000 events countered).

RNA Isolation and Quantitative Real-Time PCR

The total RNA from different tissues and hemocytes of oysters was extracted using TRIzol Reagent (Invitrogen, United States) following the manufacturer's instructions and then was treated with DNase I (TaKaRa, Japan). We checked the purity of the samples using a Nanodrop Nano-Photometer spectrophotometer (NanoDrop products IMPLEN, United States); the concentration was assessed by Nanodrop2000 (Thermo Fisher Scientific, United States), and the RNA integrity was verified using an Agilent 2100 BioAnalyzer (Agilent, United States).

The cDNA templates for the qRT-PCR were synthesized by the PrimeScript™ RT reagent (with gDNA Eraser) Kit (TaKaRa, Japan). The qRT-PCR reactions were conducted using the 2× RealStar Green Power Mixture Kit (GENE STAR, China) with the LightCycler480II System (Roche, United States), according to the manufacturer's protocol. Each qRT-PCR analysis was performed in triplicate. The transcript quantifications of the genes were calculated using the $2^{-\Delta\Delta C_T}$ method with GAPDH as the reference gene (Kenneth and Livak, 2001).

RNA-Seq Analysis

Two biological replicates of RNA samples were collected from the *Ch*Lhx9 RNAi or EGFP RNAi group. As previously reported (Mortazavi et al., 2008; Wang et al., 2009), a total of four libraries were constructed, and sequencing was performed with the sequencing platform BGISEQ-500 (BGI, China). Clean tags were generated from raw sequencing reads, which were filtered to remove the adapters, unknown biases and low-quality reads and were mapped to the *C. hongkongensis* transcriptome dataset (Tong et al., 2015). For gene expression analysis, the matched reads were calculated and then normalized to RPKM using RESM software (Li and Dewey, 2011). The significance of the differential gene expression was based on the Noiseq method (Tarazona et al., 2011) with the absolute value of $\log_2$-Ratio ≥ 1 and the divergence probability ≥ 0.8 in this research. All DEGs were further subjected to Gene Ontology (GO) and KEGG Orthology (KO) enrichment analysis by mapping the DEGs to the GO and KEGG databases followed by hypergeometric tests (Ye et al., 2006; Kanehisa et al., 2008). The reliability of the DEGs was validated by qRT-PCR, and primers (**Supplementary Table S1**) were designed using Primer 5.0 software.

Statistical Analysis

All of the statistical analyses were carried out with SPSS 18.0 software. Significant differences in the expression of *Ch*Lhx9 in different tissues and in hemocytes after bacterial challenge were analyzed by one-way analysis of variance (ANOVA) followed by Duncan's multiple range tests. Significant differences in knockdown efficiency of RNAi and flow cytometry analysis of apoptosis were analyzed by Student's t-test. Means ± SE (standard error) were determined based on three biological replicates.

[1] http://www.ncbi.nlm.nih.gov/BLAST/

[2] http://www.expasy.ch/tools/pi_tool.html

[3] http://smart.embl-heidelberg.de/

[4] http://nls-mapper.iab.keio.ac.jp/cgi-bin/NLS_Mapper_form.cgi#opennewwindow

RESULTS

Sequence Analysis of *Ch*Lhx9

The full-length cDNA sequence of the *Ch*Lhx9 gene (GenBank accession number: MG879528) contains a 5′-UTR of 286 bp, a 3′-UTR of 143 bp and an open reading frame (ORF) of 1,230 bp. The ORF is predicted to encode a protein of 409 amino acids (**Figure 1**), with a calculated molecular mass of 46.07 kDa and a theoretical isoelectric point of 7.23. The conserved domains of *Ch*Lhx9 were predicted and analyzed by the SMART program, including two LIM domains and one homeodomain, with the typical features of Lhx9 family proteins (**Figure 2A**).

A phylogenetic tree was constructed by MEGA7.0 software using the amino acid sequences of the Lhx9 from *C. hongkongensis* and other species, which reveals their clear evolutionary relationship. As shown in **Figure 2B**, the *Ch*Lhx9 was clustered with Lhx9 from other mollusks such as *C. gigas*, *Mizuhopecten yessoensis*, *Biomphalaria glabrata,* and *Leptochiton asellus* and then clustered with arthropods and vertebrates, which means that its evolution is relatively conservative in mollusks and different from vertebrates and other invertebrates.

Expression Pattern of *Ch*Lhx9 in Tissues

The mRNA expression pattern of *Ch*Lhx9 was detected via qRT-PCR for all of the examined tissues of *C. hongkongensis*, including the hemocytes, labial palps, heart, digestive gland, mantle, muscle, gonad, and gill. The results revealed that *Ch*Lhx9 was constitutively expressed in all of the examined tissues but had specific and high expression in *C. hongkongensis* hemocytes (**Figure 3**). Its expression level in hemocytes is 4.66-fold higher than in heart and 16-fold higher than in digestive gland.

*Ch*Lhx9 Localized to the Nucleus

Usually, the function of transcription factors is coupled with their nuclear localization. The NLS (nuclear localization signal) prediction results showed that *Ch*Lhx9 has one NLS (RPRKRKNHVI) that has a conserved alkaline amino acid motif (RKRK) with other proven NLSs (**Figure 4A**). Moreover, the recombinant plasmid that expresses *Ch*Lhx9-EGFP protein was transfected into HEK293T cells, and the fusion protein was visualized by fluorescence microscopy. The results showed that the *Ch*Lhx9-EGFP fusion protein was dominantly distributed in the nucleus, the majority of which overlapped with DAPI staining. As a control, the pEGFP-N1 protein was widely spread over the whole cells (**Figure 4B**).

Knockdown of *Ch*Lhx9 Results in Declining of the Apoptosis Rate of Hemocytes

To investigate the possible function of *Ch*Lhx9 in hemocytes, dsRNA was injected into the muscle to knockdown *Ch*Lhx9 mRNA expression. The results showed that the expression level of *Ch*Lhx9 was successfully knocked down to 19.18% 72 h after the *Ch*Lhx9 dsRNA injection (**Figure 5A**). At the same time, flow cytometry analysis showed that the apoptosis rate of the hemocytes declined 36.49% (including early and late apoptotic cells) in the ds*Ch*Lhx9-injected oysters (**Figures 5B,C**), which clearly implies the pro-apoptotic role of *Ch*Lhx9 in oyster hemocytes.

Global Expression Profiling of Hemocytes After Knockdown of *Ch*Lhx9

To study the pro-apoptotic mechanism of *Ch*Lhx9 in hemocytes, we further examined the effect of *Ch*Lhx9 knockdown on the whole transcription expression of *C. hongkongensis* hemocytes. Firstly, two hemocyte libraries, including the *Ch*Lhx9 dsRNA-injected and EGFP dsRNA-injected groups, were generated, and the expression levels of *Ch*Lhx9 in hemocytes of the two replicates was successfully depleted to 27.31% and 25.22% (**Supplementary Figure S1**). We summarized the sequencing and mapping results in **Supplementary Table S2**. RNA-seq analysis also showed that the square of the correlation value is 0.992 and 0.976 between two replicates within the *Ch*Lhx9 dsRNA and EGFP dsRNA injected groups, respectively (**Figure 6A**), which confirms the reliable replication in our assay. In total, more than 73% of the clean reads were aligned to references, and the detailed gene expression is listed in **Supplementary Data Sheet S1**.

Analysis of the differentially expressed genes (DEGs) reveals that 4,092 genes were down-regulated and 554 genes were up-regulated, which suggests an extensive transcriptional activation role of *Ch*Lhx9 in oyster (**Figure 6B** and **Supplementary Data Sheet S2**). Among them, 17 DEGs were selected for qRT-PCR analysis to assess the reliability of RNA-seq, which verifies a high reliability between RNA-seq and qRT-PCR (**Supplementary Figure S2**). Furthermore, pathway enrichment analysis of DEGs showed that the apoptosis pathway, hippo signaling pathway and p53 signaling pathway were significantly enriched after *Ch*Lhx9 knockdown (**Figure 6C** and **Supplementary Data Sheet S2**). Meanwhile, the vast majority of genes of these pathways were downregulated by *Ch*Lhx9 RNAi, which suggests an activating role of *Ch*Lhx9 in controlling the expression of the apoptosis-related pathways.

*Ch*Lhx9 Induced Apoptosis Through the Transactivation of *Ch*ASPP1

On the basis of several apoptosis-related pathways, the hippo signal pathway, p53 signaling pathway and apoptosis pathway were regulated by *Ch*Lhx9, and the key apoptosis-related genes were further analyzed by qRT-PCR. Among all of the apoptosis-related genes, we found that seven pro-apoptotic and one anti-apoptotic gene had significantly different expression post-*Ch*Lhx9 dsRNA injection, which was tested by qRT-PCR (**Figure 7A**). The expression of ASPP1 (apoptosis-stimulating protein of p53) and LATS1 (large tumor suppressor kinase), pro-apoptotic genes that exist extensively in the model organism, declined to 16.95% and 20.88% of the expression in the control group.

To validate the function of the downstream target genes of *Ch*Lhx9, we injected *Ch*ASPP1 dsRNA into the muscle of oysters. The relative expression of *Ch*ASPP1 was 21.45% of

```
   1 agtctcattggagaattattcactgtttgatcaaatttataagtaaatatttataaaata
  61 ggacataatcttctttttgaaagtgaaaggaaacgcgacagacgacttcatattctggag
 121 caaacgaaccaggcacgctttctttagaactcggaggaagtttgcaacagaaaaaaaatt
 181 tgcaatagagattgaagaaattaacattgcagtatgatgaaaggcacatattcccccgcg
 241 gacgaattttgacatctgattcaactgcacgcgacagcatctatatATGGTGGGACTTCA
   1                                                 M  V  G  L  Q
 301 GACTTTGAACTGCGGAATGGTAGAGAAGACAAATATGATTTTGTCCGACCATAATGCCTT
   6  T  L  N  C  G  M  V  E  K  T  N  M  I  L  S  D  H  N  A  F
 361 TCCTGACCACACGCCATGCTCCAGGGAAATGTCACAGTTTGATATCAACCAGCACCAGCA
  26  P  D  H  T  P  C  S  R  E  M  S  Q  F  D  I  N  Q  H  Q  H
 421 CCACATGCAGACCATGCCGGTGTTAAATAAATTCGAATCTCCAAGTTTCTGTGCTGGGTG
  46  H  M  Q  T  M  P  V  L  N  K  F  E  S  P  S  F  C  A  G  C
 481 CGGATCCAGAATTTTTGACCGGTATTACCTGATGGCCGTTGATAAACAGTGGCATGTGAA
  66  G  S  R  I  F  D  R  Y  Y  L  M  A  V  D  K  Q  W  H  V  N
 541 CTGCCTAAAATGTTGCGAGTGCAAAATTGGTCTGGATTCAGAACTCACCTGCTTTGCACG
  86  C  L  K  C  C  E  C  K  I  G  L  D  S  E  L  T  C  F  A  R
 601 AGACGGAAATATTTATTGTAAAGAAGATTATTACAGGAGGTATGCTGTCAAGCGATGCTC
 106  D  G  N  I  Y  C  K  E  D  Y  Y  R  R  Y  A  V  K  R  C  S
 661 GCGGTGTCATCAGGGTATCACGGCGAACGAACTAGTGATGCGCGCCAAGGACTTAGTGTT
 126  R  C  H  Q  G  I  T  A  N  E  L  V  M  R  A  K  D  L  V  F
 721 TCACATCAACTGTTTCACGTGTGCATCGTGTAATAAGACCCTTACTACGGGTGATCAGTT
 146  H  I  N  C  F  T  C  A  S  C  N  K  T  L  T  T  G  D  Q  F
 781 CGGAATGCAGGATGATTTAGTATATTGTAGAACAGACTATGAAATCATTTTTCAAGGAGA
 166  G  M  Q  D  D  L  V  Y  C  R  T  D  Y  E  I  I  F  Q  G  D
 841 CTATTTCTCGCGCATGCATCCAGCATTGCCGTGTCCAAACAACGGCCATATCCCGTTCTA
 186  Y  F  S  R  M  H  P  A  L  P  C  P  N  N  G  H  I  P  F  Y
 901 CAATGGAGTCGGAACAGCCGTGCAAAAAGGGCGGCCCAGGAAGCGGAAGAACCACGTGAT
 206  N  G  V  G  T  A  V  Q  K  G  R  P  R  K  R  K  N  H  V  I
 961 AGATCATGACGGATGTCCACCCGGCATGGGTCTTGGGCACGGTGACGGGCCGGATAGGGG
 226  D  H  D  G  C  P  P  G  M  G  L  G  H  G  D  G  P  D  R  G
1021 TGGAGATCTGATGAGACAAGATGGCGGATACGGATCACAGCCACCTCCGCGACAAAAAAG
 246  G  D  L  M  R  Q  D  G  G  Y  G  S  Q  P  P  P  R  Q  K  R
1081 AGTCCGGACATCATTTAAGCACCACCAGCTACGCACCATGAAATCTTATTTTGCACTGAA
 266  V  R  T  S  F  K  H  H  Q  L  R  T  M  K  S  Y  F  A  L  N
1141 CCACAATCCCGACGCTAAAGACCTAAAACAACTAGCCCAAAAGACTGGGTTATCCAAAAG
 286  H  N  P  D  A  K  D  L  K  Q  L  A  Q  K  T  G  L  S  K  R
1201 AGTTCTACAGGTTTGGTTCCAAAACGCAAGAGCGAAATATCGAAGAAATATGTTAAAGAG
 306  V  L  Q  V  W  F  Q  N  A  R  A  K  Y  R  R  N  M  L  K  S
1261 TGACTCGGACAAAACCGGCCAGGGTGGCAGCCAATCGAGTGACCAGTCCGCCGTGAGCCC
 326  D  S  D  K  T  G  Q  G  G  S  Q  S  S  D  Q  S  A  V  S  P
1321 GGATGACGACAAAATAAAAGATGACCAATCAATCTCCGAGTTGACAGAACTCGATGACAG
 346  D  D  D  K  I  K  D  D  Q  S  I  S  E  L  T  E  L  D  D  S
1381 CCAATCTCCGGACGCCATGTCAGACATCAGCTCCACGCCGTCATTATCTGACCTCCACAG
 366  Q  S  P  D  A  M  S  D  I  S  S  T  P  S  L  S  D  L  H  S
1441 CAACAACATGGAGTCAGACCACTCCACCAGCAGTCTGTCAGACTTATTTACTAATTCAAT
 386  N  N  M  E  S  D  H  S  T  S  S  L  S  D  L  F  T  N  S  I
1501 AAACTCGCTAAGCTGAgagattcctcgtgtcagttggtgtagtcgtgtaaagtaatgaca
 406  N  S  L  S  *
1561 agtgctactgtattatattgtaaatttgtattgtgaatttacatcactcagtcaaatttt
1621 cggaggccaaaaaaaaaaaaaaaaaaaaaaaaaaaaa
```

FIGURE 1 | The full-length cDNA and deduced amino acid sequence of *Ch*Lhx9. The two LIM domains (amino acids 61-114 and 123-177) were shadowed and the homeodomain (amino acids 263–325) was underlined.

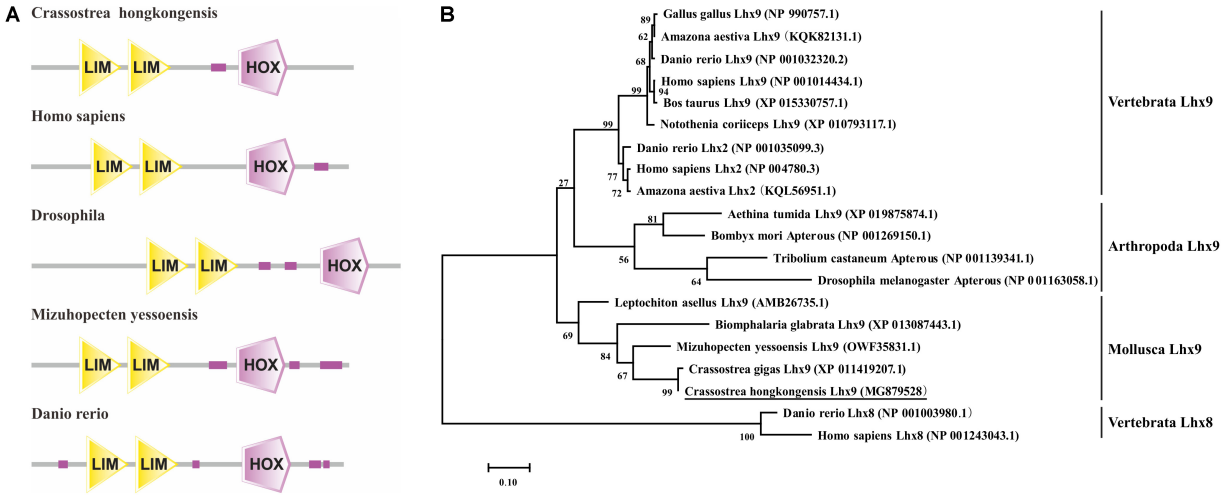

FIGURE 2 | Sequence analysis of Lhx9 proteins. **(A)** Functional domains of different species Lhx9 proteins **(B)** Phylogenetic tree analysis of the amino acid sequences of *Ch*Lhx9 protein and its homologs was constructed by the maximum likelihood method and was bootstrapped 1,000 times using the MEGA 7.0 software.

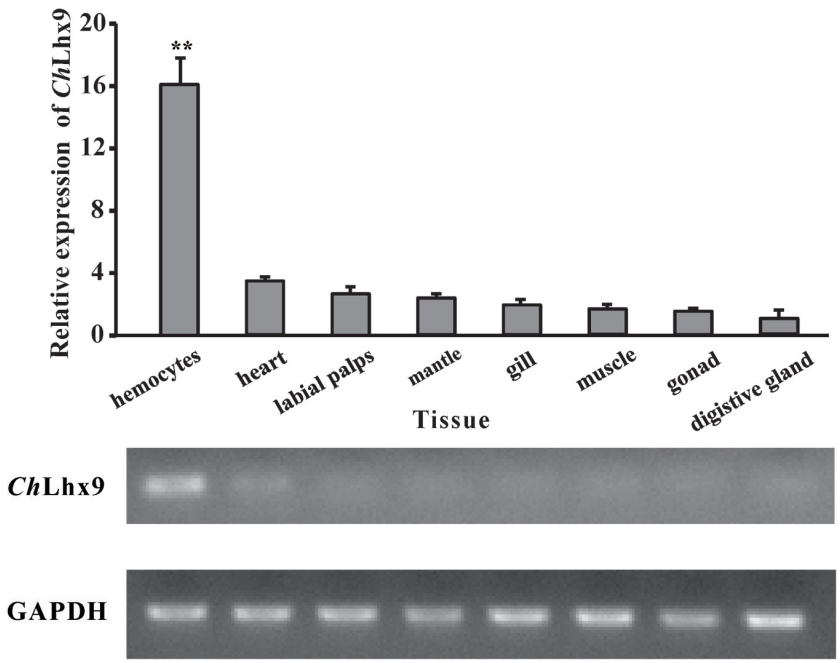

FIGURE 3 | Expression pattern of *Ch*Lhx9. Relative expression levels of *Ch*Lhx9 in different tissues. The Relative expression levels were normalized to GAPDH. **Represent $p < 0.01$.

that in the EGFP dsRNA-injected oysters and there was no significant difference in the expression levels of *Ch*Lhx9 between ASPP1-silenced oysters and control oysters (**Figure 7B** and **Supplementary Figure S3**). Compared with the EGFP dsRNA-injected oyster, the hemocyte apoptosis rate of the *Ch*ASPP1 dsRNA-injected oysters declined by 38.92% (**Figures 7C,D**), which verifies that *Ch*ASPP1 was one of the functional targets of *Ch*Lhx9 in the regulation of hemocyte apoptosis.

*Ch*Lhx9 Regulates Apoptosis in Immune Responses

The expression levels of *Ch*Lhx9 in hemocytes were significantly increased in response to two different pathogen challenges. When challenged by *V. alginolyticus*, the expression level initially significantly increased at 3 h post-challenge (3.8-fold), and it reached the highest level at 6 h post-infection (8.4-fold), compared to the treatment with PBS (**Figure 8A**).

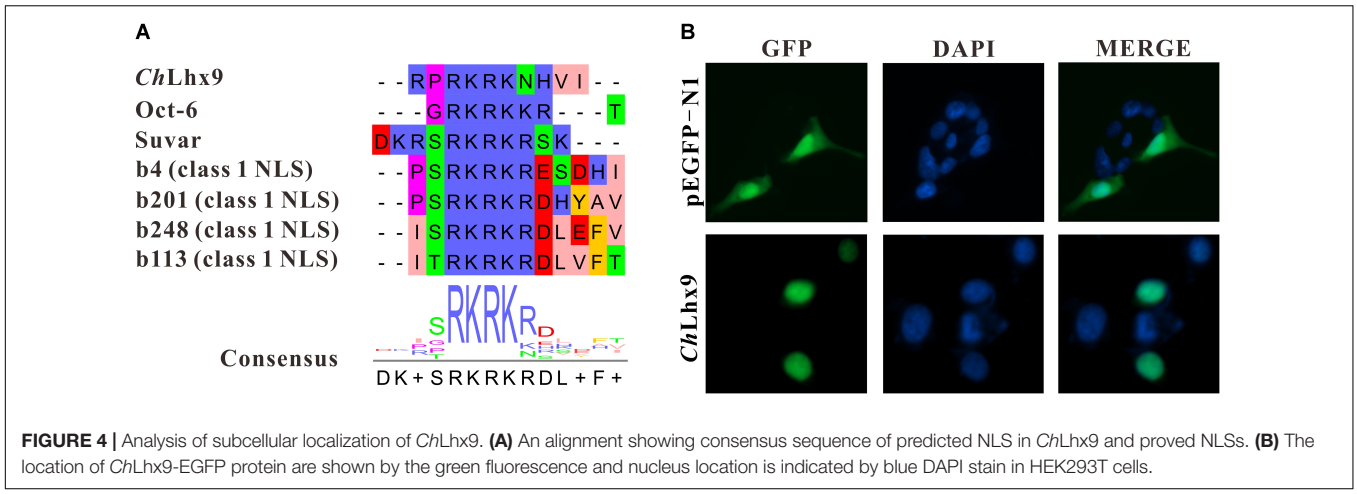

FIGURE 4 | Analysis of subcellular localization of *Ch*Lhx9. **(A)** An alignment showing consensus sequence of predicted NLS in *Ch*Lhx9 and proved NLSs. **(B)** The location of *Ch*Lhx9-EGFP protein are shown by the green fluorescence and nucleus location is indicated by blue DAPI stain in HEK293T cells.

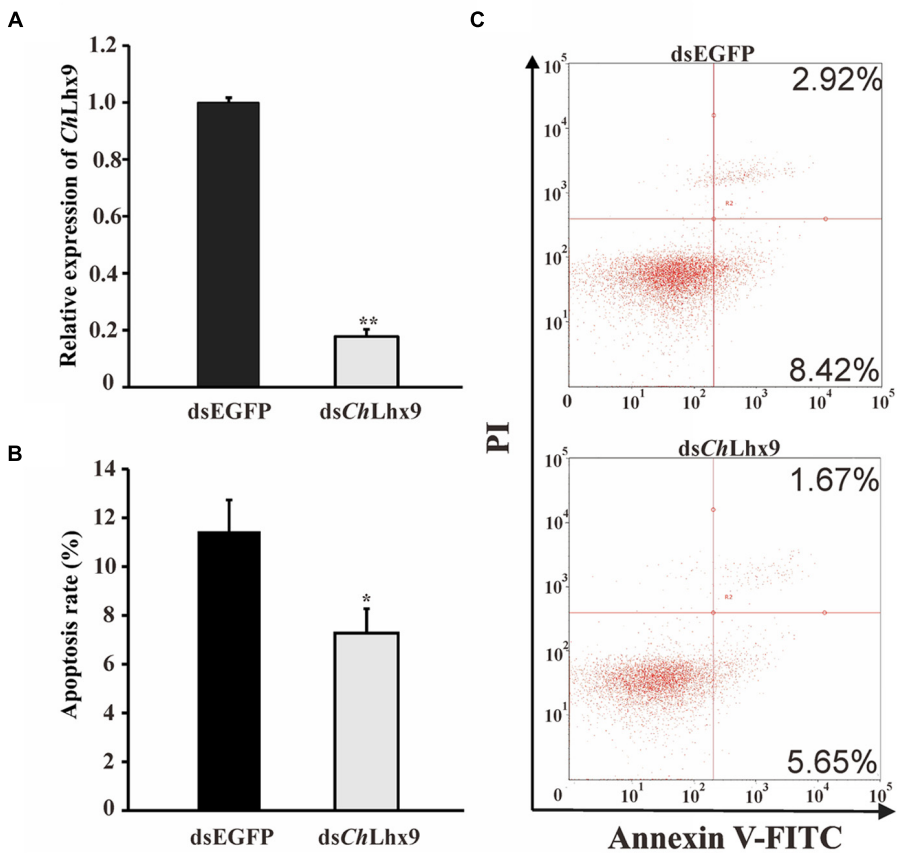

FIGURE 5 | ds*Ch*Lhx9 RNA significantly inhibited apoptosis in *C. hongkongensis* hemocytes. **(A)** Expression levels of *Ch*Lhx9 after RNAi. Significant differences are indicated by an asterisk (* and ** represent $p < 0.05$ and $p < 0.01$, respectively). **(B)** Histogram showing results obtained from three independent experiments presented **(C)** Representative images of flow cytometry analysis of apoptosis after double staining of *C. hongkongensis* hemocytes with Annexin V-FITC and PI; $n = 3$. Top right region, lower right region and bottom left region represent the late apoptotic cells, early apoptotic cells and living cells respectively.

When challenged by *S. haemolyticus*, the level of *Ch*Lhx9 mRNA was also significantly increased at 3 h and 6 h post-infection, the early stage of infection, and then it recovered to an equal level between the challenge and PBS groups.

Twenty-four hours after the *V. alginolyticus* challenge, the apoptosis rate of the hemocytes was significantly increased with an increased expression of *Ch*Lhx9 (**Figures 8A,B**). The apoptosis rate of hemocytes in the dsEGFP infection group was dramatically increased by 45% compared with the dsEGFP

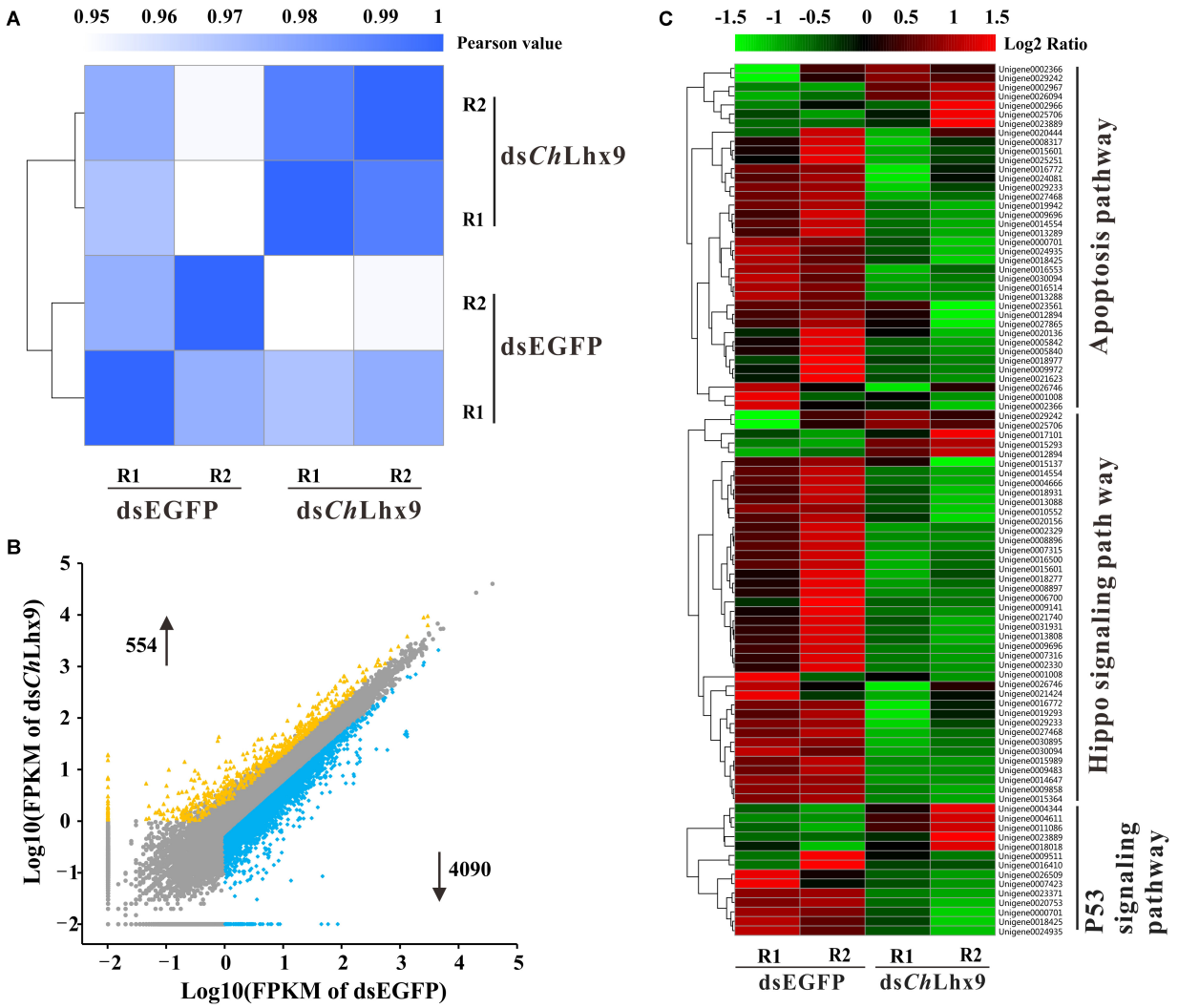

FIGURE 6 | Global expression profile after *Ch*Lhx9 dsRNAi was analyzed by means of RNA-seq quantification. **(A)** Heatmap showing the square of correlation value from two biological replicates in dsEGFP and ds*Ch*Lhx9 groups. The square of correlation value was assessed by using the Pearson correlation. R1 and R2 indicate two independent biological replicates. **(B)** Scatter plot presents the DEGs in hemocytes after *Ch*Lhx9 dsRNAi, DEGs were calculated based on an algorithm of Noiseq, with a cutoff of the absolute $\log_2$ (RPKM ratio) ≥ 1 and probability ≥ 0.8. **(C)** Three functional gene clusters involved in cell apoptosis were regulated after *Ch*Lhx9 dsRNAi, the color code indicates the fold change of the gene abundance in the form of a logarithm. The RPKM of genes is normalized in each row, and the dendrograms are constructed based on an algorithm of hierarchical clustering.

uninfected group. Although the apoptosis rate in the ds*Ch*Lhx9 group was observed to be augmented after *V. alginolyticus* challenge, it still declined 34.48% compared with the dsEGFP infection group.

DISCUSSION

The LIM homeobox gene Lhx9, which controls the proliferation, differentiation and migration of cells, is essential for organogenesis in vertebrates (the formation of the brain and glands) (Birk et al., 2000; Hobert and Westphal, 2000; Mazaud et al., 2002; Yamazaki et al., 2015; Tandon et al., 2016). The typical Lhx9 protein consists of two LIM domains and one homeodomain that is located C-terminally of the second LIM domain (Hobert and Westphal, 2000), which has the DNA-binding ability to regulate the transcription of downstream genes and is recognized by some co-factors that mediate Lhx9 function (Pomerantz et al., 1995; Jurata and Gill, 1998; Hobert and Westphal, 2000). In this study, the full-length cDNA of *Ch*Lhx9 was cloned from the invertebrate *C. hongkongensis*, which shares conserved domain structure with homologs from other species. Previous studies show that Lhx9 is mainly expressed in the epithelium, developing limbs and the nervous system (Bertuzzi et al., 1999; Mazaud et al., 2002; Tzchori et al., 2009; Yang and Wilson, 2015). However, we found Lhx9 to be specific and highly expressed in hemocytes of oyster (Tong et al., 2015), which demonstrates a species-specific expression pattern during

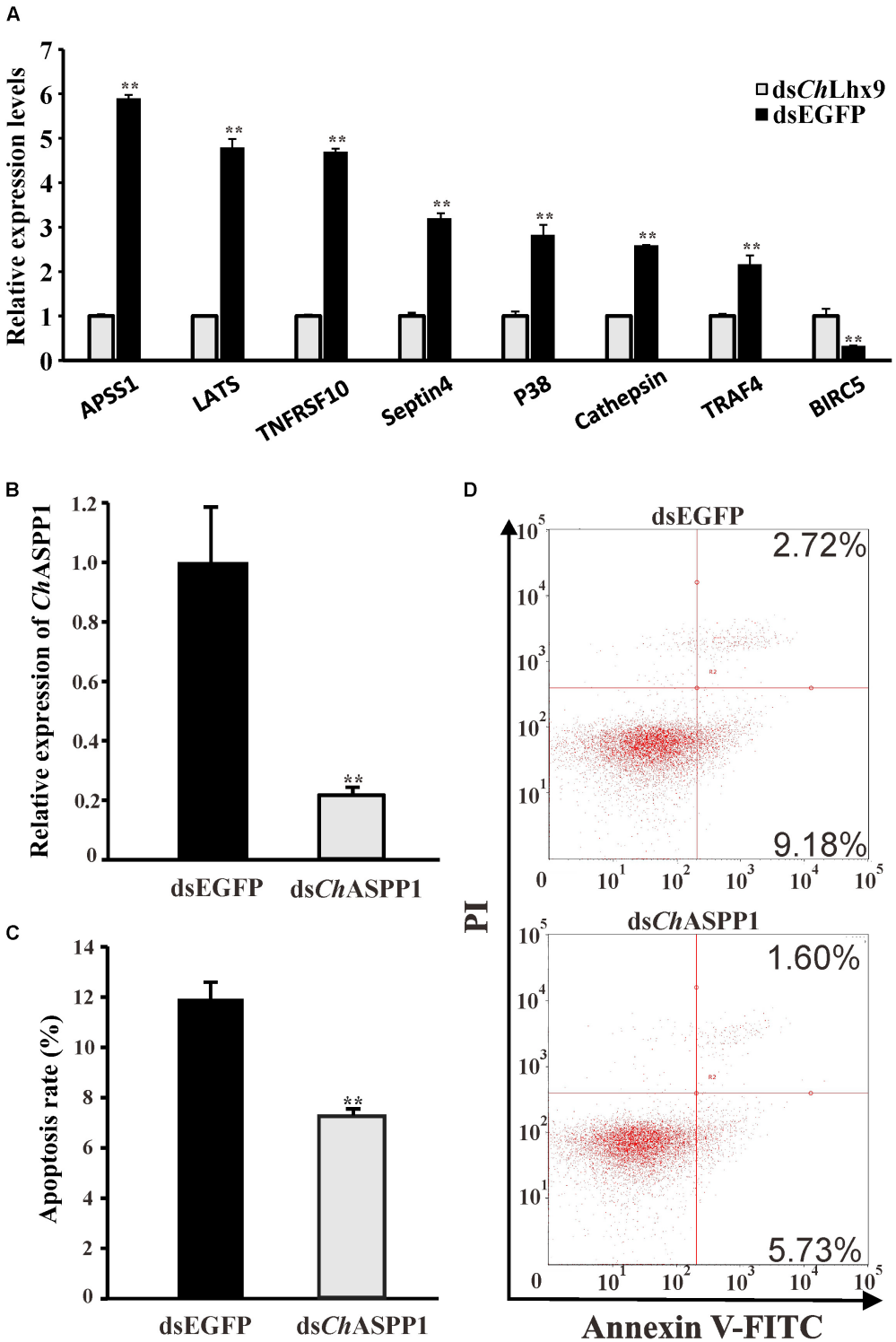

FIGURE 7 | Relative expression levels of selected DEGs and function identification of *Ch*ASPP1. **(A)** Relative expression of apoptosis-related DEGs verified by qRT-PCR. Each qRT-PCR reaction run in three replicates with GAPDH as an internal control. **(B)** Expression levels of *Ch*ASPP1 after RNAi. Significant differences are indicated: $^{**}p < 0.01$. **(C)** Histogram showing results obtained from three independent experiments presented. **(D)** Representative images of fow cytometry analysis of apoptosis after double staining of *C. hongkongensis* hemocytes with Annexin V-FITC and PI; $n = 3$. Top right region, lower right region and bottom left region represent the late apoptotic cells, early apoptotic cells and living cells respectively.

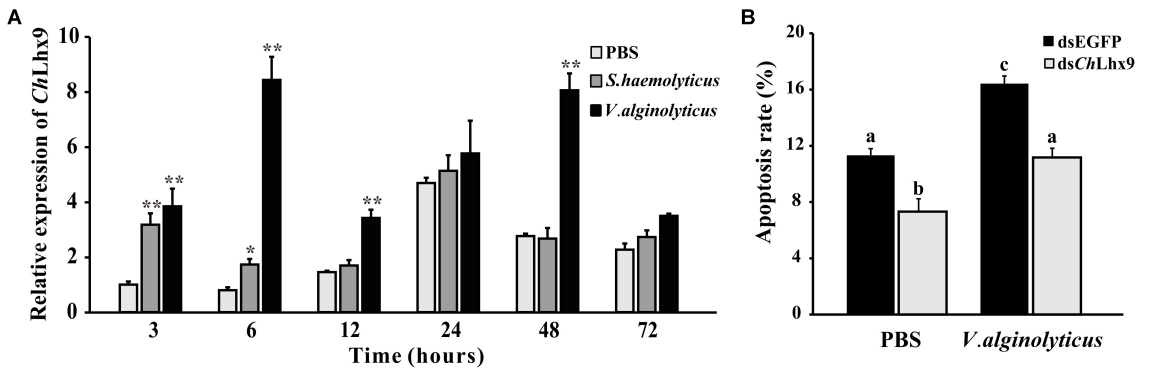

FIGURE 8 | *Ch*Lhx9 involved in immune response and apoptosis check. **(A)** Relative expression levels of *Ch*Lhx9 in hemocytes after by *S. haemolyticus* and *V. alginolyticus* challenge. Each bar represents the mean of the normalized expression levels of the replicates ($N = 3$). Significant differences are indicated by an asterisk (* and ** represent $p < 0.05$ and $p < 0.01$, respectively). **(B)** Histogram showing results obtained from three independent experiments presented, significant differences are indicated by different letters ($p < 0.05$).

evolution. Thus, it is appealing to explore the possible function of *Ch*Lhx9 in hemocytes and the non-conserved function of Lhx9 in evolution. After the knockdown of *Ch*Lhx9 in oysters, the apoptosis rate of hemocytes declined significantly compared with the control group, which was the first evidence of the pro-apoptosis role of an Lhx9 homolog in oyster. We consider that Lhx9 controls cell proliferation, adhesion and migration in the central nervous system in mouse (Bertuzzi et al., 1999; Rétaux et al., 1999; Tandon et al., 2016). That *Ch*Lhx9 induced the apoptosis of hemocytes in oysters revealed a divergent evolution in Lhx9 function.

To gain comprehensive insight into how *Ch*Lhx9 affects the apoptosis of *C. hongkongensis* hemocytes, global gene expression profiling after *Ch*Lhx9 knockdown revealed that substantial genes were extensively transactivated. More specifically, several crucial pathways that are associated with apoptosis are targets of *Ch*Lhx9, including hippo signaling, p53 signaling and apoptosis pathways. The hippo signaling pathway plays profound roles in both cell density control and anti-tumor because LATS1/2 phosphorylates the transcriptional coactivators, promoting its cytoplasmic localization, preventing the expression of anti-apoptotic genes and inducing apoptosis and restricting cell density (Zhao et al., 2010, 2011). The p53 signaling pathway influences cell cycle arrest, cellular senescence or apoptosis through enhancing or attenuating the functions of the p53 protein (Balint-E and Vousden, 2001; Thorenoor et al., 2016). The tumor suppressor p53 has recently been characterized as an apoptosis-inducing gene in oyster, as it was capable to activate pro-apoptotic genes and induce apoptosis in Pacific oyster, *C. gigas* (Savitskaya and Onishchenko, 2015; Li et al., 2017). Therefore, these evidences revealed that *Ch*Lhx9 can manipulate hemocyte apoptosis through the activation of a variety of apoptotic pathways.

To further define the target genes of *Ch*Lhx9-mediated apoptosis, seven key pro-apoptotic genes, including ASPP1, LATS1, Septin4, TNFRSF10, p38, Cathepsin and TRAF4 and one anti-apoptotic gene, BIRC5, were examined (Xia et al., 1995; Guicciardi et al., 2000; Sax and El-Deiry, 2003; Aylon et al., 2010; Lamers et al., 2011; Shi et al., 2011; Zhao et al., 2014; Zhou et al., 2014; Jeon et al., 2016). The results indicated that seven pro-apoptotic genes were significantly down-regulated and one anti-apoptotic gene was significantly up-regulated in the *Ch*Lhx9 knockdown oysters, which is consistent with the pro-apoptotic role of *Ch*Lhx9. Among them, ASPP1 (apoptosis-stimulating protein of p53) was one of the targets of *Ch*Lhx9 with the highest responsibility in our assay, which has been reported to induce apoptosis by stimulating the selection of proapoptotic genes (Levine, 1997). Additionally, recently, researchers have demonstrated that a blockade of the ASPP-p53 pathway attenuates the apoptosis of retinal ganglion cells (Wilson et al., 2013). In oyster hemocytes, an abatement of the apoptosis rate by knockdown of *Ch*ASPP1 also confirms the conserved function of ASPP1 in apoptosis induction. In addition, LATS1 kinase phosphorylates YAP and TAZ to inhibit cell growth and induce apoptosis (Qi, 2002; Halder et al., 2012), and its homolog, LATS2, phosphorylates ASPP1 and drives its translocation into the nucleus to activate the p53 signaling pathway (Aylon et al., 2010), which implies that its targets could have a synergistic effect on the promotion of apoptosis. However, this system still needs to be investigated further.

Considering the crucial role of hemocytes in immune defense, we believe that *Ch*Lhx9 is involved in the oyster immune system. When challenged with *V. alginolyticus* and *S. haemolyticus*, the expression levels of *Ch*Lhx9 were induced significantly at an early stage of infection. Consistently, the apoptosis rate was also raised under bacterial challenge in oyster, and such a phenomenon was also observed in other marine mollusks (Liu et al., 2017). At the same time, silencing of *Ch*Lhx9 attenuates the apoptosis caused by bacterial infection, which suggests that *Ch*Lhx9 could be an important apoptotic inducer under immune responses. Previous studies have revealed that apoptosis is essential for the development and maintenance of cellular homeostasis of the immune system, to ensure that the host maintains its numbers of immune cells at reasonable levels (Opferman and Korsmeyer, 2003;

Hildeman et al., 2007). In addition, the induction of hemocyte apoptosis could prevent autoimmunity and excessive immune response during inflammation (Feig and Peter, 2007). Hence, *Ch*Lhx9-induced apoptosis in hemocytes could play an essential role in homeostasis of the immune responses during infection.

In summary, we first identified a tissue-specific transcription factor Lhx9 homolog (*Ch*Lhx9), which plays a pro-apoptotic role in hemocytes through the transactivation of multiple apoptosis factors or signaling pathways. These results could contribute to a better understanding of hemocyte renewal or homeostasis of immune responses in oyster. However, further studies are required for intensively illustrating a concrete mechanism for how the transcription factor *Ch*Lhx9 regulates the expression of these genes.

AUTHOR CONTRIBUTIONS

YiZ, YaZ, and ZY designed the research. YiZ performed all of the experiments with the help of ZH, FM, and JL. SX, YuZ, HM, and ZX cultured and processed the experimental oysters. YiZ and YaZ analyzed the data and drafted the paper. YaZ and ZY critically revised the manuscript and approved the final version to be published.

FUNDING

This research was supported by the Guangdong Natural Science Funds for Distinguished Young Scholars (No. 2015A030306003), the National Science Foundation of China (Nos. 31572640 and 31572661), the Guangdong Special Support Program of Youth Scientific and Technological Innovation (No. 2015TQ01N139), and the Science and Technology Planning Project of Guangzhou, China (201707010177 and 2017B030314052).

SUPPLEMENTARY MATERIAL

The Supplementary Material for this article can be found online at: https://www.frontiersin.org/articles/10.3389/fphys.2018.00612/full#supplementary-material

FIGURE S1 | The knockdown efficiency of ds*Ch*Lhx9 RNAi in RNA-seq. **(A,B)** Represent two biological replicates respectively. Significant differences are indicated: $^{**}p < 0.01$.

FIGURE S2 | The correlation coefficient between RNA-seq and qRT-PCR data from 17 genes. The fold change is calculated by gene expression level in dsEGFP group dived by that in ds*Ch*Lhx9 group.

FIGURE S3 | The expression level of *Ch*Lhx9 after knockdown of *Ch*ASPP1.

TABLE S1 | Primers used in this study.

TABLE S2 | Overview of the RNA-seq analysis of *C. hongkongensis* hemocytes: Summary of transcriptome sequencing and mapping results of two replicates are presented in the table.

DATA SHEET S1 | List of the FPKM value of *C. hongkongensis* genes.

DATA SHEET S2 | List and annotation of differentially expressed genes after ds*Ch*Lhx9 RNAi.

REFERENCES

Agulnick, A. D., Taira, M., Breen, J. J., Tanaka, T., Dawid, I. B., and Westphal, H. (1996). Interactions of the LIM-domain-binding factor Ldb1 with LIM homeodomain proteins. *Nature* 384, 270–272. doi: 10.1038/384270a0

Arefin, B., Kucerova, L., Krautz, R., Kranenburg, H., Parvin, F., and Theopold, U. (2015). Apoptosis in hemocytes induces a shift in effector mechanisms in the drosophila immune system and leads to a pro-inflammatory state. *PLoS One* 10:e0136593. doi: 10.1371/journal.pone.0136593

Aylon, Y., Ofir-Rosenfeld, Y., Yabuta, N., Lapi, E., Nojima, H., Lu, X., et al. (2010). The Lats2 tumor suppressor augments p53-mediated apoptosis by promoting the nuclear proapoptotic function of ASPP1. *Genes Dev.* 24, 2420–2429. doi: 10.1101/gad.1954410

Balint-E, E., and Vousden, K. (2001). Activation and activities of the p53 tumour suppressor protein. *Br. J. Cancer* 85, 1813–1823. doi: 10.1054/bjoc.2001.2128

Bertuzzi, S., Porter, F. D., Pitts, A., Kumar, M., Agulnick, A., Wassif, C., et al. (1999). Characterization of Lhx9, a novel LIM/homeobox gene expressed by the pioneer neurons in the mouse cerebral cortex. *Mech. Dev.* 81, 193–198. doi: 10.1016/S0925-4773(98)00233-0

Birk, O. S., Casiano, D. E., Wassif, C. A., Cogliati, T., Zhao, L., Zhao, Y., et al. (2000). The LIM homeobox gene Lhx9 is essential for mouse gonad formation. *Nature* 403, 909–913. doi: 10.1038/35002622

Bourgouin, C., Lundgren, S. E., and Thomas, J. B. (1992). Apterous is a Drosophila LIM domain gene required for the development of a subset of embryonic muscles. *Neuron* 9, 549–561. doi: 10.1016/0896-6273(92)90192-G

Chu, F. L. E. (1988). "Humoral defense factors in marine bivalves," in *Disease Processes in Marine Bivalve Molluscs*, ed. W.S. Fisher (Bethesda, MD: American Fisheries Society Special publication).

Dawid, I. B., Toyama, R., and Taira, M. (1995). LIM domain proteins. *C. R. Acad. Sci. III* 318, 295–306.

Dedera, D. A., Waller, E. K., LeBrun, D. P., Sen-Majumdar, A., Stevens, M. E., Barsh, G. S., et al. (1993). Chimeric homeobox gene E2A-PBX1 induces proliferation, apoptosis, and malignant lymphomas in transgenic mice. *Cell* 74, 833–843. doi: 10.1016/0092-8674(93)90463-Z

Feig, C., and Peter, M. E. (2007). How apoptosis got the immune system in shape. *Eur. J. Immunol.* 37, S61–S70. doi: 10.1002/eji.200737462

Feng, S. Y. (1988). "Cellular defense mechanisms of oysters and mussels," in *Disease Processes in Marine Bivalve Molluscs*, Vol. 18, ed. W.S. Fisher (Bethesda, MD: American Fisheries Society Special Publication), 153–168.

Ghosh, S., Singh, A., Mandal, S., and Mandal, L. (2015). Active hematopoietic hubs in drosophila adults generate hemocytes and contribute to immune response. *Dev. Cell* 33, 478–488. doi: 10.1016/j.devcel.2015.03.014

Guicciardi, M. E., Deussing, J., Miyoshi, H., Bronk, S. F., Svingen, P. A., Peters, C., et al. (2000). Cathepsin B contributes to TNF-alpha-mediated hepatocyte apoptosis by promoting mitochondrial release of cytochrome c. *J. Clin. Invest.* 106, 1127–1137. doi: 10.1172/JCI9914

Halder, G., Dupont, S., and Piccolo, S. (2012). Transduction of mechanical and cytoskeletal cues by YAP and TAZ. *Nat. Rev. Mol. Cell Biol.* 13, 591–600. doi: 10.1038/nrm3416

Hildeman, D., Jorgensen, T., Kappler, J., and Marrack, P. (2007). Apoptosis and the homeostatic control of immune responses. *Curr. Opin. Immunol.* 19, 516–521. doi: 10.1016/j.coi.2007.05.005

Hobert, O., and Westphal, H. (2000). Functions of LIM-homeobox genes. *Trends Genet.* 16, 75–83. doi: 10.1016/S0168-9525(99)01883-1

Hughes, F. M., Foster, B., Grewal, S., and Sokolova, I. M. (2010). Apoptosis as a host defense mechanism in *Crassostrea virginica* and its modulation by *Perkinsus marinus*. *Fish Shellfish Immunol.* 29, 247–257. doi: 10.1016/j.fsi.2010.03.003

Jeon, T. W., Yang, H., Lee, C. G., Oh, S. T., Seo, D., Baik, I. H., et al. (2016). Electro-hyperthermia up-regulates tumour suppressor Septin 4 to induce apoptotic cell

death in hepatocellular carcinoma. *Int. J. Hyperthermia* 32, 1–9. doi: 10.1080/02656736.2016.1186290

Jurata, L. W., and Gill, G. N. (1998). Structure and function of LIM domains. *Curr. Top. Microbiol. Immunol.* 228, 75–113. doi: 10.1007/978-3-642-80481-6_4

Kanehisa, M., Araki, M., Goto, S., Hattori, M., Hirakawa, M., Itoh, M., et al. (2008). KEGG for linking genomes to life and the environment. *Nucleic Acids Res.* 36, D480–D484.

Kenneth, J., and Livak, T. D. (2001). Analysis of relative gene expression data using real-time quantitative PCR and the $2^{-\Delta\Delta C_T}$ method. *Method* 25, 402–408. doi: 10.1006/meth.2001.1262

Kocak, H., Ackermann, S., Hero, B., Kahlert, Y., Oberthuer, A., Juraeva, D., et al. (2013). Hox-C9 activates the intrinsic pathway of apoptosis and is associated with spontaneous regression in neuroblastoma. *Cell Death Dis.* 4:e586. doi: 10.1038/cddis.2013.84

Lam, K., and Morton, B. (2003). Mitochondrial DNA and morphological identification of a new species of *Crassostrea* (Bivalvia: Ostreidae) cultured for centuries in the Pearl River Delta, Hong Kong, China. *Aquaculture* 228, 1–13. doi: 10.1016/S0044-8486(03)00215-1

Lamers, F., Ploeg, I. V. D., Schild, L., Ebus, M. E., Koster, J., Bo, R. H., et al. (2011). Knockdown of survivin (BIRC5) causes apoptosis in neuroblastoma via mitotic catastrophe. *Endocr. Relat. Cancer* 18, 657–668. doi: 10.1530/ERC-11-0207

Lavine, M. D., and Strand, M. R. (2002). Insect hemocytes and their role in immunity. *Insect Biochem. Mol. Biol.* 32, 1295–1309. doi: 10.1016/S0965-1748(02)00092-9

Levine, A. J. (1997). p53, the cellular gatekeeper for growth and division. *Cell* 88, 323–331. doi: 10.1016/S0092-8674(00)81871-1

Li, B., and Dewey, C. N. (2011). RSEM: accurate transcript quantification from RNA-Seq data with or without a reference genome. *BMC Bioinformatics* 12:323. doi: 10.1186/1471-2105-12-323

Li, Y., Zhang, L., Qu, T., Tang, X., Li, L., and Zhang, G. (2017). Conservation and divergence of mitochondrial apoptosis pathway in the Pacific oyster, *Crassostrea gigas*. *Cell Death Dis.* 8:e2915. doi: 10.1038/cddis.2017.307

Liu, R., Cheng, Q., Wang, X., Chen, H., Wang, W., Zhang, H., et al. (2017). The B-cell translocation gene 1 (CgBTG1) identified in oyster *Crassostrea gigas* exhibit multiple functions in immune response. *Fish Shellfish Immunol.* 61, 68–78. doi: 10.1016/j.fsi.2016.12.005

Lohmann, I., Mcginnis, N., Bodmer, M., and Mcginnis, W. (2002). The *Drosophila Hox* gene *Deformed* sculpts head morphology via direct regulation of the apoptosis activator *reaper*. *Cell* 110, 457–466. doi: 10.1016/S0092-8674(02)00871-1

Mazaud, S., Oréal, E., Guigon, C. J., Carréeusèbe, D., and Magre, S. (2002). Lhx9 expression during gonadal morphogenesis as related to the state of cell differentiation. *Gene Expr. Patterns* 2, 373–377. doi: 10.1016/S1567-133X(02)00050-9

Mcginnis, W., Garber, R. L., Wirz, J., Kuroiwa, A., and Gehring, W. J. (1984). A homologous protein-coding sequence in drosophila homeotic genes and its conservation in other metazoans. *Cell* 37, 403–408. doi: 10.1016/0092-8674(84)90370-2

Mortazavi, A., Williams, B. A., Mccue, K., Schaeffer, L., and Wold, B. (2008). Mapping and quantifying mammalian transcriptomes by RNA-Seq. *Nat. Methods* 5, 621–628. doi: 10.1038/nmeth.1226

Opferman, J. T., and Korsmeyer, S. J. (2003). Apoptosis in the development and maintenance of the immune system. *Nat. Immunol.* 4, 410–415. doi: 10.1038/ni0503-410

Pearson, J. C., Lemons, D., and Mcginnis, W. (2005). Modulating Hox gene functions during animal body patterning. *Nat. Rev. Genet.* 6, 893–904. doi: 10.1038/nrg1726

Petrini, M., Felicetti, F., Bottero, L., Errico, M. C., Morsilli, O., Boe, A., et al. (2013). HOXB1 restored expression promotes apoptosis and differentiation in the HL60 leukemic cell line. *Cancer Cell Int.* 13:101. doi: 10.1186/1475-2867-13-101

Pomerantz, J. L., Pabo, C. O., and Sharp, P. A. (1995). Analysis of homeodomain function by structure-based design of a transcription factor. *Proc. Natl. Acad. Sci. U.S.A.* 92, 9752–9756. doi: 10.1073/pnas.92.21.9752

Qi, H. (2002). LATS1 tumor suppressor regulates G2/M transition and apoptosis. *Oncogene* 21, 1233–1241. doi: 10.1038/sj.onc.1205174

Raman, V., Martensen, S. A., Reisman, D., Evron, E., Odenwald, W. F., Jaffee, E., et al. (2000). Compromised HOXA5 function can limit p53 expression in human breast tumours. *Nature* 405, 974–978. doi: 10.1038/35016125

Rétaux, S., Rogard, M., Bach, I., Failli, V., and Besson, M. J. (1999). Lhx9: a novel LIM-homeodomain gene expressed in the developing forebrain. *J. Neurosci.* 19, 783–793. doi: 10.1523/JNEUROSCI.19-02-00783.1999

Sanchezgarcia, I., and Rabbitts, T. H. (1994). THE LIM DOMAIN - A NEW STRUCTURAL MOTIF FOUND IN ZINC-FINGER-LIKE PROTEINS. *Trends Genet.* 10, 315–320. doi: 10.1016/0168-9525(94)900345

Savitskaya, M. A., and Onishchenko, G. E. (2015). Mechanisms of apoptosis. *Biochemistry* 80, 1393–1405. doi: 10.1134/S0006297915110012

Sax, J. K., and El-Deiry, W. S. (2003). Identification and characterization of the cytoplasmic protein TRAF4 as a p53-regulated proapoptotic gene. *J. Biol. Chem.* 278, 36435–36444. doi: 10.1074/jbc.M303191200

Shi, Y., Yang, S., Troup, S., Lu, X., Callaghan, S., Park, D. S., et al. (2011). Resveratrol induces apoptosis in breast cancer cells by E2F1-mediated up-regulation of ASPP1. *Oncol. Rep.* 25, 1713–1719. doi: 10.3892/or.2011.1248

Sokolova, I. M. (2009). Apoptosis in molluscan immune defense. *Inv. Surv. J.* 6, 49–58.

Tandon, P., Wilczewski, C. M., Williams, C. E., and Conlon, F. L. (2016). The Lhx9-Integrin pathway is essential for positioning of the proepicardial organ. *Development* 143, 831–840. doi: 10.1242/dev.129551

Tarazona, S., García-Alcalde, F., Dopazo, J., Ferrer, A., and Conesa, A. (2011). Differential expression in RNA-seq: a matter of depth. *Genome Res.* 21, 2213–2223. doi: 10.1101/gr.124321.111

Thorenoor, N., Faltejskova-Vychytilova, P., Hombach, S., Mlcochova, J., Kretz, M., Svoboda, M., et al. (2016). Long non-coding RNA ZFAS1 interacts with CDK1 and is involved in p53-dependent cell cycle control and apoptosis in colorectal cancer. *Oncotarget* 7, 622–637. doi: 10.18632/oncotarget.5807

Tong, Y., Zhang, Y., Huang, J., Xiao, S., Zhang, Y., Li, J., et al. (2015). Transcriptomics analysis of *Crassostrea hongkongensis* for the discovery of reproduction-related genes. *PLoS One* 10:e0134280. doi: 10.1371/journal.pone.0134280

Tzchori, I., Day, T. F., Carolan, P. J., Zhao, Y., Wassif, C. A., Li, L., et al. (2009). LIM homeobox transcription factors integrate signaling events that control three-dimensional limb patterning and growth. *Development* 136, 1375–1385. doi: 10.1242/dev.026476

Volety, A. K., Genthner, F. J., Oliver, L. M., and Fisher, W. S. (1999). A rapid tetrazolium dye reduction assay to assess the bactericidal activity of oyster (*Crassostrea virginica*) hemocytes against Vibrio parahaemolyticus. *Aquaculture* 172, 205–222. doi: 10.1016/S0044-8486(98)00438-4

Wang, Z., Gerstein, M., and Snyder, M. (2009). RNA-Seq: a revolutionary tool for transcriptomics. *Nat. Rev. Genet.* 10, 57–63. doi: 10.1038/nrg2484

White, K., Grether, M. E., Abrams, J. M., Young, L. Y., Farrell, K., and Steller, H. (1994). Genetic control of programmed cell death in *Drosophila*. *Science* 264, 677–683. doi: 10.1126/science.8171319

Wilson, A. M., Morquette, B., Abdouh, M., Unsain, N., Barker, P. A., Feinstein, E., et al. (2013). ASPP1/2 regulate p53-dependent death of retinal ganglion cells through PUMA and Fas/CD95 activation *in vivo*. *J. Neurosci.* 33, 2205–2216. doi: 10.1523/JNEUROSCI.2635-12.2013

Xia, Z., Dickens, M., Raingeaud, J., Davis, R. J., and Greenberg, M. E. (1995). Opposing effects of ERK and JNK-p38 MAP kinases on apoptosis. *Science* 270, 1326–1331. doi: 10.1126/science.270.5240.1326

Yamazaki, F., Møller, M., Fu, C., Clokie, S. J., Zykovich, A., Coon, S. L., et al. (2015). The Lhx9 homeobox gene controls pineal gland development and prevents postnatal hydrocephalus. *Brain Struct. Funct.* 220, 1497–1509. doi: 10.1007/s00429-014-0740-x

Yang, Y., and Wilson, M. J. (2015). Lhx9 gene expression during early limb development in mice requires the FGF signalling pathway. *Gene Expr. Patterns* 19, 45–51. doi: 10.1016/j.gep.2015.07.002

Ye, J., Fang, L., Zheng, H., Zhang, Y., Chen, J., Zhang, Z., et al. (2006). WEGO: a web tool for plotting GO annotations. *Nucleic Acids Res.* 34, W293–W297. doi: 10.1093/nar/gkl031

Zhao, B., Li, L. Q., and Guan, K. L. (2010). The Hippo-YAP pathway in organ size control and tumorigenesis: an updated version. *Genes Dev.* 24, 862–874. doi: 10.1101/gad.1909210

Zhao, B., Tumaneng, K., and Guan, K. L. (2011). The Hippo pathway in organ size control, tissue regeneration and stem cell self-renewal. *Nat. Cell Biol.* 13, 877–883. doi: 10.1038/ncb2303

Zhao, X., Liu, X., and Su, L. (2014). Parthenolide induces apoptosis via TNFRSF10B and PMAIP1 pathways in human lung cancer cells. *J. Exp. Clin. Cancer Res.* 33:3. doi: 10.1186/1756-9966-33-3

Zhou, X. H., Yang, C. Q., Zhang, C. L., Gao, Y., Yuan, H. B., and Wang, C. (2014). RASSF5 inhibits growth and invasion and induces apoptosis in osteosarcoma cells through activation of MST1/LATS1 signaling. *Oncol. Rep.* 32, 1505–1512. doi: 10.3892/or.2014.3387

Conflict of Interest Statement: The authors declare that the research was conducted in the absence of any commercial or financial relationships that could be construed as a potential conflict of interest.

frontiers in Physiology

ORIGINAL RESEARCH
published: 21 August 2018
doi: 10.3389/fphys.2018.01173

Integrative Biomarker Assessment of the Influence of Saxitoxin on Marine Bivalves: A Comparative Study of the Two Bivalve Species Oysters, *Crassostrea gigas*, and Scallops, *Chlamys farreri*

Ruiwen Cao[1,2,3], Dan Wang[1], Qianyu Wei[1], Qing Wang[1,2], Dinglong Yang[1,2], Hui Liu[1,2], Zhijun Dong[1,2], Xiaoli Zhang[1,2], Qianqian Zhang[1,2] and Jianmin Zhao[1,2]**

[1] Muping Coastal Environmental Research Station, Yantai Institute of Coastal Zone Research, Chinese Academy of Sciences, Yantai, China, [2] Key Laboratory of Coastal Biology and Biological Resources Utilization, Yantai Institute of Coastal Zone Research, Chinese Academy of Sciences, Yantai, China, [3] University of Chinese Academy of Sciences, Beijing, China

OPEN ACCESS

Edited by:
Xiaotong Wang,
Ludong University, China

Reviewed by:
Baojun Tang,
Chinese Academy of Fishery Sciences, China
Daniel Carneiro Moreira,
Universidade de Brasília, Brazil

***Correspondence:**
Qianqian Zhang
qqzhang@yic.ac.cn
Jianmin Zhao
jmzhao@yic.ac.cn

Specialty section:
This article was submitted to Aquatic Physiology, a section of the journal Frontiers in Physiology

Received: *20 June 2018*
Accepted: *06 August 2018*
Published: *21 August 2018*

Citation:
Cao R, Wang D, Wei Q, Wang Q, Yang D, Liu H, Dong Z, Zhang X, Zhang Q and Zhao J (2018) Integrative Biomarker Assessment of the Influence of Saxitoxin on Marine Bivalves: A Comparative Study of the Two Bivalve Species Oysters, Crassostrea gigas, and Scallops, Chlamys farreri. Front. Physiol. 9:1173. doi: 10.3389/fphys.2018.01173

Harmful algae blooms have expanded greatly in recent decades, and their secreted toxins pose a severe threat to human health and marine ecosystems. Saxitoxin (STX) is a main paralytic shellfish poison naturally produced by marine microalgae of the genus *Alexandrium*. Despite numerous studies have assessed the impacts of STX on marine bivalves, comparative *in vivo* study on the toxicity of STX on bivalves with distinct accumulation ability (such as oysters and scallops) has been seldom investigated. The aim of this study was to identify whether distinct sensitivity exists between oysters, *Crassostrea gigas*, and scallops, *Chlamys farreri* under the same amount of STX exposure using multiple biomarker responses. The responses of different biochemical markers including oxidative stress markers (catalase, superoxide dismutase, glutathione *S*-transferase, and lipid peroxidation) and immunotoxicity biomarkers (hemocyte phagocytosis rate, reactive oxidative species production, and DNA damages) were evaluated in bivalves after 12, 48, and 96 h of exposure to STX. The integrated biomarker responses value combined with two-way ANOVA analysis suggested that STX posed slightly severer stress on scallops than oysters for the extended period of time. This study provided preliminary results on the usefulness of a multi-biomarker approach to assess the toxicity associated with STX exposure in marine bivalves.

Keywords: saxitoxin, *Crassostrea gigas*, *Chlamys farreri*, oxidative stress, immunotoxicity

INTRODUCTION

In recent decades, harmful algae blooms (HABs) have increased in frequency and expanded in spatial extent worldwide, which represents a risk for marine ecosystems due to the excreted toxins of HABs (Bricelj and Shumway, 1998; Lagos, 1998; Wang and Wu, 2009; Klemas, 2011; Rodrigues et al., 2012). Marine bivalves constitute a major taxonomic group in estuarine and coastal

regions, and play important roles in community structure and ecosystem functioning (Dumbauld et al., 2009). In the meantime, bivalve species encounter mass mortalities while confronting HABs (Anderson et al., 2000). In recent studies, negative effects on neural function and energy metabolism, combined with behavioral functions such as feeding, valve closure, cardiac activity and respiration, have been observed in bivalve species exposed to harmful marine algae and their released toxins (Perovic et al., 2000; Moroño et al., 2001; Colin and Dam, 2003; Twiner et al., 2004; Estrada et al., 2007; Ramos and Vasconcelos, 2010; Haberkorn et al., 2011; Basti et al., 2016). In addition, some types of marine toxins can lead to reduced growth, reproduction, and survival rates of bivalve species (Blanco et al., 2006; Shumway et al., 2006; Samson et al., 2008).

Saxitoxin is a marine toxin produced in large quantities during the massive episodic proliferation of dinoflagellates of the ubiquitous and hazardous genera *Alexandrium* and *Gymnodinium* (Lagos, 1998; Rodrigues et al., 2012). STX can lead to detrimental effects in marine species and cause paralytic shellfish poisoning (PSP) in humans through trophic transfer along the food chain (Landsberg et al., 2006). STX is known as a neurotoxin that specifically targets voltage-dependent sodium channels and calcium and potassium channels, resulting in neuromuscular paralysis and metabolic stress (Narahashi, 1998; Llewellyn, 2006). In addition to acting as a neurotoxin, STX can also induce severe oxidative stress in vertebrate cell lines (Melegari et al., 2012). As suspension-feeders, bivalves readily concentrate and bioaccumulate toxins by ingesting harmful algae (Bricelj and Shumway, 1998; Estrada et al., 2010). STX may induce declined reproduction and growth rates in marine bivalves, which could be a major cause of mortality in natural populations (Shumway et al., 2006).

In the meantime, STX has also shown to cause various biochemical and cellular alterations in bivalves, including antioxidant responses, immune defenses, and detoxification processes (Mello et al., 2013; Núñez-Acuña et al., 2013; Astuya et al., 2015; Detree et al., 2016; Abi-Khalil et al., 2017). Despite numerous studies have investigated the impacts of STX on marine bivalves, those studies mainly focus on few facets of the toxic effects caused by STX. Due to the variation in the mechanisms involved in the organisms when they are exposed to the pollutant, results interpretation from a combination of the biomarkers has more advantage than interpreting single biomarker results. As results interpretation from multi-biomarker could provide the overall impact of a specific pollutant (i.e., STX), the integrated biomarker responses (IBRs), as an indicator of environment stress, has been widely used in stress responses and ecological risk assessment of marine pollutants including toxins (Beliaeff and Burgeot, 2002; Wang et al., 2011, 2018; Pain-Devin et al., 2014; Yan et al., 2014; Martínez-Ruiz and Martínez-Jerónimo, 2015, 2017; Nogueira et al., 2015; Meng et al., 2016; Teles et al., 2016; Vieira et al., 2016; Devin et al., 2017; Duarte et al., 2017; Li et al., 2017; Luna-Acosta et al., 2017; Sanchez-García et al., 2017; Sobjak et al., 2017; Valerio-García et al., 2017). In addition, the integrated approach combining conventional toxicological bioassays with predictive biomarkers in native mussels might represent an additional tool for Control Agencies and Administrators dealing with management of human risk and economical damage caused by STX secreted by harmful algal blooms (Beliaeff and Burgeot, 2002).

Recently, differences in the sensitivity to environmental stressors, including toxic chemicals, were observed in various bivalve species (Smolowitz and Shumway, 1997; May et al., 2010; Mello et al., 2010; Ballanti et al., 2012; Ivanina and Sokolova, 2013; Carregosa et al., 2014; Götze et al., 2014; Simões et al., 2015; Velez et al., 2016; Breitwieser et al., 2017; Prasetiya et al., 2017), which may be due to the differential adaptation of organisms under certain conditions. It should also be noted that there is great variation between different shellfish species in the phycotoxins accumulation capability (Shumway, 1990). In general, oysters and mussels show rapid detoxification rates in competition with other bivalve species such as scallops (Shumway, 1995; Bricelj and Shumway, 1998). Takata et al. (2008) has found that oysters released 62% of paralytic shellfish toxin (PST) within 48 h of being held in running seawater. In contrast, scallops accumulate toxins in their tissues to a greater extent because of their low metabolic rate (Young-Lai and Aiken, 1986), and toxic retention in scallops can last up to several months from the cessation of the toxic algal bloom (Shumway, 1990). Thus, we suppose that the different accumulation ability between oysters and scallops might lead to distinct sensitivity of these two bivalve species to STX. However, to the best of our knowledge, there is to date no study investigating the different sensitivity between oysters and scallops under STX exposure through using IBRs.

Thus, multi-biomarker responses of oyster, *Crassostrea gigas*, and scallop, *Chlamys farreri*, under the same amount of STX exposure were investigated in this study. Because digestive glands serve as the main organ for toxin accumulation and detoxification (Bricelj and Shumway, 1998), the physiological and biochemical parameters investigated in this study were measured in this tissue. Specifically, the present study evaluated oxidative stress markers [catalase (CAT), superoxide dismutase (SOD), glutathione *S*-transferase (GST), and lipid peroxidation (LPO)], and immunotoxic effects [hemocyte phagocytosis rate, reactive oxidative species (ROS) production, and DNA damages] of adult oysters and scallops after exposure to STX for 12, 48, and 96 h. The mRNA expression of cytochrome P450 (CYP 450) and heat-shock protein-90 (HSP 90) transcripts were also evaluated to determine the stress and detoxification responses of bivalve species in response to STX exposure. Furthermore, the IBR index was applied as a general comparison of the potential toxicity of STX on these two bivalve species.

MATERIALS AND METHODS

Reagent

STX (NRC CRM-STX-f) was obtained from the Institute for Marine Biosciences (National Research Centre, Halifax Regional Municipality, NS, Canada), and stored in the dark at 4°C to avoid photolysis. The stock solution was diluted to 20 μg /L in filter-sterilized seawater (FSSW).

Experimental Conditions

Adult oysters, *C. gigas* (5–7 cm long) and scallops, *C. farreri* (4–6 cm long) were collected from an aquaculture farm located in a relatively pristine area (Yantai, Shandong, China). The oysters and scallops (soft body weight was about 10–20 g for both oysters and scallops) were acclimated for 2 weeks in aerated seawater (salinity 31.2 ± 0.5‰) at a temperature of 15.3 ± 0.2°C. The bivalves were fed daily with commercial algal blends during the acclimation period.

After acclimation, two treatment groups of each bivalve species were established (experimental STX and control group). The exposure concentration of STX (approximately 10–20 μg STX eq. 100 g^{-1} shellfish meat) used in this study is at the range of accumulated level in bivalves collected in HAB outbreak regions (0.2 to 127 × 10^3 μg STX eq. 100 g^{-1} shellfish meat) (Bricelj and Shumway, 1998; Turner et al., 2014), which is far lower than the current EU regulation limit for human consumption of shellfish (80 μg STX eq. 100 g^{-1} shellfish meat). After the preliminary acclimation, the two bivalve species were either STX- or FSSW-injected. In the STX treatment, the oysters and scallops were directly injected with 100 μL of 20 μg/L STX. The organisms from the control group were injected with 100 μL of FSSW. The challenge experiment was carried out in 40 L aquaria with 40 organisms in each aquarium. Three replicate aquaria were used in each treatment (total of 120 individuals in each treatment), with different species separately exposed. After injection, the organisms were put back into their respective aquaria and sampled at 12, 48, and 96 h. No oyster mortality was recorded in any of the treatments during the exposure period.

At each sampling period, the digestive glands from the oysters and scallops were carefully excised and immediately frozen in liquid nitrogen and stored at −80°C for subsequent biomarker analysis. At the same time, the bivalve hemolymph samples were collected at each sampling period for the measurement of hemocyte parameters. For the measurement of oxidative stress biomarkers, a total of 12–18 individual samples (digestive glands) were dissected at each time point and pooled into six independent replicates to minimize biological variation. Also, six independent pooled samples from 12 to 18 individual samples (digestive glands) were used for real-time quantitative PCR analyses.

Oxidative Stress Markers

The samples of the digestive glands were homogenized in phosphate buffer (50 mM potassium dihydrogen phosphate; 50 mM potassium phosphate dibasic; 1 mM EDTA; pH 7.0) and centrifuged at 10,000 *g* for 20 min at 4°C. The supernatants were used to assay the antioxidant enzymatic activities and lipid peroxidation level.

The catalase activity was determined at 240 nm based on the method described by Aebi (1984). The SOD activity was assayed by measuring its ability to inhibit the reduction of nitroblue tetrazolium (NBT), which was determined by the method described by Beauchamp and Fridovich (1971). The GST activity was determined at 340 nm according to Habig et al. (1974). The LPO level was assessed by measuring malondialdehyde (MDA) content as described by Ohkawa et al. (1979). The protein concentration was determined according to the Bradford method (Bradford, 1976), using bovine γ-globuline as a standard. All the measured parameters in this experiment were normalized for the total protein concentration of each sample.

Hemocyte Phagocytosis and Reactive Oxygen Species Production

The hemolymph samples were withdrawn from the adductor muscle of the oysters and scallops using a 21G needle attached to a 1-ml syringe and kept on ice to avoid cell clumping. Six independent pooled samples of hemolymph were prepared using 12–18 individuals to minimize biological variation. The hemolymph sample was filtered through an 80-μm mesh sieve, centrifuged at 4°C, and then washed twice with phosphate-buffered saline (PBS) buffer (137 mM NaCl, 2.7 mM KCl, 8.1 mM Na_2HPO_4, and 1.5 mM KH_2PO_4, pH 7.4). The cells were re-suspended in 500 μL of PBS as working solution. Each pooled sample was divided into two aliquots to measure the phagocytic rate and reactive oxygen species (ROS) production.

The hemocyte phagocytosis was measured according to the method of Delaporte et al. (2003). Briefly, the hemolymph was mixed with 2.3% yellow-green FluoSpheres (YG 2.0 microns, Polyscience, Eppelheim, Germany), and then incubated at 18°C for 1 h in the dark, followed by addition of 6% formalin solution to terminate the reaction. Hemocytes were analyzed by flow cytometry using the FL-1 tunnel. The phagocytic capacities were defined as the percentage of hemocytes that engulfed three or more beads.

The determination of the intracellular ROS content was adapted from Hégaret et al. (2003). Hemocytes were incubated with 5 μL of fluorescent probe DCFH-DA (0.01 mM) at 18°C for 1 h in the dark. A FACSCalibur flow cytometer (Becton-Dickinson, San Diego, CA, United States) equipped with a 488 nm argon laser was used for functional analyses of hemocytes at the end of the incubation. The results were expressed as the geometric mean of the fluorescence [in arbitrary units (AUs)] detected in each hemolymph sample.

Comet Assay

Six independent pooled samples of hemolymph were prepared using 12–18 individuals for the measurement of comet assay in each treatment group. A comet assay was performed following the protocol proposed by Danellakis et al. (2011) with slight modifications. Briefly, 40 μL of hemocyte suspension and 75 μL of 1.0% LMA (low melting point agar) were mixed and pipetted over a slide pre-coated with 2.0% normal melting point agarose. After the agarose was polymerized, the cover slides were removed, and a third layer of LMA was added to the slides. Then, the slides were immersed into ice-cold lysis buffer (2.5 M of NaCl, 100 mM of EDTA, 10 mM of Tris, 1% Triton X-100, 10% DMSO, pH 10.0) for 1 h. At the end of the lysis period, the slides were immersed in an alkaline electrophoresis buffer (300 mM of NaOH and 1 mM of EDTA, pH 13.0) for 20 min at 4°C, and then electrophoresis was run in the same buffer for 10 min at 25 V (300 mA, E = 0.66 V/cm). After electrophoresis, the slides were neutralized in Tris buffer (0.4 M of Tris-HCl, pH 7.5). The DNA

was stained with SYBR Green I (Molecular Probe, Eugene, OR, United States) and examined with a fluorescence microscope (Olympus FV 1000, Tokyo, Japan). For each treatment group, six slides were prepared and 50 nuclei were analyzed per slide. The DNA damage was expressed as the percentage of DNA in the comet tail (% DNA in tail).

Real-Time Quantitative PCR Analyses

The gene HSP 90 and gene CYP 450 were selected in this study for qRT-PCR assay. In addition, the gene EF-1α (AB122066.1) and gene 18S RNA (FJ588641) were used as an internal control in quantitative gene expression studies of selected genes in adult oysters and scallops, respectively. The total RNA was extracted from digestive gland tissue of the oysters and scallops using TRIzol reagent (Invitrogen, United States) following the manufacturer's directions. The cDNA was synthesized from the DNase I-treated (Promega, United States) RNA and then mixed with 10 μL of 2× Master Mix (Applied Biosystems, United States), 4.8 μL DEPC-treated H_2O and 0.4 μL (0.2 μM) of each forward and reverse primer to a final volume of 20 μl. Real-time quantitative PCR (qPCR) was carried out using standard protocols on an Applied Biosystems 7500 fast Real-Time PCR System (Applied Biosystems, United States). The list of primers designed for quantitative RT-PCR is shown in **Table 1**. The specificity of the qPCR products was analyzed by a dissociation curve analysis of the amplification products. The expression level of the selected genes was analyzed by using the comparative $2^{-\Delta\Delta CT}$ method (Livak and Schmittgen, 2001) with target genes normalized with the selected endogenous control.

Integrated Biomarker Response

To integrate all the measured biomarker responses into one general "stress index," the IBR index was calculated as described by Beliaeff and Burgeot (2002) and modified by Sanchez et al. (2013). In this study, the IBR index was applied to assess the potential toxicity of STX to *C. gigas* and *C. farreri* at the three different time points (12, 48, and 96 h). The procedure for calculating the IBR index is briefly described as follows. Individual biomarker data (Xi) were compared to the reference data (X0) and log transformed to yield Yi = log Xi/X0. The general mean (μ) and standard deviation (s) of each biomarker Yi were calculated for all treatments, and Yi was standardized as Zi = (Yi-μ)/s. The biomarker deviation index (A) was calculated by using the mean of the standardized biomarker response (Zi) and the mean of the reference biomarker data (Z0) to yield Ai = Zi-Z0. To obtain IBRv2, the absolute values of A parameters calculated for each biomarker were summed to yield IBRv2 = Σ|A|. Finally, the data for each biomarker were represented in radar type graphs, and the biomarker deviation index (A) was depicted in a star plot indicating the deviation of the investigated biomarker of the STX group compared to the control group. The area above 0 reflects biomarker induction, and the area below 0 indicates biomarker inhibition.

Statistical Analysis

All statistical analyses were performed using SPSS 13.0 statistical software (SPSS 13.0, Chicago, IL, United States). The data were expressed as the means ± standard deviation (SD). A Shapiro–Wilk test was performed to test the normality of the data. Then, the raw data were analyzed statistically by two-way analysis of variance (ANOVA). Significant differences between treatments were assessed by ANOVA combined with least significant difference (LSD) *post hoc* tests. The differences were considered statistically significant at $P < 0.05$; $P < 0.01$ was considered extremely significant.

RESULTS

Oxidative Stress Markers

In oysters, the activity of CAT increased significantly ($P < 0.05$) in digestive glands under STX exposure at 96 h (**Figure 1A**). The SOD activity was one-fifth stimulated under STX exposure at 12 h compared with individuals in control group (**Figure 1B**). However, the SOD activity in STX-exposed oysters decreased significantly ($P < 0.05$) at 96 h compared to individuals at 12 h. Meanwhile, there was a significant increase ($P < 0.05$) in the GST activity and LPO level in the STX-treated group as compared to non-injected individuals at 48 and 96 h, respectively (**Figures 1C,D**).

In scallops, CAT activities in the STX treatment group were significantly ($P < 0.01$) increased compared to the control treatment at all three sampling time points (**Figure 2A**). Concerning the SOD activity, a significant increase ($P < 0.01$) was observed in the STX-treated scallops at 48 h compared to other treatments (**Figure 2B**). In addition, the scallop GST activity was one-sixth stimulated ($P < 0.05$) under STX exposure compared to non-exposed individuals at 96 h (**Figure 2C**). Furthermore, the LPO level increased significantly ($P < 0.01$) in the STX treatment compared to the control group at both 48 and 96 h (**Figure 2D**). Also, significant higher ($P < 0.01$) LPO level was observed in STX-exposed scallops at 48 and 96 h compared to individuals at 12 h (**Figure 2D**). Besides, significant interaction ($P < 0.05$) between STX and time was observed in SOD activity and LPO levels of scallops (**Table 2**).

Hemocytic Parameters

In oyster hemocytes, the phagocytosis rate decreased significantly ($P < 0.01$) in the STX-treated group compared to the non-injected individuals at 12 and 96 h (**Figure 3A**). There was a slight decrease in oyster hemocyte ROS production under STX exposure at 12 and 96 h, but no significant differences were observed between exposed and non-exposed individuals (**Figure 3B**). However, the results of the comet assay showed a significant increase ($P < 0.01$) in DNA damage values in the hemocytes of oysters at 48 and 96 h (**Figure 3C**). Significant ($P < 0.01$) interaction between STX and time was observed in DNA damage of oysters (**Table 2**).

In scallops, there was a significant decrease ($P < 0.05$) in the hemocyte phagocytosis rate in the STX-treated group compared to non-exposed individuals at 48 and 96 h (**Figure 3D**). Under STX exposure, scallop hemocyte phagocytosis rate was reduced by one-third at 48 h compared to individuals at 12 h ($P < 0.05$).

TABLE 1 | Primers used for real-time quantitative PCR analysis.

	Gene name	Forward primer (5′–3′)	Reverse primer (5′–3′)	GenBank accession number
Oysters	EF1α	GAGCGTGAACGTGGTATCAC	ACAGCACAGTCAGCCTGTGA	AB122066.1
	HSP 90	GGTGAATGTTACCAAGGAAGG	GTTACGATACAGCAAGGAGATG	EF687776.1
	CYP 450 2C8	CCCTACGGTCCCTTTCCTAG	GGAGCCCGTGATCAGACTAA	XM_011451620
Scallops	18S RNA	CGTTCTTAGTTGGTGGAGCG	AACGCCACTTGTCCCTCTAA	FJ588641
	HSP 90	AACACAGTCAGTTCATCGGCTAC	TCTTCTACCTTTGGCTTGTCATC	AY362761.1
	CYP 450 family 4	TCGAGGGCGTCGTAATCC	TCTTGGTCCTGCTGAAAATGG	FJ588641

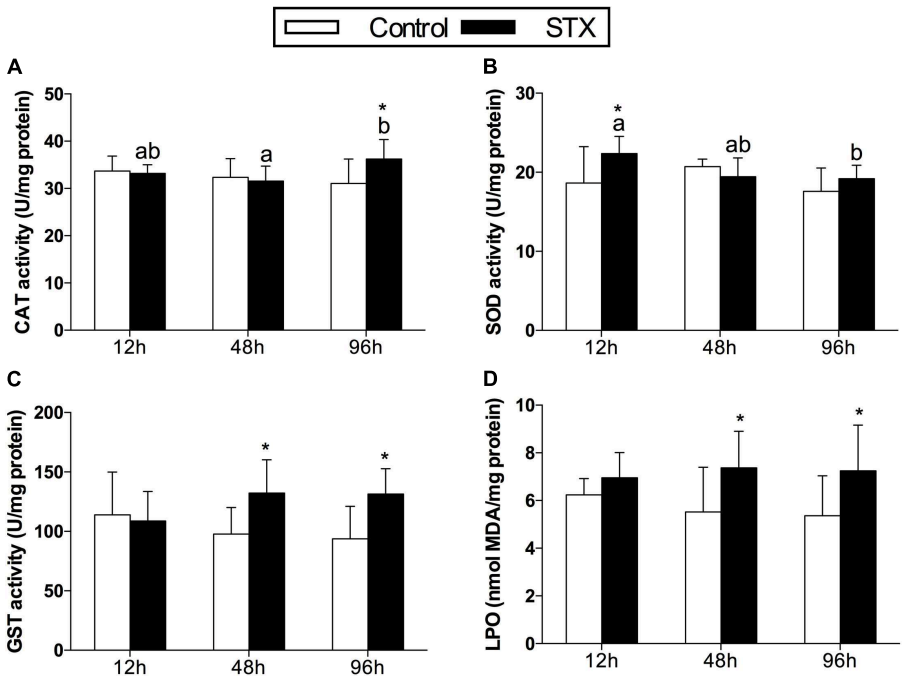

FIGURE 1 | Antioxidant enzyme activities and LPO (lipid peroxidation) level in the digestive glands of *Crassostrea gigas* post-STX exposure. **(A)** CAT (catalase); **(B)** SOD (superoxide dismutase); **(C)** GST (glutathione *S*-transferase); **(D)** LPO. Each bar represents the mean ± SD ($n = 6$). Different letters indicate significant differences among treatments at the same concentration of STX exposure ($P < 0.05$). Asterisks indicate significant differences between the values for the control and STX-exposed groups (*$P < 0.05$, **$P < 0.01$).

Moreover, an extremely significant ($P < 0.01$) increase in ROS production was observed in the STX treatment group at both 48 and 96 h (**Figure 3E**). Furthermore, the results of the comet assay revealed a one increase ($P < 0.01$) in DNA strand breaks in the scallop hemocytes under STX exposure at 96 h (**Figure 3F**). In addition, there is significant interaction ($P < 0.05$) between STX and time on all the immune parameters measured in scallop hemocytes (**Table 2**).

Gene Expression of HSP 90 and CYP 450

In oysters, the mRNA expression of HSP 90 was significantly stimulated ($P < 0.05$) in the STX-treated group compared to non-exposed individuals at 48 and 96 h (**Figure 4A**). Besides, significant elevation in the mRNA expression of HSP 90 was observed as the exposure time increases. In STX-exposed oyster hemocytes HSP 90 transcript levels at 96 h were two-third fold higher than that at 48 h. Additionally, significantly ($P < 0.05$) stimulated expression of a CYP 450 gene (CYP 450 2C8) was observed in the oyster digestive glands after 48 h of STX exposure (**Figure 4B**). Meanwhile, there is significant interaction ($P < 0.05$) between STX and time on the mRNA expression of HSP 90 and CYP 450 2C8 in oysters (**Table 2**).

In scallops, there was a threefold increase ($P < 0.05$) in the mRNA expression of HSP 90 under STX exposure at 96 h compared to non-exposed individuals at this time point (**Figure 4C**). In addition, the mRNA expression of a CYP 450 gene (CYP 450 family 4) was increased significantly ($P < 0.01$) in the STX treatment group compared to the control group after 12 and 96 h of exposure (**Figure 4D**). In STX-exposed scallops, significant decrease ($P < 0.05$) in the mRNA expression of CYP 450 family 4 was observed at 48 h compared with individuals at 12 and 96 h. Meanwhile, mRNA expression of CYP 450 family 4 was twofold higher ($P < 0.05$) in STX-exposed scallops at 96 h than STX-exposed individuals at 12 h. Significant ($P < 0.01$) interaction between STX and time was observed in mRNA expression of CYP 450 family 4 of scallops (**Table 2**).

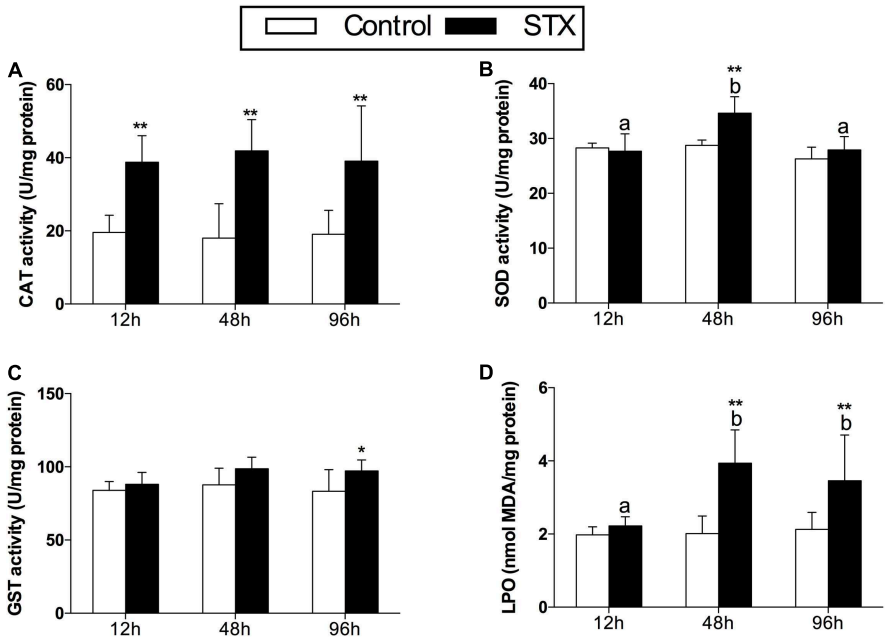

FIGURE 2 | Antioxidant enzyme activities and LPO (lipid peroxidation) level in the digestive glands of *Chlamys farreri* post-STX exposure. **(A)** CAT (catalase); **(B)** SOD (superoxide dismutase); **(C)** GST (glutathione *S*-transferase); **(D)** LPO. Each bar represents the mean ± SD ($n = 6$). Different letters indicate significant differences between timepoints at the same treatment conditions ($P < 0.05$). Asterisks indicate significant differences between the values for the control and STX-exposed groups ($^*P < 0.05$, $^{**}P < 0.01$).

Integrated Biomarker Response (IBR)

The transformed data of all the biomarkers at the different time points are presented as star plots in **Figure 5**. The IBR index was also calculated for each time point and showed differences in the STX-treated group in relation to the baseline (**Figure 6**). The value of the IBR index was increased with prolonged exposure to STX in the STX-treated oysters, with the highest value observed at 96 h (26.4, **Figure 6**), indicating the induction of the antioxidant enzyme responses, cellular damage, hemocyte genotoxicity, and heat-shock protein expression and the inhibition of the hemocyte phagocytosis rate and ROS production (**Figure 5C**). Similarly, the IBR index at 96 h in the STX-treated scallops was the highest among all three time points (29.2, **Figure 6**). Here, we observed stimulated antioxidant enzyme responses, cellular damage, hemocyte ROS production and genotoxicity and increased mRNA expression of HSP 90 and CYP 450 (**Figure 5F**). Additionally, the hemocyte phagocytosis rate was greatly inhibited in scallops under STX exposure (**Figure 5F**).

Meanwhile, at 48 and 96 h, the IBR index was slightly higher in scallops (10.5, 26.4) than oysters (12.5, 29.2), suggesting scallops were under severer stress than oysters in response to the same amount of STX exposure. Correspondingly, from our star graph (**Figure 5**), higher IBR value was observed in scallops than oysters at 48 h, which was associated with higher stimulation in CAT activity, SOD activity and ROS production in scallops compared with oysters. In addition, higher stimulation in ROS production and CYP 450 expression in scallops compared with oysters was observed at 96 h, which was associated with higher IBR value observed in this species than oysters at this time points.

DISCUSSION

Harmful algae blooms have been reported with increasing frequency worldwide due to climate change and anthropogenic activities (Heisler et al., 2008; Wang and Wu, 2009; Lapointe et al., 2015; Visser et al., 2016). Thus, the toxic mechanisms of marine biotoxins and more accurate risk evaluations associated with marine biotoxins have received increasing attention from scientific community (Accoroni et al., 2011; Munday, 2011; Trainer et al., 2014).

Recent laboratory studies have found that the toxic species associated with HABs and their secreted toxins could alter antioxidant responses and lead to cellular damage in marine organisms (Estrada et al., 2007; Amado and Monserrat, 2010; Fabioux et al., 2015; Kim et al., 2017). For example, PST-exposed clam *Ruditapes philippinarum* displayed significantly altered antioxidant enzyme activity and increased LPO levels (Choi et al., 2006). Previous *in vitro* studies on various cell lines also indicated oxidative stress induction by STX (Melegari et al., 2012). The increased oxidative stress on aquatic organisms caused by STX is expected because ROS can be produced during the process of xenobiotic detoxification (Kelly et al., 1998; Vinothini and Nagini, 2010).

Oxidative stress in organisms is mainly caused by excessive ROS production (Lushchak, 2011; Melegari et al., 2012; Zhang

et al., 2013; Wang et al., 2017). High levels of ROS can be toxic to important cellular components including lipids, DNA and protein, leading to cell injury and even death in aquatic organisms (Lushchak, 2011). A wide array of low molecular weight scavengers and antioxidant enzymes function to prevent the adverse effects of ROS and maintain cellular redox homeostasis (Regoli and Giuliani, 2014). As an important antioxidant enzyme, CAT prevents the formation of excessive H_2O_2 through decomposing H_2O_2 once it is formed (Halliwell, 1974), while SOD functions as an antioxidant enzyme by catalyzing excess O_2^- radicals into H_2O_2 and O_2 (Halliwell, 1974). As a phase II detoxification enzyme, GST protects cells and tissues against oxidative stress by catalyzing the conjugation of the reduced form of glutathione to various xenobiotic substrates (Hayes and Strange, 1995). The above-mentioned antioxidant enzyme activities alteration has been widely used as biochemical biomarkers for oxidative stress caused by environmental stressors (Matozzo et al., 2013; Nogueira et al., 2015; Freitas et al., 2017). Based on this study, antioxidant enzymes (CAT, SOD, and GST) were generally stimulated in the digestive glands of both oysters and scallops, indicating that the antioxidant system was activated in response to the induction of oxidative stress caused by STX exposure. Correspondingly, increased CAT activity was also found in mussels, *Mytilus edulis,* exposed to the toxic cyanobacterium *Nodularia spumigena* (Kankaanpää et al., 2007). These authors suggested that the detoxification reactions

TABLE 2 | Two-way ANOVA: effects of STX exposure and time on the physiological parameters and gene expression in oyster *C. gigas* and scallop *C. farreri*.

			Factors/interaction		
			STX	**Time**	**STX × Time**
Oysters	Antioxidant enzymes activities	CAT	$F(1,30) = 0.98$	$F(2,30) = 0.74$	$F(2,30) = 2.45$
			$P = 0.330$	$P = 0.484$	$P = 0.104$
		SOD	$F(1,30) = 2.24$	$F(2,30) = 2.08$	$F(2,30) = 2.60$
			$P = 0.145$	$P = 0.143$	$P = 0.091$
		GST	**$F(1,30) = 6.14$**	$F(2,30) = 0.06$	$F(2,30) = 2.32$
			$P = 0.019$	$P = 0.943$	$P = 0.116$
		LPO	**$F(1,30) = 8.58$**	$F(2,30) = 0.11$	$F(2,30) = 0.57$
			$P = 0.006$	$P = 0.896$	$P = 0.570$
	Immune-related parameters	Phagocytosis	**$F(1,30) = 20.28$**	$F(2,30) = 1.56$	$F(2,30) = 0.76$
			$P < 0.001$	$P = 0.231$	$P = 0.477$
		ROS	$F(1,30) = 1.13$	$F(2,30) = 0.89$	$F(2,30) = 0.53$
			$P = 0.296$	$P = 0.422$	$P = 0.593$
		DNA damage	**$F(1,30) = 70.54$**	**$F(2,30) = 46.34$**	**$F(2,30) = 35.57$**
			$P < 0.001$	**$P < 0.001$**	**$P < 0.001$**
	Gene expression	HSP 90	**$F(1,30) = 11.46$**	**$F(2,30) = 17.50$**	**$F(2,30) = 15.48$**
			$P = 0.002$	**$P < 0.001$**	**$P < 0.001$**
		CYP 450	$F(1,30) = 0.81$	$F(2,30) = 3.10$	**$F(2,30) = 3.50$**
			$P = 0.375$	$P = 0.060$	**$P = 0.044$**
Scallops	Antioxidant enzymes activities	CAT	**$F(1,30) = 46.91$**	$F(2,30) = 0.032$	$F(2,30) = 0.22$
			$P < 0.001$	$P = 0.968$	$P = 0.807$
		SOD	**$F(1,30) = 9.20$**	**$F(2,30) = 13.61$**	**$F(2,30) = 6.22$**
			$P = 0.005$	**$P < 0.001$**	**$P = 0.006$**
		GST	**$F(1,30) = 8.87$**	$F(2,30) = 1.65$	$F(2,30) = 0.80$
			$P = 0.006$	$P = 0.209$	$P = 0.459$
		LPO	**$F(1,30) = 24.98$**	**$F(2,30) = 5.24$**	**$F(2,30) = 4.45$**
			$P < 0.001$	**$P = 0.011$**	**$P = 0.020$**
	Immune-related parameters	Phagocytosis	**$F(1,30) = 3.68$**	$F(2,30) = 2.01$	**$F(2,30) = 6.28$**
			$P = 0.065$	$P = 0.151$	**$P = 0.005$**
		ROS	**$F(1,30) = 17.70$**	**$F(2,30) = 20.20$**	**$F(2,30) = 3.58$**
			$P < 0.001$	**$P < 0.001$**	**$P = 0.042$**
		DNA damage	**$F(1,30) = 70.54$**	**$F(2,30) = 46.34$**	**$F(2,30) = 35.57$**
			$P < 0.001$	**$P < 0.001$**	**$P < 0.001$**
	Gene expression	HSP 90	$F(1,30) = 3.90$	$F(2,30) = 1.06$	$F(2,30) = 0.87$
			$P = 0.058$	$P = 0.360$	$P = 0.428$
		CYP 450	**$F(1,30) = 28.25$**	**$F(2,30) = 15.07$**	**$F(2,30) = 13.79$**
			$P < 0.001$	**$P < 0.001$**	**$P < 0.001$**

Significant effects are highlighted in bold.

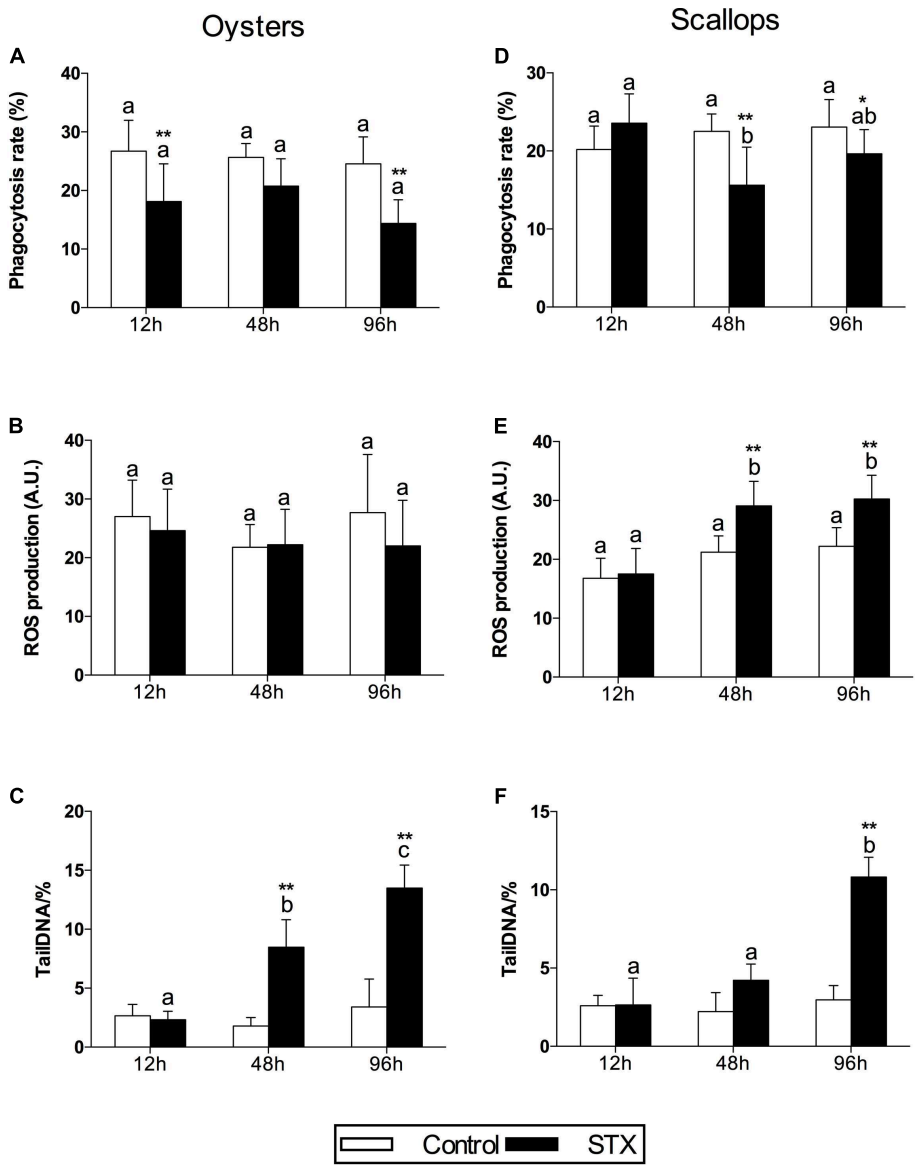

FIGURE 3 | Immunotoxicity biomarkers in hemocytes of *C. gigas* **(A–C)** and *C. farreri* **(D–F)** exposed to STX for 12, 48, and 96 h. **(A,D)** Hemocyte phagocytosis rate, **(B,E)** ROS (reactive oxidative species) production, **(C,F)** DNA damage. Each bar represents the mean ± SD ($n = 6$). Different letters indicate significant differences between timepoints at the same treatment conditions ($P < 0.05$). Asterisks indicate significant differences between the values for the control and STX-exposed groups ($^*P < 0.05$, $^{**}P < 0.01$).

could be responsible for the increased production of oxidative species. Meanwhile, the earlier stimulation of CAT activity in scallops compared with oysters might indicated higher sensitivity of scallops to STX toxicity. In addition, compared with the unchanged SOD activity in oysters, the elevated SOD activity in scallops at 48 h indicated that this taxa was under more severe oxidative stress at this time point.

However, the overwhelmed antioxidant system resulting from excessive ROS production could lead to LPO (Sevgiler et al., 2004). Elevated LPO level is a major indicator of cellular oxidative damage in organisms and is a major contributor to the loss of cell function under environmental perturbations, including toxins released by harmful algae (Moreira et al., 2016; Ricevuto et al., 2016; Valerio-García et al., 2017). Based on our results, cellular damage, as indicated by lipid peroxidation, increased significantly in both oysters and scallops after 48 and 96 h of exposure to STX. It seems that, although the antioxidant mechanisms were activated, they could not efficiently eliminate the excessive ROS, resulting in cellular damage in both bivalve species. Meanwhile, the baseline levels of LPO are threefold higher in oysters than in scallops. The differences in baseline LPO levels between the two studied species may reflect adaptations of the intertidal-dwelling oysters to higher LPO baseline levels, compared to the subtidal species such as scallops.

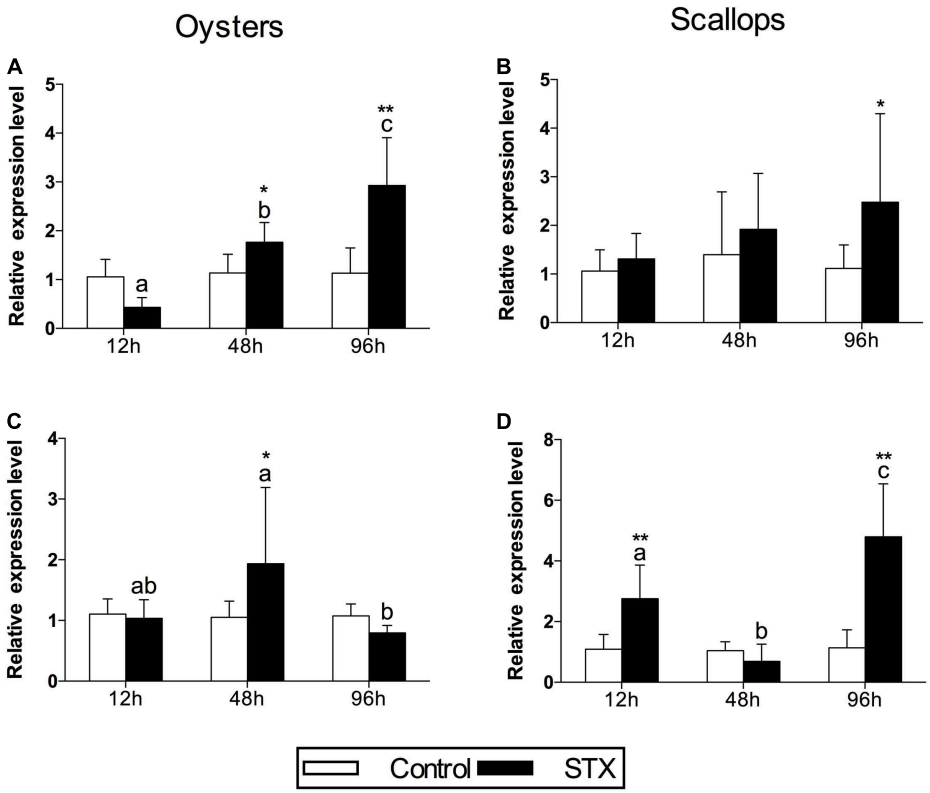

FIGURE 4 | The mRNA expression profiles of the genes HSP 90 and CYP 450 in the digestive glands of oysters and scallops post-STX exposure. **(A,C)** HSP 90, **(B)** CYP 450 2C8, **(D)** CYP 450 family 4. Each bar represents the mean ± SD ($n = 6$). Different letters indicate significant differences between timepoints at the same treatment conditions ($P < 0.05$). Asterisks indicate significant differences between the values for the control and STX-exposed groups ($^*P < 0.05$, $^{**}P < 0.01$).

In addition, time posed significant effects on the elevation of the scallop LPO level, which might suggest that STX pose severer oxidative damage to scallops than oysters with prolonged time exposure.

Additionally, bivalves hemocytes function as the first line of immune responses including phagocytosis, ROS production, opsonization, nodule formation and the release of immune mediators (Thomas, 1996). Inhibited phagocytosis rate and increased DNA damage of oyster and scallop hemocytes were observed in this study. Similarly, phagocytosis inhibition and genotoxicity of STX on oyster hemocytes has been observed in previous *in vitro* study (Mello et al., 2013; Abi-Khalil et al., 2017). The suppressed immune system in two bivalve species, as indicated by the inhibition of phagocytosis rate and induction of DNA damage in STX-treated oyster and scallop hemocytes, might sensitize them to future pathogen infection. In this study, STX posed no significant effect on ROS production in oyster hemocytes. Similarly, Mello et al. (2013) has found that *Alexandrium minutum* and STX could negatively affect immnunocompetence of *C. gigas* by decreasing the phagocytosis and ROS production of *C. gigas* hemocyte. However, significant stimulation of ROS production was observed in STX-exposed scallop at 48 and 96 h, which might suggest higher toxicity posed by STX on scallops than oysters with prolonged exposure. In addition, excessive ROS production in hemocytes could pose severe oxidative stress to scallops, and ROS are highly reactive molecules known to interact with sulfhydryl groups on proteins. Previous study has suggested that ROS production might be associated with the actin filament disruption in bivalve hemocytes treated with benzo(a)pyrene (Gómez-Mendikute et al., 2002). Since a bivalve's ability to mount an efficient immune response is reliant upon the integrity and efficient functioning of hemocytes, thus, the disturbed hemocyte actin filament caused by ROS production might be partially associated with the immune suppression effect caused by STX in scallops. In addition, Abi-Khalil et al. (2017) has discovered that PSTs including STX were shown to be directly responsible for inducing apoptosis in hemocytes, a process dependent on caspase activation and independent of ROS production. Thus, we suppose that the increased DNA damage observed in oysters could be directly caused by STX toxicity rather than excessive ROS, as the ROS level in oyster hemocytes showed no change under STX exposure.

The proteins of the cytochrome P450 (CYP 450) family are known to be involved in the biotransformation of various xenobiotics in aquatic invertebrates (Snyder, 2000), and their expression was found to be disturbed in bivalve species exposed to HABs and/or their associated toxins (Mello et al., 2012, 2013; García-Lagunas et al., 2013; Huang et al., 2015). Heat shock proteins (HSPs) are molecular chaperones that assist in the refolding of stress-damaged proteins and are usually

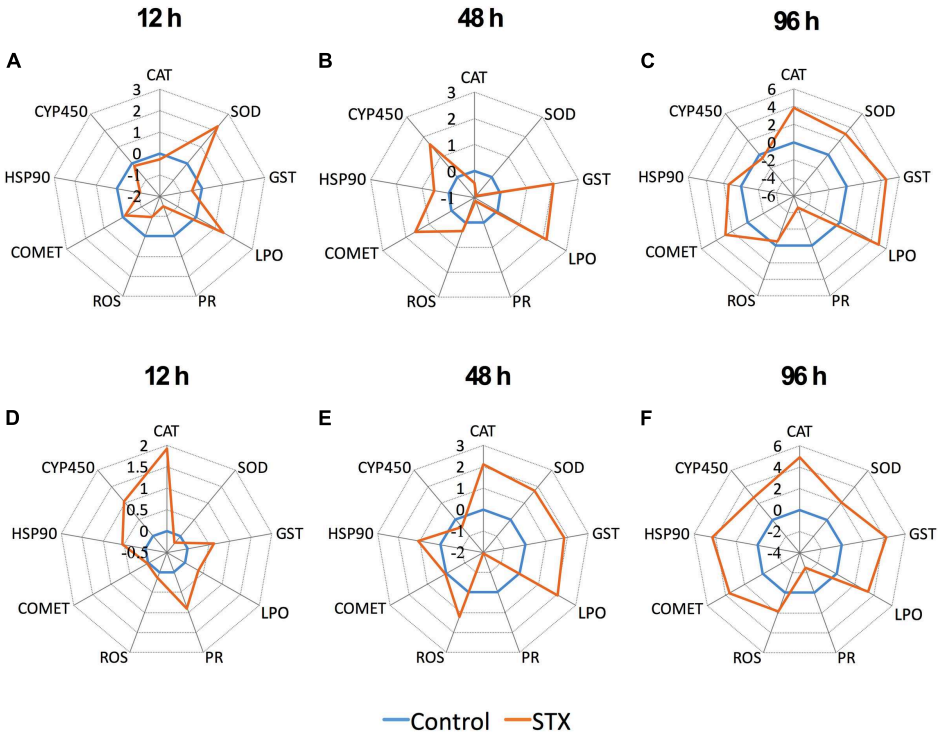

FIGURE 5 | Biomarker star plots of multiple biomarker responses of *C. gigas* **(A–C)** and *C. farreri* **(D–F)** exposed to STX for 12, 48, and 96 h. CAT, catalase; SOD, superoxide dismutase; GST, glutathione *S*-transferase; LPO, lipid peroxidation; PR, hemocyte phagocytosis rate; ROS, reactive oxidative species production in hemocytes; COMET, hemocyte DNA damage; HSP 90, heat-shock protein-90; CYP 450, cytochrome P450.

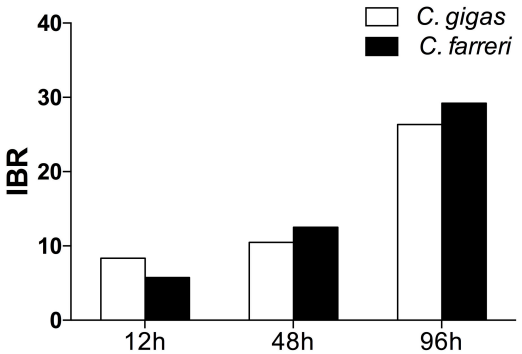

FIGURE 6 | Calculated IBR index using the molecular and biochemical biomarkers measured in *C. gigas* and *C. farreri* after exposure to STX for 12, 48, and 96 h.

induced under stressful conditions (Moraga et al., 2005; Dong et al., 2014; Alaraby et al., 2015). The increased expression of HSP transcripts has been reported in a variety of marine organisms exposed to toxins excreted by harmful algae (da Silva et al., 2011; El Golli-Bennour and Bacha, 2011; Jiang et al., 2012; Mello et al., 2012; Núñez-Acuña et al., 2013). Correspondingly, the expression of HSP 90 and CYP 450 transcripts was upregulated in the digestive glands of oysters and scallops in the present study, indicating positive regulation by these two bivalves as part of stress responses and detoxification processes following STX exposure. However, stimulated stress responses and detoxification processes were not enough to protect the cells of the digestive glands from the toxicity caused by accumulated STX, as indicated by the increased oxidative stress and immunotoxicity in both bivalve species. The expression of HSP 90 showed similar pattern in oysters and scallops. Meanwhile, significant stimulation in the expression of a CYP 450 gene (CYP 450 family 4) were observed in STX-exposed scallops at 96 h, which was in contrast with expression of the CYP 450 gene (CYP 450 2C8) in STX-exposed oysters (showing no alteration at this timepoint). We suppose that higher STX might be accumulated in scallops than oysters at this time point, thus more CYP 450 needs to be synthesized to fulfill the complication of STX detoxification.

In this study, the IBR index was applied to compare the overall stress of STX on oysters, *C. gigas*, and scallops, *C. farreri*. This approach provides a simple tool for the visualization of biological effects by integrating different biomarker signals (Beliaeff and Burgeot, 2002). The IBR analysis showed a general stimulation of antioxidant enzyme activity, cellular damage, and immunotoxicity in the two bivalve species under STX exposure at all three investigated time points (**Figure 6**). In general, IBR index increased with extended time exposure to STX in both oysters and scallops. The highest IBR index was observed at 96 h, indicating the highest stress level at this time point. However, slightly higher IBR value was observed in STX-exposed scallops

than STX-exposed oysters at both 48 and 96 h, suggesting higher stress level in scallops than oysters with prolonged exposure to STX.

Also, from our two-way ANOVA analysis results, we observed that time pose much more significant effects on scallops than oysters. Meanwhile, the significant interacted effects of STX and time on scallops were observed in most of the tested biomarkers, while only three parameters (hemocyte DNA damage, mRNA expression of HSP 90 and CYP 450) tested in oysters observed the significant interacted effects of STX and time. From both our IBR results and two-way ANOVA analysis, we conclude that STX pose severer stress on scallops than oysters as the exposure time increases. The much lower toxin detoxification ability of scallops compared with oysters, which has been investigated in previous literatures (Shumway, 1990, 1995; Bricelj and Shumway, 1998; Takata et al., 2008), might be associate with the higher sensitivity of this species than oysters in response to STX as indicated in this study. Furthermore, the different resistance capabilities between oysters and scallops could also attribute to their distinct habitats. Living in estuarine and intertidal regions, oysters are confronted with harsh and dynamic environmental stresses, including toxins excreted by harmful algae (Zhang et al., 2016). Hence, the high level of resistance and adaptive recovery of this species in response to STX acidification toxicity is expected. However, scallops live in subtidal conditions, with low levels of environmental perturbations, which could explain the high sensitivity of this species to STX toxicity, regardless of the distinct accumulation and detoxification ability between these two investigate species under STX exposure.

In the present paper, while not being lethal to oysters and scallops, STX exposure induced oxidative stress, cellular damage, and immunotoxicity indiscriminately in both oysters and scallops. Although the exposure time in this experiment is very short, the present study clearly suggested slightly higher sensitivity of scallops than oysters under exposure to the common level of STX. Thus, toxicity assessment on different bivalve species especially with distinct phycotoxin accumulation capability needs to be tested in order to better predict the ecological risk of toxins excreted by harmful algal. Meanwhile, longer time exposure to STX by oysters and scallops are required to be investigated in our future study to test whether significant difference in sensitivity to STX exists between these two bivalve species. In conclusion, the overall results of this study highlighted that the multi-biomarker analysis in bivalves might be profitably considered as an integrative tool for assessing the impact of STX, therefore should be considered in the future assessment of the environment risks of STX released during harmful algal blooms.

ETHICS STATEMENT

All organisms used for this research were marine invertebrate bivalves and as such were not subject to Institutional Animal Care and Use Committee (IACUC; China) oversight. However, care was taken in designing experiments to limit and reduce the number animals sacrificed during the course of research. All organisms prior to and after experimentation were adequately fed, maintained at optimal densities, and routinely cared for.

AUTHOR CONTRIBUTIONS

RC, DW, QyW, QW, DY, HL, ZD, XZ, and QZ performed the experiments. RC, QZ, and JZ conceived and designed the experimental plan, analyzed the data, and drafted the manuscript.

FUNDING

This research was supported by grants from the Strategic Priority Research Program of the Chinese Academy of Sciences (Grant No. XDA11020305), the Key Research Program of the Chinese Academy of Sciences (Grant No. KZZDEW-14), the Informatization Engineering of Scientific Research (Grant No. XXH13506-305), the Instrument Developing Project of the Chinese Academy of Sciences (Grant No. YJKYYQ20170071), and the Youth Innovation Promotion Association, CAS (Grant No. 2016196).

REFERENCES

Abi-Khalil, C., Finkelstein, D. S., Conejero, G., Du Bois, J., Destoumieux-Garzon, D., and Rolland, J. L. (2017). The paralytic shellfish toxin, saxitoxin, enters the cytoplasm and induces apoptosis of oyster immune cells through a caspase-dependent pathway. *Aquat. Toxicol.* 190, 133–141. doi: 10.1016/j.aquatox.2017.07.001

Accoroni, S., Romagnoli, T., Colombo, F., Pennesi, C., Di Camillo, C. G., Marini, M., et al. (2011). *Ostreopsis* cf. *ovata* bloom in the northern Adriatic Sea during summer 2009: ecology, molecular characterization and toxin profile. *Mar. Pollut. Bull.* 62, 2512–2519. doi: 10.1016/j.marpolbul.2011.08.003

Aebi, H. (1984). [13] Catalase in vitro. *Methods Enzymol.* 105, 121–126. doi: 10.1016/S0076-6879(84)05016-3

Alaraby, M., Demir, E., Hernández, A., and Marcos, R. (2015). Assessing potential harmful effects of CdSe quantum dots by using *Drosophila melanogaster* as in vivo model. *Sci. Total Environ.* 53, 66–75. doi: 10.1016/j.scitotenv.2015.05.069

Amado, L. L., and Monserrat, J. M. (2010). Oxidative stress generation by microcystins in aquatic animals: why and how. *Environ. Int.* 36, 226–235. doi: 10.1016/j.envint.2009.10.010

Anderson, D. M., Hoagland, P., Kaoru, Y., and White, A. W. (2000). *Estimated Annual Economic Impacts from Harmful Algal Blooms (HABs) in the United States (No. WHOI-2000-11)*. Woods Hole, MA: Woods Hole Oceanographic Institution.

Astuya, A., Carrera, C., Ulloa, V., Aballay, A., Núñez-Acuña, G., Hégaret, H., et al. (2015). Saxitoxin modulates immunological parameters and gene transcription in *Mytilus chilensis* hemocytes. *Int. J. Mol. Sci.* 16, 15235–15250. doi: 10.3390/ijms160715235

Ballanti, L. A., Tullis, A., and Ward, P. D. (2012). Comparison of oxygen consumption by *Terebratalia transversa* (Brachiopoda) and two species of pteriomorph bivalve molluscs: implications for surviving mass extinctions. *Paleobiology* 38, 525–537. doi: 10.1666/11020.1

Basti, L., Nagai, S., Watanabe, S., Oda, T., and Tanaka, Y. (2016). Neuroenzymatic activity and physiological energetics in Manila clam, *Ruditapes philippinarum*,

during short-term sublethal exposure to harmful alga, *Heterocapsa circularisquama*. *Aquat. Toxicol.* 176, 76–87. doi: 10.1016/j.aquatox.2016.04.011

Beauchamp, C., and Fridovich, I. (1971). Superoxide dismutase: improved assays and an assay applicable to acrylamide gels. *Anal. Biochem.* 44, 276–287. doi: 10.1016/0003-2697(71)90370-8

Beliaeff, B., and Burgeot, T. (2002). Integrated biomarker response: a useful tool for ecological risk assessment. *Environ. Toxicol. Chem.* 21, 1316–1322. doi: 10.1002/etc.5620210629

Blanco, J., Cano, J., Mariño, M., del, C., and Campos, M. J. (2006). Effect of phytoplankton containing paralytic shellfish and amnesic shellfish toxins on the culture of the king scallop *Pecten maximus* in Málaga (SE Spain). *Aquat. Living Resour.* 19, 267–273. doi: 10.1051/alr:2006027

Bradford, M. M. (1976). A rapid and sensitive method for the quantitation of microgram quantities of protein utilizing the principle of protein-dye binding. *Anal. Biochem.* 72, 248–254. doi: 10.1016/0003-2697(76)90527-3

Breitwieser, M., Viricel, A., Churlaud, C., Guillot, B., Martin, E., Stenger, P.-L., et al. (2017). First data on three bivalve species exposed to an intra-harbour polymetallic contamination (La Rochelle, France). *Comp. Biochem. Physiol. C Toxicol. Pharmacol.* 199, 28–37. doi: 10.1016/j.cbpc.2017.02.006

Bricelj, V. M., and Shumway, S. E. (1998). Paralytic shellfish toxins in bivalve molluscs: occurrence, transfer kinetics, and biotransformation. *Rev. Fish. Sci.* 6, 315–383. doi: 10.1016/j.aquatox.2013.11.011

Carregosa, V., Velez, C., Soares, A. M. V. M., Figueira, E., and Freitas, R. (2014). Physiological and biochemical responses of three Veneridae clams exposed to salinity changes. *Comp. Biochem. Physiol. B Biochem. Mol. Biol.* 17, 1–9. doi: 10.1016/j.cbpb.2014.08.001

Choi, N. M.-C., Yeung, L., Siu, W. H. L., So, I. M. K., Jack, R. W., Hsieh, D. P. H., et al. (2006). Relationships between tissue concentrations of paralytic shellfish toxins and antioxidative responses of clams, *Ruditapes philippinarum*. *Mar. Pollut. Bull.* 52, 572–597. doi: 10.1016/j.marpolbul.2006.01.009

Colin, S. P., and Dam, H. G. (2003). Effects of the toxic dinoflagellate *Alexandrium fundyense* on the copepod *Acartia hudsonica*: a test of the mechanisms that reduce ingestion rates. *Mar. Ecol. Prog. Ser.* 248, 55–65. doi: 10.3354/meps248055

da Silva, C. A., Oba, E. T., Ramsdorf, W. A., Magalhães, V. F., Cestari, M. M., Oliveira Ribeiro, C. A., et al. (2011). First report about saxitoxins in freshwater fish *Hoplias malabaricus* through trophic exposure. *Toxicon* 57, 141–147. doi: 10.1016/j.toxicon.2010.10.015

Danellakis, D., Ntaikou, I., Kornaros, M., and Dailianis, S. (2011). Olive oil mill wastewater toxicity in the marine environment: alterations of stress indices in tissues of mussel *Mytilus galloprovincialis*. *Aquat. Toxicol.* 101, 358–366. doi: 10.1016/j.aquatox.2010.11.015

Delaporte, M., Soudant, P., Moal, J., Lambert, C., Quéré, C., Miner, P., et al. (2003). Effect of a mono-specific algal diet on immune functions in two bivalve species – *Crassostrea gigas* and *Ruditapes philippinarum*. *J. Exp. Biol.* 206, 3053–3064. doi: 10.1242/jeb.00518

Detree, C., Núñez-Acuña, G., Roberts, S., and Gallardo-Escárate, C. (2016). Uncovering the complex transcriptome response of *Mytilus chilensis* against saxitoxin: implications of harmful algal blooms on mussel populations. *PLoS One* 11:e0165231. doi: 10.1371/journal.pone.0165231

Devin, S., Buffet, P. E., Châtel, A., Perrein-Ettajani, H., Valsami-Jones, E., and Mouneyrac, C. (2017). The integrated biomarker response: a suitable tool to evaluate toxicity of metal-based nanoparticles. *Nanotoxicology* 11, 1–6. doi: 10.1080/17435390.2016.1269374

Dong, Y., Han, G., and Huang, X. (2014). Stress modulation of cellular metabolic sensors: interaction of stress from temperature and rainfall on the intertidal limpet *Cellana toreuma*. *Mol. Ecol.* 23, 4541–4554. doi: 10.1111/mec.12882

Duarte, I. A., Reis-Santos, P., França, S., Cabral, H., and Fonseca, V. F. (2017). Biomarker responses to environmental contamination in estuaries: a comparative multi-taxa approach. *Aquat. Toxicol.* 189, 31–41. doi: 10.1016/j.aquatox.2017.05.010

Dumbauld, B. R., Ruesink, J. L., and Rumrill, S. S. (2009). The ecological role of bivalve shellfish aquaculture in the estuarine environment: a review with application to oyster and clam culture in West Coast (USA) estuaries. *Aquaculture* 290, 196–223. doi: 10.1016/j.aquaculture.2009.02.033

El Golli-Bennour, E., and Bacha, H. (2011). Hsp70 expression as biomarkers of oxidative stress: mycotoxins' exploration. *Toxicology* 287, 1–7. doi: 10.1016/j.tox.2011.06.002

Estrada, N., de Jesús Romero, M., Campa-Córdova, A., Luna, A., and Ascencio, F. (2007). Effects of the toxic dinoflagellate, *Gymnodinium catenatum* on hydrolytic and antioxidant enzymes, in tissues of the giant lions-paw scallop *Nodipecten subnodosus*. *Comp. Biochem. Physiol. C Toxicol. Pharmacol.* 146, 502–510. doi: 10.1016/j.cbpc.2007.06.003

Estrada, N., Rodríguez-Jaramillo, C., Contreras, G., and Ascencio, F. (2010). Effects of induced paralysis on hemocytes and tissues of the giant lions-paw scallop by paralyzing shellfish poison. *Mar. Biol.* 157, 1401–1415. doi: 10.1007/s00227-010-1418-4

Fabioux, C., Sulistiyani, Y., Haberkorn, H., Hégaret, H., Amzil, Z., and Soudant, P. (2015). Exposure to toxic *Alexandrium minutum* activates the detoxifying and antioxidant systems in gills of the oyster *Crassostrea gigas*. *Harmful Algae* 48, 55–62. doi: 10.1016/j.hal.2015.07.003

Freitas, J. S., Teresa, F. B., and de Almeida, E. A. (2017). Influence of temperature on the antioxidant responses and lipid peroxidation of two species of tadpoles (*Rhinella schneideri* and *Physalaemus nattereri*) exposed to the herbicide sulfentrazone (Boral 500SC®). *Comp. Biochem. Physiol. C Toxicol. Pharmacol.* 197, 32–44. doi: 10.1016/j.cbpc.2017.04.005

García-Lagunas, N., Romero-Geraldo, R., and Hernández-Saavedra, N. Y. (2013). Genomics study of the exposure effect of *Gymnodinium catenatum*, a paralyzing toxin producer, on *Crassostrea gigas*' defense system and detoxification genes. *PLoS One* 8:e72323. doi: 10.1371/journal.pone.0072323

Gómez-Mendikute, A., Etxeberria, A., Olabarrieta, I., and Cajaraville, M. P. (2002). Oxygen radicals production and actin filament disruption in bivalve haemocytes treated with benzo(a)pyrene. *Mar. Environ. Res.* 54, 431–436. doi: 10.1016/S0141-1136(02)00177-0

Götze, S., Matoo, O. B., Beniash, E., Saborowski, R., and Sokolova, I. M. (2014). Interactive effects of CO2 and trace metals on the proteasome activity and cellular stress response of marine bivalves *Crassostrea virginica* and *Mercenaria mercenaria*. *Aquat. Toxicol.* 149, 65–82. doi: 10.1016/j.aquatox.2014.01.027

Haberkorn, H., Tran, D., Massabuau, J.-C., Ciret, P., Savar, V., and Soudant, P. (2011). Relationship between valve activity, microalgae concentration in the water and toxin accumulation in the digestive gland of the Pacific oyster *Crassostrea gigas* exposed to *Alexandrium minutum*. *Mar. Pollut. Bull.* 62, 1191–1197. doi: 10.1016/j.marpolbul.2011.03.034

Habig, W. H., Pabst, M. J., and Jakoby, W. B. (1974). Glutathione S-transferases: the first enzymatic step in mercapturic acid formation. *J. Biol. Chem.* 249, 7130–7139.

Halliwell, B. (1974). Superoxide dismutase, catalase and glutathione peroxidase: solutions to the problems of living with oxygen. *New Phytol.* 73, 1075–1086. doi: 10.1111/j.1469-8137.1974.tb02137.x

Hayes, J. D., and Strange, R. C. (1995). Invited commentary potential contribution of the Glutathione S-transferase supergene family to resistance to oxidative stress. *Free Radic. Res.* 22, 193–207. doi: 10.3109/10715769509147539

Hégaret, H., Wikfors, G. H., and Soudant, P. (2003). Flow cytometric analysis of haemocytes from eastern oysters, *Crassostrea virginica*, subjected to a sudden temperature elevation: II. *Haemocyte* functions: aggregation, viability, phagocytosis, and respiratory burst. *J. Exp. Mar. Biol. Ecol.* 293, 249–265. doi: 10.1016/S0022-0981(03)00235-1

Heisler, J., Glibert, P. M., Burkholder, J. M., Anderson, D. M., Cochlan, W., Dennison, W. C., et al. (2008). Eutrophication and harmful algal blooms: a scientific consensus. *Harmful Algae* 8, 3–13. doi: 10.1016/j.hal.2008.08.006

Huang, L., Zou, Y., Weng, H., Li, H.-Y., Liu, J.-S., and Yang, W.-D. (2015). Proteomic profile in *Perna viridis* after exposed to *Prorocentrum lima*, a dinoflagellate producing DSP toxins. *Environ. Pollut.* 196, 350–357. doi: 10.1016/j.envpol.2014.10.019

Ivanina, A. V., and Sokolova, I. M. (2013). Interactive effects of pH and metals on mitochondrial functions of intertidal bivalves *Crassostrea virginica* and *Mercenaria mercenaria*. *Aquat. Toxicol.* 14, 303–309. doi: 10.1016/j.aquatox.2013.10.019

Jiang, J., Shi, Y., Shan, Z., Yang, L., Wang, X., and Shi, L. (2012). Bioaccumulation, oxidative stress and HSP70 expression in *Cyprinus carpio* L. exposed to microcystin-LR under laboratory conditions. *Comp. Biochem. Physiol. C Toxicol. Pharmacol.* 155, 483–490. doi: 10.1016/j.cbpc.2011.12.008

Kankaanpää, H., Leiniö, S., Olin, M., Sjövall, O., Meriluoto, J., and Lehtonen, K. K. (2007). Accumulation and depuration of cyanobacterial toxin nodularin and biomarker responses in the mussel *Mytilus edulis*. *Chemosphere* 68, 1210–1217. doi: 10.1016/j.chemosphere.2007.01.076

Kelly, K. A., Havrilla, C. M., Brady, T. C., Abramo, K. H., and Levin, E. D. (1998). Oxidative stress in toxicology: established mammalian and emerging piscine model systems. *Environ. Health Perspect.* 106, 375–384. doi: 10.1289/ehp.98106375

Kim, Y. D., Kim, W. J., Shin, Y. K., Lee, D.-H., Kim, Y.-J., Kim, J. K., et al. (2017). Microcystin-LR bioconcentration induces antioxidant responses in the digestive gland of two marine bivalves *Crassostrea gigas* and *Mytilus edulis*. *Aquat. Toxicol.* 188, 119–129. doi: 10.1016/j.aquatox.2017.05.003

Klemas, V. (2011). Remote sensing of algal blooms: an overview with case studies. *J. Coast. Res.* 28, 34–43. doi: 10.2112/JCOASTRES-D-11-00051.1

Lagos, N. (1998). Microalgal blooms: a global issue with negative impact in Chile. *Biol. Res.* 31, 375–386.

Landsberg, J. H., Hall, S., Johannessen, J. N., White, K. D., Conrad, S. M., Abbott, J. P., et al. (2006). Saxitoxin puffer fish poisoning in the United States, with the first report of *Pyrodinium bahamense* as the putative toxin source. *Environ. Health Perspect.* 114, 1502–1507. doi: 10.1289/ehp.8998

Lapointe, B. E., Herren, L. W., Debortoli, D. D., and Vogel, M. A. (2015). Evidence of sewage-driven eutrophication and harmful algal blooms in Florida's Indian River Lagoon. *Harmful Algae* 43, 82–102. doi: 10.1016/j.hal.2015.01.004

Li, Y., Men, B., He, Y., Xu, H., Liu, M., and Wang, D. (2017). Effect of single-wall carbon nanotubes on bioconcentration and toxicity of perfluorooctane sulfonate in zebrafish (*Danio rerio*). *Sci. Total Environ.* 60, 509–518. doi: 10.1016/j.scitotenv.2017.06.140

Livak, K. J., and Schmittgen, T. D. (2001). Analysis of relative gene expression data using Real-Time quantitative PCR and the $2^{-\Delta\Delta C_T}$ method. *Methods* 25, 402–408. doi: 10.1006/meth.2001.1262

Llewellyn, L. E. (2006). Saxitoxin, a toxic marine natural product that targets a multitude of receptors. *Nat. Prod. Rep.* 23, 200–222. doi: 10.1039/b501296c

Luna-Acosta, A., Bustamante, P., Thomas-Guyon, H., Zaldibar, B., Izagirre, U., and Marigómez, I. (2017). Integrative biomarker assessment of the effects of chemically and mechanically dispersed crude oil in Pacific oysters, *Crassostrea gigas*. *Sci. Total Environ.* 598, 713–721. doi: 10.1016/j.scitotenv.2017.04.001

Lushchak, V. I. (2011). Environmentally induced oxidative stress in aquatic animals. *Aquat. Toxicol.* 101, 13–30. doi: 10.1016/j.aquatox.2010.10.006

Martínez-Ruiz, E. B., and Martínez-Jerónimo, F. (2015). Nickel has biochemical, physiological, and structural effects on the green microalga *Ankistrodesmus falcatus*: an integrative study. *Aquat. Toxicol.* 169, 27–36. doi: 10.1016/j.aquatox.2015.10.007

Martínez-Ruiz, E. B., and Martínez-Jerónimo, F. (2017). Exposure to the herbicide 2,4-D produces different toxic effects in two different phytoplankters: a green microalga (*Ankistrodesmus falcatus*) and a toxigenic cyanobacterium (*Microcystis aeruginosa*). *Sci. Total Environ.* 619–620, 1566–1578. doi: 10.1016/j.scitotenv.2017.10.145

Matozzo, V., Chinellato, A., Munari, M., Bressan, M., and Marin, M. G. (2013). Can the combination of decreased pH and increased temperature values induce oxidative stress in the clam *Chamelea gallina* and the mussel *Mytilus galloprovincialis*? *Mar. Pollut. Bull.* 72, 34–40. doi: 10.1016/j.marpolbul.2013.05.004

May, S. P., Burkholder, J. M., Shumway, S. E., Hégaret, H., Wikfors, G. H., and Frank, D. (2010). Effects of the toxic dinoflagellate *Alexandrium monilatum* on survival, grazing and behavioral response of three ecologically important bivalve molluscs. *Harmful Algae* 9, 281–293. doi: 10.1016/j.hal.2009.11.005

Melegari, S. P., Perreault, F., Moukha, S., Popovic, R., Creppy, E. E., and Matias, W. G. (2012). Induction to oxidative stress by saxitoxin investigated through lipid peroxidation in Neuro 2A cells and *Chlamydomonas reinhardtii* alga. *Chemosphere* 89, 38–43. doi: 10.1016/j.chemosphere.2012.04.009

Mello, D. F., da Silva, P. M., Barracco, M. A., Soudant, P., and Hégaret, H. (2013). Effects of the dinoflagellate *Alexandrium minutum* and its toxin (saxitoxin) on the functional activity and gene expression of *Crassostrea gigas* hemocytes. *Harmful Algae* 26, 45–51. doi: 10.1016/j.hal.2013.03.003

Mello, D. F., de Oliveira, E. S., Vieira, R. C., Simoes, E., Trevisan, R., Dafre, A. L., et al. (2012). Cellular and transcriptional responses of *Crassostrea gigas* hemocytes exposed in vitro to brevetoxin (PbTx-2). *Mar. Drugs* 10, 583–597. doi: 10.3390/md10030583

Mello, D. F., Proença, L. A., de, O., and Barracco, M. A. (2010). Comparative study of various immune parameters in three bivalve species during a natural bloom of *Dinophysis acuminata* in Santa Catarina Island, Brazil. *Toxins* 2, 1166–1178. doi: 10.3390/toxins2051166

Meng, L., Yang, S., Feng, M., Qu, R., Li, Y., Liu, J., et al. (2016). Toxicity and bioaccumulation of copper in *Limnodrilus hoffmeisteri* under different pH values: impacts of perfluorooctane sulfonate. *J. Hazard. Mater.* 305, 219–228. doi: 10.1016/j.jhazmat.2015.11.048

Moraga, D., Meistertzheim, A.-L., Tanguy-Royer, S., Boutet, I., Tanguy, A., and Donval, A. (2005). Stress response in Cu2 + and Cd2 + exposed oysters (*Crassostrea gigas*): an immunohistochemical approach. *Comp. Biochem. Physiol. C Toxicol. Pharmacol.* 141, 151–156. doi: 10.1016/j.cca.2005.05.014

Moreira, A., Figueira, E., Soares, A. M. V. M., and Freitas, R. (2016). The effects of arsenic and seawater acidification on antioxidant and biomineralization responses in two closely related *Crassostrea* species. *Sci. Total Environ.* 545, 569–581. doi: 10.1016/j.scitotenv.2015.12.029

Moroño, A., Franco, J., Miranda, M., Reyero, M. I., and Blanco, J. (2001). The effect of mussel size, temperature, seston volume, food quality and volume-specific toxin concentration on the uptake rate of PSP toxins by mussels (*Mytilus galloprovincialis* Lmk). *J. Exp. Mar. Biol. Ecol.* 257, 117–132. doi: 10.1016/S0022-0981(00)00336-1

Munday, R. (2011). Palytoxin toxicology: animal studies. *Toxicon* 57, 470–477. doi: 10.1016/j.toxicon.2010.10.003

Narahashi, T. (1998). Mechanism of tetrodotoxin and saxitoxin action. *Mar. Toxins Venoms* 3, 185–210.

Nogueira, L., Garcia, D., Trevisan, R., Sanches, A. L. M., da Silva Acosta, D., Dafre, A. L., et al. (2015). Biochemical responses in mussels Perna perna exposed to diesel B5. *Chemosphere* 134, 210–216. doi: 10.1016/j.chemosphere.2015.04.034

Núñez-Acuña, G., Aballay, A. E., Hégaret, H., Astuya, A. P., and Gallardo-Escárate, C. (2013). Transcriptional responses of *Mytilus chilensis* exposed in vivo to saxitoxin (STX). *J. Molluscan Stud.* 79, 323–331. doi: 10.1093/mollus/eyt030

Ohkawa, H., Ohishi, N., and Yagi, K. (1979). Assay for lipid peroxides in animal tissues by thiobarbituric acid reaction. *Anal. Biochem.* 95, 351–358. doi: 10.1016/0003-2697(79)90738-3

Pain-Devin, S., Cossu-Leguille, C., Geffard, A., Giambérini, L., Jouenne, T., Minguez, L., et al. (2014). Towards a better understanding of biomarker response in field survey: a case study in eight populations of zebra mussels. *Aquat. Toxicol.* 155, 52–61. doi: 10.1016/j.aquatox.2014.06.008

Perovic, S., Tretter, L., Brümmer, F., Wetzler, C., Brenner, J., Donner, G., et al. (2000). Dinoflagellates from marine algal blooms produce neurotoxic compounds: effects on free calcium levels in neuronal cells and synaptosomes. *Environ. Toxicol. Pharmacol.* 8, 83–94. doi: 10.1016/S1382-6689(99)00035-6

Prasetiya, F. S., Comeau, L. A., Gastineau, R., Decottignies, P., Cognie, B., Morançais, M., et al. (2017). Effect of marennine produced by the blue diatom *Haslea ostrearia* on behavioral, physiological and biochemical traits of juvenile *Mytilus edulis* and *Crassostrea virginica*. *Aquaculture* 467, 138–148. doi: 10.1016/j.aquaculture.2016.08.029

Ramos, V., and Vasconcelos, V. (2010). Palytoxin and analogs: biological and ecological effects. *Mar. Drugs* 8, 2021–2037. doi: 10.3390/md8072021

Regoli, F., and Giuliani, M. E. (2014). Oxidative pathways of chemical toxicity and oxidative stress biomarkers in marine organisms. *Mar. Environ. Res.* 93, 106–117. doi: 10.1016/j.marenvres.2013.07.006

Ricevuto, E., Lanzoni, I., Fattorini, D., Regoli, F., and Gambi, M. C. (2016). Arsenic speciation and susceptibility to oxidative stress in the fanworm *Sabella spallanzanii* (Gmelin) (Annelida, Sabellidae) under naturally acidified conditions: an in situ transplant experiment in a Mediterranean CO2 vent system. *Sci. Total Environ.* 544, 765–773. doi: 10.1016/j.scitotenv.2015.11.154

Rodrigues, S. M., de Carvalho, M., Mestre, T., Ferreira, J. J., Coelho, M., Peralta, R., et al. (2012). Paralytic shellfish poisoning due to ingestion of *Gymnodinium catenatum* contaminated cockles – application of the AOAC HPLC official method. *Toxicon* 59, 558–566. doi: 10.1016/j.toxicon.2012.01.004

Samson, J. C., Shumway, S. E., and Weis, J. S. (2008). Effects of the toxic dinoflagellate, *Alexandrium fundyense* on three species of larval fish: a food-chain approach. *J. Fish Biol.* 72, 168–188. doi: 10.1111/j.1095-8649.2007.01698.x

Sanchez, W., Burgeot, T., and Porcher, J.-M. (2013). A novel "Integrated Biomarker Response" calculation based on reference deviation concept. *Environ. Sci. Pollut. Res.* 20, 2721–2725. doi: 10.1007/s11356-012-1359-1

Sanchez-García, A., Rodríguez-Fuentes, G., Díaz, F., Galindo-Sánchez, C. E., Ortega, K., Mascaró, M., et al. (2017). Thermal sensitivity of O. maya embryos as a tool for monitoring the effects of environmental warming in the Southern

of Gulf of Mexico. *Ecol. Indic.* 72, 574–585. doi: 10.1016/j.ecolind.2016.08.043

Sevgiler, Y., Oruç, E. Ö, and Üner, N. (2004). Evaluation of etoxazole toxicity in the liver of *Oreochromis niloticus*. *Pestic. Biochem. Physiol.* 78, 1–8. doi: 10.1016/j.pestbp.2003.09.004

Shumway, S. E. (1990). A review of the effects of algal blooms on shellfish and aquaculture. *J. World Aquac. Soc.* 21, 65–104. doi: 10.1111/j.1749-7345.1990.tb00529.x

Shumway, S. E. (1995). "Management of shellfish resources," in *Manual on Harmful Marine Microalgae, IOC Manuals and Guides No. 33*, eds G. M. Hallegraeff, D. M. Anderson, A. D. Cembella, and H. O. Enevoldsen (Paris: UNESCO), 433–461.

Shumway, S. E., Burkholder, J. M., and Springer, J. (2006). Effects of the estuarine dinoflagellate *Pfiesteria shumwayae* (Dinophyceae) on survival and grazing activity of several shellfish species. *Harmful Algae* 5, 442–458. doi: 10.1016/j.hal.2006.04.013

Simões, E., Vieira, R. C., Schramm, M. A., Mello, D. F., Pontinha, V. D. A., da Silva, P. M., et al. (2015). Impact of harmful algal blooms (Dinophysis acuminata) on the immune system of oysters and mussels from Santa Catarina, Brazil. *J. Mar. Biol. Assoc. U.K.* 95, 773–781. doi: 10.1017/S0025315414001702

Smolowitz, R., and Shumway, S. E. (1997). Possible cytotoxic effects of the dinoflagellate, *Gyrodinium aureolum*, on juvenile bivalve molluscs. *Aquac. Int.* 5, 291–300. doi: 10.1023/A:1018355905598

Snyder, M. J. (2000). Cytochrome P450 enzymes in aquatic invertebrates: recent advances and future directions. *Aquat. Toxicol.* 48, 529–547. doi: 10.1016/S0166-445X(00)00085-0

Sobjak, T. M., Romão, S., do Nascimento, C. Z., dos Santos, A. F. P., Vogel, L., and Guimarães, A. T. B. (2017). Assessment of the oxidative and neurotoxic effects of glyphosate pesticide on the larvae of *Rhamdia quelen* fish. *Chemosphere* 182, 267–275. doi: 10.1016/j.chemosphere.2017.05.031

Takata, K., Takatsuji, H., and Seno, M. (2008). Detoxification of the oyster *Crassostrea gigas* contaminated. (with)paralytic shellfish poison (PSP) by cultivation in filtered seawater. *Nippon Suisan Gakkaishi Jpn.* 74, 78–80. doi: 10.2331/suisan.74.78

Teles, M., Fierro-Castro, C., Na-Phatthalung, P., Tvarijonaviciute, A., Trindade, T., Soares, A. M. V. M., et al. (2016). Assessment of gold nanoparticle effects in a marine teleost (*Sparus aurata*) using molecular and biochemical biomarkers. *Aquat. Toxicol.* 177, 125–135. doi: 10.1016/j.aquatox.2016.05.015

Thomas, C. (1996). Hemocytes: forms and functions. *East. Oyster Crassostrea Virginica* 1, 75–93.

Trainer, V. L., Sullivan, K., Eberhart, B.-T. L., Shuler, A., Hignutt, E., Kiser, J., et al. (2014). Enhancing shellfish safety in Alaska through monitoring of harmful algae and their toxins. *J. Shellfish Res.* 33, 531–539. doi: 10.2983/035.033.0222

Turner, A. D., Stubbs, B., Coates, L., Dhanji-Rapkova, M., Hatfield, R. G., Lewis, A. M., et al. (2014). Variability of paralytic shellfish toxin occurrence and profiles in bivalve molluscs from Great Britain from official control monitoring as determined by pre-column oxidation liquid chromatography and implications for applying immunochemical tests. *Harmful Algae* 31, 87–99. doi: 10.1016/j.hal.2013.10.014

Twiner, M. J., Dixon, S. J., and Trick, C. G. (2004). Extracellular organics from specific cultures of *Heterosigma akashiwo* (Raphidophyceae) irreversibly alter respiratory activity in mammalian cells. *Harmful Algae* 3, 173–182. doi: 10.1016/j.hal.2003.10.003

Valerio-García, R. C., Carbajal-Hernández, A. L., Martínez-Ruíz, E. B., Jarquín-Díaz, V. H., Haro-Pérez, C., and Martínez-Jerónimo, F. (2017). Exposure to silver nanoparticles produces oxidative stress and affects macromolecular and metabolic biomarkers in the goodeid fish *Chapalichthys pardalis*. *Sci. Total Environ.* 583, 308–318. doi: 10.1016/j.scitotenv.2017.01.070

Velez, C., Figueira, E., Soares, A. M. V. M., and Freitas, R. (2016). Native and introduced clams biochemical responses to salinity and pH changes. *Sci. Total Environ.* 56, 260–268. doi: 10.1016/j.scitotenv.2016.05.019

Vieira, C. E. D., Costa, P. G., Lunardelli, B., de Oliveira, L. F., da Costa, Cabrera, L., et al. (2016). Multiple biomarker responses in *Prochilodus lineatus* subjected to short-term in situ exposure to streams from agricultural areas in Southern Brazil. *Sci. Total Environ.* 542, 44–56. doi: 10.1016/j.scitotenv.2015.10.071

Vinothini, G., and Nagini, S. (2010). Correlation of xenobiotic-metabolizing enzymes, oxidative stress and NF-κB signaling with histological grade and menopausal status in patients with adenocarcinoma of the breast. *Clin. Chim. Acta* 411, 368–374. doi: 10.1016/j.cca.2009.11.034

Visser, P. M., Verspagen, J. M. H., Sandrini, G., Stal, L. J., Matthijs, H. C. P., Davis, T. W., et al. (2016). How rising CO2 and global warming may stimulate harmful cyanobacterial blooms. *Harmful Algae* 54, 145–159. doi: 10.1016/j.hal.2015.12.006

Wang, C., Lu, G., Peifang, W., Wu, H., Qi, P., and Liang, Y. (2011). Assessment of environmental pollution of Taihu Lake by combining active biomonitoring and integrated biomarker response. *Environ. Sci. Technol.* 45, 3746–3752. doi: 10.1021/es1037047

Wang, J., Tang, H., Zhang, X., Xue, X., Zhu, X., Chen, Y., et al. (2018). Mitigation of nitrite toxicity by increased salinity is associated with multiple physiological responses: a case study using an economically important model species, the juvenile obscure puffer (*Takifugu obscurus*). *Environ. Pollut.* 232, 137–145. doi: 10.1016/j.envpol.2017.09.026

Wang, J., and Wu, J. (2009). Occurrence and potential risks of harmful algal blooms in the East China Sea. *Sci. Total Environ.* 407, 4012–4021. doi: 10.1016/j.scitotenv.2009.02.040

Wang, Z., Zhang, J., Li, E., Zhang, L., Wang, X., and Song, L. (2017). Combined toxic effects and mechanisms of microsystin-LR and copper on *Vallisneria Natans* (Lour.) Hara seedlings. *J. Hazard. Mater.* 328, 108–116. doi: 10.1016/j.jhazmat.2016.12.059

Yan, Z., Yang, X., Lu, G., Liu, J., Xie, Z., and Wu, D. (2014). Potential environmental implications of emerging organic contaminants in Taihu Lake, China: comparison of two ecotoxicological assessment approaches. *Sci. Total Environ.* 47, 171–179. doi: 10.1016/j.scitotenv.2013.09.092

Young-Lai, W. W., and Aiken, D. E. (1986). Biology and culture of the giant scallop *Placopecten magellanicus*: a review. *Can. Tech. Rep. Fish. Aquat. Sci.* 1478:21.

Zhang, D. L., Hu, C. X., Li, D. H., and Liu, Y. D. (2013). Lipid peroxidation and antioxidant responses in zebrafish brain induced by *Aphanizomenon flos-aquae* DC-1 aphantoxins. *Aquat. Toxicol.* 14, 250–256. doi: 10.1016/j.aquatox.2013.10.011

Zhang, G., Li, L., Meng, J., Qi, H., Qu, T., Xu, F., et al. (2016). Molecular basis for adaptation of oysters to stressful marine intertidal environments. *Annu. Rev. Anim. Biosci.* 4, 357–381. doi: 10.1146/annurev-animal-022114-110903

Conflict of Interest Statement: The authors declare that the research was conducted in the absence of any commercial or financial relationships that could be construed as a potential conflict of interest.

frontiers in Physiology

ORIGINAL RESEARCH
published: 03 April 2019
doi: 10.3389/fphys.2019.00377

Anthropogenic Noise Aggravates the Toxicity of Cadmium on Some Physiological Characteristics of the Blood Clam *Tegillarca granosa*

*Wei Shi, Yu Han, Xiaofan Guan, Jiahuan Rong, Xueying Du, Shanjie Zha, Yu Tang and Guangxu Liu**

College of Animal Science, Zhejiang University, Hangzhou, China

Widespread applications of cadmium (Cd) in various products have caused Cd contamination in marine ecosystems. Meanwhile, human activities in the ocean have also generated an increasing amount of noise in recent decades. Although anthropogenic noise and Cd contaminants could be present simultaneously in marine environments, the physiological responses of marine bivalve mollusks upon coexposure to anthropogenic noise and toxic metal contaminants, including Cd remain unclear. Therefore, the combined effects of anthropogenic noise and Cd on the physiological characteristics of the blood clam *Tegillarca granosa* were investigated in this study. The results showed that 10 days of coexposure to anthropogenic noise and Cd can enhance adverse impacts on metabolic processes, as indicated by the clearance rate, respiration rate, ammonium excretion rate, and O:N ratio of *T. granosa*. In addition, both the ATP content, ATP synthase activity and genes encoding important enzymes in ATP synthesis significantly declined after coexposures to anthropogenic noise and Cd, which have resulted from reduced feeding activity and respiration. Furthermore, the expressions of neurotransmitter-related genes (MAO, AChE, and mAChR3) were all significantly down-regulated after coexposure to anthropogenic noise and Cd, which suggests an enhanced neurotoxicity under coexposure. In conclusion, our study demonstrated that anthropogenic noise and Cd would have synergetic effects on the feeding activity, metabolism, and ATP synthesis of *T. granosa*, which may be due to the add-on of stress responses and neurotransmitter disturbances.

Keywords: anthropogenic noise, cadmium, *Tegillarca granosa*, physiological characteristics, neurotoxic

OPEN ACCESS

Edited by:
Youji Wang,
Shanghai Ocean University, China

Reviewed by:
Amaya Albalat,
University of Stirling, United Kingdom
Aibin Zhan,
Research Center for Eco-environmental Sciences (CAS), China

****Correspondence:***
Guangxu Liu
guangxu_liu@zju.edu.cn

Specialty section:
This article was submitted to Aquatic Physiology, a section of the journal Frontiers in Physiology

Received: *17 November 2018*
Accepted: *18 March 2019*
Published: *03 April 2019*

Citation:
Shi W, Han Y, Guan X, Rong J, Du X, Zha S, Tang Y and Liu G (2019) Anthropogenic Noise Aggravates the Toxicity of Cadmium on Some Physiological Characteristics of the Blood Clam Tegillarca granosa. Front. Physiol. 10:377. doi: 10.3389/fphys.2019.00377

INTRODUCTION

As a byproduct of the zinc, lead and copper refinery, cadmium (Cd) has been recognized as one of the most dangerous toxic metals for many years (Järup, 2003; Kim et al., 2014). The widespread applications of Cd in both consumer and industrial products, such as plastics, ceramics, glass and vehicle tires, have resulted in the consistent presence of Cd contamination in marine ecosystems, which was reported to be as high as 50 μg/L in several heavily polluted areas (Vinarao et al., 2014). Due to its intrinsic ionic similarity to calcium, Cd can be accidentally ingested by marine bivalves

and enter into their cells through calcium channels (Vercauteren and Blust, 1999; Shi et al., 2018a), which would subsequently provoke a series of physiological responses, such as a decreased filtration rate, a hampered metabolism, and an altered sex ratio (Liu et al., 2014; Peng et al., 2015a; Shi et al., 2016; Wu et al., 2017). More importantly, many researches have proven that the harmful effects of Cd may occur at a much lower concentration than previously estimated (Zhang et al., 2008).

In the last few decades, human activities have not only brought chemical pollution but also generated an increasing amount of anthropogenic noise in both the open ocean and coastal areas (Peng et al., 2015b). Anthropogenic noise emitted from various ways, such as facility construction, resource exploration and maritime transportation, has led to a new type of pollution, noise pollution (Engås et al., 1996; Vasconcelos et al., 2007). Compared with other environmental disturbances, noise pollution is considered to be extremely harmful because of its universal and uncontrollable characteristics (André, 2009). Anthropogenic noise can directly or indirectly affect a wide variety of marine organisms by disturbing their biological processes and physiological functions, including acoustic communication (Codarin et al., 2009), auditory sensitivity (Popper et al., 2005; Codarin et al., 2009), individual behavior (Popper et al., 2003; Bruintjes and Radford, 2013), and population distribution (Lagardère, 1982; Soto et al., 2013). However, to date, only a few acoustic studies have been conducted with marine invertebrates, especially bivalve mollusks (Peng et al., 2015b). Limited studies have shown that exposure to anthropogenic noise could lead to physiological alterations such as hampered metabolism in marine invertebrates (Peng et al., 2016). For example, an altered O:N ratio and the expression of metabolism-related genes were detected in razor clams, *Sinonovacula constricta*, in response to anthropogenic noise at intensities of ∼80 and ∼100 dB re 1 μPa (Peng et al., 2016).

Anthropogenic noise and Cd contaminants could be present simultaneously in marine environments, especially in polluted coastal areas. Inhabiting the coastal zone, many marine bivalve species are often challenged by multiple environmental stressors (Rocha et al., 2015; Shi et al., 2018a,b; Guan et al., 2018). However, to date, little is known about the physiological responses of marine bivalve mollusks upon coexposure to anthropogenic noise and toxic metal contaminants. To the best of our knowledge, only one recent study investigated the synergetic impacts of anthropogenic noise and trace metal contamination in bivalve mollusks (Charifi et al., 2018). The results showed that compared to that of the control without ship noise, coexposure to cargo ship noise (150 dB re 1 μPa) and waterborne Cd (0.5 μg/L) led to 58.97% reduction in bioaccumulation of Cd in gills and resulted in a decrease in the growth rate of the oyster *Magallana gigas* (Charifi et al., 2018).

Although it remains unclear in marine invertebrates, since the neuroendocrine alterations were often reported along with the physiological adverse impacts in marine vertebrates (Romano et al., 2004; Anderson et al., 2011), it is generally accepted that noise may cause physiological impacts by affecting the neuroendocrine regulation pathway. Similarly, the neurotoxicity of Cd has been well studied in a variety of organisms (Gabbiani et al., 1967; Méndez-Armenta and Ríos, 2007). Therefore, theoretically, coexposure to noise and Cd may show an add-on or an offset effect on the physiological responses, such as metabolism, of an organism through their synergetic impacts on neuroendocrine regulation. However, whether this speculation holds true in bivalve mollusks needs to be verified by empirical data.

As an important aquaculture bivalve species, the blood clam, *Tegillarca granosa* is naturally distributed in the Indo-Pacific region (Liu et al., 2014; Shao et al., 2016). Due to its ecological importance in sediment nutrient cycling and ecosystem carbon flow, many studies have been performed on various aspects of *T. granosa* (Liu et al., 2016; Shi et al., 2017a,b; Zhao et al., 2017). However, the synergetic impacts of noise and Cd on the metabolism of bivalve mollusks, including blood clams, remain unknown to date. Therefore, to obtain a better understanding of the physiological responses of bivalve mollusks to coexposure to Cd and simulated anthropogenic noise, the clearance rate, respiration rate, ammonium excretion rate, O:N ratio, ATP content, activities of ATP synthases, activity of AChE, and expression of neurotransmitter- and ATP synthesis-related genes of *T. granosa* were investigated in this study. The data obtained could help the community to further understand the potential risk of emerging pollution in marine environments.

MATERIALS AND METHODS

Collection and Acclimation of Bivalves

Specimens of adult *T. granosa* (mean ± SE, shell length of 18.23 ± 1.34 mm) were collected from Yueqing Bay (28° 280′ N and 121°110′ E), Zhejiang, China in June 2018. To obtain the background concentration of Cd, seawater was sampled and analyzed in triplicate following the methods described by Shi et al. (2018a). The background concentration of Cd was found to be under the detection limits (< 0.01 μg/L). After cleaning off the epizoa, clams were acclimatized for 10 days in a 1000 L indoor tank with filtered seawater (temperature 21.4 ± 1.2°C, pH 8.09 ± 0.03, salinity 20.7 ± 0.1‰) before the experiment. During the acclimation process, the clams were fed twice daily with the microalgae *Tetraselmis chuii* at a rate of 5% of the tissue dry weight, and half the volume of the seawater was replaced with fresh filtered seawater daily. No mortality occurred during this experiment.

Exposure Experiments

$CdCl_2$ (>99% purity) was purchased from Aladdin Chemical Co, China. Stock solutions were prepared in deionized water at 1 M, a concentration high enough to prevent weighing errors and salinity fluctuation during the adding of stock solution to obtain the desired exposure concentrations (Shi et al., 2016). On the basis of previous studies (Chan, 1995), 50 μg/L of Cd^{2+} was chosen in this study to simulate the Cd concentration in heavily polluted coastal areas. The sound broadcast system was composed of an underwater loudspeaker (UW-30, Electro-Voice®, Indiana, United States; frequency response 0.1–10 kHz;

power-handling capacity 30 watts) connected to a power amplifier player (AV-296, SAST®, Guangdong, China; power-handling capacity 150 watts) as described in our previous study (Peng et al., 2016). According to preliminary survey results and reported data (Arveson and Vendittis, 2000; Zou et al., 2004), underwater sound levels of ∼70 and ∼100 dB re 1 μPa were used in this study to simulate sound levels with different degrees of anthropogenic noise input. An ambient aeration sound level of the culture system without any addition of anthropogenic sound input was used as a control. A downloaded pile-driving noise record reported in a previous study was used in this study as the source of anthropogenic sound input (Solan et al., 2016).

In the present study, three experimental groups and one control group were set up as follows: (1) control group without Cd and anthropogenic sound input, (2) Cd treatment group with 50 μg/L Cd^{2+} without anthropogenic sound input, (3) coexposure group with 50 μg/L Cd and 70 dB re 1 μPa anthropogenic noise input, and (4) coexposure group with 50 μg/L Cd and 100 dB re 1 μPa anthropogenic noise input. After acclimation, 480 clams were randomly assigned to 12 individual 160 L buckets (4 treatments × 3 replicate tanks) containing 50 cm deep filtered seawater with slight aeration. The submersible loudspeaker was suspended in the center position of the bucket at a depth of 20 cm below the water surface and oriented to the floor of the bucket to generate the experimental noise effect. The concentrations of Cd^{2+} in each treatment were measured using a graphite furnace atomic absorption spectrophotometer every 2 days during the experiment, as described previously (Shi et al., 2018a; **Table 1**). The action acoustic conditions during the experiment were measured using acoustics recording units with a bioacoustics recorder (Song Meter SM2+, Wildlife Acoustics®, MA, United States; 96 kHz sampling rate). The working sound pressure levels were measured with a hydrophone near the bottom of the tank at 5, 15, and 25 cm away from the center (**Table 2**). Then, acoustic analyses were performed using Soundscape Analysis Software SACS V1.0 (Register number: 2014SR216788) in MATLAB R2013a (The Math-Works Inc., United States) following the method described previously (Peng et al., 2016). The experiment lasted for 10 days, and no individual mortality was observed throughout the experimental period. The clams were fed with *T. chuii* as mentioned above, and the whole volume of seawater was replaced daily with newly added Cd^{2+} at the designed concentration after feeding.

Physiological Measurements

Clearance Rate

After 10 days of exposure, the clams were fasted for 12 h to empty their digestive tracts prior to the clearance rate measurement. Six blood clam individuals from each replicate tank were randomly selected and transported to a 2 L chamber filled with filtered seawater. Three identical chambers without blood clams were used as the blank control. After approximately 30 min of acclimation, when the valves of the individuals were reopened, the microalgae *T. chuii* was added to the chamber to achieve an initial concentration of 2×10^5 cells mL^{-1} (Zhao et al., 2017). The experiment lasted for 2 h. The microalgae cell concentrations at the beginning and end of the measurements were counted three times using a Neubauer hemocytometer (XB-K-25, Anxin Optical Instrument) under a microscope (BX53, Olympus, Tokyo, Japan). The microalgae cell concentrations in the control tanks did not show any significant variation during the measurements. After the measurements, the soft tissues of the clams were dissected and dried in an oven at 70°C for 72 h. The clearance rate was calculated according to previous studies (Zhao et al., 2017):

$$CR = V \times (LnC_0 - LnC_t)/(W \times T)$$

where CR represents the clearance rate (L g^{-1} h^{-1}); V represents the filtered seawater volume in the chamber (L); C_0 represents the initial microalgae concentration (cells mL^{-}); Ct represents the microalgae concentration at time T (cells mL^{-1}); W represents the dry weight of soft tissues (g); and T is the experimental time (h).

TABLE 1 | The working sound pressure levels (dB re 1 μPa) in the experimental setup at different measuring positions.

Distance to the center	5 cm	15 cm	25 cm
Control	54.53[a] (52.77∼57.23)	54.09[a] (52.38∼56.73)	53.45[a] (51.90∼55.97)
Cd treatment	53.91[a] (52.99∼56.74)	53.57[a] (52.47∼56.03)	52.95[a] (51.75∼55.77)
Co-exposure with 70 dB re 1 μPa noise input	73.78[a] (70.85∼75.09)	72.15[a] (69.62∼74.38)	71.52[a] (68.79∼73.83)
Co-exposure with 100 dB re 1 μPa noise input	101.56[a] (93.55∼108.05)	100.86[a] (92.89∼107.57)	98.36[a] (89.94∼104.37)

Significant differences at different positions of each experimental setup (data in the same line) are indicated by different superscripts.

TABLE 2 | Waterborne Cd^{2+} concentrations measured for the different groups.

Group	Control	Cd treatment	Co-exposure with 70 dB re 1 μPa noise input	Co-exposure with 100 dB re 1 μPa noise input
Concentration (μg/L)	Not detected	49.72 ± 3.5[a]	50.21 ± 4.3[a]	49.37 ± 2.66[a]

Significant differences are indicated by different superscripts.

Respiration Rate, Ammonium Excretion Rate, and Oxygen to Nitrogen Ratio

Six clam individuals were randomly sampled from each bucket after 10 days of exposure. After 12 h of depuration, these clams were transported into a closed glass respirometer (2 L) filled with oxygen-saturated filtered seawater. After incubation for approximately 30 min, when the valves of the individuals were reopened, the measurements started with the respirometers sealed off for 2 h. Three identical respirometers without clams were used as the blank control. The dissolved oxygen concentrations at the beginning and the end within the respirometers were measured by an oxygen meter (Multi 3410 SET4, WTW, Germany). The concentrations of ammonia produced by the clams were measured by the phenol-hypochlorite method (Solórzano, 1969). The dry weight of the soft tissues was obtained as mentioned above. The respiratory rate and ammonium excretion rate of the blood clams were calculated according to the following formula:

$$R(E) = V \times (C1 - C2)/(W \times T)$$

where R(E) represents the respiration (or ammonium excretion) rate (mg g^{-1} h^{-1}); V represents the volume of seawater in each respirometer (L); C_1 and C_2 represent the dissolved oxygen (or ammonia) concentrations (mg L^{-1}) at the beginning and end of the measurement, respectively, W represents the dry weight of the soft tissues (g); and T is the experimental time (h). The ratio of oxygen consumption to ammonia excretion expressed as atomic equivalents (O:N) was calculated to assess the utilization of the different biochemical compositions for energy metabolism (Peng et al., 2016).

Measurements of ATP Content and the Activities of ATP Synthases

Six clams from each bucket were randomly sampled to determine their ATP contents and the activities of 6-phosphofructokinase (PFK) and pyruvate kinase (PK) in their whole tissues after 10 days of corresponding treatment. A volume of 0.1–0.3 g of tissue from each individual was homogenized, and then ice-cold saline at quadruple the volume of the tissue was added to each sample. The homogenates were immediately centrifuged at 4°C and 2000 r/min for 10 min. The total protein concentrations of these samples were determined with a commercial kit (P0006, Beyotime Institute of Biotechnology, China) using the Bradford method (Hammond and Kruger, 1988). The collected supernatants were used for the determination of the ATP content and the activities of the ATP synthases.

The amount of ATP in the whole tissue was determined using a commercial ATP assay kit (A095 Nanjing Jiancheng Bioengineering Institute, China) according to the manufacturer's instructions and expressed as μmol per mg protein. The activities of PFK and PK were measured using commercial kits (A001 and A007, Nanjing Jiancheng Bioengineering Institute, China) with a spectrophotometer (UV-2100, Shanghai Jinghua Instruments, China) at an absorption wavelength of 340 nm following the manufacturer's protocols. All the enzyme activities were calculated as U per mg protein, where U was defined as the enzyme causing the conversion of 1 μmol of substrate min^{-1}.

Determination of AChE Activity

After 10 days of treatment, five clams from each bucket were used to determine the activity of AChE in their whole tissues. The activity of AChE was measured using commercial kits (A024, Nanjing Jiancheng Bioengineering Institute, China) with a microplate reader (Thermo Multiskan Go, United States) at an absorption wavelength of 412 nm and expressed as U per mg protein, where U was defined as the amount of enzyme decomposing 1/6 μmol of substrate per mg protein per minute at a temperature of 37°C. The total protein contents of tissues were determined as mentioned above.

Gene Expression Analysis

The expression levels of the genes encoding the key modulating enzymes or their receptors, including monoamine oxidase (MAO), AChE, and muscarinic acetylcholine receptor M3 (mAChR3), which encode dopamine (DA), acetylcholinesterase (AChE), and ACh receptors, respectively, were investigated in this study (Gainey and Greenberg, 2003; Hermida-Ameijeiras et al., 2004; Guan et al., 2018). Furthermore, the genes encoding the important modulating enzymes in ATP synthesis, including citrate synthase (CS), dihydrolipoamide dehydrogenase (DLD) and 2-oxoglutarate dehydrogenase (SucA), were also examined (Owen et al., 2002; Koubaa et al., 2013). The total RNA was isolated from the gill tissue of 5 individuals from each bucket after 10 days of exposure as described in our previous study (Shi et al., 2017b). The RNA quality and the concentration were verified by gel electrophoresis and a NanoDrop 1000 UV/visible spectrophotometer (Thermo Fisher Scientific, United States), respectively. First strand cDNA was synthesized from high-quality total RNA (>500 ng/μL) using the PrimeScript RT reagent Kit (TaKaRa, RR037A) following the manufacturer's instructions. The amplifications were performed in a total volume of 10 μL containing of 5 μL of SYBR Green Master Mix (Q111-2, Vazyme, China), 0.2 μL of each primer (10 μM), 0.2 μL of ROX Reference Dye (Q111-2, Vazyme, China), 1 μL of cDNA template, and 3.4 μL of double-distilled water. Real-time quantitative PCR was conducted on the StepOnePlus Real-Time PCR System (Applied Biosystems, United States) in triplicate according to the following procedure: 95°C for 5 min, followed by 40 cycles (95 °C for 10 s, 60°C for 30 s). A melting curve analysis was used to confirm the specificity and reliability of the PCR products. The 18S rRNA gene was utilized as an internal reference, and the $2^{-\Delta\Delta CT}$ method was applied to analyze the relative expression levels of the genes investigated. The primers used are listed in **Table 3**, and all the primers were synthesized by TsingKe Biotech (Beijing, China).

Statistical Analysis

One-way ANOVAs followed by Tukey's *post hoc* tests were conducted to compare the clearance rate, respiration rate, ammonium excretion rate, O:N ratio, ATP content and the activities of the enzymes among the experimental groups. For all the analyses, Levene's test and Shapiro-Wilk's test

TABLE 3 | Primer sequences for the genes used in the real-time PCR analysis.

Gene	Forward primer (5′–3′)	Reverse primer (5′–3′)	Accession no.
MAO	GGTCCTGAACTGTGAGTGTCCTTC	GGATGTCATCGTTATTGGAGGAGGT	MH156850
AChE	CCTCACTAGGAGTTGTATTTGGGTT	CTTGGGAAGATGTGCTTGATGCTA	MH156845
mAChR3	GCCCGTGAGTAACTTCCCATAAACA	CCAGACAACATCGTTCTTCGCAAAT	MH156849
CS	CCCGATACACTTGTCAGAGAGAATT	TTGCCTTGCCTTGTTCTAAGAGTAC	MK170247
DLD	ACGCATGTAACTTCTGCTCCTA	GGTGCCCTGTCGCTAGAGAA	MK170248
SucA	CCTGGTCCACAATCATAGCATGTCT	TTGGATTGGTCAACTGCTGAAGC	MK170249
18S	CTTTCAAATGTCTGCCCTATCAACT	TCCCGTATTGTTATTTTTCGTCACT	JN974506.1

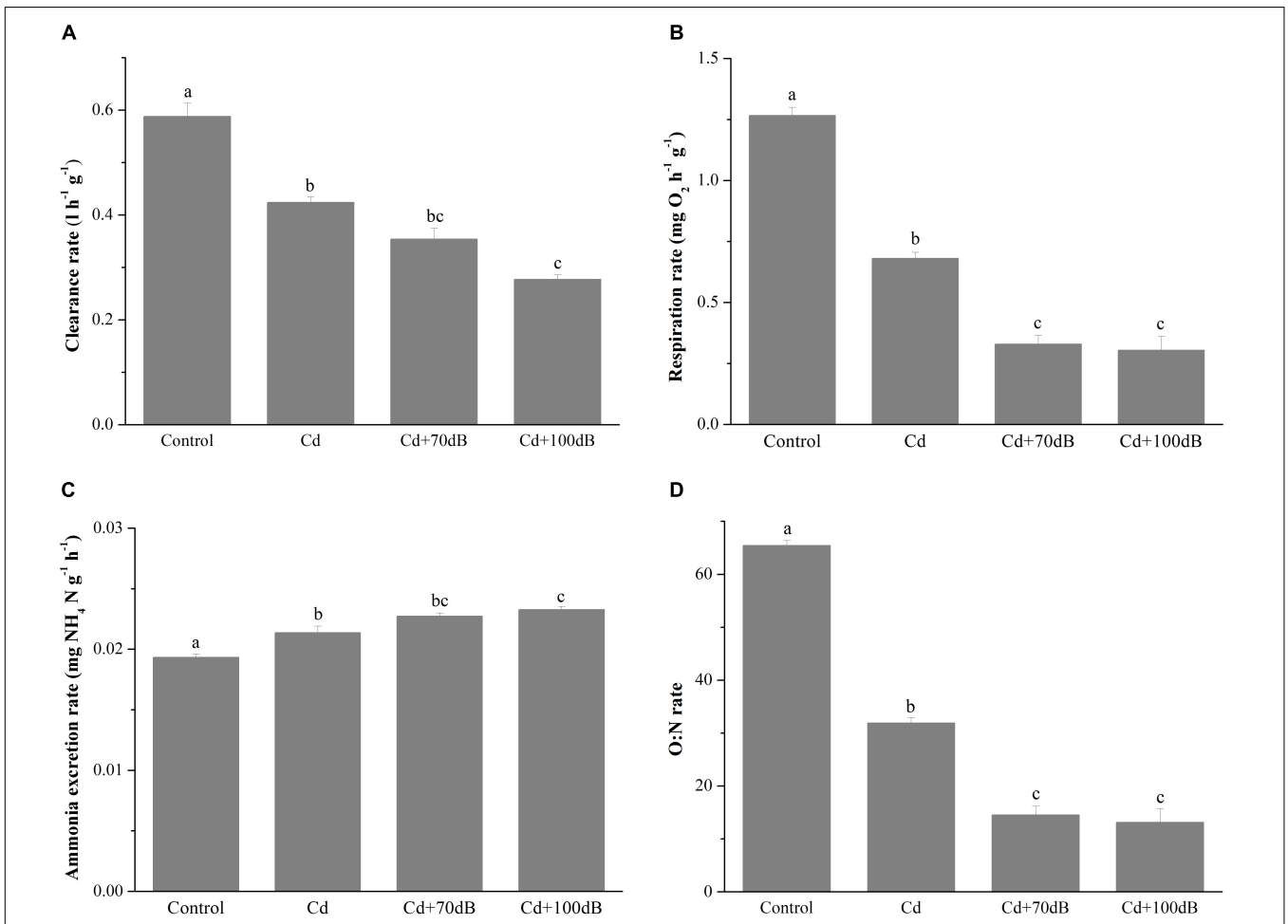

FIGURE 1 | Clearance rates **(A)**, respiration rates **(B)**, ammonium excretion rates **(C)**, and the corresponding oxygen to nitrogen (O:N) ratios **(D)** of the blood clams after 10 days of exposure to a control (without Cd and anthropogenic noise), 50 μg/L Cd, 50 μg/L Cd + 70 dB re 1 μPa anthropogenic noise, and 50 μg/L Cd + 100 dB re 1 μPa anthropogenic noise. Means not sharing the same superscript are significantly different.

were used to verify the homogeneity of the variances and normality, respectively. In cases where these assumptions were not satisfied by the raw data, the data were arcsine square root transformed prior to analysis. The gene expression levels were analyzed using the Duncan multiple range test. All the statistical analyses were carried out using the Origin-Pro 8 software package. All of the data are presented as the mean ± SE, and a p-value less than 0.05 indicated a statistically significant difference.

RESULTS

Metabolic Responses to Cd Exposure and Anthropogenic Noise

Exposure to 50 μg/L Cd alone significantly suppressed the clearance rate of the blood clams ($p < 0.05$) (**Figure 1A**), which was decreased to approximately 72.2% of that of the control. In addition, coexposure to Cd and anthropogenic noise led to a further decline in the clearance rates ($p < 0.05$), which were

reduced to approximately 83.5 and 65.3% of the Cd exposure group for coexposure groups with anthropogenic noise at 70 or 100 dB re 1 μPa, respectively.

Similar results were also observed in the respiration rates of the blood clams after 10 days of exposure to Cd and/or anthropogenic noise (**Figure 1B**). When exposed to 50 μg/L Cd alone, the respiration rate dropped to approximately 53.8% of that of the control. Coexposure to Cd and anthropogenic noise aggravated the suppression of the respiration rates, which declined to approximately 26.0 and 24.0% of the control for groups coexposed to Cd and 70 or 100 dB re 1 μPa anthropogenic noise, respectively (**Figure 1B**).

Unlike the clearance rate and respiration rate, the ammonium excretion rates were significantly induced by exposure of the blood clams to Cd and/or anthropogenic noise ($p < 0.05$, **Figure 1C**). Compared with those of the control, the ammonium excretion rates of the blood clams were significantly elevated to approximately 110% in seawater with 50 μg/L Cd and further increased to 118 and 120% when 70 or 100 dB re 1 μPa anthropogenic noise was copresent with Cd.

Due to both the reduction in respiration rates and the increase in the ammonium excretion rates, the O:N ratios were significantly reduced by Cd exposure alone and coexposure to Cd and anthropogenic noise (**Figure 1D**, $p < 0.05$). The O:N ratio of clams reduced to approximately 48.7% of the control when exposed to 50 μg/L Cd alone for 10 days and further declined to approximately 22.2 and 20.1% of the control for the groups coexposed to Cd and 70 or 100 dB re 1 μPa anthropogenic noise, respectively (**Figure 1D**).

Effects of Cd and Anthropogenic Noise Exposure on ATP Content and the Activities of Synthases

Both exposure of the clams to Cd alone and coexposure to Cd and anthropogenic noise significantly reduced the ATP contents of the clams (**Figure 2**, $p < 0.05$). After 10 days of exposure to 50 μg/L Cd alone, the ATP content of the clams was significantly decreased to approximately 77.0% that of the control. Although the ATP content was not further reduced by the copresence of anthropogenic noise at 70 dB re 1 μPa, coexposure to 100 dB re 1 μPa anthropogenic noise significantly aggravated the suppression of ATP content compared to that of the group exposed to Cd alone, which was only approximately 72.9% of that of the group exposed to Cd alone.

Similarly, compared to that of the control, the activities of PFK and PK significantly declined to approximately 86.4 and 70.6% of the control, respectively (**Figure 3** and $p < 0.05$) when the clams were exposed to 50 μg/L Cd. Although this suppression effect was not significantly aggravated by the copresence of anthropogenic noise at 70 dB re 1 μPa, the activities of PFK and PK were further reduced to 64.4 and 57.3% of that of the control for PFK and PK, respectively, when 100 dB re 1 μPa anthropogenic noise was introduced along with 50 μg/L Cd.

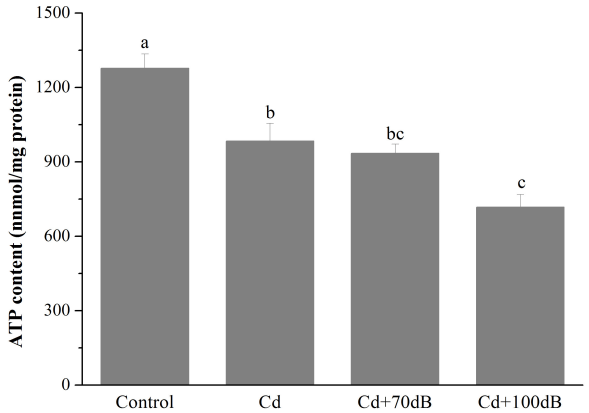

FIGURE 2 | ATP content in the tissues of the blood clams after 10 days of exposure to the control (without Cd and anthropogenic noise), 50 μg/L Cd, 50 μg/L Cd + 70 dB re 1 μPa anthropogenic noise, and 50 μg/L Cd + 100 dB re 1 μPa anthropogenic noise. Means not sharing the same superscript are significantly different.

Effects of Cd and Anthropogenic Noise Exposure on the Activity of AChE

Compared to the control, the activity of AChE in the blood clams was significantly lowered by exposure to Cd and/or anthropogenic noise for 10 days (**Figure 4**, $p < 0.05$). The blood clams exposed to Cd-contaminated seawater had a significantly lower AChE activity, which was approximately 57.9% of that of the control. However, coexposure to Cd and anthropogenic noise at 70 or 100 dB re 1 μPa did not lead to a further reduction in the activity of AChE when compared to the group exposed to Cd alone.

Effects of Cd and Anthropogenic Noise Exposure on Gene Expression

All three key genes (CS, SucA, and DLD) encoding enzymes for ATP synthesis showed a similar relative expression pattern, with the highest expression detected in the blood clams of the control followed by those in the Cd exposure group and then the lowest expression in the coexposure groups (**Figure 5**, $p < 0.05$). In addition, when coexposed to Cd and anthropogenic noise, the expression levels of SucA and DLD significantly declined with the increase in sound levels of the anthropogenic noise investigated. Similarly, the downregulation of neurotransmitter-related genes (MAO, AChE and mAChR3) was significantly ($p < 0.05$) aggravated by the copresence of anthropogenic noise (**Figure 6**, $p < 0.05$).

DISCUSSION

As a benthic filter feeder, the blood clam, similar to many other sessile marine bivalves, may be challenged by multiple environmental stressors, such as toxic trace metals and anthropogenic noise (Sokolova et al., 2004; Shi et al., 2016; Peng et al., 2016). Constrained by their limited locomotion ability,

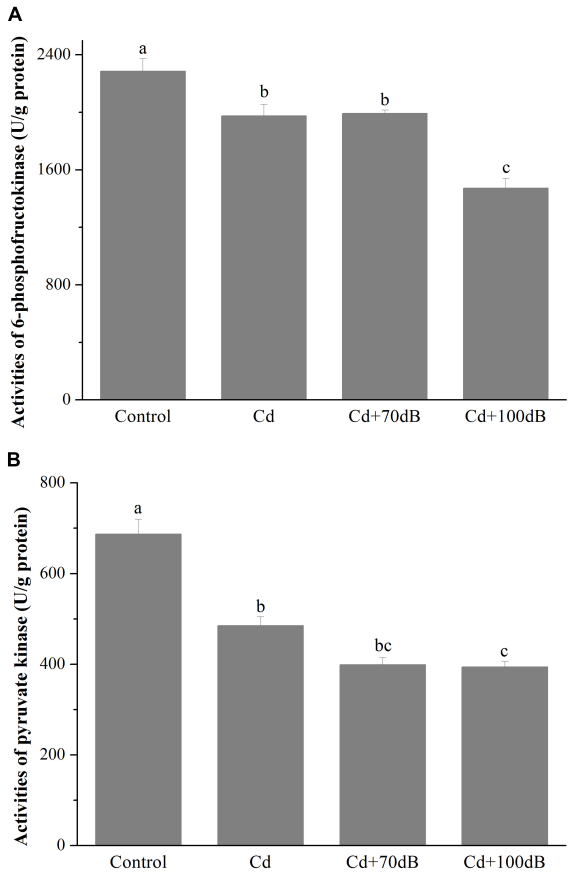

FIGURE 3 | Activities of 6-phosphofructokinase (PFK) **(A)** and pyruvate kinase (PK) **(B)** in the tissues of the blood clams after 10 days of exposure to the control (without Cd and anthropogenic noise), 50 μg/L Cd, 50 μg/L Cd + 70 dB re 1 μPa anthropogenic noise, and 50 μg/L Cd + 100 dB re 1 μPa anthropogenic noise. Means not sharing the same superscript are significantly different.

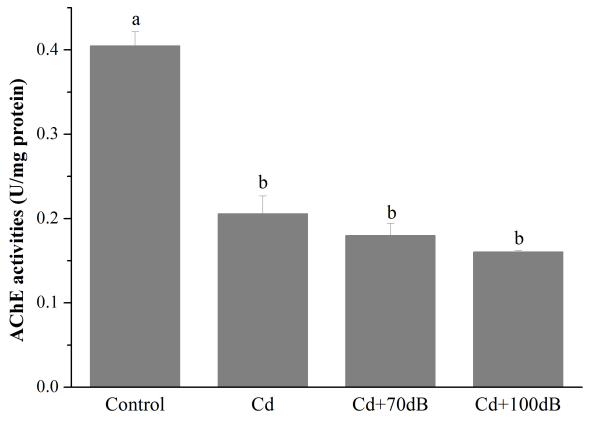

FIGURE 4 | Activities of acetylcholine esterase (AChE) in the tissues of the blood clams after 10 days of exposure to the control (without Cd and anthropogenic noise), 50 μg/L Cd, 50 μg/L Cd + 70 dB re 1 μPa anthropogenic noise, and 50 μg/L Cd + 100 dB re 1 μPa anthropogenic noise. Means not sharing the same superscript are significantly different.

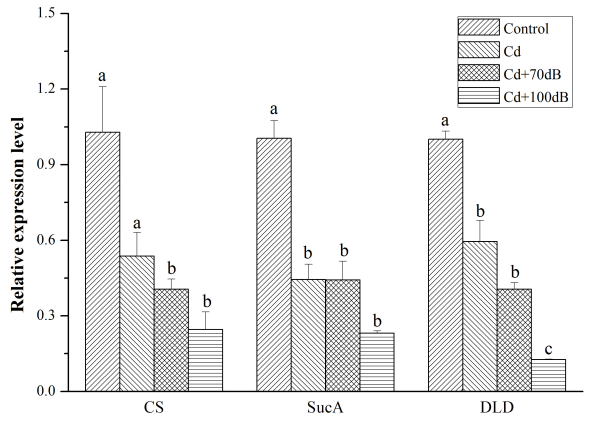

FIGURE 5 | Relative expression levels of the genes in ATP synthesis after 10 days exposure to the control (without Cd and anthropogenic noise), 50 μg/L Cd, 50 μg/L Cd + 70 dB re 1 μPa anthropogenic noise, and 50 μg/L Cd + 100 dB re 1 μPa anthropogenic noise. Means not sharing the same superscript are significantly different.

sessile bivalves have difficulty escaping from these stressors and therefore may be potentially threatened by these stressors. However, the physiological responses of bivalve mollusks to coexposure to anthropogenic noise and toxic trace metals are still largely unknown. In addition, little is known about the molecular mechanism manifesting these physiological impacts.

The results obtained in the present study suggested that coexposure to anthropogenic noise and Cd enhances the adverse impacts on metabolic processes, indicated by the clearance rate, respiration rate, ammonium excretion rate, and O:N ratio of the marine bivalve mollusks. The reduction in the clearance rate detected indicated that the feeding activity of *T. granosa* was significantly suppressed. The Cd-induced reduction in feeding activity was also reported in other marine bivalve species, such as the green-lipped mussel *Perna canaliculus* (Chandurvelan et al., 2012) and the oyster *Crassostrea hongkongensis* (Pan and Wang, 2012). Furthermore, the result that noise exposure reinforces the suppression of the feeding activity of *T. granosa* exposed to Cd in the present study may offer an explanation for the reduction in metal accumulation under the noisy scenario reported, since less Cd will be ingested through feeding (Charifi et al., 2018). In marine bivalves, clearance behavior and respiration are closely linked together, as both processes occur in the water filtration process over the gills during the opening of the valves. It has been shown recently that coexposure to anthropogenic noise and Cd led to an increase in the valve closure duration in the oyster *Magallana gigas* (Charifi et al., 2018). Therefore, both the reduced clearance and respiration rate obtained in this study can result from the suppression of ventilation (Pan and Wang, 2012).

Due to the reduction in respiration and the increase in ammonium excretion, the O:N ratio of the blood clams was significantly downregulated in response to Cd and anthropogenic

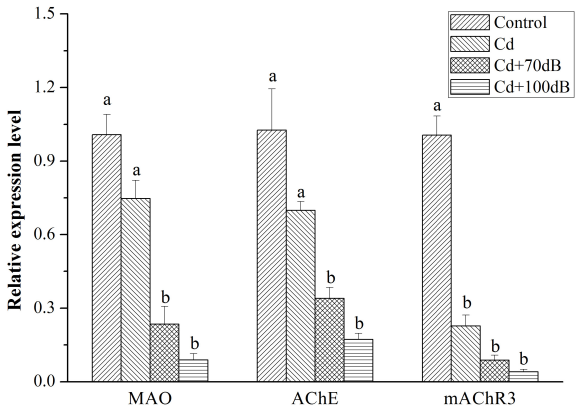

FIGURE 6 | Relative expression levels of the genes encoding neurotransmitter modulatory enzymes and receptors after 10 days of exposure to the control (without Cd and anthropogenic noise), 50 μg/L Cd, 50 μg/L Cd + 70 dB re 1 μPa anthropogenic noise, and 50 μg/L Cd + 100 dB re 1 μPa anthropogenic noise. Means not sharing the same superscript are significantly different.

noise exposures. The O:N ratio is widely considered an indicator of the physiological state of organisms by showing the usage of three substrates (carbohydrates, lipids and proteins) in energy metabolism (Mayzaud and Conover, 1988; Anestis et al., 2010). For example, higher O:N ratios (<30) usually indicate a catabolism of carbohydrates and lipids, while O:N lower ratios (<30) suggest an elevated turnover of proteins under stressful conditions in mussels (Langenbuch and Pörtner, 2002). Therefore, the increase in the ammonium excretion rate along with the reduction in O:N ratio detected suggest that more protein substrates were used to provide energy for the clams, and this phenomenon can be due to the declined energy availability through feeding (Sokolova et al., 2005). In this study, both the ATP content and ATP synthase activity in *T. granosa* significantly declined after stress exposure. In addition, the genes encoding the important enzymes in ATP synthesis were significantly downregulated as well. These ATP synthesis-related results indicated that energy availability was significantly constrained by Cd and anthropogenic noise exposures, which could be a physiological response to the reductions in feeding activity and respiration.

Reduced metabolism is widely adopted as an adaptive mechanism for marine organisms to cope with various environmental stresses, such as toxic metals, ocean acidification and anthropogenic noise (Pan and Wang, 2012; Peng et al., 2016 Zhao et al., 2017). For example, reductions in feeding and respiration may help in reducing the direct contact of the soft tissues to waterborne chemical contaminants such as toxic metals (Pan and Wang, 2012). Although little is known about the physiological impacts of noise on bivalve mollusks, one study has demonstrated that anthropogenic noise may cause razor clams to enter a metabolically inactive state through sending a stress signal via water proton movement sensed by the sensory palps on the mantle and gills (Peng et al., 2016). Therefore, the additive effects of Cd and anthropogenic noise on the metabolism of the blood clams could be simply due to the add-on of their inhibitory impacts.

When exposed to stress conditions, the physiological responses of animals are often regulated through the neuroendocrine pathway (Ravindran et al., 2005; Naqvi et al., 2012). Although the neurotoxic impacts of Cd and anthropogenic noise have been well elaborated in model organisms, the impacts remain unclear in bivalve mollusks especially under combined noise and toxic metal stress. The results obtained in the present study demonstrated that anthropogenic noise can enhance the neurotoxicity of waterborne Cd to bivalves in terms of downregulating the expression of neurotransmitter-related genes. The downregulation of AChE and MAO, which encode the modulatory enzymes for ACh and DA, respectively, could lead to decreased amounts of modulatory enzymes and subsequently constrain the hydrolysis of the corresponding neurotransmitters (Hermida-Ameijeiras et al., 2004; Guan et al., 2018). It has been confirmed that neurotransmitters play important roles in regulating various physiological functions, such as the feeding activity, of many other organisms (Panksepp and Bishop, 1979; Naqvi et al., 2012). For example, a significant inhibitory effect on food intake was observed in Chinese perch, *Siniperca chuatsi*, after 1 h postinjection of 5 μg DA (He et al., 2018). Therefore, exposure to anthropogenic noise may reinforce the physiological impacts of Cd on blood clams through its synergetic effects on disturbing neurotransmitters.

CONCLUSION

In conclusion, our study demonstrated that anthropogenic noise and Cd would have synergetic effects on the feeding activity, metabolism, and ATP synthesis of *T. granosa*, which may be due to the add-on of stress responses and neurotransmitter disturbances. This study suggests that although Cd and anthropogenic noise significantly differ in their intrinsic physical and chemical characteristics, the physiological responses provoked are somehow common.

AUTHOR CONTRIBUTIONS

WS and GL contributed to conception and design of the experimental plan. WS, YH, XG, JR, XD, YT, and SZ performed the experiments. WS and GL performed the statistical analysis and wrote the manuscript.

FUNDING

This work was funded by National Key R&D Program of China (2018YFD0900603), National Natural Science Foundation of China (No. 31672634), Open Fund of Key Laboratory for Marine Ecosystem and Biogeochemistry, SOA (No. LMEB201708), and Open Fund of Key Laboratory of Eco-Environment & Disaster Preservation of Shandong, North China Sea Branch of SOA (No. 201704).

REFERENCES

Anderson, P. A., Berzins, I. K., Fogarty, F., Hamlin, H. J., and Guillette, L. J. (2011). Sound, stress, and seahorses: the consequences of a noisy environment to animal health. *Aquaculture* 311, 129–138. doi: 10.1016/j.aquaculture.2010.11.013

André, M. (2009). The sperm whale sonar: monitoring and use in mitigation of anthropogenic noise effects in the marine environment. *Nucl. Instrum. Meth. A* 602, 262–267. doi: 10.1016/j.nima.2008.12.223

Anestis, A., Pörtner, H. O., Karagiannis, D., Angelidis, P., Staikou, A., and Michaelidis, B. (2010). Response of *Mytilus galloprovincialis* (L.) to increasing seawater temperature and to marteliosis: metabolic and physiological parameters. *Comp. Biochem. Physiol. A* 156, 57–66. doi: 10.1016/j.cbpa.2009.12.018

Arveson, P. T., and Vendittis, D. J. (2000). Radiated noise characteristics of a modern cargo ship. *J. Acoust. Soc. Am.* 107, 118–129. doi: 10.1121/1.428344

Bruintjes, R., and Radford, A. N. (2013). Context-dependent impacts of anthropogenic noise on individual andsocial behaviour in a cooperatively breeding fish. *Anim. Behav.* 85, 1343–1349. doi: 10.1016/j.anbehav.2013.03.025

Chan, K. M. (1995). Concentrations of copper, zinc, cadmium and lead in rabbitfish (*Siganus oramin*) collected in Victoria Harbour, Hong Kong. *Mar. Pollut. Bull.* 31, 277–280. doi: 10.1016/0025-326X(95)00136-B

Chandurvelan, R., Marsden, I. D., Gaw, S., and Glover, C. N. (2012). Impairment of green-lipped mussel (*Perna canaliculus*) physiology by waterborne cadmium: relationship to tissue bioaccumulation and effect of exposure duration. *Aquat. Toxicol.* 124-125, 114–124. doi: 10.1016/j.aquatox.2012.07.013

Charifi, M., Miserazzi, A., Sow, M., Perrigault, M., Gonzalez, P., Ciret, P., et al. (2018). Noise pollution limits metal bioaccumulation and growth rate in a filter feeder, the Pacific oyster *Magallana gigas*. *PLoS One* 13:e0194174. doi: 10.1371/journal.pone.0194174

Codarin, A., Wysocki, L. E., Ladich, F., and Picciulin, M. (2009). Effects of ambient and boat noise on hearing and communication in three fish species living in a marine protected area (Miramare, Italy). *Mar. Pollut. Bull.* 58, 1880–1887. doi: 10.1016/j.marpolbul.2009.07.011

Engås, A., Løkkeborg, S., Ona, E., and Soldal, A. V. (1996). Effects of seismic shooting on local abundance and catch rates of cod ((*Gadus morhua*) and haddock)(*Melanogrammus aeglefinus*). *Can. J. Fish. Aquat. Sci.* 53, 2238–2249. doi: 10.1139/f96-177

Gabbiani, G., Baic, D., and Déziel, C. (1967). Toxicity of cadmium for the central nervous system. *Exp. Neurol.* 18, 154–160. doi: 10.1016/0014-4886(67)90037-4

Gainey, L. F., and Greenberg, M. J. (2003). Nitric oxide mediates seasonal muscle potentiation in clam gills. *J. Exp. Biol.* 206, 3507–3520. doi: 10.1242/jeb.00573

Guan, X., Shi, W., Zha, S., Rong, J., Su, W., and Liu, G. (2018). Neurotoxic impact of acute TiO2 nanoparticle exposure on a benthic marine bivalve mollusk, *Tegillarca granosa*. *Aquat. Toxicol.* 200, 241–246. doi: 10.1016/j.aquatox.2018.05.011

Hammond, J. B., and Kruger, N. J. (1988). The Bradford method for protein quantitation. *Methods Mol. Biol.* 3, 25–32. doi: 10.1385/0-89603-126-8:25

He, Y., Li, L., Liang, X., He, S., Zhao, L., and Zhang, Y. (2018). Inhibitory neurotransmitter serotonin and excitatory neurotransmitter dopamine both decrease food intake in Chinese perch (*Siniperca chuatsi*). *Fish Physiol. Biochem.* 44, 175–183. doi: 10.1007/s10695-017-0422-8

Hermida-Ameijeiras, Á, Méndez-Álvarez, E. A., Sánchez-Iglesias, S. A., Sanmartın-Suárez, C., and Soto-Otero, R. (2004). Autoxidation and MAO-mediated metabolism of dopamine as a potential cause of oxidative stress: role of ferrous and ferric ions. *Neurochem. Int.* 45, 103–116. doi: 10.1016/j.neuint.2003.11.018

Järup, L. (2003). Hazards of heavy metal contamination. *Brit. Med. Bull.* 68, 167–182. doi: 10.1093/bmb/ldg032

Kim, E., Jee, J., Steiner, H., Cormet-Boyaka, E., and Boyaka, P. (2014). Chronic exposure to cadmium alters gut immune homeostasis and innate immunity (MUC8P.810). *J. Immunol.* 192(1 Suppl.), 198.111.

Koubaa, M., Cocuron, J. C., Thomasset, B., and Alonso, A. P. (2013). Highlighting the tricarboxylic acid cycle: liquid and gas chromatography-mass spectrometry analyses of 13 C-labeled organic acids. *Anal. Biochem.* 436, 151–159. doi: 10.1016/j.ab.2013.01.027

Lagardère, J. P. (1982). Effects of noise on growth and reproduction of *Crangon crangon* in rearing tanks. *Mar. Biol.* 71, 177–185. doi: 10.1007/BF00394627

Langenbuch, M., and Pörtner, H. O. (2002). Changes in metabolic rate and N excretion in the marine invertebrate *Sipunculus nudus* under conditions of environmental hypercapnia. *J. Exp. Biol.* 205, 1153–1160.

Liu, G., Shu, M., Chai, X., Shao, Y., Wu, H., Sun, C., et al. (2014). Effect of chronic sublethal exposure of major heavy metals on filtration rate, sex ratio, and gonad development of a bivalve species. *B. Environ. Contam. Tox.* 92, 71–74. doi: 10.1007/s00128-013-1138-9

Liu, S., Shi, W., Guo, C., Zhao, X., Han, Y., Peng, C., et al. (2016). Ocean acidification weakens the immune response of blood clam through hampering the NFκβ and toll-like receptor pathways. *Fish Shellfish Immunol.* 54, 322–327. doi: 10.1016/j.fsi.2016.04.030

Mayzaud, P., and Conover, R. (1988). O:N atomic ratio as a tool to describe zooplankton metabolism. *Mar. Ecol. Prog. Ser.* 45, 289–302. doi: 10.3354/meps045289

Méndez-Armenta, M., and Ríos, C. (2007). Cadmium neurotoxicity. *Environ. Toxicol. Phar.* 23, 350–358. doi: 10.1016/j.etap.2006.11.009

Naqvi, F., Haider, S., Batool, Z., Perveen, T., and Haleem, D. J. (2012). Sub-chronic exposure to noise affects locomotor activity and produces anxiogenic and depressive like behavior in rats. *Pharmacol. Rep.* 64, 64–69. doi: 10.1016/S1734-1140(12)70731-4

Owen, O. E., Kalhan, S. C., and Hanson, R. W. (2002). The key role of anaplerosis and cataplerosis for citric acid cycle function. *J. Biol. Chem.* 277, 30409–30412. doi: 10.1074/jbc.R200006200

Pan, K., and Wang, W. (2012). Reconstructing the biokinetic processes of oysters to counteract the metal challenges: physiological acclimation. *Environ. Sci. Technol.* 6, 10765–10771. doi: 10.1021/es302040g

Panksepp, J., and Bishop, P. (1979). Neurohumoral and endocrine control of feeding. *Psychoneuroendocrino.* 4, 89–106. doi: 10.1016/0306-4530(79)90023-4

Peng, C., Zhao, X., Han, Y., Shi, W., Liu, S., and Liu, G. (2015a). Toxic effects of chronic sub-lethal Cu^{2+}, Pb^{2+} and Cd^{2+} on antioxidant enzyme activities in various tissues of the blood cockle, *Anadara granosa*. *J. Res. Sci. Tech.* 12, 125–131.

Peng, C., Zhao, X., and Liu, G. (2015b). Noise in the sea and its impacts on marine organisms. *Int. J. Environ. Res. Public Health* 12, 12304–12323. doi: 10.3390/ijerph121012304

Peng, C., Zhao, X., Liu, S., Shi, W., Han, Y., Guo, C., et al. (2016). Effects of anthropogenic sound on digging behavior, metabolism, Ca^{2+}/Mg^{2+} ATPase activity, and metabolism-related gene expression of the bivalve *Sinonovacula constricta*. *Sci. Rep.* 6:24266. doi: 10.1038/srep24266

Popper, A. N., Fewtrell, J., Smith, M. E., and Mccauley, R. D. (2003). Anthropogenic sound: effects on the behavior and physiology of fishes. *Mar. Technol. Soc. J.* 37, 35–40. doi: 10.4031/002533203787537050

Popper, A. N., Smith, M. E., Cott, P. A., Hanna, B. W., Macgillivray, A. O., Austin, M. E., et al. (2005). Effects of exposure to seismic airgun use on hearing of three fish species. *J. Acoust. Soc. Am.* 117, 3958–3971. doi: 10.1121/1.1904386

Ravindran, R., Rathinasamy, S. D., Samson, J., and Senthilvelan, M. (2005). Noise-stress-induced brain neurotransmitter changes and the effect of *Ocimum sanctum* (Linn) treatment in albino rats. *J. Pharmacol. Sci.* 98, 354–360. doi: 10.1254/jphs.FP0050127

Rocha, T. L., Gomes, T., Sousa, V. S., Mestre, N. C., and Bebianno, M. J. (2015). Ecotoxicological impact of engineered nanomaterials in bivalve molluscs: an overview. *Mar. Environ. Res.* 111, 74–88. doi: 10.1016/j.marenvres.2015.06.013

Romano, T. A., Keogh, M. J., Kelly, C., Feng, P., Berk, L., Schlundt, C. E., et al. (2004). Anthropogenic sound and marine mammal health: measures of the nervous and immune systems before and after intense sound exposure. *Can. J. Fish. Aquat. Sci.* 61, 1124–1134. doi: 10.1139/f04-055

Shao, Y., Chai, X., Xiao, G., Zhang, J., Lin, Z., and Liu, G. (2016). Population genetic structure of the blood clam, *Tegillarca granosa*, along the pacific coast of asia: isolation by distance in the sea. *Malacologia* 59, 303–312. doi: 10.4002/040.059.0208

Shi, W., Guan, X., Han, Y., Guo, C., Rong, J., Su, W., et al. (2018a). Waterborne Cd2+ weakens the immune responses of blood clam through impacting Ca2+ signaling and Ca2+ related apoptosis pathways. *Fish Shellfish Immunol.* 77, 208–213. doi: 10.1016/j.fsi.2018.03.055

Shi, W., Guan, X., Han, Y., Zha, S., Fang, J., Xiao, G., et al. (2018b). The synergic impacts of TiO2 nanoparticles and 17β-estradiol (E2) on the immune responses, E2 accumulation, and expression of immune-related genes of the blood clam,

Tegillarca granosa. *Fish Shellfish Immunol.* 81, 29–36. doi: 10.1016/j.fsi.2018.07.009

Shi, W., Han, Y., Guo, C., Zhao, X., Liu, S., Su, W., et al. (2017a). Immunotoxicity of nanoparticle nTiO2 to a commercial marine bivalve species, *Tegillarca granosa*. *Fish Shellfish Immunol.* 66, 300–306. doi: 10.1016/j.fsi.2017.05.036

Shi, W., Han, Y., Guo, C., Zhao, X., Liu, S., Su, W., et al. (2017b). Ocean acidification hampers sperm-egg collisions, gamete fusion, and generation of Ca2+ oscillations of a broadcast spawning bivalve, *Tegillarca granosa*. *Mar. Environ. Res.* 130, 106–112. doi: 10.1016/j.marenvres.2017.07.016

Shi, W., Zhao, X., Han, Y., Che, Z., Chai, X., and Liu, G. (2016). Ocean acidification increases cadmium accumulation in marine bivalves: a potential threat to food safety. *Sci. Rep.* 6:20197. doi: 10.1038/srep20197

Sokolova, I. M., Evans, S., and Hughes, F. M. (2004). Cadmium-induced apoptosis in oyster hemocytes involves disturbance of cellular energy balance but no mitochondrial permeability transition. *J. Exp. Biol.* 207, 3369–3380. doi: 10.1242/jeb.01152

Sokolova, I. M., Sokolov, E. P., and Ponnappa, K. M. (2005). Cadmium exposure affects mitochondrial bioenergetics and gene expression of key mitochondrial proteins in the eastern oyster *Crassostrea virginica* Gmelin (Bivalvia: Ostreidae). *Aquat. Toxicol.* 73, 242–255. doi: 10.1016/j.aquatox.2005.03.016

Solan, M., Hauton, C., Godbold, J. A., Wood, C. L., Leighton, T. G., and White, P. (2016). Anthropogenic sources of underwater sound can modify how sediment-dwelling invertebrates mediate ecosystem properties. *Sci. Rep.* 6:20540. doi: 10.1038/srep20540

Solórzano, L. (1969). Determination of ammonia in natural waters by the phenolhypochlorite method. *Limnol. Oceanogr.* 14, 799–801. doi: 10.4319/lo.1969.14.5.0799

Soto, N. A. D., Delorme, N., Atkins, J., Howard, S., Williams, J., and Johnson, M. (2013). Anthropogenic noise causes body malformations and delays development in marine larvae. *Sci. Rep.* 3:2831. doi: 10.1038/srep02831

Vasconcelos, R. O., Amorim, M. C., and Ladich, F. (2007). Effects of ship noise on the detectability of communication signals in the Lusitanian toadfish. *J. Exp. Biol.* 210, 2104–2112. doi: 10.1242/jeb.004317

Vercauteren, K., and Blust, R. (1999). Uptake of cadmium and zinc by the mussel *Mytilus edulis* and inhibition by calcium channel and metabolic blockers. *Mar. Biol.* 135, 615–626.

Vinarao, R. T., Salem, G. M., and Ragaza, R. J. (2014). "Distribution of Cd, Pb, As and Hg in oyster tissue, sediment and water in Lingayen Gulf, Philippines," in *Molluscan Shellfish Safety*, ed. G. Sauvé (Dordrecht: Springer), 137–154. doi: 10.1007/978-94-007-6588-7_12

Wu, H., Xu, L., Yu, D., and Ji, C. (2017). Differential metabolic responses in three life stages of mussels *Mytilus galloprovincialis* exposed to cadmium. *Ecotoxicology* 26, 1–7. doi: 10.1007/s10646-016-1741-8

Zhang, W., Pang, F., Huang, Y., Yan, P., and Lin, W. (2008). Cadmium exerts toxic effects on ovarian steroid hormone release in rats. *Toxicol. Lett.* 182, 18–23. doi: 10.1016/j.toxlet.2008.07.016

Zhao, X., Shi, W., Han, Y., Liu, S., Guo, C., Fu, W., et al. (2017). Ocean acidification adversely influences metabolism, extracellular pH and calcification of an economically important marine bivalve, *Tegillarca granosa*. *Mar. Environ. Res.* 125, 82–89. doi: 10.1016/j.marenvres.2017.01.007

Zou, C., Chen, D., and Hua, H. (2004). Study on characteristics of ship underwater radiation noise. *J. Ship Mech.* 8, 113–124.

Conflict of Interest Statement: The authors declare that the research was conducted in the absence of any commercial or financial relationships that could be construed as a potential conflict of interest.

frontiers in Physiology

ORIGINAL RESEARCH
published: 05 December 2018
doi: 10.3389/fphys.2018.01536

Molecular Characterization of the Hedgehog Signaling Pathway and Its Necessary Function on Larval Myogenesis in the Pacific Oyster *Crassostrea gigas*

Huijuan Li[1], *Qi Li*[1,2]* *and Hong Yu*[1,2]

[1] Key Laboratory of Mariculture, Ministry of Education, Ocean University of China, Qingdao, China, [2] Laboratory for Marine Fisheries Science and Food Production Processes, Qingdao National Laboratory for Marine Science and Technology, Qingdao, China

Hedgehog signaling pathway participates in a chain of necessary physiological activities and dysregulation of the hedgehog signaling has been implicated in birth defects and diseases. Although substantial studies have uncovered that the hedgehog pathway is both sufficient and necessary for patterning vertebrate muscle differentiation, limited knowledge is available about its role in molluscan myogenesis. Here, the present study firstly identified and characterized the key genes (CgHh, CgPtc, CgSmo, CgGli) in the hedgehog pathway of the Pacific oyster *Crassostrea gigas*, and investigated the function of this pathway in embryonic myogenesis of *C. gigas*. Bioinformatics analysis revealed that the functional domains of the key genes were highly conserved among species. Quantitative analysis indicated that CgHh, CgPtc, CgGli mRNA began to accumulate during the blastula to gastrulation stages and accumulated throughout trochophore and into the D-shaped stage. RNA localization patterns by whole-mount *in situ* hybridization revealed that the key genes own the strongest specific staining in gastrulation, trochophore, and D-shaped stage. Hedgehog pathway genes showed a high expression level in myogenesis stage including trochophore and D-shaped stages, suggesting that the hedgehog pathway would be involved in myogenesis of *C. gigas*. In adult oysters, the key genes were expressed at various tissues, indicating that hedgehog pathway governed a series of development events. To further examine the role of hedgehog signaling in *C. gigas* myogenesis, we used cyclopamine treatment in *C. gigas* larvae to inhibit the signaling pathway. The quantification of the expression of the key genes in hedgehog pathway showed that expressions of key genes were severely down-regulated in treated larvae compared with normal larvae. The velum retractors, ventral retractors, anterior adductor, and posterior adductor muscles of larvae treated with cyclopamine at 4–6 μM for 6–12 h were severely destroyed, suggesting that the hedgehog pathway took part in the myogenesis of *C. gigas*. These findings provide a foundation for uncovering the molecular mechanisms of hedgehog signaling in molluscan physiological activity and enable us to better understand the signaling pathway involving in molluscan physiological activity.

Keywords: hedgehog, pathway, myogenesis, cyclopamine, pacific oyster

OPEN ACCESS

Edited by:
Xiaotong Wang,
Ludong University, China

Reviewed by:
Annalisa Grimaldi,
Università degli Studi dell'Insubria, Italy
Fenglian Xu,
Saint Louis University, United States

***Correspondence:**
Qi Li
qili66@ouc.edu.cn

Specialty section:
This article was submitted to Aquatic Physiology, a section of the journal Frontiers in Physiology

Received: *09 July 2018*
Accepted: *11 October 2018*
Published: *05 December 2018*

Citation:
Li H, Li Q and Yu H (2018) Molecular Characterization of the Hedgehog Signaling Pathway and Its Necessary Function on Larval Myogenesis in the Pacific Oyster Crassostrea gigas. Front. Physiol. 9:1536. doi: 10.3389/fphys.2018.01536

INTRODUCTION

Embryogenesis is a complex biological process and regulated by a mass of important cell-to-cell signaling cascades (Villavicencio et al., 2000). The principal inductive signaling pathways involved in embryogenesis are generally conserved, including TGF-β (transforming growth factor β), Wnt (Wingless and INT-1), Receptor tyrosine kinase, Notch, and hedgehog (Ingham and McMahon, 2001; Lee et al., 2001; Cornell and Eisen, 2005; Kirilly et al., 2005; Huangfu and Anderson, 2006). As one member of those cell-cell signaling pathways, hedgehog signaling is an evolutionarily conserved pathway and governs a chain of necessary embryonic development events ranging from cell proliferation, differentiation, apoptosis to morphogenesis of tissue, and organs (Weed et al., 1997). Hedgehog signaling participates in the correct development of various organs and tissue in both vertebrates and invertebrates (Heretsch et al., 2010). Furthermore, hedgehog signaling plays important roles in tissue homeostasis and dysregulation of the hedgehog pathway is relevant with developmental disorders and some diseases involving in birth defects or cancers during embryonic development (Østerlund and Kogerman, 2006).

The proteins involved in the hedgehog signaling pathway are highly conserved and include hedgehog (Hh), Patched (Ptc), Smoothened (Smo), and Gli family. Molecular characterization of the hedgehog ligands, receptors and downstream members are best understood in vertebrate and *Drosophila* (Huangfu and Anderson, 2006; Ingham and Placzek, 2006). Hh, a secreted protein, is the start of the hedgehog pathway (Villavicencio et al., 2000). Hh is firstly found in *Drosophila* to participate in embryonic segment polarity (Nüsslein-Volhard and Wieschaus, 1980). Afterward, the existence of the Hh homologs in vertebrates is proved to be a widespread phenomenon. For example, the Hh homologs are identified in mouse and chick, and they play a role in pattering of the neural tube and limb (Echelard et al., 1993; Riddle et al., 1993; Roelink et al., 1994). There are five Hh homologs in zebrafish and three of them participate in embryonic patterning (Currie and Ingham, 1996). In the mouse, there are three Hh homologs and all of them play important roles in embryonic development (Zhang et al., 2001). Hh ligand binds to the plasma membrane receptor Ptc, a 12-transmembrane protein that is a negative regulator of the pathway and highly conserved among species (Huangfu and Anderson, 2006; Østerlund and Kogerman, 2006). Ptc represses the downstream signaling when the absence of ligand, and binding of Hh ligand excuses the repression. Smo, a seven-transmembrane (TM) protein, acts downstream of Ptc and an necessary positive regulator of the hedgehog signaling (Østerlund and Kogerman, 2006). The seven-TM region structure of Smo is relatively conserved among species and strongly resembles the Frizzled protein family (Nusse, 2003). Gli is the downstream transcription factor and the end of the pathway. Active Smo regulates the bifunctional transcription factor Gli. Full-length form Gli protein is a transcriptional activator while broken or incomplete Gli protein becomes a transcriptional repressor and blocks the activity of hedgehog signaling (Matus et al., 2008). During the absence of Hh ligand, Ptc as an inhibitor blocks the ability of Smo to activate the hedgehog signaling (**Figure 1**). On this occasion, the downstream transcription factor Gli is phosphorylated and processed by an intracellular protein complex including PKA, Slimb, GSK3β and Fused. Then the incomplete Gli functions as a transcriptional inhibitor and represses the activity of the hedgehog signaling pathway (Jia et al., 2002; Price and Kalderon, 2002). When Hh is present, binding of Hh ligand to Ptc alleviates the inhibition of Smo (**Figure 1**). Subsequently, Smo represses the activity of the protein complex that destroys the structure and function of the Gli. The full-length form of Gli is protected and transported into nucleus where it activates transcription (Méthot and Basler, 2000).

Hedgehog signaling has been defined as an important regulator of myogenesis in vertebrates. Hedgehog signaling determines the fast and slow muscle fate and affects the muscle types in zebrafish embryo (Currie and Ingham, 1996; Blagden et al., 1997; Du et al., 1997).Overexpression of Hh in zebrafish is able to convert the entire myotome into slow muscle fibers (Blagden et al., 1997; Du et al., 1997). Hedgehog signaling also has a later effect on regulating the differentiation of the dermomyotome in zebrafish. Hedgehog signaling has no roles in the initial formation of the dermomyotome but is related with its differentiation into fast muscle fibers (Feng et al., 2006). Hh governs the proliferation and differentiation of myoblasts during chick limb muscle and mouse hypaxial muscle development (Duprez et al., 1998; Kruger et al., 2001). In mice, Myod is a myogenic regulatory factor that is in charge of the survival and proliferation of myoblasts (Braun et al., 1992). Pax 3 has a role in development of the somatic mesoderm muscles (Goulding et al., 1994). Hedgehog signaling has a role in expression of the Pax-3 and MyoD in mouse (Duprez et al., 1998). The ectopic expression of Hh results in the upregulation of myogenic regulatory factors (MRFs) in mice hypaxial musculature.

Though there are abundant data showing that hedgehog signaling is related with the vertebrate muscle differentiation, knowledge on the role of this pathway in invertebrate myogenesis is little (Grimaldi et al., 2008). A Hh-related gene was discovered to participate in the normal development of obliquely striated muscles in leech proboscis (Kang et al., 2003). In Mollusca, the role of hedgehog signaling in myogenesis is investigated only in *Sepia officinalis*. The hedgehog signaling is involved in correct patterning of obliquely striated muscle fibers in cuttlefish mantle (Grimaldi et al., 2008).

The Pacific oyster *Crassostea gigas* is the most widely cultivated marine bivalves and widely distributed throughout the world (Zhu et al., 2016). *C. gigas* is also becoming an interesting model species in the developmental biology because it owns the typical molluscan development stages, including planktonic laravae and metamorphosis. Though *C. gigas* possess highly economic and scientific value, knowledge about the molecular mechanisms of myogenesis is still obscure up to now. Here, we choose the *C. gigas* as a bivalve animal model to further study the conserved role of Hedgehog signaling in myogenesis. We obtained the full length cDNA of *C. gigas* Hh, Ptc, Smo, Gli (CgHh, CgPtc, CgSmo, CgGli). Subsequently, a detailed bioinformatics analysis on the molecular characterization of the hedgehog pathway genes was conducted.

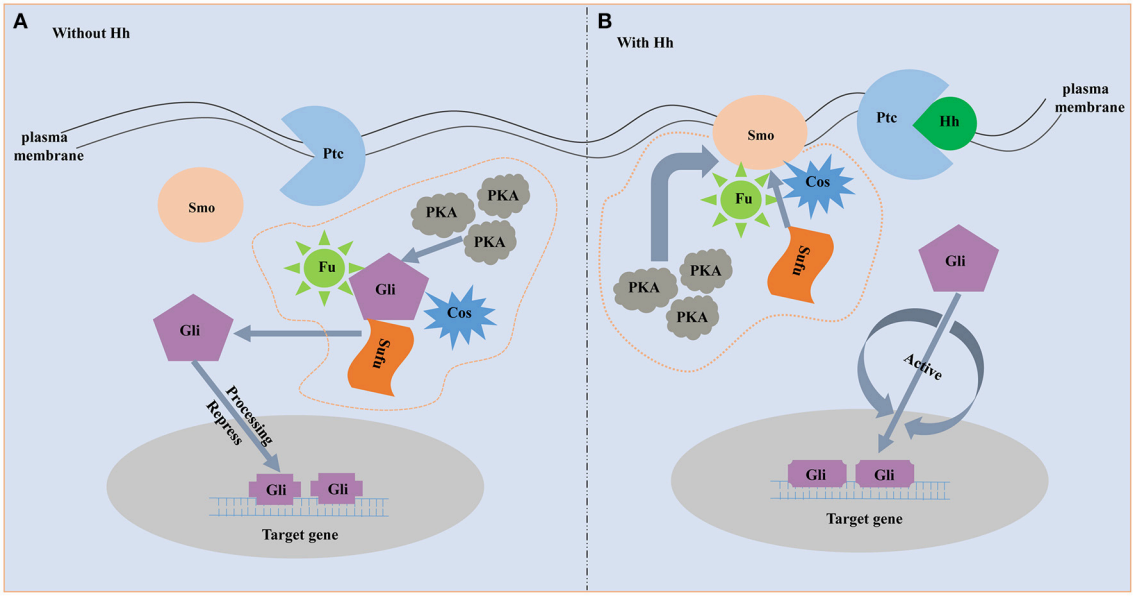

FIGURE 1 | The schematic diagram of hedgehog signaling pathway. **(A)** Without Hh ligand. Fu, Su(fu) and Cos can form a complex. In the absence of Hh, the complex is able to bind to microtubules or membranes, and Gli can undergo phosphorylation by the PKA. Then the incomplete Gli functions as a transcriptional inhibitor and represses Hh target genes. **(B)** With Hh ligand. When Hh is present, binding of Hh ligand to Ptc alleviates the inhibition of Smo. Smo represses the activity of the protein complex that destroys the structure and function of the Gli. The full-length form of Gli is protected and transported into nucleus where it activates transcription.

The spatial and temporal expression pattern of the hedgehog signaling members was studied using RT-qPCR and whole-mount *in situ* hybridization methods. To reveal the function on *C. gigas* myogenesis of hedgehog signaling, we inhibited the signaling with cyclopamine treatment in *C.gigas* embryo. Then the expression profiles of target genes and F-actin were analyzed by mean of RT-qPCR and fluorescent phalloidin staining respectively. The study was not only the first to reveal the molecular characterization and expression files of hedgehog signaling primary genes in bivalva, but also the first to investigate its function on bivalve myogenesis. The results would provide a foundation for analyzing the molecular mechanisms of hedgehog signaling in invertebrate and enable us to better understand the function of hedgehog signaling in invertebrate myogenesis.

MATERIALS AND METHODS

Samples Collection

Adult *C.gigas* were collected from an oyster farm in Laizhou in Shandong province, China. Adult tissue including gonad, hemolymph, mantle, striated, and smooth adductor muscles, gill, labial palp, digestive gland were frozen in liquid nitrogen and then stored at −80°C until further processed. Larval culture was executed as Wang et al. described (Wang et al., 2012). Embryo and larvae were sampled at the following stages: fertilized eggs, two-cell stage, four-cell stage, blastula stage, gastrula stage, trochophore, D-shaped larvae, unbo larvae and eyed larvae. Samples stored at RNA store (Dongsheng Biotech, China) at −20°C were used for extraction of RNA. For whole-mount *in situ* hybridization, samples were fixed in 4% paraformaldehyde (PFA) in 0.1 M phosphate buffered saline (PBS, pH = 7.3) for 2–3 h at 4°C. Afterwards, the larvae were rinsed three times for 10 min in methanol and then were stored at −20 °C in methanol. Samples including D-shaped larvae, umbo larvae and eyed larvae were anesthetized with 7.5% $MgCl_2$ prior to fixation. Samples used for fluorescent phalloidin staining were fixed in 4% PFA in 0.1 M PBS for 2–3 h at room temperature (RT). Afterwards, the samples were rinsed three times for 10 min in 0.1 M PBS at RT and then were stored at 4°C in 0.1 M PBS with 0.1% NaN_3.

Total RNA Isolation and Synthesis of cDNA

TRIzol reagent (Invitrogen, USA) was used to extract the total RNA from *C.gigas* samples following the manufacturer's protocol. Agarose gel (1%) electrophoresis with 10× loading buffer (Takara) was used to detect the quality of RNA. The RNA concentration and purity were verified at optical density (OD)260/(OD)280 with a NanoDrop 2000 (Thermo Scientific) spectrophotometer. PrimeScriptTM Reverse Transcription Kit (Takara) was used to synthesize first-strand cDNA according to the manufacturer's instructions. The cDNA was preserved at −20°C.

Cloning the Full-Length cDNA of Hedgehog Signaling Genes

The internal fragment of hedgehog genes were amplified by PCR according to the bioinformatics prediction of the gene models (Hh: LOC105317164; Smo: LOC105318081; Ptc: LOC105326154; Gli: LOC105322770). The template was the cDNA reverse translated from RNA of *C.gigas* adductors. Specific primers were designed by the Primer Premier 5.0 software (Premier

Biosoft International, Palo Alto, CA) based on the predicted sequence. The thermocycling program of the PCR was performed as follows: pre-denaturation at 94°C for 3 min, 94°C for 30 s, Tm for 30 s, 72°C for 45 s, 35 cycles; 72°C for 5 min. The PCR products were detected by 1.5% agarose gel electrophoresis and then sequenced using an ABI 3730 Genetic Analyzer (Applied Biosystems).

According to the obtained internal fragment sequence, the specific primers for 3′ and 5′ RACE reactions were designed. The 3′ and 5′ terminal cDNA were cloned using the RACE method with the SMARTer® RACE 5′/3′ Kit (Clontech). The 3′ and 5′ RACE PCR reactions were amplified with Tks Gflex™ DNA Polymerase (Takara) according to the following conditions: 98°C for 1 min; 98°C for 10 s, Tm for 10 s, 68°C for 20 s, 35 cycles. The PCR products were purified using DNA purified kit (Tiangen, China) and ligated into the pEASY-simple Blunt vector (Trans Biotech, China) and sequenced in both directions (Sangon Biotech, China).

Molecular Characteristic and Phylogenetic Analysis

The 3′, 5′ terminal sequence and internal fragment were assembled using SeqMan (DNAStar) software to acquire the full length cDNA of hedgehog signaling genes. The DNAMAN (Lynnon Biosoft) software was used to predict the open reading frame and translate the cDNA sequence to the protein sequence. The isoelectric point (pI) and molecular weight (MW) of the deduced amino acid sequences were predicted using the Compute pI/MW Tool at the ExPAsy site (http://web.expasy.org/compute_pi/). The TMHMM server v.2.0 (http://www.cbs.dtu.dk/services/TMHMM-2.0/) was used to predict transmembrane helices. The NetPhos server (http://www.cbs.dtu.dk/services/NetPhos) was used to generate neural network predictions for phosphorylation sites. The ScanProsite program (https://prosite.expasy.org/scanprosite/) was used to analyze the conserved motif. The PredictProtein program (https://ppopen.informatik.tu-muenchen.de/) was used to predict the secondary structure and transmembrane helices of protein. The signal peptide and three-dimensional structure of the protein were analyzed with the SignalP 4.1 (http://www.cbs.dtu.dk/services/SignalP/) and PHYRE2 servicer (http://www.sbg.bio.ic.ac.uk/phyre2). The ClustalW (Lynnon Biosoft, Los Angeles, CA) was used to align the protein sequences and modified by the ESPript 3.0 (Robert and Gouet, 2014). A phylogenetic tree was constructed by the Neighbor-Joining analysis with 1,000 bootstrap replicates using MEGA 7.0 software (Kumar et al., 2016). Protein sequence logos were generated using the Java application LogoBar (Pérez-Bercoff et al., 2005).

Expression Analysis of Key Genes by Real-Time Quantitative PCR

The qRT-PCR primers for the hedgehog signaling genes were designed, and their specificities were detected by conventional PCR and melting curve analyses. Ribosomal protein S18 (RS18) and elongation factor 1-α (EF1-α) were used as the internal control in the larvae and adult samples respectively (Du et al., 2013). cDNAs of hedgehog signaling genes were amplified using SYBR® Premix Ex Taq™ II kit (Takara) in a LightCycler® 480 real-time PCR system (Roche) according to the manufacture's protocols. The 10 μL qRT-PCR reaction contained 5 μL 2× SYBR Premix ExTaq (Takara), 1.8 μL of each primer, and 1 μL diluted cDNA. The RT-qPCR amplification was conducted at 95°C for 30 s, followed by 40 cycles at 95°C for 5 s, 60°C for 20 s and 72°C for 20 s. The relative expression was calculated by the $2^{-\Delta\Delta Ct}$ method (Livak and Schmittgen, 2001). All data were given in the light of relative mRNA expression levels as means ± SE ($n = 6$). The IBM SPSS Statistics 22 was used to analyze the significant differences between the means. All the data analyses were performed using one-way ANOVA followed by a multiple comparison. Differences were considered statistically significant at $P < 0.05$.

Whole-Mount *in situ* Hybridization

Whole mount *in situ* hybridization was performed using digoxigenin-labeled sense and anti-sense probes synthesized following SP6- and T7-mediated *in vitro* transcription (MEGAscript kit, Ambion) using a DIG-RNA labeling Kit (Roche) from the clone of cDNAs fragment of target genes. The experiment was conducted using the protocol described by Thisse and Thisse (2008) with some adjustments. Stored samples were rehydrate stepwise into PBST for 30 min, and then prehybridized with hybridization buffer (50% formamide, 50 μg/ml of heparin, 5 × SSC, 500 μg/ml tRNA, 9.2 mM citric acid, 0.1% Tween-20). Sense or anti-sense probes concentrations was 1.0 to 2.0 ng/μl and hybridizations were performed at 65°C overnight. Unbound probes were rinsed by a series of low-salt (2 × SSC, 0.2 × SSC) and samples were incubated in blocking solution for 2–4 h. embryo and larvae were incubated in anti-digoxigenin antibody (Roche) at 1:5,000 in blocking solution overnight at 4°C. Samples were then washed several times in MABT (150 mM sodium chloride, 100 mM maleic acid, 0.1% Tween-20, pH 7.5), and in alkaline Tris buffer for 3 × 5 min. Color reactions were performed with 2% NBT/BCIP solution for 2 h in at room temperature or overnight at 4°C. Specimens were photographed on a fluorescence light microscope (Olympus BX53) with digital camera (Olympus DP73).

Cyclopamine Treatment

Cyclopamine, a known blocker of hedgehog signaling pathway from invertebrates and vertebrates (Incardona et al., 2000; Kang et al., 2003), was diluted to a final concentration of 0.5, 1, 2, 4, 6 μM in sea water (from a stock solution 10 Mm in ethanol). Embryos were selected for treatments when they developed into trochophore stage. Experimental embryos (trochophore stage) were cultured in cyclopamine for 12 h (up to D-shaped stage). Control embryos were cultured in sea water with 0.1% ethanol. Treatments were done in 12 L bucket with 10 L of filtered fresh seawater. The rearing conditions retained same for control and experiment embryos. Water temperature was maintained at 23–24°C, with salinity at 30 psu and densities at 10 embryo/ml. Samples were collected and fixed for RNA extraction and F-actin staining, as described above.

F-Actin Staining and Confocal Microscopy

The specimens were permeabilized in PBS containing 2% Triton-X 100 (PBT, pH = 7.3) overnight at room temperature. Actin staining was conducted by fluorescence labeling of filamentous F-actin with Phalloidin-iFluor^{TM} 488 Conjugate (AAT Bioquest) in a 1:1,000 dilution in PBT for 24 h in the dark. Then the larvae were washed three times for 10 min each and mounted in Fluoromount G (Southern Biotech) between two coverslips to allow scanning from both sides. Acquisition of confocal images were performed on a Nikon ECLIPSE Ti confocal laser scanning microscope equipped with the software NIS-Elements (Version 4.0). Optimization and adjustment of brightness and contrast was conducted with Image J software (National Institutes of Health) and Photoshop CS5 (Adobe).

RESULTS

cDNA Cloning and Sequence Analysis of Key Hedgehog Pathway Genes

The full-length cDNA fragment of CgHh was 3,676 bp, containing a 5′-untranslated region (5′-UTR) of 1,176 bp, a 3′-untranslated region (3′-UTR) of 1,276 bp, and a putative open reading frame (ORF) of 1,224 bp encoding a 407-amino acid protein with an ATG start codon and TGA stop codon. A polyadenylation signal, AATAAA, was found 12 bases upstream from the poly (A) tail. The nucleotide and deduced amino acid sequences of Hh were shown in **Figure 1**. According to the amino acid sequence, the predicted molecular mass and the isoelectric point of CgHh were 44.99 kDa and 7.67, respectively. The total number of positivity (Arg + Lys) and negativity (Asp + Glu) in the amino acid composition of CgHh was 44 and 43, respectively. A signal petide was predicted by the SignalP 4.1 Server: the signal peptide cleavage sites of CgHh were Ala16 and Phe17, suggesting that it was a secretory protein. The CgHh protein contained HH-signal, Hint-N, and Hint-C conserved domains predicted by SMART software. The HH-signal domain is the N-terminal domain of CgHh protein, which is responsible for signaling following cleavage from the C-terminal domain. The Hint-N and Hint-C represented the C-terminal and intein domain of CgHh protein. The Hint domain was split to accommodate large insertions of endonucleases. A conserved intein N-terminal splicing motif were detected in the Hint-N domain (**Figures S1**, **S5**). The putative protein secondary structure of CgHh contained eight alpha helices and twenty one beta strand structures. The tertiary structure of Hh protein was based on template c3m1nB, which shared 78% identity with CgHh protein.

The full length CgPtc cDNA was 5,266 bp, including a 288 bp 5′-UTR, a 3,957 bp ORF encoding a 1,318 amino acid protein with predicted molecular weight of 146.51 kDa and a pI of 6.46 and a 1,021 bp 3′-UTR with a typical polyadenylation signal sequence AATAAA and a poly (A) tail. CgPtc was not a secreted protein for the reason that no signal peptide was detected in the Ptc protein according to SignalP 4.1 analysis with the D-score of 0.105 (cutoff score of 0.450). CgPtc protein included a Sterol-sensing domain and a Patched domain at the position 433–587 and 908–1,155 respectly. CgPtc protein owned one conserved Sterol-sensing domain (SSD) motif (**Figures S2**, **S6**). CgPtc is a protein with 12 transmembrane domains and its transmembrane helix region were at located among amino acid positions 56–78, 407–429, 442–464, 468–490, 518–540, 550–572, 724–746, 1002–1024, 1026–1048, 1058–1080, 1101–1123, 1133–1155. The secondary structure prediction showed that 55% of the total amino acids were in alpha helix and 5% formed beta strand. There were 27 Serine, 4 Tyrosine and 8 Threonine phosphorylation sites by protein kinase A (PKA) and casein kinase I (CKI).

The full length of cDNA CgSmo contained a 5′-UTR of 387 bp and a 3′-UTR of 802 bp with a poly (A) tail (**Figure 3**). The ORF of Smo was 3,021 bp encoding 1,006 amino acids with predicted theoretical isoelectric point of 9.51 and molecular weight of 112.3 kDa. The CgSmo was a secretory protein and the signal pepide cleavage sites of CgSmo were Ser21 and Thr22. Smo protein contained the FRI and Frizzled conserved functional domains. Seven transmembrane helix region detected by the TMHMM program were at located among amino acid positions 204–226, 233–255, 290–312, 333–355, 375–397, 426–448, 490–512, 683–700 (**Figure S3**). The predicted phosphorylated sites of CgSmo were mainly located in the C-terminal tail (**Figures S3**, **S7**). There were 27 Serine, 8 Tyrosine and 4 Threonine phosphorylation sites by protein kinase A (PKA) and casein kinase I (CKI). Two conserved motifs were found in accordance with CgSmo amino acids, including a Fruzzled (FZ) and G-protein coupled receptors family motifs at the positions of 26–150 and 202–467 respectively (**Figure S3**).

The cDNA of CgGli was 5,278 bp, containing 402 bp 5′-UTR, 4,749 bp ORF and 127 bp 3′-UTR. The ORF of 4,749 bp was predicted to encode a 1,582 amino acid. The estimated molecular weight and pI were 176.37 kDa and 7.84 respectively. There was no signal peptide and transmembrane domains in CgGli protein. The CgGli protein included five conserved ZnF_C2H2 functional domains. The zinc finger domains were relatively small protein motifs which contained multiple finger-liker protrusions that made tandem contacts with their target molecule. There were four zinc finger C2H2 type motifs in CgGli protein (**Figures S4**, **S8**). The tertiary structure of CgGli protein was based on template c2gliA, which shared 81% identity with CgGli protein.

Homology and Phylogenetic Analysis of Key Hedgehog Pathway Genes

The amino acid sequence alignment of CgHh with Hh from other vertebrate and invertebrate species showed a moderate degree of sequence similarity. It exhibited high similarity to Hh of the genus *Crassostrea* such as *Crassostrea virginica* (91%). A high sequence similarity was detected in other Bivalva species such as *Mizuhopecten yessoensis* (59%), *Nucula tumidula* (57%). In Mollusk, A high similarity was founded in Gastropoda, Cephalopoda, Scaphopoda, Polyplacophora, including *Patella vulgate* (55%), *Lottia gigantean* (57%); *Idiosepius notoides* (55%), *Euprymna scolopes* (53%), *Octopus bimaculoides* (53%); *Antalis entails* (50%); *Acanthochitona crinite* (55%). Furthermore, A moderate similarity was analyzed in other invertebrates: Annelida (50–51%), Insecta (47–52%); vertebrates: Osteichthyes

(48%), Chondrichthyes (50%), Aves (49–50%), Mammalia (48%). In addition, the Hedge_signal domain and Hint-C partial domain were evolutionally conserved among the vertebrates and invertebrates (**Figure 2A**). The phylogenetic analysis of Shh showed that the *Crassostrea* species was clustered together, and was closely related to the *M. yessoensis* (**Figure 2B**). All the Mollusca species were clustered together and formed two branches. The Bivalva, Polyplacophora and Gastropoda were clustered together, the Scaphopoda and Cephalopoda were clustered together as another branch.

Sequence alignment of CgPtc with Ptc from other species showed that it displayed an extremely high similarity to Ptc of the *C. virginica* (89%; **Figure 3A**). A moderate degree of amino acid sequence similarity was found in other mollusks such as *M. yessoensis* (63%), *Terebratalia transversa* (55%), and *Biomphalaria glabrata* (56%). It also exhibited moderate similarity to Ptc form other species: *Novocrania anomala* (59%), *Lingula anatine* (55%), *Limulus Polyphemus* (50%), *Patiria miniata* (48%), *Octodon degus* (46%) and *Acanthaster planci* (45%). In addition, the transmembrane helical region, sterol-sensing domain and patched domain were evolutionally conserved among vertebrates and invertebrate species. A majority of phosphorylation sites were highly conserved located in the position of 121, 169, 261, 373, 409, 451, 515, 545, 613, 676, 685, 894, 916, 954, 984, 1,054. The phylogenetic analysis showed that all the invertebrates were clustered together and formed three branches: Bivalvia, Gastropoda and Brachiopoda. *C. gigas*, *C. virginica,* and *M.yessoensis* were clustered together. *B.glabrata* and *L.anatina* were clustered together as another branch. The vertebrates were clustered together and formed two branches including Aves and Mammalia (**Figure 3B**).

Multiple sequence alignment of Smo showed that CgSmo had the highest identity with *C.virginica* at 87% in the *Crassostrea* species (**Figure 4A**). A moderate degree of sequence similarity was found in mollusks including *M.yessoensis* (53%), *B.glabrata* (49%), *L.anatina* (49%). The transmembrane helical region, FRI domain and Frizzled domain were highly conserved among invertebrates and vertebrates. The ligand binding sites at the position of 374, 451, 454, 458, 488, 493, 497 were absolutely conserved among species. According to deduced amino acid sequences of CgSmo from other species, a neighbor–joining phylogenetic tree was formed to identify the evolutionary position of CgSmo. In general, species from the same class were clustered together and developed into a separated subgroup. All the Mollusca species were clustered together and formed two branches including Bivalvia and Gastropoda; Brachiopoda species including *L.anatina* and *T. transversa* were clustered together as another branch (**Figure 4B**). In general, the phylogenetic results were consistent with traditional taxonomy.

Similar to CgHh, CgPtc and CgSmo, CgGli showed a high similarity to *C. virginica* (91%) and a moderate degree identity among other mollusks including *M. yessoensis* (55%), *O. bimaculoides* (62%), *B. glabrata* (55%). For *Brachiopoda*, CgGli exhibited a moderate similarity such as *L.anatina* (55%) and T. transversa (44%; **Figure 5A**). The putative nucleic acid binding sites at the position 555, 558, 559, 563, 567, 568, 583, 585, 586, 589, 590, 593, 594, 598 were highly conserved. The Zn binding sites owning a C-C-H-H conserved feature residue pattern and five ZnF_C2H2 domain showed a high identity among species. All the invertebrates were clustered together and came into being four groups including Bivalvia, Gastropoda, Cephalopoda and Brachiopoda. In Bivalvia, *Crassostrea* species were clustered together and had a closer relationship with *M.yessoensis*. Three branches including Osteichthyes, Reptilia and Aves were established in vertebrates (**Figure 5B**).

Temporal Expression Patterns of Key Hedgehog Pathway Genes

The temporal expression patterns among different embryo-larval developmental stages and different adult tissues of several key hedgehog pathway genes were examined by RT- qPCR (**Figure 6**). CgHh mRNA was not detected until blastula stage ($P < 0.05$) during the embryo stages. CgHh mRNA began to accumulate during blastula stage to trochophore stage and peaked in D-shaped stage ($P < 0.05$). During umbo larvae and eyed larvae, CgHh gene expression showed a sharply decrease ($P < 0.05$). The CgHh mRNA expression levels in different tissues including the female gonad, male gonad, gill, mantle, digestive gland, labial palp, striated adductor muscle, smooth adductor muscle, and hemolymph were investigated. The highest expression level was detected in smooth adductor muscle ($P < 0.05$), followed by gill, digestive gland, labial palp and striated adductor muscle. Relatively low expression were discovered in mantle, gonad and hemolymph ($P < 0.05$). CgPtc mRNA expression was relatively low during fertilized egg and four-cell stage until development into blastula stage ($P < 0.05$). CgPtc gene expression showed an overall increase pattern from blastula stage through gastrula stage and trochophore stage into D-shaped stage. A small decreased expression was observed in umbo larvae. Similar to CgHh, CgPtc mRNA expression showed a highest level in the smooth adductor muscle and a higher level in the gill and striated adductor muscle. A lower expression was detected in the labial palp, mantle, gonad, digestive gland and hemdymph ($P < 0.05$). CgSmo mRNA expression began fertilized egg and increased throughout the blastula stages and gastrula stage. A sharply decrease expression was observed from trochophore stage to eyed larvae ($P < 0.05$). CgSmo mRNA was expressed in a variety of tissues and had a highest expression in gonad tissue. A lower expression was observed in hemolymph, gill, labial palp and adductor muscles. CgGli mRNA was expressed in a similar pattern to CgHh. There was an overall increasing trend from the blastula stage through trochophore stage and a large increase at the eyed larvae stage. The CgGli gene was expressed in all tested tissues and the highest expression level was founded in gill. Relatively lower expression levels were detected in labial palp, gill, mantle, and adductor muscle.

RNA Localization Patterns of Key Hedgehog Pathway Genes

The RNA localization patterns of key hedgehog pathway genes from fertilized eggs to eyed larvae was studied using whole-mount *in situ* hybridization (**Figures 7**, **8**). The CgHh RNA localization pattern in early gastrula stage was a stained cell

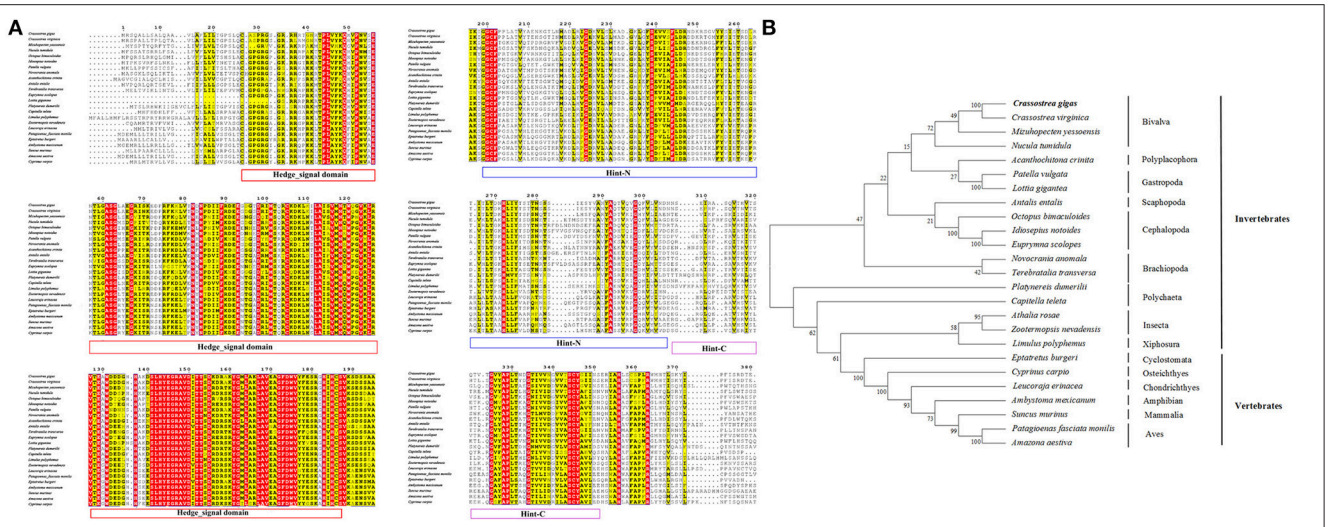

FIGURE 2 | (A) Multiple sequence alignment of the CgHh amino acid sequence among species. The conserved functional structure are marked in box. Identical residues are shown as white letters with red background, and similar residues are shown as black letters with yellow background. **(B)** Neighbor-joining phylogenetic tree based on the amino acid sequences of the CgHh.

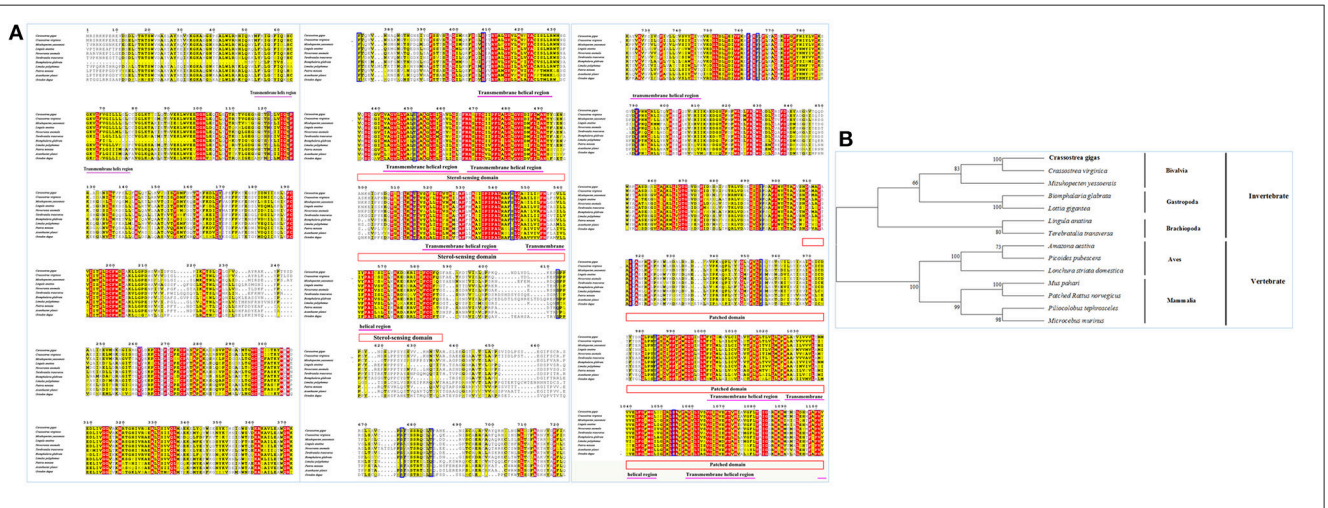

FIGURE 3 | (A) Multiple sequence alignment of the CgSmo amino acid sequence among species. The conserved functional structure are marked in box. Identical residues are shown as white letters with red background, and similar residues are shown as black letters with yellow background. **(B)** Neighbor-joining phylogenetic tree based on the amino acid sequences of the CgSmo.

clusters at the middle of the embryo. The one cell clusters have an increase in number and size during gastrula stages. Several cell clusters were distributed randomly in the body of larvae in trochopore stage. The specific signal was observed in the velum position during umbo and eyed larvae stage. The RNA localization pattern of CgSmo was several stained clusters that were located symmetrically with respect to the midline of the larval body during gastrula stages. One cell cluster was observed from trochopore stage and D-shaped larvae stage. The CgSmo gene location was restricted to the gut and stomach domain in umbo stage. The specific staining was detectable at the foot in eyed stage. Similar to CgHh, the specific signaling of CgPtc was one cell cluster in early gastrula stage. The cell clusters were increased in embryos and larvae during gastrula and early trochopore stage larvae. The specific staining were clustered together and widespread during late trochopore stage and early D-shaped larvae. However, the specific signaling decreased in late D-shaped stage and located at the gut domain in the umbo larvae and adductor muscle domain in eyed larvae. The CgGli specific staining was one cell cluster in early gastrula stage and became more and more in late gastrula stage. The specific signaling was stronger and the distribution was widespread throughout the larval body during trochopore and early D-shaped larvae. One cell cluster

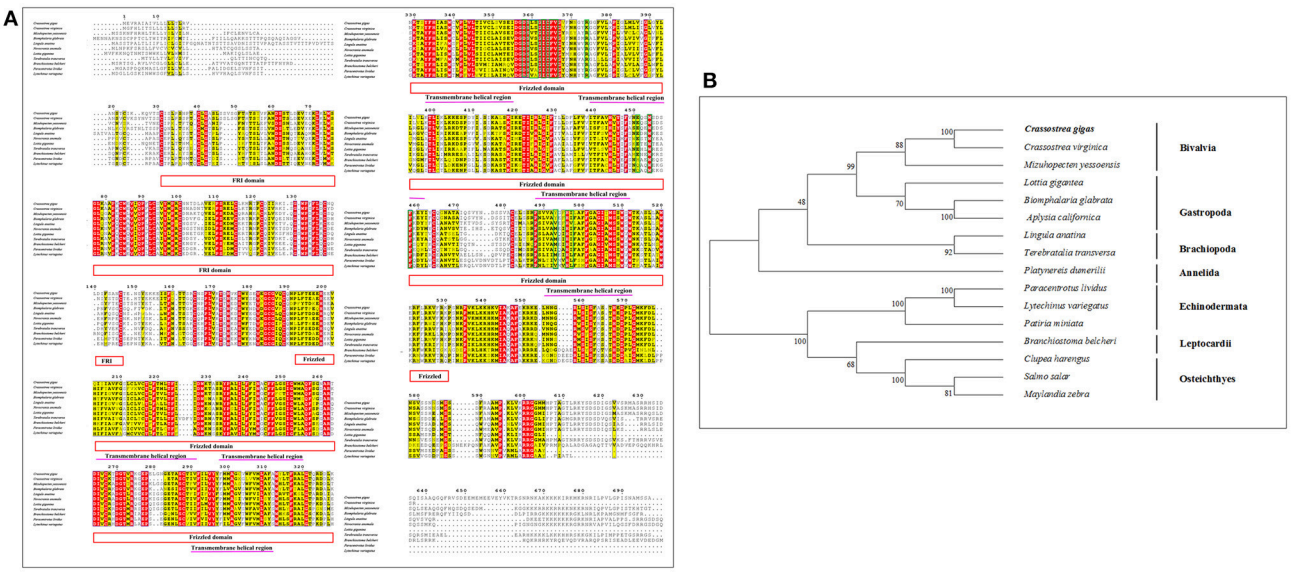

FIGURE 4 | (A) Multiple sequence alignment of the CgPtc amino acid sequence among species. The conserved functional structure are marked in box. Identical residues are shown as white letters with red background, and similar residues are shown as black letters with yellow background. **(B)** Neighbor-joining phylogenetic tree based on the amino acid sequences of the CgPtc.

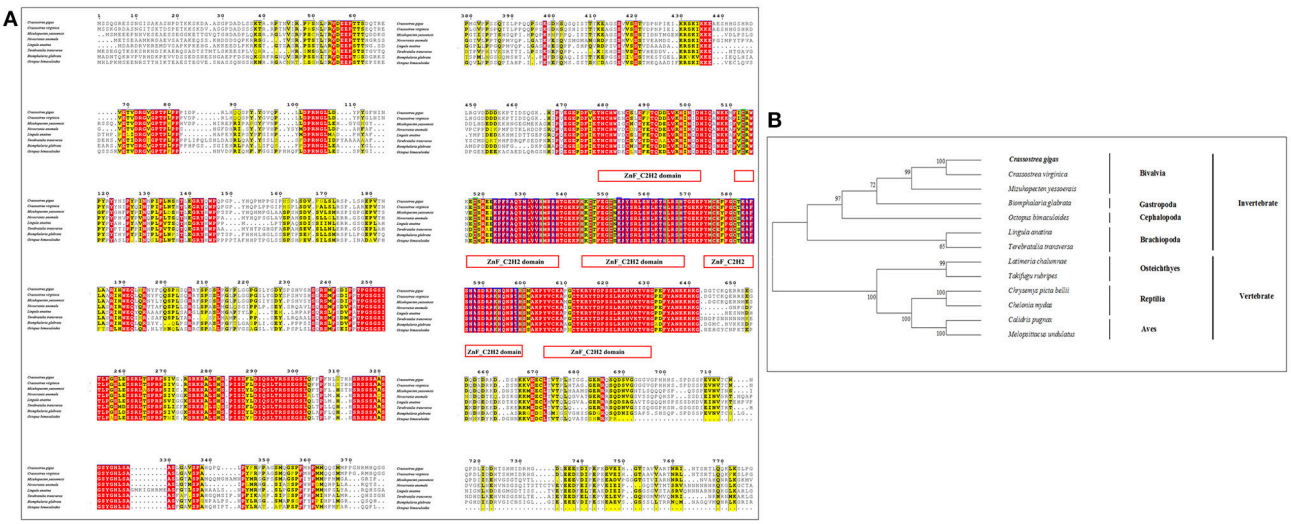

FIGURE 5 | (A) Multiple sequence alignment of the CgGli amino acid sequence among species. The conserved functional structure are marked in box. Identical residues are shown as white letters with red background, and similar residues are shown as black letters with yellow background. **(B)** Neighbor-joining phylogenetic tree based on the amino acid sequences of the CgGli.

was observed in adductor muscle domain in umbo and eyed larvae.

Quantification of the Inhibitory Effect of Cyclopamine on the Expression of Key Hedgehog Pathway Genes

To evaluate if the expression of key hedgehog pathway genes was blocked by cyclopamine, we quantified the expression by means of RT- qPCR (**Figure 9**). We found that the expression of key genes were severely down-regulated in cyclopamine treated embryos. The effective inhibition concentration of CgHh and CgPtc was 0.5 μM. The expression of CgSmo and CgGli had a significant reduction when the embryos were treated with cyoclopamine at 2 and 1μM, respectively ($P < 0.05$). Results also showed that the expression level of CgPtc decreased with the increase of cyclopamine concentration.

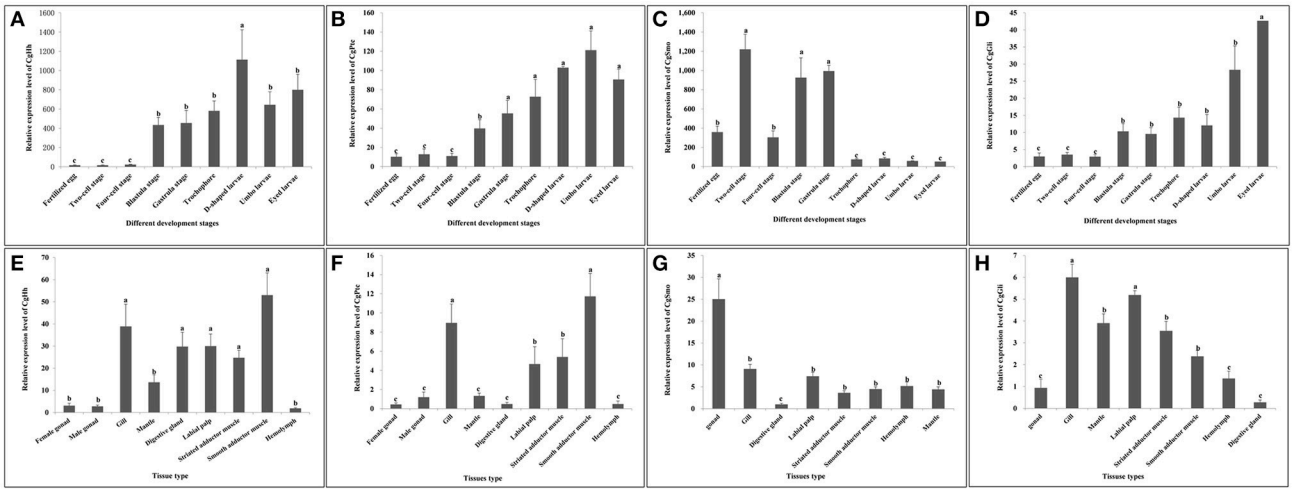

FIGURE 6 | (A–D) Expression profiles of key genes during embryo-larval developmental stages. **(E–H)** Expression profiles of key genes in adult different tissues. Different letters indicated significantly different ($P < 0.05$). The letters "a," "b," and "c" indicate the significance of the differences between two groups. Firstly, the whole mean of gene expression is ranked from large to small. The maximum average is marked the letter "a" and this average is compared with the following averages. Where the difference is not significant, the letter "a" is marked; otherwise, the letter "b" is marked. Secondly, the maximum average marked "b" is used as the standard deduction and compared with the following unmarked averages. Where the difference is not significant, the letter "b" is marked; otherwise, the letter "c" is marked.

The Hedgehog Pathway Was Required for Normal Myogenesis in *C. gigas*

To examine if the hedgehog pathway was involved in normal muscle development in *C.gigas*, we investigated the myogenesis progress of cyclopamine treated larvae by fluorescence labeling of filamentous F-actin with Phalloidin-iFluor^{TM} 488 Conjugate. Here, treatment with cyclopamine at 0.5, 1 and 2 μM for 12 h had no damage effect on muscle development and the muscle system of treatment groups was same to control groups which owned three pairs velum retractors, anterior adductor muscle and posterior adductor (**Figure 10**). The velum retractors and adductor muscles of larvae treated with cyclopamine at 4 μM for 6–12 h was significantly destroyed. The damage on larval muscle was mild after 6 h treatment and was severe after 12 h treatment. The damage effect on larval muscle was observed until the larvae were treated for 6 h at 6 μM and the larval velum retractor was destroyed severely. When the larvae were treated by cyclopamine at 6 μM for 8 h, the larval velum retractor was hardly presented. The damaged effect on larvae musculature in 12 h treatment was stronger than that in 6 h and the major musculature including velum retractor and adductor muscle of larvae was vanished.

DISCUSSION

The Sequence Characteristics of Key Hedgehog Pathway Genes

The complete cDNA sequence and characterization of the hedgehog pathway genes in *C.gigas* were analyzed in the present study. The N-terminal of Hh was responsible for signaling, and the C-terminal autoprocessing Hint domain was in charge of adding cholesterol moiety to the N-terminal signaling domain (Gallet et al., 2003; Bijlsma et al., 2004). C-terminal to the Hint domain is a sterol recognition region [SSR; Thomas et al., 2008]. The CgHh owned conserved functional motifs including the N-terminal HH-signal domain and the C-terminal autoprocessing Hint domain. Moreover, a conserved intein N-terminal splicing motif were also detected in the Hint-N domain. These findings revealed that the CgHh possessed the primary structural and functional domains as present in typical Hh family. The high sequence similarity suggested the conserved function of Hh gene among Mollusca. In addition, similar to most invertebrates, there was only one Hh gene in *C.gigas*. In general, the obvious difference between invertebrates and vertebrates is that the key hedgehog pathway genes have been duplicated in vertebrates (Huangfu and Anderson, 2006). For example, there are five Hh homologs in zebrafish and three Hh homologs in the mouse respectively (Ekker et al., 1995; Bitgood et al., 1996; Zhang et al., 2001). However, there are only one Hh gene in most invertebrates such as *Drosophila* (Huangfu and Anderson, 2006), sea urchin (Warner et al., 2013), *Sepia officinalis* (Grimaldi et al., 2008). As an important receptor of Hh in hedgehog pathway, Ptc turns off the downstream signaling pathway in the absence of Hh ligand (Huangfu and Anderson, 2006). Based on the deduced amino acid sequence of CgPtc, we predicted that it contained a sterol-sensing domain (SSD) and patch domain, which were hallmarks of Ptc family members (Huangfu and Anderson, 2006). In addition, CgPtc owned 12 transmembrane domains which showed a high similarity among Mollusca (>70%). Apparently, this 12 transmembrane domains (TM) is common within the family of vertebrates and invertebrates including mouse (Goodrich et al., 1996), chicken (Marigo et al., 1996), *Drosophila* (Huangfu and Anderson, 2006), and *Sepia officinalis* (Grimaldi et al., 2008). Moreover, the phosphorylation sites of

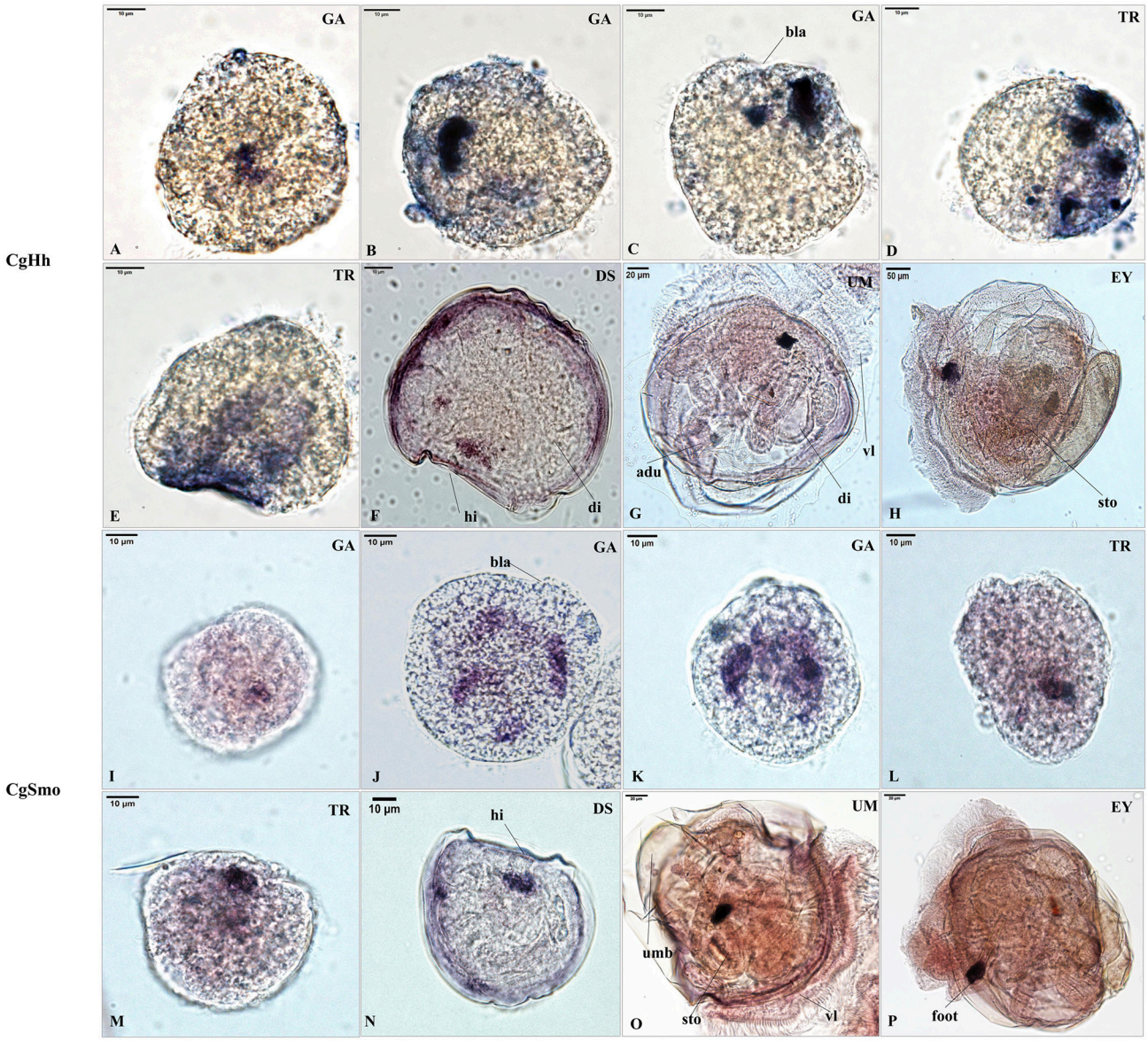

FIGURE 7 | RNA localization patterns of key hedgehog pathway genes during embryonic to larval stage. **(A–C)** RNA localization patterns of CgHh during gastrula stages. **(D,E)** RNA localization patterns of CgHh during trochopore stages. **(F)** RNA localization patterns of CgHh during D-shaped stages. **(G)** RNA localization patterns of CgHh during umbo stages. **(H)** RNA localization patterns of CgHh during eyed stages. **(I–K)** RNA localization patterns of CgSmo during gastrula stages. **(L,M)** RNA localization patterns of CgSmo during trochopore stages. **(N)** RNA localization patterns of CgSmo during D-shaped stages. **(O)** RNA localization patterns of CgSmo during umbo stages. **(P)** RNA localization patterns of CgSmo during eyed stages. GA, gastrulae stage; TR, trochophore stage; DS, D-shaped stage; UM, umbo larvae stage; EY, eyed-larvae stage; bla, blastopore; hi, hinge; di, digest gland; vl, vlum; um, umbo; fo, foot; adu, adductor.

CgPtc was highly conserved among molluscan species (>70%). There was only one Ptc gene in *C.gigas* and it was consistent with the phenomenon that the key hedgehog pathway genes have been duplicated in vertebrates compared to invertebrates (Huangfu and Anderson, 2006). For example, both mice and zebrafish have two ptc homologs, while *Ciona* and *Drosophila* only oppose one Ptc gene (Goodrich et al., 1997; Wolff et al., 2003; Huangfu and Anderson, 2006). Smo is a membrane protein owning a seven TM domain structure (Alcedo et al., 1996). In *C. gigas*, CgSmo contained most common features of Smo including the 7-TM domain structure, FRI/ Frizzled conserved functional domains, Fruzzled (FZ) and G-protein coupled receptors family motifs. Multiple sequence alignment of Smo among invertebrates showed that the TM region was relatively conserved among species, while significant difference exists in the C-terminal domain (CTD). It was also found in *Drosophila* and experiments in the fly have demonstrated that the CTD is important for Smo activity (Jia et al., 2003; Nakano et al., 2004). In addition, similar to *Drosophila* we found that the predicted phosphorylated sites of CgSmo were

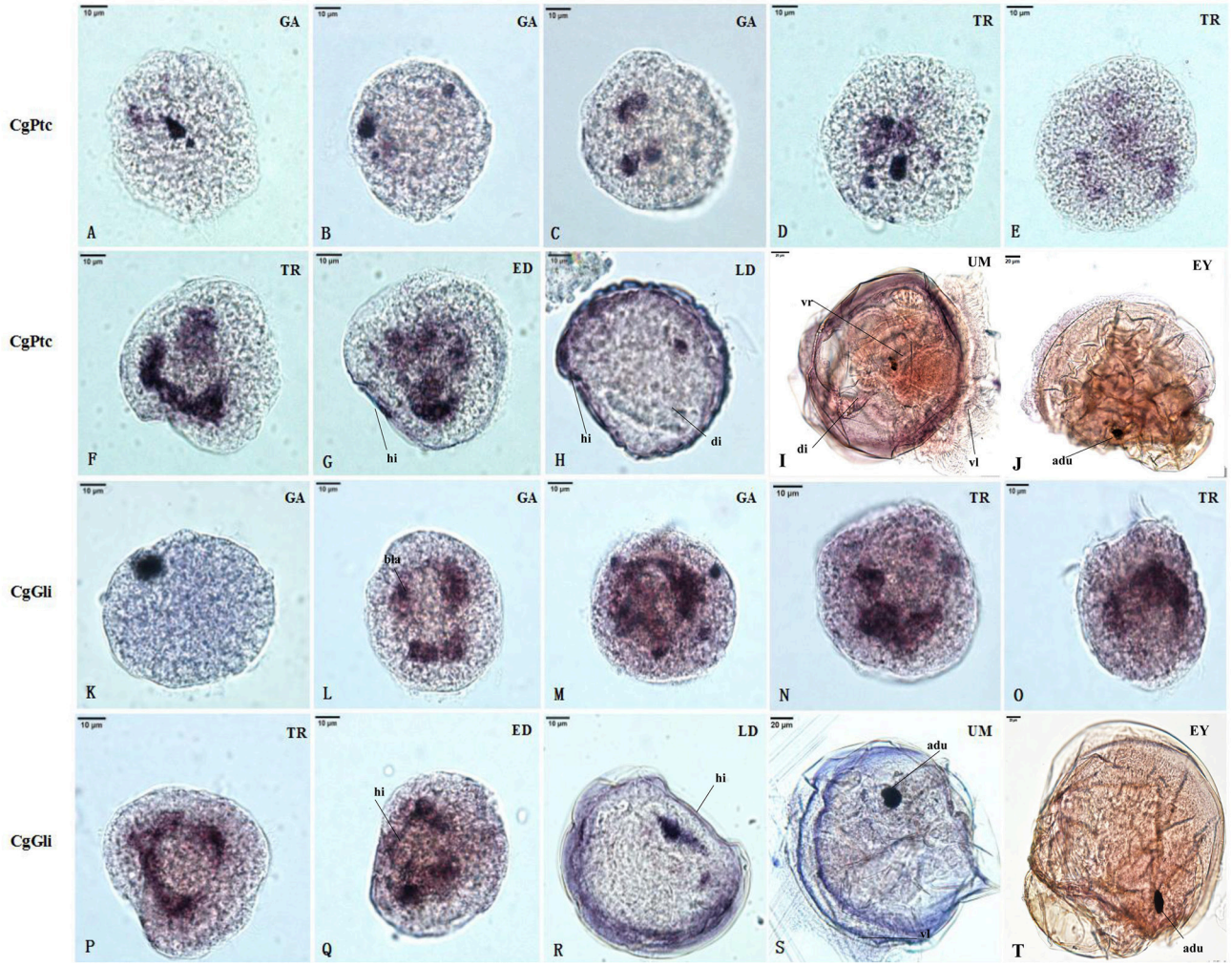

FIGURE 8 | RNA localization patterns of key hedgehog pathway genes during embryonic to larval stage. **(A–C)** RNA localization patterns of CgPtc during gastrula stages. **(D–F)** RNA localization patterns of CgPtc during trochopore stages. **(G)** RNA localization pattern of CgPtc during the early D-shaped stage. **(H)** RNA localization pattern of CgPtc during the late D-shaped stage. **(I)** RNA localization patterns of CgPtc during umbo stages. **(J)** RNA localization patterns of CgPtc during eyed stages. **(K–M)** RNA localization patterns of CgGli during gastrula stages. **(N–P)** RNA localization patterns of CgGli during trochopore stages. **(Q)** RNA localization pattern of CgGli during the early D-shaped stage. **(R)** RNA localization pattern of CgGli during the late D-shaped stage. **(S)** RNA localization patterns of CgGli during umbo stages. **(T)** RNA localization patterns of CgGli during eyed stages. GA, gastrulae stage; TR, trochophore stage; ED, early D-shaped stage; LD, late D-shaped stage; UM, umbo larvae stage; EY, eyed-larvae stage; bla, blastopore; hi, hinge; di, digest gland; vl, vlum; um, umbo; fo, foot; adu, adductor.

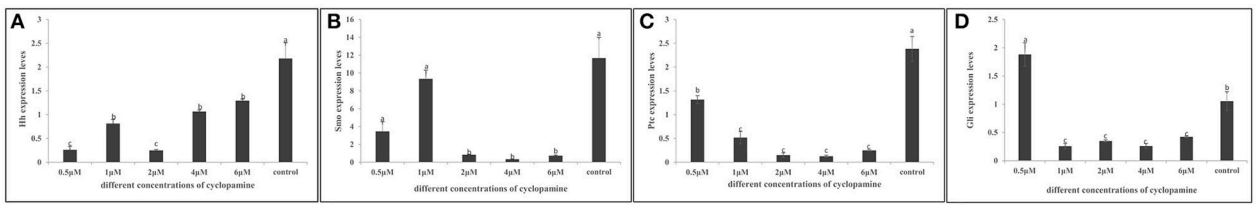

FIGURE 9 | (A–D) Inhibitory effect of cyclopamine on the RNA Expression levels of key hedgehog pathway genes. The larvae in the figures was in the D-shaped stage. Different letters indicated significantly different ($P < 0.05$). The letters "a," "b," and "c" indicate the significance of the differences between two groups. Firstly, the whole mean of gene expression is ranked form large to small. The maximum average is marked the letter "a" and this average is compared with the following averages. Where the difference is not significant, the letter "a" is marked; otherwise, the letter "b" is marked. Secondly, the maximum average marked "b" is used as the standard deduction and compared with the following unmarked averages. Where the difference is not significant, the letter "b" is marked; otherwise, the letter "c" is marked. ad, adductor muscle; vr, velum retractor muscle; lr, larval retractor.

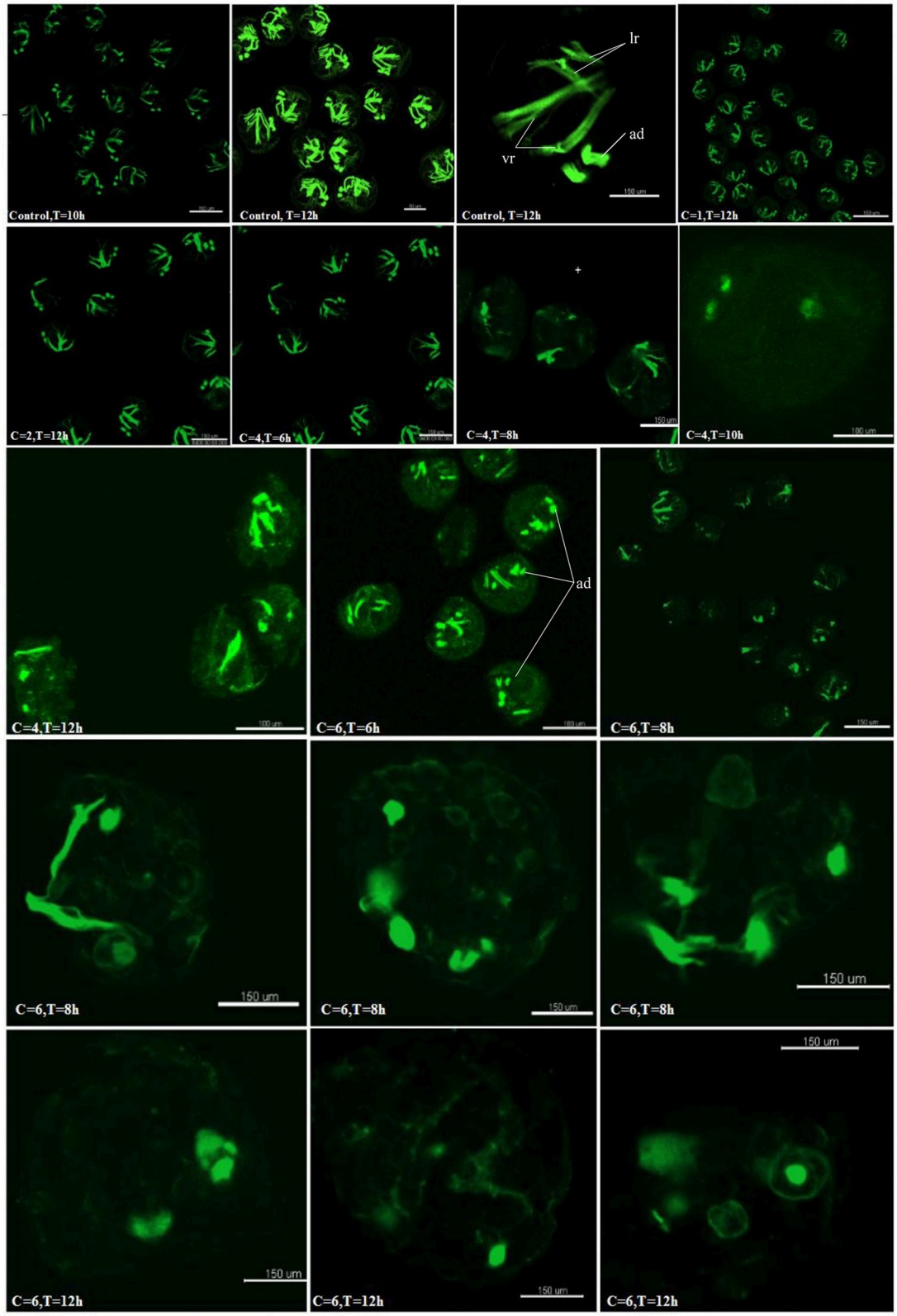

FIGURE 10 | Myogenesis of cyclopamine treated larvae. C represent the concentration of the cyclopamine (μM), T represent the treated time (hour).

mainly located in the C-terminal tail. Though the CTD of Smo was discrepant, the phosphorylation sites by protein kinase A (PKA) and casein kinase I (CKI) was conserved among invertebrates (Denef et al., 2000; Zhang et al., 2004). Because Smo phosphorylation coordinates Hh activation (Denef et al., 2000), we speculated that the function on Hh activation of Smo was conserved among invertebrates. Gli is a member of zinc-finger transcription, which has been identified as a downstream mediator of the hedgehog signaling pathway (Yang et al., 1997). According to the deduced amino acid sequence, CgGli owned most common structures including five conserved ZnF_C2H2 functional domains and zinc finger DNA binding domains. These results suggested that Gli was a relatively conserved genes among invertebrates.

Temporal Expression Patterns of Key Hedgehog Pathway Genes

Quantitative analysis of the key genes in embryo-larval stages indicated that CgHh, CgPtc, CgGli mRNA began to accumulate during the blastula to gastrulation stages and accumulated throughout trochophore and into the D-shaped stage. Similar results were also found in the previous studies on sea urchin (Walton et al., 2006). In conclusion, the key genes mRNA expression levels were observed higher in the gastrulation and trochopore stags which were an early stage of muscle development. It suggests that hedgehog pathway was mainly involved in early muscle development such as the differentiation of mesodermal muscle. The key genes were expressed in all tested tissues, indicating that the hedgehog pathway participated in various physiological activities in *C.gigas*. The highest expression level of CgHh and CgPtc were observed in adductor smooth muscle, suggesting that the hedgehog pathway was connected with muscle development in *C. gigas*. Similar phenomenon also occurred in sea urchin (Warner et al., 2013).

RNA Localization Patterns of Key Hedgehog Pathway Genes

The RNA localization patterns of CgHh and CgSmo were similar during gastrula and trochopore stages. In these stages, the irregular cell clusters were distributed randomly at the body of larvae. The specific staining of CgPtc and CgGli became stronger compared to CgHh and CgSmo during gastrula and trochopore stages. Moreover, the specific signal of CgPtc and CgGli were observed in velum retractors during the early D-shaped stages. The location patterns were accordance with myosin essential light chain (MELC) which was one muscle marker in *C. gigas* (Yu et al., 2017). These results suggested that CgPtc and CgGli were concerned with larval myogenesis in *C.gigas*. Similar data was also found in mouse (Wolff et al., 2003), *Sepia officinalis* (Grimaldi et al., 2008). The key pathway genes except CgSmo had a common localization that was near the hinge position during late D-shaped stage. The specific signals were observed in the velum, gut, stomach, adductor domain during umbo, and eyed larvae stage, suggesting that the signaling pathway might be involved in these organ development in *C. gigas*. Similarly, hedgehog signaling pathway have been confirmed to participate in muscle and gut development in chicken (Sukegawa et al., 2000), Amphioxus (Shimeld, 1999), zebrafish (Strähle et al., 1996), leech (Kang et al., 2003).

Inhibitory Effect of Cyclopamine on the RNA Expression Levels of Key Hedgehog Pathway Genes

Cyclopamine, an antagonist of the hedgehog signaling, inhibits the pathway activation by binding directly to Smo (Chen et al., 2002). Hence, cyclopamine was often used to investigate the function of hedgehog pathway in various species including chicken (Incardona et al., 1998), Zebrafish (Wolff et al., 2003), *Sepia officinalis* (Grimaldi et al., 2008). In the study, we inhibited the hedgehog pathway with cyclopamine treatment in *C. gigas* larvae. The RNA expression levels of four key genes were severely down-regulated in treated larvae compared with normal larvae. Similarly, the RNA expression of Ptc and Hh was reduced significantly in cyclopamine- treated embryos in chicken (Incardona et al., 1998). Same phenomenon was also found in Zebrafish and *Sepia officinalis* that the expression levels of Ptc was down-regulated in treatment groups (Wolff et al., 2003; Grimaldi et al., 2008). In addition, the effective inhibition concentration was different among species. In present study, we suggested that the effective inhibition concentration of CgHh and CgPtc was 0.5 μM. The effective concentration of CgSmo was 2 μM. The expression level of Ptc in zebrafish and *Sepia officinalis* was reduced significantly when the drug concentration was 15 and 10 μM respectively (Wolff et al., 2003; Grimaldi et al., 2008). We speculated the discrepancy on effective inhibition concentration of cyclopamine might be relevant to some reasons including the size of embryos, the treated stage or treated time. Our results also found that there was only the expression level of CgPtc decreased with the increase of cyclopamine concentration. Though the expression levels of CgHh, CgSmo and CgGli were down-regulated in treatment groups, there was no a consistent trend as the concentration of cyclopamine increases. We speculated that this situation might be due to the fact that the larvae used for analysis are mixed sample.

A Conserved Role for Hedgehog Signaling in Muscle Development

To verify if the hedgehog pathway was involved in normal muscle development in *C. gigas*, we investigated the changes in larval muscle phenotype by fluorescence labeling of F-actin. The data showed that as the treatment concentration and time increased, the degree of damage on larval muscle was more serious. Similar phenomenon was also found in zerbrafish (Wolff et al., 2003). Moreover, we suggested that hedgehog signaling pathway had a conserved role in muscle development among species. In sea urchin embryo, hedgehog signaling was vital for gut muscle development (Walton et al., 2006). In cuttlefish, the hedgehog pathway was involved in the formation of striated muscle fibers (Grimaldi et al., 2008). Hedgehog signaling was also proved to promote the proliferation and differentiation of muscle cells in zebrafish (Feng et al., 2006).

CONCLUSION

The present study suggested that hedgehog signaling pathway was a conserved pathway in sequence characteristic, expression profile and physiological function among invertebrates. For physiological function, we thought hedgehog pathway was involved in myogenesis of *C.gigas*. Firstly, the key genes of hedgehog pathway had a relatively high expression level in gastrulation or trochophore stage when myogenesis was just beginning to develop. Next, cyclopamine blocked the pathway and lead to RNA expression levels of CgHh, CgPtc and CgSmo were severely down-regulated. The velum retractors and adductor muscles of larvae treated with cyclopamine were significantly destroyed. In conclusion, we thought that hedgehog signaling pathway participated in myogenesis of *C.gigas*, but detailed regulatory mechanism of the signaling on muscle development is not yet clear and remains to explore.

AUTHOR CONTRIBUTIONS

HL performed the experiments, analyzed the data, drafted the manuscript, and generated all figures. HY designed the study, supervised the research, contributed to data interpretation, and writing of the manuscript. QL supervised the project and contributed to data interpretation and writing of the manuscript. All authors provided input and read and approved the final version of the manuscript.

ACKNOWLEDGMENTS

This study was supported by the grants from National Natural Science Foundation of China (31772843), the Fundamental Research Funds for the Central Universities (201762014), Taishan Scholars Seed Project of Shandong, and Industrial Development Project of Qingdao City (17-3-3-64-nsh). Open Project Program of Laboratory for Marine Fisheries Science and Food Production Processes, Qingdao National Laboratory for Marine Science, and Technology (2016LMFS-A06).

SUPPLEMENTARY MATERIAL

The Supplementary Material for this article can be found online at: https://www.frontiersin.org/articles/10.3389/fphys.2018.01536/full#supplementary-material

REFERENCES

Alcedo, J., Ayzenzon, M., Von Ohlen, T., Noll, M., and Hooper, J. E. (1996). The Drosophila smoothened gene encodes a seven-pass membrane protein, a putative receptor for the hedgehog signal. *Cell* 86, 221–232. doi: 10.1016/S0092-8674(00)80094-X

Bijlsma, M. F., Spek, C. A., and Peppelenbosch, M. P. (2004). Hedgehog: an unusual signal transducer. *Bioessays* 26, 387–394. doi: 10.1002/bies.20007

Bitgood, M. J., Shen, L., and McMahon, A. P. (1996). Sertoli cell signaling by Desert hedgehog regulates the male germline. *Curr. Biol.* 6, 298–304. doi: 10.1016/S0960-9822(02)00480-3

Blagden, C. S., Currie, P. D., Ingham, P. W., and Hughes, S. M. (1997). Notochord induction of zebrafish slow muscle mediated by Sonic hedgehog. *Genes Dev.* 11, 2163–2175. doi: 10.1101/gad.11.17.2163

Braun, T., Rudnicki, M. A., Arnold, H. H., and Jaenisch, R. (1992). Targeted inactivation of the muscle regulatory gene Myf-5 results in abnormal rib development and perinatal death. *Cell* 71, 369–382. doi: 10.1016/0092-8674(92)90507-9

Chen, J. K., Taipale, J., Cooper, M. K., Beachy, P. A. (2002). Inhibition of Hedgehog signaling by direct binding of cyclopamine to smoothened. *Genes Dev.* 16, 2743–2748. doi: 10.1101/gad.1025302

Cornell, R. A., and Eisen, J. S. (2005). Notch in the pathway: the roles of Notch signaling in neural crest development. *Semin. Cell Dev. Biol.* 16, 663–672. doi: 10.1016/j.semcdb.2005.06.009

Currie, P. D., and Ingham, P. W. (1996). Induction of a specific muscle cell type by a hedgehog-like protein in zebrafish. *Nature* 382, 452–55. doi: 10.1038/382452a0

Denef, N., Neubuser, D., Perez, L., and Cohen, S. M. (2000). Hedgehog induces opposite changes in turnover and subcellular localization of patched and smoothened. *Cell* 102, 521–531. doi: 10.1016/S0092-8674(00)00056-8

Du, S. J., Devoto, S. H., Westerfield, M., and Moon, R. T. (1997). Positive and negative regulation of muscle cell identity by members of the hedgehog and TGF-beta gene families. *J. Cell Biol.* 139, 145–156. doi: 10.1083/jcb.139.1.145

Du, Y., Zhang, L., Xu, F., Huang, B., Zhang, G., and Li, L. (2013). Validation of housekeeping genes as internal controls for studying gene expression during Pacific oyster (Crassostrea gigas) development by quantitative real-time PCR. *Fish. Shellfish. Immunol.* 24, 939–945. doi: 10.1016/j.fsi.2012.12.007

Duprez, D., Fournier-Thibault, C., and Le Douarin, N. (1998). Sonic hedgehog induces proliferation of committed skeletal muscle cells in the chick limb. *Development* 125, 495–505.

Echelard, Y., Epstein, D. J., St-Jacques, B., Shen, L., Mohler, J., McMahon, J., et al. (1993). Sonic hedgehog, a member of a family of putative signaling molecules, is implicated in the regulation of CNS polarity. *Cell* 75, 1417–1430. doi: 10.1016/0092-8674(93)90627-3

Ekker, S. C., Ungar, A. R., Greenstein, P., von Kessler, D. P., Porter, J. A., Moon, R. T., et al. (1995). Patterning activities of vertebrate hedgehog proteins in the developing eye and brain. *Curr. Biol.* 5, 944–955. doi: 10.1016/S0960-9822(95)00185-0

Feng, X., Adiarte, E. G., and Devoto, S. H. (2006). Hedgehog acts directly on the zebrafish dermomyotome to promote myogenic differentiation. *Dev. Biol.* 300, 736–746. doi: 10.1016/j.ydbio.2006.08.056

Gallet, A., Rodriguez, R., Ruel, L., and Therond, P. P. (2003). Cholesterol modification of hedgehog is required for trafficking and movement, revealing an asymmetric cellular response to hedgehog. *Dev. Cell* 4, 191–204. doi: 10.1016/S1534-5807(03)00031-5

Goodrich, L. V., Johnson, R. L., Milenkovic, L., McMahon, J. A., and Scott, M. P. (1996). Conservation of the hedgehog/patched signaling pathway from flies to mice: induction of a mouse patched gene by hedgehog. *Genes Dev.* 10, 301–312. doi: 10.1101/gad.10.3.301

Goodrich, L. V., Milenkovic, L., Higgins, K. M., and Scott, M. P. (1997). Altered neural cell fates and medulloblastoma in mouse patched mutants. *Science* 277, 1109–1113. doi: 10.1126/science.277.5329.1109

Goulding, M., Lumsden, A., and Paquette, A. J. (1994). Regulation of Pax-3 expression in the dermomyotome and its role in muscle development. *Development* 120, 957–971.

Grimaldi, A., Tettamanti, G., and Acquati, F. (2008). A hedgehog homolog is involved in muscle formation and organization of *Sepia officinalis* (mollusca) mantle. *Dev. Dyn.* 237, 659–671. doi: 10.1002/dvdy.21453

Heretsch, P., Tzagkaroulaki, L., and Giannis, A. (2010). Modulators of the hedgehog signaling pathway. *Bioorg. Med. Chem.* 18, 6613–6624. doi: 10.1016/j.bmc.2010.07.038

Huangfu, D., and Anderson, K. V. (2006). Signaling from Smo to Ci/Gli: conservation and divergence of hedgehog pathways from Drosophila to vertebrates. *Development* 133, 3–14. doi: 10.1242/dev.02169

Incardona, J. P., Gaffield, W., and Kapur, R. P. (1998). The teratogenic Veratrum alkaloid cyclopamine inhibits sonic hedgehog signal transduction. *Development* 125, 3553–3562.

Incardona, J. P., Gaffield, W., Lange, Y., Cooney, A., Pentchev, P. G., Liu, S., et al. (2000). Cyclopamine inhibition of Sonic hedgehog signal transduction is not

mediated through effects on cholesterol transport. *Dev. Biol.* 224, 440–452. doi: 10.1006/dbio.2000.9775

Ingham, P. W., and McMahon, A. P. (2001). Hedgehog signaling in animal development: paradigms and principles. *Genes Dev.* 15, 3059–3087. doi: 10.1101/gad.938601

Ingham, P. W., and Placzek, M. (2006). Orchestrating ontogenesis: variations on a theme by sonic hedgehog. *Nat. Rev. Genet.* 7, 841–850. doi: 10.1038/nrg1969

Jia, J., Amanai, K., Wang, G., Tang, J., Wang, B., and Jiang, J. (2002). Shaggy/GSK3 antagonizes hedgehog signalling by regulating cubitus interruptus. *Nature* 416, 548–552. doi: 10.1038/nature733

Jia, J., Tong, C., and Jiang, J. (2003). Smoothened transduces hedgehog signal by physically interacting with Costal2/fused complex through its C-terminal tail. *Genes Dev.* 17, 2709–2720. doi: 10.1101/gad.1136603

Kang, D., Huang, F., Li, D., Shankland, M., Gaffield, W., and Weisblat, D. A. (2003). A hedgehog homolog regulates gut formation in leech Helobdella. *Development* 130, 1645–57. doi: 10.1242/dev.00395

Kirilly, D., Spana, E. P., Perrimon, N., Padgett, R. W., and Xie, T. (2005). BMP signaling is required for controlling somatic stem cell self-renewal in the Drosophila ovary. *Dev. Cell* 9, 651–662. doi: 10.1016/j.devcel.2005.09.013

Kruger, M., Mennerich, D., Fees, S., Schafer, R., Mundlos, S., and Braun, T. (2001). Sonic hedgehog is a survival factor for hypaxial muscles during mouse development. *Development* 128, 743–752.

Kumar, S., Stecher, G., and Tamura, K. (2016). MEGA7: molecular evolutionary genetics analysis version 7.0 for bigger datasets. *Mol. Biol. Evol.* 33, 1870–1874. doi: 10.1093/molbev/msw054

Lee, C. S., Buttitta, L., and Fan, C. M. (2001). Evidence that the WNT-inducible growth arrest-specific gene 1 encodes an antagonist of sonic hedgehog signaling in the somite. *Proc. Natl. Acad. Sci. U.S.A.* 98, 11347–11352. doi: 10.1073/pnas.201418298

Livak, K. J., and Schmittgen, T. D. (2001). Analysis of relative gene expression data using realtime quantitative PCR and the 2(-Delta Delta C (T)) method. *Methods* 25, 402–408. doi: 10.1006/meth.2001.1262

Marigo, V., Scott, M. P., and Johnson, R. L. (1996). Conservation in hedgehog signaling: induction of a chicken patched homolog by Sonic hedgehog in the developing limb. *Development* 122, 1225–1233.

Matus, D. Q., Magie, C. R., and Pang, K. (2008). The Hedgehog gene family of the cnidarian, Nematostella vectensis, and implications for understanding metazoan hedgehog pathway evolution. *Dev. Biol.* 313, 501–518. doi: 10.1016/j.ydbio.2007.09.032

Méthot, N., and Basler, K. (2000). Suppressor of fused opposes hedgehog signal transduction by impeding nuclear accumulation of the activator form of Cubitus interruptus. *Development* 127, 4001–4010.

Nakano, Y., Nystedt, S., Shivdasani, A. A., Strutt, H., Thomas, C., and Ingham, P. W. (2004). Functional domains and sub-cellular distribution of the hedgehog transducing protein smoothened in Drosophila. *Mech. Dev.* 121, 507–518. doi: 10.1016/j.mod.2004.04.015

Nusse, R. (2003). Wnts and hedgehogs: lipid-modified proteins and similarities in signaling mechanisms at the cell surface. *Development* 130, 5297–5305. doi: 10.1242/dev.00821

Nüsslein-Volhard, C., and Wieschaus, E. (1980). Mutations affecting segment number and polarity in Drosophila. *Nature* 287, 795–801. doi: 10.1038/287795a0

Østerlund, T., and Kogerman, P. (2006). Hedgehog signalling: how to get from Smo to Ci and Gli. *Trends. Cell. Biol.* 16, 176–180. doi: 10.1016/j.tcb.2006.02.004

Pérez-Bercoff, Å., Koch, J., and Bürglin, T. R. (2005). LogoBar: bar graph visualization of protein logos with gaps. *Bioinformatics* 22, 112–114. doi: 10.1093/bioinformatics/bti761

Price, M. A., and Kalderon, D. (2002). Proteolysis of the hedgehog signaling effector cubitus interruptus requires phosphorylation by glycogen synthase kinase 3 and casein kinase 1. *Cell* 108, 823–835. doi: 10.1016/S0092-8674(02)00664-5

Riddle, R. D., Johnson, R. L., Laufer, E., and Tabin, C. (1993). Sonic hedgehog mediates the polarizing activity of the ZPA. *Cell* 75, 1401–1416. doi: 10.1016/0092-8674(93)90626-2

Robert, X., and Gouet, P. (2014). Deciphering key features in protein structures with the new ENDscript server. *Nucl. Acids Res.* 42, 320–324. doi: 10.1093/nar/gku316

Roelink, H., Augsburger, A., Heemskerk, J., Korzh, V., Norlin, S., Ruiz, I., et al. (1994). Floor plate and motor neuron induction by vhh-1, a vertebrate homolog of hedgehog expressed by the notochord. *Cell* 76, 761–775. doi: 10.1016/0092-8674(94)90514-2

Shimeld, S. M. (1999). The evolution of the hedgehog gene family in chordates: insights from amphioxus hedgehog. *Dev. Genes Evol.* 209, 40–47. doi: 10.1007/s004270050225

Strähle, U., Blader, P., and Ingham, P. W. (1996). Expression of axial and sonic hedgehog in wildtype and midline defective zebrafish embryos. *Int. J. Dev. Biol.* 40, 929–940.

Sukegawa, A., Narita, T., Kameda, T., Saitoh, K., Nohno, T., Iba, H., et al. (2000). The concentric structure of the developing gut is regulated by Sonic hedgehog derived from endodermal epithelium. *Development* 127, 1971–1980.

Thisse, C., and Thisse, B. (2008). High resolution *in situ* hybridization on whole-mount zebrafish embryo. *Nat. Protoc.* 3, 59–69. doi: 10.1038/nprot.2007.514

Thomas, N. A., Koudijs, M., van Eeden, F. J. M., Joyner, A. L., and Yelon, D. (2008). Hedgehog signaling plays a cell-autonomous role in maximizing cardiac developmental potential. *Development* 135, 3789–3799. doi: 10.1242/dev.024083

Villavicencio, E. H., Walterhouse, D. O., and Iannaccone, P. M. (2000). The sonic hedgehog–patched-gli pathway in human development and disease. *Am. J. Hum. Genet.* 67, 1047–1054. doi: 10.1016/S0002-9297(07)62934-6

Walton, K. D., Croce, J. C., Glenn, T. D., Croce, J. C., Glenn, T. D., Wu, S. Y., et al. (2006). Genomics and expression profiles of the Hedgehog and Notch signaling pathways in sea urchin development. *Dev. Biol.* 300, 153–164. doi: 10.1016/j.ydbio.2006.08.064

Wang, Q., Li, Q., Kong, L., and Yu, R. (2012). Response to selection for fast growth in the second generation of Pacific oyster (*Crassostrea gigas*). *J. Ocean Univ. China* 11, 413–418. doi: 10.1007/s11802-012-1909-7

Warner, J. F., McCarthy, A. M., and Morris, R. L. (2013). Hedgehog signaling requires motile cilia in the sea urchin. *Mol. Biol. Evol.* 31, 18–22. doi: 10.1093/molbev/mst176

Weed, M., Mundlos, S., and Olsen, B. R. (1997). The role of sonic hedgehog in vertebrate development. *Matrix Biol.* 16, 53–58. doi: 10.1016/S0945-053X(97)90072-X

Wolff, C., Roy, S., and Ingham, P. W. (2003). Multiple muscle cell identities induced by distinct levels and timing of hedgehog activity in the zebrafish embryo. *Curr. Biol.* 13, 1169–81. doi: 10.1016/S0960-9822(03)00461-5

Yang, J. T., Liu, C. Z., and Villavicencio, E. H. (1997). Expression of human GLI in mice results in failure to thrive, early death, and patchy Hirschsprung-like gastrointestinal dilatation. *Mol. Med.* 3:826. doi: 10.1007/BF03401719

Yu, H., Li, H., and Li, Q. (2017). Molecular characterization and expression profiles of myosin essential light chain gene in the Pacific oyster Crassostrea gigas. *Comp. Biochem. Physiol. B Biochem. Mol. Biol.* 213, 1–7. doi: 10.1016/j.cbpb.2017.07.007

Zhang, C., Williams, E. H., Guo, Y., Lum, L., and Beachy, P. A. (2004). Extensive phosphorylation of smoothened in hedgehog pathway activation. *Proc. Natl. Acad. Sci. U.S.A.* 101, 17900–17907. doi: 10.1073/pnas.0408093101

Zhang, X. M., Ramalho-Santos, M., and McMahon, A. P. (2001). Smoothened mutants reveal redundant roles for Shh and Ihh signaling including regulation of L/R symmetry by the mouse node. *Cell* 106, 781–92. doi: 10.1016/S0092-8674(01)00385-3

Zhu, Q., Zhang, L., Li, L., Que, H., and Zhang, G. F. (2016). Expression characterization of stress genes under high and low temperature stresses in the Pacific oyster, *Crassostrea gigas*. *Mar. Biotechnol.* 18, 176–188. doi: 10.1007/s10126-015-9678-0

Conflict of Interest Statement: The authors declare that the research was conducted in the absence of any commercial or financial relationships that could be construed as a potential conflict of interest.

frontiers in Physiology

ORIGINAL RESEARCH
published: 19 July 2018
doi: 10.3389/fphys.2018.00944

Metabolomics Responses of Pearl Oysters (*Pinctada fucata martensii*) Fed a Formulated Diet Indoors and Cultured With Natural Diet Outdoors

Chuangye Yang[1†], *Ruijuan Hao*[1†], *Xiaodong Du*[1,2], *Yuewen Deng*[1,2*], *Ruijiao Sun*[3] *and Qingheng Wang*[1,2*]

[1] *Fisheries College, Guangdong Ocean University, Zhanjiang, China,* [2] *Pearl Breeding and Processing Engineering Technology Research Centre of Guangdong Province, Zhanjiang, China,* [3] *Zhejiang Hengxing Food Co., Ltd., Jiaxing, China*

OPEN ACCESS

Edited by:
Xiaotong Wang,
Ludong University, China

Reviewed by:
Shengkang Li,
Shantou University, China
Jeremie Zander Lindeque,
North-West University, South Africa
Tiziana Cappello,
Università degli Studi di Messina, Italy

***Correspondence:**
Yuewen Deng
dengyw@gdou.edu.cn
Qingheng Wang
wangqingheng_haida@163.com

[†]*These authors have contributed equally to this work.*

Specialty section:
This article was submitted to Aquatic Physiology, a section of the journal Frontiers in Physiology

Received: *26 March 2018*
Accepted: *28 June 2018*
Published: *19 July 2018*

Citation:
Yang C, Hao R, Du X, Deng Y, Sun R and Wang Q (2018) Metabolomics Responses of Pearl Oysters (Pinctada fucata martensii) Fed a Formulated Diet Indoors and Cultured With Natural Diet Outdoors. Front. Physiol. 9:944. doi: 10.3389/fphys.2018.00944

Natural disasters and environmental pollution are the main problems in traditional offshore cultivation. While culturing pearl oysters through industrial farming can avoid these problems, food availability in this case is limited. This study compares the metabolomics responses of pearl oysters, *Pinctada fucata martensii*, fed a formulated diet indoors with those of oysters cultured with natural diet outdoors by using a gas chromatography time-of-flight mass spectrometry (GC-TOF/MS)-based metabolomics approach. The animals were divided into two groups as follows: the experimental group (EG) was fed a formulated diet indoors and the control group (CG) was cultured with natural diet outdoors. After 45 days of feeding, the survival rate of EG was significantly higher than that of CG. The absolute growth rate (AGR) of the total weight of EG did not significantly differ from that of CG, but the AGRs of the shell length, shell height, and shell width of CG were significantly higher than those of EG. EG showed significantly higher amylase activities than CG, and the hexokinase and glucose-6-phosphate isomerase concentrations of the former were significantly lower than those of the latter. Metabolomics revealed 125 metabolites via mass spectrum matching with a spectral similarity value > 700 in the hepatopancreas, and 48 metabolites were considered to be significantly different between groups (VIP > 1 and $P < 0.05$). Pathway analysis results indicated that these significantly different metabolites were involved in 34 pathways. Further integrated key metabolic pathway analysis showed that, compared with CG, EG had lower capabilities for cysteine and methionine metabolism, sulfur metabolism, and starch and sucrose metabolism. This study demonstrated that the formulated diet could be an excellent substitute for natural diet; however, its nutrients were insufficient. Effective strategies should be developed to enhance the utilization of formulated diets.

Keywords: metabolomics, formulated diet, nutritional requirements, GC–MS, *Pinctada fucata martensii*

INTRODUCTION

Pinctada fucata martensii is the main pearl oyster species cultured for marine pearl production in China and Japan. In Southern China, production of this organism peaked in the 1990s with an annual yield of 20 tons (Yang et al., 2017a). However, pearl yield has steadily declined because of the slow growth and mass mortality of the cultured stock and environmental deterioration (Qiu et al., 2014). Thus, various methods, including new strain development (Deng et al., 2009; Deng Y.W et al., 2010), pearl culturing techniques (Deng C.M et al., 2010), and culture modes (Wang et al., 2016), have been applied to restore pearl yields. Traditional raft-culture models depend on natural microalgae and are highly susceptible to natural disasters and environmental pollution. These disadvantages can be avoided through industrial farming, where, unfortunately, the food demand is high and the available formulated diets for bivalves are limited.

Diet quality greatly affects an animal's performance. When animals are fed diets of different quality, alterations in key metabolic pathways are difficult to characterize by using traditional nutritional methods. Metabolomics is an effective omic technique to detect the overall complexity of and determine essential changes in diverse biological systems (Liu et al., 2016; Cappello et al., 2017, 2018). Low-molecular-weight metabolites, including lipids, sugars, and amino acids, can be quantified in biological samples by utilizing metabolomics approaches, such as ^{1}H-nuclear magnetic resonance (NMR), gas chromatography–mass spectrometry (GC–MS), and liquid chromatography–mass spectrometry (LC–MS) (Ye et al., 2016; Maherizo et al., 2017; Venter et al., 2018). The identification and integrative analysis of these metabolites may enable the comprehensive characterization of metabolic mechanisms at the molecular and cellular levels under internal or external stimulating conditions. Among the metabolomics technologies currently available, gas chromatography time-of-flight mass spectrometry (GC–TOF/MS) is the most widely used because of its high resolution, high detection sensitivity, and numerous open-access spectral libraries (Sun et al., 2015; Collette et al., 2016; Hao et al., 2018). Thus, it can effectively assess the effects of food shortage (Tuffnail et al., 2009; Kullgren et al., 2010; Baumgarner and Cooper, 2012; Cipriano et al., 2015; Sheedy et al., 2016), nutrient supplementation (Andersen et al., 2014, 2015; Wagner et al., 2014), differences in nutrient levels (Jin et al., 2015), and dietary protein or lipid substitution (Abro et al., 2014; Cheng et al., 2016; Ma et al., 2017; Wei et al., 2017; Yang et al., 2018) in aquatic animals via metabolomics approaches.

The present study compares the metabolomics responses of pearl oysters *P. f. martensii* fed a formulated diet indoors with those of oysters cultured with natural diet outdoors by using a GC–TOF/MS-based metabolomics approach. The results can help enhance our understanding of the different mechanisms of *P. f. martensii* fed different diets and assist in the development of optimized nutritional requirements and feeding regimes.

MATERIALS AND METHODS

Experimental Diet and Procedures

The experimental diet was formulated according to the recommendations of previous research (Yang et al., 2017b, 2018); this diet had a typical proximate composition of 35% crude protein and 10% crude lipid and was stored at −20°C until use. Lipids were obtained from fish oils, while proteins were obtained from yeast powder and fish meal. The formulation and approximate composition of this diet were described by Yang et al. (2018). Pearl oysters [44.79 ± 1.25 mm in mean shell length (SL)] were assigned to the experimental group (EG) or control group (CG) randomly, and three replicates were prepared for both groups. Each replicate had 210 animals. The animals in EG were fed the formulated diet indoors, and the volume of water was 1,000 L. Diet doses for EG were specified according to a previous work (Wang et al., 2016), and the pearl oysters were fed every 6 h. Water was replaced daily at a volume of 300 L. CG was cultured with a natural diet outdoors. The experimental period lasted 45 days, and the following parameters were maintained: dissolved oxygen in water at 5.00 mg/L, water temperature at 20.5–22.5°C, and salinity at 30%. *P. f. martensii* is a lower invertebrate, and therefore, the study was not subject to ethical approval.

Survival Rate and Growth Rate

At the beginning and end of the experiment, the total number and growth performance of pearl oysters in each replicate were determined. SL, shell height (SH), and shell width (SW) were measured with a digital caliper (0.02 mm accuracy). Total weight (TW) was obtained with an electronic balance (0.01 g accuracy), and survival rates and absolute growth rates (AGRs) were calculated in accordance with the methods described by Yang et al. (2017b).

Sample Collection

At the end of the experiment, hepatopancreatic tissues from each animal were dissected, immediately kept in liquid nitrogen, and then stored at −80°C until analysis.

Biochemical Measurements

Eight hepatopancreatic tissues were collected from each replicate for biochemical measurements. Tissues were homogenized, and homogenates were centrifuged (10,000 × g for 20 min at 4°C) using a high-speed refrigerated centrifuge. The supernatant was transferred to new 2.0 mL tubes, and amylase activity was determined using commercial kits (Nanjing Jiancheng Bioengineering Research Institute, Nanjing, China) according to the manufacturer's instructions. Hexokinase (HK) and glucose-6-phosphate isomerase (G6PI) concentrations were also determined using commercial kits (Beijing Dongge Weiye Technology Co., Ltd., Beijing, China) according to the manufacturer's instructions. All assays were conducted within 24 h after extraction.

Preparation for GC–MS Analysis

Each replicate included 8 samples, and 24 samples were collected from each group for GC–MS analysis. Frozen

hepatopancreas samples of approximately 100 mg were obtained from four individuals, transferred into 2 mL microcentrifuge tubes, and mixed with 0.5 mL of methanol extraction liquid ($V_{methanol}$:$V_{chloroform}$ = 3:1) and 20 μL of L-2-chlorophenylalanine (1 mg/mL stock in dH_2O) as an internal standard. The samples were vortexed for 30 s, homogenized in a ball mill for 4 min at 45 Hz, subjected to ultrasound for 5 min, incubated in ice water, and centrifuged for 15 min at 12,000 rpm and 4 °C. The supernatant (0.45 mL) was transferred into fresh 2 mL GC–MS glass vials, dried in a vacuum concentrator without heating, added with 80 μL of methoxylamine hydrochloride (20 mg/mL in pyridine), and incubated for 30 min at 80°C. Approximately 100 μL of bis-(trimethylsilyl)-trifluoroacetamide reagent (1% trimethylchlorosilane, v/v) was added to the samples, which were then incubated for 2 h at 70°C.

GC–MS Analysis

GC–TOF/MS analysis was performed using an Agilent 7890 gas chromatograph system coupled to a Pegasus HT TOF/MS instrument. The system was equipped with a DB-5MS capillary column coated with 5% diphenyl cross-linked with 95% dimethylpolysiloxane (30 m × 250 μm inner diameter, 0.25 μm film thickness; J&W Scientific, Folsom, CA, USA). A 1 μL aliquot of the analyte was injected in split-less mode, and helium was used as the carrier gas. The front inlet purge flow was 3 mL min^{-1}, and the gas flow rate through the column was 1 mL min^{-1}. The initial temperature was maintained at 50°C for 1 min, raised to 310°C at a rate of 10°C min^{-1}, and then maintained at 310°C for 8 min. The injection, transfer line, and ion source temperatures were 280, 270, and 220°C, respectively, and the energy was set to −70 eV in electron impact mode. Mass spectrometry data were acquired in full-scan mode over the *m*/*z* range of 50–500 at a rate of 20 spectra per second after a solvent delay of 6 min.

Data Analysis

Chroma TOF 4.3X software (LECO Corporation) and the LECO-Fiehn Rtx5 database were used for raw peak exaction, data baseline filtering and calibration, peak alignment, deconvolution analysis, peak identification, and peak area integration (Kind et al., 2009). The retention index (RI) was utilized to identify peaks, and an RI tolerance of 5,000 was set. The three-dimensional data obtained, including the peak number, sample name, and normalized peak area, were inputted into SIMCA14.1 (V14.1, MKS Data Analytics Solutions, Umea, Sweden) for principal component analysis (PCA) and orthogonal projections to latent structure–discriminate analysis (OPLS–DA). PCA showed the distribution of the original data. Supervised OPLS–DA was applied to obtain high-level group separation and enhance our understanding of the variables responsible for classification. The OPLS–DA model was employed with the first principal component of variable importance in the projection (VIP) values (VIP > 1) combined with Student's *t*-test ($P < 0.05$) to determine significantly different metabolites (SDMs) between the two groups. The fold change (FC) of each metabolite was calculated by comparing the mean values of the peak areas obtained from EG and CG. Commercial databases, including KEGG (http://www.genome.jp/kegg/), were utilized to search for the pathways of metabolites. MetaboAnalyst, a free Web-based tool that uses high-quality KEGG metabolic pathways as the backend knowledge base, was used for pathway analysis (http://www.metaboanalyst.ca).

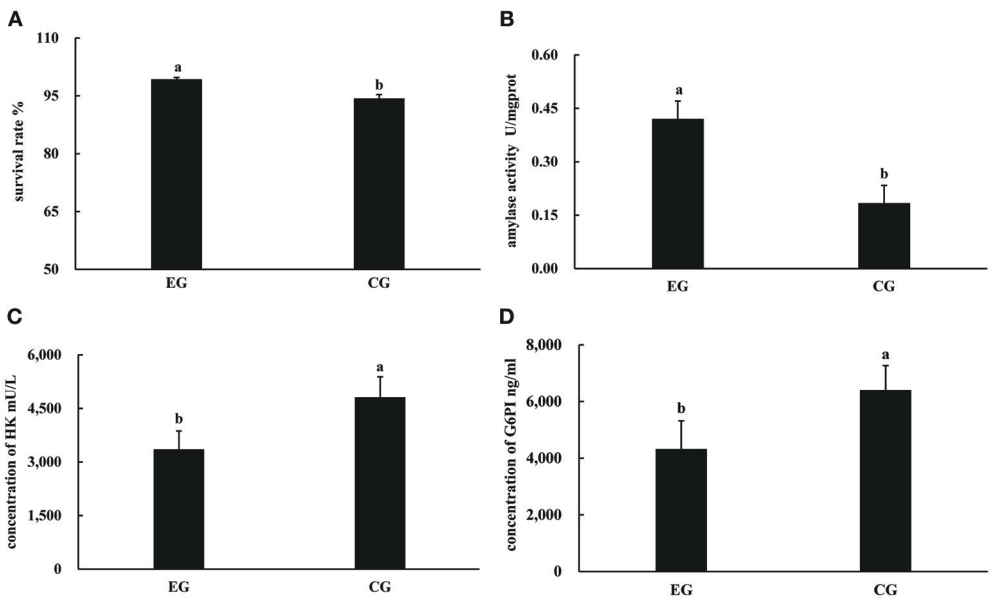

FIGURE 1 | Survival rates, activities of amylase, concentrations of HK and G6PI in the hepatopancreas of *P. f. martensii* fed formulated diet indoors (EG) and cultured with a natural diet outdoors (CG). Means with the same letters are not significantly different ($P > 0.05$). **(A)** survival rates; **(B)** activities of amylase; **(C)** concentrations of HK; **(D)** concentrations of G6PI.

TABLE 1 | Growth performance of pearl oyster (*P. f. martensii*) fed a formulated diet indoors (EG) and cultured with natural diet outdoors (CG).

	EG	CG
Shell length	3.90 ± 0.10*b*	4.42 ± 0.29*a*
Shell width	1.22 ± 0.22*b*	1.63 ± 0.39*a*
Shell height	3.97 ± 0.46*b*	4.26 ± 0.39*a*
Total weight	4.03 ± 0.32*a*	4.28 ± 0.36*a*

Means with the same letters within a row are not significantly different (P >0.05).

The results of the growth and biochemical data were expressed as mean ± SEM, and significant differences ($P < 0.05$) among each variable were detected using *t*-test. All analyses were conducted using IBM SPSS Statistics 19 (IBM, USA).

RESULTS

Growth, Survival Rate, and Biochemical Parameters in the Hepatopancreas

At the end of the experiment, the survival rates of pearl oysters in both groups ranged from 94.31 to 99.31%. The survival rate of CG was significantly lower than that of EG ($P < 0.05$, **Figure 1**), and the growth performance of the latter differed from that of the former (**Table 1**). Although the AGRs of the SL, SW, and SH of CG were significantly higher than those of EG ($P < 0.05$), the AGR of TW between EG and CG was not significantly different ($P > 0.05$). Pearl oysters in EG showed significantly higher amylase activity than those in CG ($P < 0.05$, **Figure 1**). By contrast, HK and G6PI concentrations in the hepatopancreas of the former were significantly lower than those of the latter ($P < 0.05$ **Figure 1**).

Total Ion Chromatograms (TICs) of Hepatopancreas Samples

Typical GC-TOF/MS TICs of *P. f. martensii* hepatopancreas samples from the two groups are shown in **Figure 2**. The standard deviation of the internal standard (L-2-chlorophenylalanine) retention time was 0.00255. The shape and number of peaks differed between EG and CG, and a total of 1,059 valid peaks were identified in the hepatopancreas. No drift was observed in any of the peaks that displayed a stable retention time. Thus, the TICs obtained by GC–TOF/MS could directly reflect differences in the metabolite profiles of EG and CG.

PCA

Gross changes in metabolic physiology are easily detectable by using the PCA of the entire set of measured analytes. The GC–TOF/MS metabolic profiles of the hepatopancreas between EG and CG showed markedly separated clusters in each score scatter plot of the PCA model (**Figure 3A**). Compared with that of CG, the R^2X value of the PCA model representing the explained variance in the hepatopancreas of EG was 0.516. All of the samples in the score plots were within the 95% Hotelling's T-squared ellipse, thereby indicating no outlier present among the analyzed samples.

OPLS-DA

OPLS-DA was conducted to enhance our understanding of different metabolic patterns. The parameters used to assess the quality of the OPLS-DA model in the hepatopancreas of EG could be represented by validation plots (**Figure 3B**). The parameters considered for classification from the software were $R^2X = 0.455$, $R^2Y = 1$, and $Q^2 = 0.961$, all of which are stable and effective for fitness and prediction. The R^2 and Q^2 intercept values determined after 200 permutations were 0.96 and−0.72, respectively. The low values of the Q^2 intercept indicate that the robustness of the models presents low risk of overfitting and reliability. **Figure 3C** displays the score scatter plots of the OPLS-DA model comparing EG and CG. All of the samples in the score plots were within the 95% Hotelling's T-squared ellipse, and clear separation and discrimination were found between the pair-wise groups. These findings indicate that the OPLS-DA model could be utilized to identify differences between the pair-wise groups.

Metabolite Identification and Comparison

A total of 1,015 peaks remained after filtering and denoising. The LECO/Fiehn Rtx5 Metabolomics Library suggested that most of the peaks detected were endogenous metabolites, although some may be by-product derivatives. A total of 562 metabolites were quantified, including 206 analytes (similarity value of > 0), and a total of 125 metabolites were identified by mass spectrum matching, with a spectral similarity value of > 700 (Supplemental Table 1). FC values were utilized to indicate specific variable quantities between EG and CG. Metabolite distribution could be visually divided into upregulated and downregulated metabolites. Among the 125 metabolites detected, 75 were downregulated in EG compared with CG (Supplemental Table 1). On the other hand, among 562 metabolites, 150 SDMs (VIP > 1 and $P < 0.05$) were determined in the hepatopancreas between EG and CG (**Figure 4** and Supplemental Table 2). Among these 150 SDMs, 48 yielded a similarity value of > 700. These SDMs include 15 metabolites belonging to amino acids, peptides, and analogs, such as sarcosine, valine, alanine, and glutamic acid; 7 carbohydrate metabolites, including maltose, glucose, and mannose; 10 organic acids and derivatives, such as pyruvic acid and succinic acid; 11 lipid metabolites; and 5 other metabolites (**Table 2**). Among the 150 SDMs in the hepatopancreas, 54 yielded higher concentrations in EG than in CG (**Figure 4** and Supplemental Table 2). By contrast, 96 metabolites in EG were significantly downregulated compared with those in CG.

Characterization and Functional Analysis of Key Metabolic Pathways

KEGG pathway analysis of SDMs was conducted by using MetaboAnalyst 3.0. Thirty-four pathways were found when the SDMs between EG and CG were imported into KEGG (Supplemental Table 3). However, only five of these pathways yielded an impact value of > 0.1, which is the relevance cut-off value, after the identified pathways were subjected to enrichment and pathway topology analyses (Supplemental Table 3). The impact values of sulfur metabolism, phenylalanine metabolism, pyruvate metabolism, cysteine and methionine metabolism, and starch and sucrose metabolism were 0.333, 0.308, 0.177, 0.161,

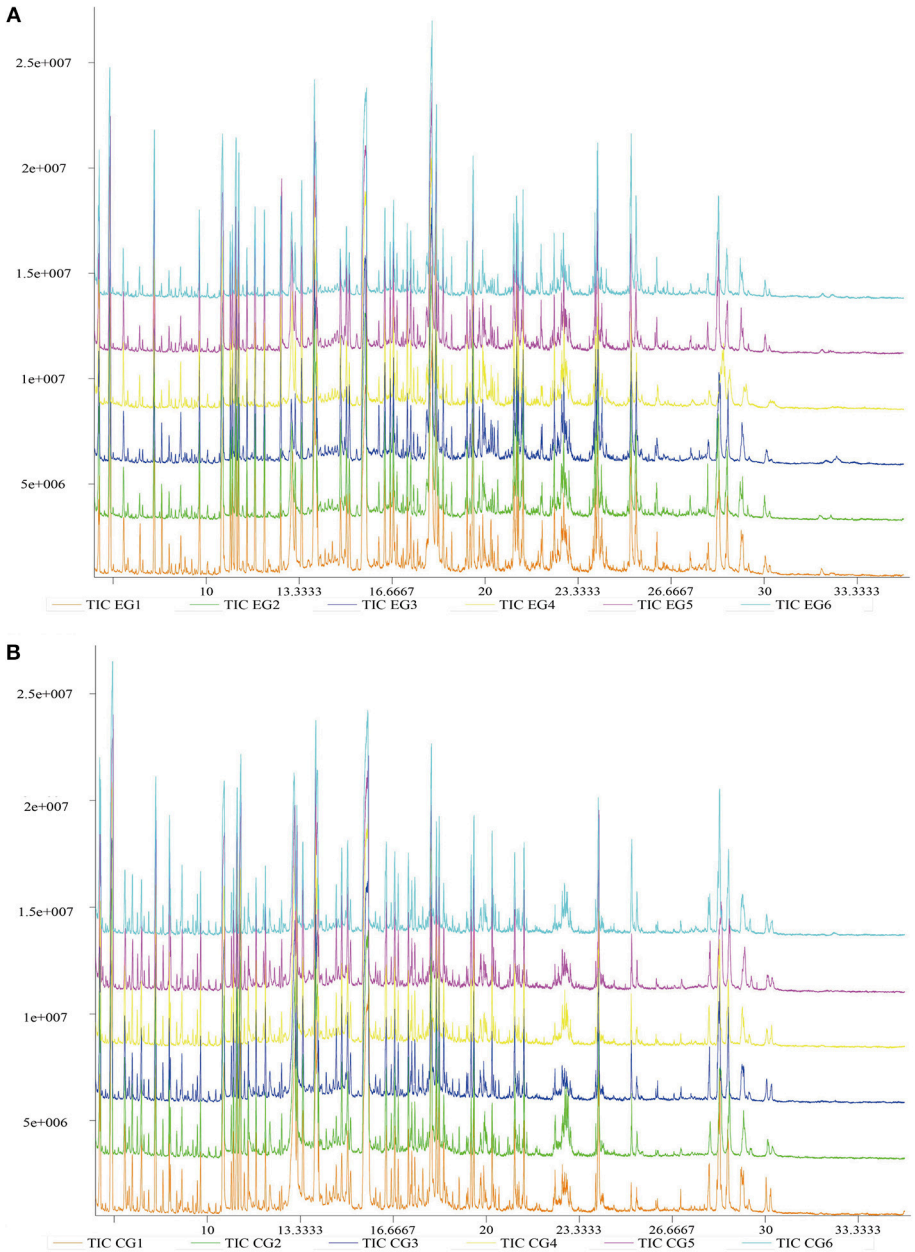

FIGURE 2 | Typical GC–TOF/MS TICs of *P. f. martensii* hepatopancreas samples of EG and CG. The ordinate shows the relative mass abundance, and the abscissa shows the retention time. **(A)** Typical GC-TOF/MS TICs of EG; **(B)** Typical GC-TOF/MS TICs of CG.

and 0.161, respectively. Cysteine and methionine metabolism, sulfur metabolism, and starch and sucrose metabolism were characterized as relevant pathways based on P and impact values (**Figure 5**). In **Table 3**, the pyruvic acid, L-cysteine, L-cysteate, and *O*-acetyl-L-serine contents of EG were lower than those of CG, whereas the L-homoserine content was upregulated in cysteine and methionine metabolism. Similarly, the succinate, L-cysteine, and *O*-acetyl-L-serine contents of EG were lower than those of CG, whereas the L-homoserine content was upregulated in sulfur metabolism. The pyruvic acid, D-fructose-6-phosphate, and sucrose contents of EG were lower than those of CG, whereas the content of D-glucose, maltose, and isomaltose were upregulated in starch and sucrose metabolism.

DISCUSSION

Like many other bivalves, the pearl oyster *P. f. martensii* filters water-suspended particles, such as bacteria, organic debris, microalgae, and microzooplankton (Wang et al., 2016). However, microalgal culturing is labor intensive and difficult to control

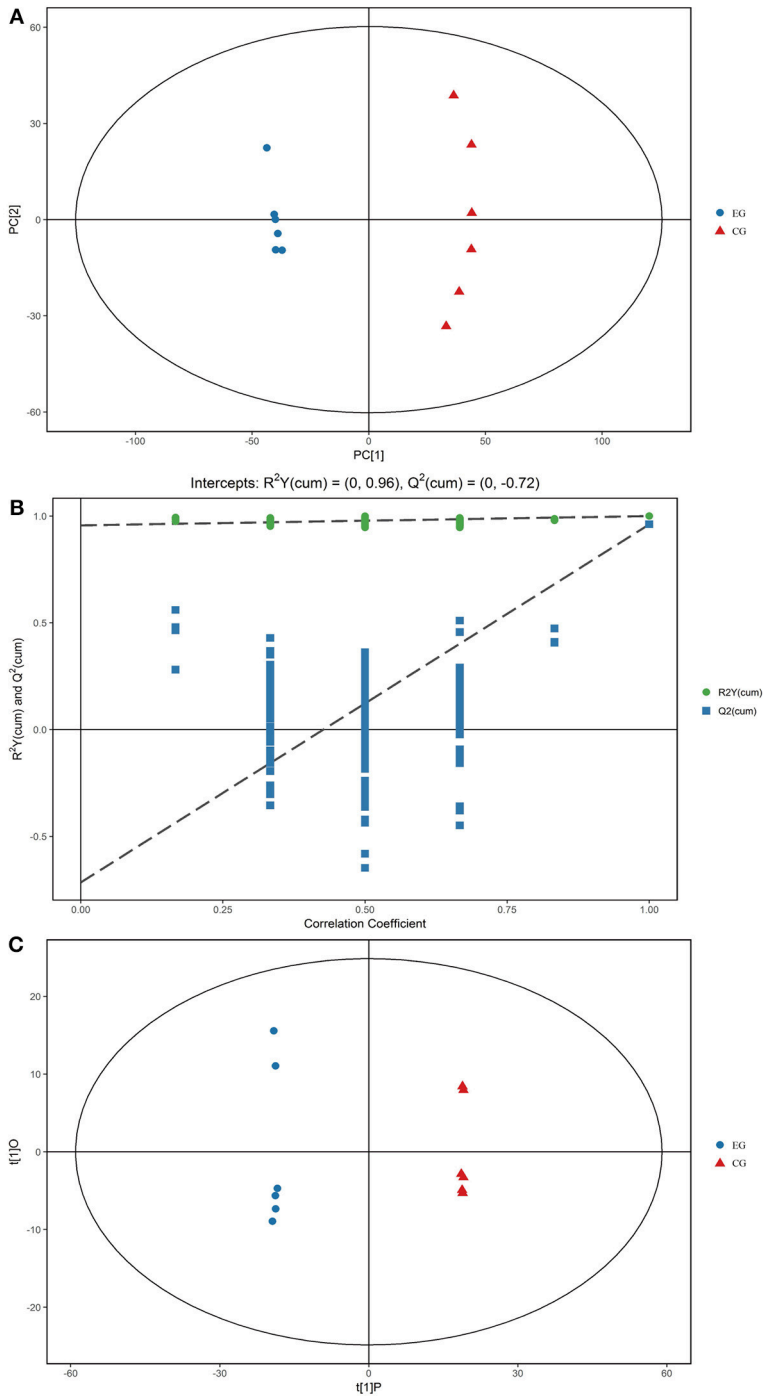

FIGURE 3 | PCA score plots, OPLS-DA corresponding validation plots, and OPLS-DA score plots derived from the GC–TOF/MS metabolite profiles of the hepatopancreas of *P. f. martensii*. **(A)** PCA score plots; **(B)** OPLS-DA corresponding validation plots; **(C)** OPLS-DA score plots.

in large-scale production. Therefore, this process hardly satisfies food requirements for industrial farming development. In previous studies, formulated diets were shown to partially or completely replace microalgae in bivalves (Nevejan et al., 2009; Gui et al., 2016; Wang et al., 2016; Yang et al., 2017a,b). Nevertheless, commercially and biologically reliable artificial diets have yet to be prepared to substitute live microalgal feed for pearl oysters.

Yang et al. (2018) proved that yeast powder is a better protein source of formulated diet for pearl oysters than corn gluten via GC–TOF/MS-based metabolomics. Thus, to determine whether diets formulated with yeast powder as a major protein source

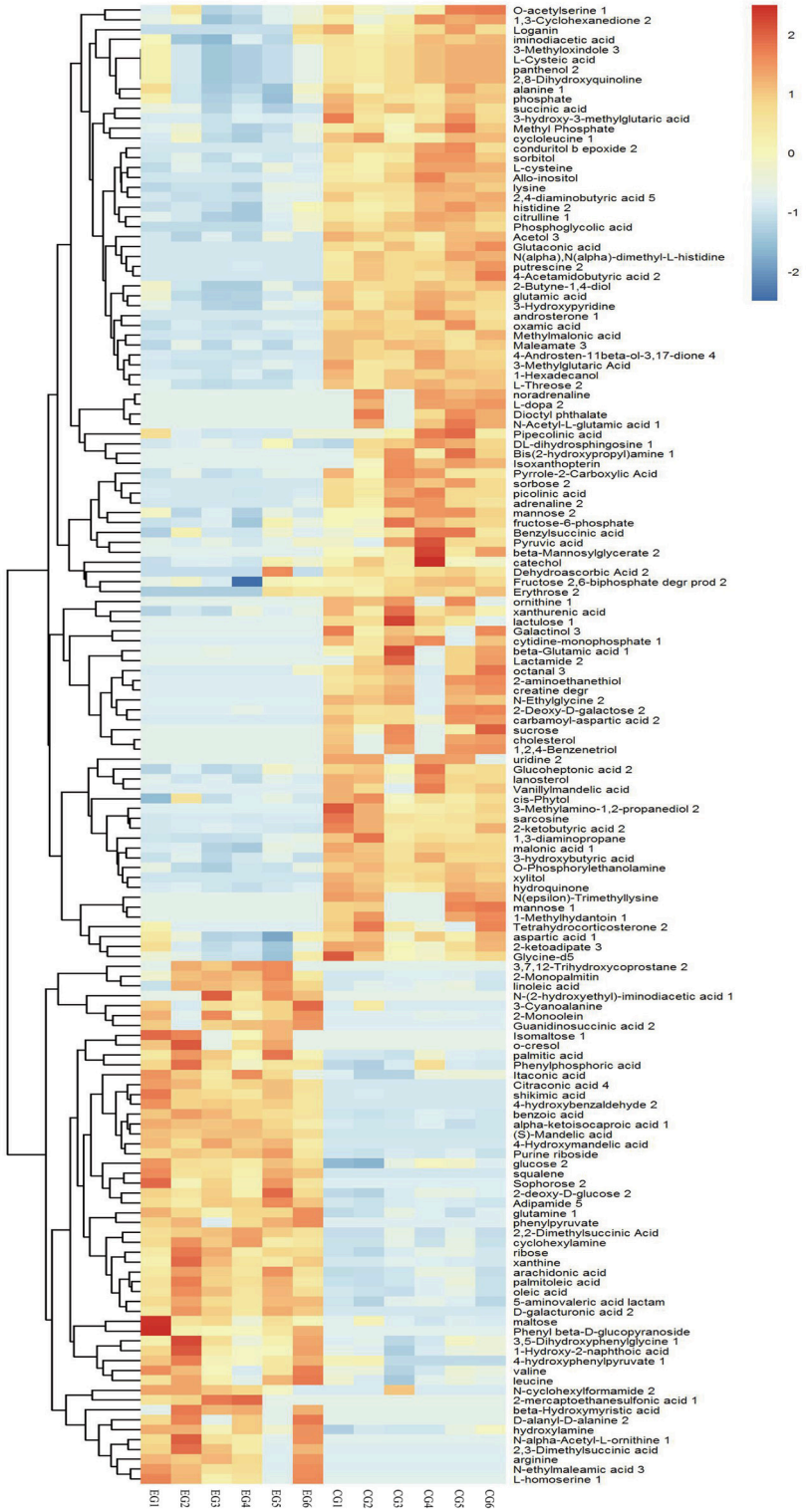

FIGURE 4 | Hierarchical clustering analysis for SDMs. The relative metabolite level is depicted according to the color scale. Red indicates upregulation, while blue indicates downregulation.

TABLE 2 | Identification of SDMs with similarity (Sim) > 700 in hepatopancreas between EG and CG groups.

Metabolites	Sim	VIP	*P*-value	FC	Log_2FC	CT
Palmitoleic acid	948	1.527	0.000	3.041	1.605	↑
Pyruvic acid	948	1.133	0.027	0.692	−0.531	↓
Oleic acid	947	1.559	0.000	2.804	1.487	↑
Sarcosine	945	1.603	0.000	0.020	−5.660	↓
Maltose	932	1.296	0.009	4.296	2.103	↑
Oleic acid	927	1.605	0.000	8.696	3.120	↑
Palmitic acid	926	1.396	0.002	1.361	0.445	↑
Glucose 2	923	1.306	0.001	1.501	0.586	↑
Valine	921	1.129	0.021	1.390	0.475	↑
O-Phosphorylethanolamine	921	1.561	0.000	0.640	−0.645	↓
Picolinic acid	918	1.593	0.000	0.201	−2.314	↓
Alanine 1	916	1.229	0.004	0.717	−0.481	↓
Phosphate	909	1.373	0.000	0.598	−0.742	↓
Glutamic acid	908	1.507	0.000	0.618	−0.693	↓
Cholesterol	908	1.162	0.026	0.000	−17.419	↓
Lysine	905	1.495	0.000	0.259	−1.950	↓
Xanthurenic acid	904	1.444	0.000	0.496	−1.012	↓
Beta-Mannosylglycerate 2	902	1.613	0.012	0.000	−21.091	↓
Glutamine 1	894	1.525	0.000	2.037	1.027	↑
Itaconic acid	888	1.302	0.002	1.635	0.709	↑
Mannose 2	882	1.376	0.001	0.581	−0.784	↓
Succinic acid	881	1.488	0.000	0.372	−1.425	↓
Isomaltose 1	880	1.113	0.049	344489.857	18.394	↑
Squalene	875	1.615	0.000	4231511.014	22.013	↑
Mannose 1	872	1.165	0.031	0.000	−18.522	↓
L-cysteine	871	1.503	0.000	0.317	−1.659	↓
Alpha-ketoisocaproic acid 1	863	1.535	0.000	11.302	3.499	↑
5-aminovaleric acid lactam	860	1.478	0.000	4.655	2.219	↑
citrulline 1	860	1.464	0.000	0.504	−0.989	↓
Ornithine 1	860	1.159	0.027	0.000	−25.208	↓
Methyl Phosphate	853	1.424	0.000	0.572	−0.807	↓
3-Hydroxypyridine	853	1.543	0.000	0.540	−0.890	↓
2-Monopalmitin	841	1.538	0.001	8.212	3.038	↑
Benzoic acid	818	1.596	0.000	2.423	1.277	↑
Putrescine 2	805	1.467	0.000	0.004	−7.796	↓
Uridine 2	804	1.162	0.025	0.000	−16.290	↓
Arachidonic acid	802	1.507	0.000	2.524	1.336	↑
2-Monopalmitin	801	1.616	0.000	4539096.110	22.114	↑
Sophorose 2	801	1.614	0.003	470699.180	18.844	↑
Ribose	800	1.501	0.000	2.332	1.221	↑
Pipecolinic acid	800	1.060	0.046	0.431	−1.213	↓
Galactinol 3	778	1.377	0.012	0.000	−18.881	↓
Conduritol b epoxide 2	758	1.615	0.000	0.000	−22.243	↓
Glucoheptonic acid 2	754	1.382	0.000	0.285	−1.810	↓
4-Hydroxymandelic acid	738	1.616	0.000	1213342.746	20.211	↑
histidine 2	718	1.385	0.000	0.354	−1.498	↓
2-Monoolein	703	1.176	0.012	66.257	6.050	↑
Leucine	703	1.236	0.004	1.756	0.812	↑

FC represent Fold change; CT represent Change trend; ↑ and ↓ indicate that the metabolites were upregulated and downregulated in EG than CG, respectively.

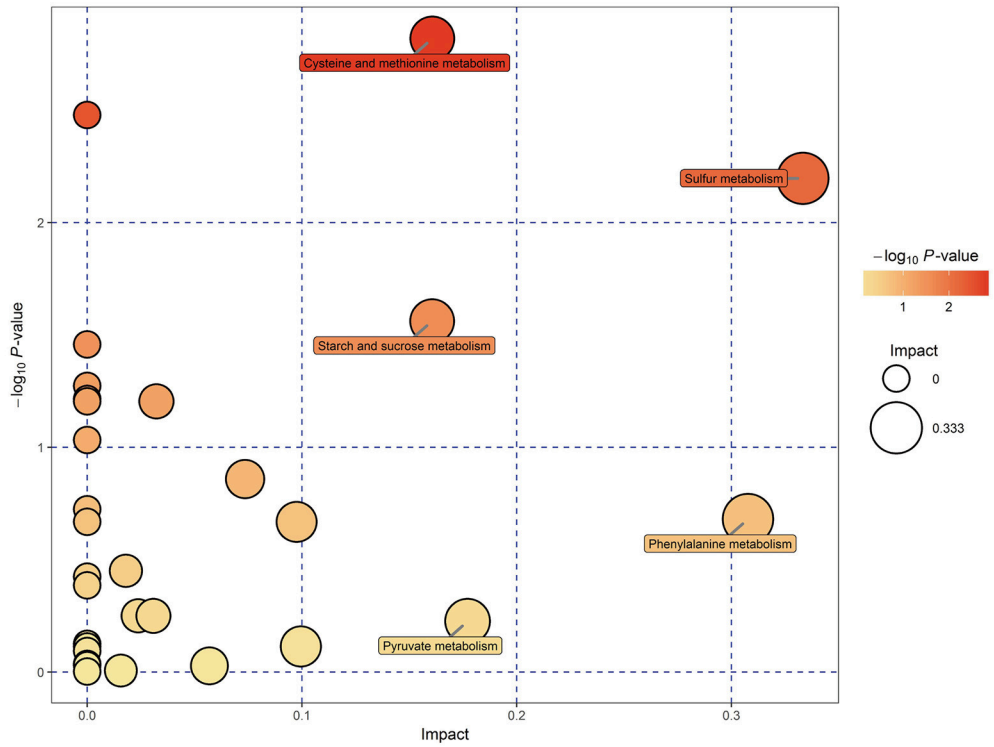

FIGURE 5 | Metabolomic view map of significant metabolic pathways characterized in the hepatopancreas of *P. f. martensii* in EG and CG. This figure illustrates significantly changed pathways based on enrichment and topology analysis. The x-axis represents pathway enrichment, and the y-axis represents pathway impact. Large sizes and dark colors represent great pathway enrichment and high pathway impact values, respectively.

achieves the ideal effects for breeding aquatics, comparison of pearl oysters fed formulated or natural diets in general is necessary. In the present study, the effects of a formulated diet on pearl oysters grown indoors were evaluated and compared with those of pearl oysters cultured with natural diet outdoors. At the end of the trials, the survival rate of EG was significantly higher than that of CG, which indicates that the formulated diet did not negatively affect *P. f. martensii*. The AGRs of EG for SL, SW, and SH of EG were lower than those of CG, but the two groups exhibited similar gains in TW. These results suggest that the formulated diet is an excellent substitute for natural diet.

Exploration of the mechanism behind the phenomenon is necessary to develop optimized nutritional requirements and feeding regimes and achieve optimum growth rates in aquaculture. Aquatic nutritional metabolomics research is an emerging field. To determine differences between the formulated and natural diets, we performed GC–TOF/MS-based metabolomics analysis, compared the metabolites, and detected changes in the hepatopancreas of pearl oysters between the two groups. Metabolomics is uniquely applicable to the assessment of metabolic responses to nutritional deficiencies or excesses. GC-TOF/MS-based metabolomics can detect low-molecular-weight metabolites and their intermediates and provide additional information on metabolic processes (Sun et al., 2015). In the present study, while 1,059 valid peaks were detected, the number of metabolites detected by GC–MS in plasma has been shown to vary among animal taxa in other studies (Kodama et al., 2014; Zaitsu et al., 2014). For example, 53 metabolites from the serum of tiger puffer fish (*Takifugu rubripes*) were obtained (Kodama et al., 2014), and 218 metabolites were found in the serum of cow (Sun et al., 2015). Although the metabolites in blood samples are secreted, excreted, or discarded from different animal tissues in response to physiological requirements or stress (Psychogios et al., 2011), the number of metabolites detected by GC–MS in serum is usually less than that in animal tissues. Ma et al. (2017) identified 222 peaks from the serum of *Eriocheir sinensis* but found that only 69 metabolites shared a similarity value of >700. In the present study, 562 peaks were detected in the hepatopancreas of the oysters, but only 125 of these peaks achieved a similarity value of >700. Among the 150 SDMs found between EG and CG, only 48 components showed a similarity value of >700. The number of metabolites with a similarity value of >700 in the present study was more than that (72 metabolites) obtained in the ovarian tissue of *Coilia nasus* (Xu et al., 2016).

Metabolomics is a useful approach to obtain a whole-organism overview of affected pathways. The metabolic pathways identified from the SDMs represent the typical characteristics of dietary or medical intervention on organisms (Sun et al., 2015; Ma et al., 2017). The integrated key metabolic pathways are manually linked together based on the results of common

TABLE 3 | Metabolic pathways identified on the SDMs from the hepatopancreas between EG and CG groups.

Metabolic pathway	SDMs
Cysteine and methionine metabolism	(0.692) Pyruvic acid* ↓
	(0.317) L-Cysteine ↓
	(347353.442) L-Homoserine ↑
	(0.753) L-Cysteate ↓
	(0.710) O-Acetyl-L-serine ↓
Starch and sucrose metabolism	(1.501) D-Glucose ↑
	(0.509) D-Fructose 6-phosphate ↓
	(0.026) Sucrose ↓
	(4.296) Maltose ↑
	(344489.857) Isomaltose ↑,
	(0.692) Pyruvic acid ↓
Sulfur metabolism	(0.372) Succinate ↓
	(0.317) L-Cysteine ↓
	(347353.442) L-Homoserine ↑
	(0.710) O-Acetyl-L-serine ↓
Phenylalanine metabolism	(0.692) Pyruvic acid ↓
	(0.372) Succinate ↓
	(477736.542) Phenylpyruvate ↑
	(2.423) Benzoate ↑
Pyruvate metabolism	(0.692) Pyruvic acid ↓
	(0.372) Succinate ↓

**The number in the parentheses represents the value of Fold change (EG/CG); ↑ and ↓ indicate that the metabolites were upregulated and downregulated in EG than CG, respectively.*

key metabolic pathways and significantly changed pathways from different metabolites in the hepatopancreas. Three key metabolic pathways, including cysteine and methionine metabolism, sulfur metabolism, and starch and sucrose metabolism, were identified (**Figure 6**); these pathways are involved in amino acid metabolism, energy metabolism, and carbohydrate metabolism, respectively.

While L-homoserine levels in EG were significantly higher than those in CG, O-acetyl-L-serine and L-cysteine levels were downregulated in this group compared with those in CG. These observations suggest the effects of the formulated diet on cysteine and methionine metabolism and sulfur metabolism. L-homoserine is a nonessential amino acid that serves as the precursor of threonine and methionine; while it acts as an important functional amino acid, this acid does not participate in protein synthesis (Li et al., 2016). Low L-homoserine levels can improve growth traits and show similar threonine bioactivity in young chicks (Bryant et al., 2009). Zeng et al. (2017) reported that exogenous administration of glucose to fish upregulates L-homoserine content and greatly enhances their survival after infection. However, Bryant et al. (2009) confirmed that high levels of supplemental L-homoserine are noxious for chicks. Hao et al. (2018) surmised that high L-homoserine levels may affect glycine, serine, and threonine metabolism, as well as cysteine and methionine metabolism, thereby resulting in different growth performances in pearl oyster (*P. maxima*). Therefore, we propose that high L-homoserine levels in the hepatopancreas may influence amino acid metabolism, including cysteine and methionine metabolism and sulfur metabolism, and result in poorer growth performance of pearl oysters in EG compared with those in CG. However, the mechanisms underlying these modes of action have yet to be established and further investigated.

During starch and sucrose metabolism, the maltose, isomaltose, and D-glucose levels of EG were higher than those of CG. This finding proves that pearl oysters can break down α-starch in the formulated diet to produce glucose and is consistent with the higher amylase activity found in EG compared with that in CG. However, the glucose-6-phosphate, D-fructose-6-phosphate, and pyruvic acid levels in EG were downregulated (Supplemental Table 1) compared with those in CG. A decrease in levels of pyruvic acid, which is a product of glycolysis, implies a decline in glucose utilization (Rocha et al., 2011). The first step of intracellular glucose utilization is catalyzed by HK (Hall et al., 2009), and EG exhibits lower HK and G6PI concentrations compared with CG; such downregulation may result in the downregulation of D-fructose-6-phosphate and pyruvic acid. Therefore, the carbohydrate metabolism of EG is lower than that of CG, which could partly explain the poorer growth performance of pearl oysters in the former compared with those in the latter. The carbohydrate content of a diet can affect HK activity in aquatic animals (Enes et al., 2008; Moreira et al., 2008). For example, when dietary carbohydrate levels were maintained near the maximum tolerable level for metabolic utilization of carbohydrates by European sea bass juveniles, their liver HK did not increase vitality (Moreira et al., 2008). Thus, higher dietary carbohydrate levels may lead to lower HK and G6PI concentrations. This premise requires further investigations, and the effects of different dietary carbohydrate levels on pearl oyster should be studied.

β-oxidation is the catabolic process by which fatty acid molecules are broken down for energy production (Houten and Wanders, 2010). In the present study, some fatty acids such as 2-Monopalmitin ($\log_2$FC=22.114), 2-Monoolein ($\log_2$FC = 6.050), oleic acid ($\log_2$FC = 8.696), and arachidonic acid ($\log_2$FC = 1.336) had very high FC values in EG2 (**Table 2**), attesting to the high fatty acid catabolic activity in EG2. Considering this, it can be hypothesized that the pearl oysters in EG2 required more energy via catabolism of fatty acids, which caused the poorer growth performance of pearl oysters in EG2 than those in CG. A similar phenomenon was also observed in farmed *Haliotis midae* (Venter et al., 2018). Squalene is the intermediate of cholesterol metabolism, and cholesterol is essential for membrane structure and hormone and steroid biosynthesis (Kalogeropoulos et al., 2010), such as cholecalciferol (VD3) biosynthesis, which can promote Ca^{2+} transport, absorption, and utilization, thereby regulating the biomineralization of pearl oyster shell. However, pearl oysters in EG achieved significantly higher squalene level ($\log_2$FC = 22.013) and significantly lower cholesterol level ($\log_2$FC = −17.419) than those in CG. This metabolic disorder could also cause a poor growth performance of pearl oysters in EG.

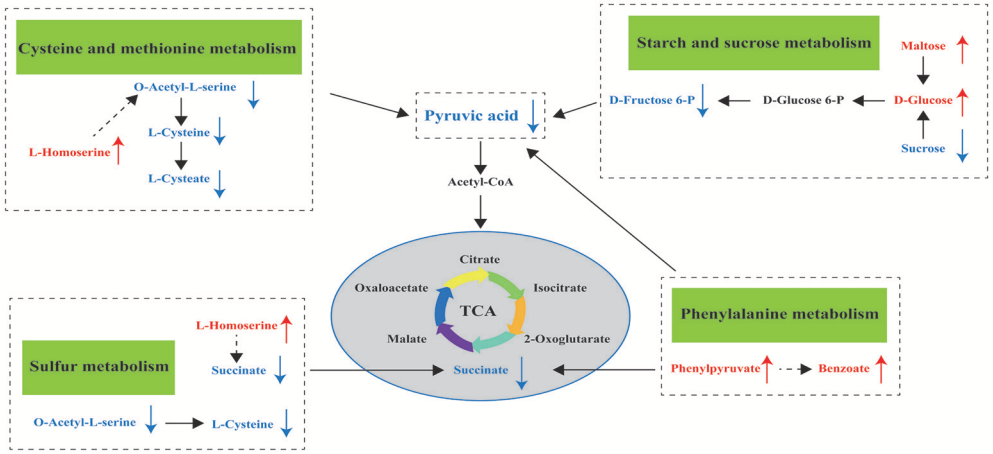

FIGURE 6 | Hypothesized scheme of the metabolomics responses of pearl oysters *P. f. martensii* fed a formulated diet indoors or cultured with natural diet outdoors.

CONCLUSIONS

Comparison of the growth performance and metabolic profiles of pearl oysters in EG and CG shows that the formulated diet could be an excellent substitute for natural diet. However, the formulated diet contains insufficient nutrients that may affect cysteine and methionine metabolism, sulfur metabolism, and starch and sucrose metabolism. Thus, modification of the dietary levels of these compounds in the formulated diet are required to achieve better growth performance, such as dietary carbohydrate level. Moreover, other strategies, such as formulating more effective diets and setting better feeding regimes, should be developed to enhance the utilization of formulated diets and improve pearl production and quality.

AUTHOR CONTRIBUTIONS

YD, CY, RS, and XD designed the research. CY, RH, and YD conducted the research. CY and RH analyzed data. CY, RH, QW, XD, and YD contributed to the final writing of the paper. CY and RH wrote the manuscript. All authors have read and approved the final manuscript.

ACKNOWLEDGMENTS

This work was supported by the Department of Science and Technology of Guangdong Province (Grant number: 2014A020208122), the Graduate Education Innovation Program of Guangdong Ocean University (Grant number: 201720), Innovation Team Project (grant number: 2017KCXTD016) from the Department of Education of Guangdong Province, and the Guangdong Marine and Fishery Bureau (Grant numbers: Z2014009 and B201601-Z10). We thank Zhe Zheng, Ronglian Huang and Yu Jiao for helpful discussions. Our data analysis was assisted by Biotree Biotech Co., Ltd. (Shanghai, China).

SUPPLEMENTARY MATERIAL

The Supplementary Material for this article can be found online at: https://www.frontiersin.org/articles/10.3389/fphys.2018.00944/full#supplementary-material

REFERENCES

Abro, R., Moazzami, A. A., Lindberg, J. E., and Lundh, T. (2014). Metabolic insights in Arctic charr (*Salvelinus alpinus*) fed with zygomycetes and fish meal diets as assessed in liver using nuclear magnetic resonance (NMR) spectroscopy. *Int. Aquat. Res* 6, 1–11. doi: 10.1007/s40071-014-0063-9

Andersen, S. M., Assaad, H. I., Lin, G., Wang, J., Wu, G., and Aksnes, A. (2015). Metabolomic analysis of plasma and liver from surplus arginine fed Atlantic salmon. *Front. Biosci. (Elite. Ed).* 7, 67–78. doi: 10.2741/718

Andersen, S. M., Taylor, R., Holen, E., Aksnes, A., and Espe, M. (2014). Arginine supplementation and exposure time affects polyamine and glucose metabolism in primary liver cells isolated from *Atlantic salmon*. *Amino Acids* 46, 1225–1233. doi: 10.1007/s00726-014-1684-4

Baumgarner, B. L., and Cooper, B. R. (2012). Evaluation of a tandem gas chromatography/time-of-flight mass spectrometry metabolomics platform as a single method to investigate the effect of starvation on whole-animal metabolism in rainbow trout (*Oncorhynchus mykiss*). *J. Exp. Biol.* 215, 1627–1632. doi: 10.1242/jeb.059873

Bryant, K. I., Dilger, R. N., Parsons, C. M., and Baker, D. H. (2009). Dietary L-homoserine spares threonine in chicks. *J. Nutr.* 139, 1298–1302. doi: 10.3945/jn.109.104372

Cappello, T., Giannetto, A., Parrino, V., Maisano, M., Oliva, S., Marcoet, G. D., et al. (2018). Baseline levels of metabolites in different tissues of mussel *Mytilus galloprovincialis* (Bivalvia: Mytilidae). *Comp. Biochem. Physiol. D Genomics Proteomics* 26, 32–39. doi: 10.1016/j.cbd.2018.03.005

Cappello, T., Maisano, M., Mauceri, A., and Fasulo, S. (2017). ^{1}H NMR-based metabolomics investigation on the effects of petrochemical contamination in posterior adductor muscles of caged mussel *Mytilus galloprovincialis*. *Ecotoxicol. Environ. Saf.* 142, 417–422. doi: 10.1016/j.ecoenv.2017.04.040

Cheng, K., Wagner, L., Moazzami, A. A., Gómez-Requeni, P., Schiller Vestergren, A., Brännäs, E., et al. (2016). Decontaminated fishmeal and fish oil from the

Baltic Sea are promising feed sources for Arctic char (*Salvelinus alpinus* L.)-studies of flesh lipid quality and metabolic profile. *Eur. J. Lipid Sci. Technol.* 118, 862–873. doi: 10.1002/ejlt.201500247

Cipriano, R. C., Smith, M. L., Vermeersch, K. A., Dove, A. D., and Styczynski, M. P. (2015). Differential metabolite levels in response to spawning-induced inappetence in Atlantic salmon *Salmo salar*. *Comp. Biochem. Physiol. D Genomics Proteomics* 13, 52–59. doi: 10.1016/j.cbd.2015.01.001

Collette, T. W., Skelton, D. M., Davis, J. M., Cavallin, J. E., Jensen, K. M., Kahl, M. D., et al. (2016). Metabolite profiles of repeatedly sampled urine from male fathead minnows (*Pimephales promelas*) contain unique lipid signatures following exposure to anti-androgens. *Comp. Biochem. Physiol. D Genomics Proteomics* 19, 190–198. doi: 10.1016/j.cbd.2016.01.001

Deng, C. M., Liang, F. L., Fu, S., and Deng, Y. W. (2010). Research of preoperative treatment of *Pinctada martensii* and pearl culture. *Trans. Oceanol. Limnol.* 4, 124–128. doi: 10.13984/j.cnki.cn37-1141.2010.04.019

Deng, Y. W., Du, X. D., and Wang, Q. H. (2010). Selection for fast growth in the Chinese pearl oyster, *Pinctada martensii*: response of the first generation line. *J. World Aquac. Soc.* 40, 843–847. doi: 10.1111/j.1749-7345.2009.00307.x

Deng, Y. W., Fu, S., Du, X. D., and Wang, Q. H. (2009). Realized heritability and genetic gain estimates of larval shell length in the Chinese pearl oyster *Pinctada martensii* at three different salinities. *N. Am. J. Aquac.* 71, 302–306. doi: 10.1577/A08-024.1

Enes, P., Panserat, S., Kaushik, S., and Oliva-Teles, A. (2008), Growth performance and metabolic utilization of diets with native and waxy maize starch by gilthead sea bream (*Sparus aurata*) juveniles. *Aquaculture* 274, 101–108. doi: 10.1016/j.aquaculture.2007.11.009

Gui, Y., Kaspar, H., Zamora, L., Dunphy, B., and Jeffs, A. (2016). Capture efficiency of artificial food particles of post-settlement juveniles of the Greenshell^{TM} mussel, *Perna canaliculus*. *Aquaculture* 464, 1–7. doi: 10.1016/j.aquaculture.2016.06.011

Hall, J. R., Short, C. E., Petersen, L. H., Stacey, J., Gamperl, A. K., and Driedzic, W. R. (2009). Expression levels of genes associated with oxygen utilization, glucose transport and glucose phosphorylation in hypoxia exposed Atlantic cod (*Gadus morhua*). *Comp. Biochem. Physiol. D Genomics Proteomics s* 4, 128–138. doi: 10.1016/j.cbd.2008.12.007

Hao, R. J., Wang, Z. M., Yang, C. Y., Deng, Y. W., Zheng, Z., Qingheng Wang, Q. H., et al. (2018). Metabolomic responses of juvenile pearl oyster *Pinctada maxima* to different growth performances. *Aquaculture* 491, 258–265. doi: 10.1016/j.aquaculture.2018.03.050

Houten, S. M., and Wanders, R. J. A. (2010). A general introduction to the biochemistry of mitochondrial fatty acid β-oxidation. *J. Inherit. Metab. Dis.* 33, 469–477. doi: 10.1007/s10545-010-9061-2

Jin, Y., Tian, L. X., Xie, S. W., Guo, D. Q., Yang, H. J., Liang, G. Y., et al. (2015). Interactions between dietary protein levels, growth performance, feed utilization, gene expression and metabolic products in juvenile grass carp (*Ctenopharyngodon idella*). *Aquaculture* 437, 75–83. doi: 10.1016/j.aquaculture.2014.11.031

Kalogeropoulos, N., Chiou, A., Gavala, E., Christea, M., and Andrikopoulos, N. K. (2010). Nutritional evaluation and bioactive microconstituents (carotenoids, tocopherols, sterols and squalene) of raw and roasted chicken fed on dha-rich microalgae. *Food Res. Int.* 43, 2006–2013. doi: 10.1016/j.foodres.2010.05.018

Kind, T., Wohlgemuth, G., Lee, D. Y., Lu, Y., Palazoglu, M., Shahbaz, S., et al. (2009). Fiehnlib-mass spectral and retention index libraries for metabolomics based on quadrupole and time-of-flight gas chromatography/mass spectrometry. *Anal. Chem.* 81, 10038–10048. doi: 10.1021/ac9019522

Kodama, H., Otani, K., Iwasaki, T., Takenaka, S., Horitani, Y., and Togase, H. (2014). Metabolomic investigation of pathogenesis of myxosporean emaciation disease of tiger puffer fish *Takifugu rubripes*. *J. Fish Dis.* 37, 619–627. doi: 10.1111/jfd.12154

Kullgren, A., Samuelsson, L. M., Larsson, D. G., Björnsson, B. T., and Bergman, E. J. (2010). A metabolomics approach to elucidate effects of food deprivation in juvenile rainbow trout (*Oncorhynchus mykiss*). *Am. J. Physiol. Regul. Integr. Comp. Physiol.* 299, 1440–1448. doi: 10.1152/ajpregu.00281.2010

Li, H., Wang, B. S., Zhu, L. H., Cheng, S., Li, Y. R., Zhang, L., et al. (2016). Metabolic engineering of *Escherichia coli*, W3110 for L-homoserine production. *Process Biochem.* 51, 1973–1983. doi: 10.1016/j.procbio.2016.09.024

Liu, S. L., Zhou, Y., Ru, X. S., Zhang, M. Z., Cao, X. B., and Yang, H. S. (2016). Differences in immune function and metabolites between aestivating and non-aestivating *Apostichopus japonicus*. *Aquaculture* 459, 36–42. doi: 10.1016/j.aquaculture.2016.03.029

Ma, Q. Q., Chen, Q., Shen, Z. H., Li, D. L., Han, T., Qin, J. G., et al. (2017). The metabolomics responses of Chinese mitten-hand crab (*Eriocheir sinensis*) to different dietary oils. *Aquaculture* 479, 188–199. doi: 10.1016/j.aquaculture.2017.05.032

Maherizo, G. F., Catherine, R., Yann, G., Julie, L., Sandrine, L., Joëlle, D., et al. (2017). Fungi isolated from Madagascar shrimps investigation of the *Aspergillus niger* metabolism by combined LC-MS and NMR metabolomics studies. *Aquaculture* 479, 750–758. doi: 10.1016/j.aquaculture.2017.07.015

Moreira, I. S., Peres, H., Couto, A., Enes, P., and Olivateles, A. (2008). Temperature and dietary carbohydrate level effects on performance and metabolic utilisation of diets in European sea bass (*Dicentrarchus labrax*) juveniles. *Aquaculture* 274, 153–160. doi: 10.1016/j.aquaculture.2007.11.016

Nevejan, N., Davis, J., Little, K., and Kiliona, A. (2009). Use of a formulated diet for mussel spat *Mytilus galloprovincialis* (Lamarck 1819) in a commercial hatchery. *J. Shellfish Res.* 26, 357–363. doi: 10.2983/0730-8000(2007)26[357:UOAFDF]2.0.CO;2

Psychogios, N., Hau, D. D., Peng, J., Guo, A. C., Mandal, R., Bouatra, S., et al. (2011). The human serum metabolome. *PLoS ONE* 6:e16957. doi: 10.1371/journal.pone.0016957

Qiu, Y., Lu, H., Zhu, J. T., Chen, X. F., Wang, A. M., and Wang, Y. (2014). Characterization of novel EST-SSR markers and their correlations with growth and nacreous secretion traits in the pearl oyster *Pinctada martensii* (Dunker). *Aquaculture* 420–421, S92–S97. doi: 10.1016/j.aquaculture.2013.09.040

Rocha, C. M., Carrola, J., Barros, A. S., Gil, A. M., Goodfellow, B. J., Carreira, I. M., et al. (2011). Metabolic signatures of lung cancer in biofluids: NMR-based metabonomics of blood plasma. *J. Proteome Res.* 10, 4314–4324. doi: 10.1021/pr200550p

Sheedy, J. R., Lachambre, S., Gardner, D. K., and Day, R. W. (2016). ^{1}H-NMR metabolite profiling of abalone digestive gland in response to short-term starvation. *Aquacult. International* 24, 503–521. doi: 10.1007/s10499-015-9941-4

Sun, H. Z., Wang, D. M., Wang, B., Wang, J. K., Liu, H. Y., Guan, L. L., et al. (2015). Metabolomics of four biofluids from dairy cows: potential biomarkers for milk production and quality. *J. Proteome Res.* 14, 1287–1298. doi: 10.1021/pr501305g

Tuffnail, W., Mills, G. A., Cary, P., and Greenwood, R. (2009). An environmental, ^{1}H NMR metabolomic study of the exposure of the marine mussel, *Mytilus edulis*, to atrazine, lindane, hypoxia and starvation. *Metabolomics* 5, 33–43. doi: 10.1007/s11306-008-0143-1

Venter, L., Vosloo, A., Du, T. L., Mienie, L. J., Rensburg, P. J. J. V., and Lindeque, J. Z. (2018). Characterising the metabolic differences related to growth variation in farmed *Haliotis midae*. *Aquaculture* 493, 144–152. doi: 10.1016/j.aquaculture.2018.04.052

Wagner, L., Trattner, S., Pickova, J., Gómez-Requeni, P., and Moazzami, A. A. (2014). ^{1}H NMR-based metabolomics studies on the effect of sesamin in Atlantic salmon (*Salmo salar*). *Food Chem.* 147, 98–105. doi: 10.1016/j.foodchem.2013.09.128

Wang, Q. H., Yang, C. Y., Du, X. D., Liu, X. W., Sun, R. J., and Deng, Y. W. (2016). Growth performance and biochemical composition of juvenile pearl oyster *Pinctada martensii* fed on artificial diets. *Aquacult. Int.* 24, 995–1005. doi: 10.1007/s10499-015-9966-8

Wei, Y., Liang, M., Mai, K., Zheng, K., and Xu, H. (2017). ^{1}H NMR-based metabolomics studies on the effect of size-fractionated fish protein hydrolysate, fish meal and plant protein in diet for juvenile turbot (*Scophthalmus maximus*, L.). *Aquaculture Nutrition* 23, 523–536. doi: 10.1111/anu.12420

Xu, G. C., Du, F. K., Li, Y., Nie, Z. J., and Xu, P. (2016). Integrated application of transcriptomics and metabolomics yields insights into population-asynchronous ovary development in *Coilia nasus*. *Sci. Rep.* 6:31835. doi: 10.1038/srep31835

Yang, C. Y., Hao, R. J., Deng, Y. W., Liao, Y. S., Wang, Q. H., Sun, R. J., et al. (2017b). Effects of protein sources on growth, immunity and antioxidant capacity of juvenile pearl oyster *Pinctada fucata martensii*. *Fish Shellfish Immunol.* 67, 411–418. doi: 10.1016/j.fsi.2017.06.037

Yang, C. Y., Hao, R. J., Du, X. D., Wang, Q. H., Deng, Y. W., Sun, R. J., et al. (2018). GC–TOF/MS-based metabolomics studies on the effect of protein sources in

formulated diet for pearl oyster *Pinctada fucata martensii*. *Aquaculture* 486, 139–147. doi: 10.1016/j.aquaculture.2017.12.020

Yang, C. Y., Wang, Q. H., Hao, R. J., Liao, Y. S., Du, X. D., and Deng, Y. W. (2017a). Effects of replacing microalgae with an artificial diet on pearl production traits and mineralization-related gene expression in pearl oyster *Pinctada fucata martensii*. *Aquac. Res.* 48, 5331–5337. doi: 10.1111/are.13346

Ye, Y. F., Xia, M. J., Mu, C. K., Li, R. H., and Wang, C. L. (2016). Acute metabolic response of *Portunus trituberculatus*, to *Vibrio alginolyticus*, infection. *Aquaculture* 463, 201–208. doi: 10.1016/j.aquaculture.2016.05.041

Zaitsu, K., Miyawaki, I., Bando, K., Horie, H., Shima, N., Katagi, M., et al. (2014). Metabolic profiling of urine and blood plasma in rat models of drug addiction on the basis of morphine, methamphetamine, and cocaine-induced conditioned place preference. *Anal. Bioanal. Chem.* 406, 1339–1354. doi: 10.1007/s00216-013-7234-1

Zeng, Z. H., Du, C. C., Liu, S. R., Li, H., Peng, X. X., and Peng, B. (2017). Glucose enhances tilapia against *Edwardsiella tarda* infection through metabolome reprogramming. *Fish Shellfish Immunol.* 61, 34–43. doi: 10.1016/j.fsi.2016.12.010

Conflict of Interest Statement: The authors declare that the research was conducted in the absence of any commercial or financial relationships that could be construed as a potential conflict of interest.

frontiers in Physiology

ORIGINAL RESEARCH
published: 16 July 2018
doi: 10.3389/fphys.2018.00811

PiggyBac Transposon-Mediated Transgenesis in the Pacific Oyster (*Crassostrea gigas*) – First Time in Mollusks

*Jun Chen[1†], Changlu Wu[1†], Baolu Zhang[2†], Zhongqiang Cai[3], Lei Wei[1], Zhuang Li[1], Guangbin Li[1], Ting Guo[1], Yongchuan Li[1], Wen Guo[4] and Xiaotong Wang[1]**

[1] School of Agriculture, Ludong University, Yantai, China, [2] Consultation Center, State Oceanic Administration, Beijing, China, [3] Changdao Enhancement and Experiment Station, Chinese Academy of Fishery Sciences, Yantai, China, [4] Center for Mollusc Study and Development, Marine Biology Institute of Shandong Province, Qingdao, China

As an effective method of transgenesis, the plasmid of *PiggyBac* transposon containing GFP (*PiggyBac*) transposon system has been widely used in various organisms but not yet in mollusks. In this work, *piggyBac* containing green fluorescent protein (GFP) was transferred into the Pacific oyster (*Crassostrea gigas*) by sperm-mediated gene transfer with or without electroporation. Fluorescent larvae were then observed and isolated under an inverted fluorescence microscope, and insertion of *piggyBac* was tested by polymerase chain reaction (PCR) using genomic DNA as template. Oyster larvae with green fluorescence were observed after transgenesis with or without electroporation, but electroporation increased the efficiency of sperm-mediated transgenesis. Subsequently, the recombinant *piggyBac* plasmid containing *gGH* (*piggyBac-gGH*) containing GFP and a growth hormone gene from orange-spotted grouper (*gGH*) was transferred into oysters using sperm mediation with electroporation, and fluorescent larvae were observed and isolated. The insertion of *piggyBac-gGH* was tested by PCR and genome walking analysis. PCR analysis indicated that *piggyBac-gGH* was transferred into oyster larvae; genome walking analysis further showed the detailed location where *piggyBac-gGH* was inserted in the oyster genome. This is the first time that *piggyBac* transposon-mediated transgenesis has been applied in mollusks.

Keywords: Pacific oyster, transgenesis, *piggyBac* transposons, sperm-mediated gene transfer, electroporation

OPEN ACCESS

Edited by:
Menghong Hu,
Shanghai Ocean University, China

Reviewed by:
Weiwei You,
Xiamen University, China
Vengatesen Thiyagarajan,
University of Hong Kong, Hong Kong

***Correspondence:**
Xiaotong Wang
wangxiaotong999@163.com

† These authors have contributed equally to this work.

Specialty section:
This article was submitted to Aquatic Physiology, a section of the journal Frontiers in Physiology

Received: *09 April 2018*
Accepted: *08 June 2018*
Published: *16 July 2018*

Citation:
Chen J, Wu C, Zhang B, Cai Z, Wei L, Li Z, Li G, Guo T, Li Y, Guo W and Wang X (2018) PiggyBac Transposon-Mediated Transgenesis in the Pacific Oyster (Crassostrea gigas) – First Time in Mollusks. Front. Physiol. 9:811. doi: 10.3389/fphys.2018.00811

INTRODUCTION

Many methods can be employed to achieve genetic transformation, including viral vectors, non-viral vectors and transposons. Among these relatively effective methods of transgenesis, transposons have the ability to integrate into chromosomes, and gene expression from transposons is permanent (Ivics and Izsvak, 2006). Transposons are mobile elements that can transpose between vectors and a target genome. The original *piggyBac* transposon was first identified and isolated from the genome of the cabbage looper moth, *Trichoplusia ni,* in the late 1980s (Cary et al., 1989). Later,

Abbreviations: CMV, human cytomegalovirus; GFP, green fluorescent protein; *gGH*, a growth hormone gene from orange-spotted grouper; MCS, multiple cloning site; PCR, polymerase chain reaction; *piggyBac*, the plasmid of *PiggyBac* transposon containing GFP; *piggyBac-gGH*, the recombinant *piggyBac* plasmid containing *gGH*.

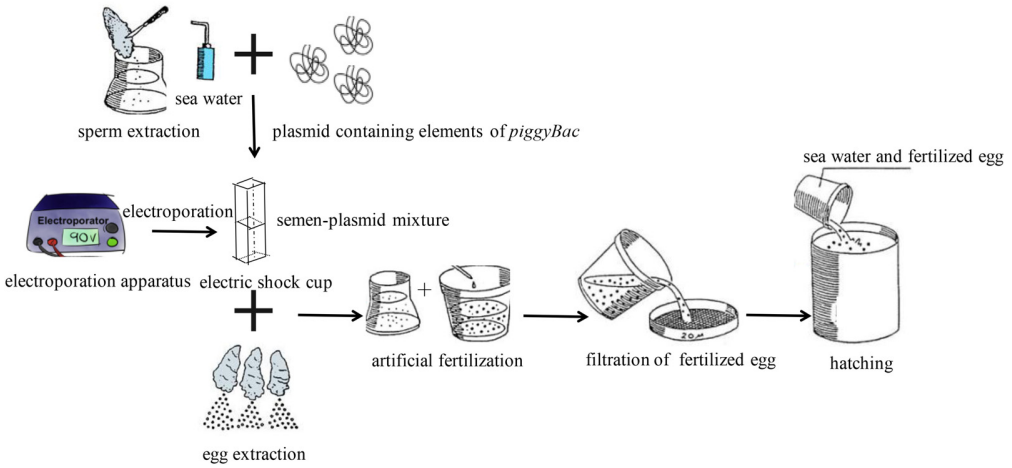

FIGURE 1 | Schematic diagram of procedures for transfection of *piggyBac* into Pacific oyster.

other *piggyBac*-like transposons were identified in different insect species (Wu et al., 2011; Depra et al., 2012; Sormacheva et al., 2012), frogs (Lam et al., 1996; Leaver, 2001), fish (Cocca et al., 2011; Costa et al., 2013), and mammals (Jurka, 2000; Sarkar et al., 2003). The original *piggyBac* element is approximately 2.4 kb, with identical 13 bp inverted terminal repeats and additional asymmetric 19 bp internal repeats (Elick et al., 1997; Li et al., 2001, 2005). Previous data have shown that the original *piggyBac* transposon can effectively transfer up to 9.1 kb of transgene sequence into chromosomes with the help of the *piggyBac* transposase enzyme from a separate plasmid (Ding et al., 2005). *PiggyBac* allows "cut and paste" transfer of genes of interest between inverted terminal repeats and internal repeats into a host genome at TTAA nucleotide elements (Fraser et al., 1996; Bauser et al., 1999; O'Brochta et al., 2003; Wu and Burgess, 2004). *PiggyBac* transposon can insert into gene regions and cause mutagenesis, which contributes to infer function of the inserted gene (Ding et al., 2005). Furthermore, *PiggyBac* transposon can introduce exogenous genes into the genome for constructing transgenic organisms or testing gene function (Yusa, 2015). Thus, *piggyBac* transposons have been successfully used as a promising tool for basic genetic studies (Wang et al., 2008; Kaji et al., 2009; Woltjen et al., 2009; Yusa et al., 2009), gene therapies (Carlson et al., 2005) and construction of transgenic animals (Ding et al., 2005). Studies have also shown that the original *piggyBac* transposon has a broad host spectrum ranging from yeast to mammals, and this mobile element has been widely used for a variety of applications in a diverse range of organisms. However, the *piggyBac* transposition system has not yet been utilized or characterized in mollusks.

It has been reported that exogenous DNA can stick to spermatozoa and then be carried into an egg via fertilization. This method of sperm mediation is widely used for gene transfer (Parrington et al., 2011). Previous research has also investigated approaches for increasing the proportion of spermatozoa carrying exogenous DNA to improve the efficiency of transgenesis. One effective method is electroporation of spermatozoa during transformation, which increases the capacity of DNA bound by sperm in fish (Patil and Khoo, 1996) and mollusks (Tsai, 2000).

Pacific oyster is one of the most economically important cultivated oysters in the world. Genome sequencing of Pacific oyster has been completed (Zhang et al., 2012). However, the functions of most Pacific oyster genes are unknown due to a lack of effective research methods, such as transgenesis technology. In this work, we demonstrate that the *piggyBac* transposon system is suitable for Pacific oyster transgenesis.

MATERIALS AND METHODS

Plasmid Construction

The donor plasmid *piggyBac* Dual Promoter and helper plasmid HA-mPB were constructed by Applied Biosystems. *PiggyBac* Dual Promoter carries the CMV promoter upstream of a MCS.

TABLE 1 | Primers used in this study.

Primer	Sequence (5′→3′)	Purpose
GFP-F	TGACCAACAAGATGAAGAGCACC	Cloning of GFP gene
GFP-R	TCCACGTCACCGCATGTTAGAAGA	Cloning of GFP gene
GH-F	CGGAATTCATGGACCGA GTCGTCCTCCTG	Cloning of GH gene
GH-R	CGGGATCCCTACAGGGTA CAGTTGGCCTC	Cloning of GH gene
GH-GFP-F	AACTGCTGGCTTGTTTCA	Cloning of GH-GFP gene
GH-GFP-R	CGATGCGGGTGTTGGTGT	Cloning of GH-GFP gene
SP1	ATTCCACACAACATACGAGCCG	Genome walking
SP2	CTGGGGTGCCTAATGAGTGAGC	Genome walking
SP3	GGGAGAGGCGGTTTGCGTATTG	Genome walking

The base sequences of restriction enzyme cutting sites are underlined.

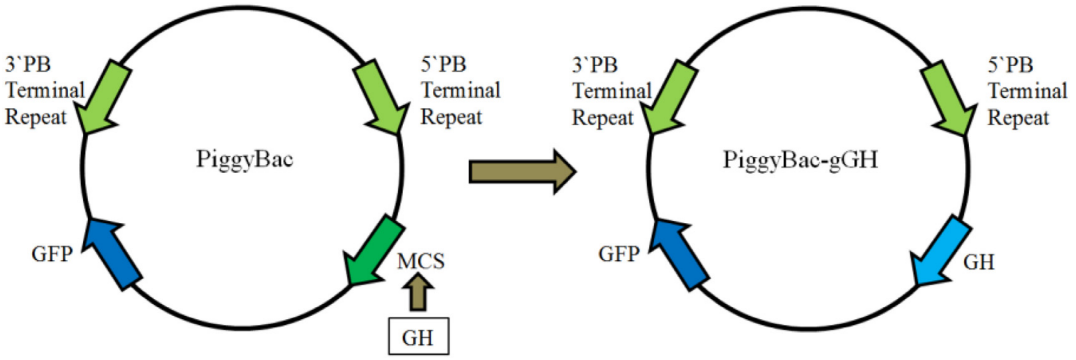

FIGURE 2 | Construction of plasmid *piggyBac-gGH*. The left is the plasmid *PiggyBac*, the right the recombinant plasmid *piggyBac-gGH*. PB, *piggyBac*; GFP, green fluorescent protein; MCS, multiple clone sites; gGH, growth hormone gene of orange-spotted grouper.

Downstream of the expression cassette is an EF1alpha promoter driving the expression of a GFP+Puro marker. The entire cassette is flanked by genomic insulator elements to stabilize expression and *piggyBac* ITR for mobilization and integration. The helper plasmid HA-mPB contains the mPB transposase coding sequence in a pcDNA3-Kz-HA backbone, and it features a 5′ HS4 insulator to support robust transcription from the rPolr2A promoter.

Sequence encoding the mature GH peptide of orange-spotted grouper was amplified by primers GH-F and GH-R, with EcoRI at the 5′ end and BamHI at the 3′ end, using grouper pituitary cDNA as template. Then, the resultant GH fusion gene was digested with EcoRI and BamHI, purified and ligated into the EcoRI and BamHI sites of plasmid *piggyBac* to construct *piggyBac-gGH*.

Transfection of *piggyBac* Into Pacific Oysters

Five hundred μL of semen sampled from mature male Pacific oysters was collected into conical polystyrene sample cups, and then diluted to a concentration of 10^5 sperm/mL. Then, a combination of "helper-independent" transposase (15 μg) and transposon (30 μg) were added to the semen, and the mixture was incubated for 5 min at 20°C. For sperm-mediated gene transfer, approximately 10^4 eggs collected from mature female Pacific oysters were added to the semen-plasmid mixture, and then the mixture was incubated for 5 min. Finally, seawater was added into the mixture to activate fertilization.

For electroporation-mediated gene transfer, the semen-plasmid mixture was transferred into an electric shock cup, and then treated five times with an electroporation apparatus (Scientz, Wuhan, China) with the following parameters: resistance, 100 Ω; voltage, 300 V; capacitance, 100 μF. And each electric pulse duration was 20 ms, and the interval between two pulses was 100 ms. Then, fertilization was carried out as described above. Finally, fertilized ova were cultured in a 10-L tank at 20°C. During transgenesis, the same treatment was performed without plasmid as a negative control. All treatments were repeated three times, and three individual experiments were performed. Additionally, Schematic diagram of procedures for transfection of *piggyBac* into Pacific Oysters was shown in **Figure 1**.

Microscopic Observation of Fluorescent Oyster Larvae and Calculation of Transfection Efficiency and Relative Transfection Efficiency

Survival rates of oyster larvae were initially estimated by counting the density of oyster larvae using an optical microscope 0 and 72 h after fertilization. Oyster larvae transfected with both donor and helper plasmids were observed at 72 h post-transfection using a fluorescence microscope (IX71, Olympus, Japan), under which the expressed fluorescence appeared green. Fluorescent oyster larvae were photographed, counted and isolated.

Next, the efficiency of transfection (%) and relative efficiency of transfection (%) were calculated as below. Efficiency of transfection (%) = Number of larvae expressing fluorescence/Total number of fertilized eggs; relative efficiency of transfection (%) = Number of larvae expressing fluorescence/Total number of larvae at 72 h.

PCR and Sequence Analysis

QIAamp® DNA Micro Kit (Qiagen, United States) was used for trace DNA extraction from oyster larvae. Primers specific for GFP, GH, GH-GFP and the sequence downstream of GFP were used to confirm that *piggyBac-GFP* and *piggyBac-gGH* were successfully inserted and to identify the insertion site within the Pacific oyster genome (primers are shown in **Table 1**). Briefly, PCR amplification for GFP, GH, or GH-GFP sequences was conducted with 35 cycles of 95°C for 20 s, 60°C/60°C/56°C for 20 s, and 72°C for 50 s/1 min/1 min 20 s. PCR products were analyzed by agarose gel electrophoresis and sequencing. Additionally, the oyster genomic insertion site was analyzed using a genome walking kit (Takara, Japan). All primers are shown in **Table 1**.

Statistical Analysis

All data were analyzed using SPSS 20.0 software (Chicago, IL, United States) with one-way variance (ANOVA) followed by Student–Newman–Keuls multiple comparisons test. Differences were considered statistically significant when $p < 0.05$.

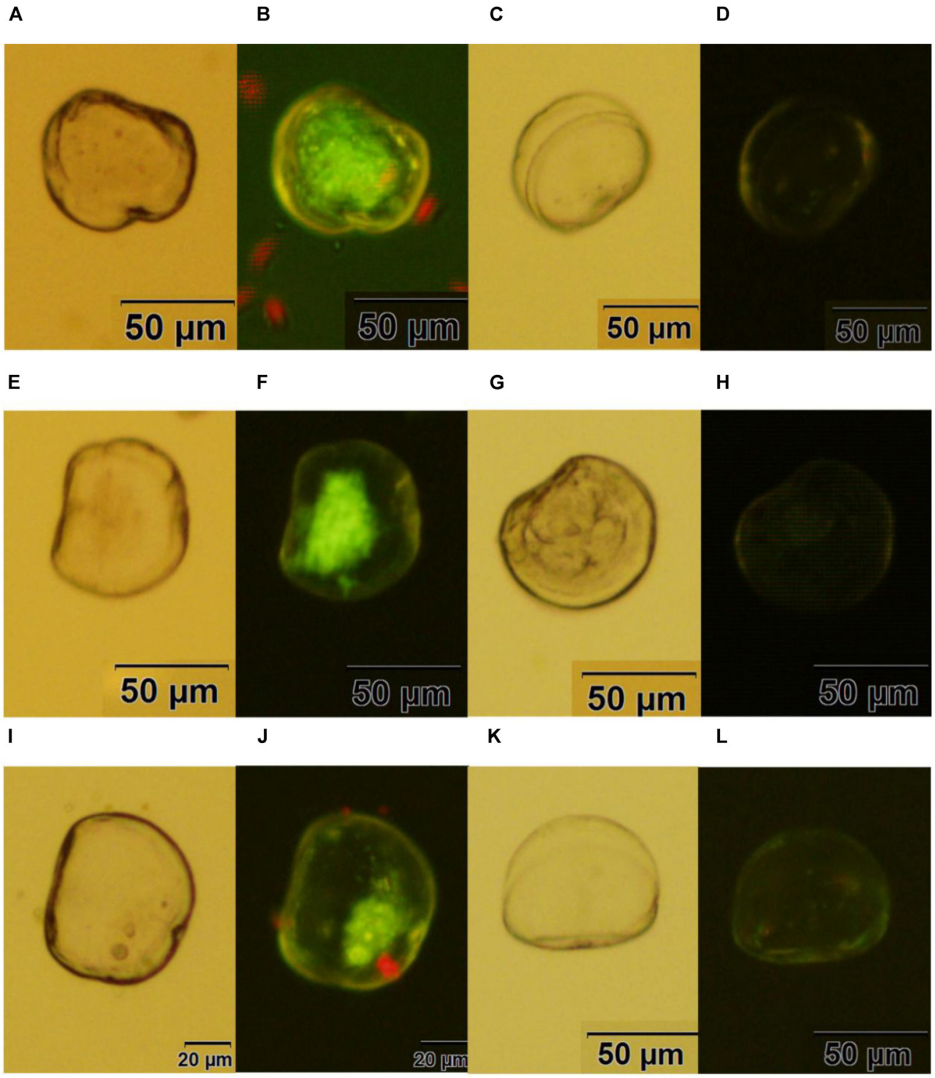

FIGURE 3 | Transgenic oyster larvae and controls. **(A,B)** Oyster larvae transfected with *piggyBac* using sperm mediation without electroporation under white light or green fluorescence; **(C,D)** non-transfected oyster larvae as a control for **(A,B)**; **(E,F)** oyster larvae transfected with piggyBac using sperm mediation with electroporation under white light or green fluorescence; **(G,H)** non-transfected oyster larvae as a control for **(E,F)**; **(I,J)** oyster larvae transfected with *piggyBac-gGH* using sperm mediation with electroporation under white light or green fluorescence; **(K,L)** non-transfected oyster larvae as a control for **(I,J)** Red spots are the algae *Isochrysis galbana* used as food for oyster larvae.

RESULTS

Construction of *piggyBac-gGH*

As shown in **Figure 2**, a fusion gene encoding the mature *GH* peptide of orange-spotted grouper was subcloned upstream of *GFP* in the donor plasmid *PiggyBac*, producing the recombinant plasmid *piggyBac-gGH*.

Observation of Fluorescent Larvae and Efficiency of Transfection

Fluorescent oyster larvae transfected with helper and donor plasmids were observed and counted using a confocal microscope, and then were isolated 72 h after transfection. As shown in **Figure 3**, Pacific oyster larvae with green fluorescence were observed after transformation with *piggyBac* without electroporation (**Figure 3B**), with electroporation (**Figure 3F**) or with *piggyBac-gGH w*ith electroporation (**Figure 3J**), while green fluorescence was not observed in the control group (**Figures 3D,H,L**).

As shown in **Figure 4A**, the survival rates of oyster larvae were approximately 10 and 1% after gene transfer of *piggyBac* without or with electroporation, respectively. The survival rate of the electroporation group was significantly lower than that of the control group or the group without electroporation ($p < 0.01$). However, the results (**Figure 4B**) showed that the efficiency of *piggyBac* transfection with electroporation (0.4%) was significantly higher than without electroporation (0.03%).

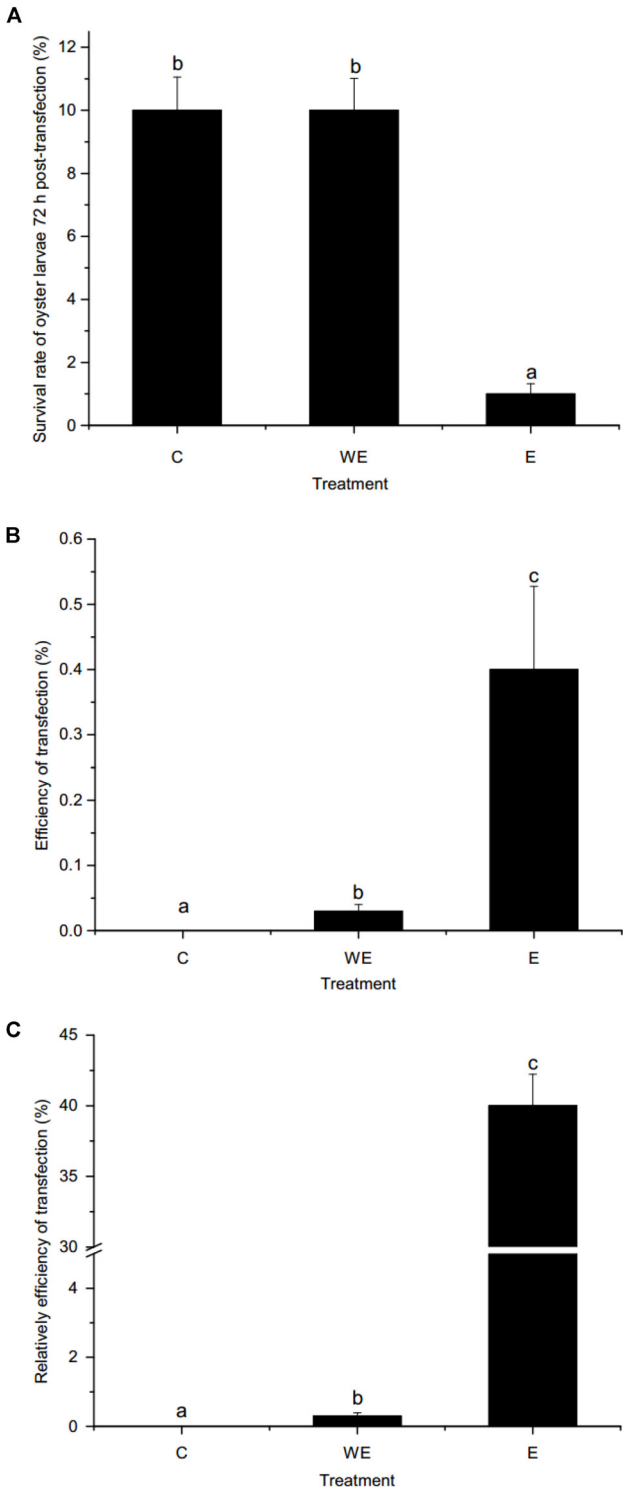

FIGURE 4 | Survival rate and transfection efficiency using *piggyBac* system in oyster larvae. **(A)** Survival rate of oyster larvae 72 h post-transfection; **(B)** efficiency of transfection; **(C)** relative efficiency of transfection. C, non-transfected control group. WE, sperm-mediated transfection without electroporation. E, sperm-mediated transfection with electroporation. Data are shown as the means ± SEM (standard error of mean, SEM), $n = 3$. Different letters indicate statistically significant differences ($p < 0.05$).

In addition, the relative efficiency of *piggyBac* transfection with electroporation was dramatically higher than transfection without electroporation (40 vs. 0.3%, **Figure 4C**).

Characterization of Exogenous Gene Insertion

Polymerase chain reaction and agarose gel electrophoresis detected the target gene segment in fluorescent oyster larvae, but not in non-fluorescent oyster larvae. As shown in **Figure 5A**, the GFP gene was detected in oyster larvae transfected with *piggyBac*. Both the GFP and GH genes were amplified from genomic DNA of oyster larvae transfected with *piggyBac-gGH* (**Figure 5B**), and sequencing results showed that their sequences matched the appropriate gene sequences in *piggyBac-gGH* (**Supplementary Figures S1**, **S2**). Meanwhile, segments covering partial sequences of GFP and GH were amplified using GH-GFP-F and GH-GFP-R as primers, which indicated that the GFP and GH genes were inserted into the oyster genome together (**Figure 5C** and **Supplementary Figure S3**). Additionally, the genomic insertion site of *piggyBac-gGH* was identified using the method of genome walking, and as shown in **Figure 6**, GFP-GH had been inserted into Scaffold200 of Pacific oyster genome at the sequence "AAGA."

DISCUSSION

Sperm-mediated transformation in mollusks has been reported in previous studies with or without electroporation (Tsai et al., 1997; Guerra et al., 2005; Guerra and Esponda, 2006), and CRISPR/Cas9-mediated transformation has also been utilized (Perry and Henry, 2015). In this work, our transgenesis of Pacific oysters with the *piggyBac* transposon system is the first time this system has been used in mollusks.

Our study showed that transgenic fluorescent oyster larvae can be acquired with the *piggyBac* transposon system, and PCR amplification of target genes from the genomes of transgenic fluorescent oyster larvae indicated that exogenous genes were integrated into Pacific oyster genomes. Genome walking is commonly used to identify regions upstream and downstream from known DNA sequences (Rishi et al., 2004; Leoni et al., 2008, 2011; Shapter and Waters, 2014). In this study, the DNA sequence of unknown genomic regions flanking the *piggyBac-gGH* insertion were determined by genome walking, then these sequences were aligned with the oyster genome sequence to determine the insertion site. These results further showed that *piggyBac* transposons can mediate integration of exogenous genes into the oyster genome. However, the insertion site of *piggyBac-gGH* in this study was different from previous studies, which reported that *piggyBac* insertions showed a high preference for genomic TTAA nucleotide elements (Fraser et al., 1995; Balu et al., 2005; Ding et al., 2005; Su et al., 2012; Yusa, 2015).

In this study, the efficiency of transfection using electroporation in Pacific oysters was approximately 0.4%, which is similar to reported rates of 0.1–10% in insects (Fraser, 2012);

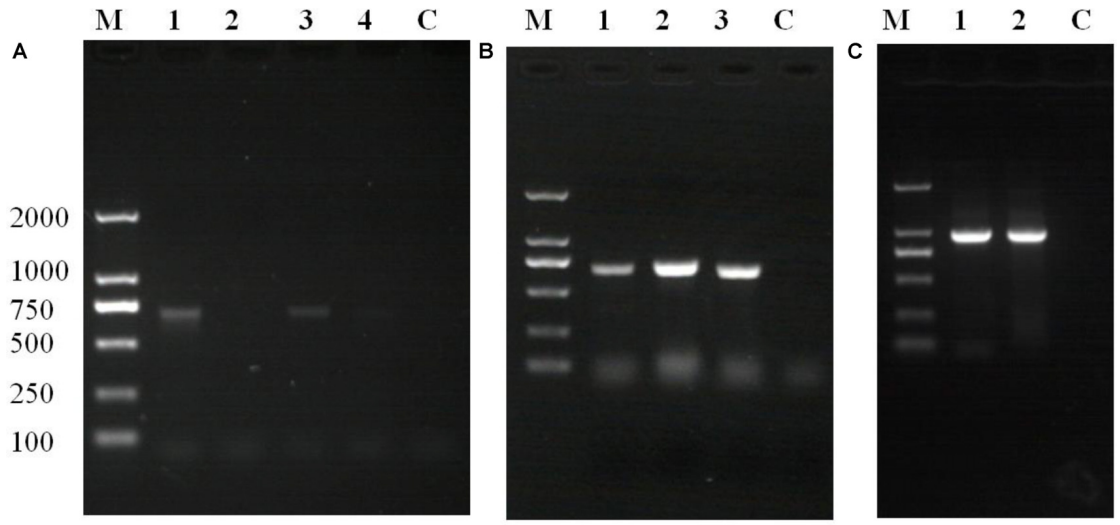

FIGURE 5 | Polymerase chain reaction (PCR) amplification of target genes using the transgenic oyster genome as template. **(A)** GFP gene products amplified from oyster larvae transformed with *piggyBac*: lane M, marker; lane 1, amplification of GFP gene using fluorescent larvae from transgenesis experiment without electroporation; lane 2, amplification of GFP gene using non-fluorescent larvae from transgenesis experiment without electroporation; lane 3, amplification of GFP gene using fluorescent oyster larvae in transgenesis experiment with electroporation; lane 4, amplification of GFP gene using non-fluorescent larvae from transgenesis experiment with electroporation; lane C, control. **(B)** Gene products amplified from oyster larvae transformed with *piggyBac* or *piggyBac-gGH* with electroporation: lane M, marker; lane 1, amplification of GFP gene using fluorescent larvae transfected with *piggyBac*; lane 2, amplification of GFP gene using fluorescent larvae transfected with *piggyBac-gGH*; lane 3, amplification of GH gene using fluorescent larvae transfected with *piggyBac-gGH*; lane C, control. **(C)** Gene products covering partial sequences of GFP and GH genes amplified from oyster larvae transformed with *piggyBac-gGH* with electroporation: lane M, marker; lanes 1 and 2, amplification of segments covering GH and GFP genes using genome walking; lane C, control.

FIGURE 6 | Sequence obtained by genome walking using genomic DNA from transgenic oyster larvae as template. The sequence in red corresponds to partial vector sequence downstream of the GFP gene in *piggyBac-gGH*, and sequence in blue aligns with the scaffold200 in Pacific oyster genome (http://www.oysterdb.com/FrontToolsAction.do?method=blastInit).

electroporation of the mixture of spermatozoa and transposase–transposon vectors resulted in about 10-fold higher efficiency of transgenesis than without electroporation, in agreement with earlier research (Patil and Khoo, 1996; Tsai, 2000). These results indicated that electroporation of the mixture of spermatozoa and vectors increased the efficiency of transgenesis. However, data in this study revealed that survival rate of Pacific oysters was decreased by electroporation prior to gene transfer, maybe because spermatozoa were damaged by the electrical impulse.

In addition, the present work would support a new method, *piggyBac* transposon system, for the research fields of genome and gene function in oyster. Firstly, some genes related with economic importance, such as resistance gene, growth hormone gene, or glycogenesis gene, could be introduced into oyster genome by *piggyBac* transposon system to improve the quality of oyster. Moreover, the genes with unknown function also could be transferred into oyster genome and their physiological functions could be deduced according to the phenotype of the transgenic oysters.

CONCLUSION

This study demonstrated that the *piggyBac* transposon system can be used for transgenesis of Pacific oysters. This work provides a new chance for studying the gene function of mollusks. And

our further research will focus on enhancing the transfection efficiency of Pacific oysters.

AUTHOR CONTRIBUTIONS

XW and BZ conceived and designed the experiments. JC, CW, ZC, LW, and ZL performed the experiments. GL, TG, and YL analyzed the data. WG contributed reagents, materials, analysis tools. XW, JC, and CW wrote the paper. All authors reviewed the manuscript.

FUNDING

This research was supported by the Shandong Provincial Natural Science Foundation, China (Grant Nos. ZR2013CM026, ZR2014CP009, and ZR2017BC058), the Modern Agricultural Industry Technology System of Shandong Province, China (Grant No. SDAIT-14-03), Key R&D program of Shandong Province, China (Grant No. 2018GHY115027), the Key R&D Program of Yantai City, China (Grant No. 2017ZH054), the Innovation Plan for Marine/Fishery Science and Technology of Shandong Province, China (Grant No. 2017YY03), and A Project of Shandong Province Higher Educational Science and Technology Program (Grant No. J17KA129).

SUPPLEMENTARY MATERIAL

The Supplementary Material for this article can be found online at: https://www.frontiersin.org/articles/10.3389/fphys.2018.00811/full#supplementary-material

FIGURE S1 | Sequence alignment between *piggyBac* sequence and GFP segment amplified using the genome of the oyster transfected with *piggyBac* as template (PCR amplification using primers GFP-F and GFP-R).

FIGURE S2 | Sequence alignment between *piggyBac-gGH* sequence and GH segment amplified using the genome of the oyster transfected with *piggyBac-gGH* as template (PCR amplification using primers GH-F and GH-R).

FIGURE S3 | Sequence alignment between *piggyBac-gGH* sequence and GH-GFP segment amplified using the genome of the oyster transfected with *piggyBac-gGH* as template (PCR amplification using primers GH-GFP-F and GH-GFP-R). The sequence at upstream of the first red arrow is GH segment, that between the two red arrows is the partial plasmid sequence, and that at downstream of the second red arrow is GFP segment.

REFERENCES

Balu, B., Shoue, D. A., Fraser, M. J. Jr., and Adams, J. H. (2005). High-efficiency transformation of *Plasmodium falciparum* by the lepidopteran transposable element piggyBac. *Proc. Natl. Acad. Sci. U.S.A.* 102, 16391–16396. doi: 10.1073/pnas.0504679102

Bauser, C. A., Elick, T. A., and Fraser, M. J. (1999). Proteins from nuclear extracts of two lepidopteran cell lines recognize the ends of TTAA-specific transposons *piggyBac* and tagalong. *Insect. Mol. Biol.* 8, 223–230. doi: 10.1046/j.1365-2583.1999.820223.x

Carlson, C. M., Frandsen, J. L., Kirchhof, N., Mcivor, R. S., and Largaespada, D. A. (2005). Somatic integration of an oncogene-harboring Sleeping Beauty transposon models liver tumor development in the mouse. *Proc. Natl. Acad. Sci. U.S.A.* 102, 17059–17064. doi: 10.1073/pnas.0502974102

Cary, L. C., Goebel, M., Corsaro, B. G., Wang, H. G., Rosen, E., and Fraser, M. J. (1989). Transposon mutagenesis of baculoviruses: analysis of *Trichoplusia ni* transposon IFP2 insertions within the FP-locus of *Nuclear polyhedrosis viruses*. *Virology* 172, 156–169. doi: 10.1016/0042-6822(89)90117-7

Cocca, E., De Iorio, S., and Capriglione, T. (2011). Identification of a novel helitron transposon in the genome of Antarctic fish. *Mol. Phylogenet. Evol.* 58, 439–446. doi: 10.1016/j.ympev.2010.12.020

Costa, G. W., Cioffi, M. B., Bertollo, L. A., and Molina, W. F. (2013). Transposable elements in fish chromosomes: a study in the marine cobia species. *Cytogenet. Genome Res.* 141, 126–132. doi: 10.1159/000354309

Depra, M., Ludwig, A., Valente, V. L., and Loreto, E. L. (2012). *Mar*, a MITE family of *hAT* transposons in *Drosophila*. *Mob. DNA* 3:13. doi: 10.1186/1759-8753-3-13

Ding, S., Wu, X., Li, G., Han, M., Zhuang, Y., and Xu, T. (2005). Efficient transposition of the *piggyBac* (PB) transposon in mammalian cells and mice. *Cell* 122, 473–483. doi: 10.1016/j.cell.2005.07.013

Elick, T. A., Lobo, N., and Fraser, M. J. Jr. (1997). Analysis of the cis-acting DNA elements required for *piggyBac* transposable element excision. *Mol. Gen. Genet.* 255, 605–610. doi: 10.1007/s004380050534

Fraser, M. J. Jr. (2012). Insect transgenesis: current applications and future prospects. *Annu. Rev. Entomol.* 57, 267–289. doi: 10.1146/annurev.ento.54.110807.090545

Fraser, M. J., Cary, L., Boonvisudhi, K., and Wang, H. G. (1995). Assay for movement of Lepidopteran transposon IFP2 in insect cells using a baculovirus genome as a target DNA. *Virology* 211, 397–407. doi: 10.1006/viro.1995.1422

Fraser, M. J., Ciszczon, T., Elick, T., and Bauser, C. (1996). Precise excision of TTAA-specific lepidopteran transposons *piggyBac* (IFP2) and *tagalong* (TFP3) from the baculovirus genome in cell lines from two species of Lepidoptera. *Insect. Mol. Biol.* 5, 141–151. doi: 10.1111/j.1365-2583.1996.tb00048.x

Guerra, R., Carballada, R., and Esponda, P. (2005). Transfection of spermatozoa in bivalve molluscs using naked DNA. *Cell Biol. Int.* 29, 159–164. doi: 10.1016/j.cellbi.2004.11.018

Guerra, R., and Esponda, P. (2006). Transfection of eggs in the bivalve mollusc *Chamelea gallina* (Bivalvia, Veneridae). *J. Submicrosc. Cytol. Pathol.* 38, 5–10.

Ivics, Z., and Izsvak, Z. (2006). Transposons for gene therapy! *Curr. Gene Ther.* 6, 593–607.

Jurka, J. (2000). Repbase update: a database and an electronic journal of repetitive elements. *Trends Genet.* 16, 418–420. doi: 10.1016/S0168-9525(00)02093-X

Kaji, K., Norrby, K., Paca, A., Mileikovsky, M., Mohseni, P., and Woltjen, K. (2009). Virus-free induction of pluripotency and subsequent excision of reprogramming factors. *Nature* 458, 771–775. doi: 10.1038/nature07864

Lam, W. L., Seo, P., Robison, K., Virk, S., and Gilbert, W. (1996). Discovery of amphibian Tc1-like transposon families. *J. Mol. Biol.* 257, 359–366. doi: 10.1006/jmbi.1996.0168

Leaver, M. J. (2001). A family of Tc1-like transposons from the genomes of fishes and frogs: evidence for horizontal transmission. *Gene* 271, 203–214. doi: 10.1016/S0378-1119(01)00530-3

Leoni, C., Gallerani, R., and Ceci, L. R. (2008). A genome walking strategy for the identification of eukaryotic nucleotide sequences adjacent to known regions. *Biotechniques* 44, 229, 232–235. doi: 10.2144/000112680

Leoni, C., Volpicella, M., De Leo, F., Gallerani, R., and Ceci, L. R. (2011). Genome walking in eukaryotes. *FEBS J.* 278, 3953–3977. doi: 10.1111/j.1742-4658.2011.08307.x

Li, X., Harrell, R. A., Handler, A. M., Beam, T., and Hennessy, K. (2005). *piggyBac* internal sequences are necessary for efficient transformation of target genomes. *Insect. Mol. Biol.* 14, 17–30. doi: 10.1111/j.1365-2583.2004.00525.x

Li, X., Lobo, N., Bauser, C. A., and Fraser, M. J. Jr. (2001). The minimum internal and external sequence requirements for transposition of the eukaryotic transformation vector piggyBac. *Mol. Genet. Genomics* 266, 190–198. doi: 10.1007/s004380100525

O'Brochta, D. A., Sethuraman, N., Wilson, R., Hice, R. H., Pinkerton, A. C., Levesque, C. S., et al. (2003). Gene vector and transposable element behavior in mosquitoes. *J. Exp. Biol.* 206, 3823–3834. doi: 10.1242/jeb.00638

Parrington, J., Coward, K., and Gadea, J. (2011). Sperm and testis mediated DNA transfer as a means of gene therapy. *Syst. Biol. Reprod. Med.* 57, 35–42. doi: 10.3109/19396368.2010.514022

Patil, J. G., and Khoo, H. W. (1996). Nuclear internalization of foreign DNA by zebrafish spermatozoa and its enhancement by electroporation. *J. Exp. Zool.* 274, 121–129. doi: 10.1002/(SICI)1097-010X(19960201)274:2<121::AID-JEZ5>3.0.CO;2-R

Perry, K. J., and Henry, J. Q. (2015). CRISPR/Cas9-mediated genome modification in the mollusc, *Crepidula fornicata*. *Genesis* 53, 237–244. doi: 10.1002/dvg.22843

Rishi, A. S., Nelson, N. D., and Goyal, A. (2004). Genome walking of large fragments: an improved method. *J. Biotechnol.* 111, 9–15. doi: 10.1016/j.jbiotec.2004.03.008

Sarkar, A., Sim, C., Hong, Y. S., Hogan, J. R., Fraser, M. J., Robertson, H. M., et al. (2003). Molecular evolutionary analysis of the widespread *piggyBac* transposon family and related "domesticated" sequences. *Mol. Genet. Genomics* 270, 173–180. doi: 10.1007/s00438-003-0909-0

Shapter, F. M., and Waters, D. L. (2014). Genome walking. *Methods Mol. Biol.* 1099, 133–146. doi: 10.1007/978-1-62703-715-0_12

Sormacheva, I., Smyshlyaev, G., Mayorov, V., Blinov, A., Novikov, A., and Novikova, O. (2012). Vertical evolution and horizontal transfer of CR1 non-LTR retrotransposons and Tc1/mariner DNA transposons in Lepidoptera species. *Mol. Biol. Evol.* 29, 3685–3702. doi: 10.1093/molbev/mss181

Su, H., Liu, X., Yan, W., Shi, T., Zhao, X., Blake, D. P., et al. (2012). *piggyBac* transposon-mediated transgenesis in the apicomplexan parasite *Eimeria tenella*. *PLoS One* 7:e40075. doi: 10.1371/journal.pone.0040075

Tsai, H. J. (2000). Electroporated sperm mediation of a gene transfer system for finfish and shellfish. *Mol. Reprod. Dev.* 56, 281–284. doi: 10.1002/(SICI)1098-2795(200006)56:2+<281::AID-MRD15>3.0.CO;2-B

Tsai, H. J., Lai, C. H., and Yang, H. S. (1997). Sperm as a carrier to introduce an exogenous DNA fragment into the oocyte of Japanese abalone (*Haliotis divorsicolor suportexta*). *Transgenic Res.* 6, 85–95. doi: 10.1023/A:1018413318223

Wang, W., Lin, C., Lu, D., Ning, Z., Cox, T., Melvin, D., et al. (2008). Chromosomal transposition of *piggyBac* in mouse embryonic stem cells. *Proc. Natl. Acad. Sci. U.S.A.* 105, 9290–9295. doi: 10.1073/pnas.0801017105

Woltjen, K., Michael, I. P., Mohseni, P., Desai, R., Mileikovsky, M., Hamalainen, R., et al. (2009). *piggyBac* transposition reprograms fibroblasts to induced pluripotent stem cells. *Nature* 458, 766–770. doi: 10.1038/nature07863

Wu, M., Sun, Z., Luo, G., Hu, C., Zhang, W., and Han, Z. (2011). Cloning and characterization of piggyBac-like elements in lepidopteran insects. *Genetica* 139, 149–154. doi: 10.1007/s10709-010-9542-0

Wu, X., and Burgess, S. M. (2004). Integration target site selection for retroviruses and transposable elements. *Cell Mol. Life Sci.* 61, 2588–2596. doi: 10.1007/s00018-004-4206-9

Yusa, K. (2015). *piggyBac* Transposon. *Microbiol. Spectr.* 3, MDNA3–MDNA0028. doi: 10.1128/microbiolspec.MDNA3-0028-2014

Yusa, K., Rad, R., Takeda, J., and Bradley, A. (2009). Generation of transgene-free induced pluripotent mouse stem cells by the *piggyBac* transposon. *Nat. Methods* 6, 363–369. doi: 10.1038/nmeth.1323

Zhang, G., Fang, X., Guo, X., Li, L., Luo, R., Xu, F., et al. (2012). The oyster genome reveals stress adaptation and complexity of shell formation. *Nature* 490, 49–54. doi: 10.1038/nature11413

Conflict of Interest Statement: The authors declare that the research was conducted in the absence of any commercial or financial relationships that could be construed as a potential conflict of interest.

frontiers in Physiology

ORIGINAL RESEARCH
published: 23 October 2018
doi: 10.3389/fphys.2018.01476

Two Novel Short Peptidoglycan Recognition Proteins (PGRPs) From the Deep Sea Vesicomyidae Clam *Archivesica packardana*: Identification, Recombinant Expression and Bioactivity

*Xue Kong[1,2], Helu Liu[1], Yanan Li[1,2] and Haibin Zhang[1]**

[1] Institute of Deep-Sea Science and Engineering, Chinese Academy of Sciences, Sanya, China, [2] College of Earth and Planetary Sciences, University of Chinese Academy of Sciences, Beijing, China

Vesicomyidae clams are common species living in cold seeps, which incorporates symbiotic bacteria into their body maintaining endosymbiosis relationship. As members of pattern recognition receptor (PRR) family, peptidoglycan recognition proteins (PGRPs) recognize pathogen associated molecular patterns and play an important role in innate immunity. In present study, two short PGRPs (ApPGRP-1 and -2) were first identified from Vesicomyidae clam *Archivesica packardana*. Sequences analysis showed that they have both conserved Zn^{2+} binding sites (H-H-C) and amidase catalytic sites (H-Y-H-T-C), and phylogenetic tree indicated that they clustered with short PGRPs of other molluscs. PGN assay showed that ApPGRPs could bind Lys-type PGN from *Staphylococcus aureus* and Dap-type PGN from *Bacillus subtilis*, and revealed amidase activity with selective zinc ion dependence. rApPGRP-1 and -2 (recombinant ApPGRP-1 and -2) could bind six bacteria with a broad spectrum and had both zinc-dependent and -independent bactericidal activity. ApPGRPs had the complete functions of effectors and partial functions of receptors from PGRPs. Further analyses showed that ApPGRPs from *A. packardana* might be involved in the endosymbiosis relationship between the host clam and endosymbiotic bacteria as a regulator. The results of these experiments suggested that ApPGRPs were involved in cold seep clams' immune response. This study provides basic information for further research on the immune mechanisms of deep sea organisms.

Keywords: innate immunity, *Archivesica packardana*, PGRP, antibacterial activity, endosymbiosis

OPEN ACCESS

Edited by:
Xiaotong Wang,
Ludong University, China

Reviewed by:
Xian De Liu,
Jimei University, China
Camino Gestal,
Consejo Superior de Investigaciones Científicas (CSIC), Spain

****Correspondence:***
Haibin Zhang
hzhang@idsse.ac.cn

Specialty section:
This article was submitted to Aquatic Physiology, a section of the journal Frontiers in Physiology

Received: *04 June 2018*
Accepted: *28 September 2018*
Published: *23 October 2018*

Citation:
Kong X, Liu H, Li Y and Zhang H (2018) Two Novel Short Peptidoglycan Recognition Proteins (PGRPs) From the Deep Sea Vesicomyidae Clam Archivesica packardana: Identification, Recombinant Expression and Bioactivity. Front. Physiol. 9:1476. doi: 10.3389/fphys.2018.01476

INTRODUCTION

The immune system contains innate immunity and adaptive immunity (Janeway, 1989). Innate immune system is the frontline of defense and almost the only defense mechanism for invertebrates to protect the host from invasion by microbes in the surrounding environment (Janeway, 1989). Innate immunity can be triggered by a set of specific receptors termed PRRs. PRRs could recognize

Abbreviations: PAMPs, pathogen associated molecular patterns; PRRs, pattern-recognition receptors; PGRPs, Peptidoglycan recognition proteins; PO, Phenoloxidase; IMD, Immune Deficiency; AMP, Antimicrobial peptide.

the conserved, invariant components on the cell surface of microbes named PAMPs (Yang et al., 2013). PRRs include Toll-like receptors, PGRP, scavenger receptor (SRCR), thioester-containing proteins (TEP), lipopolysaccharide and beta-1,3-glucan binding protein (LGBP), and lectins (Janeway and Medzhitov, 2002; Hoffmann, 2003).

As a subset of PRRs, PGRP recognizes peptidoglycan (PGN) which is a crucial cell wall component of microorganisms (Steiner, 2002). In PGN, *N*-acetylglucosamine (GlcNAc) and *N*-acetylmuramic acid (MurNAc) are linked by beta (1-4)-glycoside bond. MurNAc can be linked to short peptides that have three to five commutative L and D amino acids (Chen and Lv, 2014). Therefore, PGN could be divided into two types: L-lysine-type (Lys-type) and meso-diaminopimelic acid-type (Dap-type) according to the third residue of the short peptides (Yao et al., 2012). PGRPs were divided into three types: small extracellular PGRPs (PGRP-S, 20–25 KDa), long PGRPs (PGRP-L, >90 KDa), and intermediate PGRPs (PGRP-I, 40–45 KDa) (Ni et al., 2007).

Peptidoglycan recognition proteins are identified in multiple species, from insects to mammals (Dziarski, 2003; Dziarski and Gupta, 2006). Generally, their functions include three classes. Firstly, as receptors, PGRPs recognize microbes and then activate Toll or IMD pathways for AMP synthesis to remove invasive bacteria (Tzou, 2002; Dziarski, 2003). Secondly, as regulators, PGRPs act as negative factors to diminish or shut down IMD pathways to maintain the homeostasis of symbiotic bacteria (Guo et al., 2014). PGRPs can also enhance phagocytosis (Garver et al., 2006; Royet and Dziarski, 2007). Finally, as effectors, PGRPs can kill bacteria with amidase activity, which disrupt the lactylamide bond between muramic acid and L-alanine (Gelius et al., 2003; Kim et al., 2003; Chen et al., 2014).

Compared with those in insects and mammals, studies on marine organisms PGRPs were also carried out. In fish, researchers have shown that PGRPs from *Pseudosciaena crocea*, *Sciaenops ocellatus*, *Branchiostoma japonicum*, *Ctenopharyngodon idella*, *Ictalurus punctatus*, *Cynoglossus semilaevis*, *Oreochromis niloticus,* and *Scophthalmus maximus L.* were all constitutively expressed or up-regulated in response to pathogen or PAMP challenge (Yong et al., 2010; Li et al., 2012, 2014a,b; Yao et al., 2012; Sun et al., 2014; Sun and Sun, 2015; Gan et al., 2016; Zhang et al., 2016). In Echinodermata, PGRP-S2a from European sea star *Asterias rubens* breaks down peptidoglycan and stimulates phagocytosis of *Micrococcus luteus* through sea star phagocytes (Coteur et al., 2007). In molluscs, studies of PGRPs from *Argopecten irradians* (Ni et al., 2007), *Crassostrea gigas* (Itoh and Takahashi, 2009), *Solen grandis* (Wei et al., 2012), *Hyriopsis cumingi* (Yang et al., 2013), and *Haliotis discus discus* (Premachandra et al., 2014) have been conducted. For an example, in *C. gigas* PGRP, mRNA level was up-regulated after *Vibrio tubiashii* and *Marinococcus halophilus* challenge (Itoh and Takahashi, 2009). These data suggested that PGRPs from marine organisms play a crucial role in the innate immunity defense mechanisms against infections.

The *Bathymodiolus* mussel and Vesicomyidae clam are common species in hydrothermal vents and cold seeps (Barros et al., 2015). They have methane-oxidizing (MOX) bacteria or sulfur-oxidizing (SOX) bacteria in their gills as symbionts (Martins et al., 2014). Expression level of *BaPGRP* was up-regulated at 12 h but down-regulated at 24 h in the hydrothermal vents mussel *Bathymodiolus azoricus* that had been challenged with live *V. alginolyticus* (Martins et al., 2014). PGRPs from the cold seep mussel *B. platifrons* had different binding modes to peptidoglycan (PGN) from Gram-negative and Gram-positive microorganisms (Yue et al., 2015). These results suggested that pattern recognition receptors and related molecules are involved in the immune response of deep sea vent/seep organisms, but little information about Vesicomyidae clam is available.

The Vesicomyidae clam *A. packardana*, previously named Ca*lyptogena packardana*, which has been collected from cold seeps (Johnson et al., 2016). In present study, we study the roles of PGRP in immune system of this species. The primary objectives of the present research are: (1) identification and sequence analysis of ApPGRP-1 and -2 molecules; (2) combination and degradation of PGN by rApPGRP-1 and -2; (3) combination and inhibition of microbes by rApPGRP-1 and -2. The roles of PGRPs in the endosymbiosis relationship between the clam and endosymbiotic bacteria have also been discussed.

MATERIALS AND METHODS

Sample Collection

Clams were collected from the Malibu Mound (33.902, -118.735) at a depth of 520 m during a MBARI expedition in 2014. Once clams were brought to the deck, the adductor muscle and gill were immediately removed and stored in RNAlater (Ambion, Austin, TX, United States). Total RNA was extracted and quality was assessed using gel electrophoresis and a spectrophotometer (Nanodrop2000, Thermo Scientific^{TM} NanoDrop^{TM}, United States). Then, the RNA samples were sent out for sequencing at SeqMatic LLC (Fremont, CA, United States) on a HiSeq^{TM} 2000 platform. Over 6 Gbp clean data were obtained for each tissue library.

Gene Identification and Expression Vector Construction

Homologs of the peptidoglycan recognition protein (PGRP) gene were found through searching the *A. packardana* transcriptome (data not yet published) using TBLASTN[1] with previously published PGRP genes as a query. Two new PGRPs (ApPGRP-1 and -2) were identified.

cDNA was synthesized and amplified using a PrimeScript^{TM} II 1st Strand cDNA Synthesis Kit (Takara, Dalian, China) according to the manufacturer's instructions. The open reading frame (ORF) of ApPGRP-1, -2 were amplified by PCR with primer pairs P1-1, P1-2 and P2-1, P2-2 (**Table 1**), and then the PCR products were inserted into plasmid expression vector pCOLDII(Takara, Dalian, China). The recombinant plasmids (pCOLDII-ApPGRP-1 and -2) were transformed into *Escherichia coli* Chaperone Competent Cells pG-KJE8/BL21 (Takara, Dalian, China). Colonies containing the appropriate vectors were verified by sequencing.

[1]http://www.ncbi.nlm.nih.gov/BLAST/

TABLE 1 | Primers used in the present study.

Primer	Sequence (5′–3′)	Sequence information
P1-1 (sense)	ATGGAGCCACTTGTACA	ORF primer
P1-2 (antisense)	CTACCTTGTCATCTGATAC	ORF primer
P1-3 (sense)	CGGGATCCATGGAGCCACTT GTACA	Recombinant primer
P1-4 (antisense)	AACTGCAGCCTTGTCATCT GATAC	Recombinant primer
P2-1 (sense)	ATGCACGTGTATTCAATGT	ORF primer
P2-2 (antisense)	TTACGATGTTAGCTTATTCC CATCC	ORF primer
P2-3 (sense)	CGGGATCCAGGCACGTGGG CAGTTGTTCTGGCA	Recombinant primer (Signal peptide deleted)
P2-4 (antisense)	AACTGCAGCGATGTTAGCTT ATTCCCATCC	Recombinant primer

Restriction enzyme target sites are underlined.

Sequence Analyses

Sequence comparison was conducted in the BLAST program[1]. We calculated theoretical isoelectric point and molecular weight in the ProtParam program[2]. SignalIP4.1[3] was used to predict the signal peptide, and the SMART program (Letunic and Bork, 2018)[4] was used to predict functional domains. Multiple protein sequences were aligned by using Clustal W program (Larkin et al., 2007) (version1.83[5]). A neighbor-joining (NJ) tree was established based on the deduced amino acid sequences with 1,000 bootstrap replicates by using MEGA v5.0 software (Tamura et al., 2011)[6]. The predicted tertiary structures were constructed in the SWISS-MODEL program[7] and checked in Deepview/Swiss-Pdb Viewer 4.0[8] (Guex and Peitsch, 1997).

Expression, Purification and Western Blotting of Recombinant Proteins

Verified transformants were cultured in LB medium (yeast extract, 5 g, tryptone, 10 g, sodium chloride, 10 g of 1 L) with 100 μg/ml ampicillin, 20 μg/ml chloramphenicol, 0.5 mg/ml L-arabinose. The culture temperature was set at 37°C with shaking at 200 rpm. Two hours later, tetracycline was added into the LB medium to a final concentration of 2 ng/ml. L-arabinose and tetracycline are inducers of chaperone proteins dnaK-dnaJ-grpE and groES-groEL, respectively. Chloramphenicol is the resistance marker of plasmid pG-KJE8. When optical density at 600 nm (OD_{600}) reached 0.5, the medium was cooled to 15°C and incubated for more than 30 min. After that, Isopropyl-h-d-thiogalactoside (IPTG) was added and the final concentration was 0.1 mM. The medium was cultured for another 24 h at 15°C. Then, bacteria were precipitated at 8,000 g for 5 min at 4°C. The recombinant proteins pCOLD II-ApPGRP-1 and -2 were present in the supernatant after sonication. Proteins were purified with Ni-NTA-Sefinose Column (Sangon Biotech, Shanghai, China), and eluted with 300 mM imidazole under non-denaturing conditions. The obtained proteins were dialysed, concentrated, and then stored at −80°C before use. The protein samples (before induction, after induction, the supernatant and precipitate after sonication) were separated in 10% SDS-polyacrylamide gel electrophoresis (SDS–PAGE). Western blotting procedures were set as follows: proteins were transferred from gels to PVDF membranes (Immobilon-membrane, Millipore, MA, United States) by Trans-Blot SD Semi-Dry Electrophoretic Transfer Cell (DYCP-40C, Beijingliuyi, Beijing, China). After that, the primary anti-6 × His antibody (diluted 1: 5000 with 5% skim milk; ab18184, abcam, Cambridge, United Kingdom) was incubated overnight with the membranes. The membrane was then washed with TBST (50 mM Tris–HCl, 50 mM NaCl, 0.05% Tween20, pH 7.2) three times. After that, secondary antibody (diluted 1: 10000; ab6789, abcam, Cambridge, United Kingdom) was incubated with the PVDF membranes for 2 h, followed by three washes with TBST. The membranes were incubated for 5 min with Pierce ECL Western Blotting Substrate (Thermo Scientific, MA, United States), and the Chemiluminescence imaging system (ChemStudio, Analytikjena, Jena, Germany) was used to detect chemical signals.

Binding Analysis of rApPGRP-1, -2 to PGN

The assay was done as previous study (Yang et al., 2013) with slight modifications. We first incubated 40 μg of rApPGRP-1 or -2 proteins in 200 μl TBS buffer (50 mM Tris–HCl, 50 mM NaCl, pH 7.2) with L- PGN from *Staphylococcus. aureus* (Catalog No. 77140, Sigma-Aldrich, MA, United States; 100 μg, 1 mg/ml) and D-PGN from *Bacillus subtilis* (Sigma-Aldrich, MA, United States; 100 μg, 1 mg/ml). Then, bound and unbound proteins were obtained by centrifugation at 13,000 rpm for 15 min after incubation at 4°C for 3 h. TBS was used to wash the pellets (bound fraction) three times. After that, 2 × SDS–PAGE loading buffer was used to separate bound proteins from PGN by boiling at 95°C for 5 min. Samples were analyzed in 10% SDS–PAGE. Western blotting with anti-6 × His antibody was used to detect the target proteins as above.

Binding Analysis of rApPGRP-1, -2 to Microbial Cells

The assay was done as described by Feng et al. (2012) with slight modifications. *S. aureus*, *M. luteus*, *B. subtilis*, *E. coli*, *Pichia pastoris*, and *Saccharomyces cerevisiae* colonies were grown in culture medium (LB medium for Gram-positive bacteria, Gram-negative bacteria; YPD medium for fungi). LB medium was the same as above, and YPD medium (1 L) includes: 10 g yeast extract, 20 g peptone, 20 g dextrose. When the OD_{600} was close to 0.8 (ca. 1.6×10^8 cells/ml), 4 ml of each medium was centrifuged at 5,000 *g* and the pellets were washed twice with TBS buffer. Microbial cells were re-suspended in 50 μl of TBS buffer and then mixed with 40 μg of rApPGRP-1 or -2 dissolved in 200 μl of TBS buffer. The mixture was incubated for 3 h

[2]http://www.expasy.ch/tools/protparam.html
[3]http://www.cbs.dtu.dk/services/SignalP/
[4]http://smart.embl-heidelberg.de/
[5]http://www.clustal.org/clustal2/
[6]http://www.megasoftware.net/mega4/
[7]http://swissmodel.expasy.org/
[8]https://spdbv.vital-it.ch/

at 4°C, and centrifuged at 12,000 *g* at 4°C for 15 min. The cell pellets were washed three times with TBS buffer and then suspended in 50 μl of 2 × SDS sample buffer. The samples were heated at 95°C for 5 min to get the bound protein. The bound proteins from six kinds of microorganisms were checked in 10% SDS–PAGE and detected using western blotting as above.

Analysis of Amidase Activities

Amidase activity of PGRP could cleave the lactylamide bond between muramic acid and L-alanine, and further cause the dissolution of the PGN (Foster, 2004). The assay was done as described by Mellroth et al. (2003), Yang et al. (2013) with slight modifications. 40 μg L, D-PGN (1 mg/ml) was incubated with 50 μg of rApPGRP-1 or -2 protein in TBS-$ZnCl_2$ solution (50 mM Tris–HCl, 50 mM NaCl, 100 μM $ZnCl_2$, pH 7.2). 40 μg PGN (1 mg/ml) was mixed with TBS buffer which was set as a control. OD_{540} was measured per 30 min during a 300 min period by using Varioskan LUX Multimode Microplate Reader (Thermo Fisher Scientific, MA, United States).

Analysis of Antimicrobial Activities

The assay was done as described by Chen et al. (2014) with slight modification. *S. aureus*, *M. luteus*, *B. subtilis*, *E. coli*, *P. pastoris*, and *S. cerevisiae* were cultured to an OD_{600} of 0.6 in LB medium at 37°C or YPD medium at 28°C (Fungi). 200 μl aliquots of the cultures were pelleted by centrifugation at 5,000 *g* for 5 min at 4°C and washed with TBS buffer twice. The pellets were re-suspended in 200 μl TBS buffer. After a 1:50 dilution, 10 μl of the suspensions was mixed with 25 μl 200 μg/ml rApPGRP-1, or 200 μg/ml rApPGRP-2, or TBS (as control), with 10 or 100 μM $ZnCl_2$ existed. The mixtures were shaken on a Tube Tumbler for 6 h at 26°C, and then 1 ml LB or YPD medium was added separately. The cultures were shaken at 37°C or 28°C overnight before absorbance measurement at 600 nm.

Statistical Analyses

Statistical analysis was performed in SPSS22.0 (IBM Company, NY, United States). Duncan test of one-way ANOVA was used among mean values from different groups. The *P*-value is 0.05.

RESULTS

Sequence Characteristics of ApPGRP-1 and -2

The open reading frame of ApPGRP-1 and ApPGRP-2 obtained using local blast are 567- and 675-bp, respectively (Genbank Nos. MH286797, MH306208, separately). ApPGRP-1 has 188 amino acids. Its theoretical isoelectric point and predicted molecular weight are 5.58, 21.38 kDa, respectively. ApPGRP-2 has 244 amino acids. Its theoretical isoelectric point and predicted molecular weight are 6.91, 24.94 kDa, respectively. ApPGRP-2 has a putative signal peptide in the N-terminus (**Figure 1**), but ApPGRP-2 doesn't have. The Zn^{2+}-dependent amidase domains are located in ApPGRP-1 and ApPGRP-2 at positions 10(V)–158(G) and 28(I)–177(G), respectively.

Alignment and Phylogenetic Analysis of ApPGRP-1 and ApPGRP-2

Online BLAST analysis showed that amino acid sequences of ApPGRP-1 and -2 are highly homologous with PGRPs from other species. ApPGRP-1 is homologous with PGRPs from *H. cumingii* (AHK22786.1), *H. discus discus* (AHB30456.1), and the similarities are 58% and 53%, respectively. In addition, it also has a high homology with an *Octopus bimaculoides* protein (XP_014778613.1) with 56% identity. ApPGRP-2 has high similarity with PGRPs from *C. gigas* (XP_011422763.1) and *Pinctada fucata* (JAS03318.1), and the similarities are 56% and 52%, respectively. ApPGRP-1 and -2 have 44% similarity with each other.

Alignment analysis of these two ApPGRPs and other animals' PGRPs showed that the C-portion of the PGRPs is highly

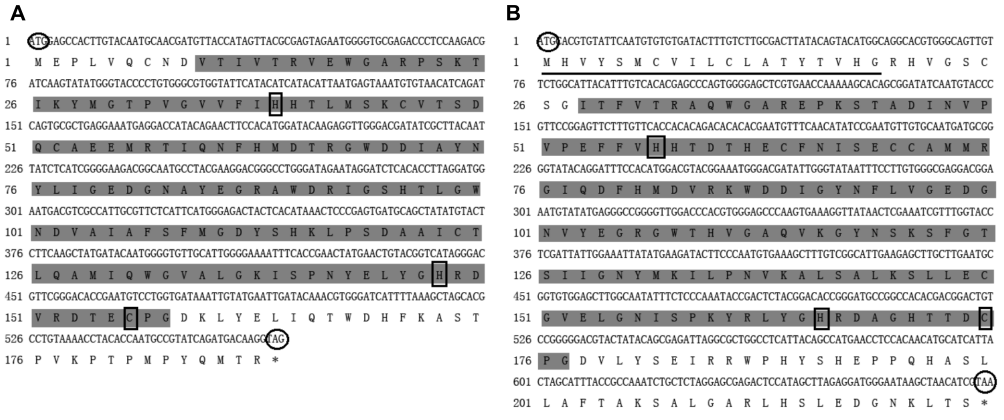

FIGURE 1 | Nucleotide and deduced amino acid sequences of ApPGRP-1 **(A)** and ApPGRP-2 **(B)**. The predicted signal peptide is underlined, and the predicted start and termination codons are circled. The amidase/PGRP domain predicted in SMART program is highlighted in gray, and the black boxes indicate Zn^{2+} binding sites.

similar and conserved, whereas the N-terminal region is relatively diversified (**Figure 2**). In ApPGRP-1, the Zn^{2+} binding sites (H39, H148, and C156) and amidase catalytic sites (H39, Y74, H148, T154, and C156) are both very conserved (**Figure 2**). The Zn^{2+} binding sites (H57, H166, and C175) and amidase catalytic sites (H57, Y92, H166, T173, and C175) are also conserved in ApPGRP-2 (**Figure 2**).

Phylogenetic analysis of ApPGRP-1, -2 and other species' PGRPs showed that ApPGRP-1 clustered with short PGRPs from abalone *H. discus discus* and freshwater pearl mussel *H. cumingii*, and ApPGRP-2 clustered with three short PGRPs from oyster *C. gigas*, and then these two branches were grouped together (**Figure 3**).

Potential Tertiary Structures of ApPGRP-1 and -2

The SWISS-MODEL prediction algorithm was used to predict the tertiary structures of ApPGRP-1, ApPGRP-2 and PGRP-SC2 from *Drosophila melanogaster* (CAD89187). The tertiary and secondary protein structure of ApPGRP-1 and -2 are well conserved by comparing with model *Drosophila* PGRP-SC2 (**Figure 4**). ApPGRP-1 was predicted to have four α-helices and seven β-strands (refer to the whole protein sequences). ApPGRP-2 was predicted to have five α-helices and eight β-strands (refer to the whole protein sequences). PGRP from *D. melanogaster* has a typical PGRP structure including five β-strands and five α-helices. The Zn^{2+} binding sites and amidase catalytic sites in ApPGRP-1 and-2 are both well conserved (**Figure 2**), while H50-H159-C167 and H50-Y85-H159-T165-C167 are present in PGRP-SC2 from *D. melanogaster* (**Figure 4**).

Bioassay of Recombinant ApPGRP-1 and -2 Proteins

A clear band with a molecular mass of ∼24 kDa (containing partial vector sequences; **Figure 5A-A5**) was detected (→ label), which match predicted protein size of rApPGRP-1 (**Figures 5A-A1–A4**). The western blotting results in **Figure 5A-A6**. Lane B5 in **Figure 5B** showed a unique ∼28 kDa protein representing rApPGRP-2.

Binding of Recombinant Protein ApPGRP-1 and -2 to L, D-PGN

Binding of rApPGRP-1 and -2 to PGN (L-PGN and D-PGN) was analyzed using western blotting. For the TBS group in **Figure 6**, most of the rApPGRP-1 and -2 protein was present in the supernatant. For the L-PGN group, rApPGRP-1 bound it, although there was also an obvious band corresponding to the unbound fraction. Binding of rApPGRP-2 to L-PGN was relatively strong as there was no clear band in the unbound part. For the D-PGN group, a similar pattern was existed

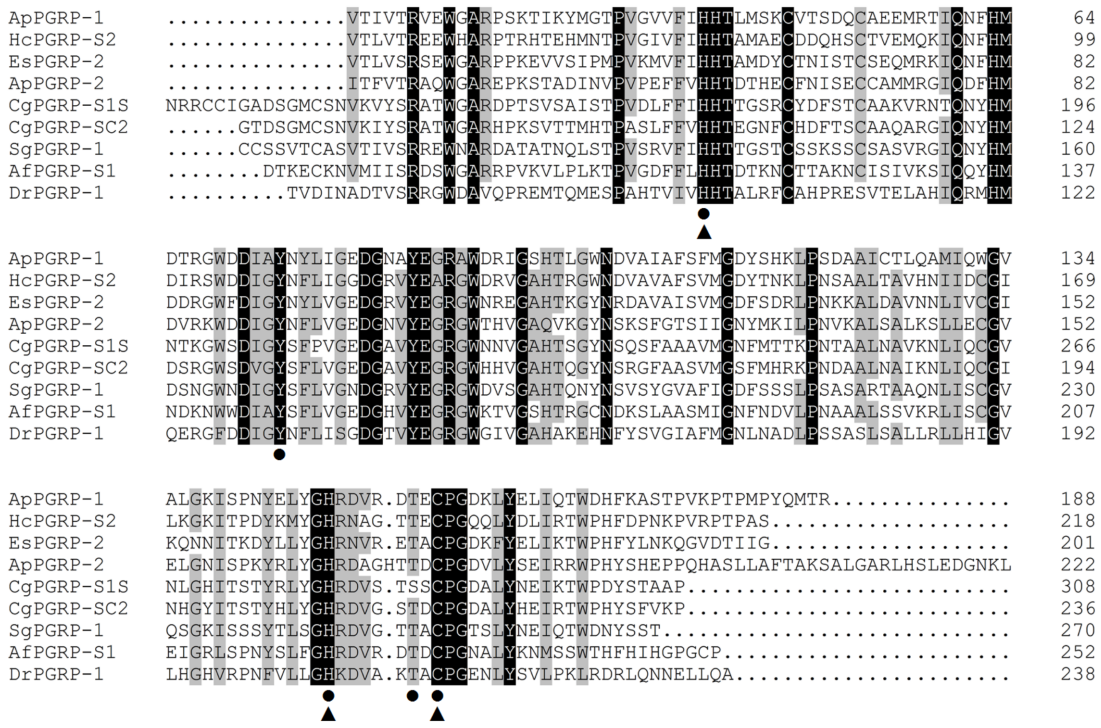

FIGURE 2 | Alignments of amino acid sequences of ApPGRP-1 and -2 with other species. Zn^{2+} binding sites and amidase catalytic sites are marked with triangles ▲ and cycles ●, respectively. Amino acid residues that are conserved in at least 75% sequences are shaded in gray, and 100% identity amino acids are shaded in black. Species include CgPGRP-S1S (*Crassostrea gigas*, BAG31896), AfPGRP-S1 (*Azumapecten farreri*, AAY53765), SgPGRP-1 (*Solen grandis*, JN642118), EsPGRP-2 (*Euprymna scolopes*, AAY27974) and DrPGRP-1 (*Danio rerio*, NP_001037786), HcPGRP-S2 (*Hyriopsis cumingii*, AHK22786.1), and CgPGRP-SC2 (*C. gigas*, EKC26200.1).

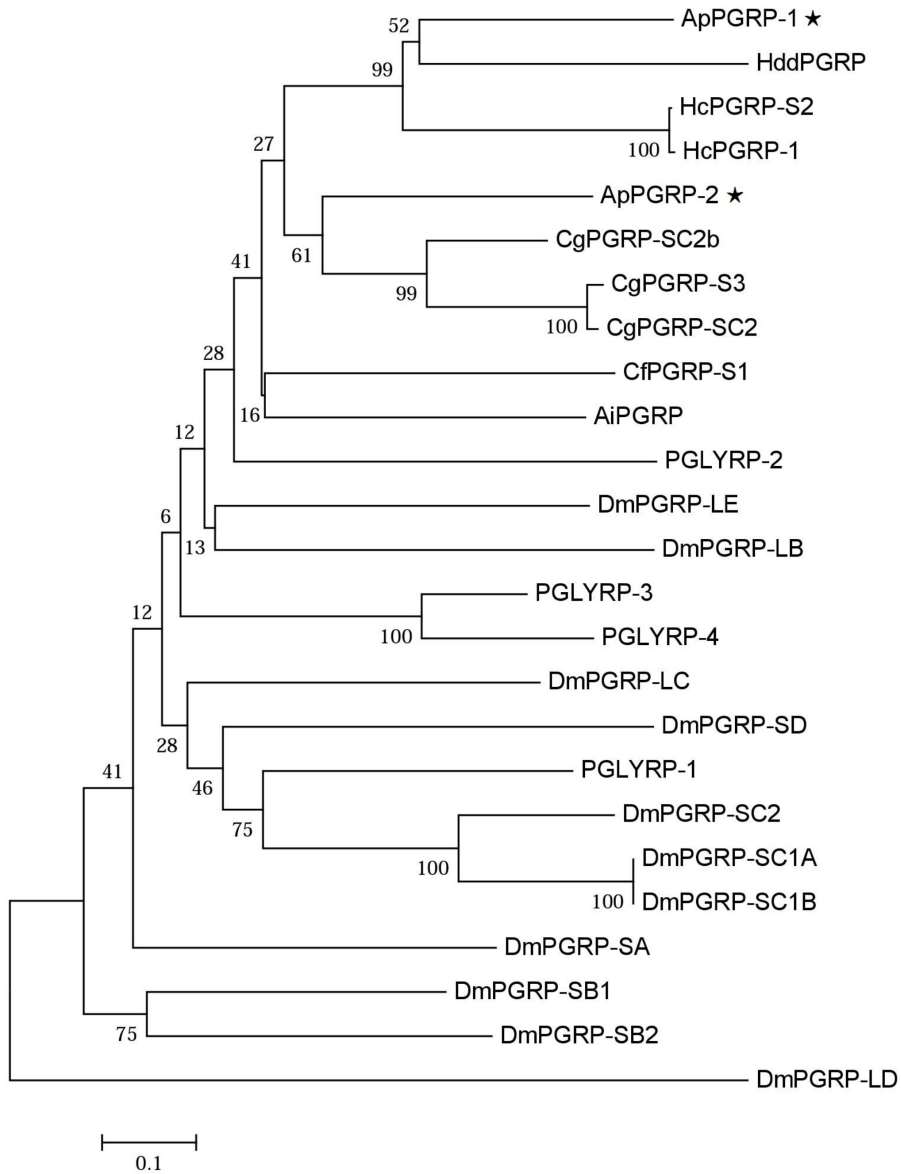

FIGURE 3 | Phylogenetic tree of ApPGRP-1 and ApPGRP-2 with other PGRPs. CgPGRP-SC2 (XP_011422762.1), CgPGRP-SC2b (XP_011422763.1), and CgPGRP-S3 (BAG31899.1) from *C. gigas*, CfPGRP-S1 (AAY53765) from *Chlamys farreri*, AiPGRP (AAR92030) from *Argopecten irradians*, HcPGRP-1 (AGU68334.1) and HcPGRP-S2 (AHK22786.1) from *H. cumingi*, HddPGRP (AHB30456.1) from *Haliotis discus discus*, DmPGRP-LE (AAF48519), -SA (AAF48056), -LF (NP_648299), -LBa (AAF54643), -LCa (NP_729468), -LDa (NP_001027113), -SC1a (CAD89163), -SC1b (CAD89164), -SD (CAD89198), -SC2 (CAD89178), -SB1 (CAD89129), -SB2 (CAD89140), and -LAa (AAK00295) from *Drosophila melanogaster*, PGLYRP-1 (O75594), PGLYRP-2 (Q96PD5), PGLYRP-3 (Q96LB9), and PGLYRP-4 (Q96LB8) from *Homo sapiens*. The tree was established using the neighbor-joining (NJ) method using the Mega7.0 program based on coding sequences. Bootstrap values of 1,000 replicates (%) are indicated for the branches. ApPGRPs are labeled with ⋆.

(**Figure 6**). Both rApPGRP-1 and -2 could bind L- PGN or D-PGN.

Binding of Recombinant ApPGRP-1 and -2 Proteins to Microbial Cells

Microbe binding assay was done to analyze whether rApPGRP-1 and -2 bound Gram-negative bacteria, Gram-positive bacteria and fungi. Clear bands were detected which suggested that rApPGRP-1 and -2 could bind to six microbes (**Figure 7**). The band intensities of E.c (lane 4, **Figure 7**) were weaker than other bands. No bands were observed for the negative control (data not shown). Seeing from these data, the ApPGRPs proteins could bind a wide spectrum of bacteria.

Amidase Activities of rApPGRP-1 and -2

With L- and D-PGN as substrates, we estimated relative amidase activities of rApPGRP-1 and -2 through measuring OD_{540} value. The OD_{540} value went down dramatically within

FIGURE 4 | Predicted tertiary structures of ApPGRP-1, -2 and *Drosophila* PGRP-SC2 (CAD89187) using SWISS-MODEL. **(A,B)**: ApPGRP-1, -2; **(C)**: *Drosophila* PGRP-SC2. The Zn^{2+} binding sites and amidase catalytic sites are labeled in red.

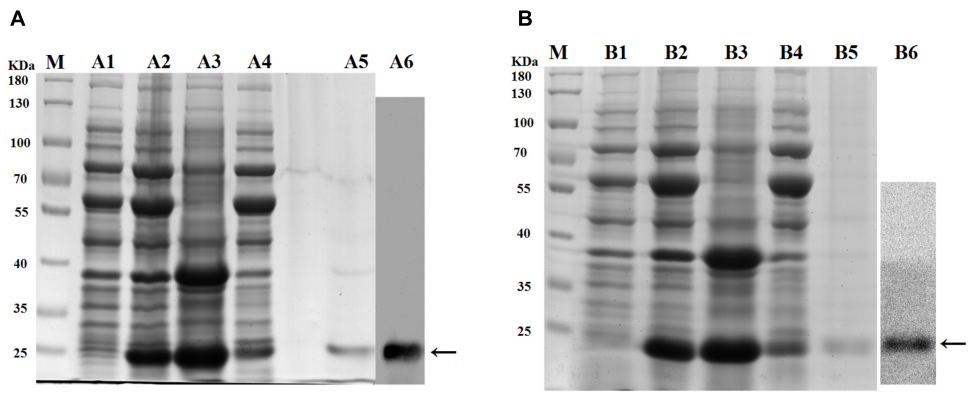

FIGURE 5 | SDS–PAGE of recombinant proteins and western blotting. **(A)**: rApPGRP-1, **(B)**: rApPGRP-2. lane M, molecular mass standards; lane A1, B1, total cellular extracts from *Escherichia. coli* Chaperone Competent Cells pG-KJE8/BL21 with pCold II before induction; lanes A2, B2, total cellular extracts from IPTG induced *E. coli* cells (containing expression vector); lanes A3, B3, pellet of total cellular extracts from IPTG induced *E. coli* (containing expression vector); lanes A4, B4, supernatant of total cellular extracts from IPTG induced *E. coli* (containing expression vector); lanes A5, B5, purified rApPGRP-1 and rApPGRP-2; lanes A6, B6, western blot. The bands of target protein are labled by ←.

300 min when the TBS group was incubated with L-PGN or D-PGN (**Figure 8**). rApPGR-1 and -2 degraded L-PGN in the existence of Zn^{2+} (except D-PGN + rApPGRP-1 + 100 μMZn group and D-PGN + rApPGRP-2 + 100 μMZn group). rApPGRP-1 degraded D-PGN in the absence of Zn^{2+} (ANOVA, $F(1,5) = 6.036$, $P = 0.07$; **Figure 8A2**). Zn^{2+} did not enhance this amidase activity as no change was found between D-PGN + rApPGRP-1 group and D-PGN + rApPGRP-1 + 100 μMZn group. A similar result could be seen in rApPGRP-2 (**Figure 8B2**), whereas Zn^{2+} might slightly inhibit rApPGRP-2 from degrading D-PGN. As there are conserved catalytic residues in rApPGRP-1 and -2, we concluded that rApPGRP-1 and -2 have amidase activity against both Lys-type and Dap-type PGN (**Figure 8**).

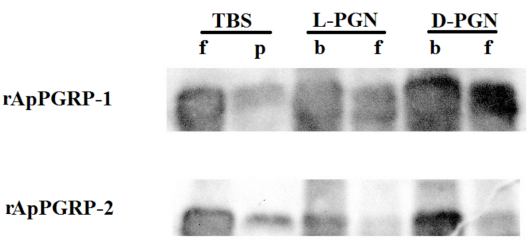

FIGURE 6 | rApPGRP-1 and -2 bind Lys-type PGN from *S. aureus* and Dap-type PGN from *B. subtilis*. f, free; p, pellet; b, bound.

Antimicrobial Activities of rApPGRP-1 and -2

For Gram-positive bacteria, when zinc ions didn't exist, rApPGRP-2 had antibacterial activity against *B. subtilis*, but no antibacterial activity against *S. aureus* or *M. luteus*. In the participation of zinc ions, rApPGRP-1 + 100 μMZn group significantly inhibited *S. aureus*, which was significant different from the rApPGRP-1 or 100 μMZn groups ($P < 0.01$), indicating that rApPGRP-1 had strong enough amidase activity to achieve bactericidal activity in the presence of zinc ions. Similarly, rApPGRP-2 + 100 μMZn group showed analogous activity against *B. subtilis* and rApPGRP-1 + 100 μMZn group showed activity against *M. luteus* (**Figure 9**).

For *E. coli*, *S. cerevisiae* and *P. pastoris*, we chose 10 μM Zn^{2+} for antibacterial experiments, as 100 μM Zn^{2+} alone had a strong antibacterial effect on these microorganisms.

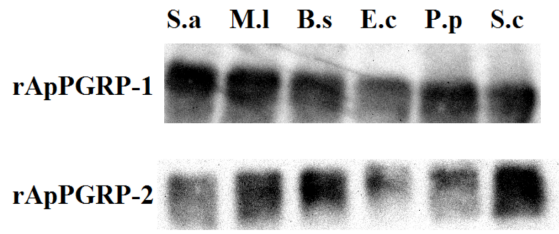

FIGURE 7 | The combination of rApPGRP-1 and -2 with live microbes as detected using western blot. S.a, *Staphylococcus aureus*; M.l, *Micrococcus lutea*; B.s, *Bacillus subtilis*; E.c, *Escherichia coli*; P.p, *Pichia pastoris*; S.c, *Saccharomyces cerevisiae.*

For *E. coli*, rApPGRP-1 and -2 had clear antimicrobial activity in the absence of 10 μM Zn^{2+}. In the presence of 10 μM Zn^{2+}, 10 μMZn group had a bacteriostatic effect but not significant. As the antibacterial effect of rApPGRP-1 + 10 μMZn group is not more than rApPGRP-1 group and there is no significant difference among these three groups: rApPGRP-1, 10 μMZn and rApPGRP-1 + 10 μMZn group ($P > 0.05$), suggested that antibacterial ability of rApPGRP-1 may not require zinc ions. A similar situation was also observed in the rApPGRP-2 + 10 μMZn group (**Figure 9**).

For fungi *S. cerevisiae*, rApPGRP-1 and -2 had no antibacterial activity in the absence of 10 μM Zn^{2+}. In the presence of 10 μM Zn^{2+}, the antibacterial activity of 10 μMZn, rApPGRP-1 + 10 μMZn and rApPGRP-2 + 10 μMZn groups were not significantly different from each other ($P > 0.05$), indicating that the antibacterial ability of rApPGRP-1 + 10 μMZn and rApPGRP-2 + 10 μMZn groups may derive from the zinc ions. For *P. pastoris*, a similar pattern to *S. cerevisiae* was also observed for rApPGRP-1 and-2 when 10 μM Zn^{2+} existed, but both proteins had significant antimicrobial activity in the absence of 10 μM Zn^{2+} ($P < 0.01$; **Figure 9**).

From these analyses, rApPGRP-1 and -2 showed zinc-dependent or -independent bactericidal activity.

DISCUSSION

In this study, two new short PGRPs (ApPGRP-1 and -2) were identified from *A. packardana*. Homology analysis indicated that ApPGRPs had relatively high similarity with PGRPs of other organisms, and phylogenetic tree analysis showed that ApPGRPs clustered with most PGRPs from molluscs with high bootstrap values. As mollusc PGRPs are commonly involved in a series of immune responses, rApPGRP-1 and -2 from *A. packardana* might also play a similar role in regulating diverse immune responses to adapt cold seep habitat.

PGN Binding Specificity and Amidase Activities of PGRPs

L-PGN or D-PGN can be specifically and preferentially recognized by PGRPs. In *Drosophila*, L-PGN from Gram-positive bacteria could trigger the toll signal pathway by PGRP-SA or

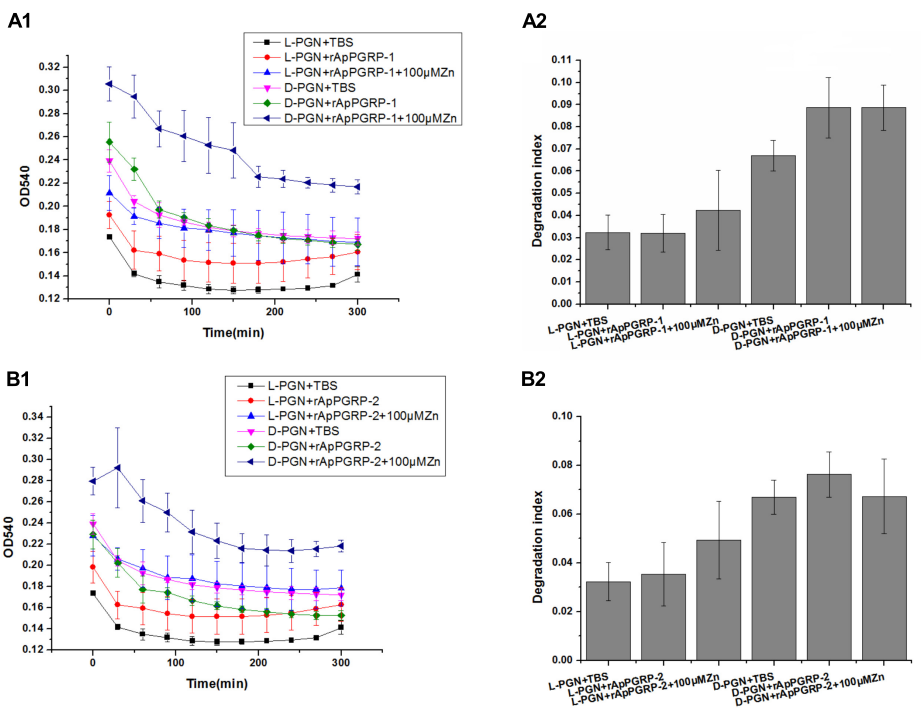

FIGURE 8 | Activity of rApPGRP-1 and -2 in the degradation of L-PGN and D-PGN. **(A1,A2)**, OD_{540} change and degradation index of rApPGRP-1, respectively; **(B1,B2)**, OD_{540} change and degradation index of rApPGRP-2, respectively. Degradation index = OD_{540}(0 min)–OD_{540}(300 min).

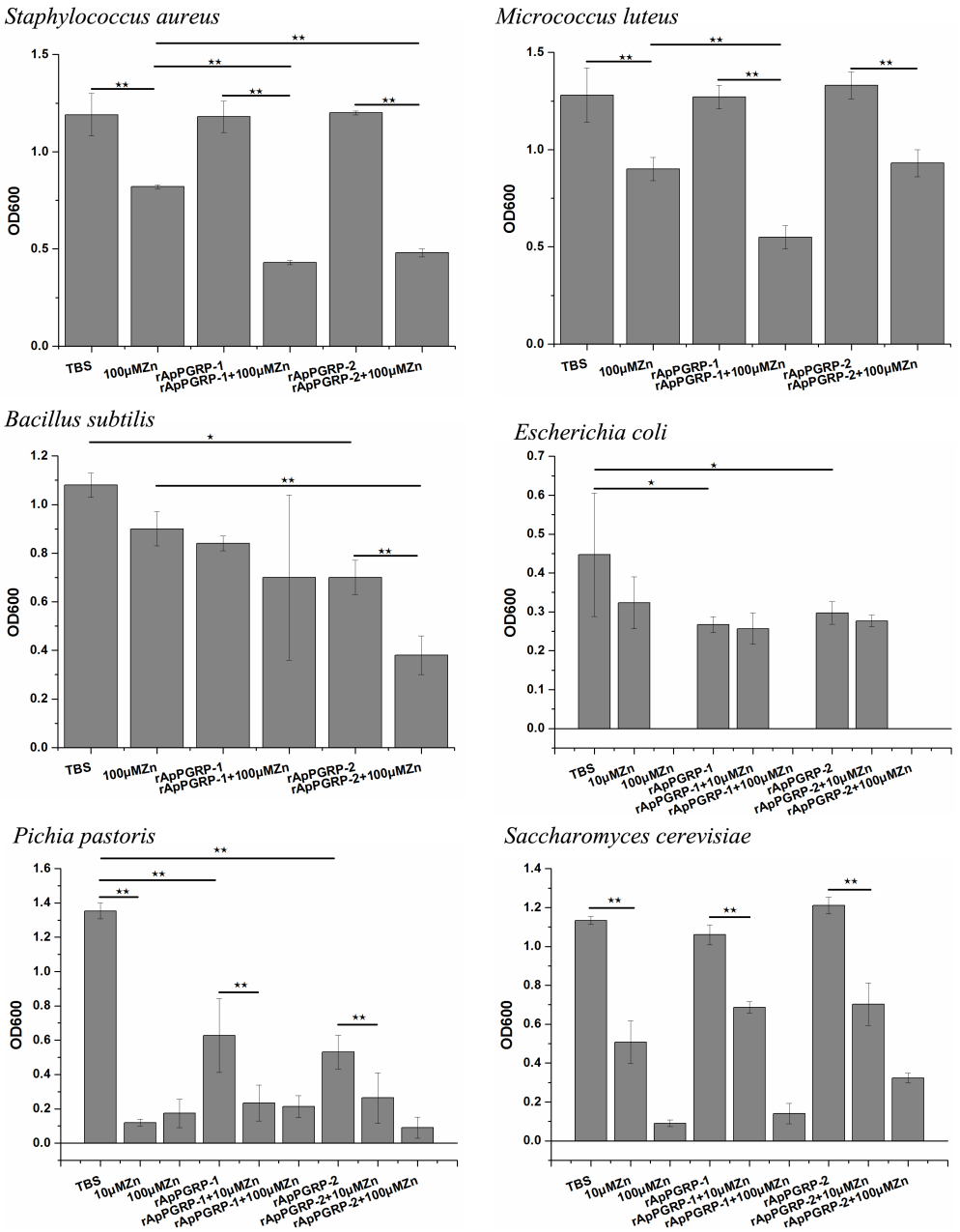

FIGURE 9 | Antimicrobial activity of rApPGRP-1 and -2. ⋆⋆ indicates $P < 0.01$, ⋆ indicates $P < 0.05$.

PGRP-SD. Dap-type PGNs from *Bacillus* and Gram-negative bacteria could stimulate the IMD pathway (Michel et al., 2001; Hoffmann, 2003; Kaneko et al., 2004). In molluscs, rCfPGRPS1 from *Chlamys farreri* displays affinity to L-PGN from *S. aureus* (Yang et al., 2010). CgPGRP-S1S from pacific oyster displays specific binding activity to D-PGN, but not to L-PGN (Iizuka et al., 2014). In this study, PGN binding assays revealed that ApPGRPs have PGN-binding activity toward D, L-PGN which was also found in HcPGRPS1 from *H. cumingi* (Yang et al., 2013). It could be seen that PGRPs from different organisms have their specific PGN binding spectrums.

We also measured amidase activities of the PGRPs. In rPGRP-S from amphioxus, with the participation of Zn^{2+}, higher hydrolyzing activity was detected when using Lys-PGN as substrate compared to Dap-type PGN (Yao et al., 2012). In the present study, rApPGRP-1 and -2 showed some but not significant degradation activity for L-PGN in the presence of Zn^{2+}. However, rApPGRP-1 also showed somehow amidase activity toward D-PGN in the absence of Zn^{2+}. These results are consistent with previous study (Chen et al., 2014). We therefore conclude that the amidase activity of these ApPGRPs is Zn^{2+}-selective dependent.

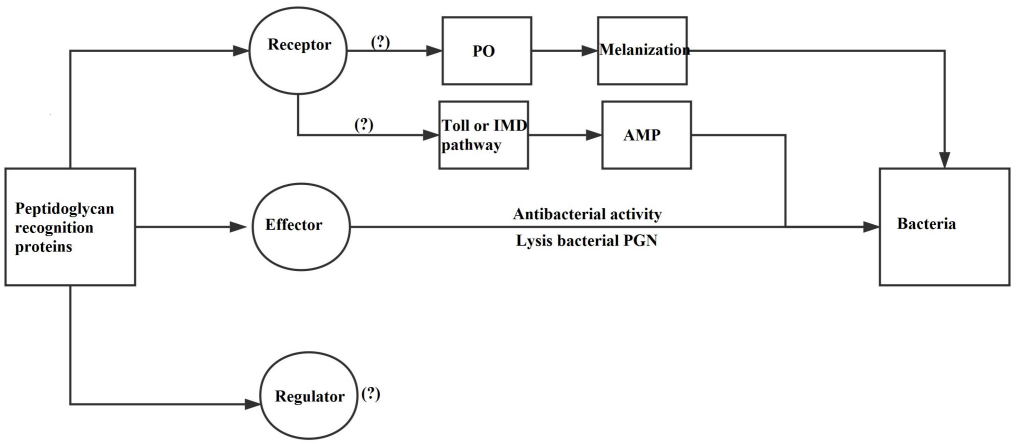

FIGURE 10 | A diagram of PGRPs' functions [modified from Chen and Lv (2014)]. PO, Phenoloxidase; IMD, Immune Deficiency; AMP, Antimicrobial peptide.

Microbial Binding Specificity and Antibacterial Activity

rApPGRP-1 and -2 bound six bacteria with a broad spectrum. Recombinant ApPGRP-1 exhibited antibacterial activity that inhibited the growth of *S. aureus* and *M. luteus* in the presence of Zn^{2+}. This is consistent with the results from *Drosophila* (Mellroth and Steiner, 2006), *C. farreri* (Yang et al., 2010). On the other hand, rApPGRP-1 and-2 had obvious antimicrobial activity for *E. coli* and *P. pastoris* in the absence of Zn^{2+}. This antimicrobial activity might similar to BmPGRP-S5 from *Bombyx mori*, which has obvious antibacterial activity toward Gram-positive bacteria *M. luteus* and *S. aureus*, Gram-negative bacteria *S. marcescens,* and *E. coli* (Chen et al., 2014). Similarly, amphioxus rPGRP-S can also suppress the growth of *P. pastoris* in the absence of Zn^{2+} (Yao et al., 2012). In our study, rApPGRP-1 and -2 displayed amidase activity and bactericidal activity in Zn^{2+}-dependent or –independent manner. These results indicated that the bactericidal effect of ApPGRPs might be a direct effect of amidase-mediated lysis of PGN as there are conserved sites (H-Y-H-T-C) for amidase activity in ApPGRP-1, -2.

Functions of ApPGRPs

Peptidoglycan recognition proteins mainly have three functions: recognition receptor, regulator, and effector (**Figure 10**; Chen and Lv, 2014). ApPGRPs bound PGN and six kinds of microorganisms, which indicate they have partial functions of PGRPs as receptors. After that, IMD, PO, or Toll pathway would be activated, and hosts produce diverse immune responses (Michel et al., 2001; Bischoff et al., 2004; Park et al., 2007; Pal and Wu, 2009). However, the roles of ApPGRPs in these pathways are still not well studied. From the result that ApPGRPs have amidase activity to degrade PGN and could kill microorganisms, we speculate that they can function as effector of PGRPs. To explore the possible roles of ApPGRPs as a regulator, further *in vivo* study is needed.

Trade Off Between Immune Response and Symbiotic Relationship Maintaining

The clam *A. packardana* in the study is from cold seep and has sulfur-oxidizing in its gills as a symbiont (Johnson et al., 2016). ApPGRPs can bind microbes, cleave PGN and display antibacterial activity, which indicated that PGRPs from *A. packardana* might play vital roles in regulating diverse immune responses. Organisms that incorporate symbiotic bacteria into their bodies must maintain a stable symbiotic relationship, therefore as a regulator, PGRPs might play important roles in this process. Given that the large amount symbionts are existed in cold seep clam gills (Johnson et al., 2016), ApPGRPs might function as a regulator (enhance or inhibit) in this tissue. To maintain a long-term symbiotic relationship, weevils from the genus *Sitophilus* express a PGRP which can decrease the biological activity of PGN from symbiotic bacteria (maybe), and therefore avoid PGN from stimulating the host to generate higher immune response (Anselme et al., 2006; Moya et al., 2008). In deep sea organisms, PGRPs' roles as regulator are not very clear. We just found that PGRPs from the Atlantic vent mussel *B. azoricus* might participate in the immune response at early point as they establish symbiotic relationship with bacteria (Martins et al., 2014). PGRPs from cold seep mussel *B. platifrons* might have different roles in different tissues, and BpPGRPs might recognize symbiont bacteria in the gill and function in the immune response in the visceral mass (Sun et al., 2017).

CONCLUSION

In conclusion, two short PGRPs from the cold seep clam *A. packardana* were identified and preliminarily analyzed. Functional assays showed that ApPGRPs have biological function and participate in the immune response. By comparison with PGRPs from other invertebrates, we hypothesize that ApPGRP might also be involved in the endosymbiosis relationship between the host and endosymbiotic bacteria as a regulator. Taken

together, our study provides some basic information for further study on the immune and symbiotic mechanisms of vent/seep molluscs.

ETHICS STATEMENT

All applicable international, national, and/or institutional guidelines for the care and use of animals were followed.

AUTHOR CONTRIBUTIONS

XK and HZ conceived and designed the experiments, analyzed the data, and wrote the paper. XK, HL, YL, and HZ performed the experiments. All authors reviewed the manuscript.

FUNDING

This work was supported by Major scientific and technological projects of Hainan Province (ZDKJ2016009), Strategic Priority Research Program of the Chinese Academy of Sciences (CAS; XDB06010104), The National Key Research and Development Program of China (2017YFC0306600), Knowledge Innovation Program of CAS (SIDSSE–201401), Hundred Talents Program of CAS (SIDSSE–BR–201401), and National Natural Science Foundation of China (41576127).

ACKNOWLEDGMENTS

The authors thank Dr. Vrijenhoek and Ms. Shannon for their kindness in providing clam samples.

REFERENCES

Anselme, C., Vallier, A., Balmand, S., Fauvarque, M.-O., and Heddi, A. (2006). Host PGRP gene expression and bacterial release in endosymbiosis of the weevil *Sitophilus zeamais*. *Appl. Environ. Microbiol.* 72, 6766–6772. doi: 10.1128/aem.00942-06

Barros, I., Divya, B., Martins, I., Vandeperre, F., Santos, R. S., and Bettencourt, R. (2015). Post-capture immune gene expression studies in the deep-sea hydrothermal vent mussel *Bathymodiolus azoricus* acclimatized to atmospheric pressure. *Fish Shellfish Immunol.* 42, 159–170. doi: 10.1016/j.fsi.2014.10.018

Bischoff, V., Vignal, C., Boneca, I. G., Michel, T., Hoffmann, J. A., and Royet, J. (2004). Function of the drosophila pattern-recognition receptor PGRP-SD in the detection of Gram-positive bacteria. *Nat. Immunol.* 5, 1175–1180. doi: 10.1038/ni1123

Chen, K., Liu, C., He, Y., Jiang, H., and Lu, Z. (2014). A short-type peptidoglycan recognition protein from the silkworm: expression, characterization and involvement in the prophenoloxidase activation pathway. *Dev. Comp. Immunol.* 45, 1–9. doi: 10.1016/j.dci.2014.01.017

Chen, K., and Lv, Z. (2014). Peptidoglycan recognition proteins (PGRPs) in insects. *Acta Entomol. Sin.* 57, 969–978.

Coteur, G., Mellroth, P., Lefortery, C. D., Gillan, D., Dubois, P., Communi, D., et al. (2007). Peptidoglycan recognition proteins with amidase activity in early deuterostomes (Echinodermata). *Dev. Comp. Immunol.* 31:790. doi: 10.1016/j.dci.2006.11.006

Dziarski, R. (2003). Recognition of bacterial peptidoglycan by the innate immune system. *Cell. Mol. Life Sci.* 60, 1793–1804. doi: 10.1007/s00018-003-3019-6

Dziarski, R., and Gupta, D. (2006). Mammalian PGRPs: novel antibacterial proteins. *Cell Microbiol.* 8, 1059–1069. doi: 10.1111/j.1462-5822.2006.00726.x

Feng, Y., Li, Z., Zhang, Y., and Zhang, S. (2012). A novel short peptidoglycan recognition protein in amphioxus: identification, expression and bioactivity. *Dev. Comp. Immunol.* 38, 332–341. doi: 10.1016/j.dci.2012.07.009

Foster, S. J. (2004). "257 - N-Acetylmuramoyl-l-alanine amidase," in *Handbook of Proteolytic Enzymes* 2nd Edn, eds A. J. Barrett, N. D. Rawlings, and J. F. Woessner (London: Academic Press), 866–868. doi: 10.1016/B978-0-12-079611-3.50265-2

Gan, Z., Chen, S., Hou, J., Huo, H., Zhang, X., Ruan, B., et al. (2016). Molecular and functional characterization of peptidoglycan-recognition protein SC2 (PGRP-SC2) from Nile tilapia (*Oreochromis niloticus*) involved in the immune response to *Streptococcus agalactiae*. *Fish Shellfish Immunol.* 54, 1–10. doi: 10.1016/j.fsi.2016.03.158

Garver, L. S., Wu, J., and Wu, L. P. (2006). The peptidoglycan recognition protein PGRP-SC1a is essential for Toll signaling and phagocytosis of *Staphylococcus aureus* in Drosophila. *Proc. Natl. Acad. Sci. U.S.A.* 103, 660–665. doi: 10.1073/pnas.0506182103

Gelius, E., Persson, C., Karlsson, J., and Steiner, H. (2003). A mammalian peptidoglycan recognition protein with N-acetylmuramoyl-L-alanine amidase activity. *Biochem. Biophys. Res. Commun.* 306, 988–994.

Guex, N., and Peitsch, M. C. (1997). SWISS-MODEL and the Swiss-PdbViewer: an environment for comparative protein modeling. *Electrophoresis* 18, 2714–2723.

Guo, L., Karpac, J., Tran, S. L., and Jasper, H. (2014). PGRP-SC2 promotes gut immune homeostasis to limit commensal dysbiosis and extend lifespan. *Cell* 156, 109–122. doi: 10.1016/j.cell.2013.12.018

Hoffmann, J. A. (2003). The immune response of Drosophila. *Nature* 426, 33–38. doi: 10.1038/nature02021

Iizuka, M., Nagasaki, T., Takahashi, K. G., Osada, M., and Itoh, N. (2014). Involvement of Pacific oyster CgPGRP-S1S in bacterial recognition, agglutination and granulocyte degranulation. *Dev. Comp. Immunol.* 43, 30–34. doi: 10.1016/j.dci.2013.10.011

Itoh, N., and Takahashi, K. G. (2009). A novel peptidoglycan recognition protein containing a goose-type lysozyme domain from the Pacific oyster, *Crassostrea gigas*. *Mol. Immunol.* 46, 1768–1774. doi: 10.1016/j.molimm.2009.01.022

Janeway, C. A. (1989). Approaching the asymptote? Evolution and revolution in immunology. *Cold. Spring Harb. Symp. Quant. Biol.* 54, 1–13.

Janeway, C. A. J., and Medzhitov, R. (2002). Innate immune recognition. *Annu. Rev. Immunol.* 20, 197–216. doi: 10.1146/annurev.immunol.20.083001.084359

Johnson, S. B., Krylova, E. M., Audzijonyte, A., Sahling, H., and Vrijenhoek, R. C. (2016). Phylogeny and origins of chemosynthetic vesicomyid clams. *Syst. Biodiv.* 15, 346–360. doi: 10.1080/14772000.2016.1252438

Kaneko, T., Goldman, W. E., Mellroth, P., Steiner, H., Fukase, K., Kusumoto, S., et al. (2004). Monomeric and polymeric gram-negative peptidoglycan but not purified LPS Stimulate the Drosophila IMD pathway. *Immunity* 20, 637–649. doi: 10.1016/S1074-7613(04)00104-9

Kim, M.-S., Byun, M., and Oh, B.-H. (2003). Crystal structure of peptidoglycan recognition protein LB from Drosophila melanogaster. *Nat. Immunol.* 4, 787–793. doi: 10.1038/ni952

Larkin, M. A., Blackshields, G., Brown, N. P., Chenna, R., McGettigan, P. A., McWilliam, H., et al. (2007). Clustal W and clustal X version 2.0. *Bioinformatics* 23, 2947–2948.

Letunic, I., and Bork, P. (2018). 20 years of the SMART protein domain annotation resource. *Nucleic Acids Res.* 46, D493–D496. doi: 10.1093/nar/gkx922

Li, J. H., Chang, M. X., Xue, N. N., and Nie, P. (2014a). Functional characterization of a short peptidoglycan recognition protein, PGRP5 in grass carp *Ctenopharyngodon idella*. *Fish Shellfish Immunol.* 42, 244–255. doi: 10.1016/j.fsi.2013.04.025

Li, J. H., Yu, Z. L., Xue, N. N., Zou, P. F., Hu, J. Y., Nie, P., et al. (2014b). Molecular cloning and functional characterization of peptidoglycan recognition protein 6 in grass carp *Ctenopharyngodon idella*. *Dev. Comp. Immunol.* 42, 244–255. doi: 10.1016/j.dci.2013.09.014

Li, M. F., Zhang, M., Wang, C. L., and Sun, L. (2012). A peptidoglycan recognition protein from *Sciaenops ocellatus* is a zinc amidase and a bactericide with a

substrate range limited to Gram-positive bacteria. *Fish Shellfish Immunol.* 32, 322–330. doi: 10.1016/j.fsi.2011.11.024

Martins, E., Figueras, A., Novoa, B., Santos, R. S., Moreira, R., and Bettencourt, R. (2014). Comparative study of immune responses in the deep-sea hydrothermal vent mussel *Bathymodiolus azoricus* and the shallow-water mussel *Mytilus galloprovincialis* challenged with Vibrio bacteria. *Fish Shellfish Immunol.* 40, 485–499. doi: 10.1016/j.fsi.2014.07.018

Mellroth, P., Karlsson, J., and Steiner, H. (2003). A scavenger function for a Drosophila peptidoglycan recognition protein. *J. Biol. Chem.* 278, 7059–7064. doi: 10.1074/jbc.M208900200

Mellroth, P., and Steiner, H. (2006). PGRP-SB1: an N-acetylmuramoyl L-alanine amidase with antibacterial activity. *Biochem. Biophys. Res. Commun.* 350, 994–999. doi: 10.1016/j.bbrc.2006.09.139

Michel, T., Reichhart, J. M., Hoffmann, J. A., and Royet, J. (2001). Drosophila Toll is activated by Gram-positive bacteria through a circulating peptidoglycan recognition protein. *Nature* 414, 756–759. doi: 10.1038/414756a

Moya, A., Pereto, J., Gil, R., and Latorre, A. (2008). Learning how to live together: genomic insights into prokaryote-animal symbioses. *Nat. Rev. Genet.* 9, 218–229. doi: 10.1038/nrg2319

Ni, D., Song, L., Wu, L., Chang, Y., Yu, Y., Qiu, L., et al. (2007). Molecular cloning and mRNA expression of peptidoglycan recognition protein (PGRP) gene in bay scallop (*Argopecten irradians*, Lamarck 1819). *Dev. Comp. Immunol.* 31, 548–558. doi: 10.1016/j.dci.2006.09.001

Pal, S., and Wu, L. P. (2009). Pattern recognition receptors in the fly: lessons we can learn from the Drosophila melanogaster immune system. *Fly* 3, 121–129.

Park, J. W., Kim, C. H., Kim, J. H., Je, B. R., Roh, K. B., Kim, S. J., et al. (2007). Clustering of peptidoglycan recognition protein-SA is required for sensing lysine-type peptidoglycan in insects. *Proc. Natl. Acad. Sci. U.S.A.* 104, 6602–6607. doi: 10.1073/pnas.0610924104

Premachandra, H. K., Elvitigala, D. A., Whang, I., and Lee, J. (2014). Identification of a novel molluscan short-type peptidoglycan recognition protein in disk abalone (*Haliotis discus discus*) involved in host antibacterial defense. *Fish Shellfish Immunol.* 39, 99–107. doi: 10.1016/j.fsi.2014.04.018

Royet, J., and Dziarski, R. (2007). Peptidoglycan recognition proteins: pleiotropic sensors and effectors of antimicrobial defences. *Nat. Rev. Microbiol.* 5, 264–277. doi: 10.1038/nrmicro1620

Steiner, H. (2002). Peptidoglycan recognition proteins: on and off switches for innate immunity. *Immunol. J.* 198, 83–96.

Sun, J., Zhang, Y., Xu, T., Zhang, Y., Mu, H., Zhang, Y., et al. (2017). Adaptation to deep-sea chemosynthetic environments as revealed by mussel genomes. *Nat. Ecol. Evol.* 1:0121. doi: 10.1038/s41559-017-0121

Sun, L., Liu, S., Wang, R., Li, C., Zhang, J., and Liu, Z. (2014). Pathogen recognition receptors in channel catfish: IV. Identification, phylogeny and expression analysis of peptidoglycan recognition proteins. *Dev. Comp. Immunol.* 46, 291–299. doi: 10.1016/j.dci.2014.04.018

Sun, Q. L., and Sun, L. (2015). A short-type peptidoglycan recognition protein from tongue sole (*Cynoglossus semilaevis*) promotes phagocytosis and defense against bacterial infection. *Fish Shellfish Immunol.* 47, 313–320. doi: 10.1016/j.fsi.2015.09.021

Tamura, K., Peterson, D., Peterson, N., Stecher, G., Nei, M., and Kumar, S. (2011). MEGA5: molecular evolutionary genetics analysis using maximum likelihood, evolutionary distance, and maximum parsimony methods. *Mol. Biol. Evol.* 28, 2731–2739. doi: 10.1093/molbev/msr121

Tzou, P. (2002). How Drosophila combats microbial infection: a model to study innate immunity and host–pathogen interactions. *Curr. Opin. Microbiol.* 5, 102–110.

Wei, X., Yang, J., Yang, D., Xu, J., Liu, X., Fang, J., et al. (2012). Molecular cloning and mRNA expression of two peptidoglycan recognition protein (PGRP) genes from mollusk *Solen grandis*. *Fish Shellfish Immunol.* 32, 178–185. doi: 10.1016/j.fsi.2011.11.009

Yang, J., Wang, W., Wei, X., Qiu, L., Wang, L., Zhang, H., et al. (2010). Peptidoglycan recognition protein of *Chlamys farreri* (CfPGRP-S1) mediates immune defenses against bacterial infection. *Dev. Comp. Immunol.* 34, 1300–1307. doi: 10.1016/j.dci.2010.08.006

Yang, Z., Li, J., Li, Y., Wu, H., and Wang, X. (2013). Molecular cloning and functional characterization of a short peptidoglycan recognition protein (HcPGRPS1) from the freshwater mussel. *Hyriopsis cumingi. Mol. Immunol.* 56, 729–738. doi: 10.1016/j.molimm.2013.06.019

Yao, F., Li, Z., Zhang, Y., and Zhang, S. (2012). A novel short peptidoglycan recognition protein in amphioxus: identification, expression and bioactivity. *Dev. Comp. Immunol.* 38, 332–341. doi: 10.1016/j.dci.2012.07.009

Yong, M., Wang, J., Zhang, Z., Ding, S., and Su, Y. (2010). Cloning, mRNA expression, and recombinant expression of peptidoglycan recognition protein II gene from large yellow croaker (*Pseudosciaena crocea*). *Mol. Biol. Rep.* 37, 3897–3908. doi: 10.1007/s11033-010-0046-x

Yue, H. W., Sun, J., He, L. S., Chen, L. G., Qiu, J. W., and Qian, P. Y. (2015). High-throughput transcriptome sequencing of the cold seep mussel *Bathymodiolus platifrons*. *Sci. Rep.* 5:16597. doi: 10.1038/srep16597

Zhang, L., Gao, C., Liu, F., Song, L., Su, B., and Li, C. (2016). Characterization and expression analysis of a peptidoglycan recognition protein gene, SmPGRP2 in mucosal tissues of turbot (*Scophthalmus maximus* L.) following bacterial challenge. *Fish Shellfish Immunol.* 56, 367–373. doi: 10.1016/j.fsi.2016.07.029

Conflict of Interest Statement: The authors declare that the research was conducted in the absence of any commercial or financial relationships that could be construed as a potential conflict of interest.

frontiers in Physiology

ORIGINAL RESEARCH
published: 22 August 2018
doi: 10.3389/fphys.2018.01166

FOXL2 and DMRT1L Are Yin and Yang Genes for Determining Timing of Sex Differentiation in the Bivalve Mollusk *Patinopecten yessoensis*

Ruojiao Li[1,2†], Lingling Zhang[1,3†], Wanru Li[1], Yang Zhang[1], Yangping Li[1], Meiwei Zhang[1], Liang Zhao[1], Xiaoli Hu[1,3], Shi Wang[1,2] and Zhenmin Bao[1,3]*

[1] MOE Key Laboratory of Marine Genetics and Breeding, Ocean University of China, Qingdao, China, [2] Laboratory for Marine Biology and Biotechnology, Qingdao National Laboratory for Marine Science and Technology, Qingdao, China, [3] Laboratory for Marine Fisheries Science and Food Production Processes, Qingdao National Laboratory for Marine Science and Technology, Qingdao, China

OPEN ACCESS

Edited by:
Xiaotong Wang,
Ludong University, China

Reviewed by:
Adam Michael Reitzel,
University of North Carolina at Charlotte, United States
Zhigang Shen,
Huazhong Agricultural University, China

***Correspondence:**
Lingling Zhang
lingling80@ouc.edu.cn

[†] These authors have contributed equally to this work

Specialty section:
This article was submitted to Aquatic Physiology, a section of the journal Frontiers in Physiology

Received: 08 May 2018
Accepted: 03 August 2018
Published: 22 August 2018

Citation:
Li R, Zhang L, Li W, Zhang Y, Li Y, Zhang M, Zhao L, Hu X, Wang S and Bao Z (2018) FOXL2 and DMRT1L Are Yin and Yang Genes for Determining Timing of Sex Differentiation in the Bivalve Mollusk Patinopecten yessoensis. Front. Physiol. 9:1166. doi: 10.3389/fphys.2018.01166

Sex determination and differentiation have long been a research hotspot in metazoans. However, little is known about when and how sex differentiation occurs in most mollusks. In this study, we conducted a combined morphological and molecular study on sex differentiation in the Yesso scallop *Patinopecten yessoensis*. Histological examination on gonads from 5- to 13-month-old juveniles revealed that the morphological sex differentiation occurred at 10 months of age. To determine the onset of molecular sex differentiation, molecular markers were screened for early identification of sex. The gonadal expression profiles of eight candidate genes for sex determination or differentiation showed that only two genes displayed sexually dimorphic expression, with *FOXL2* being abundant in ovaries and *DMRT1L* in testes. *In situ* hybridization revealed that both of them were detected in germ cells and follicle cells. We therefore developed LOG_{10}(*DMRT1L*/*FOXL2*) for scallop sex identification and confirmed its feasibility in differentiated individuals. By tracing its changes in 5- to 13-month-old juveniles, molecular sex differentiation time was determined: some scallops differentiate early in September when they are 7 months old, and some do late in December when they are 10 months old. Two kinds of coexpression patterns were found between *FOXL2* and *DMRT1L*: expected antagonism after differentiation and unexpected coordination before differentiation. Our results revealed that scallop sex differentiation co-occurs with the formation of follicles, and molecular sex differentiation is established prior to morphological sex differentiation. Our study will assist in a better understanding of the molecular mechanism underlying bivalve sex differentiation.

Keywords: Yesso scallop, sex differentiation, FOXL2, DMRT1L, LOG_{10}(*DMRT1L*/*FOXL2*)

INTRODUCTION

Sexual reproduction is one of the most universal phenomena that widely exist in animals. As a focus of this research area, sexual development encompasses sex determination and differentiation. The former is defined as the process by which sex is established under the influence of genetic or environmental factors and the latter as the process that an undifferentiated gonad uses to transform

into an ovary or a testis (Bull, 1983; Penman and Piferrer, 2008; Piferrer and Guiguen, 2008). Therefore, sexual development is a complex network that is initiated by a sex-determining trigger mediating the expression of sex differentiation genes, which ultimately gives rise to the phenotypic differences between sexes (Heule et al., 2014).

Sex determination and differentiation have received much research attention in various species. For example, in mammals, genotypic sex is defined by the presence or absence of sex-specific chromosome Y that carries the dominant male determinant SRY (Swain and Lovell-Badge, 1999; Kocer et al., 2009). In chickens that possess a ZZ/ZW sex chromosome system, DMRT1 is required for testis determination (Zarkower, 2001; Smith et al., 2009). In *Caenorhabditis elegans* and *Drosophila melanogaster*, a cascade of sex switch genes is controlled by the ratio of X chromosomes to sets of autosomes (the X:A ratio; Zarkower, 2001; Goodwin and Ellis, 2002). It seems sex is determined by sex chromosomes and controlled by some master switch genes in many organisms.

Mollusca represents the second largest phylum of invertebrates after Arthropoda. Bivalves are a large group of mollusks that exhibit different reproductive strategies: some are gonochoric, some are hermaphroditic, and some are capable of sex changes. Although much research has been done on many different bivalves, there is no clear evidence for the existence of sex chromosomes in these animals. However, some progress has been made regarding the identification of sex determination or differentiation genes. Several key sex-related genes in model species have been characterized in bivalves, including FOXL2 (Naimi et al., 2009a; Liu et al., 2012), WNT4 (Li et al., 2013; Yang et al., 2015), FST (follistatin; Ni et al., 2012), β-catenin (Li et al., 2014b; Santerre et al., 2014), DMRT (Naimi et al., 2009b; Feng et al., 2010; Yu et al., 2011; Shi et al., 2014), DAX1 (Li et al., 2014a), and SOXE (Santerre et al., 2014). Many of them display sexually dimorphic expression patterns in the gonads and are regarded as participants in the sex differentiation cascade. Meanwhile, gonadal transcriptome analyses identified some key candidate genes for sex determination or differentiation, such as FOXL2, WNT4, β-catenin, DMRT, DAX1, SOXE, and SOXH (Teaniniuraitemoana et al., 2014; Zhang et al., 2014; Tong et al., 2015; Li et al., 2016; Patnaik et al., 2016). These studies suggest that sex determination and differentiation genes may be deeply conserved in animals.

Yesso scallop *Patinopecten yessoensis* is a commercially important species widely cultured in China and Japan. It is predominantly gonochoric, with scarce hermaphroditism. Due to its commercial importance, much work has been performed to obtain an understanding of its reproductive process (Osada et al., 2004; Tanabe et al., 2010; Nagasawa et al., 2015). Recently, our group completed whole genome sequencing and gonadal transcriptome analysis of *P. yessoensis* (Li et al., 2016; Wang et al., 2017), which provide valuable resources for unraveling the molecular mechanisms underlying scallop sex differentiation. In the present study, morphological and molecular sex differentiation was examined in the Yesso scallop. Eight candidate genes for sex determination or differentiation were chosen to establish markers for sex identification and the onset of molecular sex differentiation was determined; we also compared the molecular changes in the undifferentiated and differentiated gonads. This study will pave the way for a better understanding of the regulatory network in bivalve sex differentiation.

MATERIALS AND METHODS

Sample Collection

To obtain adult scallops with known sexes, 15-month-old mature female and male individuals were selected in May 2015, cultured in separate cages, and transported to the laboratory every month from August 2015 to March 2016. Meanwhile, juvenile scallops 5–13 months of age were obtained from July 2015 to March 2016. All of these scallops were collected from the Dalian Zhangzidao Fishery Group Corporation (Liaoning Province, China) and acclimated in filtered and aerated seawater for 1 week at the temperature at which they were collected. For each month, gonads of 50 adults and/or 50 juveniles were dissected: the majority were immediately frozen in liquid nitrogen and stored at −80°C for RNA extraction, and the remainder were fixed in 4% paraformaldehyde overnight, dehydrated with serial methanol (25, 50, 75, and 100%) diluted in 0.01 M phosphate-buffered saline and then stored at −20°C for paraffin sectioning and *in situ* hybridization. Our experiments were conducted according to the guidelines and regulations established by the Ocean University of China and the local government.

Histology

The samples were transferred to ethanol, cleared in xylene, embedded in paraffin wax, and cut into 5-μm-thick sections on a rotary microtome (Leica, Wetzlar, Germany). Serial sections were tiled on glass slides, deparaffinized with xylene, hydrated with graded ethanol to water, and stained with hematoxylin. After that, the glass slides were counterstained with eosin, dehydrated with ethanol, cleared with xylene, mounted with neutral balsam, and covered with coverslips. Finally, the sections were observed under a Nikon's Eclipse E600 research microscope.

Candidate Genes Identification

Four ovary-related genes (FOXL2, WNT4, FST, β-catenin) and four testis-related genes (DMRT1L, DAX1, SOXE, and SOXH) were selected for analysis. To identify these genes, protein sequences from other organisms were collected from NCBI and used as queries against the genome (Wang et al., 2017) and gonadal transcriptomes (Li et al., 2016) by TBLASTN with an e-value threshold of $1e^{-5}$. The resultant scallop sequences were further confirmed by BLASTX against the NCBI protein sequence database.

Phylogenetic Analyses

Full-length protein sequences encoding FOXL2/3 and DMRT homologs were downloaded from NCBI. Multiple sequence alignments (**Supplementary Material**) were conducted using ClustalW2 program with default parameters (Larkin et al., 2007). The neighbor-joining phylogenetic trees were constructed using

MEGA 6 (Tamura et al., 2013), with a Poisson model and assuming uniform rates among sites. Bootstrapping with 1000 replications was conducted to evaluate the phylogenetic tree.

RNA Extraction

Total RNA was isolated using the conventional guanidinium isothiocyanate method and digested with DNase I (TaKaRa, Shiga, Japan) to remove potential DNA contamination. RNA concentration and purity were determined by Nanovue Plus spectrophotometer (GE Healthcare, Piscataway, NJ, United States), and RNA integrity was verified by agarose gel electrophoresis. Only RNA samples with clear bands corresponding to 18S and 28S rRNA on the gel, an OD260/OD280 ratio between 1.8–2.0, and an OD260/OD230 ratio higher than 2.0 were used for subsequent experiments.

Reverse Transcription Quantitative-PCR (RT-qPCR)

First-strand cDNA was synthesized from 2 μg total RNA using oligo$(dT)_{18}$ and MMLV reverse transcriptase (TaKaRa, Shiga, Japan) in a volume of 20 μl. The reaction was performed at 42°C for 90 min and terminated by heating at 70°C for 10 min. Finally, the cDNA products were diluted to 10 ng/μl and stored at −20°C. Gene-specific primers were designed using Primer Premier 5.0 and listed in **Table 1**. Amplification efficiency of each primer pair was calculated based on the standard curve generated from a twofold dilution series spanning six orders of magnitude. Quantitative-PCR was conducted using Light Cycler 480 SYBR Green I Master on a Light Cycler 480 Real-time PCR System (Roche Diagnostics, Mannheim, Germany) with the following program: 94°C for 10 min, followed by 40 cycles of 94°C for 15 s and 60°C for 1 min. For each month, six to eight samples were assayed and all reactions were conducted in triplicate. To ensure that the RT-qPCR ran properly, negative controls, including NTCs (no-template controls) and no-reverse transcription controls, and positive controls were included in each run. Melting curve analysis was performed to verify that each primer set amplified a single product (**Supplementary Figure S1**). *EF1A* (elongation factor 1-alpha), which was stably expressed throughout the entire experiment, was used as an endogenous control for the normalization of gene expression (Santerre et al., 2013; Teaniniuraitemoana et al., 2015; Li et al., 2016). The relative expression level of each gene was calculated using the $2^{-\Delta\Delta Ct}$ method. Statistical analysis was performed by Welch's *t*-tests. Pearson's correlation coefficient was calculated to explore the relationships between the two genes. *P*-values lower than 0.05 were considered statistically significant.

In situ Hybridization

To prevent cross-detection of other FOX and DMRT genes, cDNA fragments avoiding conserved DNA binding domains were amplified with specific primers (**Table 2**) containing a 5′ T7 promoter sequence (5′-TAATACGACTCACTATAGGG-3′). Purified PCR products were used as templates for *in vitro* transcription. Digoxigenin-labeled sense and anti-sense probes were generated using the DIG RNA Labeling Mix (Roche, Mannheim, Germany) and T7 RNA polymerase (Thermo, Waltham, MA, United States). Sections of the gonadal tissues were serially rehydrated in PBST (phosphate-buffered saline plus 0.1% Tween-20) and digested with 2 μg/ml proteinase K at 37°C for 15 min. After pre-hybridization at 60°C for 4 h, hybridization was performed with 1 μg/ml denatured RNA probe in hybridization buffer (50% formamide, 5× SSC, 100 μg/ml yeast tRNA, 1.5% blocking reagent, 0.1% Tween-20) at 60°C for 16 h. Then, the probes were washed away, and antibody incubation was performed in a fresh solution of anti-digoxigenin-AP Fab fragments (Roche, Mannheim, Germany) coupled with blocking buffer (diluted 1:2000) at 4°C for 16 h. After extensive

TABLE 1 | Sequences of all primers used for RT-qPCR.

Gene name	Primer sequences (5′–3′)	Amplicon length (bp)	Amplification efficiency	GenBank Acc. No
EF1A	F:CCATCTGCTCTGACAACTGA	196	1.02	XM_021500266.1
	R:GGACAATAACCTGAGCCATAA			
FOXL2	F:AACTTCTGGACATTGGACCCTGCTT	134	1.00	XM_021497746.1
	R:CCGCAGTGGTTGTCAGCAAATAAGG			
WNT4	F:ATGAATAGCGTGGCAGCAAT	141	0.97	XM_021498826.1
	R:ACTCGTCTATAGCCGAATGA			
FST	F:CCAATCCTAACTTCGTGTGT	105	1.04	XM_021490283.1
	R:CCATAGGCGATACGTATTGA			
β-catenin	F:GCAACACCAGGATGATGAAT	112	1.03	XM_021507890.1
	R:ATCCTGCATGTAGGTGTTCT			
DMRT1L	F:ACAGATTCCCTACAGATGCT	128	0.98	XM_021498039.1
	R:TTATTCATGGCGGCGTCTAT			
DAX1	F:CGTGTCCTACAACAGTAACA	117	0.98	XM_021500761.1
	R:GTGGTCCATTGCTACCTTAT			
SOXE	F:CTCTGGAGGCTTCTGAATGA	144	1.01	XM_021493168.1
	R:TCTGTCCTCCACTAGCACTT			
SOXH	F:CATGCCTGGTACCTCTATGA	172	0.99	XM_021485311.1
	R:GGCCGAGTCGAACACTGATT			

TABLE 2 | Sequences of primers used for *in situ* hybridization.

Gene name	Primer sequences (5′–3′)
FOXL2	F:CTTATTTGCTGACAACCACTGCG
	R:TAGGGGCCGAACGGAAAGG
	F-T7:TAATACGACTCACTATAGGGCTTATTTGCTGACAACCACTGCG
	R-T7:TAATACGACTCACTATAGGGTAGGGGCCGAACGGAAAGG
DMRT1L	F:GGACACCATCACGCATACCAA
	R:ACCAGAGTTCCTTCCGCCTC
	F-T7:TAATACGACTCACTATAGGGGGACACCATCACGCATACCAA
	R-T7:TAATACGACTCACTATAGGGACCAGAGTTCCTTCCGCCTC

Primers F and R were used to amplify the cDNA fragment, and the product was used for the second-round PCR with the primers F and R-T7 to generate an anti-sense probe and with primers R and F-T7 to generate a sense probe.

washing with maleic acid buffer (0.1 M maleic acid, 0.15 M NaCl, 0.1% Tween-20, pH = 7.5), sections were incubated with nitro blue tetrazolium/5-bromo-4-chloro-3-indolyl phosphate (NBT/BCIP) substrate solution and counterstained with 1% neutral red solution.

RESULTS

Histological Analysis of the Juvenile Gonads

Gonads were examined histologically in juveniles aged 5 (shell height ∼10 mm) to 13 months old (shell height ∼60 mm). **Figures 1A,B** show the morphology of 5- and 6-month-old gonads, respectively. As seen, the majority of the gonads are intestine, surrounded by gonadal tissues. In the 7-month-old gonad, some small-sized follicles have formed (**Figure 1C**). In the 8-month-old gonad, the follicles grow bigger but are basically empty, containing some follicle cells and sexually indistinguishable gonia (**Figure 1D**). The 10-month-old gonads are already morphologically differentiated, with oocytes (**Figure 1E**) or spermatocytes (**Figure 1F**) scattering in the follicles. Oogonia, oocytes, and a few mature oocytes coexist in the 11-month-old ovary (**Figure 1G**), and several layers of spermatogonia and spermatocytes are found in the 11-month-old testis (**Figure 1H**), indicating that the gonads are at the growing stage. As shown in **Figures 1I,J**, the 13-month-old gonads have reached full maturity. In the ovary, the follicles are filled with mature oocytes with a polygonal shape due to packing (**Figure 1I**). In the follicles of the testis, diverse germ cells can be detected, including spermatogonia, spermatocytes, spermatids, and spermatozoa (**Figure 1J**).

Selection of Candidate Genes for Sex Analysis

To determine the onset of molecular sex differentiation, molecular markers were screened for sex identification. All eight candidate genes (FOXL2, WNT4, FST, β-catenin, DMRT1L, DAX1, SOXE, and SOXH) were identified in the scallop genome. Their expression patterns in ovaries and testes were examined by RT-qPCR. In order to obtain genes that show sexually dimorphic expression in somatic and/or gonia cells and eliminate the effects of gametogenesis, we only used gonads at the resting stage for gene expression analysis (Yu et al., 2017). As shown in **Figure 2A**, only *FOXL2* and *DMRT1L* displayed significant ($P < 0.01$) sexually dimorphic expression, with *FOXL2* being abundant in ovaries, and *DMRT1L* in testes. Therefore, LOG_{10}(*DMRT1L*/*FOXL2*) is a potential marker for scallop sex identification, which led us to further investigate its values in the other three reproductive stages (proliferative, growing, and maturation stages). The results also confirmed that LOG_{10}(*DMRT1L*/*FOXL2*) could be used to determine the sex of differentiated scallops throughout the reproductive cycle: the

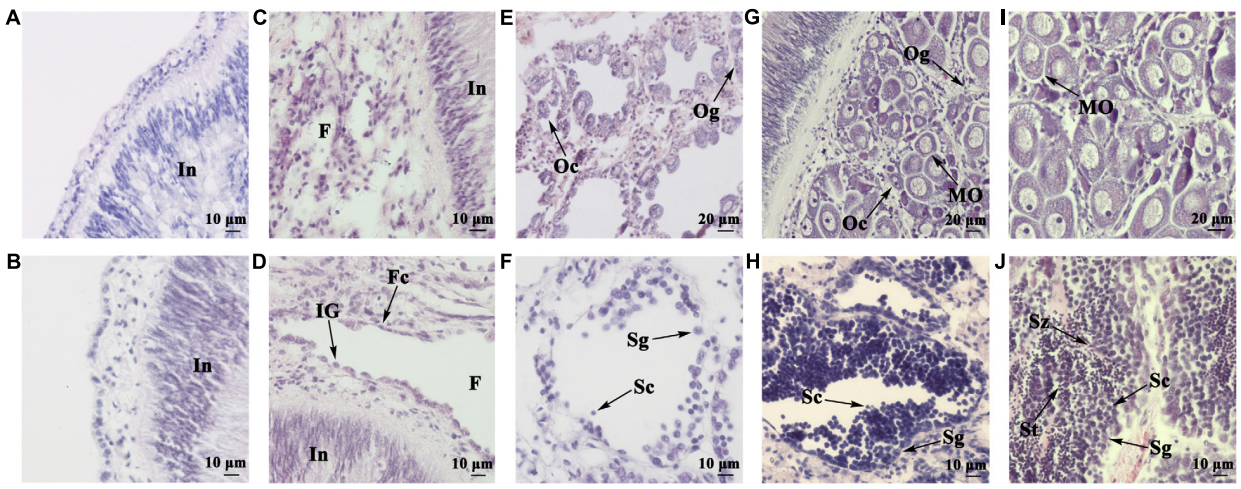

FIGURE 1 | Histological observation of juvenile gonads of different ages. **(A)** Gonad of a 5-month-old juvenile. **(B)** Gonad of a 6-month-old juvenile. **(C)** Gonad of a 7-month-old juvenile. **(D)** Gonad of an 8-month-old juvenile. **(E)** Ovary of a 10-month-old juvenile. **(F)** Testis of a 10-month-old juvenile. **(G)** Ovary of an 11-month-old juvenile. **(H)** Testis of an 11-month-old juvenile. **(I)** Ovary of a 13-month-old juvenile. **(J)** Testis of a 13-month-old juvenile. In, intestine; F, follicle; Fc, follicle cell; IG, indistinguishable gonium; Og, oogonium; Oc, oocyte; MO, mature oocyte; Sg, spermatogonium; Sc, spermatocyte; St, spermatid; Sz, spermatozoon.

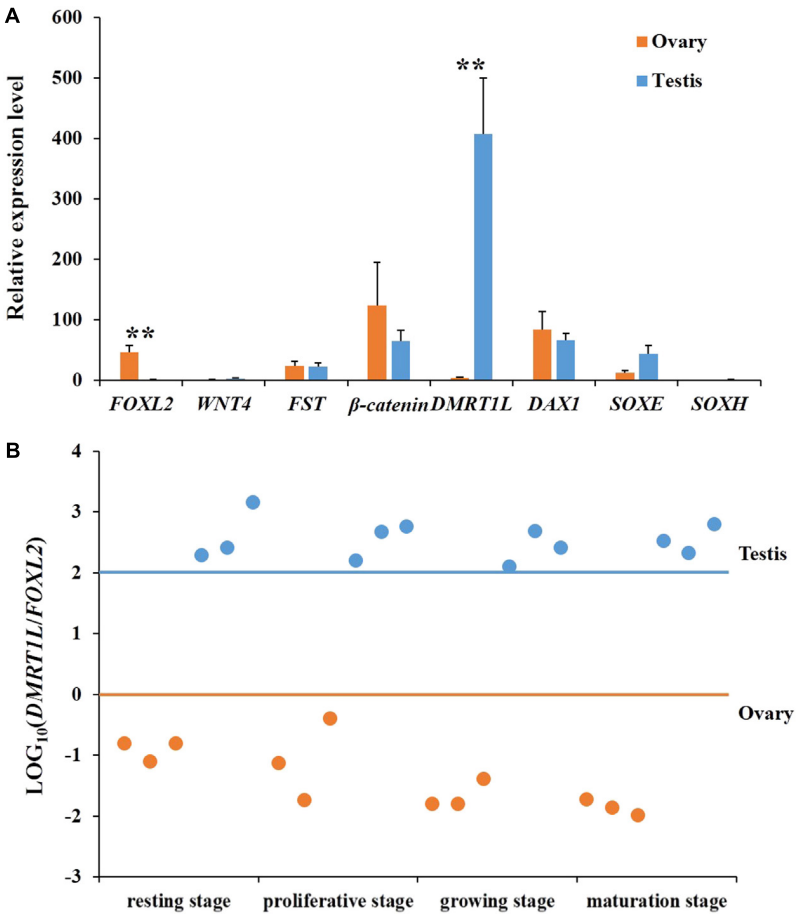

FIGURE 2 | Screening of key genes responsible for scallop sex differentiation. **(A)** Expression profiles of eight candidate genes (*FOXL2*, *WNT4*, *FST*, β-*catenin*, *DMRT1L*, *DAX1*, *SOXE*, and *SOXH*) in scallop ovaries (orange) and testes (blue) at the resting stage. The vertical bars represent the means ± SE ($N = 7$). "**" indicates differences that are statistically significant ($P < 0.01$). **(B)** The LOG_{10}(*DMRT1L*/*FOXL2*) in ovaries (orange) and testes (blue) at the resting stage, proliferative stage, growing stage, and maturation stage. For each stage, six gonads, including three ovaries and three testes, were assayed. The horizontal lines indicate the threshold for sex differentiation, i.e., orange for ovary and blue for testis, respectively.

value was always lower than 0 for ovaries and higher than 2 for testes (**Figure 2B**).

Phylogenetic Analyses of FOXL2 and DMRT1L

To determine the identity of the two sexually dimorphic expressed genes, phylogenetic analysis was conducted. As shown in **Figure 3A**, Yesso scallop FOXL2 clustered with FOXL2 from other bivalves and gastropods, and then clustered with vertebrate FOXL2 and FOXL3. In **Figure 3B**, the selected DMRT proteins were clustered into several major groups. The Yesso scallop DMRT, together with DMRT from *Mimachlamys nobilis* and *Haliotis asinina* forms a new group, namely, DMRT1L.

Localization of *FOXL2* and *DMRT1L* mRNA

Spatial expression of *FOXL2* and *DMRT1L* was detected in the ovary and testis at the proliferative stage after sex differentiation. For both genes, the signals were present in germ cells and follicle cells. Specifically, the anti-sense probe of *FOXL2* was detected in the cytoplasm of oogonia, oocytes, and follicle cells (**Figure 4A**) and faint in testis (**Figure 4B**). *DMRT1L* transcripts were located clearly in all germ cells of the ovary (**Figure 4C**) and testis (**Figure 4D**), but the signal intensity was higher in the testis than in the ovary. No signal was detected in the ovary or testis with the sense probes (**Figures 4E–H**).

Determining the Timing of Molecular Sex Differentiation

The feasibility of LOG_{10}(*DMRT1L*/*FOXL2*) for accurate sex identification enables us to determine the timing of gonadal sex differentiation in the Yesso scallop. Here, we traced the dynamic changes of LOG_{10}(*DMRT1L*/*FOXL2*) in juveniles aged 5–13 months old. According to **Figure 5A**, LOG_{10}(*DMRT1L*/*FOXL2*) values of young individuals (5 and 6 months old) are between 0 and 1, suggesting that these scallops are still undifferentiated. In 7- to 10-month-old scallops, we found a decreasing number of LOG_{10}(*DMRT1L*/*FOXL2*) falling within 0–1. This indicates

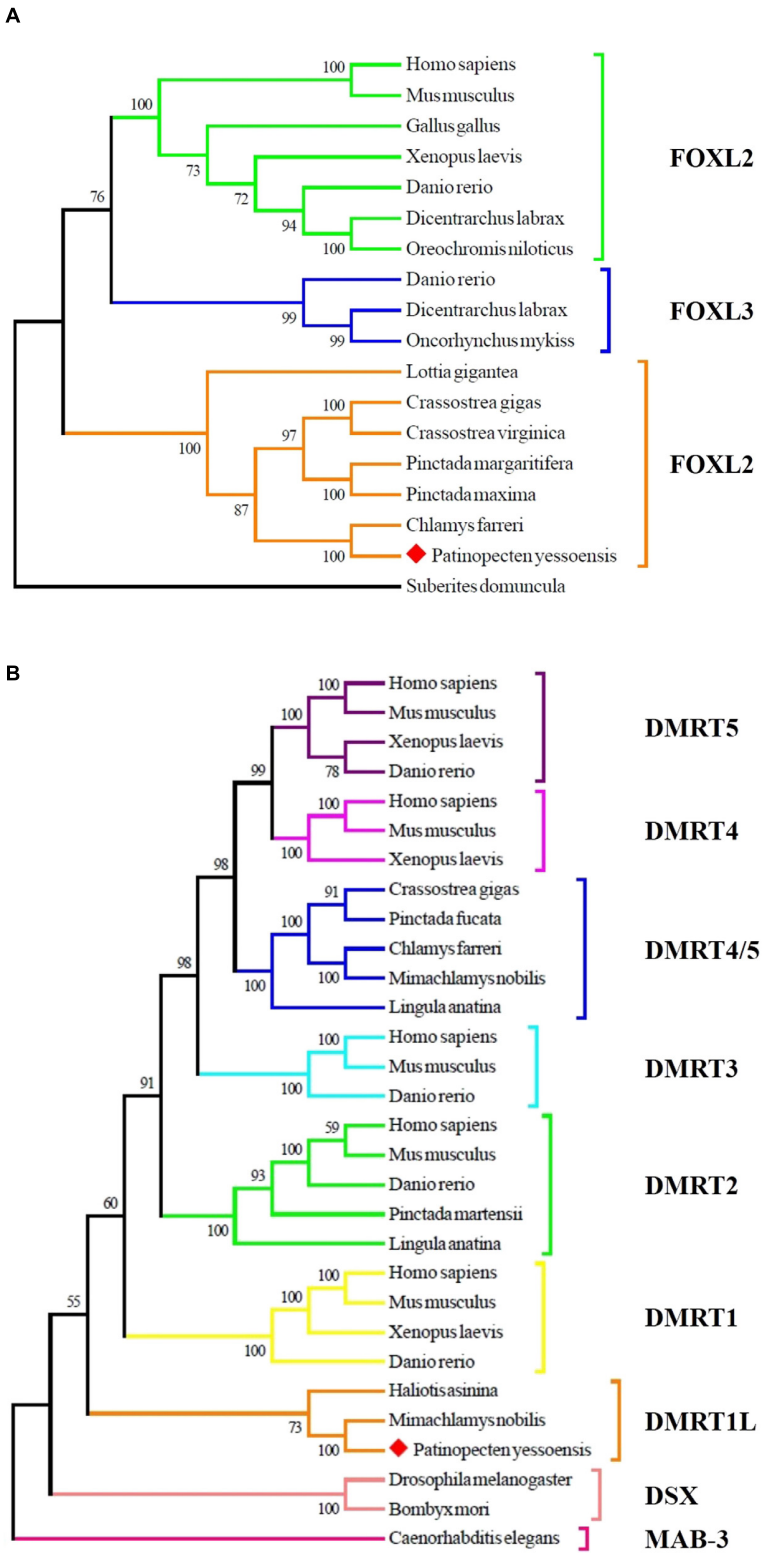

FIGURE 3 | Phylogenetic analyses of FOXL2 **(A)** and DMRT **(B)** proteins. The numbers show the bootstrap percentages (1000 replicates) obtained using neighbor-joining (NJ) method. Different branch colors denote different groups, and red diamonds indicate FOXL2 and DMRT1L of *P. yessoensis*. The protein sequences used for phylogenetic analyses include: FOXL2 of *Homo sapiens* (AAY21823.1), *Mus musculus* (NP_036150.1), *Gallus gallus* (NP_001012630.1),

(Continued)

FIGURE 3 | Continued
Xenopus laevis (BAG69484.1), *Danio rerio* (AAI16586.1), *Dicentrarchus labrax* (AGS36082.1), *Oreochromis niloticus* (AAT36328.1), *Lottia gigantea* (BAQ19215.1), *Crassostrea gigas* (ACN80999.1), *Crassostrea virginica* (XP_022345405.1), *Pinctada margaritifera* (AIE16098.1), *Pinctada maxima* (ATJ00808.1), *Chlamys farreri* (AFB35647.1), *Suberites domuncula* (CAE51212.1); FOXL3 of *Danio rerio* (AAI62838.1), *Dicentrarchus labrax* (AFV13295.1), *Oncorhynchus mykiss* (NP_001117956.1); MAB-3 of *Caenorhabditis elegans* (NP_871909.1); DSX of *Drosophila melanogaster* (NP_731197.1), *Bombyx mori* (AGS48306.1); DMRT1 of *Homo sapiens* (NP_068770.2), *Mus musculus* (NP_056641.2), *Xenopus laevis* (BAE45870.1), *Danio rerio* (AAU04562.1); DMRT1L of *Haliotis asinina* (ACC94178.1), *Mimachlamys nobilis* (AHW85419.1); DMRT2 of *Homo sapiens* (AAD40475.1), *Mus musculus* (NP_665830.1), *Danio rerio* (NP_571027.1), *Pinctada martensii* (ADD97887.1), *Lingula anatina* (XP_013397304.1); DMRT3 of *Homo sapiens* (NP_067063.1), *Mus musculus* (NP_796334.2), *Danio rerio* (AAU89440.1); DMRT4 of *Homo sapiens* (AAI30436.1), *Mus musculus* (AAN77234.1), *Xenopus laevis* (AAV66322.1); DMRT5 of *Homo sapiens* (Q96SC8.2), *Mus musculus* (AAN10254.1), *Xenopus laevis* (AAI70170.1), *Danio rerio* (AAU85258.1); DMRT4/5 of *Crassostrea gigas* (ABS88697.1), *Pinctada fucata* (AIW04133.1), *Chlamys farreri* (ADK55063.1), *Mimachlamys nobilis* (AHW85420.1), *Lingula anatina* (XP_013419494.1).

that sex differentiation does not occur simultaneously in all individuals, with some scallops differentiating early when they are 7 months old and some not differentiating until they are 10 months old. However, after reaching 11 months of age, all investigated gonads had differentiated into ovaries or testes. The histogram in **Figure 5B** shows the corresponding differentiation rate for each month based on the LOG_{10}(*DMRT1L*/*FOXL2*) values. It reveals an increase in the differentiation rate from 0 in 5- and 6-month-old individuals to 100% in 11- to 13-month-old scallops.

Coexpression of *FOXL2* and *DMRT1L* in the Juvenile Gonads

Figure 6A shows the temporal expression profiles of both *FOXL2* and *DMRT1L* in juveniles of 5- to 13-month-olds. According to the results, *FOXL2* and *DMRT1L* are relatively low in 5- to 10-month-old scallops, but expression of *FOXL2* in ovaries and *DMRT1L* in testes was dramatically increased in 11- to 13-month-old scallops. During the eight investigated months, there existed two major coexpression patterns between *FOXL2* and *DMRT1L*: (i) a significantly positive correlation for the two undifferentiated stages (r = 0.955–0.980, $P < 0.01$), with the regression equation of $y = 1.018x + 0.370$ (**Figure 6B**); (ii) significantly negative correlation after the completion of sex differentiation in the last three time points ($r = -0.791$ to -0.957, $P < 0.05$), with the regression equation of $y = -0.684x + 1.584$ (**Figure 6C**). Between the undifferentiated and fully differentiated months are three partially differentiated ones, in which correlation coefficients displayed a transition from significantly positive (0.860) to negative (−0.587).

DISCUSSION

By examining the gonadal expression of eight candidate sex determination or differentiation genes in the resting stage, we found that only two genes (*FOXL2* and *DMRT1L*) displayed sexually dimorphic expression. Both genes are transcription factors, with the former being a forkhead transcription factor and the latter encoding a DM domain-containing protein. Specific sequence information, including conserved domain alignments, has been described previously (Li et al., 2016). According to the transcriptomes of nine adult tissues/organs (Wang et al., 2017), *FOXL2* and *DMRT1L* seem to be specifically expressed in scallop gonads, and no evidence of splice isoforms was found for *DMRT1L* despite that splicing of *DMRT* is common in many animals (Nothiger et al., 1987; Kopp, 2012). Interestingly, sexually dimorphic expression of *FOXL2* (Liu et al., 2012; Teaniniuraitemoana et al., 2014; Zhang et al., 2014) and *DMRT1L* (Shi et al., 2014) occurs not only in the Yesso scallop but also in other bivalves. Therefore, FOXL2 and DMRT1L, like Yin and Yang, may be crucial genes for female and male gonadal differentiation in bivalves. Similarly, in mammals, FOXL2 is an ovarian marker that suppresses genes involved in testicular differentiation from the early embryonic gonad throughout adult life (Cocquet et al., 2002; Ottolenghi et al., 2007; Uhlenhaut et al., 2009; Liu et al., 2014). Although DMRT genes have diverse roles in development and physiology (Huang et al., 2005; Hong et al., 2007; Reitzel et al., 2016), DMRT1 is a deeply conserved gene that is involved in testis differentiation and development in various animal taxa (Naimi et al., 2009b; Kopp, 2012; Matson and Zarkower, 2012; Picard et al., 2015). In mammals, a battle between FOXL2 and DMRT1 for sex control has been proposed (Herpin and Schartl, 2011; Matson et al., 2011). We assume that this battle may be extended to invertebrates, but with different DMRT members.

Spatial expression of *FOXL2* and *DMRT1L* in the ovary and testis reveals that both genes are distributed in germ cells and follicle cells, consistent with previous research in other marine bivalves (Naimi et al., 2009a; Liu et al., 2012). The signal intensity also agrees with the RT-qPCR data. The expression patterns of *FOXL2* and *DMRT1L* make LOG_{10}(*DMRT1L*/*FOXL2*) an alternative method to histological examination for scallop sex identification. By tracking LOG_{10}(*DMRT1L*/*FOXL2*) at four gonadal developmental stages, we found the value was always lower than 0 for ovaries and higher than 2 for testes, which indicates that in the Yesso scallop, (i) there is no sex reversal once the gonads differentiate, (ii) FOXL2 and DMRT1L may play important roles in both sex maintenance and gametogenesis, and (iii) LOG_{10}(*DMRT1L*/*FOXL2*) is an effective solution for sex identification during the resting stage, which is usually indistinguishable by morphology- or histology-based approaches. Since *FOXL2* and *DMRT1L* also show sexually dimorphic expression patterns in other bivalves (Liu et al., 2012; Shi et al., 2014; Teaniniuraitemoana et al., 2014; Zhang et al., 2014), using LOG_{10}(*DMRT1L*/*FOXL2*) for sex identification may be applicable in these organisms. For oysters that are capable of sex reversal (Teaniniuraitemoana et al., 2014; Zhang et al., 2014), sex-reversing individuals may be easily screened out by examining the LOG_{10}(*DMRT1L*/*FOXL2*) values that fall between

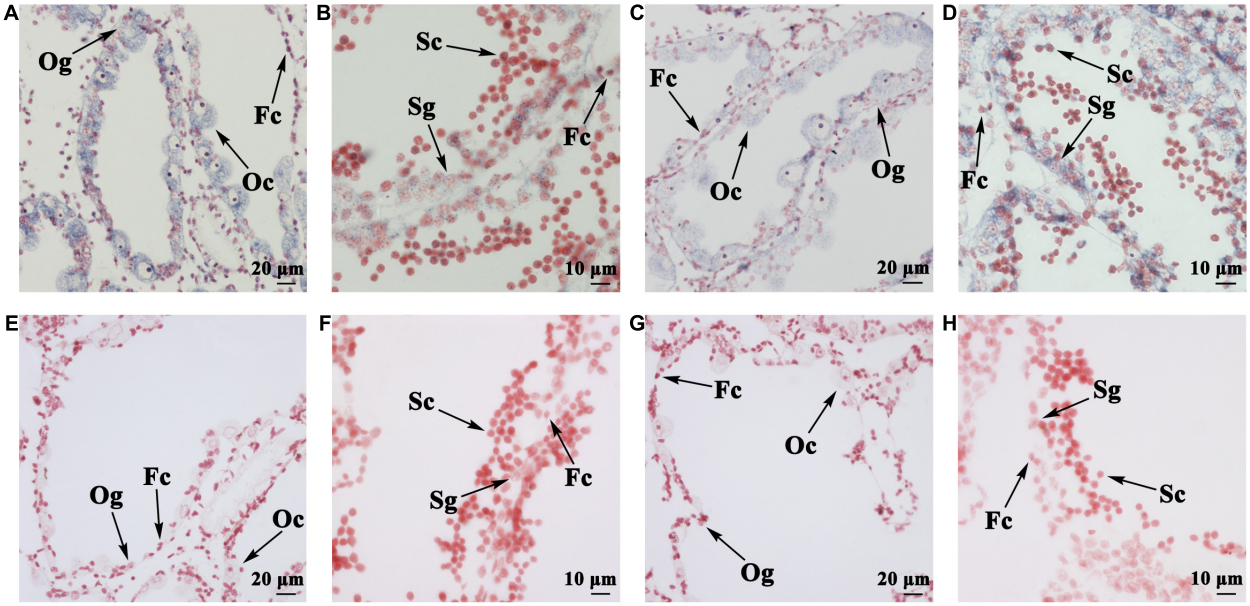

FIGURE 4 | Localization of *FOXL2* and *DMRT1L* in gonads by *in situ* hybridization. **(A)** Localization of *FOXL2* with an anti-sense probe in ovaries. **(B)** Localization of *FOXL2* with an anti-sense probe in testes. **(C)** Localization of *DMRT1L* with an anti-sense probe in ovaries. **(D)** Localization of *DMRT1L* with an anti-sense probe in testes. **(E)** Localization of *FOXL2* with a sense probe in ovaries. **(F)** Localization of *FOXL2* with a sense probe in testes. **(G)** Localization of *DMRT1L* with a sense probe in ovaries. **(H)** Localization of *DMRT1L* with a sense probe in testes. Fc, follicle cell; Og, oogonium; Oc, oocyte; Sg, spermatogonium; Sc, spermatocyte.

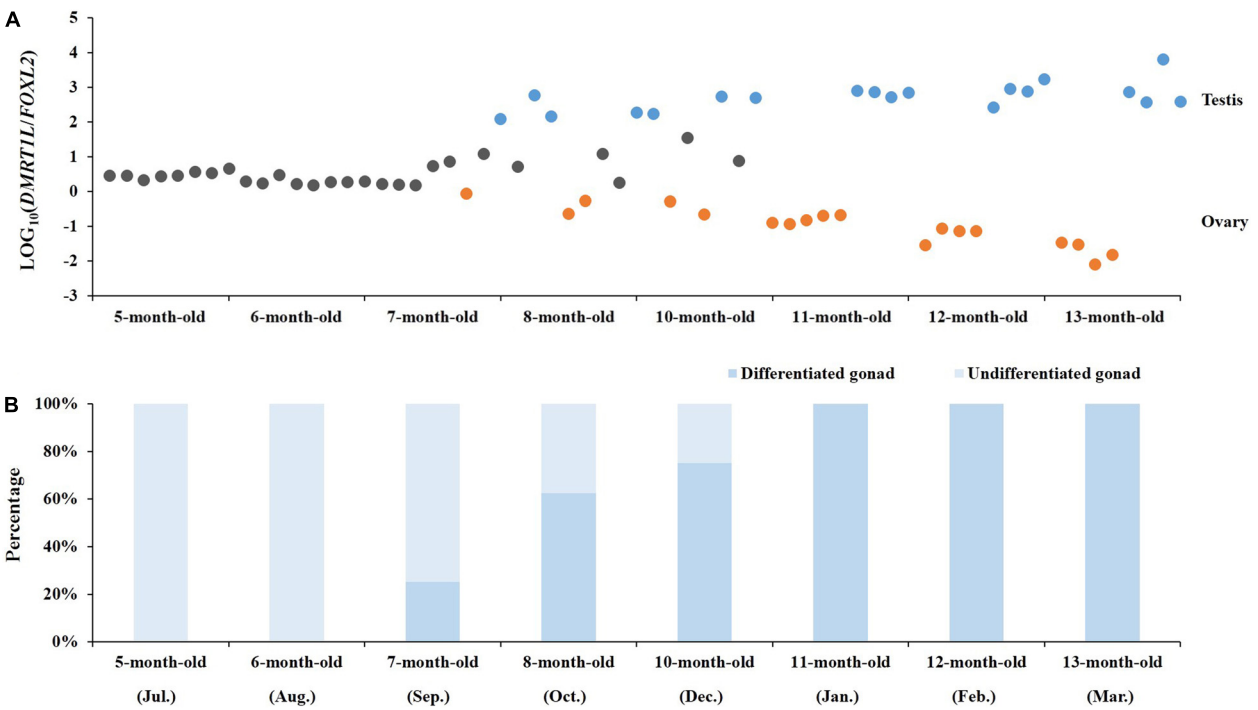

FIGURE 5 | Determination of the timing of molecular sex differentiation in juvenile scallops. **(A)** The dynamic changes in LOG_{10}(*DMRT1L*/*FOXL2*) in 5- to 13-month-old juvenile gonads (N = 8 for each month). Gray, orange, and blue dots stand for undifferentiated gonads, ovaries and testes, respectively. **(B)** The histogram indicates the corresponding percentage of undifferentiated (light blue) and differentiated gonads (blue) in each month.

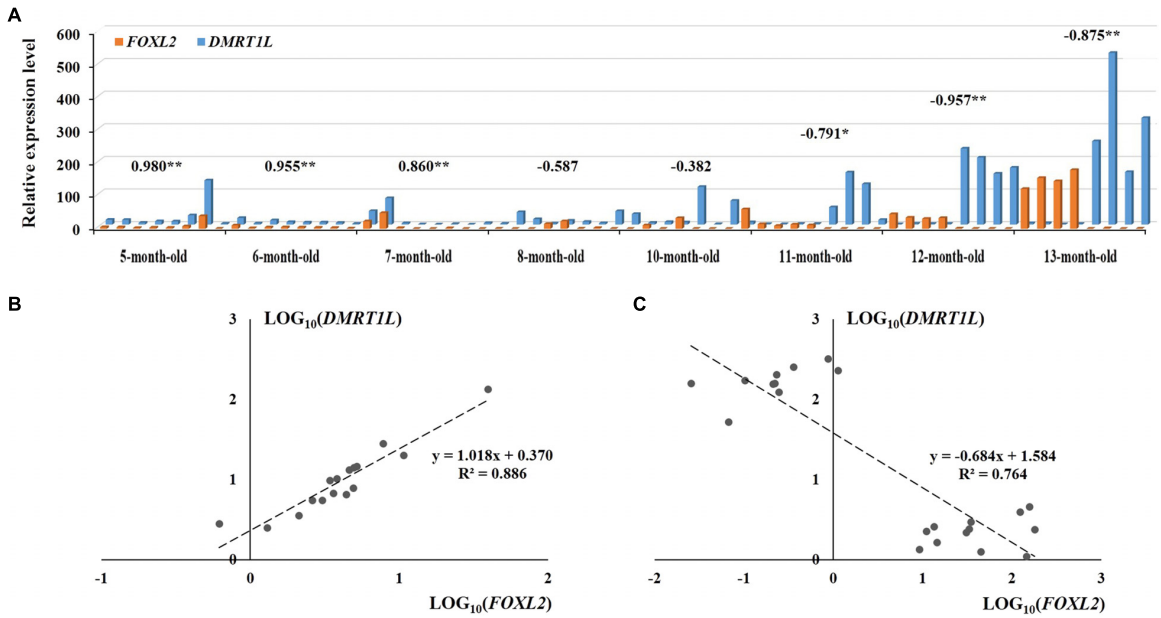

FIGURE 6 | The expression patterns of *FOXL2* and *DMRT1L* in juvenile scallops 5–13 months old. **(A)** The samples correspond to those in **Figure 5A**. The numbers above the bars are the correlation coefficients between LOG_{10}(*FOXL2*) and LOG_{10}(*DMRT1L*) in the particular months. "*" indicates $P < 0.05$; "**" indicates $P < 0.01$. **(B)** The positive correlation between LOG_{10}(*FOXL2*) and LOG_{10}(*DMRT1L*) for 5- to 6-month-old undifferentiated gonads. **(C)** The negative correlation between LOG_{10}(*FOXL2*) and LOG_{10}(*DMRT1L*) for 11- to 13-month-old differentiated gonads.

the ovary and testis thresholds, which could contribute to a better understanding of the molecular mechanisms underlying sex reversal.

Based on the histological analysis, we found that the developmental process of juvenile gonads can be classified into four stages, namely, undifferentiated, differentiated, growing, and maturation stages, which are consistent with the documentation by Shumway and Parsons (2016). Combined with the dynamic changes of LOG_{10}(*DMRT1L*/*FOXL2*) in juvenile scallops, we found that sex differentiation occurs earlier at the molecular level than at the histological level, which is similar to the findings in other organisms (Siegfried, 2010; Haugen et al., 2012; Ayers et al., 2013; Robledo et al., 2015; Tao et al., 2018). In addition, our study shows that although the onset of molecular sex differentiation varies between individuals, it always occurs from 7 to 10 months of age, and almost all of the scallops investigated completed differentiation before 11 months of age. This falls within the time frame of gonadal differentiation documented by Shumway and Parsons (2016) (between 4 months old and 1 year old). It suggests that LOG_{10}(*DMRT1L*/*FOXL2*) allows early identification of sex, and is a convenient and accurate way to assess the molecular sex differentiation period. This opens a gate for unraveling the regulatory network of sex differentiation in the Yesso scallop.

The coexpression patterns of *FOXL2* and *DMRT1L* are different before and after gonadal differentiation. Before differentiation, *FOXL2* and *DMRT1L* are relatively low but display unexpected coordinated expression patterns. Combined with the histological results showing that the follicles have not yet formed at this stage, we assume these two genes may coexpress in GSCs that are dispersed in the connective tissues. Sex differentiation co-occurs with the formation of follicles, in which relative expression of *FOXL2* vs *DMRT1L* changes, possibly leading to the differentiation of undifferentiated germ cells into spermatogonia or oogonia. Therefore, we speculate that in Yesso scallops, the undifferentiated gonads directly differentiate into either ovaries or testes. This challenges a previous opinion regarding the existence of sex reversal from male to female through an undifferentiated stage (Maru, 1978). In particular, some researchers claimed that Yesso scallops grow as males at less than one year of age; sex is thereafter reversed to female through an undifferentiated or ambiguous status in half of the scallops, resulting in a sex ratio close to 1:1; after sex reversal, the sex may become stable throughout successive periods of life (Mori et al., 1977; Maru, 1978; Otani et al., 2017). Considering that these studies are generally based on macroscopic observation of gonadal color (testis with white color, ovary with orange or pink color), which could be misleading in some cases, we assume that findings of sex reversal in Yesso scallops may be an artifact. However, since environmental factors have been demonstrated to be involved in the sex determination of many bivalves, we cannot rule out the possibility that the Yesso scallop does undergo sex reversal in Japan.

AUTHOR CONTRIBUTIONS

LinZ and SW conceived and designed the experiments. RL, WL, and YZ performed the experiments. YL, MZ, LiaZ, and XH

collected the samples. RL and LinZ analyzed the data. RL, LinZ, SW, and ZB wrote the paper. All authors read and approved the final manuscript.

FUNDING

This work was supported by the National Natural Science Foundation of China (Grant Nos. 31572600, U1706203, and 2018A07) and Fundamental Research Funds for the Central Universities (Grant Nos. 201762001 and 201841001).

SUPPLEMENTARY MATERIAL

The Supplementary Material for this article can be found online at: https://www.frontiersin.org/articles/10.3389/fphys.2018.01166/full#supplementary-material

REFERENCES

Ayers, K. L., Davidson, N. M., Demiyah, D., Roeszler, K. N., Grützner, F., Sinclair, A. H., et al. (2013). RNA sequencing reveals sexually dimorphic gene expression before gonadal differentiation in chicken and allows comprehensive annotation of the W-chromosome. *Genome Biol.* 14:R26. doi: 10.1186/gb-2013-14-3-r26

Bull, J. J. (1983). *Evolution of Sex Determining Mechanisms*. Menlo Park, CA: Benjamin/Cummings Publishing Company, Inc.

Cocquet, J., Pailhoux, E., Jaubert, F., Servel, N., Xia, X., Pannetier, M., et al. (2002). Evolution and expression of FOXL2. *J. Med. Genet.* 39, 916–921. doi: 10.1136/jmg.39.12.916

Feng, Z., Shao, M., Sun, D., and Zhang, Z. (2010). Cloning, characterization and expression analysis of Cf-dmrt4-like gene in *Chlamys farreri*. *J. Fish. Sci. China* 17, 930–940.

Goodwin, E. B., and Ellis, R. E. (2002). Turning clustering loops: sex determination in *Caenorhabditis elegans*. *Curr. Biol.* 12, R111–R120. doi: 10.1016/S0960-9822(02)00675-9

Haugen, T., Almeida, F. F., Andersson, E., Bogerd, J., Male, R., Skaar, K. S., et al. (2012). Sex differentiation in Atlantic cod (*Gadus morhua* L.): morphological and gene expression studies. *Reprod. Biol. Endocrinol.* 10:47. doi: 10.1186/1477-7827-10-47

Herpin, A., and Schartl, M. (2011). Sex determination: switch and suppress. *Curr. Biol.* 21, R656–R659. doi: 10.1016/j.cub.2011.07.026

Heule, C., Göppert, C., Salzburger, W., and Böhne, A. (2014). Genetics and timing of sex determination in the East African cichlid fish *Astatotilapia burtoni*. *BMC Genet.* 15:140. doi: 10.1186/s12863-014-0140-5

Hong, C. S., Park, B. Y., and Saintjeannet, J. P. (2007). The function of Dmrt genes in vertebrate development: it is not just about sex. *Dev. Biol.* 310, 1–9. doi: 10.1016/j.ydbio.2007.07.035

Huang, X., Hong, C. S., O'Donnell, M., and Saintjeannet, J. P. (2005). The doublesex-related gene, XDmrt4, is required for neurogenesis in the olfactory system. *Proc. Natl. Acad. Sci. U.S.A.* 102, 11349–11354. doi: 10.1073/pnas.0505106102

Kocer, A., Reichmann, J., Best, D., and Adams, I. R. (2009). Germ cell sex determination in mammals. *Mol. Hum. Reprod.* 15, 205–213. doi: 10.1093/molehr/gap008

Kopp, A. (2012). Dmrt genes in the development and evolution of sexual dimorphism. *Trends Genet.* 28, 175–184. doi: 10.1016/j.tig.2012.02.002

Larkin, M. A., Blackshields, G., Brown, N. P., Chenna, R. M., Mcgettigan, P. A., Mcwilliam, H., et al. (2007). Clustal W. clustal X version 2.0. *Bioinformatics* 23, 2947–2948. doi: 10.1093/bioinformatics/btm404

Li, H., Liu, J., Huang, X., Wang, D., and Zhang, Z. (2014a). Characterization, expression and function analysis of DAX1 gene of scallop (*Chlamys farreri* Jones and Preston 1904) during its gametogenesis. *J. Ocean Univ. China* 13, 696–704. doi: 10.1007/s11802-014-2299-9

Li, H., Zhang, Z., Bi, Y., Yang, D., Zhang, L., and Liu, J. (2014b). Expression characteristics of β-catenin in scallop Chlamys farreri gonads and its role as a potential upstream gene of Dax1 through canonical Wnt signalling pathway regulating the spermatogenesis. *PLoS One* 9:e115917. doi: 10.1371/journal.pone.0115917

Li, H., Liu, J., Liu, X., and Zhang, Z. (2013). Molecular cloning and expression analysis of wnt4 cDNA from the Zhikong scallop *Chlamys farreri*. *J. Fish. Sci. China* 20, 260–268.

Li, Y., Zhang, L., Sun, Y., Ma, X., Wang, J., Li, R., et al. (2016). Transcriptome sequencing and comparative analysis of ovary and testis identifies potential key sex-related genes and pathways in scallop patinopecten yessoensis. *Mar. Biotechnol.* 18, 453–465. doi: 10.1007/s10126-016-9706-8

Liu, X. L., Li, Y., Liu, J. G., Cui, L. B., and Zhang, Z. F. (2014). Gonadogenesis in scallop *Chlamys farreri* and Cf-foxl2 expression pattern during gonadal sex differentiation. *Aquac. Res.* 47, 1605–1611. doi: 10.1111/are.12621

Liu, X.-L., Zhang, Z.-F., Shao, M.-Y., Liu, J.-G., and Muhammad, F. (2012). Sexually dimorphic expression of foxl2 during gametogenesis in scallop *Chlamys farreri*, conserved with vertebrates. *Dev. Genes Evol.* 222, 279–286. doi: 10.1007/s00427-012-0410-z

Maru, K. (1978). Studies on the reproduction of a scallop, *Patinopecten yessoensis* (Jay), 2: gonad development in 1-year-old scallops. *Sci. Rep. Hokkaido Fish. Exp. Stn.* 20, 13–26.

Matson, C. K., Murphy, M. W., Sarver, A. L., Griswold, M. D., Bardwell, V. J., and Zarkower, D. (2011). DMRT1 prevents female reprogramming in the postnatal mammalian testis. *Nature* 476, 101–104. doi: 10.1038/nature10239

Matson, C. K., and Zarkower, D. (2012). Sex and the singular DM domain: insights into sexual regulation, evolution and plasticity. *Nat. Rev. Genet.* 13, 163–174. doi: 10.1038/nrg3161

Mori, K., Sato, R., and Osanai, K. (1977). Seasonal gonad changes in scallops under culture in Toni Bay, Iwate Prefecture [Japan]. *Bull. Jpn. Soc. Sci. Fish.* 43, 1–8. doi: 10.2331/suisan.43.1

Nagasawa, K., Oouchi, H., Itoh, N., Takahashi, K. G., and Osada, M. (2015). In Vivo administration of scallop gnrh-like peptide influences on gonad development in the yesso Scallop, *Patinopecten yessoensis*. *PLoS One* 10:e0129571. doi: 10.1371/journal.pone.0129571

Naimi, A., Martinez, A.-S., Specq, M.-L., Diss, B., Mathieu, M., and Sourdaine, P. (2009a). Molecular cloning and gene expression of Cg-Foxl2 during the development and the adult gametogenetic cycle in the oyster *Crassostrea gigas*. *Comp. Biochem. Physiol. B Biochem. Mol. Biol.* 154, 134–142. doi: 10.1016/j.cbpb.2009.05.011

Naimi, A., Martinez, A.-S., Specq, M.-L., Mrac, A., Diss, B., Mathieu, M., et al. (2009b). Identification and expression of a factor of the DM family in the oyster *Crassostrea gigas*. *Comp. Biochem. Physiol. A Mol. Integr. Physiol.* 152, 189–196. doi: 10.1016/j.cbpa.2008.09.019

Ni, J., Zeng, Z., Han, G., Huang, H., and Ke, C. (2012). Cloning and characterization of the follistatin gene from *Crassostrea angulata* and its expression during the reproductive cycle. *Comp. Biochem. Physiol. B Biochem. Mol. Biol.* 163, 246–253. doi: 10.1016/j.cbpb.2012.06.006

Nothiger, R., Leuthold, M., Andersen, N., Gerschwiler, P., Gruter, A., Keller, W., et al. (1987). Genetic and developmental analysis of the sex-determining gene 'double sex' (dsx) of *Drosophila melanogaster*. *Genet. Res.* 50, 113–123. doi: 10.1017/S001667230002351X

Osada, M., Harata, M., Kishida, M., and Kijima, A. (2004). Molecular cloning and expression analysis of vitellogenin in scallop, *Patinopecten yessoensis* (*Bivalvia, mollusca*). *Mol. Reprod. Dev.* 67, 273–281. doi: 10.1016/j.dci.2014.12.004

Otani, A., Nakajima, T., Okumura, T., Fujii, S., and Tomooka, Y. (2017). Sex reversal and analyses of possible involvement of sex steroids in scallop gonadal development in newly established organ-culture systems. *Zoolog. Sci.* 34, 86–92. doi: 10.2108/zs160070

Ottolenghi, C., Pelosi, E., Tran, J., Colombino, M., Douglass, E., Nedorezov, T., et al. (2007). Loss of Wnt4 and Foxl2 leads to female-to-male sex reversal extending to germ cells. *Hum. Mol. Genet.* 16, 2795–2804. doi: 10.1093/hmg/ddm235

Patnaik, B. B., Wang, T. H., Kang, S. W., Hwang, H.-J., Park, S. Y., Park, E. B., et al. (2016). Sequencing, de novo assembly, and annotation of the transcriptome of the endangered freshwater pearl bivalve, *Cristaria plicata*, provides novel

insights into functional genes and marker discovery. *PLoS One* 11:e0148622. doi: 10.1371/journal.pone.0148622

Penman, D. J., and Piferrer, F. (2008). Fish gonadogenesis. Part I: genetic and environmental mechanisms of sex determination. *Rev. Fish. Sci.* 16, 16–34. doi: 10.1080/10641260802324610

Picard, M. A. L., Cosseau, C., Mouahid, G., Duval, D., Grunau, C., Toulza, È, et al. (2015). The roles of *Dmrt* (double sex/male-abnormal-3 related transcription factor) genes in sex determination and differentiation mechanisms: ubiquity and diversity across the animal kingdom. *C. R. Biol.* 338, 451–462. doi: 10.1016/j.crvi.2015.04.010

Piferrer, F., and Guiguen, Y. (2008). Fish gonadogenesis. Part II: molecular biology and genomics of sex differentiation. *Rev. Fish. Sci.* 16, 35–55. doi: 10.1080/10641260802324644

Reitzel, A. M., Pang, K., and Martindale, M. Q. (2016). Developmental expression of "germline"- and "sex determination"-related genes in the ctenophore *Mnemiopsis leidyi*. *Evodevo* 7:17. doi: 10.1186/s13227-016-0051-9

Robledo, D., Ribas, L., Cal, R., Sánchez, L., Piferrer, F., Martínez, P., et al. (2015). Gene expression analysis at the onset of sex differentiation in turbot (*Scophthalmus maximus*). *BMC Genomics* 16:973. doi: 10.1186/s12864-015-2142-8

Santerre, C., Sourdaine, P., Adeline, B., and Martinez, A.-S. (2014). Cg-SoxE and Cg-β-catenin, two new potential actors of the sex-determining pathway in a hermaphrodite lophotrochozoan, the Pacific oyster *Crassostrea gigas*. *Comp. Biochem. Physiol. A Mol. Integr. Physiol.* 167, 68–76. doi: 10.1016/j.cbpa.2013.09.018

Santerre, C., Sourdaine, P., Marc, N., Mingant, C., Robert, R., and Martinez, A.-S. (2013). Oyster sex determination is influenced by temperature—first clues in spat during first gonadic differentiation and gametogenesis. *Comp. Biochem. Physiol. A Mol. Integr. Physiol.* 165, 61–69. doi: 10.1016/j.cbpa.2013.02.007

Shi, Y., Wang, Q., and He, M. (2014). Molecular identification of dmrt2 and dmrt5 and effect of sex steroids on their expressions in *Chlamys nobilis*. *Aquaculture* 426, 21–30. doi: 10.1016/j.aquaculture.2014.01.021

Shumway, S. E., and Parsons, G. J. (2016). *Scallops: Biology, Ecology, Aquaculture, and Fisheries*. New York, NY: Elsevier.

Siegfried, K. R. (2010). In search of determinants: gene expression during gonadal sex differentiation. *J. Fish Biol.* 76, 1879–1902. doi: 10.1111/j.1095-8649.2010.02594.x

Smith, C. A., Roeszler, K. N., Ohnesorg, T., Cummins, D. M., Farlie, P. G., Doran, T. J., et al. (2009). The avian Z-linked gene DMRT1 is required for male sex determination in the chicken. *Nature* 461, 267–271. doi: 10.1038/nature08298

Swain, A., and Lovell-Badge, R. (1999). Mammalian sex determination: a molecular drama. *Genes Dev.* 13, 755–767. doi: 10.1101/gad.13.7.755

Tamura, K., Stecher, G., Peterson, D., Filipski, A., and Kumar, S. (2013). MEGA6: molecular evolutionary genetics analysis version 6.0. *Mol. Biol. Evol.* 30, 2725–2729. doi: 10.1093/molbev/mst197

Tanabe, T., Yuan, Y., Nakamura, S., Itoh, N., Takahashi, K. G., and Osada, M. (2010). The role in spawning of a putative serotonin receptor isolated from the germ and ciliary cells of the gonoduct in the gonad of the Japanese scallop, *Patinopecten yessoensis*. *Gen. Comp. Endocrinol.* 166, 620–627. doi: 10.1016/j.ygcen.2010.01.014

Tao, W., Chen, J., Tan, D., Yang, J., Sun, L., Wei, J., et al. (2018). Transcriptome display during tilapia sex determination and differentiation as revealed by RNA-Seq analysis. *BMC Genomics* 19:363. doi: 10.1186/s12864-018-4756-0

Teaniniuraitemoana, V., Huvet, A., Levy, P., Gaertner-Mazouni, N., Gueguen, Y., and Le Moullac, G. (2015). Molecular signatures discriminating the male and the female sexual pathways in the pearl oyster *Pinctada margaritifera*. *PLoS One* 10:e0122819. doi: 10.1371/journal.pone.0122819

Teaniniuraitemoana, V., Huvet, A., Levy, P., Klopp, C., Lhuillier, E., Gaertner-Mazouni, N., et al. (2014). Gonad transcriptome analysis of pearl oyster *Pinctada margaritifera*: identification of potential sex differentiation and sex determining genes. *BMC Genomics* 15:491. doi: 10.1186/1471-2164-15-491

Tong, Y., Zhang, Y., Huang, J., Xiao, S., Zhang, Y., Li, J., et al. (2015). Transcriptomics analysis of *Crassostrea hongkongensis* for the discovery of reproduction-related genes. *PLoS One* 10:e0134280. doi: 10.1371/journal.pone.0134280

Uhlenhaut, N. H., Jakob, S., Anlag, K., Eisenberger, T., Sekido, R., Kress, J., et al. (2009). Somatic sex reprogramming of adult ovaries to testes by FOXL2 ablation. *Cell* 139, 1130–1142. doi: 10.1016/j.cell.2009.11.021

Wang, S., Zhang, J., Jiao, W., Li, J., Xun, X., Sun, Y., et al. (2017). Scallop genome provides insights into evolution of bilaterian karyotype and development. *Nat. Ecol. Evol.* 1:0120. doi: 10.1038/s41559-017-0120

Yang, M., Xu, F., and Liu, J. (2015). Molecular cloning and expression of Wnt4 gene in pacific oyster *Crassostrea gigas*. *Oceanol. Limnol. Sin.* 46, 35–42.

Yu, F.-F., Wang, M.-F., Zhou, L., Gui, J.-F., and Yu, X.-Y. (2011). Molecular cloning and expression characterization of Dmrt2 in Akoya pearl oysters, *Pinctada martensii*. *J. Shellfish Res.* 30, 247–254. doi: 10.2983/035.030.0208

Yu, J., Zhang, L., Li, Y., Li, R., Zhang, M., Li, W., et al. (2017). Genome-wide identification and expression profiling of the SOX gene family in a bivalve mollusc *Patinopecten yessoensis*. *Gene* 627, 530–537. doi: 10.1016/j.gene.2017.07.013

Zarkower, D. (2001). Establishing sexual dimorphism: conservation amidst diversity? *Nat. Rev. Genet.* 2, 175–185. doi: 10.1038/35056032

Zhang, N., Xu, F., and Guo, X. (2014). Genomic analysis of the Pacific oyster (*Crassostrea gigas*) reveals possible conservation of vertebrate sex determination in a mollusc. *G3* 4, 2207–2217. doi: 10.1534/g3.114.013904

Conflict of Interest Statement: The authors declare that the research was conducted in the absence of any commercial or financial relationships that could be construed as a potential conflict of interest.

frontiers in Physiology

ORIGINAL RESEARCH
published: 26 November 2018
doi: 10.3389/fphys.2018.01674

Comparison of the Biochemical Composition and Nutritional Quality Between Diploid and Triploid Hong Kong Oysters, *Crassostrea hongkongensis*

Yanping Qin[1,2,3], *Yuehuan Zhang*[1,2]*, *Haitao Ma*[1,2], *Xiangwei Wu*[1,2,3], *Shu Xiao*[1,2], *Jun Li*[1,2], *Riguan Mo*[1,2,3] *and Ziniu Yu*[1,2]*

[1] *Key Laboratory of Tropical Marine Bio-Resources and Ecology, Guangdong Provincial Key Laboratory of Applied Marine Biology, South China Sea Institute of Oceanology, Chinese Academy of Sciences, Guangzhou, China,* [2] *South China Sea Bio-Resource Exploitation and Utilization Collaborative Innovation Center, Guangzhou, China,* [3] *University of Chinese Academy of Sciences, Beijing, China*

OPEN ACCESS

Edited by:
Xiaotong Wang,
Ludong University, China

Reviewed by:
Lorenzo Gallus,
Università di Genova, Italy
Filippo Garofalo,
Università della Calabria, Italy
Weiwei You,
Xiamen University, China

***Correspondence:**
Yuehuan Zhang
yhzhang@scsio.ac.cn
Ziniu Yu
carlzyu@scsio.ac.cn

Specialty section:
This article was submitted to Aquatic Physiology, a section of the journal Frontiers in Physiology

Received: *28 August 2018*
Accepted: *08 November 2018*
Published: *26 November 2018*

Citation:
Qin Y, Zhang Y, Ma H, Wu X, Xiao S, Li J, Mo R and Yu Z (2018) Comparison of the Biochemical Composition and Nutritional Quality Between Diploid and Triploid Hong Kong Oysters, Crassostrea hongkongensis. Front. Physiol. 9:1674. doi: 10.3389/fphys.2018.01674

This study is the first systematic comparison of the biochemical composition and nutritional quality between diploid and triploid Hong Kong oysters, *Crassostrea hongkongensis*. Results showed that in the reproductive season, the glycogen content in five tissues (gill, mantle, adductor muscle, labial palps and gonad) was significantly higher ($P < 0.05$) in triploids than in diploids, with odds ratios (ORs) of 96.26, 60.17, 72.59, 53.56, and 128.52%, respectively. In the non-reproductive phase, significant differences in glycogen content ($P < 0.05$) between diploid and triploid oysters existed only in gill and gonad. In both diploid and triploid Hong Kong oysters, quantitative real-time PCR analysis of the glycogen synthesis gene (*Ch*GS) and glycogen phosphorylase gene (*Ch*GP) showed that the gene expression patterns matched the pattern of variation in glycogen content. Moreover, in both the reproductive and the non-reproductive phases, triploid Hong Kong oysters had a well balance of essential amino acids and were thus a well source of high-quality protein. Surprisingly, in both phases, significantly higher ($P < 0.05$) percentages of four essential fatty acids (α-linolenic acid, linoleic acid, eicosapentaenoic acid, and docosahexaenoic acid) were observed in triploids than in diploids. Additionally, the ratio of n-3/n-6 polyunsaturated fatty acids (PUFAs) was much higher in triploids than that in diploids. Variations in Biochemical composition were consistent with the relative expression of the citrate synthase gene (*Ch*CS) and the α-ketoglutarate dehydrogenase gene (*Ch*KD), which are key enzyme genes of the tricarboxylic acid cycle. Overall, the triploid Hong Kong oyster has a better nutritional value and taste than the diploid in terms of glycogen content, protein quality and fatty acid content.

Keywords: ***Crassostrea hongkongensis*, diploid, triploid, biochemical compositions, nutritional quality, metabolic pathways**

INTRODUCTION

Due to their rapid growth and maintaining good taste in the reproductive phase, many triploid bivalves have entered into commercial farming, including oysters (Allen and Downing, 1986; Houcke et al., 2016), scallops (Racotta et al., 2008), clams (Utting and Child, 1994; Shpigel and Spencer, 1996), and mussels (Zwaan and Zandee, 1972; Dare and Edwards, 1975). However, no solid comparative data is available on the differences in the biochemical compositions and nutritional qualities between diploid and triploid Hong Kong oysters, which are very important for promoting the application of triploid Hong Kong oysters in the industry. *Crassostrea hongkongensis* (Hong Kong oyster) is economically important and widely cultivated in southern China. However, like many other oyster species, diploid Hong Kong oysters have an inferior taste and low meat quality during the reproductive season (from May to August) each year, which can be attributed to gametogenesis (Lam and Morton, 2003; Bacca et al., 2005; Wang et al., 2015; Zhang et al., 2017). One way of solving these problems is to introduce the use of triploid oysters into the aquaculture industry (Stanley et al., 1981; Ren et al., 2003; Qin et al., 2017). Gametogenesis in triploids is retarded in the reproductive season, since triploid oysters have poorly developed gonads compared to diploids. According to previous studies on diploid *Tapes philippinarum* (Shpigel and Spencer, 1996), *Crassostrea gigas* (Soudant et al., 1999; Dridi et al., 2007; Pogoda et al., 2013), *Ostrea edulis* (Houcke et al., 2016), and *Crassostrea virginica* (Zeng et al., 2015), large changes in biochemical composition occur in response to gonad development.

Glycogen is the main molecular contributor to flavor quality in bivalves (Berthelin et al., 2000b; Racotta et al., 2008; Zhang et al., 2015). Glycogen content decreased is strongly linked with gonad development and gametogenesis in *C. gigas* (Berthelin et al., 2000b; Zeng et al., 2015). Various studies have confirmed glycogen synthesis and glycogen degradation can be altered by changes of the glycogen synthesis gene (*Ch*GS) and glycogen phosphorylase gene (*Ch*GP) (Greiwe et al., 1999; Bacca et al., 2005; Dridi et al., 2007). *Ch*GS and *Ch*GP are the key enzyme genes of glycogen synthesis and degradation, respectively, in *C. hongkongensis*. Bacca et al. (2005) confirmed that the expression level of glycogen synthase changed in a pattern consistent with seasonal variations in glycogen content in *C. gigas*, and the same phenomenon was also observed in *C. angulate* (Zeng et al., 2013).

Protein content play a important role in determing the nutritional value of food, and has a large effect on the market value (Manninen et al., 2018). At the same time, the essential amino acid composition is one of the most important factors determining the nutritional qualities of protein. Amino acid score is a good method of appraising protein quality by comparing a test amino acid content with that of the reference of the amino acid (Chen et al., 2007). When the amino acid score is calculated, it is compared to the amino acid requirements of young children. Amino acid scores are widely used for evaluating the nutritional quality of protein (Celik et al., 2004; Iqbal et al., 2006; Lv et al., 2018). In addition, it has been shown that amino acid composition is closely linked to gonad development in *C. gigas* (Kong et al., 2001; Dridi et al., 2007) and *Mytilus edulis* (Su et al., 1998).

Four essential fatty acids, namely α-linolenic acid (ALA, 18:3n-3), linoleic acid (LA, 18:2n-6), eicosapentaenoic acid (EPA, 20:5n-3), and docosahexaenoic acid (DHA, 22:6n-3) are very important for human health (Dyerberg, 1986; Coetzee and Hoffman, 2002). The nutritional quality of food is to a great extent associated with the ratio of n-3/n-6 polyunsaturated fatty acids (PUFAs). Several sources of information confirm that a higher ratio of n-3/n-6 PUFAs is desirable to reduce the incidence of many diseases (such as cardiovascular disease, asthma, breast cancer) in modern societies, especially in developed countries (Coetzee and Hoffman, 2002; Simopoulos, 2008). However, many peoples' diets are deficient in n-3 PUFAs and have excessive amounts of n-6 PUFAs (Park et al., 1994). Seafood is well known as a rich source of n-3 PUFAs, and some types of seafood have a high ratio of n-3/n-6 PUFAs (Soudant et al., 1999; Skonberg and Perkins, 2002; Celik et al., 2004; Chen et al., 2007). According to Dridi et al. (2007), PUFAs were always the dominant fatty acids in *C. gigas* throughout the year, and the ratio of n-3/n-6 PUFAs ranged from 2.45 to 3.15, indicating that *C. gigas* was a relatively nutritious food. Many researchers have found a relationship between variations in the ratio of n-3/n-6 PUFAs and gonad development; Dridi et al. (2007) confirmed that the maximum docosahexaenoic acid levels corresponded with oocyte maturation in *C. gigas*. Ojea et al. (2004) found that neutral and polar lipids increased during the period of maximum ripeness and decreased during spawning of *Ruditapes decussatus*, while Orban et al. (2002) reported high levels of n-3 polyunsaturated fatty acids during spawning of *Mytilus galloprovincialis*. However, as yet there is no study on the relationship between fatty acid composition and gonad development in *C. hongkongensis*. Our study aims to compare and assess the performance of diploid and triploid oysters during the reproductive and non-reproductive phases, from a biochemical and nutritional point of view. In addition, by illustrating the relationships between variations in biochemical composition and the gonad development of Hong Kong oysters, this study will provide important information for the application of triploid Hong Kong oysters in the aquaculture industry.

MATERIALS AND METHODS

Sample Collection and Ploidy Determination

Diploid and triploid Hong Kong oysters for use in this study were collected from Beihai, Guangxi Province, China. Triploid Hong Kong oysters were induced by blocking the release of the second polar body (PB2) in fertilized eggs using 0.5 $mg.L^{-1}$ Cytochalasin B in this research (Wang et al., 2002; Qin et al., 2017). Both diploid and triploid oysters used in this study were descendants from the same base population and were cultured under the same environmental conditions. Large numbers of triploid and diploid oysters were collected in December 2016 (non-reproductive phase) and July 2017 (reproductive phase). The oysters collected in July 2017 were at the stage 3B of gonad

development, during which the gonads of diploid oysters were dramatically developed morphologically ripe, covering all of the visceral mass, the soft parts were extremely full, and the gametes immediately scattered when put into seawater. The gonads of oysters collected in December 2016 were at stage 0. At this stage, the gonads of the oysters remained inactive and undifferentiated, and the soft parts were clear and colorless (Allen and Downing, 1986; Ojea et al., 2004; Dridi et al., 2007).

According to the protocols developed by Downing and Allen (1987) and Qin et al. (2018), the ploidy status of each individual oyster was determinated using flow cytometry using a CyFlow Ploidy Analyser (Sysmex). Then, subsamples of gill, mantle, adductor muscle, labial palps, and gonad tissue were stored at −80°C for glycogen and protein content analysis, and all tissues were lyophilized before use. The tissues were mingled to create mixed samples from 10 individuals of the same ploidy status. The same individuals used for glycogen content determination were also used for related gene expression analysis. Five tissue samples were immediately dissected from each oyster, placedin 1 mL Trizol and wholly ground with a homogenizer, then frozen at −80°C. For amino acid and fatty acid analysis of the whole oysters, three pools each of 10 diploids and 10 triploids were collected and immediately dissected, then freeze dried. All analyses were done in triplicate.

Glycogen and Protein Content Analyses

The glycogen content of the five lyophilized tissues of diploids and triploids, was analyzed using a kit for detecting glycogen content (Nanjing Jiancheng Bioengineering Institute).The kit was used according to the following procedure: after 1 mg dry weight (DW) of tissue was ground into a powder in the presence of liquid nitrogen, a 0.50 μg sample was added to a tube containing alkaline liquid. Then, the tube was heated at 100°C for 20 min in a water bath. After that, the hydrolysate was diluted 16-fold by adding sterile water. Subsequently, 2 mL of color reagent was added to the diluted hydrolysate and the samples were heated for 5 min at a 100°C in a water bath. Finally, the OD value of each sample was measured at 620 nm using a Multimode Plate Reader (Ensight) after setting the blank and standard for each group. The glycogen content was calculated according to the following formula:

$$\text{Glycogen content (mg/g, DW)} = \left(\frac{\text{OD of test group} - \text{OD of blank group}}{\text{OD of standard group} - \text{OD of blank group}}\right) \times 0.01 \times 20 \times 10 \div 1.11$$

For protein content analyses, the lyophilized tissues were wholly ground with a homogenizer and then analyzed using a fully automatic Kjeldahl analyzer (PeiOU, Skd-800). Finally, protein content was calculated by multiplying nitrogen content by a factor of 6.25 (Iqbal et al., 2006).

Amino Acid and Fatty Acid Content Assays

Amino acid analyses were performed according to the method of Chen and Zhang (Hugli and Moore, 1972; Chen and Zhang, 2007; Chen et al., 2007). Lyophilized meat samples of diploid and triploid Hong Kong oysters (three pools of 10 oysters from each group) were weighed (0.0150–0.0250 g), placed in 15 mL ampoules, and 8 mL of (6.0 N) HCl was added. Ampoules were vacuum sealed, and samples were hydrolyzed at 110°C for 24 h. Following hydrolysis, 1 mL of hydrolyzate was withdrawn and evaporated to dryness under vacuum at 45°C to remove HCl. The hydrolyzate was dissolved in 5 mL of 0.02 N HCl, and then centrifuged at 5,000 rpm and filtered. One microliter of supernatant was used for amino acid analysis. The identity and quantity of the amino acids were determined by comparison with the retention times and peak areas of each amino acid standard. The tryptophan content was determined by Guangdong Food Quality Supervision Inspection Station according to GB 5009.168-2016.

Fatty acids were analyzed according to Doan et al. (2018). In brief, 10 mg of dry tissue was dissolved in 1 mL of petroleum ether. Then, 25 μL of 2 M sodium methanolate methanol solution was added, and the closed vial was agitated vigorously for 1 min. About 20 μL of water was added, and after centrifugation the aqueous phase was removed. Then 20 μL methyl orange in 0.1 N HCl was added as a pH indicator. The mixture was agitated carefully and the derivatives were analyzed using a Hewlett-Packard Gas Chromatography Instrument.

Real-Time Quantitative PCR Analysis of Genes

According to the sequence of the *C. gigas* glycogen synthesis gene (Genbank accession bank number: NM001308922.1), glycogen phosphorylase gene (Genbank accession bank number: NM001305341.1), citrate synthase gene (Genbank accession bank number: XM011429904.2), and α-ketoglutarate dehydrogenase gene (Genbank accession bank number: XM011437307.2), and a BLAST analysis of all EST sequences from a *C. hongkongensis* hemocyte EST library which was constructed and sequenced by our lab, the open reading frames (ORF) of *Ch*GS, *Ch*GP, *Ch*CS, and *Ch*KD have already been obtained. The temporal expression of the genes in various tissues (gill, mantle, labial palps, muscle, and gonad) of the oysters during the reproductive and non-reproductive phases were investigated using real-time quantitative PCR (qPCR) analysis. We designed gene-specific primers (**Table 1**) based on ORF to amplify gene fragments ∼250 bp in length. Amplifications of actin and elongation factor 1α gene (EF1α) fragments were performed in order to confirm the steady-state level of expression of housekeeping genes, providing an internal reference for gene expression (Zhou et al., 2018).

The real-time PCR amplifications were carried out in triplicate in a total volume of 10 μL with 5 μL of 2 × Real Star Green Power mixture (Genstar), 0.50 μM each of forward and reverse primers, 1 μL of the 1:20 diluted cDNA using Light Cycler 480II (Roche). The PCR protocol was: 95°C for 10 min, followed by 40 cycles of 95°C for 15 s, 60°C for 30 s, and 72°C for 30 s. The relative expression ratio (R) of each target gene was calculated based on the threshold value (Ct) deviation of this target gene from the housekeeping gene, corresponding to the copy number of the target gene relative to the copy number of the housekeeping

TABLE 1 | Sequences of designed primers used in this study.

Primer	Sequence (5′ → 3′)	Comment
*Ch*GS-F	TCGGCTGGGAGATATGAGTT	qPCR of *Ch*GS
*Ch*GS-R	AGTTGTTGGTCTTGGTGGGG	
*Ch*GP-F	ACCACGAGAAGCGAAAGCAAATCAG	qPCR of *Ch*GP
*Ch*GP-R	CGGTGTCGCCACATTTCTATCTTTC	
*Ch*KD-F	TACTCTGGCTCGTCTCGT	qPCR of *Ch*KD
*Ch*KD-R	GCACATTCAGTCTCCCTCT	
*Ch*CS-F	TCTCCTCTCCCCAACCAT	qPCR of *Ch*CS
*Ch*CS-R	TAATGGCAGCAATGGTGG	
EFLα-F	CGGGATCCATGTATAGTCGGGAGA	qPCR of EFLα
EFLα-R	CCCAAGCTTTCACAGAGAAATCAA	

"F" indicates forward primers and "R" indicates reverse primers.

gene. So, the following formula was used:

$$R = 2^{-(Ct_{target\ gene} - Ct_{housekeeping\ gene})}$$

Statistical Analysis

All data are presented as mean ± standard deviation (SD). Multiple comparisons of the relative expression levels of target genes and biochemical makeup of different tissues from diploid and triploid oysters during the reproductive and non-reproductive phases were performed using one-way analysis of variance (ANOVA) followed by a multiple comparison test with the LSD-*t*-test using Statistical Package for the Social Sciences (SPSS18). $P < 0.05$ was considered significant, while $P < 0.01$ was considered extremely significant.

The odds ratio (OR) is defined as the percent difference in the biochemical components (glycogen, fatty acid, and amino acid contents) between the diploid (2N) and the triploid oyster (3N) performances and is calculated using the following formula (Callam et al., 2016):

$$\text{OR}\ (\%) = \left(\frac{3N - 2N}{2N}\right) \times 100$$

where a positive OR indicates that the triploid oysters performed better than the diploids, and a negative OR indicates that the triploids performed worse.

The essential amino acid score was calculated with reference to the FAO/WHO reference amino acid pattern for preschool children (2–5 years old) (FAO/WHO/UNU, 1985), according to the following formula:

$$\text{Amino acid score} = \left(\frac{\text{Test amino acid}}{\text{Reference amino acid}}\right) \times 100$$

The reason for using the requirements of young children as a reference is that, if the amino acid composition of proteins can adequately support the healthy growth of preschool children, it will be more than adequate for adults (Kirimura et al., 1969; Gatenby et al., 2003).

RESULTS

Glycogen Content and *Ch*GS and *Ch*GP mRNA Expressions

In the non-reproductive phase (December), the average glycogen content of diploids was 36.20 ± 8.59 mg/g DW in the muscle, 37.25 ± 2.98 mg/g DW in the mantle, 57.89 ± 3.88 mg/g DW in the gill, 176.69 ± 10.80 mg/g DW in the gonad, and 178.49 ± 17.41 mg/g DW in the labial palps. In triploids, the average glycogen content was 35.93 ± 4.55 mg/g DW in the muscle, 39.96 ± 7.78 mg/g DW in the mantle, 68.35 ± 3.62 mg/g DW in the gill, 185.19 ± 30.42 mg/g DW in the labial palps, and 226.03 ± 6.70 mg/g DW in the gonad (**Figure 1A**). There were statistically significant differences in gill and gonad glycogen content between diploids and triploids ($P < 0.05$), with ORs of 18.07 and 27.92%, respectively (**Table 2**). In the non-reproductive phase, triploids showed highly significant elevations in ChGS and ChGP expressions in tissues compared to diploids ($P < 0.01$) (**Figures 3A,B**).

However, in the reproductive season (July), the average glycogen content of diploids was 27.47 ± 1.81 mg/g DW in the muscle, 31.00 ± 6.45 mg/g DW in the gill, 34.30 ± 7.84 mg/g DW in the mantle, 86.39 ± 3.63 mg/g DW in the labial palps, and 88.87 ± 7.24 mg/g DW in the gonad. In triploids, the average glycogen content was 47.41 ± 10.46 mg/g DW in the muscle, 54.94 ± 4.55 mg/g DW in the mantle, 60.84 ± 3.64 mg/g DW in the gill, 132.66 ± 11.26 mg/g DW in the labial palps, and 203.09 ± 12.41 mg/g DW in the gonad. The glycogen content of all five tissues was significantly higher ($P < 0.05$) in triploids than in diploids (**Figure 1B**). The ORs of the five tissues (gill, mantle, muscle, labial lalps, and gonad) were 96.26, 60.17, 72.59, 53.56, and 128.52%, respectively (**Table 2**). In addition, we found that the glycogen content of some tissues was lower during the reproductive season than in the non-reproductive phase in diploid oysters, especially in the labial palps and gonad, which had ORs of −51.60 and −49.70% comparing the reproductive to the non-reproductive phase. By contrast, from the non-reproductive to the reproductive phase, the five triploid tissues had glycogen content ORs of −10.99, 37.49, 31.95, −28.37, and −10.15% (**Table 3**). In the reproductive phase, significantly higher ($P < 0.05$) expressions of *Ch*GS were observed in triploids than in diploids. In contrast, the expressions of *Ch*GP were significantly lower ($P < 0.05$) in triploids (**Figures 4A,B**).

Protein Content

According to our research, in the non-reproductive stage, the protein content ranged from 424.46 ± 16.00 (mantle) to 458.73 ± 6.77 mg/g DW (labial palps) in diploids and from 422.47 ± 13.78 (muscle) to 466.07 ± 8.87 mg/g DW (labial palps) in triploids, and there were no statistically significant differences in protein content between diploid and triploid oysters (**Figure 2A**, **Table 2**). In the reproductive phase, the protein content was lowest in the muscle tissue of both diploids and triploids, with 430.84 ± 16.05 and 421.79 ± 3.52 mg/g DW, respectively. Conversely, the protein content of diploid and triploid oysters was highest in the gonad and labial palps, respectively, with 491.23 ± 14.38 and 479.32 ± 7.23 mg/g DW. In addition, except

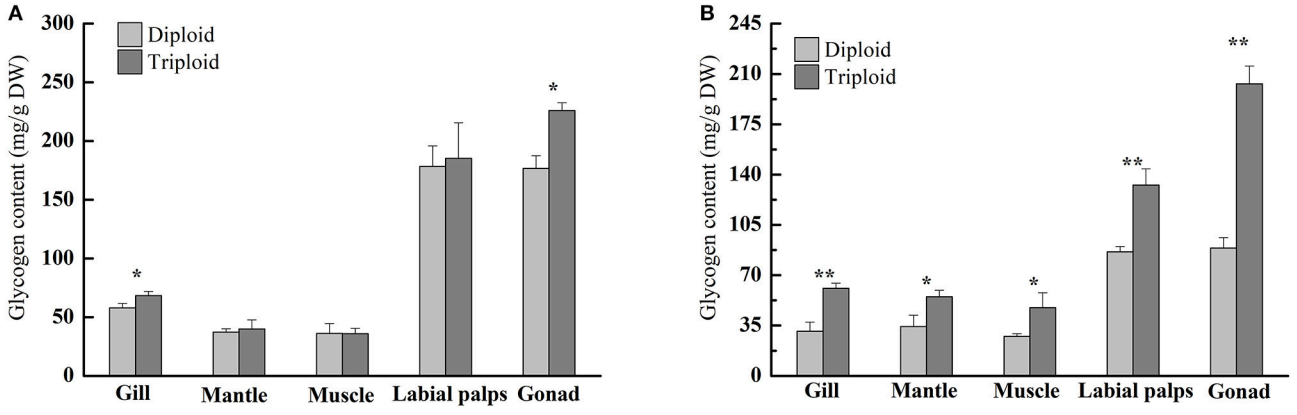

FIGURE 1 | Glycogen contents (mg/g, DW) of various tissues (gill, mantle, muscle, labial palps, and gonad) of diploid and triploid Hong Kong oysters, *Crassostrea hongkongensis*, in the non-reproductive phase **(A)** and reproductive phase **(B)**. Significant differences are indicated by asterisks (* and ** represent $P < 0.05$ and $P < 0.01$, respectively).

TABLE 2 | The odds ratios (ORs) of the glycogen and protein content of various tissues (gill, mantle, muscle, labial palps, and gonad) between diploid and triploid Hong Kong oysters, *Crassostrea hongkongensis*, in the non-reproductive and reproductive phases.

			Gill	Mantle	Muscle	Labial palps	Gonad
OR (%)	Glycogen	Non-reproductive	18.07	7.28	−0.75	3.75	27.92
		Reproductive	96.26	60.17	72.59	53.56	128.52
	Protein	Non-reproductive	−0.72	3.14	−1.67	1.60	0.52
		Reproductive	1.99	−0.22	−2.00	0.97	−11.41

TABLE 3 | The odds ratios (ORs) of the glycogen and protein content of various tissues (gill, mantle, muscle, labial palps, and gonad) of diploid and triploid Hong Kong oysters, *Crassostrea hongkongensis*, between the non-reproductive phase and the reproductive phase.

			Gill	Mantle	Muscle	Labial palps	Gonad
OR (%)	Glycogen	2N	−46.45	−7.92	−24.12	−51.60	−49.70
		3N	−10.99	37.49	31.95	−28.37	−10.15
	Protein	2N	1.03	8.57	0.18	3.49	17.72
		3N	3.79	5.03	−0.16	2.84	3.75

in the gonad ($P < 0.05$), there were no significant differences in the protein content between diploids and triploids in the reproductive phase (**Figure 2B**, **Table 2**).

Amino Acid and Fatty Acid Content

During the non-reproductive phase, the individual amino acid levels were highest for glutamic acid and lowest for methionine in both diploid and triploid oysters (**Table 4**). In the reproductive phase, the diploid Hong Kong oysters contained glutamic acid in the largest amounts (142.0 mg/g of protein), followed by aspartic acid, lysine, leucine, arginine, and glycine in descending order. Individual amino acid contents ranged from 20.2 (methionine) to 153.8 mg/g of protein (glutamic acid) in triploids (**Table 4**). When compared to the reference amino acid pattern of children, all of the essential amino acid scores in diploids and triploids were more than 100, except that of methionine, no matter in the non-reproductive phase or the reproductive phase (**Table 5**).

In the non-reproductive phase, 21 fatty acids were present in diploids and triploids. The proportion of saturated fatty acids (SFAs) was lower in triploids than in diploids, while that of PUFAs was higher, indicating that triploids have a better fatty acid composition for human consumption than diploids during the non-reproductive phase. In diploids, the proportions of individual PUFAs making up the total PUFA content ranged from 0.16 ± 0.01% for γ-linolenic acid (18:3n-6) to 11.28 ± 1.05% for DHA (22:6n-3). In triploids, the dominant PUFA was also DHA (22:6n-3), accounting for 14.30 ± 0.39% of the total fatty acid content, and there appeared to be more n-3 than n-6 fatty acids (**Table 6**). During the reproductive phase, 19 fatty acids were found in diploid and triploid Hong Kong oysters. The fatty acid compositions of the diploids and triploids in the reproductive phase are shown in **Table 6**. The fatty acid profiles of both diploids and triploids were dominated by SFAs, which made up 58.26 and 55.34% of the total fatty acids, respectively. Among the SFAs, the proportions of fatty acids in diploids ranged from 0.10 ± 0.03% for lauric acid (12:0) to 38.35 ± 0.74 for palmitic acid (16:0), which was also the dominant SFA in triploids (37.6 ± 2.00% of the total fatty acids). EPA (20:5n-3) was the dominant PUFA in both diploids and triploids, followed by DHA (22:6n-3), ALA (18:3n-3), and LA (18:2n-6) in descending order. Triploids had a greater PUFA content than diploids, with PUFAs making up 37.71% of the total fatty acid content of triploids.

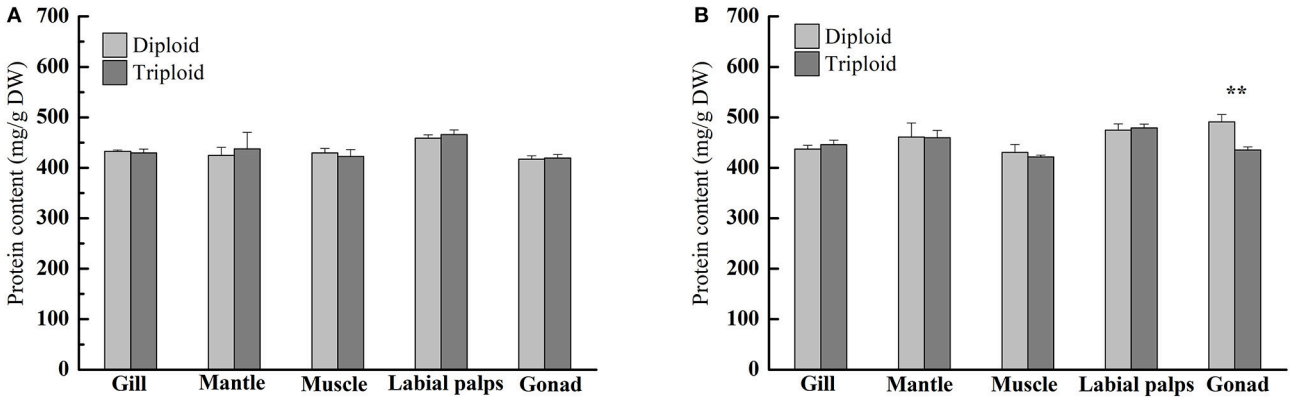

FIGURE 2 | Protein contents (mg/g, DW) of various tissues (gill, mantle, muscle, labial palps, and gonad) of diploid and triploid Hong Kong oysters, *Crassostrea hongkongensis*, in the non-reproductive phase **(A)** and reproductive phase **(B)**. Significant differences are indicated by asterisks (** represent $P < 0.01$).

TABLE 4 | Amino acid composition of diploid and triploid Hong Kong oysters, *Crassostrea hongkongensis,* in the non-reproductive and reproductive phases.

Amino acid	Non-reproductive				Reproductive			
	Content (g/100 g meat)		Content (mg/g protein)		Content (g/100 g meat)		Content (mg/g protein)	
	2N	3N	2N	3N	2N	3N	2N	3N
Aspartic acid	4.16 ± 0.60	4.27 ± 0.57	107.8	108.4	5.83 ± 0.98*a*	3.91 ± 0.07*b*	111.3	105.1
*Threonine	1.92 ± 0.27	1.93 ± 0.24	49.7	49.0	2.72 ± 0.48*a*	1.77 ± 0.04*b*	51.9	47.6
Serine	2.04 ± 0.25	2.00 ± 0.36	52.8	50.8	2.95 ± 0.64*a*	1.80 ± 0.03*b*	56.3	48.4
Glutamic acid	5.43 ± 0.66	5.86 ± 0.25	140.7	148.7	7.44 ± 1.30	5.72 ± 0.19	142.0	153.8
Proline	1.67 ± 0.28	1.81 ± 0.08	43.3	45.9	2.22 ± 0.29	1.76 ± 0.04	42.4	47.3
Glycine	2.46 ± 0.52	2.94 ± 0.38	63.7	74.6	2.97 ± 0.52	3.14 ± 0.04	56.7	84.4
Alanine	2.09 ± 0.26	2.24 ± 0.08	54.1	56.9	2.75 ± 0.48*a*	2.20 ± 0.04*b*	52.5	59.1
*Valine	2.07 ± 0.30	2.03 ± 0.30	53.6	51.5	2.88 ± 0.48*a*	1.83 ± 0.04*b*	55.0	49.2
*Methionine	0.71 ± 0.13	0.77 ± 0.03	18.4	19.5	0.95 ± 0.11*a*	0.75 ± 0.03*b*	18.1	20.2
*Isoleucine	1.73 ± 0.27	1.73 ± 0.27	44.8	43.9	2.48 ± 0.45*a*	1.55 ± 0.03*b*	47.3	41.7
*Leucine	2.78 ± 0.35	2.67 ± 0.41	72.0	67.8	3.92 ± 0.75*a*	2.45 ± 0.04*b*	74.8	65.9
Tyrosine	1.36 ± 0.13	1.38 ± 0.14	35.2	35.0	1.83 ± 0.36	1.31 ± 0.07	34.9	35.2
*Phenylalanine	2.01 ± 0.21	1.94 ± 0.32	52.1	49.2	2.87 ± 0.63*a*	1.74 ± 0.03*b*	54.8	46.8
*Lysine	3.18 ± 0.35	2.91 ± 0.51	82.4	73.9	4.32 ± 0.79*a*	2.63 ± 0.02*b*	82.4	70.7
*Histidine	0.94 ± 0.20	0.99 ± 0.16	24.4	25.1	1.22 ± 0.09*a*	0.92 ± 0.08*b*	23.3	24.7
*Arginine	2.74 ± 0.27	2.62 ± 0.28	71.0	66.5	3.71 ± 0.72*a*	2.46 ± 0.02*b*	70.8	66.1
Tryptophan	1.31 ± 0.02	1.32 ± 0.04	33.9	33.5	1.34 ± 0.10	1.26 ± 0.05	25.6	33.9
Total	38.60	39.41	999.9	1000.2	52.40	37.16	1000.1	999.0

Means ± SD followed by different letter within a line are significantly different ($P < 0.05$). "" indicate essential amino-acids.*

DISCUSSION

The Glycogen Content Variation Pattern Is Correlated With ChGS and ChGP mRNA Expression Patterns

According to our study, in the non-reproductive phase, there were statistically significant differences in gill and gonad glycogen content between diploids and triploids, as the glycogen content of triploid Hong Kong oysters increased in response to increasing translatable mRNA of *Ch*GS, especially in the labial palps and gonad. The same phenomenon has been observed in *C. gigas* and *C. virginica* (Bacca et al., 2005; Zeng et al., 2013; Guévélou et al., 2017). Pogoda et al. (2013) confirmed that *O. edulis* and *C. gigas* juveniles and adults primarily utilized glycogen to store energy, and that all tissues were capable of glycogen hydrolysis and glucose formation to provide ATP for growth. This process is known to be modulated by variations in *Ch*GS and *Ch*GP expressions. In our study, the rates of *Ch*GS and *Ch*GP transcription appeared to vary depending on the tissue and ploidy status. In the non-reproductive phase, highly significant differences ($P < 0.01$) in levels of *Ch*GS expression existed between diploid and triploid oysters in all five tissues. In the

TABLE 5 | Essential amino acid scores of diploid and triploid Hong Kong oysters, *Crassostrea hongkongensis,* in the non-reproductive and reproductive phases.

Amino acid	Reference (mg/g protein)	Non-reproductive		Reproductive	
		Score 2N	Score 3N	Score 2N	Score 3N
Threonine	34	146	144	153	140
Valine	35	153	147	157	141
Methionine	25	74	78	72	81
Isoleucine	28	160	157	169	149
Leucine	66	109	103	113	100
Phenylalanine + tyrosine	63	138	134	142	130
Lysine	58	142	127	142	122
Histidine	19	128	132	123	130
Tryptophan	11	308	304	233	308
Total	339				

Reference amino acid pattern for preschool children (2–5 years) (FAO/WHO/UNU, 1985). Each amino acid in the reference was presumed to score a value = 100. Score for each amino acid is expressed relative to the reference.

mantle, muscle, labial palps, and gonad, there were also very significant differences ($P < 0.01$) in *Ch*GP expression between diploid and triploid oysters. According to Dégremont et al. (2012) and Zhang et al. (2017), triploid oysters had a faster growth rate than diploids, and therefore had higher energy requirements for growth. Because of the faster growth in triploid Hong Kong oysters, the tissue-specific expressions of *Ch*GS and *Ch*GP (except in the gill) have been shown to be very significantly higher ($P < 0.01$) in triploids than in diploids (Zhang et al., 2017).

In the present study, significantly higher ($P < 0.05$) expressions of *Ch*GS in triploids were observed across the five tissues in the reproductive season, but expressions of *Ch*GP in all tissues were significantly lower ($P < 0.05$) in triploids than in diploids. This is in accordance with the higher glycogen content observed in all five tissues of triploid oysters. *Ch*GS and *Ch*GP mRNA expressions are closely related to glycogen content, as previously characterized in *C. gigas* (Berthelin et al., 2000a,b), so it is believed that the observed variations in *Ch*GS and *Ch*GP mRNA levels in diploid *C. hongkongensis* are closely linked to the stages of reproduction. Additionally, the OR of the glycogen content of the gonad of triploid oysters from the non-reproductive to the reproductive phase was much lower than that of diploids, indicating that much less glycogen was required to support gonad development in triploid Hong Kong oysters in the reproductive phase. Zwaan and Zandee (1972) and Berthelin et al. (2000a,b) reported the same phenomenon, finding that the storage and mobilization of glycogen was correlated with the reproductive cycle of bivalves. The glycogen storage levels of *Mytilus edulis* and *C. gigas* were lowest during the reproductive phase, while phytoplanktonic food was potentially abundant, suggesting that diploids were unable to store reserves at this time due to gametogenesis. Based on Zhang et al. (2017) and Qin et al. (2018), the gonad development and spawning stage of diploid Hong Kong oysters lasts from May to August. In our study, the diploids went through the maturation stage until July, and needed to consume large amounts of glycogen to support gonad development. In male diploid oysters, energy in the forms of glycogen would be mobilized for active production of germ cells, while in diploid females glycogen would be mobilized for vitellogenesis due to oocyte maturation, with the accumulation of yolk and other nutritive substances (Fabioux et al., 2004; Bacca et al., 2005; Zeng et al., 2013). In addition, according to Allen and Downing (1986) and Jeung et al. (2016), reproductive sterility is a common feature of triploid oysters as a result of the extra set of chromosomes, and gonadogenesis in triploids is either reduced or absent, with reduced numbers of gametes even if a small number of triploids are fertile.

From our results, together with previous studies, we conclude that in both diploid or triploid Hong Kong oysters, expressions of *Ch*GS and *Ch*GP appear to be related to glycogen content, indicating that their expressions are likely to be involved in glycogen regulation, as observed in other bivalves and mammals (Zwaan and Zandee, 1972; Towle, 1995; Berthelin et al., 2000a; Vali et al., 2000). Glycogen content is an important factor that affects taste, meaning that sterile triploid Hong Kong oysters have added value, because their increased glycogen content allows them to be marketed during the reproductive phase, when diploids suffer from low meat quality.

Crude Protein and Amino Acid Contents

Proteins are the fundamental building blocks for tissue biosynthesis and enzyme production in all animals. Dietary protein must meet the demands for tissue production and metabolic processes, and meat consumption is an important part of this for most consumers (Manninen et al., 2018). High-quality protein is generally considered most important for rapidly growing young chindren, followed by adults undergoing gametogenesis (Kirimura et al., 1969; Gatenby et al., 2003). High-quality protein content directly contributes to the nutritional value of food, and has a large effect on the market value. In the reproductive phase, there were no statistically significant differences in protein content between diploid and triploid oysters, which may indicate that the overwhelming majority of ATP supporting the fast growth of triploid Hong Kong oysters was produced thorugh glycogen metabolism. However, there was a significant difference ($P < 0.05$) between diploids and triploids in the protein content of the gonad, in agreement with a previous study done in *C. gigas* by Ren et al. (2003), in which gonad protein levels correlated positively with the gametogenic cycle, increasing with gonad development and oocyte diameter. Together with Dare and Edwards (1975), they concluded that glycogen and lipid stored in the mantle and gonad contributed to the increase in protein content in the gonad during the reproductive phase. Because of their sterility, the OR of triploids (3.75%) was smaller than that of diploids (17.72%) from the non-reproductive to the reproductive phase (**Table 3**). Based on the experiments, protein was typically the major biochemical component of diploid and triploid Hong Kong oysters and

TABLE 6 | Fatty acid composition (% of total fatty acids) of diploid and triploid Hong Kong oysters, *Crassostrea hongkongensis,* in the non-reproductive and reproductive phases.

Fatty acid	Non-reproductive		Reproductive	
	Mean ± SD/2N	Mean ± SD/3N	Mean ± SD/2N	Mean ± SD/3N
SATURATED FATTY ACID (SFA) COMPOSITION (%)				
8:0	–	–	0.25 ± 0.01	0.29 ± 0.05
12:0	–	–	0.10 ± 0.03	0.09 ± 0.02
14:0	3.04 ± 0.10	2.97 ± 0.09	6.13 ± 0.10a	3.42 ± 0.28b
15:0	1.42 ± 0.04	1.32 ± 0.04	0.98 ± 0.07	1.24 ± 0.17
16:0	38.13 ± 0.60a	33.7 ± 0.04b	38.35 ± 0.74	37.6 ± 2.00
17:0	4.25 ± 0.26a	3.79 ± 0.04b	2.64 ± 0.27	2.99 ± 0.21
18:0	11.23 ± 0.31a	9.84 ± 0.33b	9.53 ± 0.37	9.42 ± 0.67
20:0	0.21 ± 0.02	0.19 ± 0.01	0.28 ± 0.01	0.29 ± 0.03
21:0	0.10 ± 0.01	0.10 ± 0.01	–	–
22:0	0.34 ± 0.01	0.33 ± 0.01	–	–
ΣSFA	58.72	52.24	58.26	55.34
MONOUNSATURATED FATTY ACID (MUFA) COMPOSITION (%)				
16:1n-7	1.95 ± 0.06	1.94 ± 0.11	4.46 ± 0.50	3.97 ± 0.47
18:1n-9	5.39 ± 0.05	5.41 ± 0.02	4.42 ± 0.47	5.09 ± 0.30
20:1n-9	0.90 ± 0.03	0.83 ± 0.05	–	–
22:1n-9	1.28 ± 0.10a	0.98 ± 0.07b	–	–
ΣMUFA	9.52	9.16	8.88	9.06
POLYUNSATURATED FATTY ACID (PUFA) COMPOSITION (%)				
18:2n-6	2.49 ± 0.12a	2.79 ± 0.05b	2.57 ± 0.11a	3.25 ± 0.06b
18:3n-6	0.16 ± 0.01a	0.18 ± 0.01b	0.33 ± 0.02a	0.46 ± 0.02b
18:3n-3	2.88 ± 0.39a	3.85 ± 0.09b	4.25 ± 0.31a	5.13 ± 0.35b
20:2n-6	0.40 ± 0.01	0.41 ± 0.02	0.40 ± 0.04	0.35 ± 0.02
20:3n-6	0..22 ± 0.01	0.21 ± 0.01	0.28 ± 0.03	0.28 ± 0.01
20:4n-6	3.43 ± 0.08	3.35 ± 0.12	2.13 ± 0.52	2.01 ± 0.03
20:3n-3	0.20 ± 0.01	0.22 ± 0.02	0.24 ± 0.03	0.23 ± 0.02
20:5n-3	10.49 ± 0.71a	14.27 ± 0.83b	13.4 ± 0.44a	15.07 ± 0.71b
22:6n-3	11.28 ± 1.05a	14.30 ± 0.39b	8.61 ± 0.24a	10.93 ± 0.84b
ΣPUFA	31.55	39.58	32.21	37.71
ΣPUFA n-3	24.85	32.64	26.50	31.36
ΣPUFA n-6	6.70	6.94	5.71	6.35
ΣPUFA n-3/ΣPUFA n-6	3.71	4.70	4.64	4.94
ΣPUFA n-6/ΣPUFA n-3	0.27	0.21	0.22	0.20

Means ± SD followed by different letter within a line are significantly different ($P < 0.05$). "–" indicates <0.0033%.

maintained a relatively stable levels (consistently above 40% DW) compared to glycogen between the reproductive and non-reproductive phases, similar to diploid *C. gigas* (Ren et al., 2003), *O. edulis* (Ruiz et al., 1992), and *M. edulis* (Dare and Edwards, 1975). In general, we confirmed that both diploid and triploid oysters were high protein foods regardless of the phase of the reproductive cycle.

Amino acids are associated with flavors of sweetness, bitterness, sourness, saltiness, and umami, and are very important in contributing to the taste of foodstuffs. Protein quality is determined based on levels of essential amino acids for humans (Kirimura et al., 1969). In the non-reproductive phase, there were no significant differences between the levels of individual amino acids in diploid and triploid oysters. In both diploids and triploids, the methionine content was the lowest of the essential amino acids, and had scores of <100 when compared to the reference amino acid pattern for preschool children (2–5 years old) (FAO/WHO/UNU, 1985), indicating that methionine was the limiting amino acid in both diploid and triploid Hong Kong oysters (**Table 5**). Glutamic acid and aspartic acid were found to be major non-essential amino acids in diploids and triploids, as reported in *C. gigas* (Kong et al., 2001) and

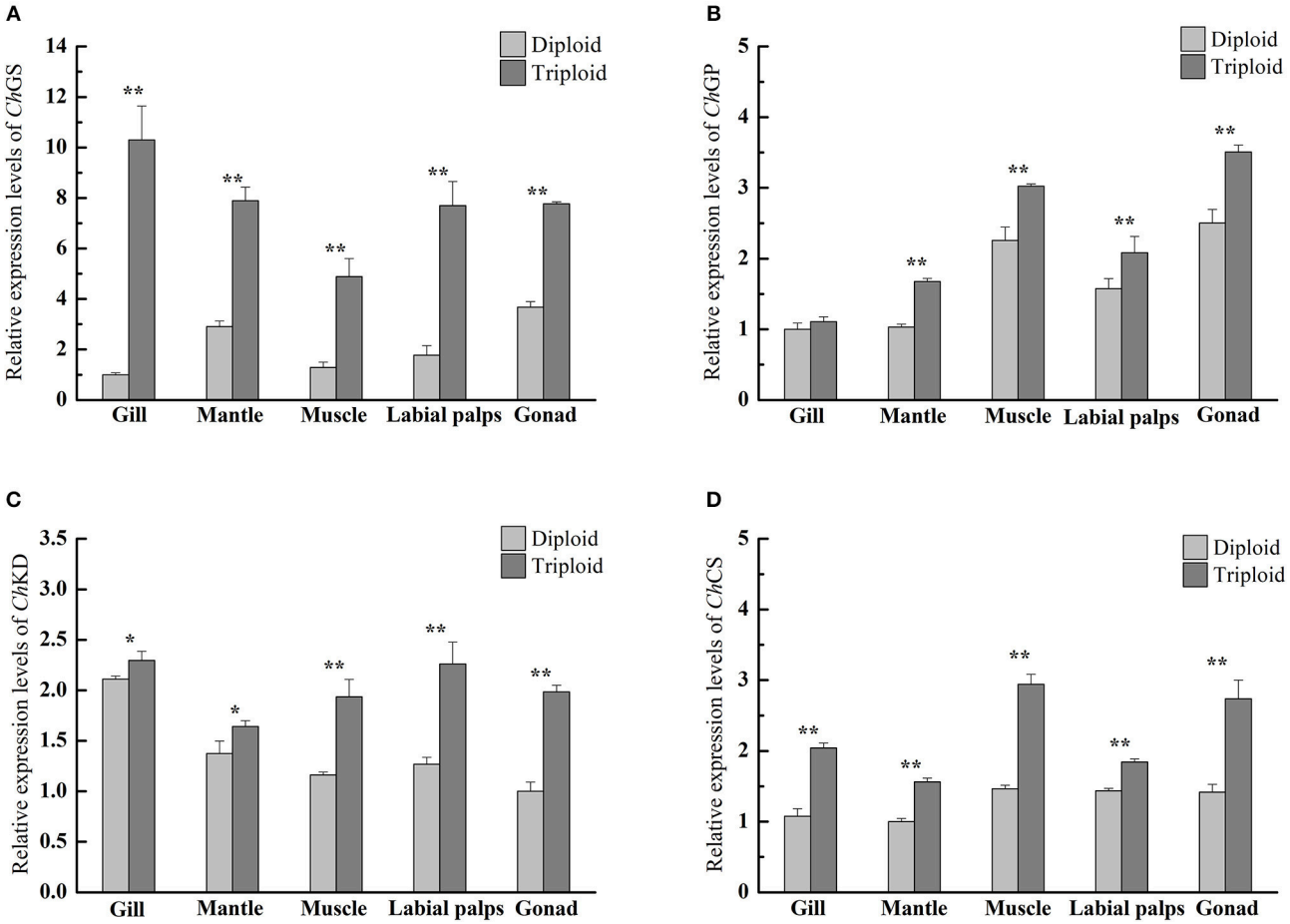

FIGURE 3 | Quantitative PCR analysis of relative mRNA expressions of *Ch*GS **(A)**, *Ch*GP **(B)**, *Ch*KD **(C),** and *Ch*CS **(D)** in various tissues (gill, mantle, muscle, labial palps, and gonad) of diploid and triploid Hong Kong oysters in the non-reproductive phase. Each bar represents the mean of the normalized expression levels of the replicates ($n = 3$). Significant differences are indicated by asterisks (* and ** represent $P < 0.05$ and $P < 0.01$, respectively).

M. edulis (Su et al., 1998). In the reproductive phase, significant differences ($P < 0.05$) existed in the individual essential amino acid levels between diploids and triploids, particularly for valine, isoleucine, leucine, phenylalanine, and lysine, which were higher in diploids and had ORs of −8.01, −6.78, −10.53, −12.38, and −11.50%, respectively. This is likely related to gonad development, as reported in *C. gigas* by Kong et al. (2001). Kong et al. (2001) also found that the amino acid composition of diploid *C. gigas* changed dramatically with gonad development, but remained relatively stable in triploids. According to the reference amino acid pattern, methionine levels did not meet the recommendations for preschool children in either diploids or triploids (scored <100); however, given that about 55% of methionine is lost when meat was hydrolyzed without performic acid oxidation, the true methionine score would likely be over 100 (Spindler et al., 1985; Chen et al., 2007). Overall, diploid and triploid Hong Kong oysters are high protein foods and are relatively well-balanced in terms of essential amino acid composition, which indicates that they are a high-quality protein source.

Fatty Acid Content

Essential fatty acids, namely ALA, LA, EPA, and DHA, are very important for human health (Coetzee and Hoffman, 2002). ALA and DHA are major components of cell membrane phospholipids and are the predominant long-chain PUFAs of the central nervous system (Dyerberg, 1986). The ratio between n-3 and n-6 long chain PUFAs (n-3/n-6) is also considered to be important (Coetzee and Hoffman, 2002; Simopoulos, 2008). Lack of n-3 PUFAs and very low n-3/n-6 ratios promote the pathogenesis of many diseases, including cancer, inflammatory, and autoimmune diseases (Park et al., 1994). In both the non-reproductive and the reproductive phases, the proportion of saturated fatty acids (SFAs) was lower and that of polyunsaturated fatty acids (PUFAs) was higher in triploids than in diploids, indicating that triploids have better fatty acid composition as a human food source (Chen and Zhang, 2007). In both phases, significant differences ($P < 0.05$) were observed between diploids and triploids in the proportions of LA, ALA, γ-linolenic acid, EPA, and DHA. EPA and DHA were the dominant PUFAs. Many researchers have also confirmed that variations in the fatty acid composition of bivalves

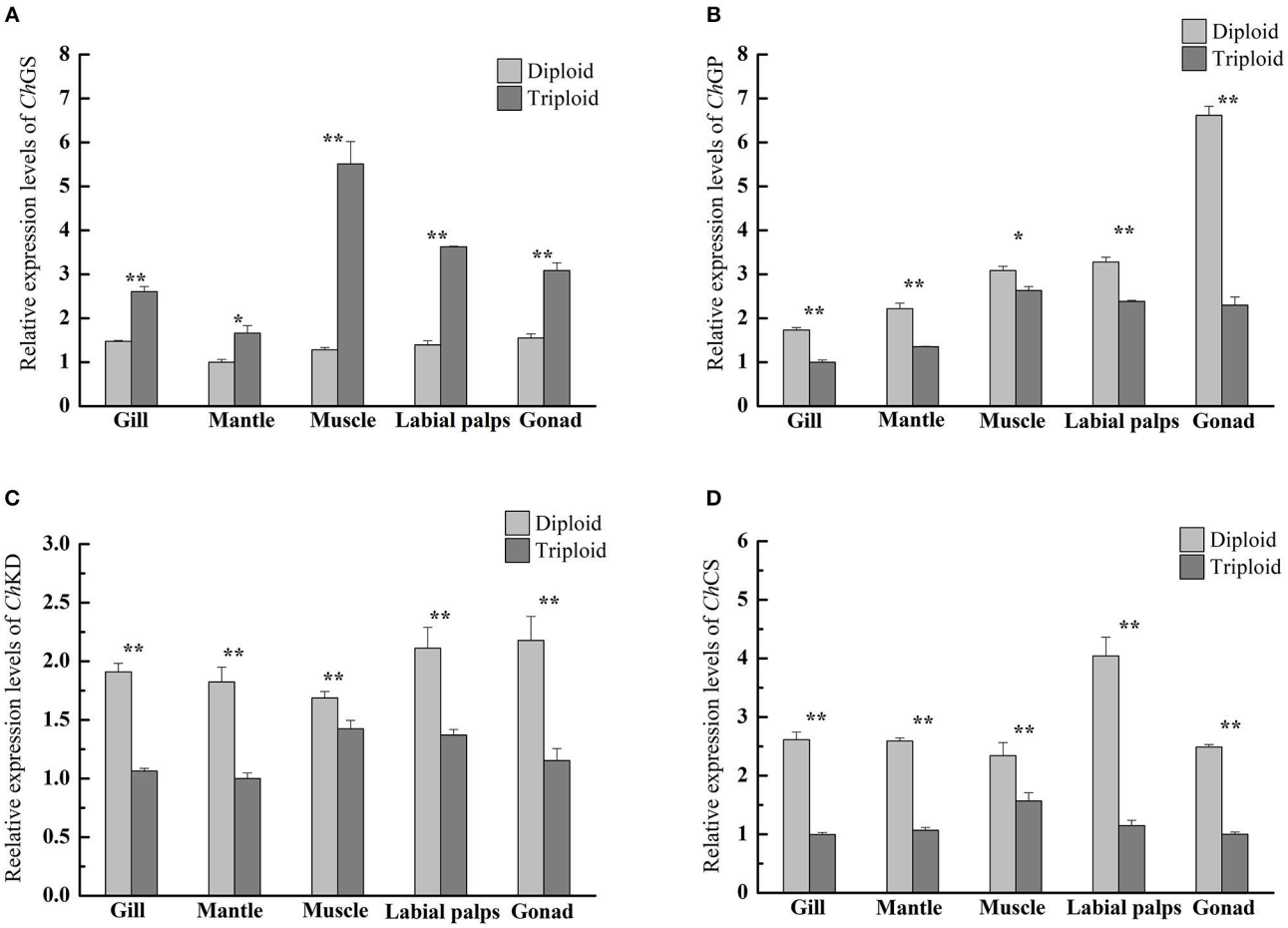

FIGURE 4 | Quantitative PCR analysis of relative mRNA expressions of *Ch*GS **(A)**, *Ch*GP **(B)**, *Ch*KD **(C),** and *Ch*CS **(D)** in various tissues (gill, mantle, muscle, labial palps, and gonad) of diploid and triploid Hong Kong oysters in the reproductive phase. Each bar represents the mean of the normalized expression levels of the replicates ($n = 3$). Significant differences are indicated by asterisks (* and ** represent $P < 0.05$ and $P < 0.01$, respectively).

were related to gametogenic cycle, such as in *C.gigas* (Dridi et al., 2007), *Subnodosus nodipecten* (Racotta et al., 2008), *R. decussatus* (Ojea et al., 2004), and *M. galloprovincialis* (Orban et al., 2002).

Furthermore, the proportion of n-3 PUFAs was significantly higher than that of n-6 in both diploid and triploid Hong Kong oysters. An increase in the levels of n-3 PUFAs in the triploid oysters effectively reduced the proportion of SFAs, making them healthier for human consumption (Celik et al., 2004). There is no question that n-3 PUFAs are important in the human diet, or that they are found in a wide variety of foods. The n-3/n-6 ratio is a good index for comparing the relative nutritional value of foods from different sources, and a high n-3/n-6 PUFA ratio has often been cited as an indicator of high nutritional value (Skonberg and Perkins, 2002). The n-3/n-6 PUFA ratio of triploid Hong Kong oysters was higher than that of diploids in both the non-reproductive (4.70 and 3.71, respectively) and reproductive (4.94 and 4.64, respectively) phases. By contrast, in *C. gigas*, the n-3/n-6 PUFA ratio was only 3.15 in the non-reproductive stage and only 2.45 in the reproductive stage (Dridi et al., 2007). The difference in fatty acid composition and the n-3/n-6 PUFA ratio between *C. gigas* and *C. hongkongensis* can be attributed to special biological traits (endogenous origins) and living environments (exogenous origins). Orban et al. (2002) confirmed a close relationship between temperature and PUFA compositions in *M. galloprovincialis*, and Napolitano et al. (1997) reported that seasonal variations in fatty acid composition of *Placopecten magellanicus* reflected the fatty acid composition of the phytoplankton. Precisely the opposite from *C. gigas*, *C. hongkongensis* live in a high temperature and low salt sea area. As *C. hongkongensis* grow slowly, it usually takes 3 years to reach the specified commercial size (Qin et al., 2018). Dyerberg noted that an increase in the ratio of n-3/n-6 PUFAs increases the availability of n-3 PUFAs, which are beneficial for human health (Dyerberg, 1986). In general, triploid Hong Kong oysters have higher nutritional value than diploids, since the ratio of n-3/n-6 PUFAs is higher than diploids.

The Tricarboxylic Acid Cycle Related to Variations in Biochemical Composition

The tricarboxylic acid (TCA) cycle is the final metabolic pathway of glycogen, lipids and proteins, and is also a hub for the metabolism of three major nutrients. The biochemical

composition of organisms is closely related to the TCA cycle. *Ch*CS and *Ch*KD are the key enzyme genes in the TCA cycle. According to our research, during the non-reproductive phase, the relative expressions of *Ch*KD and *Ch*CS were significant higher ($P < 0.05$) in all five tissues (gill, mantle, muscle, labial palps, and gonad) of triploids than in those of diploids (**Figures 3C,D**). Interestingly, the glycogen content was significantly higher in the gill and gonad of triploids than those of diploids, while there was no signiciant difference in protein content between triploids and diploids. Although the high levels of expression of *Ch*GS and *Ch*GP were related to glycogen metabolism, higher expressions of *Ch*KD and *Ch*CS in triploid oysters revealed that these oysters have a higher matabolic rate than diploid oysters, which may contribute to their faster growth. The same phenomenon was discovered by Li et al. (2017), who found that the TCA cycle was enhanced in *C. gigas* by high glycogen content in the non-reproductive stage, implying that increased energy metabolism occurs in the high-glycogen Pacific oysters.

In the reproductive phase, the glycogen contents of all five tissues (gill, mantle, muscle, labial palps, and gonad) of triploid Hong Kong oysters were significantly higher than those of diploids, but the protein content of the gonad of diploids was significantly higher than that of triploids. Correspondingly, the relative expressions of *Ch*KD and *Ch*CS in the five tissues of triploids were significantly lower ($P < 0.05$) than in diploids (**Figures 4C,D**). In addition, from the non-reproductive to the reproductive phase, the glycogen content of the diploid gonad decreased more and the protein content of the diploid gonad increased more than those of triploids. Previous studies on *O. edulis* and *C. gigas* confirmed that glycogen was a preferred energy form for supporting gametogenesis and growth (Pogoda et al., 2013; Li et al., 2017). The simultaneous glycogen decrease and protein increase may indicate the conversion of glycogen into protein during gonad development, as suggested in previous studies on other oyster species such as *C. gigas* and O. e*dulis* (Ruiz et al., 1992; Dridi et al., 2007). Moreover, triploids undergo less gonad development than diploids, and therefore require less energy to support gonad development. This may account for the variations in biochemical composition and relative expressions of *Ch*KD and *Ch*CS of diploid and triploid Hong Kong oysters.

AUTHOR CONTRIBUTIONS

YQ, ZY, and YZ designed experiments. YQ carried all of the experiments with the help of HM, XW, SX, JL, and RM. YQ analyzed the data and wrote the paper. ZY and YZ critically revised the manuscript and approved the final version to be published.

FUNDING

This research was supported by the Guangdong Province Program, China (2014B020202011; 2014A020208083; A201601A04; 2016B020233005; 2016TQ03N905), Guangdong Key Laboratory of Applied Marine Biology program (2017B030314052), the China Agriculture Research System (No. CARS-49), and the National Science Foundation of China (No. 31702340; 31572640).

REFERENCES

Allen, S. K., and Downing, S. L. (1986). Performance of triploid Pacific oysters, *Crassostrea gigas* (Thunberg). I. Survival, growth, glycogen content, and sexual maturation in yearlings. *J. Exp. Mar. Biol. Ecol.* 102, 197–208. doi: 10.1016/0022-0981(86)90176-0

Bacca, H., Huvet, A., Fabioux, C., Daniel, J. Y., Delaporte, M., Pouvreau, S., et al. (2005). Molecular cloning and seasonal expression of oyster glycogen phosphorylase and glycogen synthase genes. *Compar. Biochem. Physiol. Part B Biochem. Mol. Biol.* 140, 635–646. doi: 10.1016/j.cbpc.2005.01.005

Berthelin, C., Kellner, K., and Mathieu, M. (2000a). Histological characterization and glucose incorporation into glycogen of the Pacific oyster *Crassostrea gigas* storage cells. *Mar. Biotechnol.* 2, 136–145. doi: 10.1007/s101269900017

Berthelin, C., Kellner, K., and Mathieu, M. (2000b). Storage metabolism in the Pacific oyster (*Crassostrea gigas*) in relation to summer mortalities and reproductive cycle (west coast of France). *Compar. Biochem. Physiol. Part B* 125, 359–369. doi: 10.1016/S0305-0491(99)00187-X

Callam, B. R., Allen, S. K., and Frank-Lawale, A. (2016). Genetic and environmental influence on triploid *Crassostrea virginica* grown in Chesapeake Bay: growth. *Aquaculture* 452, 97–106. doi: 10.1016/j.aquaculture.2015.10.027

Celik, M., Tureli, C., Celik, M., Yanar, Y., Erdem, U., and Kucukgulmez, A. (2004). Fatty acid composition of the blue crab (*Callinectes sapidus* Rathbun, 1896) in the north eastern Mediterranean. *Food Chem.* 88, 271–273. doi: 10.1016/j.foodchem.2004.01.038

Chen, D.-W., and Zhang, M. (2007). Non-volatile taste active compounds in the meat of Chinese mitten crab (*Eriocheir sinensis*). *Food Chem.* 104, 1200–1205. doi: 10.1016/j.foodchem.2007.01.042

Chen, D. W., Zhang, M., and Shrestha, S. (2007). Compositional characteristics and nutritional quality of Chinese mitten crab (*Eriocheir sinensis*). *Food Chem.* 103, 1343–1349. doi: 10.1016/j.foodchem.2006.10.047

Coetzee, G. J. M., and Hoffman, L. C. (2002). Effects of various dietary n-3 / n-6 fatty acid ratios on the performance and body composition of broilers. *S. Afr. J. Anim. Sci.* 32, 175–184. doi: 10.4314/sajas.v32i3.3744

Dare, P. J., and Edwards, D. B. (1975). Seasonal changes in flesh weight and biochemical composition of mussels (*Mytilus edulis* L.) in the Conwy Estuary, North Wales. *J. Exp. Mar. Biol. Ecol.* 18, 89–97. doi: 10.1016/0022-0981(75)90066-0

Dégremont, L., Garcia, C., Frank-Lawale, A., and Allen, S. K. (2012). Triploid oysters in the chesapeake bay: comparison of diploid and triploid *Crassostrea virginica*. *J. Shellfish Res.* 31, 21–31. doi: 10.2983/035.031.0103

Doan, L. P., Thuy, N. T., Long, P. Q., Quan, P. M., Thuy, T. T. T., Minh, P. T. H., et al. (2018). Fatty acid, tocopherol, sterol compositions and antioxidant activity of three garcinia seed oils. *Rec. Nat. Prod.* 12, 323–331. doi: 10.25135/rnp.32.17.09.051054

Downing, S. L., and Allen, S. K. (1987). Induced triploidy in the Pacific oyster, *Crassostrea gigas*: optimal treatments with cytochalasin B depend on temperature. *Aquaculture* 61, 1–15. doi: 10.1016/0044-8486(87)90332-2

Dridi, S., Romdhane, M. S., and Elcafsi, M. H. (2007). Seasonal variation in weight and biochemical composition of the Pacific oyster, *Crassostrea gigas* in relation to the gametogenic cycle and environmental conditions of the Bizert lagoon, Tunisia. *Aquaculture* 263, 238–248. doi: 10.1016/j.aquaculture.2006.10.028

Dyerberg, J. (1986). Linolenate-derived polyunsaturated fatty acids and prevention of atherosclerosis. *Nutr. Rev.* 44, 125–134. doi: 10.1111/j.1753-4887.1986.tb07603.x

Fabioux, C., Pouvreau, S., Le Roux, F., and Huvet, A. (2004). The oyster vasa-like gene: a specific marker of the germline in *Crassostrea gigas*. *Biochem. Biophys. Res. Commun.* 315, 897–904. doi: 10.1016/j.bbrc.2004.01.145

FAO/WHO/UNU. (1985). *Energy and Protein Requirements*. Report of a Joint FAO/WHO/UNU expert consultation.

Gatenby, C. M., Orcutt, D. M., Kreeger, D. A., Parker, B. C., Jones, V. A., and Neves, R. J. (2003). Biochemical composition of three algal species proposed as food for captive freshwater mussels. *J. Appl. Phycol.* 15, 1–11. doi: 10.1023/A:1022929423011

Greiwe, J. S., Hickner, R. C., and Hansen, P. A. (1999). Effects of endurance exercise training on muscle glycogen accumulation in humans. *J. Appl. Physiol.* 87, 222–226. doi: 10.1152/jappl.1999.87.1.222

Guévélou, E., Matt, J. L., and Allen, S. K. (2017). Glycogen Concentration in freeze-dried tissues of eastern oyster (*Crassostrea virginica*) using near infrared reflectance spectroscopy to determine the relationship between concentrations of the tissues excised for histological sampling and the remaining tissues. *J. Shellfish Res.* 36, 325–333. doi: 10.2983/035.036.0204

Houcke, J. V., Medina, I., Linssen, J., and Luten, J. (2016). Biochemical and volatile organic compound profile of European flat oyster (*Ostrea edulis*) and Pacific cupped oyster (*Crassostrea gigas*) cultivated in the Eastern Scheldt and Lake Grevelingen, the Netherlands. *Food Control* 68, 200–207. doi: 10.1016/j.foodcont.2016.03.044

Hugli, T. E., and Moore, S. (1972). Determination of the tryptophan content of proteins by ion exchange chromatography of alkaline hydrolysates. *J. Biol. Chem.* 247, 2828–2834.

Iqbal, A., Khalil, I. A., Ateeq, N., and Khan, M. S. (2006). Nutritional quality of important food legumes. *Food Chem.* 97, 331–335. doi: 10.1016/j.foodchem.2005.05.011

Jeung, H.-D., Keshavmurthy, S., Lim, H.-J., Kim, S.-K., and Choi, K.-S. (2016). Quantification of reproductive effort of the triploid Pacific oyster, *Crassostrea gigas* raised in intertidal rack and bag oyster culture system off the west coast of Korea during spawning season. *Aquaculture* 464, 374–380. doi: 10.1016/j.aquaculture.2016.07.010

Kirimura, J., Shimizu, A., Kimizuka, A., Ninomiya, T., and Katsuya, N. (1969). Contribution of peptides and amino acids to the taste of foods. *J. Agric. Food Chem.* 17, 689–695. doi: 10.1021/jf60164a031

Kong, L., Wang, Z., Yu, R., and Wang, R. (2001). Comparison of biochemical composition and amino acid contents between diploid and triploid Pacific oyster, *Crassostrea gigas*, pre and post spawning. *Trans. Oceanol. Limnol.* 4, 44–49.

Lam, K., and Morton, B. (2003). Mitochondrial DNA and morphological identification of a new species of Crassostrea (Bivalvia: Ostreidae) cultured for centuries in the Pearl River Delta, Hong Kong, China. *Aquaculture* 228, 1–13. doi: 10.1016/S0044-8486(03)00215-1

Li, B., Song, K., Meng, J., Li, L., and Zhang, G. (2017). Integrated application of transcriptomics and metabolomics provides insights into glycogen content regulation in the Pacific oyster *Crassostrea gigas*. *BMC Genomics* 18:713. doi: 10.1186/s12864-017-4069-8

Lv, M., Mei, K., Zhang, H., Xu, D., and Yang, W. (2018). Effects of electron beam irradiation on the biochemical properties and structure of myofibrillar protein from *Tegillarca granosa* meat. *Food Chem.* 254, 64–69. doi: 10.1016/j.foodchem.2018.01.165

Manninen, H., Rotola-Pukkila, M., Aisala, H., Hopia, A., and Laaksonen, T. (2018). Free amino acids and 5'-nucleotides in Finnish forest mushrooms. *Food Chem.* 247:23. doi: 10.1016/j.foodchem.2017.12.014

Napolitano, G. E., Pollero, R. J., Gayoso, A. M., MacDonald, B. A., and Thompson, R. J. (1997). Fatty acids as trophic markers of phytoplankton blooms in the Bahía Blanca estuary (Buenos Aires, Argentina) and in Trinity Bay (Newfoundland, Canada). *Biochem. Syst. Ecol.* 25, 739–755. doi: 10.1016/S0305-1978(97)00053-7

Ojea, J., Pazos, A. J., Martinez, D., Novoa, S., Sanchez, J. L., and Abad, M. (2004). Seasonal variation in weight and biochemical composition of the tissues of *Ruditapes decussatus* in relation to the gametogenic cycle. *Aquaculture* 238, 451–468. doi: 10.1016/j.aquaculture.2004.05.022

Orban, E., Lena, G. D., Nevigato, T., Casini, I., Marzetti, A., and Caproni, R. (2002). Seasonal changes in meat content, condition index and chemical composition of mussels (*Mytilus galloprovincialis*) cultured in two different Italian sites. *Food Chem.* 77, 57–65. doi: 10.1016/S0308-8146(01)00322-3

Park, J. W., Testin, R. F., Park, H. J., Vergano, P. J., and Weller, C. L. (1994). Fatty acid concentration effect on tensile strength, elongation, and water vapor permeability of laminated edible films. *J. Food Sci.* 59, 916–919. doi: 10.1111/j.1365-2621.1994.tb08157.x

Pogoda, B., Buck, B. H., Saborowski, R., and Hagen, W. (2013). Biochemical and elemental composition of the offshore-cultivated oysters *Ostrea edulis* and *Crassostrea gigas*. *Aquaculture* 400–401, 53–60. doi: 10.1016/j.aquaculture.2013.02.031

Qin, Y., Xiao, S., Ma, H., Mo, R., Zhou, Z., Wu, X., et al. (2018). Effects of salinity and temperature on the timing of germinal vesicle breakdown and polar body release in diploid and triploid Hong Kong oysters, *Crassostrea hongkongensis*, in relation to tetraploid induction. *Aquac. Res.* 49, 3647–3657. doi: 10.1111/are.13833

Qin, Y., Zhang, Y., Zhou, Y., Wu, X., Peng, M., and Yu, Z. (2017). Comparative studies on triploidy induction using CB and 6-DMAP in *Crassostrea hongkongensis*. *J. Fish. China* 41, 250–257. doi: 10.11964/jfc.20151110167

Racotta, I. S., Palacios, E., Ibarra, A. M., Ramírez, J. L., Arcos, F., and Arjona, O. (2008). Comparative biochemical composition of ploidy groups of the lion-paw scallop (Nodipecten subnodosus Sowerby) supports the physiological hypothesis for the lack of advantage in triploid mollusc's growth in food-rich environments. *Mar. Biol.* 153, 1245–1256. doi: 10.1007/s00227-007-0897-4

Ren, J., Marsden, I., Ross, A., and Schiel, D. (2003). Seasonal variation in the reproductive activity and biochemical composition of the Pacific oyster (*Crassostrea gigas*) from the Marlborough Sounds, New Zealand. *N. Z. J. Mar. Freshw. Res.* 37, 171–182. doi: 10.1080/00288330.2003.9517155

Ruiz, C., Martinez, D., Mosquera, G., Abad, M., and Sánchez, J. L. (1992). Seasonal variations in condition, reproductive activity and biochemical composition of the flat oyster, *Ostrea edulis*, from San Cibran (Galicia, Spain). *Mar. Biol.* 112, 67–74. doi: 10.1007/BF00349729

Shpigel, M., and Spencer, B. (1996). Performance of diploid and triploid Manila clams (*Tapes philippinarum*, Adams and Reeve) at various levels of tidal exposure in the UK and in water from fish ponds at Eilat, Israel. *Aquaculture* 141, 159–171. doi: 10.1016/0044-8486(95)01236-2

Simopoulos, A. P. (2008). The importance of the omega-6/omega-3 fatty acid ratio in cardiovascular disease and other chronic diseases. *Exp. Biol. Med.* 233, 674–688. doi: 10.3181/0711-MR-311

Skonberg, D. I., and Perkins, B. L. (2002). Nutrient composition of green crab (*Carcinus maenus*) leg meat and claw meat. *Food Chem.* 77, 401–404. doi: 10.1016/S0308-8146(01)00364-8

Soudant, P., Ryckeghem, K. V., Marty, Y., Moal, J., Samain, J. F., and Sorgeloos, P. (1999). Comparison of the lipid class and fatty acid composition between a reproductive cycle in nature and a standard hatchery conditioning of the Pacific Oyster *Crassostrea gigas*. *Compar. Biochem. Physiol. Part B Biochem. Mol. Biol.* 123, 209–222. doi: 10.1016/S0305-0491(99)00063-2

Spindler, M., Stadler, R., and Tanner, H. (1985). Amino acid analysis of feedstuffs: determination of methionine and cystine after oxidation with performic acid and hydrolysis. *J. Agric. Food Chem.* 32, 24–26.

Stanley, J. G., Allen, S. K., and Hidu, H. (1981). Polyploidy induced in the American oyster, *Crassostrea virginica*, with cytochalasin B. *Aquaculture* 23, 1–10. doi: 10.1016/0044-8486(81)90002-8

Su, X., Li, T., and Ding, M. (1998). Studies on the nutritive contents of the mussel *Mytilus edulis* and *Mytilus coruscus*. *Chin. J. Mar. Drugs* 2, 30–32.

Towle, H. C. (1995). Metabolic regulation of gene transcription in mammals. *J. Biol. Chem.* 270, 23235–23238. doi: 10.1074/jbc.270.40.23235

Utting, S. D., and Child, A. R. (1994). Genetic manipulation of the Manila clam (*Tapes philippinarum*) using cytochalasin B to induce triploidy. *Aquaculture* 120, 271–282. doi: 10.1016/0044-8486(94)90084-1

Vali, S., Carlsen, R., Pessah, I., and Gorin, F. (2000). Role of the sarcoplasmic reticulum in regulating the activity-dependent expression of the glycogen phosphorylase gene in contractile skeletal muscle cells. *J. Cell. Physiol.* 185, 184–199. doi: 10.1002/1097-4652(200011)185:2<184::AID-JCP3>3.0.CO;2-T

Wang, F., Xiao, S., Zhang, Y., Zhang, Y., Liu, Y., Yan, Y., et al. (2015). ChAkt1 involvement in orchestrating the immune and heat shock responses in *Crassostrea hongkongensis*: molecular cloning and functional characterization. *Fish Shellfish Immunol.* 47, 1015–1023. doi: 10.1016/j.fsi.2015.11.009

Wang, Z. P., Guo, X., Allen, S. K., and Wang, R. C. (2002). Heterozygosity and body size in triploid Pacific oysters, *Crassostrea gigas* Thunberg, produced

from meiosis II inhibition and tetraploids. *Aquaculture* 204, 337–348. doi: 10.1016/S0044-8486(01)00845-6

Zeng, Z., Jianbin, N. I., and Caihuan, K. E. (2015). Glycogen content relative to expression of glycogen phosphorylase(GPH) and hexokinase(HK) during the reproductive cycle in the Fujian Oyster, *Crassostrea angulata*. *Acta Oceanol. Sin.* 34, 66–76. doi: 10.1007/s13131-015-0639-2

Zeng, Z., Ni, J., and Ke, C. (2013). Expression of glycogen synthase (GYS) and glycogen synthase kinase 3beta (GSK3beta) of the Fujian oyster, *Crassostrea angulata*, in relation to glycogen content in gonad development. *Compar. Biochem. Physiol. Part B Biochem. Mol. Biol.* 166, 203–214. doi: 10.1016/j.cbpb.2013.09.003

Zhang, L., Lin, Q., Feng, Y., Fan, X., Zou, F., Yuan, D. Y., et al. (2015). Transcriptomic identification and expression of starch and sucrose metabolism genes in the seeds of Chinese Chestnut (*Castanea mollissima*). *J. Agric. Food Chem.* 63, 929–942. doi: 10.1021/jf505247d

Zhang, Y., Li, J., Qin, Y., Zhou, Y., Zhang, Y., and Yu, Z. (2017). A comparative study of the survival, growth and gonad development of the diploid and triploid Hong Kong oyster, *Crassostrea hongkongensis* (Lam & Morton 2003). *Aquac. Res.* 48, 2453–2462. doi: 10.1111/are.13081

Zhou, Y., Mao, F., He, Z., Li, J., Zhang, Y., Xiang, Z. (2018). The molecular mechanism underlying pro-apoptotic role of hemocytes specific transcriptional factor Lhx9 in *Crassostrea hongkongensis*. *Front. Physiol.* 9:612. doi: 10.3389/fphys.2018.00612

Zwaan, A. D., and Zandee, D. I. (1972). Body distribution and seasonal changes in the glycogen content of the common sea mussel *Mytilus edulis*. *Compar. Biochem. Physiol. Part A Physiol.* 43, 53–58. doi: 10.1016/0300-9629(72)90468-9

Conflict of Interest Statement: The authors declare that the research was conducted in the absence of any commercial or financial relationships that could be construed as a potential conflict of interest.

Advantages of publishing in Frontiers

OPEN ACCESS
Articles are free to read for greatest visibility and readership

FAST PUBLICATION
Around 90 days from submission to decision

HIGH QUALITY PEER-REVIEW
Rigorous, collaborative, and constructive peer-review

TRANSPARENT PEER-REVIEW
Editors and reviewers acknowledged by name on published articles

Frontiers
Avenue du Tribunal-Fédéral 34
1005 Lausanne | Switzerland

Visit us: www.frontiersin.org
Contact us: info@frontiersin.org | +41 21 510 17 00

REPRODUCIBILITY OF RESEARCH
Support open data and methods to enhance research reproducibility

DIGITAL PUBLISHING
Articles designed for optimal readership across devices

FOLLOW US
@frontiersin

IMPACT METRICS
Advanced article metrics track visibility across digital media

EXTENSIVE PROMOTION
Marketing and promotion of impactful research

LOOP RESEARCH NETWORK
Our network increases your article's readership